On the afterglow of Gamma-Ray Bursts within the EMBH model

Federico Fraschetti

UNIVERSITÀ DEGLI STUDI DI TRENTO
Facoltà di Scienze Matematiche, Fisiche e Naturali
Scuola di dottorato in Fisica
XVII ciclo

On the afterglow of Gamma-Ray Bursts within the EMBH model

Supervisor
Prof. Luciano Vanzo

Candidate
Dott. Federico Fraschetti

External Supervisor:
Prof. Remo Ruffini

Accademic Year 2003–2004

(Defended November 4^{th}, 2004)

Contents

List of Figures

1 Introduction and summary

Among the variety of astrophysical phenomena, Gamma-Ray Bursts (GRBs) are the most fascinating, as witnessed by the daily frequency of publications on this subject. The feature making them unique is the huge amount of energy they emit in a short time interval as electromagnetic radiation: in one second they reach the luminosity of all stars of the whole visible universe in that second.

Until almost 40 years ago GRBs were completely unknown and no astrophysical or cosmological model predicted their existence. The GRBs were discovered by chance in 1967 by *Vela* satellites, which were part of a space US program aimed to verify the observance of a nuclear weapon band treaty.

The first revolution dates back in Spring 1991 by *BATSE* detector; the observations of *BATSE* confirmed that GRBs are isotropic: from the catalogs of more than 2000 events it has been concluded that there is not any preferential direction in space. Moreover a bimodal distribution of GRBs according to their temporal duration has been found. The second revolution occurred on February 27^{th} 1997 when the Italian-Dutch satellite *BeppoSAX* detected the late time emission called afterglow; moreover *BeppoSAX* confirmed that GRBs explode at cosmological distance, as guessed by their discoverers at beginning of '70. This discovery ruled out the wide variety of models born in the last years. The third revolution is expected to occur by *Swift* satellite, to be launched in late 2004; *Swift* is an autonomous rapid-slewing satellite for observation of transients in multiwavelength and is expected to shed light on GRB progenitors, to study ultrarelativistic outflow in cold medium and to use GRB to explore early universe out to $z > 10$.

The present work contains the study of the afterglow phase of a model for GRBs, according to which the phenomenon is triggered by the vacuum polarization process of Heisenberg-Euler-Schwinger [60, 131] in the space-time surrounding a non rotating ElectroMagnetic Black Hole (the so-called the EMBH model). The region outside the black hole horizon where the vacuum polarization occurs has been called "dyadosphere" [95, 96]. From dyadosphere an electron-positron-photon plasma optically thick expands at ultrarelativistic velocity. This plasma, which in literature is commonly called "fireball", accelerates (Pair ElectroMagnetic, or PEM, pulse phase) up to the completely inelastic collision with the baryonic matter left over in the gravitational collapse; then the plasma, loaded by baryonic matter, re-accelerates (Pair ElectroMagnetic Baryonic, or PEMB, pulse phase) up to the transparency point where all the photons are assumed to be emitted (the so-called Proper-GRB, or P-GRB [103, 104]). In the following eras the remaining baryonic matter pulse, called Accelerated Baryonic Pulse (ABM pulse) [103, 104], slows down in the collision with Interstellar Medium sweeping up the cold matter surrounding the source at large distance, from roughly 10^{14} cm to 10^{17} cm.

The other models found in literature are mostly of phenomenological nature and limit

themselves to give the kinematics of energy emission or to describe limited regions of the expansion by approximated power laws. In literature essentially a series of models facing piecewise the phenomenon can be found: either models of the inner engine which estimate by order of magnitude the main processes by satisfying energetic and time scale requirements but do not make detailed prediction of the observable quantities as time-structured luminosity emitted or time-resolved spectra, or scenarios for the expansion of the plasma, as internal or external shock to be described later on, which from initial conditions disentangled from the detailed properties of the source, as a certain fireball with given particle number density or Lorentz γ factor or electron energy distribution, try to reproduce light curves and spectra.

The uniqueness of this model is due to the possibility of predict time structured light curve and spectral distributions at any time by a specific set of equation of motion, so by studying the dynamics of the process, and by an assumption on high energy spectrum. The real advantage of this model is that the theoretical predictions of luminosity, Lorentz γ factor and spectral behaviour strongly limit the initial conditions, fixing the value of the parameters of the model.

An essential feature of the model is the dependence of the result globally on only four parameters for long bursts: the total energy emitted by the EMBH in the e^+e^- and photons plasma in the dyadosphere, called E_{dya} [116]; the amount of protostellar matter left over in the gravitational collapse B in units of E_{dya}, defined as $B = M_B c^2/E_{dya}$ [117]; an other parameter called $\mathcal{R}$ describing the porosity of the matter around the source [110]; finally the average value of number density of interstellar medium $\langle n_{ism} \rangle$ [106, 107].

The main results of this work are the contribution to find the following results:

- The most general GRB is made by an early emission (P-GRB or Proper-GRB), with a time-scale not larger than 1 or 2 seconds and an afterglow, whose light curve is characterized by an increasing phase followed by a peak and a decreasing phase. This peak has been identified with the long GRBs prompt emission. In this scenario short GRBs are not but P-GRB, while long GRBs present both a peak and a decreasing late time emission, which is the observed afterglow (see sect. 2.4.1 and [104]).

- A possible GRB/SuperNova connection is based on the process of induced gravitational collapse of a companion star of the black hole originating the GRB [105].

- A thermal distribution in the comoving frame of the expanding system is assumed for X and γ bands of the spectrum [110]. This assumption leads to a natural bending of the late time light curves making not necessary the hypothesis of a beamed emission within a collimated jet from the inner engine, which has been introduced in literature essentially to reduce the energy requirements.

These results led to a natural explanation of the bimodal distribution of *BATSE* (see sect. 2.4.1), tracing back both long and short events to the same progenitor system; show that the temporal substructure of light curves can be reproduced by modelling the density of cold InterStellar Medium around the source; kinematically agree with the GRB/Supernova observed coincidence in space and time; explain the apparently non-thermal spectrum observed as a superposition of black bodies spectra with different temperatures.

In chapter 2 we present the history of the discovery of GRBs, the main observational results which find a quite natural explanation within the EMBH model and a brief review of

the theoretical models for the progenitor and for the expanding fireball, spherically symmetric or collimated in a beaming angle. In chapter 3 the first three eras of the EMBH model are presented until the transparency point is reached, from the formation of the dyadosphere around an already formed black hole to the expansion of the PEM pulse and the collision with the baryonic remnant, to the expansion of the PEMB pulse; the identification of the parameters of the model is discussed. In chapter 4 the constitutive equations for the afterglow are written: the energy-momentum conservation equation at all orders, the relation between time at the source and time at the detector, the expression of observed luminosity taking into account the off-axis contribution; the best fit of the bolometric luminosity of the prototype GRB 991216 is presented, with the identification of the precursor as P-GRB and consequently the interpretation of the bimodal distribution of *BATSE*; a proposal for the explanation of the observed GRB-Supernova connection kinematically compatible with the observations; finally a brief discussion of the ultrarelativistic approximation of γ factor in literature. In chapter 5 the assumption of thermal origin of the X and γ radiation is presented with the prediction of the hard-to-soft spectral evolution and a comparison with the Band formula for the time-integrated spectrum again in the case of GRB 991216. In chapter 6 light curve prediction and spectral behaviour are qualitatively analyzed for the limiting case of a zero material not collapsed in the black hole, i.e. for the case of short burst. A soft-to-hard evolution is found.

The following appendixes contain the papers published on refereed journals or proceedings:

- **Appendix 1**: Ruffini R., Bianco C.L., Chardonnet P., Fraschetti F., Xue S.S., "Relative space-time transformations in GRBs", ApJ, 555, L107, 2001;
- **Appendix 2**: Ruffini R., Bianco C.L., Chardonnet P., Fraschetti F., Xue S.S., "On the interpretation of the burst structure of GRBs", ApJ, 555, L113, 2001;
- **Appendix 3**: Ruffini R., Bianco C.L., Chardonnet P., Fraschetti F., Xue S.S., "On a possible GRB-supernova time sequence", ApJ, 555, L117, 2001;
- **Appendix 4**: Ruffini R., Bianco C.L., Chardonnet P., Fraschetti F., Xue S.S., "On the physical processes which lie at the bases of time variability of GRBs", Nuovo Cimento, Vol.116 B, 99, 2001;
- **Appendix 5**: Ruffini R., Bianco C.L., Chardonnet P., Fraschetti F., Xue S.S., "On the structure of the burst and afterglow of Gamma-Ray Bursts I: the radial approximation", *International Journal of Modern Physics D*, 12, 2, 173, 2003;
- **Appendix 6**: Ruffini R., Bianco C.L., Chardonnet P., Fraschetti F., Xue S.S., "On the structures in the Afterglow Peak Emission of Gamma-Ray Bursts", ApJ, 581, L19, 2002;
- **Appendix 7**: Ruffini R., Bianco C.L., Chardonnet P., Fraschetti F., Vitagliano L., Xue S.S., "New perspectives in physics and astrophysics from the theoretical understanding of Gamma-Ray Bursts", *Proceedings of the* X *Brazilian School of Cosmology and Gravitation*, editors M. Novello, S.E. Perez Bergliaffa, AIP Conference proceedings 668, p. 16, (2003), astro-ph/0302557;

- **Appendix 8**: R. Ruffini, C.L. Bianco, P. Chardonnet, F. Fraschetti, S.-S. Xue, "The EMBH model in GRB 980425 and GRB 991216", *Proceedings of the* 3^{rd} *Workshop "Gamma-Ray Bursts in the Afterglow Era"* editors M. Feroci, F. Frontera, N. Masetti, L. Piro, ASP Conference Series, 312, p. 349, 2004, pre-print: astro-ph/0409341;

- **Appendix 9**: Ruffini R., Bernardini M.G., Bianco C.L., Chardonnet P., Fraschetti F., Xue S.S., "GRB 980425, SN1998BW and the EMBH model", *Proceedings 34th COSPAR (GRB AFTERGLOW PHYSICS) Scientific Assembly, The Second World Space Congress*, Houston, TX, USA, 10-19 October 2002, in press, astro-ph/0306246;

- **Appendix 10**: Ruffini R., Bianco C.L., Xue S.S., Chardonnet P., Fraschetti F., Gurzadyan V., "On the instantaneous spectrum of Gamma-Ray Bursts", *International Journal of Modern Physics D*, 13, 5, 843, 2004;

- **Appendix 11**: Fraschetti F., Bernardini M. G., Bianco C.L., Chardonnet P., Ruffini R., Xue S.S., "The GRB 980425-SN1998bw Association in the EMBH Model", to appear in the *Proceedings of the Los Alamos "Gamma Ray Burst Symposium"* in Santa Fe, New Mexico, USA, September 8-12 2003 (AIP Conf. Ser.), pre-print: astro-ph/0407147;

- **Appendix 12**: Corsi A., Bernardini M.G., Bianco C.L., Chardonnet P., Fraschetti F., Ruffini R., Xue S.S., "GRB 970228 Within the EMBH model", to appear in the *Proceedings of the Los Alamos "Gamma Ray Burst Symposium"*, Santa Fe, New Mexico, USA, September 8-12 2003 (AIP Conf. Ser.), pre-print: astro-ph/0407233;

- **Appendix 13**: Bernardini M.G., Bianco C.L., Chardonnet P., Fraschetti F., Ruffini R., Xue S.S., "A New Astrophysical "Triptych": GRB030329/SN2003dh/URCA-2", to appear in the *Proceedings of the Los Alamos "Gamma Ray Burst Symposium"*, Santa Fe, New Mexico, USA, September 8-12 2003 (AIP Conf. Ser.), pre-print: astro-ph/0407503;

- **Appendix 14**: Ruffini R., Fraschetti F., Vitagliano L., Xue S.S., "Observational signatures of an electromagnetic overcritical gravitational collapse", *International Journal of Modern Physics D*, in press, pre-print: astro-ph/0410233.

2 Historical overview, observations, models

In the first three sections of this chapter the history of discovery of Gamma-Ray Bursts is described. The first signal has been detected by chance in the end of '60s by *Vela* satellites whose aim was to check the observance of a nuclear weapon band treaty (sect. 2.1). Later on the *BATSE* detector has shown the isotropy of the sky distribution (sect. 2.2) and in 1997 *BeppoSAX* satellite discovered the afterglow and confirmed the cosmological origin of these events (sect. 2.3). In sect. 2.4 a general review is presented of the main observational results which find a simple and quite natural explanation within the model developed in this work, as time duration and time variability and the Band model for time integrated spectral distribution; the observed coincidence in space and time of a GRB and a Supernova. In sect. 2.5 some theoretical models for the progenitor are outlined: the coalescence of a binary system or the collapse single massive object, as the "Supranova" model. In sect. 2.6 the historical path leading from the necessity to explain the apparently non-thermal observed spectrum to the fireball scenario is presented. In sect. 2.7 the reason of the introduction of the beamed emission and the interpretation of observations invocated to justify it are outlined.

2.1 Vela satellites: discovery

In this chapter the research lines are traced which led to the identification of Gamma-Ray Bursts (GRBs) as events of cosmological nature. The *Beppo-SAX* satellite in 1997 discovered the afterglow: the phenomenon is not limited to a brief and intense explosion, but the source of the event remains active for a period of hours, days or months.

In 1963 the U.S. Air Force launched a series of satellites inspired by a recently signed band nuclear tests treaty [15]. Band signatories engaged themselves band nuclear tests in terrestrial atmosphere or in space. These satellites, called *Vela* (from spanish "velar", to watch), were aimed to treaty conditions observance inspection [141]. Satellites were launched and made operative in couple with two identical satellites in opposite points of a circular orbit with a diameter of 250.000 km (orbital period of 4 days) so that no part of Earth surface was hidden to direct observation. *Vela* satellites had on board X, γ rays and neutron detectors, designed by *Los Alamos Scientific Laboratory* (now LANL) and by *Sandia Laboratories* from Albuquerque NM to monitor space environment; simultaneous indication of an explosion by many detectors would have confirmed the nuclear event. If the explosion would occur on the hidden Moon surface or behind a thick screen, initial X flash would not be visible to

detectors, but the radioactive material expanding cloud generated by the nuclear explosion would have been detected in γ. The *Vela* satellites were progressively improved, until with *Vela* 5*a* and 5*b* (launched in 1969) and *Vela* 6*a* and 6*b* a sufficient accuracy was reached to determine the origin direction of the nuclear explosion by time delay between triggers of two satellites: the light travel time from one device to another, roughly one second, was larger than the temporal resolution, roughly 0.2 seconds.

In 1965 with the construction and launch of satellites *Vela* 3, Ray Klebesadel, from LANL, was encharged of X and γ instrumentation. He found that events that actived the detectors but that were not nuclear explosions were put aside for future studies.

In 1972 the obtained temporal resolution let Ray Klebesadel, Ian Strong and Roy Olsen, from *Los Alamos* [22, 64, 132, 147] to determine the origin direction of events which seemed nuclear detonation but apparently not originated from the Earth or the Sun. They concluded that these events were probably of cosmological origin. The data of *Vela* 4 satellites were used to build a temporal profile of the phenomenon, or the count number of photons received on the detector in a certain energy band, so the energy observed as a function of time. This result was promptly published in 1976 [134]. The resonance caused by the discovery is witnessed by the prompt and huge number [62, 89, 91] of theoretical and experimental publications on this subject.

Among the numerous theories elaborated to explain the GRB origin around middle '80s, some of these proposed that GRB originate from neutron stars in our galaxy, but late observations ruled out these models.

2.2 The BATSE detector: isotropy

A second phase in observational research of GRBs has been open by *BATSE* detectors (standing for "Burst and Transient Source Experiment") on the NASA observatory called COMPTON-GRO (COMPTON - Gamma-Ray Observatory), launched in Spring 1991 and landed in June 2000. Space missions using satellites were necessary since a flux of γ rays cannot be observed on the earth surface because they are absorbed in atmosphere at tens of kilometres from sea level.

BATSE data allowed a wide and accurate analysis of GRBs since 2700 events have been observed in roughly 9 years, while satellites *Vela* 5*a* e 5*b*, 6*a* e 6*b* recorded only 73 events from April 1969 to April 1979. The observations of *BATSE* confirmed that no preferential direction in the sky for GRBs exist: if they were originated in our Milky Way, a dominant amount of events would have been located in the galactic plane, concentrated in the direction of the center of Milky Way, and less in the surrounding halo. Furthermore the small number of soft events in *BATSE* catalog allowed to exclude the galactic neutron star model, making real the possibility of an extragalactic nature of GRBs.

The observed isotropy of these events (see fig.2.1) still left open two alternatives: GRBs could come from a spherical cloud of neutron stars surrounding solar system at small distance (about hundreds of light years), like the Oort cloud for comets, or they were objects of cosmological origin. But it was highly unlikely that this cloud would exist only in the near vicinity of solar system, making it a preferred system, so that these explosions could occur only in far away galaxies.

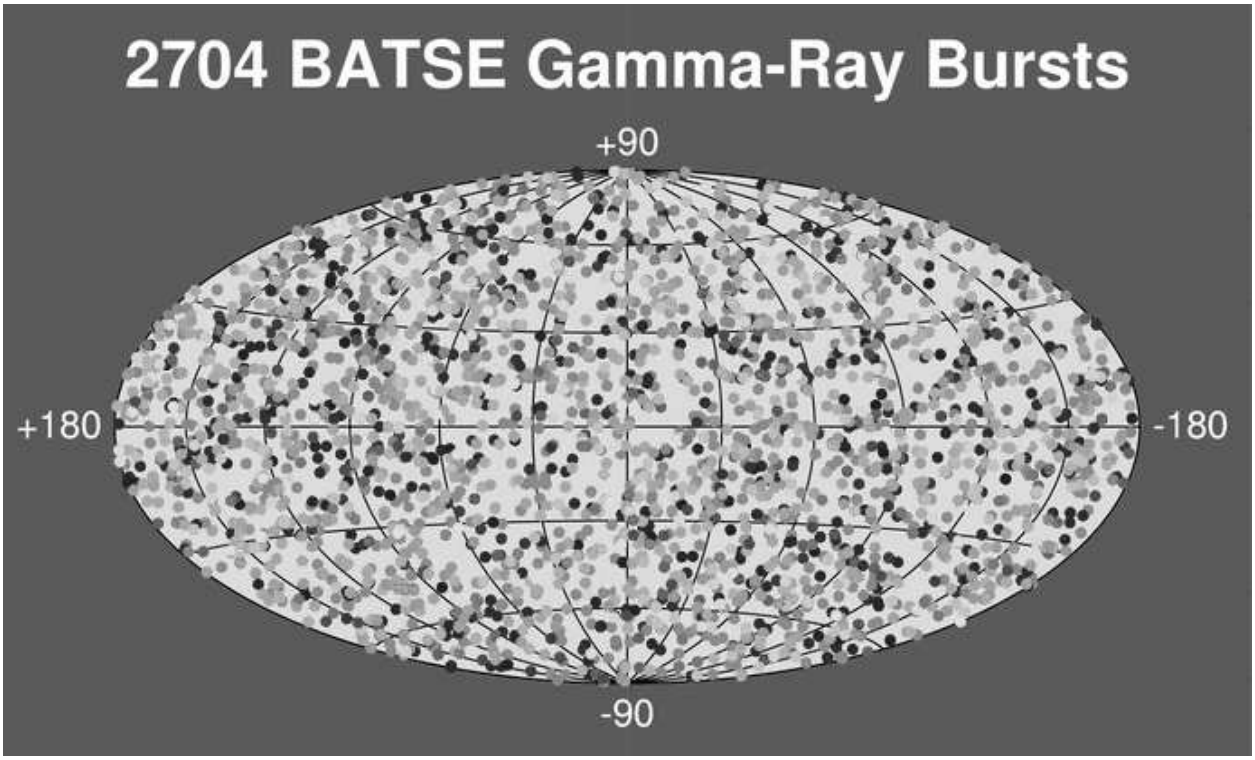

Figure 2.1: *On average roughly three times a day the sky in γ band enlights with an explosion. The map represents the sky in galactic coordinate. The points indicate the position of the* 2704 *explosions observed by BATSE from April* 5^{th} 1991 *to June* 4^{th} 2000*. The phenomenon is completely isotropic, but the cosmological distance was definitely confirmed only by BeppoSAX satellite.*

2.3 The satellite Beppo-SAX: cosmological distance

The cosmological origin of GRBs was confirmed by the Italian-Dutch satellite *Beppo-SAX* (*Satellite per Astronomia X* in honour of Giuseppe Occhialini), which on February 27^{th} 1997 discovered the "afterglow" in X band: eight hours after the main deflagration, the detectors of satellite pointed towards the event found a still active source in X band which lasted some days [25]. This observation was promptly followed by others in optical [139] and radio bands [40], which coincided with the X-ray location. Later on the publication frequency on this subject further increased [54]. Through optical absorption spectroscopy on the event of May 8^{th} 1997 (GRB 970508), a redshift $z = 0.835$ was found; similar values have been found later confirming the cosmological nature of the event.

The main consequence of the cosmological distance on the source is that they turn out to be much more energetic than expected. If the source is located at cosmological distance, in the assumption of isotropic emission from the source, it turns out from the measurements of observed flux an energy release of the order of $10^{51} - 10^{54}$ erg. Since the rest energy of the Sun is roughly $M_{\odot}c^2 \simeq 10^{54}$erg, in a brief time interval this source emits an amount of energy equal to the rest energy of a star of average dimension. This would induce us to consider GRB a relatively rare event: if a constant rate with respect to cosmic time is assumed, from *BATSE* observations a rate is estimated of one GRB per million year per galaxy which is

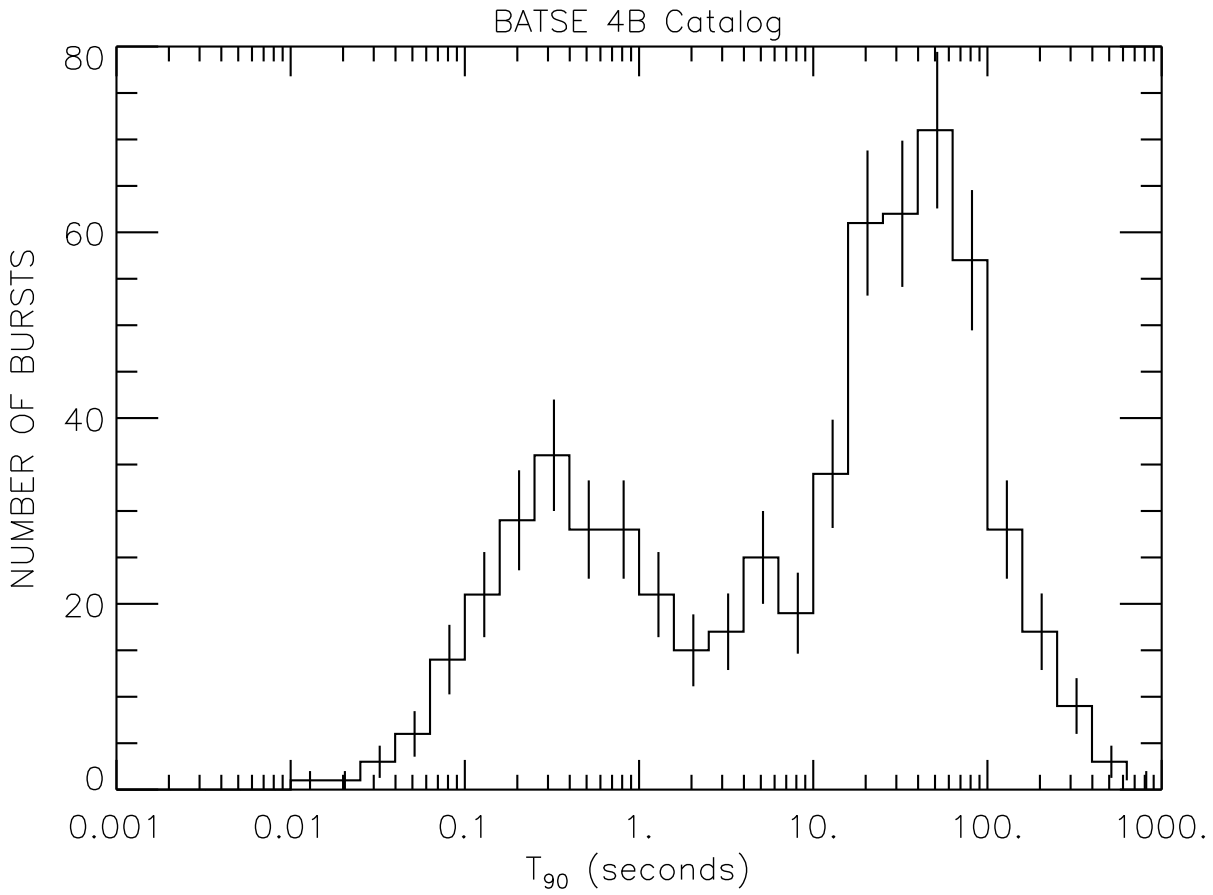

Figure 2.2: *Histogram of GRB time duration from BATSE 4B catalog [6]. The duration is computed by the T_{90} (T_{50}) criterion, according to which the duration of an event is asssumed to be the time interval during which is collected from* 5% *(*25%*) to* 95% *(*75%*) of the total energy emitted. A time interval is chosen because, due to background noise, it is never possible to determine the instant of beginning (*0%*) and of the end (*100%*) of the signal. From this histogram emerges that GRBs divide in two classes: "short GRBs" and "long GRBs".*

roughly 1/3000 the rate of Supernova [91].

It has to be noted that at present only the redshift of some tens of sources has been measured by spectroscopic observations, resulting all of the order of unity, except some next cases as GRB 980425 ($z = 0.0085$) and GRB 030329 ($z = 0.169$), so that the conclusion that GRBs are cosmological comes from an extrapolation from tens to thousands of sources. Moreover all these sources with measured redshift are long (see sect. 2.4.1), because for short events no redshift has been measured, due to the lack of afterglow observations; just in the recent short GRB 040924 an optical afterglow has been observed but the redshift is unknown yet [33].

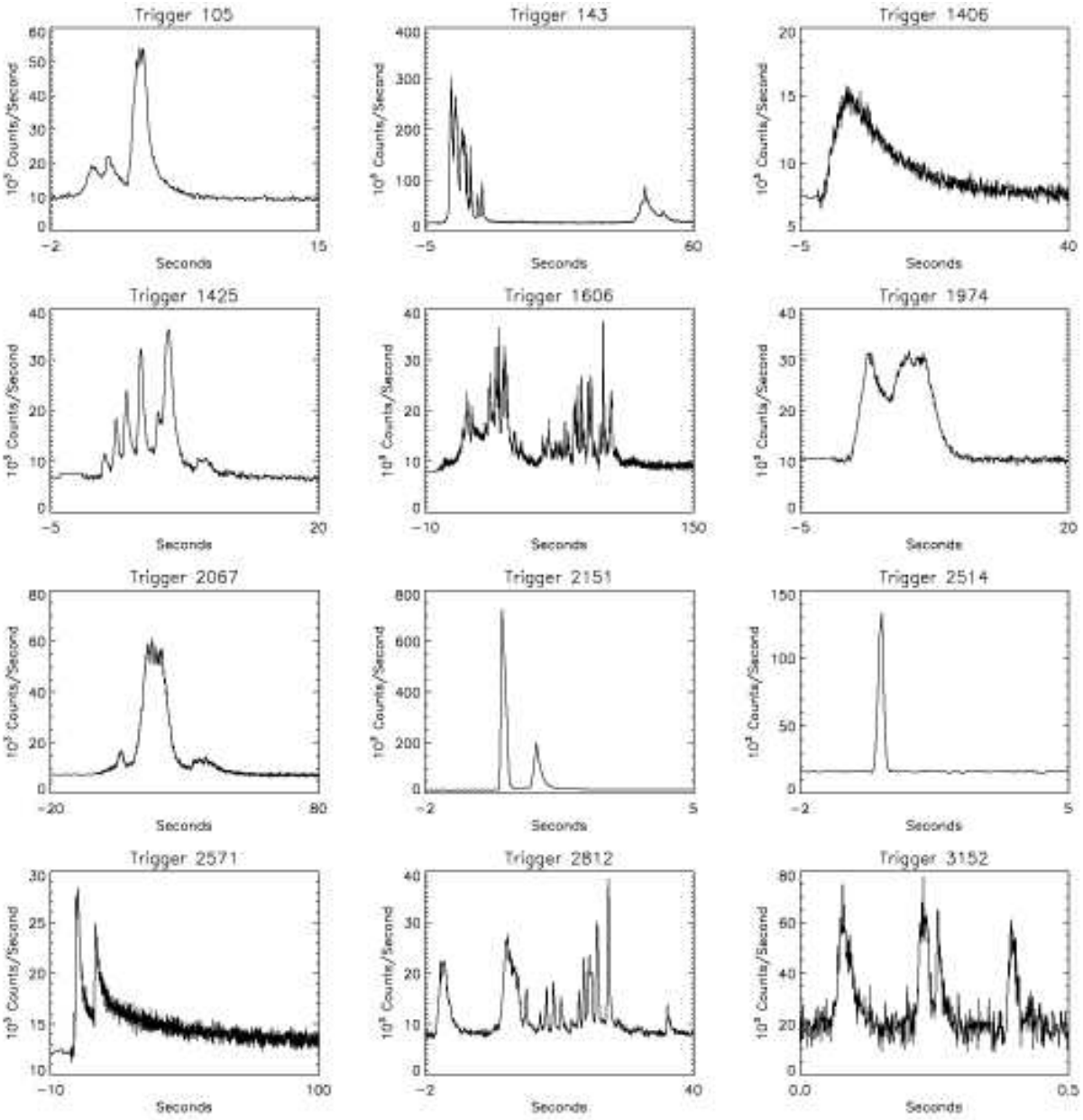

Figure 2.3: *Variability of temporal profile of a single event with time scale down to ms and difference of temporal profile between different events is shown, making evident the difficulty of building a single model reproducing all observational features. Usually "long" events present a more complicated temporal structure than "short" ones.*

2.4 Observations

2.4.1 Time duration and time variability

Among the observational features of GRBs to be underlined within the EMBH model there are the temporal duration, the temporal sub-structure, the spectral behaviour and the GRB/SN connection.

In fig. 2.2 the histogram of time duration of GRBs observed in *BATSE* 4B catalog is reported [6]. This distribution seems strongly bimodal, even if some statistical analysis conducted by a neural network agorithm [4] tried to indicate the existence of a third class of GRBs with an intermediate duration. The events in fig. 2.2 are distributed in two classes: "long GRBs" ($T_{90} > 2$ s) with a duration peaked around 50 s and "short GRBs" ($T_{90} < 2$ s) with a duration peaked around 0.3 s [65]. Apparently short events are in ratio one to three with respect to long ones. However short bursts due to their brief duration could easily have been hidden by spurious signals; this selection effect makes underestimate the rate of short events. By the analysis of the *BATSE* catalogs[1] Tavani in 1998 [137] confirmed the existence of two families of GRBs precedently identified in [65] according to their temporal duration and spectral properties. The rapid response of *Swift* instrument will shed light on the distinction between the two families.

It is still open the question whether the GRBs long and short are different phenomena, originated by progenitors of different nature or due to different mechanisms of emission of electromagnetic radiation, not simply the same phenomenon at different time scales. The EMBH model provides an interesting answer to the previous question: from the same progenitor, an electromagnetic black hole (EMBH), the internal energy released by the source and kept inside the adiabatically expanding system is emitted entirely in short burst when the transparency condition with respect to Thomson scattering is reached; in the following eras the internal energy developed in the collision of the expanding system with the cold interstellar medium is emitted in the long burst. For a further discussion see fig. 4.7 and sect. 4.8.

Other relevant features of GRBs are the variability of profile of the light curve between one GRB and another one and the very high irregularity of the single temporal profile [35]. This irregularity clearly emerges in fig. 2.3. The temporal profiles range from a simple *FRED* structure (*Fast Rise and Exponential Decay*, indicating a very rapid rise followed by a slower exponential decay) to a multipeak structure with a rise time down to $\delta T \sim 10$ msec in which the first peak is not always the most intense and, when is the case, the second peak is not significantly less intense than the first one. If a time variability index N is defined in the form $N = \delta T/T$, a value $N \simeq 10^{-3} - 10^{-4}$ is often found. High temporal variability ($N \ll 1$) has been observed also in a significant sample of short bursts *BATSE* 4B catalog [80]. Within EMBH model the complex temporal structure of light curve is correlated to inhomogeneities of ISM, as explained in sect. 4.9.

[1] see http://f64.nsstc.nasa.gov/batse/grb/catalog/4b/ maintained by W.S. Paciesas et al.

2.4.2 Spectral distribution

GRBs are characterized by an apparently non-thermal observed spectrum. Among the models trying to explain the energy distribution of the observed radiation, the most refereed one is the Band model [5], based on an empirical formula for time integrated spectrum not directly related to the underlying physical processes, but introduced in order to provide a unified description of the spectral features of GRBs. The Band function is essentially made of two smoothly connected power laws:

$$N(E) = \begin{cases} A\left(\dfrac{E}{100\ \mathrm{keV}}\right)^{\alpha} \exp\left(-\dfrac{E}{E_0}\right) & \text{for } E \leq (\alpha-\beta)\,E_0 \\ \\ AE^{\beta}\left[\dfrac{(\alpha-\beta)E_0}{100\ \mathrm{keV}}\right]^{\alpha-\beta} \exp(\beta-\alpha) & \text{for } E \geq (\alpha-\beta)\,E_0 \end{cases} \tag{2.1}$$

where $N(E)$ is the photon count number in photons $\mathrm{cm}^{-2}\ \mathrm{s}^{-1}\ \mathrm{keV}^{-1}$. The free parameters are A, the normalization constant at 100 keV; α, the low energy power law spectral index; β, the high energy power law spectral index; E_0, related to the peak energy in the $E - F_E$ diagram (F_E is the flux in counts/cm^2sec) by $E_{peak} = (\alpha+2)E_0$; E_{peak} represents the energy at which most of the luminosity is emitted. Moreover Band parameters do not have universal values but vary from burst to burst: from an analysis of the spectra of twelve bursts with known redshifts [3], a large dispersion in Band parameters has been found. In a recent work [52] a further distintion between short and long events has been found in the average low energy power law index of time integrated spectrum: $< \alpha >= -0.58$ and $< \alpha >= -1.05$ respectively. However due to the "shape-shifting" [26] of instantaneous spectra, the time integrated spectra can loose distinguishing features of the parameters as time evolution of low energy index α. Moreover a model consistent with time integrated spectra can be inconsistent with time resolved spectra. In chapt. 5 we show that EMBH model reproduces both integrated and resolved spectra in agreement with observations.

A model proposed to explain the observed spectra is based on the assumption that optically thin plasma of relativistic electrons behind the shock front of the expanding system accelerated in a magnetic field emit synchrotron radiation, if energy distribution of the relativistic electrons has a single power law form. However in [94, 51] the authors have shown that the standard model of synchrotron emission does not give a good explanation of the whole observed spectra since the theoretically predicted limit of the low energy spectral index α for time resolved and time integrated spectra is violated for a non negligible part of the *BATSE* sample. This at least indicates that synchrotron shock model can not be the only emission mechanism of GRBs and a significant energy fraction must follow other spectral distributions.

Sometimes spectral lines has been observed as the emission iron line in GRB 991216 at roughly 37 hours since trigger [93]. The presence of iron or X-ray lines in the spectra is a useful tool to estimate the redshift for those puzzling bursts detected in X rays but not optically, e.g. because of dust absorption of the host galaxy.

2.4.3 GRB/SN connection

A correlation between the GRBs and Supernova events exists and has been established by many works [48, 49, 66, 140]. On April 25^{th} 1998 a prompt emission was detected by GRBM of *BeppoSAX* in (40-700)keV [46, 86, 87] and by *BATSE* in (50-300)keV. The source was then localized by WFC of *BeppoSAX* [46, 86, 87]. The great novelty was that the GRB was observed almost in coincidence in time and space direction as SN1998bw, a type Ic Supernova exceedingly bright in optical and radio. The peculiarity of this GRB is the atipically low energy ($E_{tot} \sim 10^{48}$ erg) and the atipically low distance ($z = 0.00835$). In addition to the source GRB 980425 and the supernova SN1998bw, two X-ray sources have been found by *BeppoSAX* in the error box for the location of GRB 980425: a source *S1* and a source *S2* [87]. Since the nature of the two sources *S1* and *S2* was not clear, a variety of slopes in the decaying part of the afterglow have been proposed (see fig. 7(c) in [87]). In 1998 Kulkarni and collaborators [66] have proposed to explain both the supernova SN1998bw and the GRB 980425 observations by a new class of GRBs, distinctly different from the cosmological ones due to its very low redshift, both originated by a single unusual supernova event. Due to the very large value of kinetic energy of the ejecta (roughly 10^{52} erg), much larger than for any observed supernova, it has been tried to identify [63] the supernova and GRB event with the "hypernova" described for the first time by Paczyński [83] (see Sect. 2.5).

The extremely low value of total energy emitted in GRB 980425 ($E_{tot} \simeq 10^{48}$erg) with respect to the energy estimate of SN 1998bw ($E_{tot}/E_{SN} \simeq 10^{-1}$) made possible observation of light curve of the underlying Supernova which if connected to a more energetic GRB could remain hidden by its predominant emission. This indicates that the rate of SN events associated to GRBs could be at present underestimated.

More recent is the case of GRB 030329. GRB 030329 has been detected on March 29^{th}, 2003. Its very high fluence for the prompt emission (1.2×10^{-4} in the $30 - 400\, keV$ band, as measured by *HETE* [101]) and the bright X-ray afterglow observed by *Rossi–XTE* [71, 72], and by *XMM–Newton* [136] provided a wealth set of observational data. As GRB 980425 this event has been observed at quite low distance: the redshift of its host galaxy is $z = 0.1685$ [16, 56]. From the optical afterglow 7 days after the burst, it has been found the spectroscopic evidence of the underlying Type Ic supernova SN2003dh with a large expansion velocity [61, 133]. At variance from GRB 980425, the GRB 030329 is supposed energetically dominant on the underlying supernova.

The observational data left open any possible time sequence between GRB and SN explosion, because the time of SN is extrapolated back from the form of spectra, so that it is model dependent and uncertain [74]. Within the EMBH model a time sequence GRB-SN has been proposed: in a binary system made by the EMBH and a metastable white dwarf, the photons and eventually the neutrinos emitted at transparency of expanding plasma induce the gravitational collapse of the white dwarf which gives rise to SN explosion; the supernova remnant expanding from the newly born Neutron Star is then enlightened by the afterglow.

2.5 Other models for the progenitor

Before *BATSE* launch there were more GRB progenitor models than GRBs effectively

observed; the confirmation of cosmological origin allowed to exclude large part of them. Theoretical models trying to explain the GRB phenomenon are distributed in two main groups:

1. Coalescence of binary systems (e.g. Neutron Star-White Dwarf, Neutron Star-Neutron Star, Neutron Star-Black Hole) leading to the formation of a rotating black hole; in this process a large fraction of energy would be released in emission of low energy neutrinos or gravitational radiation, but enough energy would remain for GRB; the explanation of the most luminous GRBs (as GRB 990123 or GRB 990510 or GRB 991216) would require a very narrow jet emission;

2. Explosion of massive and rotating objects in star forming regions such as the Collapsars (from "collapsing-stars"), or the Supranova; in both cases the GRB energy is supplied by accretion of matter on the disk surrounding the newly born black hole and originated from the debris of Supernova explosion.

An other possibility were the Active Galactic Nuclei (AGN), but the temporal variability of GRBs requires for energy source a stellar mass object [18]; so this third possibility has been excluded.

From a statistical analysis of some tens of long GRBs [14] a net probability emerged favouring massive objects as progenitors of long GRBs.

The location of GRBs within a galaxy provides an important clue in order to discriminate between different progenitors. Explosion of massive stars occurs near the birth place, likely in star forming regions. On the other hand BH-BH systems merge quickly so that they are expected to merge near the birth place. Systems as BH-NS or NS-NS requiring at least one supernova explosion, are to be characterized, if the explosion is asymmetric, by a certain "kick" velocity imparted to the resulting Neutron Star [59, 47]. The binary systems survived the supernova explosion are expected to receive a boost to a velocity of the order of some km/s, which ejects them from the originary galaxy. The two components of the binary system will then merge by angular momentum loss in a location far away their birth place.

The "Collapsar" is a one step event. According to the Collapsar model GRB arises from the collapse of a rapidly rotating massive star (failed Type Ib Supernova) [149]. Paczynski [83] pointed out the evidence that some GRB (e.g. GRB 970228, GRB 9709508) were close to star forming regions and this strengthens the connection of GRBs with death of massive stars. The "Hypernova" model [83], derives its name from the explosive nature of the phenomenon, much more luminous and energetic than any Supernova. The Supernova itself is assumed to originate in the process of gravitational collapse to a black hole of a massive progenitor star ($\sim 40 M_{\odot}$) with a particularly large angular momentum and strong magnetic field. A large rotational energy of the black hole extracted with a strong magnetic field would explain the explosion of this "hypernova" leading both to the GRB and the supernova. Later on a computation began [69] showing the effect of collimation of the jet by the stellar envelop. The massive iron core of the star collapses to a black hole; an accretion disk forms around the black hole and a funnel forms around the rotation axis. The relativistically expanding jet is collimated by the mantle enveloping the collapsing star. In this model bumps emerging on the afterglow light curve are expected.

Among the models with a massive progenitors, the "Supranova model" is one of the most well known [142]. The Supranova is a two steps event. The first one is the explosion of a SuperNova (SN), much more energetic than usually, which leaves a SuperMassive Neutron Star

(SMNS). The second step, the collapse of the SMNS, is due to losses of angular momentum through, for instance, magnetic dipole radiation, which has also the effect of reducing the baryon contamination of the environment. The consequent reduction of centrifugal forces is such that it can no longer counterbalance the gravitational attraction and the system implodes into a black hole. The main feature of this model is that the SN explosion which gives origin to the SMNS cleans up the space region surrounding in the very proximity the source so that the implosion of the remnant neutron star in black hole occurs in a baryon clean environment making possible very high Lorentz γ of the ejecta. The preceeding SN explosion enriches the space region around of heavy elements, up to Fe synthesized by the exploded system. The GRB is powered by the accretion on the disk surrounding the newly born black hole. The observations [2, 93] are consistent with the presence of Fe near the birthplace of the GRBs. The main difficulty of Supranova model is the time delay between SN explosion and GRB which could be of order of weeks or months; this is in disagreement with the observational evidence for GRB 030329 [61].

It has been proposed also a model based on the gravitational collapse in a Neutron Star of accreting white dwarfs with anomalously high magnetic fields in binaries [138]. The energy available in this case would be the rotational and magnetic energy of NS which are of the order of 10^{51} erg for a NS near break up.

To the emission of γ rays in GRB is likely to be associated a class of different bursts of high energy cosmic rays [144], neutrinos [78, 143] or gravitational radiation. The study of the link between these phenomena and GRB is now going on.

2.6 Fireball scenario

In this section we will briefly show how the scenario of a relativistically expanding fireball describing both the prompt emission and the afterglow phase is advocated in literature to obtain an apparently observed non-thermal spectrum. Consider a typical burst whose source is at rest with respect to the earth; cosmological effects change the following treatment by numerical factors of order unity that are neglected in the present discussion. It is assumed that the size of the source emitting the observed radiation is determined back by the observed variability time scale: the rapid temporal variability on a time scale $\delta T \approx 10\ msec$ would imply a size of the source $R_i < c\delta T \approx 3000$ km. It is possible to show that the opacity τ of the high energy gamma-ray to e^+e^- pair production would be in this case $\tau_{\gamma\gamma} \sim 10^{13}$ [89], i.e. optically thick, in contradiction with the apparently non-thermal observed spectra, which would imply $\tau_{\gamma\gamma} < 1$; this is the so-called compactness problem. The conclusion would be that the compactness problem arises from the assumption that the size of the sources emitting the observed radiation is determined back by the observed variability time scale.

Consider instead a source of radiation that is moving towards an observer at rest with a relativistic velocity characterized by a Lorentz factor $\gamma = 1/\sqrt{1 - v^2/c^2} \gg 1$. Since the observed energy of a single emitted photon $h\nu_{obs}$ is blue-shifted, its energy at the source was $\approx h\nu_{obs}/\gamma$; this implies that a less number of photons can produce pairs, thus reducing optical thickness of the system. Moreover the radius from which the radiation is emitted would be given roughly by $R_e < \gamma^2 c\delta T$, in the assumption that the γ is constant; the latter value of R_e is larger than the previous value, $R_e < c\delta T$, by a factor of γ^2. These two modifications

for a source moving relativistically towards us with a Lorentz factor $\gamma > 10^2$ give $\tau_{\gamma\gamma} < 1$ allowing a solution of the compactness problem.

The point of view in EMBH model is radically different: the apparently non-thermal observed spectrum does not imply a non-thermal spectrum at the source [12, 110] (see chapt. 5).

Quite generally it is found in literature that the mechanisms of conversion of kinetic energy in electromagnetic radiation for GRBs are essentially two: the "internal shock" [99, 82] and the "external shock" [76]. The internal shock originates from an inner engine which in a steady activity emits shells at different Lorentz γ factor; when an inner faster shell with Lorentz factor γ_2 reaches an outer slower shell with Lorentz factor γ_1, they collide completely inelastically and the kinetic energy is converted in radiation. This internal shock is advocated to reproduce the complex observed temporal substructure of prompt emission. However only the relative kinetic energy between the two shells can be dissipated, and since the Lorentz γ' of the second shell relative to the first shell is $\gamma' \simeq \gamma_2/\gamma_1$ a wide distribution of γ of the shells emitted by the source is necessary [53]; moreover only a small fraction of the dissipable energy is available for electrons, highly reducing the efficiency of the process.

The external shock model occurs when a single ultrarelativistic shell ejected by the inner engine collides with the clouds of the external medium. This model relates the GRB light curves and time variabilities to external medium distribution. The interesting possibility has been also recognized within this model, that GRB light curves "are tomographic images of the density distribution of the medium surrounding the sources of GRBs" [31] (see also [30, 32] and references therein). In this case, the structure of the burst is assumed not to depend directly on the inner engine (see e.g. [90] and references therein).

General consensus has been recently reached on the role of external shock scenario to explain the afterglow of GRB. The solution of the relativistic Rankine-Hugoniot equation governing the propagation of a shock wave has been given by Taub [135]. The application of this solution to adiabatic and radiative regimes of afterglow in ultrarelativistic case has been presented in [11, 89]. In sect. 4.11 is presented an analysis of the approximations which can be found in literature made to obtain the power law behaviour of the dynamical quantities in the slowing down phase of Gamma-Ray Bursts within the external shock scenario; in particular we focus on the radial dependence the Lorentz γ factor of the bulk.

2.7 Collimated emission

The possibility of a collimated jet emission from the source has been introduced in order to reduce the energy requirements [70] which in the assumption of isotropic emission from the source can arrive to roughly $E_{tot} \simeq 10^{54}$erg. Sometimes the observed light curves in X, optical and radio apparently have a change of slope which at late times becomes steeper. The supposed impossibility of explaining this steepening by an expanding system with spherical symmetry has been interpreted as further proof of jet emission: when the angle of visible area ϑ_{max} equals the physical angle of the jet $\vartheta_\circ$, a steepening of light curve must occur. The GRB 991216 is considered by Halpern et al. [58] an example of jet emission: the light curve in optical band steepens and the value of X decay slope ($\alpha \simeq -1.6$) is discrepant from the predicted value which for spherical symmetry should be $\alpha \geq -1.47$. Within EMBH model a

complex behaviour of light curve is found different from a power law (see fig. 5.1 and fig. 5.4) in the assumption of spherical symmetry. It is argued that from the determination of the instant of time at the detector in which an achromatic steepening in the light curve would be observed [89] the beaming angle can be deduced; however this procedure appears quite uncertain due to the difficulties of determining unequivocally this instant of time and to the dependence on several parameters of the relation between this instant and beaming angle. Moreover the achromaticity of the breaking necessary to prove the existence of a collimation angle in many cases has not been observed because optical data were not available. The determination of the peak in the distribution of the jet opening angle [42] led to the result of a unique value of total energy available in GRB: $E_{tot} \simeq 10^{51}$erg. Within EMBH model no restriction on the total energy exists but a range of six orders of magnitude is spanned by the sources fit until now, from one of the most energetic ever observed (GRB 991216) to the weakest one (GRB 980425).

3 The EMBH model: the first three eras

Observations have shown that GRBs are bursts essentially in X and γ bands, with a late time emission at lower energies (optical and radio). The main features are the energy range 10 keV - 100 MeV and temporal duration between 0.1 sec and 100 sec with tails at times of order of days or months. Therefore any theoretical model aiming to the explanation of the origin of GRBs must reproduce both the luminosity as a function of the time at the detector and the spectral distribution. Many models have been proposed to explain GRB origin and the difference between them is both in the identification of the inner engine and in the mechanism of emission of the observed radiation.

The following sections are dedicated to the description of a GRB model, called EMBH model since an ElectroMagnetic Black Hole is assumed as inner engine. This model is based on the process of vacuum polarization of Heisenberg-Euler-Schwinger [60, 131] in the space time region surrounding an electromagnetic black hole. In the very beginning of the EMBH model, in 1975, the vacuum polarization process has been applied to the more complicated case of a black hole electrically charged and rotating [27]. In the following for the sake of simplicity the rotation has been omitted and a pure Reissner-Nordstrøm black hole has been considered. Therefore the work presented here aims to extract all the detectable consequences of the simplifying assumption of a Reissner-Nordstrøm metric, neglecting the even small rotation which characterizes any astrophysical object. Nevertheless, the farther from the inner engine we predict observations, the less dependence on the black hole parameters as rotation has to be expected. This is valid for the whole work here presented, except the chapt. 6, where the early time predictions give information about the central black hole.

3.1 General sketch of the model

A large part of models or scenarios found in literature are mostly of phenomenological nature and limit themselves to give the kinematics of energy emission or to describe limited regions of the process by approximated power laws [129, 99, 82, 76]. In literature essentially a series of models facing piecewise the phenomenon can be found: either models of the inner engine which estimate by order of magnitude the main processes by satisfying energetic and time scale requirements but do not make detailed prediction of the observable quantities as time-structured luminosity emitted or time-resolved spectra, or scenarios for the expansion of the plasma, as internal or external shock to be described later on, which from initial conditions disentangled from the source, as a certain fireball with given particle number density or Lorentz γ factor or electron energy distribution in a given magnetic field, try to reproduce light curves and spectra.

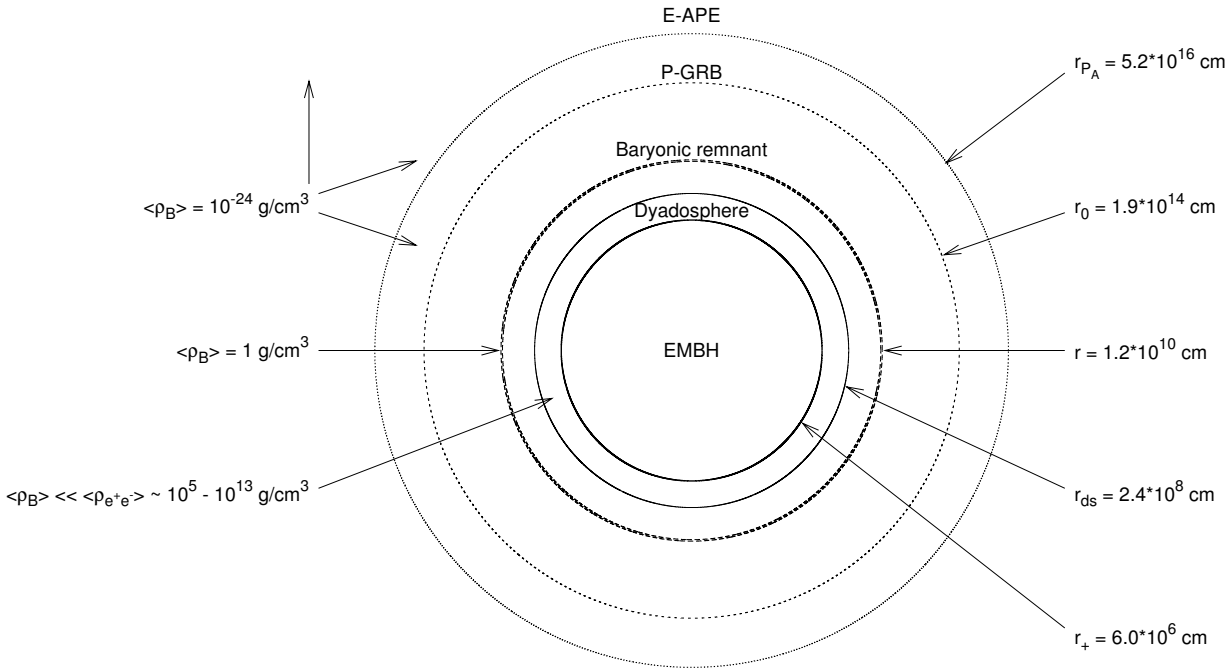

Figure 3.1: *Selected events in the EMBH model are represented. For each one the values of the energy density of the medium and the distances from the EMBH in the laboratory frame are given for the prototype GRB 991216; logarithmic scale is used.*

The EMBH model instead furnishes a dynamical explanation by equations of motion and well specified initial conditions. The advantage is that the result strongly constrains the arbitrariness of initial conditions.

From the EMBH a plasma of pairs e^+e^- and photons initially optically thick with respect to scattering Thomson expands at ultrarelativistic velocity, collides inelastically with baryonic matter not collapsed and then reaccelerates up to the transparency point, when it is assumed that after e^+e^- pair recombination all the electromagnetic radiation is emitted. The baryonic matter remained in the pulse slows down in the collision with cold InterStellar Medium (ISM) until the non-relativistic regime (see fig. 3.1).

This model presents two peculiarities: the GRB is originated by an electromagnetic and non-rotating black hole whose surrounding space time is described by Reissner-Nordstrøm geometry; most observed astrophysical objects have an even small rotational energy but this choice is aimed to simplicity of treatment. The second peculiarity is that for the black hole is necessary a ratio of electric charge Q over the mass M satisfying $Q/\sqrt{G}M > 10^{-6}$. It can be useful to recall that an extreme black hole has a charge to mass ratio 10^{18} times smaller than the nuclear matter; this means that a quantum of charge over 10^{18} neutral nucleons is enough to make extremal an EMBH.

The discussion about the possibility of vacuum polarization process during the gravitational collapse of a charged system has been proceeded in [118, 119] and its observational consequences has been derived for the first time in [122].

If the two previous assumptions are accepted, by using the parameters of the model, several predictions can be found; many sources up to present moment have been fit in their

complicated temporal structure of light curve and in their spectral evolution.

3.2 The dyadosphere

Let us assume that the gravitational collapse of a body of mass greater than the critical mass for neutron star brings in general to a black hole characterized by the three fundamental parameters: the mass M, angular momentum L and electric charge Q. In this model we limit ourselves to a black hole with $L = 0$. The spacetime is therefore described by the Reissner-Nordstrøm square line element, given by:

$$ds^2 = g_{tt}(r)d^2t + g_{rr}(r)d^2r + r^2d^2\theta + r^2\sin^2\theta d^2\phi \ , \tag{3.1}$$

where

$$g_{tt}(r) = -\left[1 - \frac{2GM}{c^2 r} + \frac{Q^2 G}{c^4 r^2}\right] \equiv -\alpha^2(r) \tag{3.2}$$

$$g_{rr}(r) = \alpha^{-2}(r). \tag{3.3}$$

It has been shown that a large fraction of the mass-energy E of a Reissner-Nordstrøm black hole (up to 50%) can be stored in the form of electromagnetic energy extractable in the sense of Christodoulou, Ruffini [21]. The formula of Christodoulou-Ruffini for mass-energy of Reissner-Nordstrøm black hole is:

$$E^2 = M^2c^4 = \left(M_{\rm irr}c^2 + \frac{Q^2}{2r_+}\right)^2, \tag{3.4}$$

$$S = 4\pi {r_+}^2 = 16\pi\left(\frac{G^2}{c^4}\right)M_{\rm irr}^2 \tag{3.5}$$

where c is the light velocity in vacuum, $M_{\rm irr}$ is the irreducible mass of a black hole, the minimum mass value to which a black hole can be reduced by extraction energy process, r_+ is the radius of event horizon given by

$$r_+ = \frac{GM}{c^2}\left[1 + \sqrt{1 - \frac{Q^2}{GM^2}}\right], \tag{3.6}$$

with G Newton gravitational constant, S the area of surface horizon.

According to the classical treatment of Heisenberg-Euler [60], formulated in relativistic invariant form by Schwinger [131], if in a parallel plate capacitor with a separation between plates $d = \hbar/mc$, where m is electron mass and $\hbar$ is the Planck constant divided by 2π, the electric field reaches the value $\mathcal{E}_{\rm c}$ such that $e\mathcal{E}_{\rm c}\dfrac{\hbar}{mc} = mc^2$, where e is the electron charge, pair e^+e^- creation is possible. The critical value of field $\mathcal{E}_{\rm c}$ above which this can happen is $\mathcal{E}_{\rm c} = m^2c^3/\hbar e$ [96]. In a suitable reference frame the electric field has only the radial component, having the same form of minkowskian space-time: $\mathcal{E} = Q/r^2$. The region

between radius of horizon r_+ and radius $r_{\rm ds}$ at which the electric field reaches the critical value $\mathcal{E}_{\rm c} = Q/r_{\rm ds}^2$ has been called "dyadosphere" [102], while $r_{\rm ds}$ is given by

$$r_{\rm ds} = \sqrt{Q\frac{\hbar e}{m^2c^3}}. \tag{3.7}$$

If we define the adimensional quantities

$$\mu = M/M_\odot, \quad \xi = Q/(\sqrt{G}M) \tag{3.8}$$

the radius $r_{\rm ds}$ can be rewritten as

$$r_{\rm ds} = 1.1 \cdot 10^8\sqrt{\mu\xi}\ {\rm cm}, \tag{3.9}$$

while horizon radius can be rewritten as

$$r_+ = \frac{GM}{c^2}\left[1+\sqrt{1-\frac{Q^2}{GM^2}}\right] = 1.5\cdot 10^5\mu\left(1+\sqrt{1-\xi^2}\right)\ {\rm cm}. \tag{3.10}$$

The dyadosphere can be formed just if electric field reaches critical value outside horizon; therefore the disequality $Q/{r_+}^2 > \mathcal{E}_{\rm c}$ must hold; this gives a lower limit to the values of electric charge per unit of mass $\xi_{\rm min}$:

$$\frac{Q}{\left[\frac{GM}{c^2}\left[1+\sqrt{1-\frac{Q^2}{GM^2}}\right]\right]^2} > \frac{m^2c^3}{\hbar e}; \tag{3.11}$$

the $\xi_{\rm min}$ is implicitly defined in

$$\frac{\xi_{\rm min}}{\left[1+\sqrt{1-\xi_{\rm min}^2}\right]^2} = 10^{-6}\mu. \tag{3.12}$$

Moreover holds $Q \le \sqrt{G}M = Q_{max}$ or $\xi \le 1$; so that $\xi_{\rm min} \le \xi \le 1$. The values of μ are between $3.2M_\odot$, upper limit for neutron stars, and $6\cdot 10^5 M_\odot$ (in correspondence of $\xi = 1$), above which electric field does not reach the critical value $\mathcal{E}_{\rm c}$.

The pair number density in dyadosphere can be modelled by imagining dyadosphere as a sequence of thin spherical shell concentric capacitors with a thickness

$$\delta \simeq \frac{\hbar}{mc} \tag{3.13}$$

and a number of created pairs [96]

$$\Delta N(r) = \frac{Q}{e}\left[1-\left(\frac{r}{r_{\rm ds}}\right)^2\right]\ . \tag{3.14}$$

The local number density of electron and positron pairs created in this region as a function of radius is given by [96]

$$n_{e^+e^-}(r) = \frac{Q}{4\pi r^2\left(\frac{\hbar}{mc}\right)e}\left[1-\left(\frac{r}{r_{\rm ds}}\right)^2\right]\ . \tag{3.15}$$

In a time of order $\frac{\hbar}{mc^2} \simeq 10^{-21}$s many pairs are created and during this process the dyadosphere can be considered a set of shells causally disconnected. The inner layer of inner shell, containing charges opposite to black hole charge, is attracted by black hole reducing its charge to the value $Q_c = r_+^2 \mathcal{E}_{\rm c}$, the electric field below the critical value breaking the polarization process. As an example, if $\mu = 10^3$ and $\xi = 0.1$, the number of pairs created in the dyadosphere turns out to be $N_{e^+e^-} \sim 10^{60}$.

If final electric field is $\mathcal{E}_{\rm c}$, the final electrostatic energy density is $\rho_f(r) = {\mathcal{E}_{\rm c}}^2/8\pi$. Therefore the energy density of pairs deposited inside dyadosphere as a function of radial coordinate can be computed as difference between initial and final electrostatic energy density:

$$\rho_{e^+e^-}(r) = \frac{1}{8\pi}\left(\mathcal{E}_{\rm i}^2(r) - \mathcal{E}_{\rm c}^2\right) \ . \tag{3.16}$$

The total energy released is

$$E_{dya} \equiv E^{\rm tot}_{e^+e^-} = \frac{1}{2}\frac{Q^2}{r_+}\left(1 - \frac{r_+}{r_{\rm ds}}\right)\left(1 - \left(\frac{r_+}{r_{\rm ds}}\right)^4\right). \tag{3.17}$$

In the limit $\frac{r_+}{r_{\rm ds}} \to 0$, for the dyadosphere energy $E_{dya} \to \frac{Q^2}{2r_+}$ holds, corresponding to the maximal energy extractable from a black hole in reversible processes, i.e. $E - M_{\rm irr} = \frac{Q^2}{2r_+}$. Due to the huge number of pairs created and to the order of magnitude of the cross section for the process $e^+ + e^- \to \gamma + \gamma$, the system in dyadosphere is expected to thermalize to a plasma with $N_{e^-} = N_{e^+} = N_p = N_\gamma$, where N_p is the number of pairs. The plasma begins to expand from the black hole assumed at rest at ultrarelativistic velocity; this phase has been called PEM pulse [116]. The pairs and photons at each instant of time reach thermodynamic equilibrium during expansion.

It has been assumed for the sake of simplicity that pair energy density in dyadosphere and then in the PEM pulse is given at first approximation by its average value (see fig. 3.2), i.e. ratio of total energy to volume of dyadosphere:

$$\bar{\rho}_{e^+e^-} = \frac{E^{\rm tot}_{e^+e^-}}{\frac{4\pi}{3}\left(r_{\rm ds}^3 - r_+^3\right)}. \tag{3.18}$$

In fact we expect that the dyadosphere will form not around an already collapsed black hole but more realistically during the same gravitational collapse and the black hole formation. The study of dynamical formation of the dyadosphere during the gravitational collapse has received recently a new form [19].

The process described up to now can be called era zeroth. Following eras involve the expansion in vacuum from the progenitor star and the completely inelastic collision with the protostellar baryonic matter left over in the gravitational collapse. The collision with baryonic remnant brings a characteristic observable contribution to the GRB phenomenon. In the remaining part of this chapter we will separately analyze the phases up to the transparency point of this system.

We recall that the interval of time Δt measured in the frame of observer on the earth and the one in which the central black hole is at rest are connnected by simple cosmological transformation, while the fireball of plasma emerging at ultrarelativistic velocity from the black hole defines a Lorentz frame with respect to the observer on the earth.

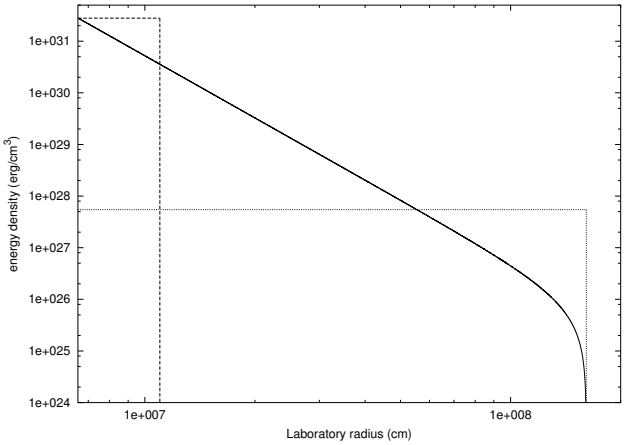

Figure 3.2: *Two different approximations for the energy density profile inside the dyadosphere. The first one (dashed line) fixes the energy density equal to its peak value, and computes an "effective" dyadosphere radius accordingly. The second one (dotted line) fixes the dyadosphere radius to its correct value, and assumes an uniform energy density over the dyadosphere volume. The total energy in the dyadosphere is the same in both cases. The solid curve represents the real energy density profile.*

3.3 Era I: expansion of PEM pulse

After the explosion from the dyadosphere a thermal plasma of e^+e^- pairs and photons optically thick with respect to Thomson scattering processes begins to expand at ultra-relativistic velocity. In this era the expansion takes place in a region of very low baryonic contamination.

Recalling Eq.(3.15) the limit on such baryonic contamination, where ρ_{B_c} is the mass-energy density of baryons, is given by

$$\rho_{B_c} \ll m_p n_{e^+e^-}(r) = 3.2 \cdot 10^8 \left(\frac{r_{ds}}{r}\right)^2 \left[1 - \left(\frac{r}{r_{ds}}\right)^2\right] (g/cm^3). \tag{3.19}$$

Near the horizon $r \simeq r_+$, this gives

$$\rho_{B_c} \ll m_p n_{e^+e^-}(r) = 1.86 \cdot 10^{14} \left(\frac{\xi}{\mu}\right) (g/cm^3)\,, \tag{3.20}$$

and near the radius of the dyadosphere r_{ds}:

$$\rho_{B_c} \ll m_p n_{e^+e^-}(r) = 3.2 \cdot 10^8 \left[1 - \left(\frac{r}{r_{ds}}\right)^2\right]_{r \to r_{ds}} (g/cm^3)\,. \tag{3.21}$$

Such conditions could be easily satisfied in the collapse to an EMBH. Consequently we have solved the equations governing a plasma composed solely of e^+e^--pairs and photons, starting at time zero from the two dyadosphere configurations corresponding to constant density (see fig. 3.2).

The plasma of e^+e^- pairs and photons is described by the following energy-momentum tensor:

$$T^{\mu\nu} = pg^{\mu\nu} + (p+\rho)\,U^\mu U^\nu + \Delta T^{\mu\nu} \tag{3.22}$$

where ρ and p are respectively total proper energy density and pressure in the comoving system; U^μ are contravariant components of 4-velocity and $\Delta T^{\mu\nu}$ takes into account of dissipative effects due to heat conduction and viscosity, but in this treatment it has been neglected. In general we have $g_{\mu\nu}U^\mu U^\nu = -1$; for a spherically symmetric motion this reduces to $g_{tt}(U^t)^2 + g_{rr}(U^r)^2 = -1$, where U^t and U^r are respectively temporal and radial controvariant components of 4-velocity U^μ.

It is assumed that the gravitational energy of interaction of the PEM pulse with central black hole is negligible with respect to the total energy of PEM pulse such that a fluid expansion with special relativistic equations can be considered.

Moreover it is assumed that photons remain trapped inside the fireball until complete transparency, i.e. the emission of electromagnetic radiation is negligible during the first phases of expansion, being therefore adiabatic [116]. This assumption is valid until the photon mean free path is negligible with respect to the thickness of pulse [97].

The thermodynamic quantities used to describe the process are the proper internal energy density of all species particles in the pulse ϵ, given by $\epsilon = \epsilon_{e^+} + \epsilon_{e^-} + \epsilon_\gamma$, where ϵ_{e^+} (ϵ_{e^-}) is the proper internal energy density of electrons (positrons) and ϵ_γ the proper internal energy density of photons. The proper number density of pairs $n_{e^\pm}$, if the system is in thermodynamic equilibrium initially at temperature T of order $T \sim MeV$, enough for e^+e^- pair creation, equals the proper number density of photons n_γ. This is not valid at lower temperature [10]. The total pressure is $p = p_{e^+} + p_{e^-} + p_\gamma$, where $p_{e^\pm}$ are electrons and positrons pressures and p_γ is photons pressure. The system is highly relativistic, so the equation of state $p = \epsilon/3$ can be considered valid. The equation of state for this plasma is represented with thermal index Γ:

$$\Gamma = 1 + \frac{p}{\epsilon}. \tag{3.23}$$

3.3.1 Fermi integrals

Thermodynamical quantities before introduced are expressed and numerically computed in terms of integrals over Bose distribution for photons and Fermi distribution for e^+e^- pairs with zero chemical potentials μ_γ and $\mu_{e^\pm}$. We begin from the reaction $e^+ + e^- \rightarrow \gamma + \gamma$. From statistical mechanics it is known that given a thermodynamic system at temperature T kept inside a volume V and made of a variable number of particles N, the thermodynamic equilibrium is expressed by the condition that the potential free energy of Helmholtz $F(T, V, N)$ is stationary with respect to N variations:

$$\left(\frac{\partial F}{\partial N}\right)_{T,V} = 0; \tag{3.24}$$

by definition, chemical potential μ is given by

$$\mu = \left(\frac{\partial F}{\partial N}\right)_{T,V}; \tag{3.25}$$

so that for a system made by a photon gas at equilibrium with matter with respect to creation and absorption processes, we have $\mu_\gamma = 0$ [67]. Therefore the chemical potential of electrons and positrons associated to the reaction $e^+ + e^- \rightarrow \gamma + \gamma$ is equal and opposite: $\mu_{e^-} = -\mu_{e^+} = \mu$. The proper number density of electrons [146], as other thermodynamical quantities, is given by Fermi integrals:

$$\begin{aligned} n_{e^-}(m,T,\mu_{e^-}) &= \frac{2}{h^3}\int \frac{d^3p}{e^{\frac{\sqrt{(pc)^2+(mc^2)^2}}{kT}+\frac{\mu}{kT}}+1} = \\ &= \frac{8\pi}{h^3}\int_0^{+\infty} \frac{p^2}{e^{\frac{\sqrt{(pc)^2+(mc^2)^2}}{kT}+\frac{\mu}{kT}}+1}dp = \\ &= \frac{aT^3}{k}\frac{7}{4}\frac{1}{A}\int_0^{+\infty} \frac{z^2}{e^{\sqrt{z^2+(mc^2/kT)^2}+\frac{\mu}{kT}}+1}dz, \end{aligned} \tag{3.26}$$

where $z = pc/kT$, m is the electron mass, T[MeV] is the temperature of fireball in comoving frame, a is a constant given by $a = 8\pi^5k^4/15h^3c^3 = 1.37 \cdot 10^{26} erg/cm^3 MeV^4$, k is the Boltzmann constant and A is a numerical constant ($A = \frac{7}{4}\frac{\pi^4}{15} = 11.36$) introduced for convenience.

Moreover also μ must be zero since the total electric charge of fireball is zero: if Q is total electric charge of fireball, we have

$$Q = e\left[n_{e^-}(m,T,\mu) - n_{e^+}(m,T,-\mu)\right] = 0 \tag{3.27}$$

where $n_{e^-}(m,T,\mu)$ is given by Eq.(3.26); so that $\mu = 0$.

The proper internal energy density for photons is given by

$$\epsilon_\gamma = \frac{2}{h^3}\int \frac{h\nu}{e^{\frac{h\nu}{kT}}-1}d^3p = aT^4 \tag{3.28}$$

where $p = h\nu/c$. The proper internal energy density for electrons is given by:

$$\begin{aligned} \epsilon_{e^-} &= \frac{2}{h^3}\int \frac{\sqrt{(pc)^2+(mc^2)^2}}{e^{\frac{\sqrt{(pc)^2+(mc^2)^2}}{kT}}+1}d^3p = \\ &= \frac{8\pi}{h^3}\int_0^{+\infty} \frac{p^2\sqrt{(pc)^2+(mc^2)^2}}{e^{\frac{\sqrt{(pc)^2+(mc^2)^2}}{kT}}+1}dp = \\ &= aT^4\frac{7}{4}\frac{1}{A}\int_0^{+\infty} \frac{z^2\sqrt{z^2+(mc^2/kT)^2}}{e^{\sqrt{z^2+(mc^2/kT)^2}}+1}dz \end{aligned} \tag{3.29}$$

where $z = pc/kT$. Therefore the total proper internal energy density of the PEM pulse, summing up all the contributions of photons and e^+e^- pairs, is given by

$$\epsilon_{tot} = aT^4\left[1 + \frac{7}{4}\frac{2}{A}\int_0^{+\infty} \frac{z^2\sqrt{z^2+(mc^2/kT)^2}}{e^{\sqrt{z^2+(mc^2/kT)^2}}+1}dz\right] \tag{3.30}$$

where the factor 2 in front of the integral takes into account of electrons and positrons. About the pressure of the photons, the relativistic equation of state gives

$$p_\gamma = \frac{\epsilon_\gamma}{3} = \frac{aT^4}{3}; \tag{3.31}$$

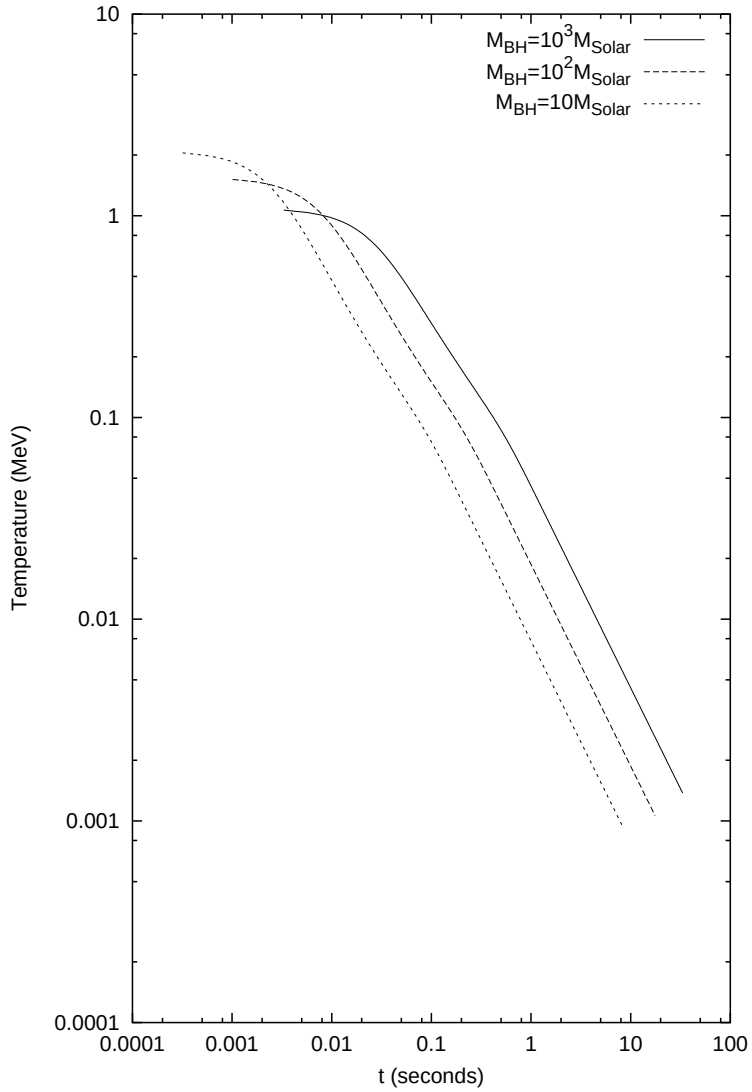

Figure 3.3: *Temperature in comoving system as a function of laboratory time for different values of black hole mass μ.*

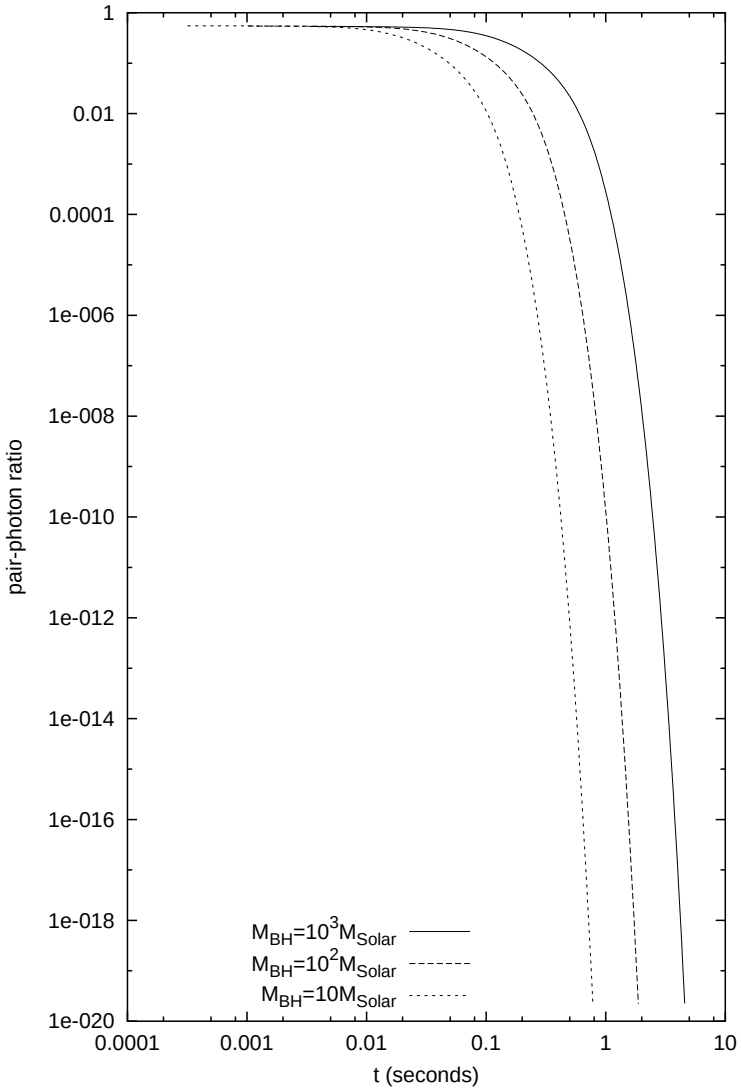

Figure 3.4: *Ratio between number density of pairs e^+e^- $n_{e^\pm}$ and number density of photons $n_\gamma(T)$ as a function of laboratory time for different values of black hole mass μ.*

and about the pressure of electrons

$$\begin{aligned} p_{e^-} &= \frac{2}{3h^3}\int \frac{1}{e^{\frac{\sqrt{(pc)^2+(mc^2)^2}}{kT}}+1}\cdot\frac{(pc)^2}{\sqrt{(pc)^2+(mc^2)^2}}d^3p = \\ &= \frac{8\pi}{3h^3}\int_0^{+\infty}\frac{p^2}{e^{\frac{\sqrt{(pc)^2+(mc^2)^2}}{kT}}+1}\cdot\frac{(pc)^2}{\sqrt{(pc)^2+(mc^2)^2}}dp = \\ &= \frac{aT^4}{3}\frac{7}{4}\frac{1}{A}\int_0^{+\infty}\frac{z^4}{e^{\sqrt{z^2+(mc^2/kT)^2}}+1}\cdot\frac{1}{\sqrt{z^2+(mc^2/kT)^2}}dz. \end{aligned} \tag{3.32}$$

Therefore the total pressure of PEM pulse is given by

$$p_{tot} = \frac{aT^4}{3}\left[1+\frac{7}{4}\frac{2}{A}\int_0^{+\infty}\frac{z^4}{e^{\sqrt{z^2+(mc^2/kT)^2}}+1}\cdot\frac{1}{\sqrt{z^2+(mc^2/kT)^2}}dz\right]. \tag{3.33}$$

3.3.2 Numerical code

In the following we recall a zeroth order approximation of the fully relativistic equations of the previous section [116]:
(i) Since we are mainly interested in the expansion of the e^+e^- plasma away from the EMBH, we neglect the gravitational interaction.
(ii) We describe the expanding plasma by a special relativistic set of equations.

In the PEM pulse phase the expansion in vacuum is described by a set of equations expressing:

- entropy conservation, because of the assumption that emission of electromagnetic radiation is negligible up to transparency;
- energy conservation: the increase of kinetic energy is compensated by a decrease of total internal energy.

For the expansion of a single shell, the adiabaticity is given by

$$d\left(V\epsilon\right)+pdV = dE+pdV = 0\ , \tag{3.34}$$

where V is the volume of the shell in the comoving frame and $E = V\epsilon$ is the proper internal energy of all species particles in the plasma. By using the equation of state (3.23) we find

$$dln\epsilon+\Gamma dlnV = 0 \tag{3.35}$$

and, by integrating, we find

$$\frac{\bar{\epsilon}_\circ}{\bar{\epsilon}} = \left(\frac{V}{V_\circ}\right)^\Gamma; \tag{3.36}$$

recalling that the volume of the fireball in the comoving frame is given by $V = \mathcal{V}\bar{\gamma}$, where $\mathcal{V}$ is the volume in the laboratory frame, we find

$$\frac{\bar{\epsilon}_\circ}{\bar{\epsilon}} = \left(\frac{V}{V_\circ}\right)^\Gamma = \left(\frac{\mathcal{V}}{\mathcal{V}_\circ}\right)^\Gamma\left(\frac{\bar{\gamma}}{\bar{\gamma}_\circ}\right)^\Gamma. \tag{3.37}$$

The total energy conservation of the shell implies [116]:

$$(\Gamma\bar{\epsilon})\mathcal{V}\bar{\gamma}^2 = (\Gamma\bar{\epsilon}_\circ)\mathcal{V}_\circ\bar{\gamma}_\circ^2\,; \tag{3.38}$$

and this gives the evolution for $\bar{\gamma}$:

$$\bar{\gamma} = \bar{\gamma}_\circ\sqrt{\frac{\bar{\epsilon}_\circ\mathcal{V}_\circ}{\bar{\epsilon}\mathcal{V}}}\,. \tag{3.39}$$

Substituting this expression for $\bar{\gamma}$ in (3.37) the final equation for proper internal energy density is found

$$\bar{\epsilon} = \bar{\epsilon}_\circ\left(\frac{\mathcal{V}_\circ}{\mathcal{V}}\right)^{\frac{\Gamma}{2-\Gamma}}\,. \tag{3.40}$$

Since the thermodynamic equilibrium is assumed and in all cases considered the initial temperature is larger than e^+e^- pairs creation threshold ($T \simeq 1$ MeV), the proper number density of electrons is roughly equal to that one of photons:

$$n_{e^\pm} \sim n_{e^-}(T) \sim n_\gamma(T)\,, \tag{3.41}$$

where $n_{e^\pm}(T)$ is the total proper number density of electrons and positrons in comoving frame at thermodynamic equilibrium in the process $e^+ + e^- \rightarrow \gamma + \gamma$ ($n_{e^-}(m,T) \sim n_\gamma(T)$), $n_{e^\pm}$ is the total proper number density of electrons and positrons in comoving frame at a generic time before reaching the equilibrium. In these conditions the number of particles is conserved:

$$\left(n_{e^\pm}U^\mu\right)_{,\mu} = 0. \tag{3.42}$$

Later on, for $T \ll 1$MeV (see fig. 3.3), e^+e^- pairs still annihilate but can not be created anymore, therefore

$$n_\gamma(T) > n_{e^\pm} > n_{e^\pm}(T) \tag{3.43}$$

as shown in fig. 3.4.

The evolution of a plasma of e^+e^- pairs and photons should be treated by general relativistic hydrodynamics equations describing the variation of the number of particles in the process. The 4-vector number density of pairs is defined ($n_{e^\pm}U^\mu$), which in the comoving frame reduces to the 4-vector $(n_{e^\pm}, 0, 0, 0)$. The law of number conservation for pairs is

$$\begin{aligned}\left(n_{e^\pm}U^\mu\right)_{;\mu} &= \frac{1}{\sqrt{-g}}\left(\sqrt{-g}n_{e^\pm}U^\mu\right)_{,\mu} = \\ &= \left(n_{e^\pm}U^t\right)_{,t} + \frac{1}{r^2}\left(r^2 n_{e^\pm}U^r\right)_{,r} = 0\end{aligned} \tag{3.44}$$

where $g = \parallel g^{\mu\nu} \parallel = -r^4 sin^2\theta$ is the determinant of Reissner-Nordstrøm metric. In the plasma processes of creation and annihilation of particles occur due to collisions between particles. If the number of particles is conserved, it holds $\left(n_{e^\pm}U^\mu\right)_{;\mu} = 0$; if instead it is not conserved, in the assumptions that only binary collisions occur between particles and in the assumption of molecular caos [34], the Eq.(3.44) becomes

$$\left(n_{e^\pm}U^\mu\right)_{;\mu} = \overline{\sigma v}\left[n_{e^-}(T)n_{e^+}(T) - n_{e^-}n_{e^+}\right] \tag{3.45}$$

where σ is the cross section for the process of creation and annihilation of pairs, given by

$$\sigma = \frac{\pi {r_e}^2}{\alpha+1}\left[\frac{\alpha^2+4\alpha+1}{\alpha^2-1}ln\left(\alpha+\sqrt{\alpha^2-1}\right) - \frac{\alpha+3}{\sqrt{\alpha^2-1}}\right], \tag{3.46}$$

with $\alpha = \frac{E}{mc^2}$ and E total energy of positrons in the laboratory frame, and $r_e = \frac{e^2}{mc^2}$ the classical radius of electron, v is the sound velocity in the fireball:

$$v = c\sqrt{\frac{p_{tot}}{\epsilon_{tot}}}, \tag{3.47}$$

and $\overline{\sigma v}$ is the mean value of σv, where σ in first approximation can be equal to Thomson cross section, $\sigma_T = 0.665 \cdot 10^{-24} cm^2$.
Using the approximation of special relativity, the 4-velocity is written $U^\mu = (\gamma, \gamma\frac{v}{c})$; substituting to $n_{e^\pm}(T)$ the $\bar{n}_{e^\pm}(T)$ and to $n_{e^\pm}$ the $\bar{n}_{e^\pm}$, Eq.(3.45) in hybrid form becomes

$$\frac{\partial\left(n_{e^\pm}\gamma\right)}{\partial t} = -\frac{1}{r^2}\frac{\partial}{\partial r}\left(r^2 n_{e^\pm}\gamma V^r\right) + \overline{\sigma v}\left(n_{e^\pm}^2(T) - n_{e^\pm}^2\right), \tag{3.48}$$

valid for electrons and positrons.
Now we have a complete set of equations for numerical integration: (3.39), (3.40) and the (3.48).

If we now turn from a single shell to a finite distribution of shells, we can introduce the average values of the proper internal energy density and pair number densities $(\bar{\epsilon}, \bar{n}_{e^\pm})$ for the PEM pulse; the average $\bar{\gamma}$ factor is defined by

$$\bar{\gamma} = \frac{1}{\mathcal{V}}\int_{\mathcal{V}} \gamma(r) d\mathcal{V}, \tag{3.49}$$

and $\mathcal{V}$ is the total volume of the shell in the laboratory frame [116].

3.3.3 Slab approximation

In principle we could have an infinite number of possible schemes to define geometry of the expanding shell. Three different possible schemes have been proposed [116]:

- Sphere. An expansion with radial component of 4-velocity proportional to the distance to the black hole $U_r(r) = U\dfrac{r}{\mathcal{R}(t)}$, where U is the radial component of 4-velocity on the external surface of PEM pulse (having radius $\mathcal{R}(t)$), the factor $\bar{\gamma}$ from (3.49) is

  $$\bar{\gamma} = \frac{3}{8U^3}\left[2U\left(1+U^2\right)^{\frac{3}{2}} - U\left(1+U^2\right)^{\frac{1}{2}} - ln\left(U+\sqrt{1+U^2}\right)\right]; \tag{3.50}$$

  this distribution corresponds to a uniform and time decreasing density, like in Friedmann model for the universe;

- Slab 1. An expansion with thickness of fireball $\mathcal{D} = r_{ds} - r_+$ constant in laboratory frame in which the black hole is at rest, with $U_r(r) = U_r = cost$ and $\bar{\gamma} = \sqrt{1+{U_r}^2}$; this distribution does not require an average;

- Slab 2. An expansion with thickness of fireball constant in comoving frame of PEM pulse.

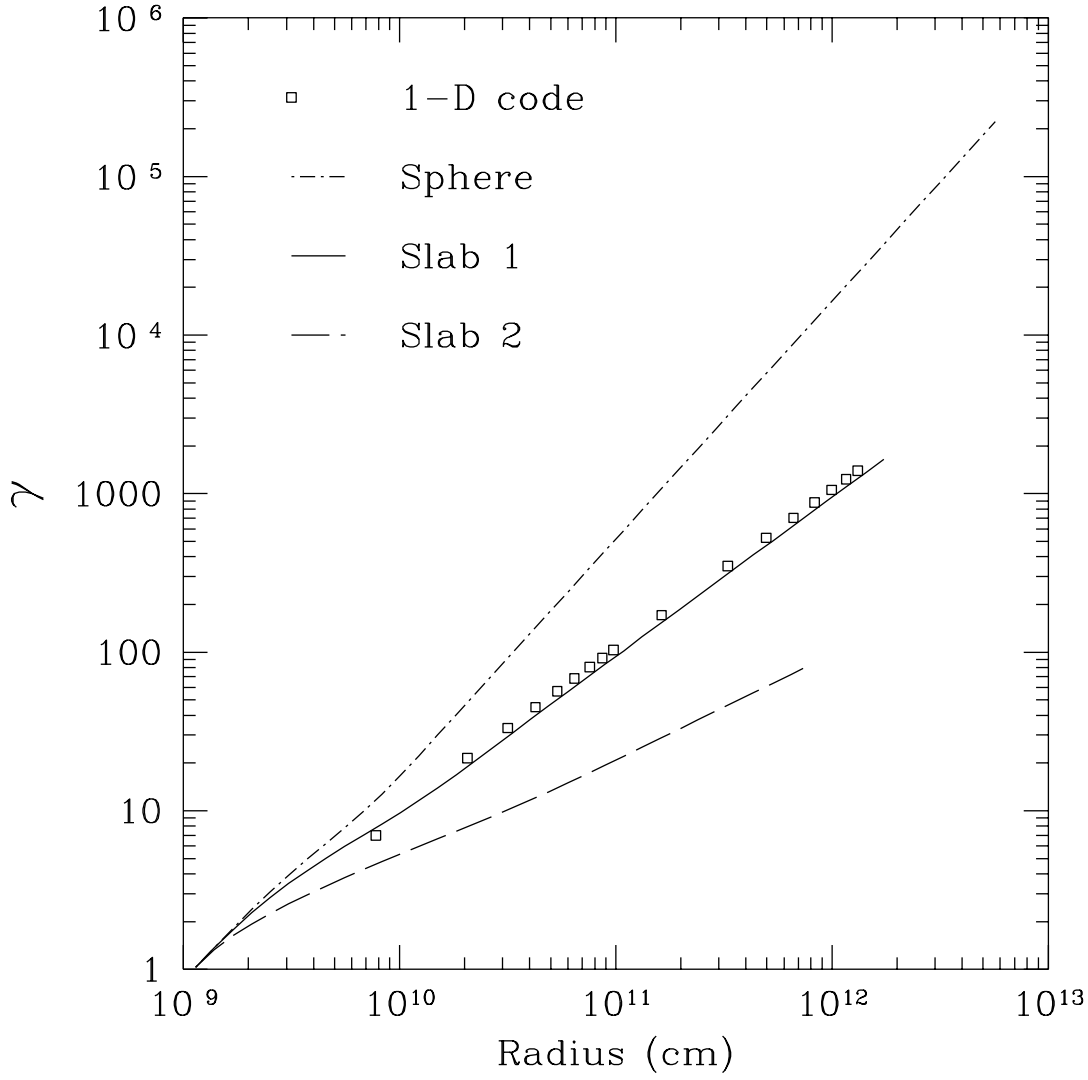

Figure 3.5: *Lorentz $\bar{\gamma}$ factor as a function of radial coordinate. Three schemes of expansion of PEM pulse (see text) are compared with solution of hydrodynamics relativistic equations numerically integrated for a black hole with $\mu = 10^3$ and $\xi = 0.1$. The result is in accordance with the scheme of a fireball with constant thickness in laboratory frame.*

The result of simulation with the code presented in subsects. (3.3.2, 3.3.1) has been compared with the one of hydrodynamic equation in general relativity [116] (see fig. 3.5). Excellent agreement has been found with the scheme in which the thickness of fireball is constant in laboratory frame: what happens is that the thickness in comoving frame increases, but due to the Lorentz contraction, it is kept constant in laboratory frame and equal to $\mathcal{D} = (r_{\rm ds} - r_+)$. In this case $U_r = \sqrt{\bar{\gamma}^2 - 1}$, where $\bar{\gamma}$ is computed by conservation equations. For a further discussion of the slab approximation in presence of baryonic contamination see sect. 3.4.

Let us discuss the emission from this slab. Even if the PEM pulse is optically thick in this era, photons located at a distance from the external surface less their mean free path can escape and reach the observer at infinity. The mean free path in the comoving frame is given in the first part of this era by roughly $L_\gamma = 1/\sigma n_{e^+e^-} \sim 10^{-6} cm$ while in laboratory frame is given by $\lambda = L_\gamma/\bar{\gamma} \sim 10^{-8}$cm. However the luminosity emitted at this stage is negligible, since the ratio between λ and the thickness of the fireball $\mathcal{D}$ in the laboratory frame (with $\mathcal{D} = (r_{ds} - r_+) \sim 10^9$cm) is of the order of $\lambda/\mathcal{D} \simeq 10^{-17}$.

As can be seen from fig. 3.5, in the slab 1 approximation the qualitative behaviour of γ is $\gamma \sim r$, in accordance with results in literature [89]. We found that due to the Lorentz contraction, the width of the pulse appears to be constant in the laboratory frame. A similar situation occurs for the observed temperature of PEM pulse. In the comoving frame the temperature decreases as $T' \sim r^{-1}$. Since γ monotonically increases as $\gamma \sim r$ [103], in laboratory frame $T = \gamma T' \sim$ *constant* [117] (see fig.4.9); photons are blue-shifted in laboratory frame in such a way that, at least in the first era, the temperature measured by an observer at infinity is constant. The numerical value of the temperature of equilibrium at each instant is found by equating (3.30) numerically computed and (3.40).

3.4 Era II: interaction of the PEM pulse with remnant

The PEM pulse expands initially in a region of very low baryonic contamination created by the process of gravitational collapse. As it moves outside, the baryonic remnant (see fig. 3.1) of the progenitor star is swept up. The existence of such a remnant is necessary in order to guarantee the overall charge neutrality of the system: the collapsing core has the opposite charge of the remnant and the system as a whole is neutral. The number of extra charges in the baryonic remnant negligibly affects the overall charge neutrality of the PEM pulse.

The baryonic matter remnant is assumed to be distributed well outside the dyadosphere in a shell of thickness Δ between an inner radius $r_{\rm in}$ and an outer radius $r_{\rm out} = r_{\rm in} + \Delta$ at a distance from the EMBH not so big that the PEM pulse expanding in vacuum has not yet reached transparency and not so small that the system will reach sufficiently high value of Lorentz γ in order to not be stopped in the collision (see fig. 3.6 and fig. 3.10). For the sake of an example we choose

$$r_{\rm in} = 100 r_{\rm ds}, \quad \Delta = 10 r_{\rm ds}. \tag{3.51}$$

The total baryonic energy-mass $M_B c^2 = N_B m_p c^2$ is assumed to be a fraction of the dyadosphere initial total energy ($E_{\rm dya}$). The total baryon-number N_B is then expressed as a

function of the dimensionless parameter B given by

$$B = \frac{N_B m_p c^2}{E_{\rm dya}}\,, \tag{3.52}$$

where B is a parameter in the range $10^{-8} - 10^{-2}$ and m_p is the proton mass. We shall see below the role of B in the determination of the features of the GRBs. We will see in sect. 3.6 the sense in which B and E_{dya} can be considered free parameters of the EMBH model for the entire GRB family of "long bursts". For the so-called "short bursts" the EMBH model depends on the other parameters μ, ξ, since in that case $B \leq 10^{-8}$ or $B = 0$, equivalently because the dynamics is not significantly modified, (see sect. 4.8) and the energy in the pulse is emitted at transparency. The baryon number density n_B° is assumed to be a constant

$$\bar{n}_B^\circ = \frac{N_B}{\mathcal{V}_B}, \quad \bar{\rho}_B^\circ = m_p \bar{n}_B^\circ c^2. \tag{3.53}$$

where $\mathcal{V}_B$ is the volume of the remnant shell at rest in the laboratory frame. As the PEM pulse reaches the region $r_{\rm in} < r < r_{\rm out}$, it interacts with the baryonic matter which is assumed to be at rest. In our model we make the following assumptions to describe this interaction:

- the PEM pulse does not change its geometry during the interaction;
- the collision between the PEM pulse and the baryonic matter is assumed to be completely inelastic,
- the baryonic matter reaches thermal equilibrium with the photons and pairs of the PEM pulse.

These assumptions are valid if: (i) the total energy of the PEM pulse is much larger than the total mass-energy of baryonic matter M_B, $10^{-8} < B < 10^{-2}$, (ii) the PEM pulse has a large value of the γ factor ($\bar{\gamma} > 100$) and (iii) the ratio of the comoving number density of pairs and baryons at the moment of collision $n_{e^+e^-}/n_B^\circ$ is very high (e.g., $10^6 < n_{e^+e^-}/n_B^\circ < 10^{12}$).

In the collision between the PEM pulse and the baryonic matter at $r_{\rm in} < r < r_{\rm out}$, we impose total conservation of energy and momentum. We consider the collision process between two radii r_1, r_2 satisfying $r_{\rm in} < r_1 < r_2 < r_{\rm out}$ and $r_2 - r_1 \ll \Delta$. The amount of baryonic mass acquired by the PEM pulse is

$$\Delta M = \frac{M_B}{V_B}\frac{4\pi}{3}(r_2^3 - r_1^3). \tag{3.54}$$

As for energy density of dyadosphere, here also we choose a simplification for the energy density: in fact during the passage of the shell the material deposites on the external surface of the PEM pulse; however we neglected this effect and assumed that this material after collision diffuses instantaneously in the pulse with a constant density:

$$n'_B = \frac{N'_B}{V}, \tag{3.55}$$

where N'_B is the number of particle of the remnant shell swept up by the pulse and V is the comoving volume of the pulse.

The conservation of total energy in the laboratory frame, where the quantities before collision are indicated with "$\circ$" leads to

$$(\Gamma\bar{\epsilon}_\circ + \bar{\rho}_B^\circ)\gamma_\circ^2\mathcal{V}_\circ + \Delta M = (\Gamma\bar{\epsilon} + \bar{\rho}_B + \frac{\Delta M}{V} + \Gamma\Delta\bar{\epsilon})\gamma^2\mathcal{V}, \tag{3.56}$$

where $\Delta\bar{\epsilon}$ is the corresponding increase of internal energy due to the collision and Γ is the thermal index. Similarly the momentum-conservation gives

$$(\Gamma\bar{\epsilon}_\circ + \bar{\rho}_B^\circ)\gamma_\circ U_r^\circ\mathcal{V}_\circ = (\Gamma\bar{\epsilon} + \bar{\rho}_B + \frac{\Delta M}{V} + \Gamma\Delta\bar{\epsilon})\gamma U_r\mathcal{V}, \tag{3.57}$$

where the radial component of the four-velocity of the PEM pulse is $U_r^\circ = \sqrt{\bar{\gamma}_\circ^2 - 1}$. We then find the solution of the two previous Eq.(3.56) and Eq.(3.57) :

$$\Delta\bar{\epsilon} = \frac{1}{\Gamma}\left[(\Gamma\bar{\epsilon}_\circ + \bar{\rho}_B^\circ)\frac{\gamma_\circ U_r^\circ\mathcal{V}_\circ}{\gamma U_r\mathcal{V}} - (\Gamma\bar{\epsilon} + \bar{\rho}_B + \frac{\Delta M}{V})\right], \tag{3.58}$$

$$\gamma = \frac{a}{\sqrt{a^2-1}}, \quad a \equiv \frac{\gamma_\circ}{U_r^\circ} + \frac{\Delta M}{(\Gamma\bar{\epsilon}_\circ + \bar{\rho}_B^\circ)\gamma_\circ U_r^\circ\mathcal{V}_\circ}. \tag{3.59}$$

These equations determine the γ factor and the internal energy density $\bar{\epsilon} = \bar{\epsilon}_\circ + \Delta\bar{\epsilon}$ in the capture process of baryonic matter by the PEM pulse.

In this phase of expansion, another thermodynamic quantity has to be considered: the chemical potential μ of the electrons from ionization of baryonic remnant. The chemical potential is numerically computed from the definition of the proper number density of electrons of ionization:

$$n_{e^-}^b(m,T,\mu) = \frac{aT^3}{k}\frac{7}{4}\frac{1}{A}\int_0^{+\infty}\frac{z^2}{e^{\sqrt{z^2+(mc^2/kT)^2}+\frac{\mu}{kT}}+1}dz. \tag{3.60}$$

Therefore the equations for this phase are (3.58), (3.59), (3.55), (3.48) and (3.60).

The collision of the PEM pulse with the baryonic remnant leads to the following consequences:

- a reheating of the plasma in the comoving frame but not in the laboratory frame (see fig. 3.6), therefore an increase of the number of e^+e^- pairs; moreover an increase of free electrons originated from the ionization of atoms in the baryonic remnant; correspondingly these effect give an overall increase of the opacity of the pulse;
- the more the amount of baryonic matter swept up, the more internal energy of the pulse is converted in kinetic energy of baryons.

By describing the interaction of PEM pulse with remnant as completely inelastic collision, one can compute by the energy-momentum conservation equation the decrease of Lorentz γ and the increase of internal energy as function of B parameter; the ultrarelativistic approximation ($\gamma_\circ \to \infty$) interesting in our case is also given:

1. an abrupt decrease of the γ factor given by

$$\gamma_{coll} = \gamma_\circ\frac{1+B}{\sqrt{{\gamma_\circ}^2(2B+B^2)+1}} \quad \underset{\gamma_\circ\to\infty}{\longrightarrow} \quad \frac{B+1}{\sqrt{B^2+2B}} \tag{3.61}$$

where $\gamma_\circ$ is the γ factor of the PEM pulse before the collision,

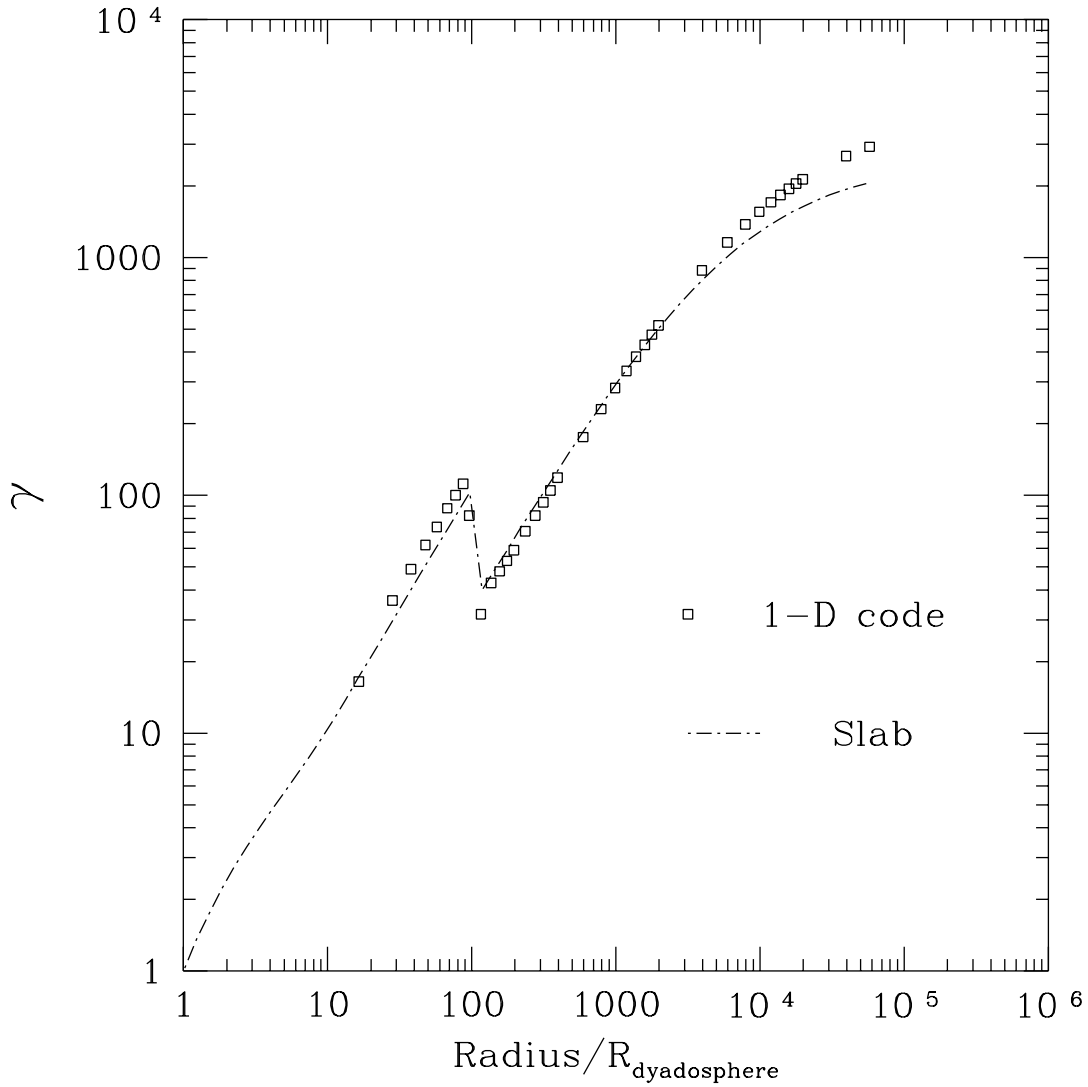

Figure 3.6: *Lorentz $\bar{\gamma}$ factor as a function of radial coordinate from the PEMB pulse simulation is compared with the $\bar{\gamma}$ factor as solution of hydrodynamics general relativistic equations numerically integrated (open squares) for $E_{dya} = 3.1 \times 10^{54} erg$ and $B = 1.3 \times 10^{-4}$, $r_{\rm in} = 100 r_{\rm ds}$ and $\Delta = 10 r_{\rm ds}$. The result is again in accordance with the scheme of a fireball with constant thickness in laboratory frame which is valid up to $B = 10^{-2}$.*

2. an increase of the internal energy in the comoving frame E_{coll} developed in the collision given by

$$\frac{E_{coll}}{E_{dya}} = \frac{\sqrt{\gamma_\circ{}^2\,(2B+B^2)+1}}{\gamma_\circ} - \left(\frac{1}{\gamma_\circ}+B\right) \quad \underset{\gamma_\circ \to \infty}{\longrightarrow} \quad -B+\sqrt{B^2+2B} \tag{3.62}$$

This approximation applies when the final γ factor at the end of the PEM pulse era $\gamma_\circ$ is larger than γ_{coll} (see fig. 3.10).

3.5 Era III: expansion of PEMB pulse

After the engulfment of the baryonic matter of the remnant the plasma of e^+e^--pairs, photons and baryonic matter expands again as a sharp pulse, namely the PEMB pulse. The calculation is continued as the plasma fluid expands, cools and the e^+e^- pairs recombine until it becomes optically thin:

$$\int_{\Delta R} dr(n_{e^\pm} + \bar{Z} n_B)\sigma_T \simeq O(1), \tag{3.63}$$

where $\sigma_T = 0.665 \cdot 10^{-24}\mathrm{cm}^2$ is the Thomson cross-section and the integration is over the radial interval of the PEMB pulse in the comoving frame. In order to study the PEMB pulse expansion the validity of the slab approximation adopted for the PEM pulse phase has to be verified; otherwise the full hydrodynamics general relativistic equations should be integrated. The PEMB pulse evolution firstly has been simulated by integrating the general relativistic hydrodynamical equations with the Livermore codes, for a total energy in the dyadosphere $E_{dya} = 3.1 \times 10^{54}$ erg and a baryonic shell of thickness $\Delta = 10 r_{\mathrm{ds}}$ at rest at a radius of $100 r_{\mathrm{ds}}$ and $B \simeq 1.3 \cdot 10^{-4}$ (see fig. 3.6).

In analogy with the special relativistic treatment for the PEM pulse, presented in section 3.3 (see also [116]), for the adiabatic expansion of the PEMB pulse in the constant-slab approximation described by the Rome codes the following hydrodynamical equations with $\bar{\rho}_B \neq 0$ has been found

$$\frac{\bar{n}_B^\circ}{\bar{n}_B} = \frac{V}{V_\circ} = \frac{\mathcal{V}\gamma}{\mathcal{V}_\circ \gamma_\circ}, \tag{3.64}$$

$$\frac{\bar{\epsilon}_\circ}{\bar{\epsilon}} = \left(\frac{V}{V_\circ}\right)^\Gamma = \left(\frac{\mathcal{V}}{\mathcal{V}_\circ}\right)^\Gamma \left(\frac{\gamma}{\gamma_\circ}\right)^\Gamma, \tag{3.65}$$

$$\gamma = \gamma_\circ \sqrt{\frac{(\Gamma\bar{\epsilon}_\circ + \bar{\rho}_B^\circ)\mathcal{V}_\circ}{(\Gamma\bar{\epsilon} + \bar{\rho}_B)\mathcal{V}}}, \tag{3.66}$$

$$\frac{\partial}{\partial t}(N_{e^\pm}) = -N_{e^\pm}\frac{1}{\mathcal{V}}\frac{\partial \mathcal{V}}{\partial t} + \overline{\sigma v}\frac{1}{\gamma^2}(N_{e^\pm}^2(T) - N_{e^\pm}^2). \tag{3.67}$$

where $N_{e^\pm}$ is the number density of pairs in laboratory frame. In these equations ($r > r_{\mathrm{out}}$) the comoving baryonic mass-density and number densities are $\bar{\rho}_B = M_B/V$ and $\bar{n}_B = N_B/V$, where V is the comoving volume of the PEMB pulse.

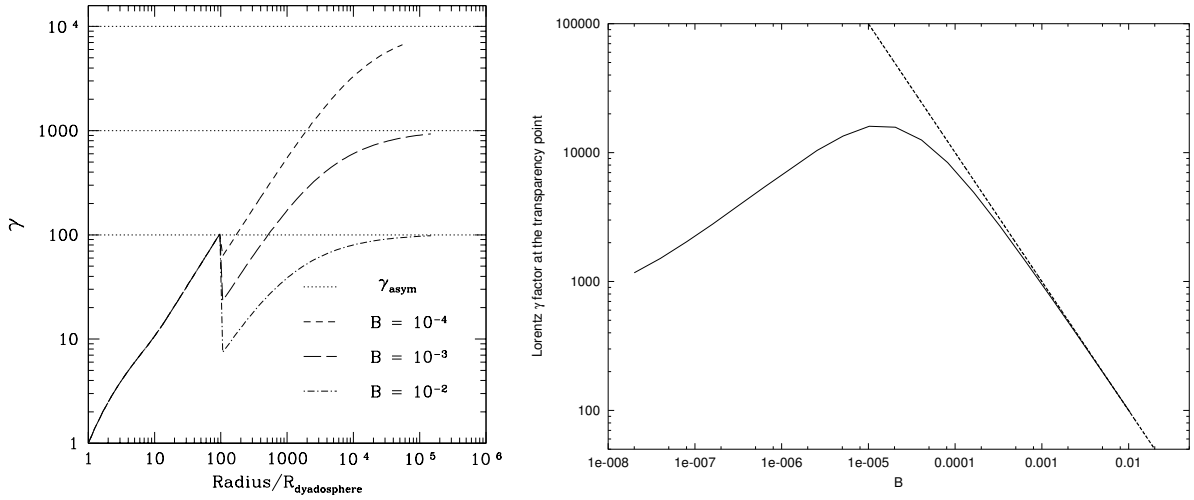

Figure 3.7: **Left)** *The γ factors are given as functions of the radius in units of the dyadosphere radius for selected values of B for the typical case $E_{dya} = 3.1 \times 10^{54}$ erg. The asymptotic values $\gamma_{\rm asym} = E_{\rm dya}/(M_B c^2) = 10^4, 10^3, 10^2$ are also plotted. The collision of the PEM pulse with the baryonic remnant occurs at $r/r_{ds} = 100$ where the jump occurs.* **Right)** *The γ factor (the solid line) at the transparency point is plotted as a function of the B parameter. The asymptotic value (the dashed line) $E_{\rm dya}/(M_B c^2)$ is also plotted.*

The result is shown in fig. 3.6 [117] where the bulk γ factor as computed from the Rome and Livermore codes are compared and very good agreement has been found. This validates the constant-thickness approximation in the case of the PEMB pulse as well. On this basis we easily estimate a variety of physical quantities for an entire range of B values.

For the same EMBH different cases have been considered [117]. The results of the integration show that for B in the parameter range the PEMB pulse propagates as a sharp pulse with constant thickness in the laboratory frame, but already for $B \simeq 1.3 \cdot 10^{-2}$ the expansion of the PEMB pulse becomes much more complex, turbolence phenomena can not be neglected any more and the constant-thickness approximation ceases to be valid. In fig. 3.7 Left we plot the γ factor of the PEMB pulse as a function of radial distance for different amounts of baryonic matter. The diagram extends to values of the radial coordinate at which the transparency condition given by Eq.(3.63) is reached.

It is also interesting to evaluate the final value of the γ factor of the PEMB pulse when the transparency condition given by Eq.(3.63) is reached as a function of B (see fig. 3.7 Right). For a given EMBH, by increasing B, the transparency occurs later, so that γ has increased further; then there is a *maximum* value of the γ factor at transparency, representing the beginning of a matter dominated regime. By further increasing the value of B the entire E_{dya} is transferred into the kinetic energy of the baryons (see also [117]). The "asymptotic" γ factor

$$\gamma_{\rm asym} \equiv \frac{E_{\rm dya}}{M_B c^2} \tag{3.68}$$

is also shown for each curve. The closer the γ value approaches the "asymptotic" value (3.68) at transparency, the smaller the intensity of the radiation emitted at transparency

and the larger the amount of kinetic energy left in the baryonic matter (see fig. 3.7 Right) to be emitted in the afterglow.

A part from the exact computation of transparency condition shown in the present section, a simple power law relation can be also found between the radius at which the PEMB pulse reaches transparency r_t and the B parameter. The transparency condition for uniform densities can be written as

$$(\bar{n}_{e^\pm} + \bar{Z}\bar{n}_B)\sigma_T\gamma\Delta \simeq \bar{Z}\bar{n}_B\sigma_T\gamma\Delta \simeq O(1) \tag{3.69}$$

where we assumed $\bar{n}_{e^\pm} \ll \bar{n}_B$ because e^+e^- pairs are completely annihilated at transparency point; here σ_T is Thomson cross-section and Δ is the thickness of PEMB pulse in laboratory frame. Using $\bar{n}_B = N_B/V$, where $V = 4\pi r_t^2\gamma\Delta$ is the volume of PEMB pulse in comoving frame, and the definition of B in Eq.(3.52), we find $r_t \simeq \sqrt{B}$. Similar behaviour has been found in [75].

3.6 Free parameters of EMBH model

Within the approximation presented in sect. 3.2 the EMBH is characterized by two parameters: μ and ξ. The energy of the dyadosphere is expressed in terms of these two parameters by Eq.(3.17).

There is an entire family of degenerate EMBH solutions with different values of μ and ξ corresponding to the same value of E_{dya} (see fig. 17 in [109]). These solutions are physically different with respect to the density of electron-positron pair distributions given by Eq.(3.15). An example of such a degeneracy is given in fig. 3.8, where in each figure the two different approximations for the energy density profile inside the dyadosphere are shown (see fig. 3.2). The total energy in the dyadosphere is the same in all cases ($E_{dya} = 3.1 \times 10^{54}$ erg). The three configurations correspond respectively to the three different pairs (μ, ξ): $(10, 0.76)$, $(10^2, 0.27)$, $(10^3, 0.10)$.

The corresponding dynamical evolution of the PEM pulse introduced in sect. 3.3 and [116] is clearly different in the three cases. When the collision with the remnant of the progenitor star is considered all these differences disappear. As usual (see sect. 3.4) we describe the baryonic content of the remnant by the parameter B. The transparency features of PEMB pulse generated after the collision with the baryonic matter depend uniquely on the two parameters E_{dya} and B. In fig. 3.9 the temperature in the laboratory frame is given for the PEM pulse and the PEMB pulse corresponding to the three configurations of fig.3.8 and $B = 4 \times 10^{-3}$. While for the PEM pulse era the three configurations are markedly different, they converge to a common behaviour in the PEMB pulse era.

If we turn now to the effect of the distance between the EMBH and the baryonic remnant, we see that this degeneracy is further extended: while the three PEM pulse eras are quite different, the PEMB pulse eras is largely insensitive to the location of the baryonic remnant (see fig. 3.10). We have plotted the three γ factors in the PEM pulse era as function of laboratory radius corresponding to the different configurations of fig. 3.8 and $B = 10^{-2}$; in the two cases the baryonic remnant is positioned at different distances from the EMBH. As shown in Eqs.(3.62, 3.63), if the PEM pulse has reached extreme relativistic regimes, the common value γ_{coll} to which the three γ factors drop in the collision with the baryonic matter

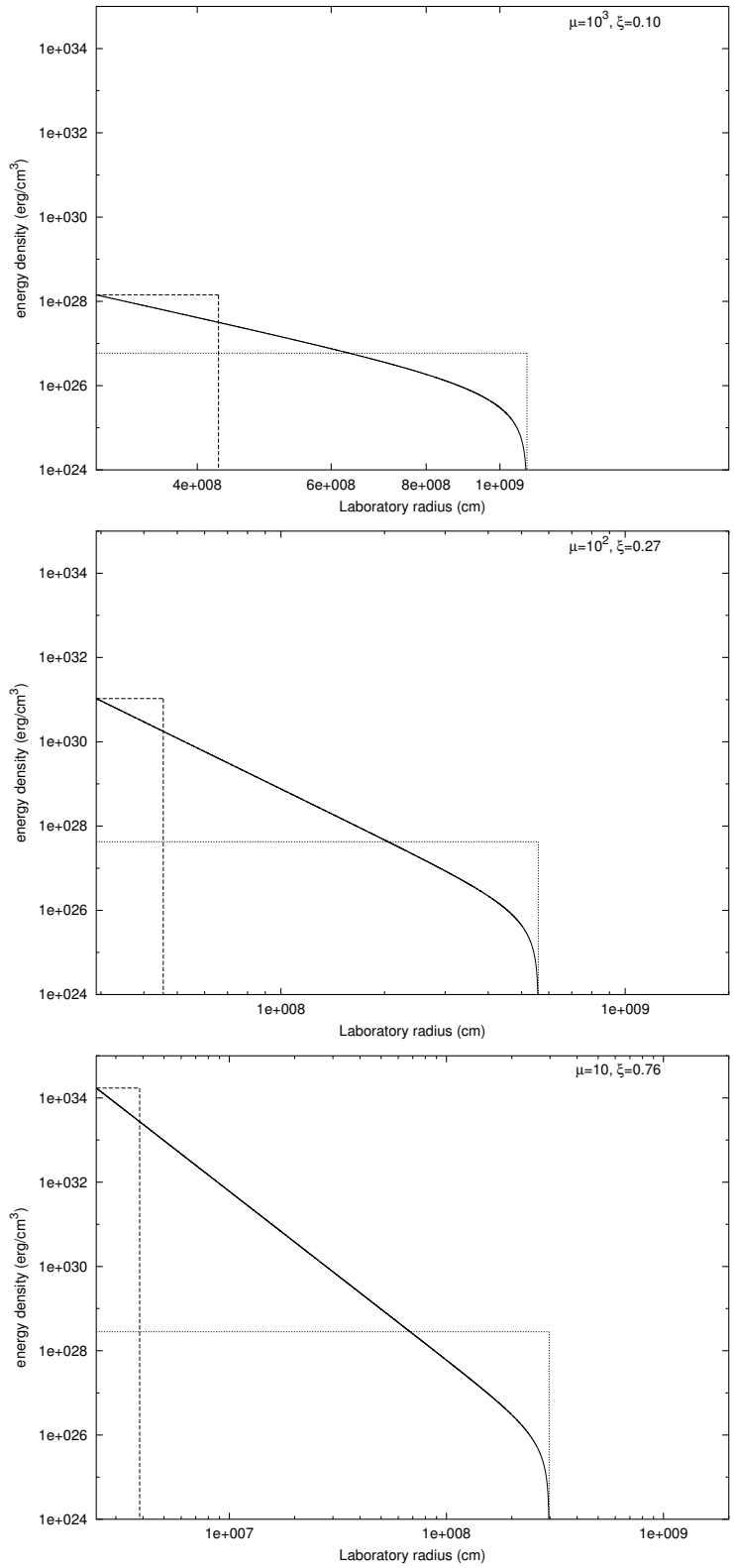

Figure 3.8: *Three different dyadospheres corresponding to the same value of energy ($E_{dya} = 3.1 \times 10^{54}$ erg) and to different values of the two parameters μ and ξ are given. The three different configurations are markedly different in their spatial extent as well as in their energy-density distribution (see text).*

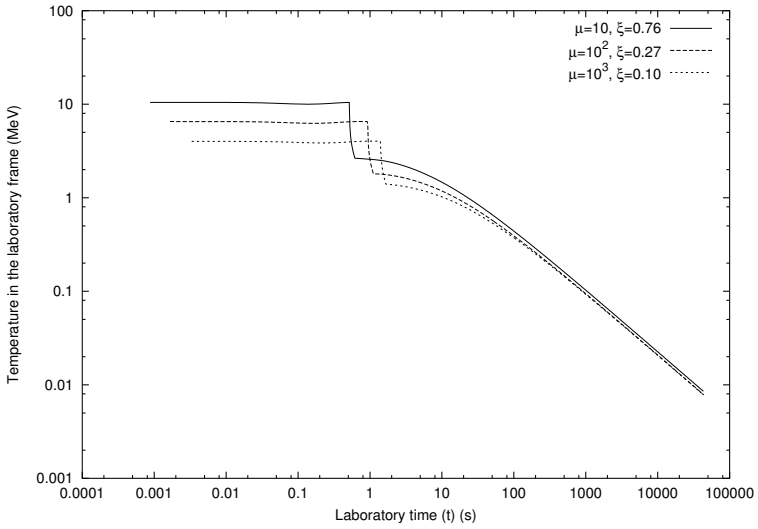

Figure 3.9: *The temperature of the plasma during the PEM pulse and PEMB pulse eras, measured in the laboratory frame, corresponding to the three (μ, ξ) pairs in fig. 3.8 is given as a function of the laboratory time. The three different curves converge to a common one in the PEMB pulse era, which is therefore only a function of the E_{dya} and B. In this case $E_{dya} = 3.1 \times 10^{54}$ erg and $B = 4 \times 10^{-3}$. The difference among the three curves in the early part of the PEMB pulse follows from having located the baryonic matter at a distance of $50(r_{\rm ds} - r_+)$, different in the three cases. Such difference becomes negligible at large distances in the later phases of the evolution of PEMB pulse.*

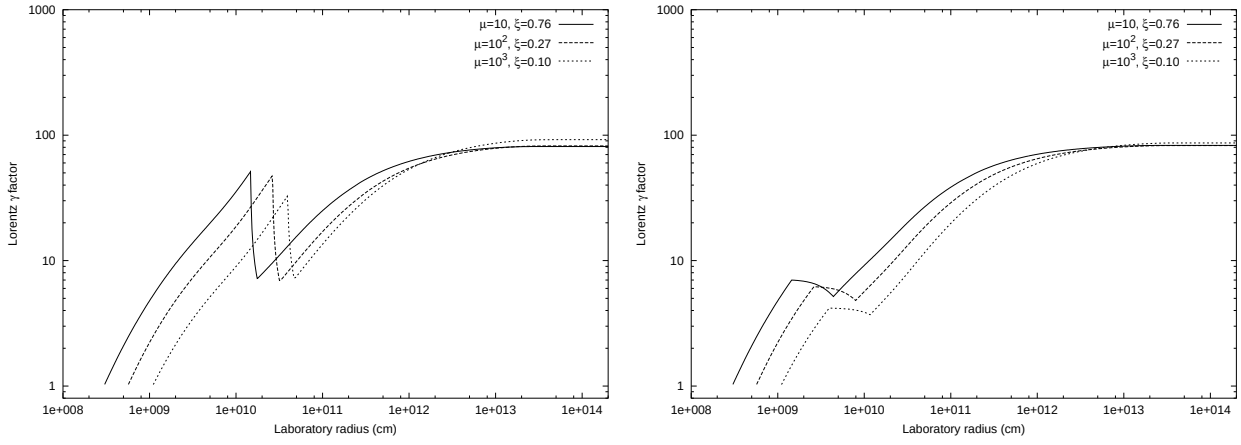

Figure 3.10: *The Lorentz γ factors for the three (μ, ξ) pairs considered in fig. 3.8 are given as a function of the radial coordinate in the laboratory frame. The two figures correspond to a baryonic remnant positioned respectively at $r_{in} = 50(r_{\rm ds} - r_+)$ (left) and at $r_{in} = 5(r_{\rm ds} - r_+)$ (right). Again the convergence to a common behaviour, uniquely a function of E_{dya} and B for the late stages of the PEMB pulse, is manifest.*

of the remnant depends only on B. As we will see in the next chapter all the information obtainable from GRBs with a large value of the parameter B will lead to the determination of the two parameters E_{dya} and B. The direct knowledge of the mass and charge of the EMBH can only be gained from the PEM pulse, i.e. from GRBs with very small values of B or "short bursts".

4 Afterglow era

After the transparency point is reached, all the photons contained in the PEMB pulse expanding in vacuum escape and the P-GRB is emitted. The remaining accelerated baryons (Accelerated Baryonic Matter pulse, or ABM pulse) collide inelastically with cold InterStellar Medium up to non relativistic region. The constitutive equations for the afterglow are written: the energy-momentum conservation equation at all orders, the relation between time at the source and time at the detector, the expression of observed luminosity taking into account the off-axis contribution; the best fit of the bolometric luminosity of the prototype GRB 991216 is presented, with the identification of the precursor as P-GRB and consequently the interpretation of the bimodal distribution of *BATSE*; finally a proposal of the GRB-Supernova connection. An overview of the standard scenario within the external shock model leading to the regime of power law of the Lorentz γ factor is given with a comparison with EMBH model.

4.1 Assumptions

The afterglow era is studied with the following assumptions:

1. the expansion of the ABM pulse through the ISM occurs keeping its width constant in the laboratory frame;
2. the expanding pulse has complete spherical symmetry;
3. the internal energy developed in the collision is emitted completely ("fully radiative" condition);
4. the temporal variability of light curve is related to ISM inhomogeneities.

In this chapter we limit ourselves to bolometric luminosity; the assumption on energy distribution of radiation will be introduced in the next chapter. The system is spherically symmetric; the declared breaking in the observed light curves is not explained as found in literature [128, 41] by a beamed emission but the assumption of thermal radiation gives a natural bending in the light curve for a spherically symmetric pulse. The slab approximation is extended by analogy with PEM and PEMB pulse phases [116, 117]; nevertheless we expect that in the non-relativistic regime the Lorentz contraction will not be so effective and the pulse width will be seen to enlarge in laboratory frame.

4.2 Era IV: ultrarelativistic regime in afterglow

We assume then that the interaction of ABM pulse with ISM can be represented by a sequence of inelastic collisions of the expanding ABM pulse with a large number of thin and cold ISM spherical shells at rest with respect to the central EMBH. Each of these swept up shells of thickness Δr has a mass $\Delta M_{\rm ism}$ and is assumed to be located between two radial distances r_1 and r_2 (where $r_2 - r_1 = \Delta r \ll r_1$) in the laboratory frame. These collisions create an internal energy $\Delta E_{\rm int}$ which is emitted completely.

We indicate by $\Delta\epsilon$ the increase in the proper internal energy density due to the collision with a single shell of ISM and by ρ_B the homogeneous proper energy density of the swept up baryonic matter. This includes the baryonic matter composing the remnant around the central EMBH, already swept up in the PEMB pulse phase, and the baryonic matter from the ISM swept up by the ABM pulse:

$$\rho_B = \frac{(M_B + M_{\rm ism})\, c^2}{V}. \tag{4.1}$$

Here V is the ABM pulse volume in the comoving frame, M_B is the mass of the baryonic remnant and $M_{\rm ism} = M_{\rm ism}(r)$ is the ISM mass swept up from the transparency point at radius $r_\circ$ up to the generic radius r in the laboratory frame:

$$M_{\rm ism}(r) = m_p n_{\rm ism} \frac{4\pi}{3} \left(r^3 - {r_\circ}^3\right) , \tag{4.2}$$

where m_p the proton mass and $n_{\rm ism}$ the number density of the ISM in the laboratory frame, not necessarily constant.

The energy conservation law in the laboratory frame at a generic step of the collision process is given by

$$\rho_{B_1} {\gamma_1}^2 \mathcal{V}_1 + \Delta M_{\rm ism} c^2 = \left(\rho_{B_1} \frac{V_1}{V_2} + \frac{\Delta M_{\rm ism} c^2}{V_2} + \Delta\epsilon\right) {\gamma_2}^2 \mathcal{V}_2, \tag{4.3}$$

where the quantities with the index "1" are calculated before the collision of the ABM pulse with an elementary shell of thickness Δr and the quantities with "2" after the collision, γ is the γ factor and $\mathcal{V}$ the volume of the ABM pulse in the laboratory frame so that $V = \gamma\mathcal{V}$.

The momentum conservation law in the laboratory frame is given by

$$\rho_{B_1} \gamma_1 U_{r_1} \mathcal{V}_1 = \left(\rho_{B_1} \frac{V_1}{V_2} + \frac{\Delta M_{\rm ism} c^2}{V_2} + \Delta\epsilon\right) \gamma_2 U_{r_2} \mathcal{V}_2, \tag{4.4}$$

where $U_r = \sqrt{\gamma^2 - 1}$ is the radial covariant component of the four-velocity vector (see [116, 117]).

We thus obtain

$$\Delta\epsilon = \rho_{B_1} \frac{\gamma_1 U_{r_1} \mathcal{V}_1}{\gamma_2 U_{r_2} \mathcal{V}_2} - \left(\rho_{B_1} \frac{V_1}{V_2} + \frac{\Delta M_{\rm ism} c^2}{V_2}\right), \tag{4.5}$$

$$\gamma_2 = \frac{a}{\sqrt{a^2 - 1}}, \quad a \equiv \frac{\gamma_1}{U_{r_1}} + \frac{\Delta M_{\rm ism} c^2}{\rho_{B_1} \gamma_1 U_{r_1} \mathcal{V}_1}. \tag{4.6}$$

We use $\Delta\varepsilon = \Delta E_{\rm int}/V_2$, because all the internal energy generated in previous collisions has been emitted (fully radiative condition). By substituting Eq.(4.6) in Eq.(4.5), we obtain:

$$\Delta E_{\rm int} = \rho_{B_1} V_1 \sqrt{1 + 2\gamma_1 \frac{\Delta M_{\rm ism} c^2}{\rho_{B_1} V_1} + \left(\frac{\Delta M_{\rm ism} c^2}{\rho_{B_1} V_1}\right)^2} - \rho_{B_1} V_1 \left(1 + \frac{\Delta M_{\rm ism} c^2}{\rho_{B_1} V_1}\right) , \tag{4.7}$$

$$\gamma_2 = \frac{\gamma_1 + \frac{\Delta M_{\rm ism} c^2}{\rho_{B_1} V_1}}{\sqrt{1 + 2\gamma_1 \frac{\Delta M_{\rm ism} c^2}{\rho_{B_1} V_1} + \left(\frac{\Delta M_{\rm ism} c^2}{\rho_{B_1} V_1}\right)^2}} . \tag{4.8}$$

These solutions in literature are often expressed at the first order approximation in the expansion parameter $\Delta M_{\rm ism} c^2/\rho_{B_1} V_1$. The Eqs.(4.1, 4.7, 4.8) make the actual set of dynamical equations we have integrated for the afterglow era in the EMBH model.

We examined under the above assumptions the effects of a possible departure from homogeneity in the interstellar medium, by introducing local step functions of the radial distance from the source built over a constant average density $\langle n_{ism}\rangle$; we did not consider any variable average density profiles as $\langle n_{ism}\rangle \sim r^{-2}$. Although these inhomogeneities are not relevant for the overall behaviour of the afterglow here treated, they are indeed relevant for the actual observed flux and its temporal structures [106]. These considerations are also affected by the angular spreading [107].

4.3 Approximations in the description of afterglow

In Eqs.(4.7, 4.8) we gave the finite expressions of internal energy developed in the collision of ABM pulse with ISM and of the Lorentz γ factor after collision. We proceed to a first approximation and expand Eqs.(4.7, 4.8) to first order in the quantity

$$\frac{\Delta M_{\rm ism} c^2}{\rho_{B_1} V_1} \ll 1 . \tag{4.9}$$

where we have used the fact that $\rho_{B_1} V_1 \equiv (M_B + M_{\rm ism})\, c^2$. We obtain the following expressions [117]:

$$dE_{\rm int} = (\gamma - 1)\, dM_{\rm ism} c^2 , \tag{4.10}$$

$$d\gamma = -\frac{\gamma^2 - 1}{M_B + M_{\rm ism}} dM_{\rm ism} . \tag{4.11}$$

where $dM_{\rm ism} = 4\pi r^2 m_p n_{\rm ism} dr = 4\pi r^2 m_p n_{\rm ism} v dt$, because $v = dr/dt$ and where the ISM number density $n_{\rm ism}$ is assumed for simplicity to be constant.

Eqs.(4.10, 4.11) are limiting cases of Taub's hydrodynamical equations [135, 68]. They have been very often referred in the GRB literature as the Blandford-McKee equations [11]. The behaviour of $\Delta M_{\rm ism} c^2/\rho_{B_1} V_1$ as a function of the radius when $M_{\rm ism} \ll M_B$ is:

$$\frac{\Delta M_{\rm ism} c^2}{\rho_{B_1} V_1} = \frac{\Delta M_{\rm ism} c^2}{(M_B + M_{\rm ism}) c^2} \sim \frac{r^2 \Delta r}{M_B} . \tag{4.12}$$

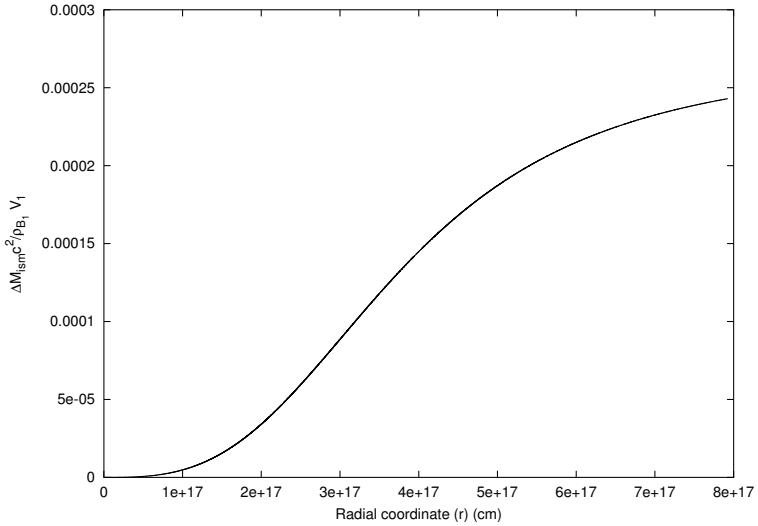

Figure 4.1: *The expansion term* $\frac{\Delta M_{\rm ism}c^2}{\rho_{B_1}V_1}$ *is represented as a function of the radial coordinate. It is manifestly an increasing function.*

The condition $M_{\rm ism} \ll M_B$ holds, e.g. in our fit for GRB 991216, during the entire evolution of the system and so Eq.(4.9) is valid (see fig. 4.1). The increase of $\Delta M_{\rm ism}c^2/\rho_{B_1}V_1$ becomes less rapid at late time of the evolution (fig. 4.1) because at late time $M_{\rm ism}$ begins to be comparable with M_B, for the choosen value of $n_{ism} \simeq 1$ particle/cm^3 making the denominator increase.

Eqs.(4.10, 4.11) can be simply solved analytically (see e.g. [11]). We then have:

$$\gamma = \frac{(M_B + M_{\rm ism})^2 + C}{(M_B + M_{\rm ism})^2 - C}, \tag{4.13}$$

where

$$C = {M_B}^2 \frac{\gamma_\circ - 1}{\gamma_\circ + 1}, \tag{4.14}$$

where we recall that $r_\circ$ and $\gamma_\circ$ are the radial coordinate and the γ factor at the transparency point and M_B is the initial baryonic mass of the ABM pulse.

Eq.(4.13) is a differential equation for $r\,(t)$, namely

$$1 - \left(\frac{dr}{cdt}\right)^2 = \left[\frac{(M_B + M_{\rm ism})^2 + C}{(M_B + M_{\rm ism})^2 - C}\right]^{-2}, \tag{4.15}$$

which can be integrated analytically with solution (see e.g. [1])

$$2c\sqrt{C}\,(t - t_\circ) = (M_B - m_i^\circ)\,(r - r_\circ) + \frac{1}{4}m_i^\circ r_\circ \left[\left(\frac{r}{r_\circ}\right)^4 - 1\right] \tag{4.16}$$

$$+\frac{Cr_\circ}{6m_i^\circ B^2}\ln\left[\frac{\left(B + \frac{r}{r_\circ}\right)^3}{B^3 + \left(\frac{r}{r_\circ}\right)^3}\frac{B^3+1}{(B+1)^3}\right] + \frac{Cr_\circ}{3m_i^\circ B^2}\left[\sqrt{3}\arctan\frac{2\frac{r}{r_\circ} - B}{B\sqrt{3}} - \sqrt{3}\arctan\frac{2-B}{B\sqrt{3}}\right]$$

where $m_i^\circ = \frac{4}{3}\pi m_p n_{\rm ism} r_\circ^3$, $B = \left(\frac{M_B - m_i^\circ}{m_i^\circ}\right)^{1/3}$ and we recall that $t_\circ$ is the laboratory time at the transparency point.

4.4 The era V: the non-relativistic slowing down

In our special relativistic equations, the expansion of the pulse is described by the very high and rapidly varying Lorentz γ. The non relativistic phase can be obtained from Eqs.(4.1, 4.3, 4.4), simply by introducing the limit $c \to \infty$. In this limit the radial velocity and not the γ is the quantity describing effectively the expansion.

4.5 Arrival time at the detector

Up to this point we presented the set of dynamical equation for description of the first three eras and of the afterglow era. In order to test our model we need now to compute the luminosity emitted by the pulse and the relation between the time in which in laboratory frame photons are emitted by pulse and the time in which those photons are detected by an observer at infinity. Actually, since the motion of the pulse is highly-relativistic ($\gamma \simeq 200 - 300$), the spherical waves emitted by external surfaces of pulse are highly distorted with respect to the observer at infinity. We will now consider this effect.

Let us indicate by t_a the arrival time of a photon emitted at a laboratory time t by the spherical surface of the relativistically expanding shell. The time t_a is measured by an observer very far from the spherical pulse but not at cosmological distance from it. Photons arriving at the same time t_a will be emitted at different t as a function of the angle ϑ, where ϑ is the angle in laboratory frame between the radial emission velocity of the photon and the line of sight; the angle ϑ satisfies the relation $(v/c) \leq \cos\vartheta \leq 1$ so that $\cos(\vartheta_{max}) = (v/c)$, where $v = v(t)$ is the expansion speed of the ABM pulse at time t. The relation between t and t_a in the case of a constant $\gamma \sim 5$ for expanding radio sources was found by Rees [98]:

$$t_a = t\left(1 - \frac{v}{c}\cos\vartheta\right) . \tag{4.17}$$

For a constant expansion speed, the radius $r(t)$ of the source is given by:

$$r(t) = vt . \tag{4.18}$$

In our case the ABM pulse Lorentz γ factor is not constant (see fig. 4.2), and so we must generalize Eqs.(4.17) to variable expansion velocity. We set $t = 0$ when the plasma starts to expand, so that $r(0) = r_{\rm ds}$, i.e. the dyadosphere radius. Let a photon be emitted at time t from the point P of the visible area of the ABM pulse. Its distance from the observer is L. The time it takes to arrive at the detector is $\frac{L}{c}$. Thus its arrival time, measured from the arrival of the first photon a time $\frac{R_0}{c}$ after its emission at $t = 0$, is:

$$t_{\rm a} = t + \frac{L}{c} - \frac{R_0}{c} , \tag{4.19}$$

where we have defined $t_{\rm a} = 0$ when a photon emitted at $t = 0$ and $\vartheta = 0$ reaches the observer after travelling the distance R_0. The distance L is clearly given by:

$$L = \sqrt{R_{\rm T}^2 + r(t)^2 - 2\,R_{\rm T}\,r(t)\cos\vartheta} , \tag{4.20}$$

where at any given value of laboratory time t, $\cos\vartheta$ can assume any value between $\left(\frac{v(t)}{c}\right)$ and 1 as noted above. Now $r\,(t)$ is less than one light year in order of magnitude while $R_{\rm T}$ corresponds to a redshift $z \sim 1$. Thus we can expand the right hand side of equation (4.20) in powers of $\frac{r(t)}{R_{\rm T}}$ to first order:

$$L \simeq R_{\rm T}\left(1 - \frac{r\,(t)}{R_{\rm T}}\,\cos\vartheta\right), \tag{4.21}$$

which corresponds to assuming L to be equal to its projection on the line of sight. Substituting (4.21) into (4.19) yields:

$$t_{\rm a} = t + \frac{r_{\rm ds}}{c} - \frac{r\,(t)}{c}\cos\vartheta\,, \tag{4.22}$$

where we have used the fact that $R_{\rm T} = R_0 + r_{\rm ds}$. For $r\,(t)$ we can use the following expression:

$$r\,(t) = \int_0^t v\,(t')\,dt' + r_{\rm ds}, \tag{4.23}$$

so that equation (4.22) can be written in the form:

$$t_{\rm a} = t - \frac{\int_0^t v\,(t')\,dt' + r_{\rm ds}}{c}\cos\vartheta + \frac{r_{\rm ds}}{c}, \tag{4.24}$$

which reduces to Eq.(4.17) only if v is constant and $r_{\rm ds}$ is negligible with respect to $r\,(t)$.

We need now to correct Eq.(4.24) for the cosmological expansion effects to get the wanted relation between t and t_a^d. We recall that

$$t_a^d = (1+z)\,t_a\,, \tag{4.25}$$

where z is the cosmological redshift. Our final relation is therefore:

$$t_a^d = (1+z)\left(t - \frac{\int_0^t v\,(t')\,dt' + r_{\rm ds}}{c}\cos\vartheta + \frac{r_{\rm ds}}{c}\right). \tag{4.26}$$

A relation very often used for arrival time of GRB signal is derived from Eq.(4.17): in radial approximation ($\vartheta = 0$), by considering $v \sim const$, in the limit $v/c \sim 1$, one can find $t_a \simeq t/2\gamma^2$. However, as can be seen in fig. 4.2, the assumption of a constant velocity can not be verified during the whole evolution.

4.6 The emitted luminosity

We now write the expression for the luminosity emitted by considering the contributions of the off-axis emission to the afterglow.

Following Eqs.(4.7–4.8), we recall that in the comoving frame of the expanding ABM pulse we suppose that the internal energy due to collision is instantaneously radiated away and that the corresponding emission is isotropic. If $\Delta\varepsilon$ is the internal energy density developed

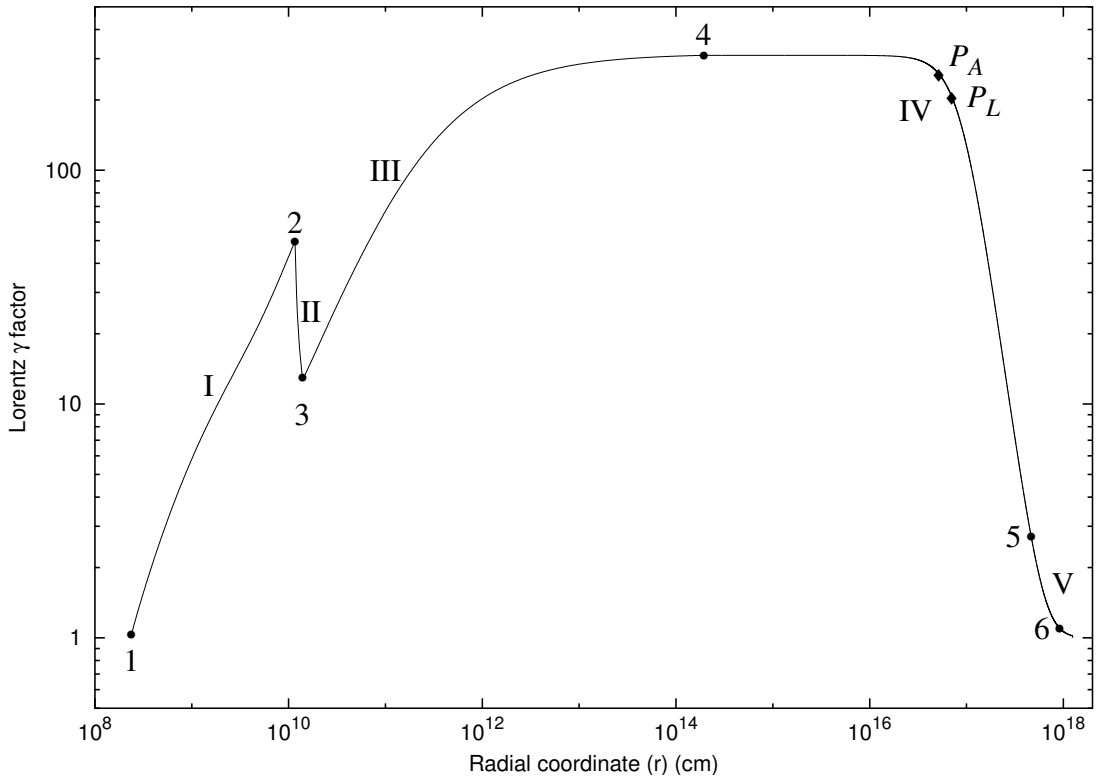

Figure 4.2: *The theoretically computed γ factor for the parameter values $E_{dya} = 4.83 \times 10^{53}$ erg, $B = 3 \times 10^{-3}$ is given as a function of the radial coordinate in the laboratory frame. The corresponding values in the comoving time, laboratory time and arrival time are given in Tab .1 in [109]. The different eras indicated by roman numerals are illustrated in the text (see sects. 3.3,3.4,3.5,4.2,4.4), while the points 1,2,3,4,5 mark the beginning and end of each of these eras. The points P_L and P_A mark the maximum of the afterglow flux, respectively in laboratory time and in arrival time (see [104] and sects. 4.5,4.6). The point 6 is the beginning of Phase D in Era V (see sects. 4.4,4.3). At point 4 the transparency condition is reached and the P-GRB is emitted. This diagram shows the inadequacy of considering the simple power-law behaviour $\gamma \propto r^{-3}$ for the relation between the radius of the source and its Lorentz γ factor as assumed in the large majority of current papers on GRBs (see e.g. [124, 145, 125, 127, 85, 89] and references therein). Actually, such a power-law behaviour with the predicted index can never be realized (see sect. 4.11).*

in the collision, in the comoving frame the energy per unit of volume and per solid angle is simply

$$\left(\frac{dE}{dV d\Omega}\right)_\circ = \frac{\Delta\varepsilon}{4\pi} \tag{4.27}$$

due to the fact that the emission is isotropic in this frame. The total number of photons emitted is an invariant quantity independent of the frame used. Thus we can compute this quantity as seen by an observer in the comoving frame (which we denote with the subscript "$\circ$") and by an observer in the laboratory frame (which we denote with no subscripts). Doing this we find

$$\frac{dN_\gamma}{dt d\Omega d\Sigma} = \left(\frac{dN_\gamma}{dt d\Omega d\Sigma}\right)_\circ \Lambda^{-3}\cos\vartheta\,, \tag{4.28}$$

where $\cos\vartheta$ comes from the projection of the elementary surface of the shell on the direction of propagation and $\Lambda = \gamma(1-\beta\cos\vartheta)$ is the Doppler factor introduced in the two following differential transformation

$$d\Omega_\circ = d\Omega \times \Lambda^{-2} \tag{4.29}$$

for the solid angle transformation and

$$dt_\circ = dt \times \Lambda^{-1} \tag{4.30}$$

for the time transformation. The surface $d\Sigma$ involved is the visible area of the ABM pulse at laboratory time t, namely with $0 \le \vartheta \le \vartheta_{max}$ (see section 4.5). An extra Λ factor comes from the energy transformation:

$$E_\circ = E \times \Lambda\,. \tag{4.31}$$

Thus finally we obtain (see also [20]):

$$\frac{dE}{dt d\Omega d\Sigma} = \left(\frac{dE}{dt d\Omega d\Sigma}\right)_\circ \Lambda^{-4}\cos\vartheta\,. \tag{4.32}$$

Doing this we identify $\left(\frac{dE}{dt d\Omega d\Sigma}\right)_\circ$ as the energy density in comoving frame up to a factor $\frac{v}{4\pi}$ (see Eq.(4.27)). Then we have:

$$\frac{dE}{dt d\Omega} = \frac{\Delta\varepsilon}{4\pi}\; v\;\cos\vartheta\;\Lambda^{-4}\;d\Sigma\,, \tag{4.33}$$

where the integration in $d\Sigma$ is performed over the ABM pulse visible area at laboratory time t, namely with $0 \le \vartheta \le \vartheta_{max}$ and ϑ_{max} defined in sect. 4.5.

Eq.(4.33) gives us the energy emitted toward the observer per unit solid angle and per unit laboratory time t in the laboratory frame. But what we really need is the energy emitted per unit solid angle and per unit detector arrival time t_a^d, so we must use the Eq.(4.26). First we have to multiply the integrand in Eq.(4.33) by the factor $\left(dt/dt_a^d\right)$ to transform the energy density generated per unit of laboratory time t into the energy density generated per unit arrival time t_a^d. Then we have to integrate with respect to $d\Sigma$ over the *equitemporal surface* (EQTS, see section 4.5) of constant arrival time t_a^d instead of the ABM pulse visible area at laboratory time t. This gives for the source luminosity in detector arrival time then:

$$\frac{dE_\gamma}{dt_a^d d\Omega} = \int_{EQTS} \frac{\Delta\varepsilon}{4\pi}\; v\;\cos\vartheta\;\Lambda^{-4}\;\frac{dt}{dt_a^d} d\Sigma\,. \tag{4.34}$$

4.7 The EMBH best fit of the GRB 991216

We use the GRB 991216 as a prototype. The data of GRB 991216 are reproduced in fig. 4.3: the data on the prompt emission as recorded by [7] and the data on the afterglow from the RXTE satellite [23] and the Chandra satellite [93] (see also [58]).

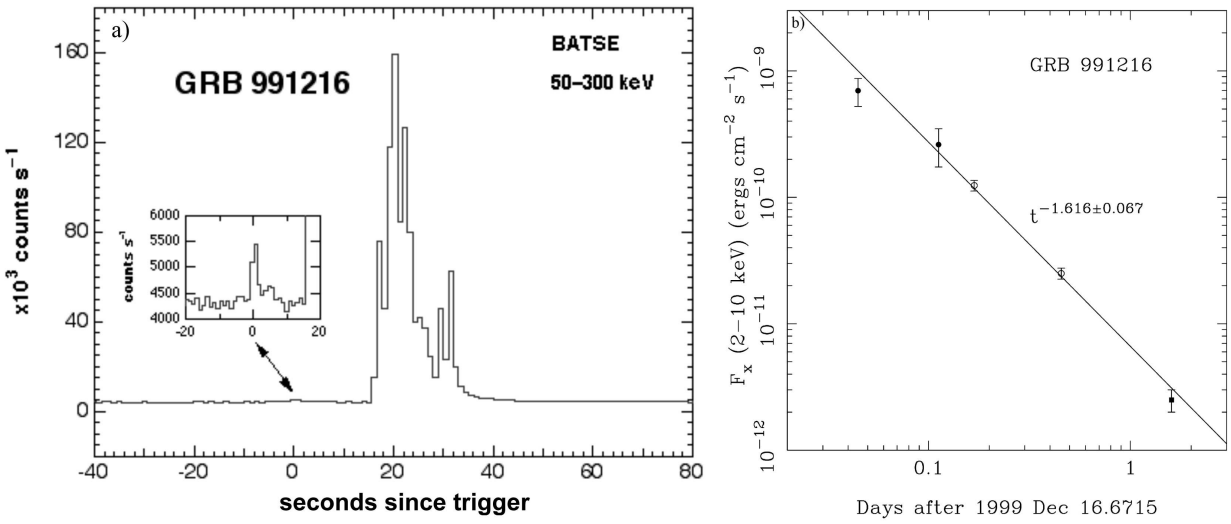

Figure 4.3: **a)** *The data on the GRB 991216 obtained by BATSE (reproduced from BATSE 1999) and* **b)** *the corresponding data for the afterglow from both RXTE and Chandra (the last point after* 10^5 *s) are given as a function of the detector arrival time (reproduced from [58]).*

The data fitting procedure relies on three basic assumptions adopted for the sake of simplicity:

1. In the light curve peak region, the source luminosity is mainly in the energy band 50–300 keV, so we consider the flux observed by *BATSE* a good approximation of the total flux.

2. In the decaying part of the afterglow, we assume that during the R-XTE and Chandra observations the source luminosity is mainly in the energy band 2–10 KeV, so we can again assume that the flux observed by these satellites is a good approximation of the total flux.

3. We have neglected in this case the lower energy contribution. In fact, even in the latest afterglow phases up to where the X-ray data are available, the optical and radio luminosities give a small contribution.

Let us apply the EMBH model by using the following parameters characterizing the afterglow: the energy of the dyadosphere, E_{dya}, the baryonic matter in the remnant of the progenitor star, parametrized by B and the average number density of ISM $\langle n_{ism} \rangle$. The location of the remnant has been assumed $\sim 10^{10}$ cm. As discussed in [103] and sect. 3.6, the PEMB pulse evolution becomes in time rather insensitive to the actual density and location of the baryonic component but they are very sensitive to the value of B [117].

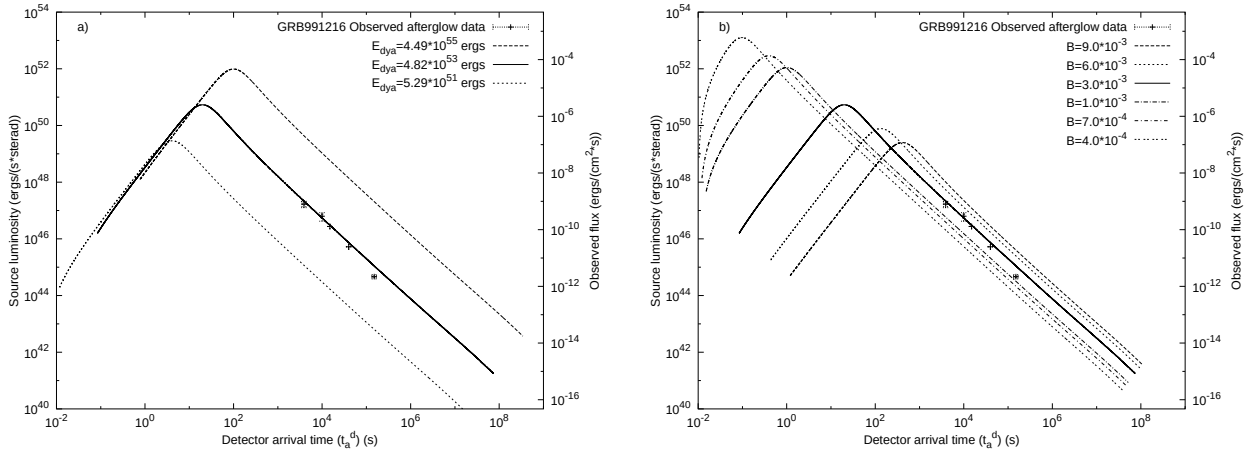

Figure 4.4: *a) Afterglow luminosity computed with fixed* $B = 3 \times 10^{-3}$ *for an EMBH of corresponding* $E_{dya} = 5.29 \times 10^{51}$ *erg,* $E_{dya} = 4.83 \times 10^{53}$ *erg,* $E_{dya} = 4.49 \times 10^{55}$ *erg. b) Afterglow luminosity computed with fixed* $E_{dya} = 4.83 \times 10^{53}$*, corresponding to* $B = 9 \times 10^{-3}$, 6×10^{-3}, 3×10^{-3}, 1×10^{-3}, 7×10^{-4}, 4×10^{-4}.

In fig. 4.4 we present the actual first results of fitting our EMBH model to the data from the R-XTE and Chandra satellites, corresponding to selected values of E_{dya} and B. For simplicity the light curve in radial approximation is shown in figs. 4.4, 4.5, 4.6; the features to be evidenced remain if we take into account the off-axis contribution. As shown in fig. 4.4 (a) the higher is the total energy E_{dya} at fixed B the later the transparency is reached, since a higher energy of the source is converted in larger number of e^+e^- pairs responsible of the opacity of the pulse. At fixed E_{dya} (fig. 4.4 (b)) by increasing the baryonic remnant, the transparency is delayed because more ionization electrons increase the opacity. Three distinct features are evident in the luminosity as a function of the arrival time at the detector for a homogeneous ISM: an initial rising part in the afterglow luminosity which reaches a peak followed by a monotonically decreasing part.

We have then proceeded to fine tune the two parameters in fig. 4.5. The main conclusions from our model are the following:

1) The slope of the bolometric afterglow in the region where the experimental data are present is $n \simeq -1.6$, in agreement with the observational data [58]. The index n in this region is rather insensitive to the values of the parameters E_{dya} and B (see fig. 4.4). The physical reason for this universality of the slope is in a variety of factors including the ultrarelativistic energy of the baryons in the ABM pulse, the assumption of constant average density in the ISM, the "fully radiative" conditions leading predominantly to X-ray emission.

2) The afterglow fit does not depend directly on the parameters μ, ξ but only through their combination E_{dya}. Thus there is a 1-parameter family of values of the pair (μ, ξ) allowed by a given viable value of E_{dya} (see fig. 17 in [109] and sect. 3.6).

3) By fine tuning the parameters of the best fit of the luminosity profile and time evolution of the afterglow the following parameters have been found: $E_{dya} = 4.83 \times 10^{53}$erg, $B = 3 \times 10^{-3}$ and $n_{ism} = 1 particle/cm^3$.

After fixing the free parameters of the EMBH model, modulo the mass-charge relationship which fixes E_{dya}, we can derive the complete space-time evolution of the pulse for GRB 991216 (see Table 1 in [109]) as well as the dependence of the γ factor as a function of

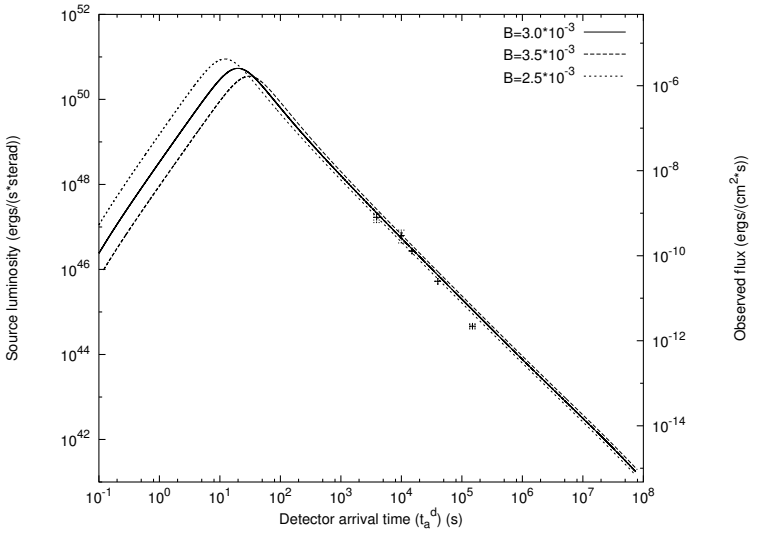

Figure 4.5: *Fine tuning of the best fit of the afterglow data of Chandra, RXTE as well as of the range of variability of the BATSE data on the prompt emission by a unique afterglow curve leading to the parameter values* $E_{dya} = 4.83 \times 10^{53} erg, B = 3 \times 10^{-3}$ *and* $n_{ism} = 1 particle/cm^3$.

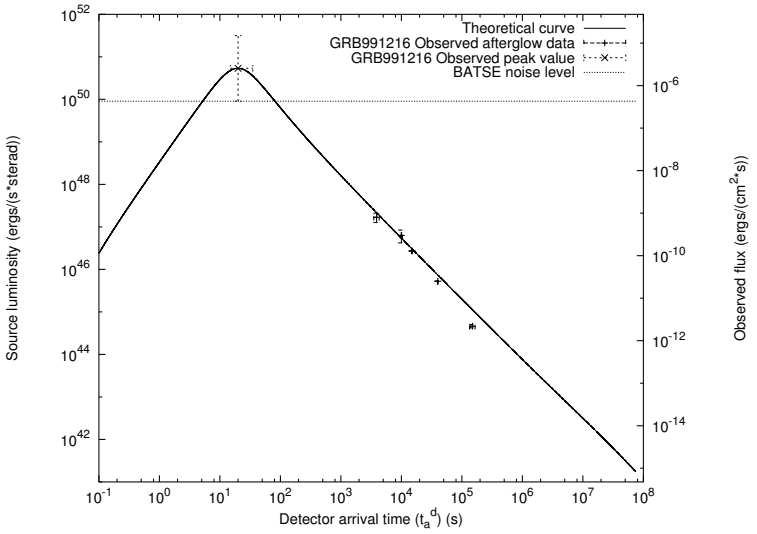

Figure 4.6: *Best bolometric fit of the afterglow data of Chandra, RXTE as well as of the range of variability of the BATSE data on the prompt emission, by a unique afterglow curve leading to the parameter values* $E_{dya} = 4.83 \times 10^{53} erg, B = 3 \times 10^{-3}$ *and* $\langle n_{ism} \rangle = 1 particle/cm^3$. *The horizontal dotted line indicates the BATSE noise threshold at time of detection. On the left axis the luminosity is given in units of the energy emitted at the source, while the right axis gives the flux as received by the detectors.*

the radial coordinate (see fig. 4.2).

4.8 Proper Gamma-Ray Burst (P-GRB)

4.8.1 Identification of the signal

Having determined the first two free parameters of the EMBH model, the bolometric luminosity is determined at all times. The average luminosity of the prompt emission observed by *BATSE* and of the afterglow emission observed by RXTE and Chandra can be fit already quite well by EMBH theoretical afterglow curve (see fig. 4.6). This led us to the identification of the long bursts observed by *BATSE* with the peak of afterglow light curve so-called Extended Afterglow Peak Emission (E-APE). The peak of this E-APE occurs at $\sim 19.87\,s$ and its intensity and time scale agree very well with the *BATSE* observations. This E-APE is not a burst, but is seen as such by *BATSE* due to its high noise threshold. This provides a natural explanation of the outstanding problem of explaining the long GRBs (see e.g. [148, 123, 90]) which are nothing but the peak of afterglow emission.

The most interesting question to be asked is: where does one find the burst which is emitted when the condition of transparency against Thomson scattering is reached? We have referred to this as the proper gamma ray burst (P-GRB) in order to distinguish it from the global GRB phenomena [103]. The answer can be found by looking at two diagrams (see fig. 4.7 and fig. 4.8). In fig. 4.7 it is shown that for a fixed value of E_{dya} the value of B uniquely determines the energy $E_{P\text{-}GRB}$ of the P-GRB and the kinetic energy $E_{Baryons}$ of the ABM pulse at transparency point which gives origin to the afterglow (see fig. 4.7). The partition of total energy budget E_{dya} is simply

$$E_{dya} = E_{P\text{-}GRB} + E_{Baryons} \tag{4.35}$$

with $E_{P\text{-}GRB}/E_{Baryons} = 1.58 \times 10^{-2}$.

The theoretical simulation fixes the coordinate of the transparency point (see Tab .1 in [109]); the prediction of the energy emitted at transparency and of the time of arrival of the average luminosity lead to the identification of the P-GRB with the just above threshold signal in the *BATSE* data preceeding the prompt emission by 20sec and apparently uncorrelated with the prompt (see fig. 4.3 **a**). We have estimated from the *BATSE* data the ratio of the P-GRB to the E-APE over the noise threshold to be $\sim 10^{-2}$, in agreement with our result. A more general and qualitative picture of time delay between P-GRB and E-APE as a function of B for different values of E_{dya} is shown in fig. 4.8.

This leads to a natural explanation of the temporal structure of GRBs: the P-GRBs coincide with the class of short events (< 2 s) discovered in the bimodal distribution of GRBs in the *BATSE* catalog [65], while the E-APEs coincide with the class of longer events (> 2 s). Therefore the absence of afterglow observations in some GRBs should be due to the fact that the amount of baryonic material in the remnant parametrized by B is so small that the afterglow signal is well below the noise level of the instrumental devices. Viceversa for long bursts the amount of baryonic matter is so dominant that almost all internal energy of

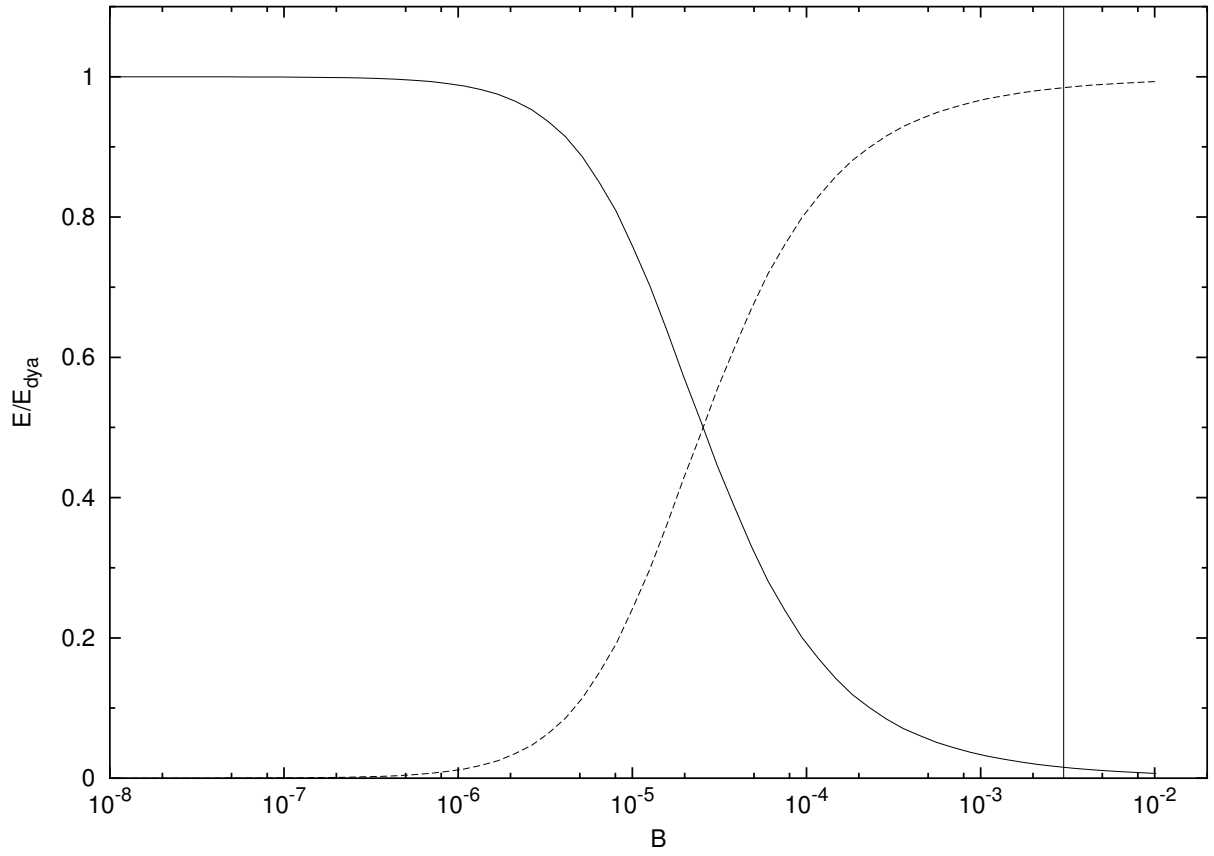

Figure 4.7: *Prediction in the EMBH model of the relative energies, in units of* $E_{dya} = 4.83 \times 10^{53}$ *erg, of P-GRB (solid line) and of afterglow (dashed line), computed as kinetic energy of baryons at transparency point. The vertical line corresponds to the value* $B = 3 \times 10^{-3}$ *of best fit of GRB 991216.*

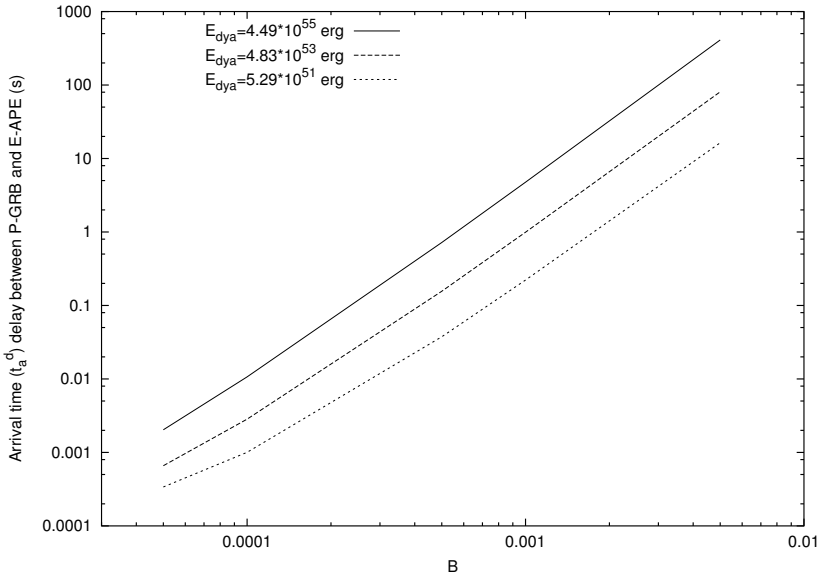

Figure 4.8: *The arrival time delay between the P-GRB and the peak of the afterglow is plotted as a function of the B parameter for three selected values of* E_{dya}.

the pulse is converted in kinetic energy of baryons. Therefore short bursts must derive from very efficiently collapsed objects, at variance from long bursts. The time scale of P-GRB is given by $\mathcal{D}/c \sim 1$ sec, coincident with the maximum duration of short bursts; here $\mathcal{D}$ is the thickness of the pulse in laboratory frame. This is the reason of the discrete distinction between short and long events in our model, in spite of a continuous B parameter. Here the predictive power of this model emerges.

This interpretation of the temporal structure of GRB will be tested by *Swift* mission, whose launch is scheduled for late 2004. The *Swift* rapid response (roughly 1 minute) will allow observations at times in which the emissions are brighter than the few hours response capabilities of current instruments.

4.8.2 Hardness of the P-GRB

Regarding the P-GRB spectrum, the initial energy of the electron-positron pairs and photons in the dyadosphere for given values of the parameters can be easily computed following the work of [96]. We obtain respectively $T = 1.95$ MeV and $T = 29.4$ MeV in the two approximations we have used for the average energy density of the dyadosphere (see section 3.6 and fig. 3.2). It is then possible to follow in the laboratory frame the time evolution of the temperature of the electron-positron pairs and photons through the different eras until transparency point, see fig. 4.9. The abrupt decrease of temperature in laboratory frame, corresponding to an increase of temperature in comoving frame, is due to the collision with remnant. In our single slab, if $B = 0$, we have $T_{obs} \sim const$ (see sect. 3.3.3). The condition of transparency is reached at temperatures in the range of $\sim 15 - 55$ keV at the detector, in agreement with the *BATSE* results. We emphasize that in the limit of B going to 10^{-8} in which the P-GRB coincides with the "short bursts" the spectrum of the P-GRB becomes

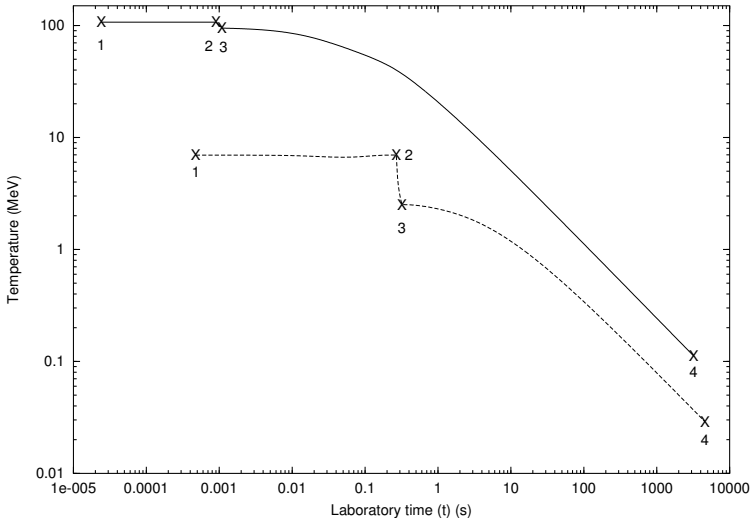

Figure 4.9: *The temperature of the pulse in the laboratory frame for the first three eras is given as a function of the laboratory time. The numbers 1, 2, 3, 4 represent the beginning and end of each era. The two curves refer to two extreme approximations adopted in the description of the dyadosphere (see section 3.6).*

harder in agreement with the observational data (see fig. 6 in [109] and [81, 5, 30, 46]).

In order to compare the EMBH theoretical results with the temporal details and spectral features of observational data on the P-GRB, inhomogeneous distributions instead of average values of number density of e^+e^- pairs, Lorentz γ factor and temperature have been introduced, obtaining the observed soft-hard spectral evolution (see Chapter 6 and [122]).

4.9 The E-APE temporal substructures taking into account off-axis emission

We now consider the problem of the relation between ISM inhomogeneity and the temporal substructures in the E-APE. We have created an ISM inhomogeneity "mask" (see fig. 4.10) with the main criteria that the density inhomogeneities and their spatial distribution fulfill $< n_{ism} >= 3\,\text{particle/cm}^3$.

The results are given in fig. 4.11 and fig. 4.12. We obtain, in agreement with the observations:

1. the theoretically computed intensity of the A, B, C peaks as a function of the ISM inhomogneities;
2. the fast rise and exponential decay shape for each peak;
3. a continuous and smooth emission between the peaks.

The points A, B, C are well fit in intensity and arrival time by the spikes of our density mask. In the case of D, the agreement with the arrival time is reached, but we do not

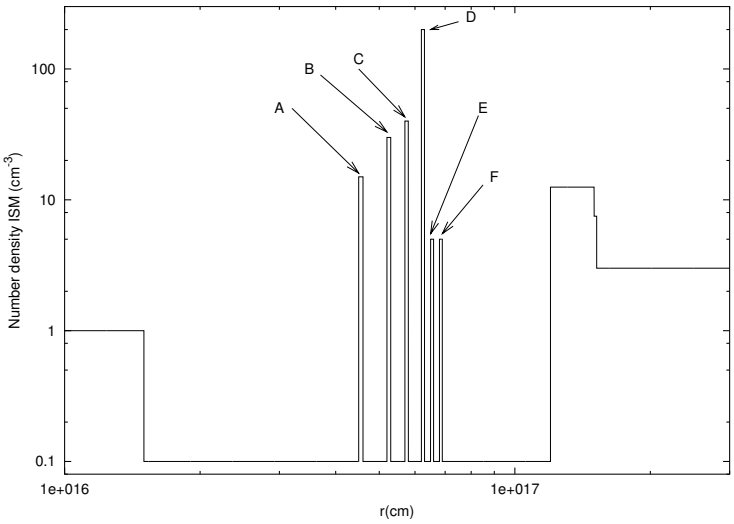

Figure 4.10: *The density profile ("mask") of ISM used to reproduce the temporal sub-structure of the peak of GRB 991216. As before, the radial coordinate is measured from the EMBH. In this cloud we have six "spikes" with overdensity separated by low density regions. Each spike has the same spatial extension of* $10^{15}\,\mathrm{cm}$*. The cloud average density is* $< n_{ism} >= 3\,\mathrm{particle/cm^3}$.

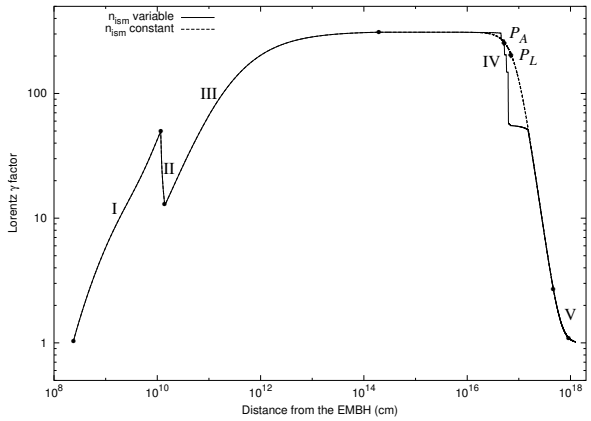

Figure 4.11: *The theoretically computed* γ *factors for the parameter values* $E_{dya} = 4.83 \times 10^{53}$ *erg,* $B = 3 \times 10^{-3}$ *are given as a function of the radial coordinate in the laboratory frame with cloud average density constant* $< n_{ism} >= 3\,\mathrm{particle/cm^3}$ *and with density mask in fig. 4.10 having the same average value (see also fig. 4.2). The different eras indicated by roman numerals are illustrated in the text (see sections 3.3,3.4,3.5,4.2,4.4). The points* P_L *and* P_A *mark the maximum of the afterglow flux, respectively in laboratory time and in arrival time (see [104] and sects. 4.5,4.6).*

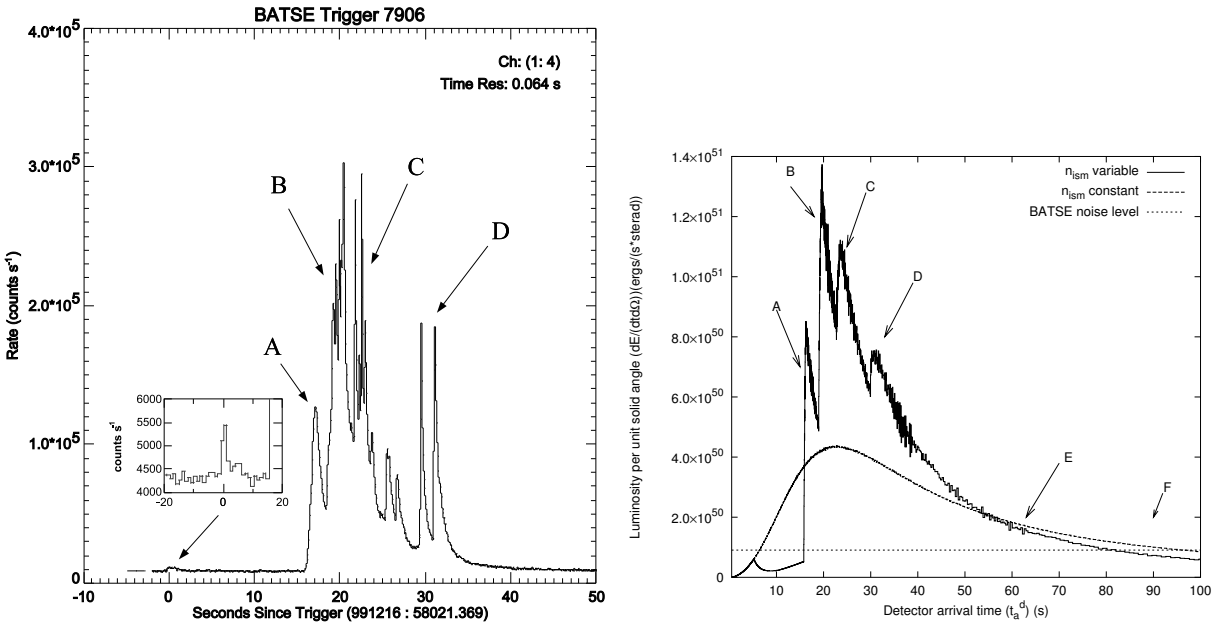

Figure 4.12: **Left)** *The BATSE data on the E-APE of GRB 991216 (source: [6]) together with an enlargement of the P-GRB data (source: [7]). For convenience each E-APE peak has been labeled by a different uppercase Latin letter.* **Right)** *The source luminosity corresponding to the mask in fig. 4.10 is given as a function of the detector arrival time (solid "spiky" line) with the corresponding curve for the case of constant* $\langle n_{ism} \rangle = 3\,\mathrm{particle/cm^3}$ *(dashed smooth line) and the BATSE noise level (dotted horizontal line).*

obtain the double peaked structure. The ABM pulse visible area diameter at the moment of interaction with the D shell is $\sim 1.0 \times 10^{15}$ cm, equal to the thickness of the ISM shell [107]. Since it is likely that the spatial scale of the ISM cloud is $\sim 1.0 \times 10^{15}$ cm also in the direction orthogonal to the ABM motion, we conclude that at point D the visible area reaches the boundary of the cloud. The additional emission from the ISM shell makes the signal of the spike D smear out. For points A, B, C, where the visible area is much less than the thickness, the approximation of the concentric shells holds very well, but not from the point D on: the disagreement with the observations makes manifest the need for a more detailed description of the three dimensional nature of the ISM cloud.

The signals from shells E and F, which have a density inhomogeneity comparable to A, are undetectable. The reason is the same as for point D, due to the even larger visible area than for point D [107].

Summarizing we can distinguish two different regimes corresponding in the afterglow of GRB 991216 respectively to $\gamma > 150$ and to $\gamma < 150$. For different sources this value may be slightly different. In the E-APE region ($\gamma > 150$) the GRB substructure intensities indeed correlate with the ISM inhomogeneities. In this limited region (see peaks A, B, C) the Lorentz γ factor of the ABM pulse ranges from $\gamma \sim 304$ to $\gamma \sim 200$. The boundary of the visible region is smaller than the thickness ΔR of the inhomogeneities. Under this condition the adopted spherical approximation is not only mathematically simpler but also fully justified. The angular spreading is not strong enough to smear out the signal from the inhomogeneity spike.

As we descend in the afterglow ($\gamma < 150$), the Lorentz γ factor decreases markedly and in the border line case of peak D $\gamma \sim 140$. For the peaks E and F we have $\gamma \sim 50$ and, under these circumstances, the boundary of the visible region becomes much larger than the thickness ΔR of the inhomogeneities. A three dimensional description would be necessary, breaking the spherical symmetry and making the computation more difficult.

Two explanations of the observed substructures can be found in literature: the one by Fenimore and collaborators (see e.g. [35, 36, 37]) and Piran and collaborators (see e.g. [126, 89, 93, 90]) on one side and the one by Dermer and collaborators [29, 30, 31] on the other side.

Fenimore et al. have focused on the specific signature to be expected in the collision of a relativistic expanding shell with the ISM, which they call a fast rise and exponential decay (FRED) shape. This feature is confirmed by our analysis (see peaks A, B, C in fig. 4.12). However they also conclude, sharing the opinion by Piran et al., that the variability observed in GRBs is inconsistent with causally connected variations in a single, spherical, relativistic shell interacting with the surrounding material ("external shocks") [36]. In their opinion the short time variability is due to the protracted activity of an unspecified "inner engine" [126] (see as well [99, 84, 77, 79, 73]).

On the other hand, Dermer et al., by considering an idealized process occurring at a fixed $\gamma = 300$, have reached the opposite conclusions: GRB light curves are tomographic images of the density distributions of the medium surrounding the sources of GRBs [31].

From our analysis we can conclude that Dermer's conclusions are correct from $\gamma \sim 300$ up to $\gamma > 150$. However, as the γ factor drops from $\gamma \sim 150$ to $\gamma \sim 1$ (see fig. 4.2), the intensity due to the inhomogeneities decreases also due to the angular spreading (events E and F). The initial Lorentz factor of the ABM pulse $\gamma \sim 310$ decreases very rapidly to $\gamma \sim 150$ as soon as ISM cloud is engulfed. We conclude that the "tomography" point of view is valid,

but just in the ISM region close to the source and for GRBs with relatively high [113] γ factor ($\gamma > 150$).

4.10 GRB-Supernova time sequence

A correlation between the GRBs and Supernova events exists and has been established by many works [13, 48, 49, 50, 66, 89, 140]. Such an association has been assumed to indicate that GRBs originate from the same massive body giving before the Supernova explosions [66].

At present at least three GRBs have unequivocally shown an observational connection with a Supernova explosion (GRB 980425, GRB 030329, GRB 031203) and not by chance they are the next ones in the whole GRB sample. We proposed [105] a GRB-SN time sequence kinematically compatible with observations of Iron line in the spectra of GRB 991216 predicting the possibility of observing a variety of pion, kaon or neutrino cooling of a newly born neutron star [17], depending on the star composition.

The idea is that a massive GRB-progenitor star P_1 of mass M_1 undergoes gravitational collapse to an EMBH. During this process the dyadosphere is formed; photons and neutrinos emitted in the P-GRB and the E-APE impact on a second supernova-progenitor star P_2 of mass M_2. Assuming that both stars were generated approximately at the same time, we expect to have $M_2 < M_1$. Under some special conditions of the thermonuclear evolution of the supernova-progenitor star P_2, the collision of the P-GRB and the E-APE with the star P_2 can induce its supernova explosion.

Especially relevant to our model are the following data from the Chandra satellite [93]: at the arrival time of 37 hr after the initial burst there is evidence of iron emission lines for GRB 991216; the emission lines are present during the observation period of 10^4 s, but the iron lines could also have been produced earlier, before Chandra was observing; the emission lines have a peak at an energy of 3.49 ± 0.06 keV which, at a redshift $z = 1.00 \pm 0.02$ corresponds to an hydrogen-like iron line at 6.97 keV at rest. This source does not appear to have any significant motion departing from the cosmological flow. Moreover the iron lines have a width of 0.23 keV consistent with a radial velocity field of $0.1c$. The iron lines are only a small fraction of the observed flux.

In order to reach an intuitive understanding of these complex computations we present a schematic very simplified diagram (not to scale) in fig. 4.13.

We now describe the sequence of events and the specific data corresponding to the time sequence proposed:

1. The two stars P_1 and P_2 are separated by a distance $D_{P_2} = 3.94 \times 10^{17}$ cm in the laboratory frame, see fig. 4.13. Both stars are at rest in the laboratory frame. At laboratory time $t = 0$ and at comoving time $\tau = 0$, the gravitational collapse of the GRB-progenitor star P_1 occurs, and the initial emission of gravitational radiation or a neutrino burst from the event then synchronizes this event with the arrival times $t_a = 0$ at the supernova-progenitor star P_2 and $t_a^d = 0$ for the distant observer at rest with the detector. The electromagnetic radiation emitted by the gravitational collapse process is instead practically zero, due to the optical thickness of the material at this stage ([10], see Tab. 1 in [109]).

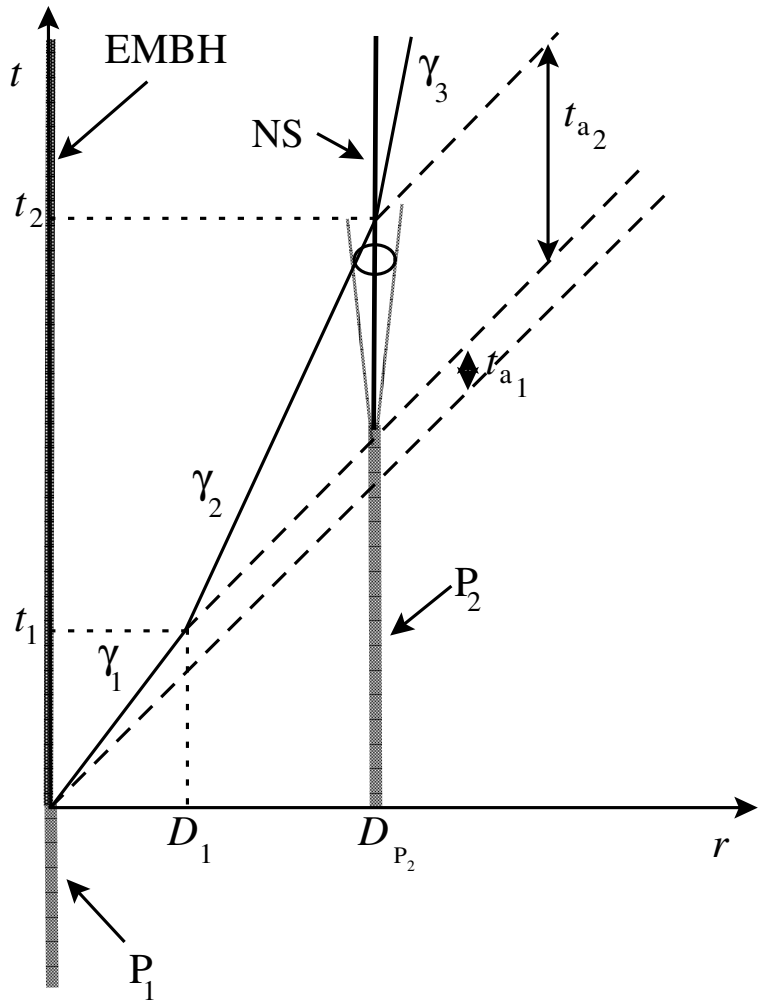

Figure 4.13: *A qualitative simplified space-time diagram (in arbitrary units) illustrating the GRB-SN connection in EMBH model. The EMBH, originating from the gravitational collapse of a massive GRB-progenitor star P_1, and the massive supernova-progenitor star P_2-neutron star (P_2-NS) system, separated by a radial distance D_{P_2}, are assumed to be at rest in the laboratory frame. Their worldlines are represented by two parallel vertical lines. The supernova shell moving at* $0.1c$ *generated by the P_2-NS transition is represented by the dotted line cone. The solid line represents the motion of the pulse, as if it would move with an "effective" constant γ factor γ_1 during the eras reaching the condition of transparency. Similarly, another "effective" constant γ factor $\gamma_2 < \gamma_1$ applies during era IV up to the collision with the P_2-NS system. A third "effective" constant γ factor $\gamma_3 < \gamma_2$ occurs during era V after the collision as the nonrelativistic regime of expansion is reached. The dashed lines at 45 degrees represent signals propagating at speed of light.*

2. From Tab. 1 in [109], at laboratory time $t_1 = 6.48 \times 10^3\, s$ and at a distance from the EMBH of $D_1 = 1.94 \times 10^{14}\, cm$, the condition of transparency for the PEMB pulse is reached and the P-GRB is emitted. This time is recorded in arrival time at the detector $t^d_{a_1} = 8.41 \times 10^{-2}\, s$, and, at P_2, at $t_{a_1} = 4.20 \times 10^{-2}\, s$. The fact that the PEMB pulse in an arrival time of $8.41 \times 10^{-2}\, s$ covers a distance of $1.94 \times 10^{14}\, cm$ gives rise to an apparent "superluminal" effect. This apparent paradox can be straightforwardly explained by introducing an "effective" γ factor, see [105].

3. At laboratory time $t = 1.73 \times 10^6\, s$ and at a distance from the EMBH of $5.18 \times 10^{16}\, cm$ in the laboratory frame, the peak of the E-APE is reached which is recorded at the arrival time $t_a = 9.93\, s$ at P_2 and $t^d_a = 19.87\, s$ at the detector. This also gives rise to an apparent "superluminal" effect.

4. At a distance $D_{P_2} = 3.94 \times 10^{17}\, cm$, the two bursts described in the above points 2) and 3) collide with the supernova-progenitor star P_2 at arrival times $t_{a_1} = 4.20 \times 10^{-2}\, s$ and $t_a = 9.93\, s$ respectively. They can then induce the supernova explosion of the massive star P_2.

5. The associated supernova shell expands with velocity $0.1c$.

6. The expanding supernova shell is reached by the ABM pulse generating the afterglow with a delay of $t_{a_2} = 18.5\, hr$ in arrival time following the arrival of the P-GRB and the E-APE. This time delay coincides with the interval of laboratory time separating the two events, since the P_2 is at rest in the laboratory frame (see [105]). The ABM pulse has travelled in the laboratory frame a distance $D_{P_2} - D_1 \simeq D_{P_2} = 3.94 \times 10^{17}\, cm$ in a laboratory time $t_2 - t_1 \simeq t_2 = 1.32 \times 10^7\, s$ (neglecting the supernova expansion).

The collision of the pulse with the supernova shell occurs at $\gamma \simeq 4.0$. By this time the supernova shell has reached a dimension of $1.997 \times 10^{14}\, cm$, which is consistent with the observations from the Chandra satellite.

In these considerations on GRB 991216 the supernova-progenitor has been assumed to be close to but not exactly along the line of sight extending from the EMBH to the observer at infinity in such a way that the P-GRB radiation is observable on the earth

The possibility of observing the supernova light curve depends on the relative intensities between the GRB and the supernova as well as on the value of the distance and the redshift of the source. In the present case of GRB 991216, the expected optical and radio emission from the supernova are many orders of magnitude smaller than the GRB intensity. The opposite situation is in GRB 980425 - SN1998bw ($z = 0.00835$) [113, 45] which is one of the closest and weakest GRBs observed. In this case, the radio and the optical emission of the supernova has been distinctively observed. For this particular case, the EMBH appears to have a significantly lower value of the parameter ξ and the validity of our scheme here is confirmed. A similar situation is found for GRB 030329 ($z = 0.168$) [9].

4.11 Ultrarelativistic approximation

In this section we present an analysis of the approximations which can be found in literature made to obtain the power law behaviour of the kinematical quantities in the slowing down phase of Gamma-Ray Bursts within the external shock scenario; here in particular we will focus on the radial dependence the Lorentz γ factor of the bulk [89, 100], e.g. used to derive the relation between time at source and time of arrival at the detector; our aim is here to clarify the regime of validity of those approximations and therefore their physical feasibility. We will present later on the approach within the EMBH model: from a numerical integration of the energy-momentum conservation equations, in the fully radiative assumption, the value of the Lorentz γ factor at any radial distance from the source is computed and it is found that the previous power law regime can not hold in any physical situation.

In the commonly accepted scenario of the external shock for the afterglow, a single ultrarelativistic shell of material slows down by colliding with matter surrounding the source. The solution of the relativistic Rankine-Hugoniot equation governing the propagation of a shock wave has been given by Taub [135]. By applying the law of conservation of energy-momentum, the slowing down of the shell is described by a series of infinitesimal inelastic collisions between the shell and infinitesimally thick external shells of mass dm [11, 89]. These equations, in analogy with Eqs.(4.10, 4.11) and if the approximation in (4.9) is valid, can be written at the first order in the form

$$\frac{d\gamma}{\gamma^2-1} = -\frac{dm}{M} \tag{4.36}$$

and

$$dE = (\gamma - 1)dm\,c^2 \tag{4.37}$$

where γ is the bulk Lorentz factor, M is the comoving energy (rest mass and internal energy), dE is the internal energy produced in this collision. The fraction of the internal energy radiated is defined as δ; so $\delta = 0$ in adiabatic case and $\delta = 1$ in fully radiative case. The total comoving energy increases according to:

$$dM\,c^2 = (1-\delta)dE + dm\,c^2 = [(1-\delta)\gamma + \delta]dm\,c^2. \tag{4.38}$$

From (4.36) and (4.38), the following relation is found [1]

$$\frac{(\gamma-1)(\gamma+1)^{1-2\delta}}{(\gamma_\circ-1)(\gamma_\circ+1)^{1-2\delta}} = (M_\circ/M)^2 \tag{4.39}$$

where $M_\circ$ and $\gamma_\circ$ are values at beginning of slowing down phase; from (4.36) and (4.39) the mass swept $m(r)$ up to a radius r is given by

$$\frac{m(r)}{M_\circ} = -\frac{(\gamma_\circ-1)^{1/2}}{(\gamma_\circ+1)^{1/2-\delta}}\int_{\gamma_\circ}^{\gamma}\frac{(\gamma'-1)^{-3/2}}{(\gamma'+1)^{-3/2+\delta}}d\gamma' \tag{4.40}$$

where r is the radial distance in laboratory frame. At this point the crucial approximation is introduced that $\gamma_0 \gg \gamma \gg 1$ in Eq.(4.40), so that, by integrating, one obtains

$$m(r) = M_\circ\frac{\gamma_\circ^{1-\delta}\gamma^{\delta-2}}{2-\delta}\left(1-\left(\frac{\gamma}{\gamma_\circ}\right)^{2-\delta}\right) \simeq \frac{M_\circ}{(2-\delta)\gamma_\circ}\left(\frac{\gamma}{\gamma_\circ}\right)^{\delta-2} \tag{4.41}$$

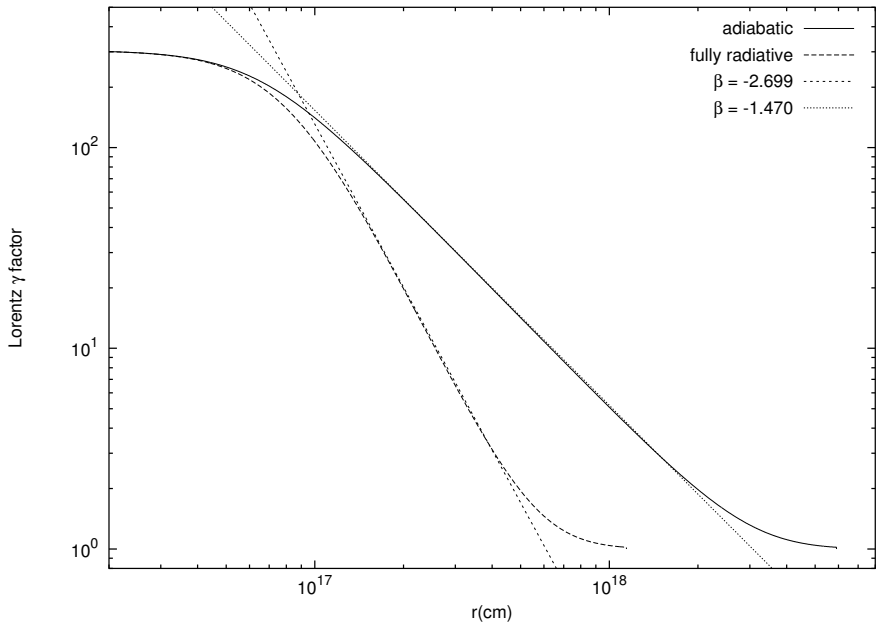

Figure 4.14: *Theoretically simulated Lorentz γ factor as a function of radial distance in laboratory frame for afterglow in adiabatic (solid line) and fully radiative (dashed line) regimes for $B = 3\times10^{-3}$. Straight lines are power laws of the form $\gamma \propto r^{-\beta}$ with $\beta = 1.47013\pm0.00052$ (adiabatic) and $\beta = 2.6996\pm0.0014$ (fully radiative). For a physical $\gamma_\circ \simeq 300$, there exists no region in which the predited power law indexes are attained in no one case.*

if $(\gamma/\gamma_\circ)^{2-\delta} \ll 1$. For a matter distribution with $m(r) \sim r^3$, the power laws of Lorentz γ are obtained:

$$\gamma(r) \propto r^{-3/(2-\delta)} \tag{4.42}$$

so that $\gamma \propto r^{-\frac{3}{2}}$ in adiabatic case and $\gamma \propto r^{-3}$ in fully radiative case. From (4.41) one can see that the validity of the approximation depends on the value of δ: the less is δ, the more the last step in Eq.(4.41) is valid. So one could expect that for sufficiently high value of $\gamma_\circ$, at least $\gamma_\circ \simeq 10^3 - 10^4$, a region could exist where γ has the predicted power law dependence.

In the EMBH model, after the so-called P-GRB in which the expanding system becomes transparent and all the internal energy is emitted as electromagnetic radiation [103, 104, 108, 109], an ultrarelativistic shell of baryonic material (ABM pulse) still expands in completely inelastic collisions with InterStellar Medium (ISM). At a generic step of the collision process, the set of constitutive equations of conservation of energy-momentum in the laboratory frame are given by

$$\rho_{B_1}{\gamma_1}^2\mathcal{V}_1 + \Delta M_{\rm ism}c^2 = \left(\rho_{B_1}\frac{V_1}{V_2} + \frac{\Delta M_{\rm ism}c^2}{V_2} + \Delta\epsilon\right){\gamma_2}^2\mathcal{V}_2 \tag{4.43}$$

$$\rho_{B_1}\gamma_1 U_{r_1}\mathcal{V}_1 = \left(\rho_{B_1}\frac{V_1}{V_2} + \frac{\Delta M_{\rm ism}c^2}{V_2} + \Delta\epsilon\right)\gamma_2 U_{r_2}\mathcal{V}_2 \tag{4.44}$$

where in this case

$$\rho_B = \frac{(M_B + M_{\rm ism})\,c^2}{V} + (1-\delta)\Delta\epsilon_{tot} \tag{4.45}$$

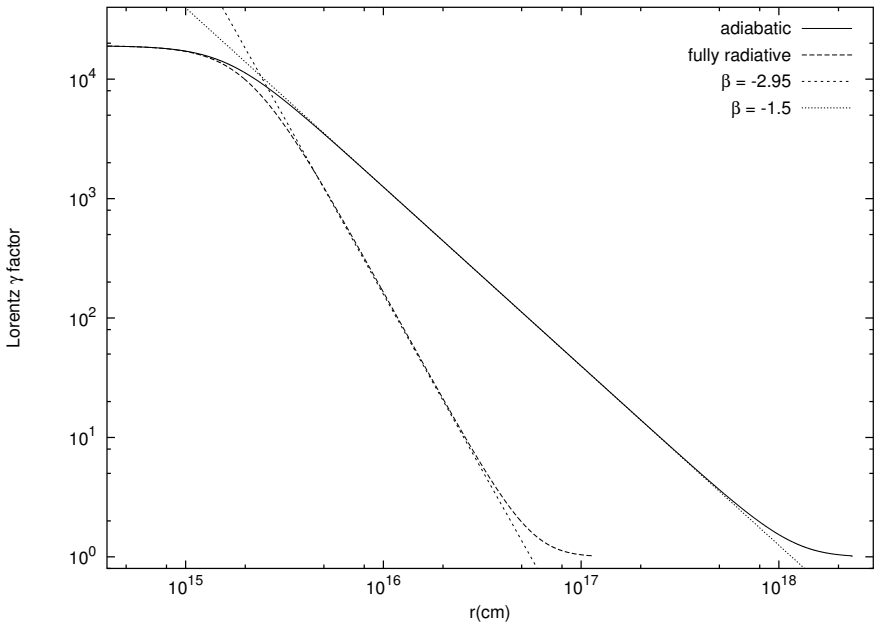

Figure 4.15: *Theoretically simulated Lorentz γ factor as a function of radial distance in laboratory frame for afterglow in adiabatic (solid line) and fully radiative (dashed line) regimes for $B = 3\times10^{-6}$. Straight lines are power laws of the form $\gamma \propto r^{-\beta}$ with $\beta = 1.50017 \pm 0.00069$ (adiabatic) and $\beta = 2.9492 \pm 0.0022$ (fully radiative). Even in the unphysical case $\gamma_\circ \simeq 10^4$, much larger than any cases fit by EMBH model, the theoretically predicted indexes power law are never reached in the fully radiative case.*

at variance from Eq. 4.1 where $\delta = 0$ (fully radiative); in Eqs.(4.43, 4.44) the quantities with the index "1" are calculated before the collision of the ABM pulse with the elementary shell of mass $\Delta M_{\rm ism}$ and the quantities with "2" after the collision; $\Delta\epsilon$ the total internal energy density created in that collision step, $\mathcal{V}$ the volume of the ABM pulse in the laboratory frame so that $V = \gamma\mathcal{V}$, $M_{\rm ism}(r) = m_p n_{\rm ism}(4/3)\pi(r^3 - {r_\circ}^3)$ with $r_\circ$ transparency radius and $U_r = \sqrt{\gamma^2 - 1}$ is the radial covariant component of the four-velocity vector (see [116, 117]). It has been shown for many fit sources that the value of Lorentz γ at transparency point $\gamma_\circ$ is of the order of $\gamma_\circ \simeq 10^2$ (see e.g. GRB 030329, GRB 020322, GRB 991216, GRB 980519, GRB 980425, GRB 970228 in [109, 111, 9, 24, 45, 113], see also fig. 4.14), while the ultrarelativistic approximation adopted in literature requires $\gamma_\circ \simeq 10^4$ or higher [44, 115]. However, even for $\gamma_\circ \simeq 10^4$, the predicted power law in the fully radiative case $\gamma \simeq r^{-3}$ is never reached (see fig. 4.15).

Our analysis shows that in the limiting cases of adiabatic and fully radiative expansion the predicted power laws in ultrarelativistic limit can never come true in any physical case of GRB, where $\gamma_\circ \sim 10^2$. Only in a restricted region and only for $\gamma_\circ > 10^4$, far above the physical value typical for GRBs, these regimes can be found.

5 Spectrum

The observed time-integrated spectra of GRBs are well reproduced by using a phenomenological formula proposed by Band [5] made of two smoothly connected power laws; the Band formula is not underlined by any physical assumption but introduced in order to provide a unified description of the spectral features of GRBs

The bolometric light curves presented up to this point are prediction of the sum of observations of all the instruments which would have observed the GRB in all frequency bands. We present an attempt to derive the GRB luminosity in selected energy bands and the GRB spectra both time resolved and time integrated from the assumption that at high energy (X and γ bands) the energy distribution of radiation in the comoving frame of ABM pulse is thermal. This energy is completely produced in the collisional shock of the ABM pulse with an ISM. We again used GRB 991216 as the prototype by comparing our theoretical predictions in the 2–300 keV range with the set of data by *BATSE* in the 50–300 keV band [7] and by R-XTE and Chandra in the 2–10 keV band [93, 23]. We also give physical reasons for the global hard-to-soft transition observed in the majority of GRBs [46, 51, 89, 92].

No evidence of beaming is found in GRB 991216. The declared breaking in the light curve is not explained in EMBH model by assuming a beamed emission from the source, but by assuming a spherically symmetric pulse a natural bending in the observed light curve is derived from a thermal radiation in the comoving frame.

5.1 The origin of the afterglow X- and γ-ray radiation

The high energy part of the spectrum finds a quite simple and natural explanation by using three basic assumptions: a) the resulting radiation as viewed in the comoving frame of the expanding pulse during the afterglow phase has a thermal spectrum; b) the ISM swept up by the front of the pulse, with a Lorentz γ factor between 300 and 2, is responsible for this thermal emission; c) the expansion occurs with spherical symmetry. These three assumptions are different from the ones adopted in the GRB literature, which are commonly based on the synchrotron radiation emitted by the relativistic electrons behind the shock front of the expanding system accelerated in a magnetic field when the jet-like ejecta encounters the external medium.

The structure of the shock is determined by mass, momentum and energy conservation, which are standard conditions in shock rest frames [150] and have already been used in our derivation (see chapt. 4 and [109]). The only additional free parameter of our model is the size of the "effective emitting area" in the shock wave front: A_{eff}. The temperature T of

the black body in the co-moving frame is then

$$T = \left(\frac{\Delta E_{\rm int}}{4\pi r^2 \Delta\tau \sigma \mathcal{R}} \right)^{1/4} , \tag{5.1}$$

where

$$\mathcal{R} = \frac{A_{eff}}{A_{abm}} \tag{5.2}$$

is the ratio between the "effective emitting area" A_{eff} and the ABM pulse surface A_{abm}, $\Delta E_{\rm int}$ is the internal energy developed in the collision with the ISM in a time interval $\Delta\tau$ in the comoving frame and σ is the Stefan-Boltzmann constant. The ratio $\mathcal{R}$, which is a priori a function that varies as the system evolves, is evaluated at every given value of the laboratory time t.

From the definition (5.1) the source luminosity at a detector arrival time t_a^d, per unit solid angle $d\Omega$ and in the energy band $[\nu_1, \nu_2]$ is given by (see sect. 4.6 and [109]):

$$\frac{dE_\gamma^{[\nu_1,\nu_2]}}{dt_a^d d\Omega} = \int_{EQTS} \frac{\Delta\varepsilon}{4\pi}\, v\, \cos\vartheta\, \Lambda^{-4}\, \frac{dt}{dt_a^d} W\left(\nu_1, \nu_2, T_{arr}\right) d\Sigma\,, \tag{5.3}$$

where $\Delta\varepsilon = \Delta E_{int}/V$ is the energy density developed in the interaction of the ABM pulse with the ISM inhomogeneities measured in the comoving frame, $\Lambda = \gamma(1 - (v/c)\cos\vartheta)$ is the Doppler factor, $W\left(\nu_1, \nu_2, T_{arr}\right)$ is an "effective weight" required to evaluate only the contributions in the energy band $[\nu_1, \nu_2]$, $d\Sigma$ is the surface element of the EQuiTemporal Surface (EQTS) at detector arrival time t_a^d on which the integration is performed, ϑ is the angle in laboratory frame between the emission line and the line of sight and T_{arr} is the observed temperature of the radiation emitted from $d\Sigma$:

$$T_{arr} = \frac{T}{\gamma\left(1 - \frac{v}{c} cos\vartheta\right)} \frac{1}{(1+z)}\,. \tag{5.4}$$

The "effective weight" $W\left(\nu_1, \nu_2, T_{arr}\right)$ is given by the ratio of the integral over the given energy band $[\nu_1, \nu_2]$ of a Planckian distribution at a temperature T_{arr} to the total integral aT_{arr}^4:

$$W\left(\nu_1, \nu_2, T_{arr}\right) = \frac{1}{aT_{arr}^4} \int_{\nu_1}^{\nu_2} \rho\left(T_{arr}, \nu\right) d \left(\frac{h\nu}{c} \right)^3 , \tag{5.5}$$

where $\rho\left(T_{arr}, \nu\right)$ is the Planckian distribution at temperature T_{arr}:

$$\rho\left(T_{arr}, \nu\right) = \frac{2}{h^3} \frac{h\nu}{\exp^{h\nu/(kT_{arr})} - 1}\,, \tag{5.6}$$

5.2 Best fit for GRB 991216 of observed flux in selected energy bands

We can now proceed to the best fit of the observed data using GRB 991216 as the prototype. The numerical integration over space-time is made over the emitting surface of EQTS

which have a known geometry. In fig. 5.1 the solid line gives the bolometric luminosity [109]. We give also in fig. 5.1 the results for the three energy bands 50–300 keV (*BATSE*), 2–10 keV (R-XTE, Chandra) and 10–50 keV. The best fit is obtained by a factor $\mathcal{R}$, which is monotonically varying in the range $3.01 \times 10^{-8} \geq \mathcal{R} \geq 5.01 \times 10^{-12}$, respectively in correspondence with the beginning of the afterglow emission and the last observation by Chandra at ~ 37 hr after the GRB. Very good agreement is obtained with the data by [7] in the energy range 50–300 keV (see dashed line in fig. 5.1) and by the R-XTE and Chandra satellites [58] in the energy range 2–10 keV (see dotted line in fig. 5.1 and fig. 5.2).

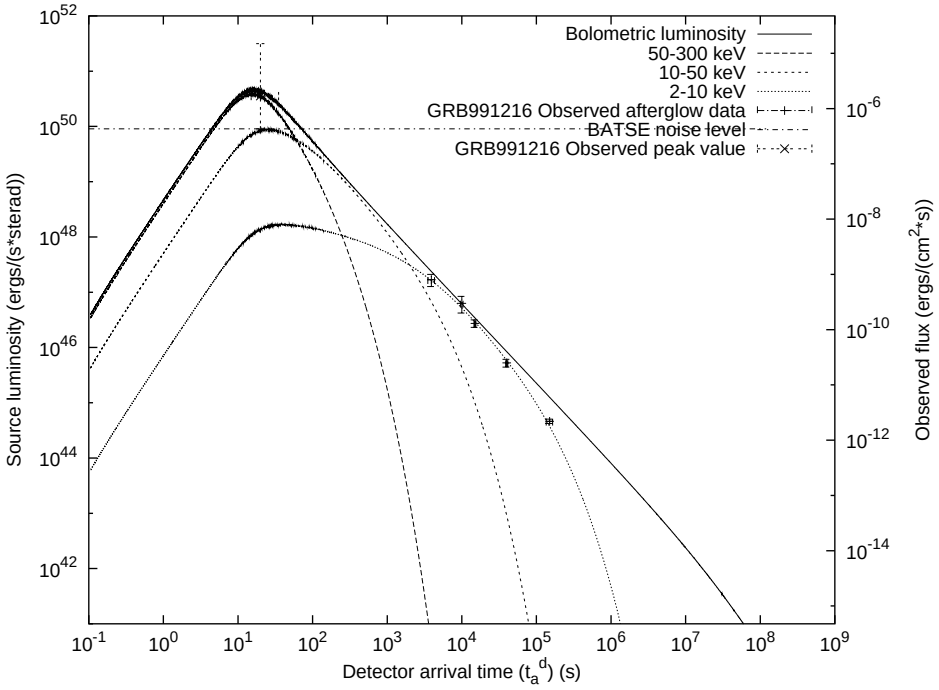

Figure 5.1: *Best fit of the afterglow data of GRB 991216. The solid curve is the bolometric luminosity. The three dotted curves correspond to the luminosities in the bands* 50–300 *keV,* 10–50 *keV and* 2–10 *keV respectively. Near the E-APE, where the BATSE data are present, the luminosity is mainly in the* 50–300 *keV band, verifying the assumption* 1) *in sect. 4.7. The afterglow data from R-XTE and Chandra [58] in the* 2–10 *keV are fit by the corresponding luminosity curve too, coincident with bolometric luminosity (assumption* 2) *in sect. 4.7). The reduced* χ^2 *value for this fit is* $\chi^2 \simeq 1.078$.

A constant ISM number density is reported $\langle n_{ism} \rangle \simeq 1$ particle/cm^3 without any radial substructure. These data are fit with a $\chi^2 \simeq 1.078$. The fit can be further improved, reaching a $\chi^2 \simeq 0.497$, when the radial dependence in $\langle n_{ism} \rangle$ from fig. 4.10 is introduced, ranging from $\langle n_{ism} \rangle \simeq 1$ particle/cm^3 in the E-APE region ($r \simeq 5 \times 10^{16}$ cm) to $\langle n_{ism} \rangle \simeq 3$ particle/cm^3 in the latest afterglow phases ($r \simeq 4 \times 10^{17}$ cm). We also verified that in the E-APE the luminosity is mainly in 50–300 keV band, while during the afterglow mainly in 2–10 keV band.

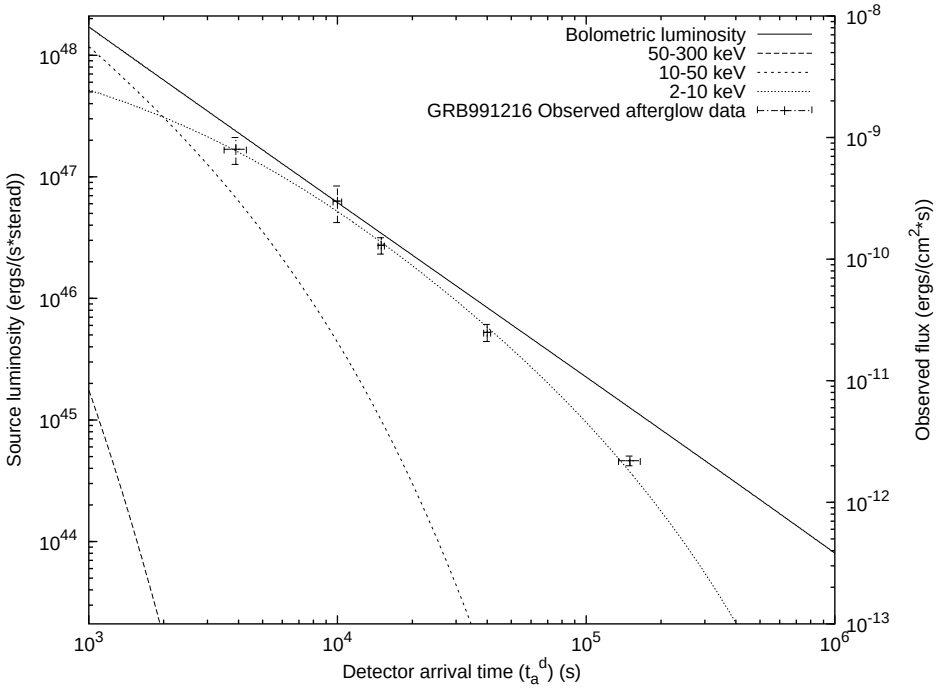

Figure 5.2: *Zoom on best fit of afterglow luminosity of GRB 991216 of fig. 5.1 in the region of the data in the* 2–10 *keV band from the R-XTE and Chandra satellites with constant number density* $n_{\rm ism}$*, showing the agreement between the theoretical curve and the observational data. The reduced* χ^2 *value for this fit is* $\chi^2 \simeq 1.078$.

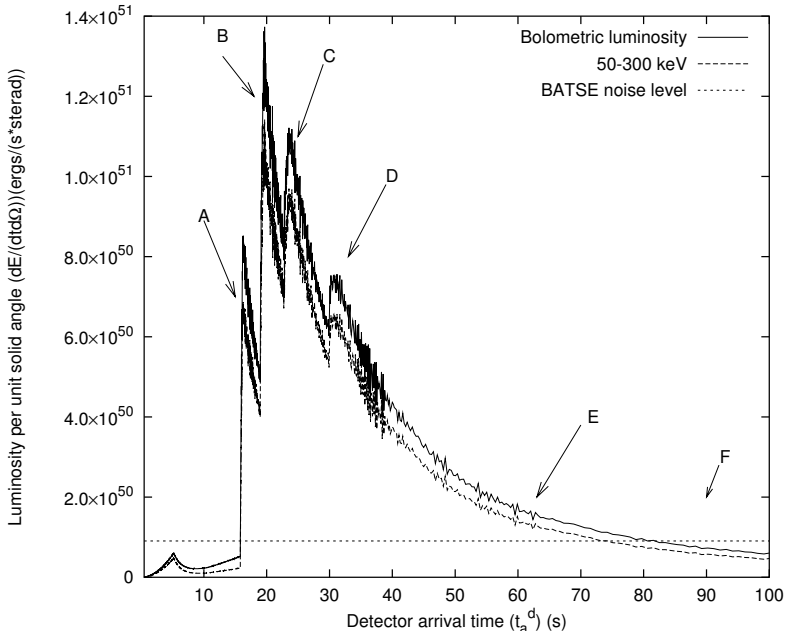

Figure 5.3: *Theoretical prediction within EMBH model of the GRB 991216 light curve in* 50–300 *keV with the number density profile given in fig. 4.10 reported with bolometric light curve and BATSE noise level. Near the E-APE, where the BATSE data are present, the bolometric luminosity is almost superposed to the* 50–300 *keV band curve, verifying the assumption* 1) *in sect. 4.7.*

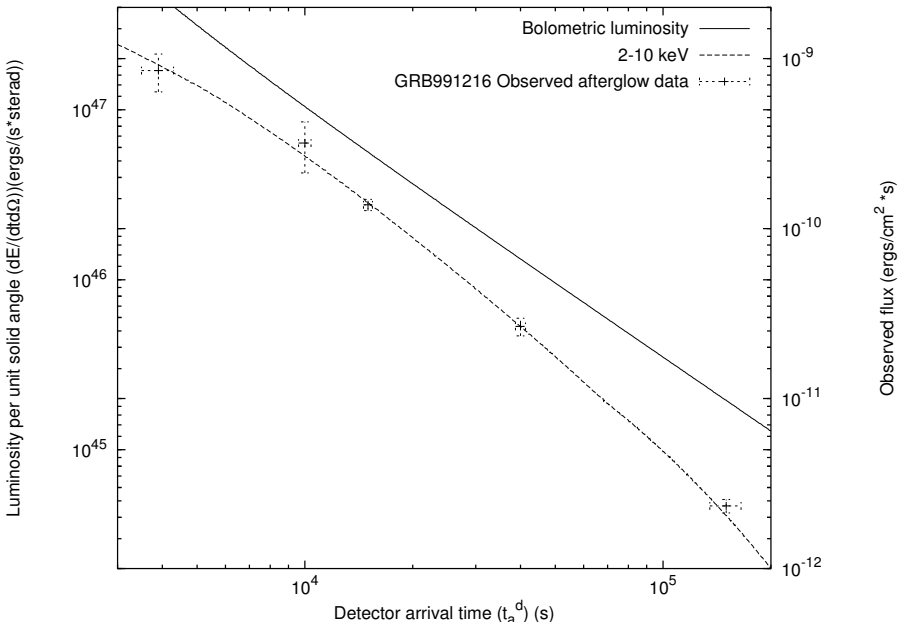

Figure 5.4: *Afterglow luminosity for GRB 991216 in* 2–10 *keV band with density mask predicted by EMBH model represented with bolometric luminosity and observational data. The reduced* χ^2 *value for this fit is* $\chi^2 \simeq 0.497$.

5.3 Hard-to-soft spectral evolution

A more stringent test of a spectral model of GRBs is not represented by time integral spectra, just useful to describe global properties of the phenomenon, but by time resolved spectra giving indication of time evolution of the parameters like power law index or energy peak. Historically the first spectral parameter of GRBs was the hardness ratio, i.e. the ratio of photon counts per second belonging to two different among the four energy channels of *BATSE* [65, 137]. Afterwards the Band formula became popular describing the global spectrum by two power law indexes at low (α) and high (β) energies and by the energy peak. Our computations are directly compared with this second set of parameters.

We turn now to the issue of the origin of the observed hard-to-soft spectral transition during the GRB observations [46, 51, 89, 92].

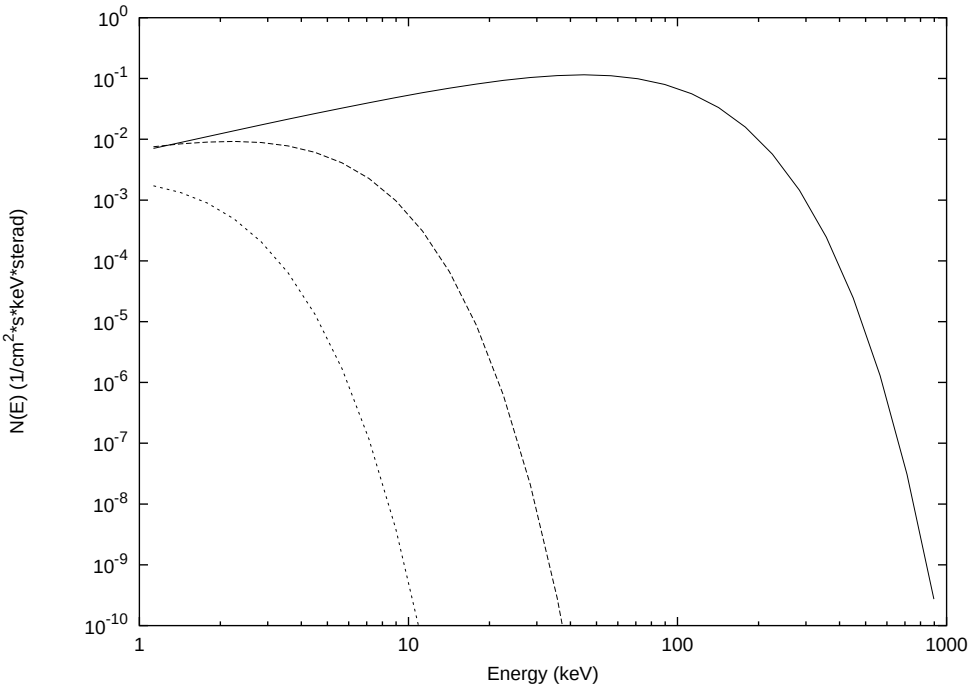

Figure 5.5: *The instantaneous spectra $N(E)$ of the radiation observed in GRB 991216 at three different arrival times respectively, from top to bottom, for $t_a^d = 10$ s, $t_a^d = 10^4$ s and $t_a^d = 1.45 \times 10^5$ s. These diagrams have been computed assuming a constant $\langle n_{ism} \rangle \simeq 1$ particle/cm^3 and explains the often quoted hard-to-soft spectral evolution in GRBs. The peak of the last time spectrum occurs below the chosen range $[1 \div 1000] keV$ due to the transition to lower energies at that time.*

We consider the instantaneous spectral distribution of the observed radiation for three different arrival time EQTS: $t_a^d = 10$ s, in the early radiation phase before the peak of the luminosity; $t_a^d = 1.45 \times 10^5$ s, at time of the last observation of the afterglow by the Chandra satellite, and $t_a^d = 10^4$ s, arbitrarily chosen in between the other two. In fig. 5.5 these time resolved spectra by $N(E)$, the photon count number in photons cm^{-2} s^{-1} keV^{-1}, are represented under the assumption of a constant ISM particle density equal to the average

$\langle n_{ism} \rangle \simeq 1$ particle/cm^3. The observed hard-to-soft spectral transition is then explained and traced back to:

1. a time decreasing temperature of the thermal spectrum measured in the comoving frame,
2. the GRB equations of motion,
3. the corresponding infinite set of relativistic transformations defining the EQTS.

A clear signature of our model is the existence of a common low-energy behavior of the instantaneous spectrum represented by a power-law with index $\alpha = +0.9$. This prediction will be possibly verified in future observations.

Starting from these instantaneous values, we integrate the spectra in arrival time obtaining what is usually fit in the literature by the Band formula [5]. Indeed we find for our integrated spectra $N(E)$ a low energy spectral index $\alpha = -1.05$ and an high energy spectral index $\beta < -16$ (see fig. 5.6). This theoretical result can be submitted to a direct confrontation with the observations of GRB 991216. The theoretical framework which we have developed can now be applied to any GRB source comparing our theoretical predictions on the luminosity in fixed energy bands with the observational data.

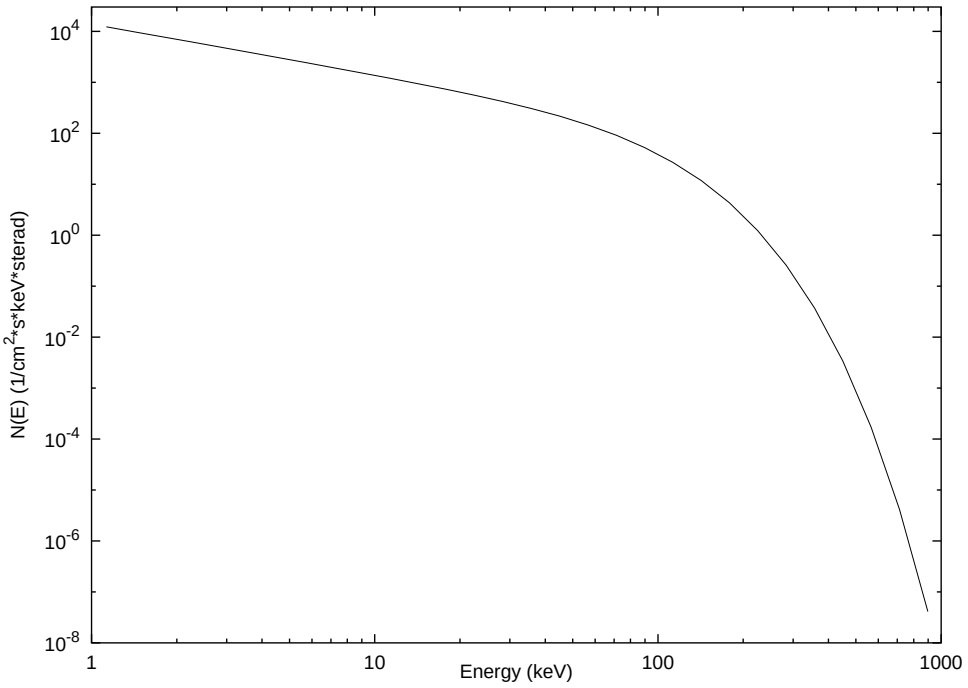

Figure 5.6: *The predicted time-integrated spectrum of the radiation observed in GRB 991216. The low energy part of the curve below* 10 *keV is fit by a power-law with index* $\alpha = -1.05$ *and the high energy part above* 500 *keV is fit by a power-law with an index* $\beta < -16$.

We have also applied our model to GRB 980425; the comparison of the theoretical light curves and time resolved spectra for early time emission with observations are shown respectively in fig. 5.7 and in fig. 5.8. It has to be noted that GRB 980425 is one of the weakest

GRBs ever observed, with an energy of the order of $\sim 10^{48}$ ergs [113]. It is remarkable that such a good agreement has been obtained by EMBH model with observations over a range of energies spanning 6 orders of magnitude. Other results on GRB 030329 and GRB 970228 are presented in [9, 24].

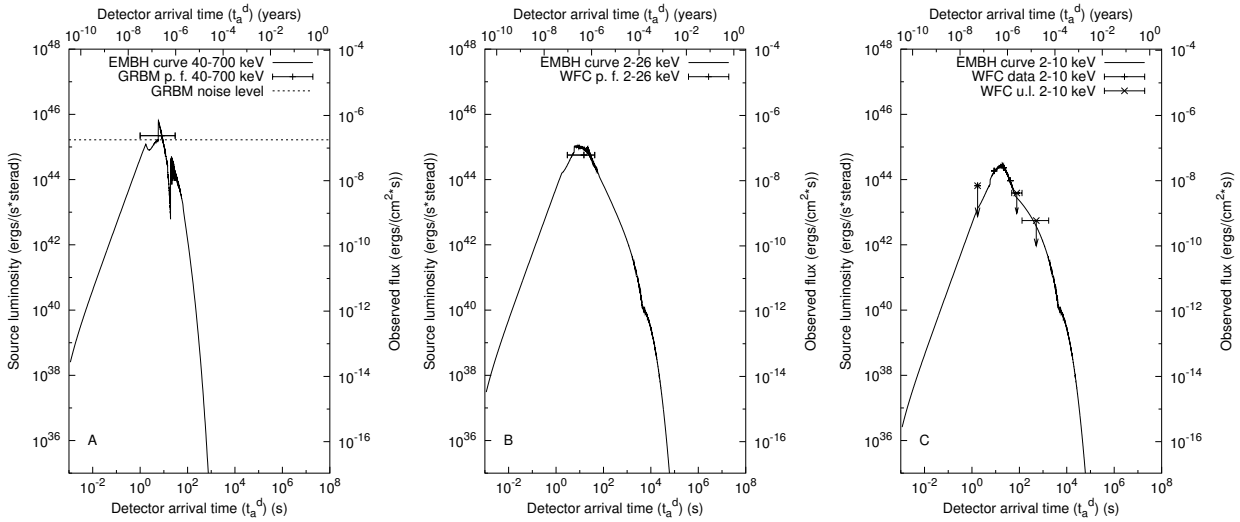

Figure 5.7: **a)** *The light curve computed within the EMBH model in γ-ray (40-700 keV) is represented for GRB 980425; the horizontal bar represents the peak flux in the 40–700 keV band measured by the GRBM [46]. The horizontal dotted line represents the noise level of the GRBM detector.* **b)** *The light curve computed within the EMBH model in hard X-rays in the 2–26 keV band with the peak flux and time duration from WFC [46].* **c)** *The light curve computed within the EMBH model in hard X-rays in the 2–10 keV band with the observational data in the same band from WFC [87].*

The new point in this work is the assumption of the thermal origin of the X and γ radiation of the afterglow in the comoving frame of the pulse. The fit of the data in fig.5.1 gives a strong support from the observations to this theoretical approach. Going back to the quoted compactness problem in sect. 2.6, it has to be noted that while in literature relativistic motion is proposed to increase the opacity and to have an optically thin system because the observed spectra look like non-thermal, in our case the relativistic motion is a consequence of the equations of motion and the assumption of black body spectrum is proposed leading to the result that the observed superposition of even perfect thermal spectra at different temperature can not be a thermal spectrum. The explanation of this is that even at fixed arrival time at the detector arrive photons emitted at different times in the laboratory frame and at different angles with respect to the line of sight; since the temperature evolves, at the detector arrive photons belonging to different black bodies; this effect is enlarged as the time goes on because the visible area increases in time [109, 107] and the range of temperature of photons observed at the same arrival time increases in correspondence [114].

After having obtained this result we were aware that in 1999 Blinnikov et al. [12] have shown that nonthermally looking GRB spectra can indeed be formed by a superposition of a set of thermal black body spectra using a temporal power-law evolution of the temperature. In our treatment not only time but also space integration on the EQTS takes place. This

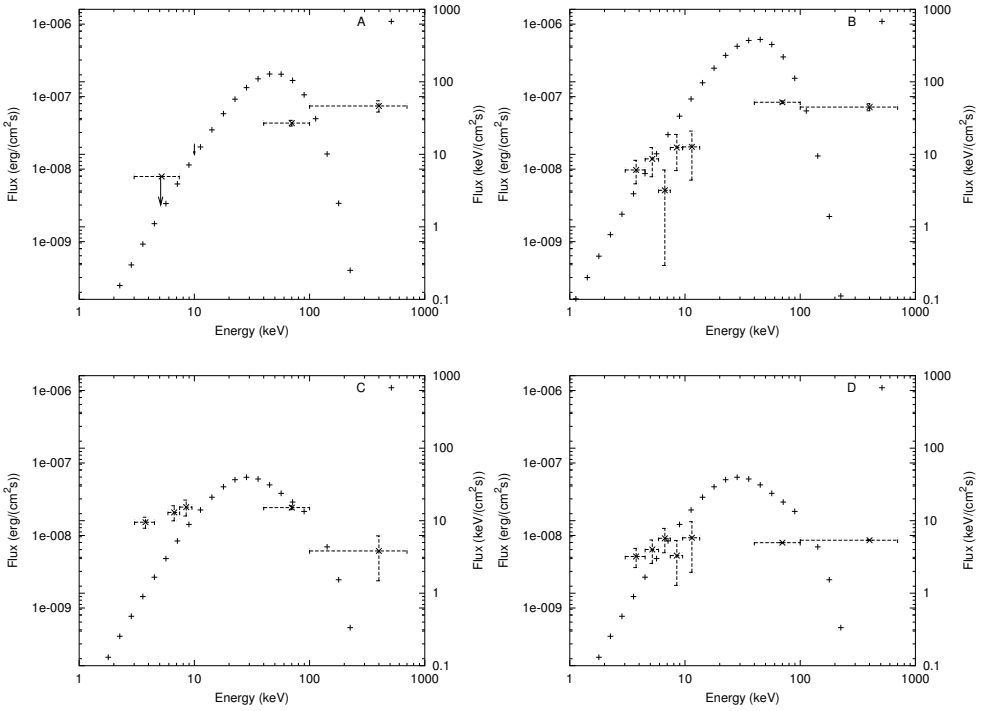

Figure 5.8: *Time resolved spectra predictions of EMBH model for four points A, B, C, D selected during the prompt phase of GRB 980425 in X and γ ranges as received at the detector, from the assumption of a thermal spectrum in the comoving frame. The observed spectra are non-thermal ones for the reasons explained in the text. A very good agreement with observations [46] is obtained.*

effect was explicitly omitted in [12]: in their work they show that a wide variety of non-thermal observed spectra can be obtained by a time integrated emission of black body spectra and state that the space integration over the emitting surface gives the same effect as the time integration, but do not make explicitly the computation; in our approach each instantaneous spectrum is derived from an infinite set of foliations of events on the EQTS, each one characterized by a different thermal spectrum in the comoving frame boosted by a different relativistic transformation obtained from the equation of motion.

We conclude that there is a marked difference (see fig. 5.1) between the bolometric intensity of the afterglow, with a simple power-law behavior with an index $n \sim -1.6$ in the decreasing part, and the actual luminosity in a fixed bandwidth, which can have a complex dependence on time. Such a complex behavior has been often interpreted in literature as a broken power-law supporting the existence of jet-like structures in GRBs, but it could be also due to the paucity of observations which hides the real complex behaviour. The sources for which a collimated emission is advocated in literature can be explained within EMBH model with a spherical symmetry. Moreover in the cases of GRB 991216 and GRB 980519, from the constraint of afterglow observations, we found lower limits on beaming angle which are larger than the corresponding values given in literature [112].

6 Observational signatures of an electromagnetic overcritical gravitational collapse

In all the previous chapters the plasma of $e^+e^-\gamma$ created by vacuum polarization is assumed to be formed in a region surrounding an already formed black hole; in fact when the gravitational collapse stops in the sense explained in [121] at time $\bar{t}$, the plasma is extended over a region which is about one order of magnitude larger than the dyadosphere. At this stage the plasma is inhomogeneous and the distribution of Lorentz γ, number density and temperature are given in [121]. These distributions can be used as initial data instead of the slab treated in previous chapters. From time $\bar{t}$ the distribution of the system is such that the gravitational effects are negligible; the expansion goes on in vacuum space until the transparency point is reached. The relevance of this analysis stands in luminosity and spectral predictions valid for short GRBs, corresponding in EMBH model to the limiting case $B = 0$. As shown in fig. 4.7, the amount of baryonic remnant B determines the relative intensity of P-GRB and afterglow; but in the case $B = 0$ no energy is transferred to baryons and the whole energy is emitted at P-GRB in a time scale of ~ 1 sec.

6.1 The expansion of the PEM pulse as a discrete set of sub-slabs

We discretize the gravitational collapse of a spherically symmetric core of mass M and charge Q by considering a set of spherical shells of plasma of constant thickness in laboratory frame Δr so that:

1. Δr is assumed to be small with respect to the core radius;
2. Δr is assumed to be large with respect to the mean free path of the particles so that the statistical description of the $e^+e^-\gamma$ plasma can be used;
3. There is no overlap among the slabs and their union describes the whole process.

We check moreover that the final results are independent of the special value of the chosen Δr. In order to describe the dynamics of the expanding plasma pulse the energy-momentum conservation law and the rate equation for the number of pairs in the Reissner-Nordstrøm

geometry external to the collapsing core have to be integrated. We use these equations to study the expansion of each sub-slab, following closely the treatment developed in [116, 117] where it was shown how a homogeneous slab of plasma expands as a pair-electromagnetic pulse (PEM pulse) of constant thickness in the laboratory frame. In the initial phase of expansion the plasma experiences the strong gravitational field of the core and a fully general relativistic description of its motion is needed. The plasma is sufficiently hot in this first phase that the e^+e^- pairs and the photons remain at thermal equilibrium in it [120]. At asymptotically late times the temperature of the plasma drops below the value 0.5 MeV and the e^+e^- pairs and the photons can no longer be considered to be in equilibrium: the full rate equation for pair annihilation needs to be used. However, the plasma is so far from the central core that gravitational effects can be neglected. In this new regime, as shown in [116], we can use Eqs.(3.37, 3.39, 3.67). At variance from our treatment, in [57] an ultrarelativistic wind of e^+e^- and photons is considered with constant energy supply from an inner engine which is not specified. In this paper, solutions to the approximate pair rate equation are discussed [88] for different values of optical depth and temperature. However we numerically found the solution to the exact rate equation for pairs as a function of time-evolution of the plasma, so that the optical depth is computed and the transparency is determined when the optical depth is one; also prediction of light curve are presented (see sect. 6.2).

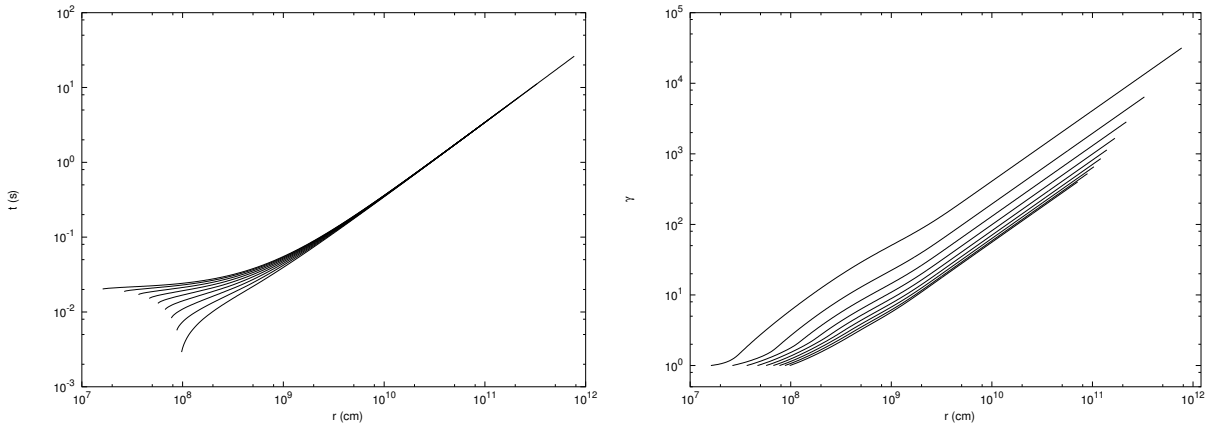

Figure 6.1: *Expansion of the plasma created around an overcritical collapsing stellar core with* $M = 10M_\odot$ *and* $Q = 0.1\sqrt{G}M$. **Left***: world lines of the plasma.* **Right***: Lorentz* γ *factors as a function of the radial coordinate* r.

6.2 Reaching of transparency

The equations of the previous two different regimes must be separately integrated and the solutions must be matched at the transition point. The integration stops when each slab of plasma reaches the optical transparency condition given by

$$\int_{\Delta R} \sigma_T n_{e^+e^-} dr \sim 1\,, \tag{6.1}$$

where σ_T is the Thomson cross-section and the integral extends over the radial thickness ΔR of each sub-slab. Since we are considering the limit case of $B = 0$ the integrand does

not contain baryonic number density n_B, at variance from Eq.(3.63). The evolution of each sub-slab occurs without any collision or interaction with the other sub-slabs: we do not find internal shock; see the Left diagram in fig. 6.1, which represents the world lines of the plasma as functions of the radius. The outer layers are colder than the inner ones and therefore reach transparency earlier; see the Right diagram in fig. 6.1, which shows the corresponding Lorentz γ factors as functions of the radius. In fig. 6.1, the solution of integration of constitutive equations is shown for $M = 10M_{\odot}$ and $Q = 0.1\sqrt{G}M$. The overall independence of the result of the dynamics on the number N of the sub-slabs adopted in the discretization process or analogously on the value of Δr has also been checked. We have repeated the integration for $N = 10$, $N = 100$ reaching analogous results for the expansion and the observed light curve (see fig. 6.2). The results in fig. 6.1 and in fig. 6.2 correspond to the case $N = 10$.

In fig. 6.2 we plot both the theoretically predicted luminosity L and the spectral hardness of the signal reaching a far-away observer as functions of the arrival time ${t_a}^d$. All three of these quantities depend in an essential way on the cosmological redshift factor z [109]; we have adopted a cosmological redshift $z = 1$ for this figure.

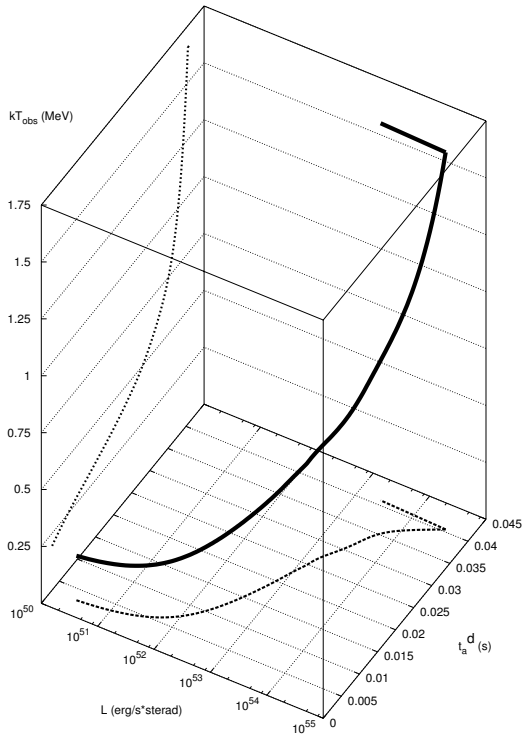

Figure 6.2: *Predicted observed luminosity and observed spectral hardness of the electromagnetic signal from the gravitational collapse of a collapsing core with* $M = 10M_{\odot}$, $Q = 0.1\sqrt{G}M$ *at* $z = 1$ *as functions of the arrival time* t_a^d *at the detector.*

As the plasma becomes transparent, gamma ray photons are emitted. The energy $\hbar\omega$ of the observed photon is roughly given by $\hbar\omega = k\gamma T/(1+z)$, where k is the Boltzmann constant, T is the temperature in the comoving frame of the pulse and γ is the Lorentz factor of the plasma at the transparency time. The initial zero of time is chosen as the time when the first photon emitted by the outer sub-shell which becomes transparent earliest is

observed; then the arrival time t_a^d of a generic photon at the detector is given by [109]:

$$t_a{}^d = (1+z)\left[t + \frac{r_0}{c} - \frac{r\,(t)}{c}\cos\theta\right] \tag{6.2}$$

where r_0 is the initial position of the slab. The projection of the plot in fig. 6.2 onto the t_a^d-L plane gives the total luminosity as the sum of the partial luminosities of the single slabs. The sudden decrease of the intensity at the time $t = 0.040466$ s corresponds to the creation of the *separatrix*, introduced in [121], defined as the radius $\bar{R}$ such that the plasma created at $R > \bar{R}$ expands to infinity, while the plasma created at $R < \bar{R}$ is trapped in the gravitational field of the collapsing core and implodes toward the singularity. We find that the duration of the electromagnetic signal emitted by the relativistically expanding pulse is given in arrival time by $\Delta t_a^d \sim 5 \times 10^{-2}$s. The projection of the plot in fig. 6.2 onto the $kT_{\rm obs}$, t_a^d plane describes the temporal evolution of the spectral hardness. We observe a precise soft-to-hard evolution of the spectrum of the gamma ray signal from $\sim 10^2$ keV monotonically increasing to ~ 1 MeV. We recall that $kT_{\rm obs} \simeq k\gamma T/\,(1+z)$.

The above quantities are clearly functions of the cosmological redshift z, of the charge Q and the mass M of the collapsing core. We present in fig. 6.3 the arrival time interval at the detector for M ranging from $M \sim 10 M_\odot$ to $10^3 M_\odot$, keeping $Q = 0.1\sqrt{G}M$. The arrival time interval is very sensitive to the mass of the black hole:

$$\Delta t_a^d \sim 10^{-2} - 10^{-1}\mathrm{s}\,. \tag{6.3}$$

Similarly the spectral hardness of the signal is sensitive to the ratio $Q/\sqrt{G}M$ [122]. Moreover the duration, the spectral hardness and luminosity are all sensitive to the cosmological redshift z [122]. All the above quantities can also be sensitive to a possible baryonic contamination of the plasma due to the remnant of the progenitor star which has undergone the process of gravitational collapse [117].

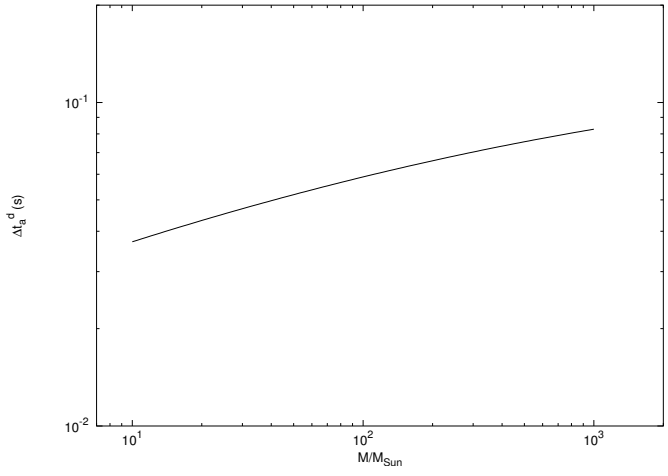

Figure 6.3: *Arrival time duration at the detector of the electromagnetic signal from the gravitational collapse of a stellar core with charge $Q = 0.1\sqrt{G}M$ as a function of the mass M of the core.*

7 Conclusion

The work presented in previous chapters is here summarized. The main feature of the model is the possibility to build the whole evolution of the emitting pulse, from the progenitor to the non-relativistic phase. Different is the situation in literature, where mainly piecewise picture of the phenomenon are presented: either models based on a progenitor satisfying the requirements of energy budget and of time scale even as brief as fractions of second but not considering in detail the late time emission in the afterglow phase where the main actor is a still ultrarelativistically expanding system; or phenomenological models defining initial conditions for a fireball so far from the progenitor that any gravitational effect is negligible and such that any assumption on the progenitor becomes not necessary.

Future perspective for the model are the theoretical prediction of the optical and radio emissions, which in some events turn out as flashes at early time with an intensity comparable with the X and γ, even if the contribution to the integrated energy in many cases result below the high energy contribution.

Many long GRBs have been fit in luminosity and spectra by EMBH model, and qualitative predictions have been computed for short events until now; so a new analysis is opening in the class of short GRBs.

The study of the association between GRB and Supernova will be improved due to the interest risen by the events GRB 980425, GRB 030329 and GRB 031203.

The rotation of the progenitor has been neglected for the sake of simplicity and a simple already formed black hole of Reissner-Nordstrøm has been considered: the predictions obtained for the afterglow should not be affected significantly by this choice. The introduction of rotation however is expected to bring new features in the early time emission.

Bibliography

[1] Abramowitz, M., Stegun, I.A., 1970, *Handbook of Mathematical Functions*, National Bureau of Standards, Washington, D.C..

[2] Amati L. et al., 2000, *Science*, 290, 953.

[3] Amati L. et al., 2002, *A&A*, 390, 81.

[4] Balastegui A., Ruiz-Lapuente P. and Canal R., 2001, *MNRAS*, 328, 283.

[5] Band D. et al., 1993, *ApJ*, 413, 281.

[6] BATSE GRB Light Curves, *http://gammaray.msfc.nasa.gov/batse/grb/lightcurve/*.

[7] BATSE Rapid Burst Response, *http://gammaray.msfc.nasa.gov/ kippen/batserbr/*.

[8] Beck S.C., Turner J.L. and Kovo O., 2000, *AJ*, 120, 244.

[9] Bernardini M.G., Bianco C.L., Chardonnet P., Fraschetti F., Ruffini R., Xue S.S., in *Proceedings of the Gamma Ray Burst Symposium*, Santa Fe, New Mexico, USA, 8-12 September 2003, in press; pre-print: astro-ph/0407503.

[10] Bianco C.L., Ruffini R., Xue S.-S., 2001, *A&A*, 368, 377.

[11] Blandford R.D., McKee C.F., 1976, *Phys. Fluids*, 19, 1130.

[12] Blinnikov S.I., Kozyreva A.V., Panchenko I.E., 1999, *Astron. Rep.*, 43, 739; preprint: astro-ph/9902378.

[13] Bloom L. et al., 1999, *Nature*, 401, 453

[14] Bloom J.S., Kulkarni S.R. and Djorgowski S.G., 2002, *AJ*, 123, 1111.

[15] Bonnell J., *http://antwrp.gsfc.nasa.gov/htmltest/jbonnell/www/grbhist.html*.

[16] Caldwell N., Garnavich P., Holland S., Matheson T. and Stanek K.Z., 2003, GCN Circ. 2053.

[17] Canuto, V., in *Physics and astrophysics of neutron stars and black holes - Proceedings of the International School of Physics "Enrico Fermi"*, ed. R. Giacconi and R. Ruffini, Bologna, Società Italiana di Fisica; Amsterdam, North Holland Publishing Co., 1978, 448.

[18] Cheng K.S. and Wang J.M., 1999, *ApJ*, 521, 502.

[19] Cherubini C., Ruffini R. and Vitagliano, L., 2002, *Phys. Rev. B*, 545, 226.

[20] Chiang J. and Dermer C.D., 1999, *ApJ*, 512, 699.

[21] Christodoulou D. and Ruffini R., 1971, *Phys. Rev. D*, 4, 3552.

[22] Cline T.L., Desai U.D., Klebesadel R.W. and Strong I.B., 1973, *ApJ*, 185, L1.

[23] Corbet R. and Smith D. A., 2000, in Rossi2000: Astrophysics with the *Rossi X-Ray Timing Explorer* (Greenbelt: NASA), E97.

[24] Corsi A., Bernardini M.G., Bianco C.L., Chardonnet P., Fraschetti F., Ruffini R.,Xue S.-S., in *Proceedings of the Gamma Ray Burst Symposium*, Santa Fe, New Mexico, USA, 8-12 September 2003, in press; pre-print: astro-ph/0407233.

[25] Costa E. et al., 1997, *Nature*, 387, 783.

[26] Crider A., Liang E. P. and Preece R. D., to appear in *Proceedings of the* IV *Huntsville Symposium on Gamma-Ray Bursts*; pre-print: astro-ph/9711100.

[27] Damour T. and Ruffini R., 1975, *Phys. Rev. Lett.*, 35, 463.

[28] Davies M.B., Benz W., Piran T. and Thielemann F.K., 1994, *ApJ*, 431, 742.

[29] Dermer C.D., 1998, *ApJ*, 501, L157.

[30] Dermer C.D., Böttcher M. and Chiang J., 1999, *ApJ*, 515, L49.

[31] Dermer C.D. and Mitman, K.E., 1999, *ApJ*, 513, L5.

[32] Dermer C.D., 2002, *ApJ*, 574, 65.

[33] Fan Y.Z., Zhang B., Kobayashi S., Mészáros P.; pre-print: astro-ph/0410060.

[34] Fanari G., Tesi di laurea, University of Rome "La Sapienza", 1988, Tutor Prof. R. Ruffini.

[35] Fenimore E.E., Madras C.D. and Nayakshin S., 1996, *ApJ*, 473, 998.

[36] Fenimore E.E., Cooper C., Ramirez-Ruiz E., Sumner M.C., Yoshida A. and Namiki M., 1999, *ApJ*, 512, 683.

[37] Fenimore E.E., 1999, *ApJ*, 518, 375.

[38] Filippenko A.V., 1997, *Annu. Rev. A&A.*, 35, 309.

[39] Fishman G. and Meegan C., 1995, *Annu. Rev. A&A*, 33, 415.

[40] Frail D. A., Kulkarni S. R., Nicastro L., Feroci M. and Taylor G. B., 1997, *Nature*, 389, 261.

[41] Frail D. et al., 2000, *ApJ*, 538, L129.

[42] Frail D. et al., 2001, *ApJ*, 562, L55.

[43] Fraschetti F., Bernardini M.G., Bianco C.L., Chardonnet P., Ruffini R.,Xue S.-S., in *Proceedings of the Gamma Ray Burst Symposium*, Santa Fe, New Mexico, USA, 8-12 September 2003, in press; pre-print: astro-ph/0407147.

[44] Fraschetti F., Bianco C.L., Ruffini R., Xue S.-S. and Chardonnet P., in *Proceedings of the X Marcel Grossmann Meeting on General Relativity*, M. Novello, S.E. Perez-Bergliaffa, R. Ruffini (eds.), 2004, World Scientific, Singapore, in press.

[45] Fraschetti F., Bernardini M.G., Bianco C.L., Ruffini R., Xue S.-S. and Chardonnet P., in *Proceedings of the X Marcel Grossmann Meeting on General Relativity*, M. Novello, S.E. Perez-Bergliaffa, R. Ruffini (eds.), 2004, World Scientific, Singapore, in press.

[46] Frontera F. et al., 2000, *ApJS*, 127, 59.

[47] Fryer C.L., 2004, *ApJ*, 601, L175.

[48] Galama T.J. et al., 1998, IAU Circ., 6895.

[49] Galama T.J. et al., 1998, *Nature*, 395, 670.

[50] Galama T.J. et al., 2000, *ApJ*, 536, 185.

[51] Ghirlanda G., Celotti A. and Ghisellini G., 2002, *A&A*, 393, 409.

[52] Ghirlanda G., Ghisellini G. and Celotti A.; pre-print: astro-ph/0310861.

[53] Ghisellini G., *Proceedings of the* 3^{rd} *Workshop "Gamma-Ray Bursts in the Afterglow Era"*, Rome, September 2002, editors M. Feroci, F. Frontera, N. Masetti, L. Piro, ASP Conference Series, 312, 319, 2004; pre-print:astro-ph/0301256

[54] Greiner J., 2001, *"Literature related to GRB afterglows"*, available on *http://www.aip.de/ jcg/grblit.html*.

[55] Greiner J., *http://www.mpe.mpg.de/ jcg/grbgen.html*.

[56] Greiner J. et al., 2003, GCN Circ. 2020.

[57] Grimsrud O.M., Wasserman I., 1998, *MNRAS*, 300, 1158.

[58] Halpern J.P. et al., 2000, *ApJ*, 543, 697.

[59] Hansen B.M.S. and Phinney E.S., 1997, *MNRAS*, 291, 569.

[60] Heisenberg W. and Euler H., 1935, *Zeits. Phys.*, 98, 714.

[61] Hjorth J. et al., 2003, *Nature*, 423, 847.

[62] Hurley K., *http://ssl.berkeley.edu/ipn3/biblionew.htm*.

[63] Iwamoto K. et al., 1998, *Nature*, 395, 672.

[64] Klebesadel R.W., Strong I.B. and Olson R.A., 1973, *ApJ*, 182, L85.

[65] Kouveliotou C. et al., 1993, *ApJ*, 413, L101.

[66] Kulkarni S.R. et al., 1998, *Nature*, 395, 663.

[67] Landau L.D. and Lifshitz E.M., *Course of Theoretical Physics - Volume 5: Statistical physics*, 3rd edition, Pergamon Press, 1980, section 63, 184.

[68] Landau L.D. and Lifshitz E.M., *Course of Theoretical Physics - Volume 6: Fluid Mechanics*, 2nd edition, paperback, 1995, Butterworth Heinemann, section 135, 510.

[69] MacFadyen A.I. and Woosley S.E., 1999, *ApJ*, 524, 262.

[70] Mao S. and Yi I., 1994, *ApJ*, 424, L131.

[71] Marshall F.E. and Swank J.H., 2003, GCN Circ. 1966.

[72] Marshall F.E., Markwardt C. and Swank J.H., 2003, GCN Circ. 2052.

[73] Mészáros P., 2002, *Annu. Rev. A&A*, 40, 137.

[74] Mészáros P., 2003, *Nature*, 423, 809.

[75] Mészáros P., Laguna P. and Rees M.J., 1993, *ApJ*, 415, 181.

[76] Mészáros P. and Rees M.J., 1993, *ApJ*, 405, 278.

[77] Mészáros P. and Rees M.J., 2000, *ApJ*, 530, 292.

[78] Mészáros P. and Rees M.J., 2000, *ApJ*, 541, L5.

[79] Mészáros P. and Rees M.J., 2001, *ApJ*, 556, L37.

[80] Nakar E. and Piran T., 2002, *MNRAS*, 330, 920.

[81] Norris J.P. et al., 1986, *ApJ*, 301, 213.

[82] Paczynski B. and Xu, G., 1994, *ApJ*, 427, 708.

[83] Paczynski B., 1998, *ApJ*, 494, L45.

[84] Panaitescu A. and Mészáros P., 1998, *ApJ*, 492, 683.

[85] Panaitescu A. and Mészáros P., 1998, *ApJ*, 501, 772.

[86] Pian E. et al., 1999, *ApJSS*, 138, 463.

[87] Pian E. et al., 2000, *ApJ*, 536, 778.

[88] Piran T., Shemi A. and Narayan R., 1993, *MNRAS*, 263, 861.

[89] Piran T., 1999, *Phys. Rep.*, 314, 575.

[90] Piran T., 2001, talk at 2000 Texas Meeting; preprint: astro-ph/0104134.

[91] Piran T., 2004; preprint: astro-ph/0405503.

[92] Piro L. et al., 1999, *ApJ*, 514, L73.

[93] Piro L. et al., 2000, *Science*, 290, 955.

[94] Preece R. D., Briggs M. S., Giblin T. W., Mallozzi R. S., Pendleton G. N., Paciesas W. S. and Band D. L., 2002, *ApJ*, 581, 1248.

[95] Preparata G., Ruffini R. and Xue S.-S., 2003, in *Proceedings of the VII Italian-Korean meeting*, ed. Journal of the Korean Physical Society, in press; preprint: astro-ph/0204080.

[96] Preparata G., Ruffini R. and Xue S.-S., 1998, *A&A*, 338, L87.

[97] Preparata G., Ruffini R. and Xue S.-S., *Il Nuovo Cimento*, Vol.115 B, N. 7-9, Luglio-Settembre 2000.

[98] Rees M.J., 1966, *Nature*, 211, 468.

[99] Rees M.J. and Mészáros P., 1994, *ApJ*, 430, L93.

[100] Rees M.J. and Mészáros P., 1998, *ApJ*, 496, L1.

[101] Ricker G.R., 2003, IAU Circ. 8101.

[102] Ruffini R., 1998, in "Black Holes and High Energy Astrophysics", Proceedings of the 49th Yamada Conference Ed. H. Sato and N. Sugiyama, Universal Ac. Press, Tokyo.

[103] Ruffini R., Bianco C.L., Chardonnet P., Fraschetti F. and Xue S.-S., 2001, *ApJ*, 555, L107.

[104] Ruffini R., Bianco C.L., Chardonnet P., Fraschetti F. and Xue S.-S., 2001, *ApJ*, 555, L113.

[105] Ruffini R., Bianco C.L., Chardonnet P., Fraschetti F. and Xue S.-S., 2001, *ApJ*, 555, L117.

[106] Ruffini R., Bianco C.L., Chardonnet P., Fraschetti F. and Xue S.-S., 2001, *Il Nuovo Cimento*, 116, 99.

[107] Ruffini R., Bianco C.L., Chardonnet P., Fraschetti F. and Xue S.-S., 2002, *ApJ*, 581, L19.

[108] Ruffini R., Bianco C.L., Chardonnet P., Fraschetti F. and Xue S.-S., 2003, *International Journal of Modern Physics D*, 12, 2, 173.

[109] Ruffini R., Bianco C.L., Chardonnet P., Fraschetti F., Vitagliano L. and Xue S.-S., *Proceedings of the* X *Brazilian School of Cosmology and Gravitation*, editors M. Novello, S.E. Perez Bergliaffa, AIP Conference proceedings 668, (2003), 16; pre-print: astro-ph/0302557.

[110] Ruffini R., Bianco C.L., Xue S.-S., Chardonnet P., Fraschetti F. and Gurzadyan V., 2004, *International Journal of Modern Physics D*, 13, 5, 843.

[111] Ruffini R., Bernardini M.G., Bianco C.L., Chardonnet P., Corsi A., Fraschetti F., Xue S.-S., in *Proceedings of the X Marcel Grossmann Meeting on General Relativity*, M. Novello, S.E. Perez-Bergliaffa, R. Ruffini (eds.), 2004, World Scientific, Singapore, in press.

[112] Ruffini R., Bernardini M.G., Bianco C.L., Chardonnet P., Fraschetti F., Xue S.-S., 2004, submitted to *ApJL.*.

[113] Ruffini R., Bianco C.L., Chardonnet P., Fraschetti F. and Xue S.-S., 2003, in "Proceedings of the 34^{th} COSPAR scientific assembly", - Houston, TX, USA, 2002, Pian, E., Masetti, N., Piro, L., editors, Elsevier, in press.

[114] Ruffini R., Bianco C.L., Chardonnet P., Fraschetti F., Gurzadyan V. and Xue S.-S., 2004, submitted to *ApJL.*

[115] Ruffini R., Bianco C.L., 2004, submitted to *A&A*.

[116] Ruffini R., Salmonson J.D., Wilson J.R. and Xue S.-S., 1999, *A&A* 350, 334; *A&A Suppl. Ser.*, 138, 511.

[117] Ruffini R., Salmonson J.D., Wilson J.R. and Xue S.-S., 2000, *A&A*, 359, 855.

[118] Ruffini R. and Vitagliano L., 2002, *Phys. Lett. B*, 545, 233.

[119] Ruffini R. and Vitagliano L., 2003, *International Journal of Modern Physics D*, 12, 121.

[120] Ruffini R., Vitagliano L. and Xue S.-S., 2003, *Phys. Lett. B*, 559, 12.

[121] Ruffini R., Vitagliano L. and Xue S.-S., 2003, *Phys. Lett. B*, 573, 33.

[122] Ruffini R., Fraschetti F., Vitagliano L. and Xue S.-S., 2004, *International Journal of Modern Physics D*, in press.

[123] Salmonson J.D., Wilson J.R. and Mathews G.J, 2001, *ApJ*, 553, 471.

[124] Sari R., 1997, *ApJ*, 489, L37.

[125] Sari R., 1998, *ApJ*, 494, L49.

[126] Sari R. and Piran T., 1997, *ApJ*, 485, 270.

[127] Sari R., Piran T. and Narayan, R., 1998, *ApJ*, 497, L17.

[128] Sari R., Piran T. and Halpern, J.P., 1999, *ApJ*, 519, L17.

[129] Sari R. and Mészáros P., 2000, *ApJ*, 535, L33.

[130] Schmidt M., 2001, *ApJ*, 559, L79.

[131] Schwinger J., 1951, *Phys. Rev.*, 82, 664.

[132] Singer S., Proceedings of the IEEE 53 December 1965, 1935.

[133] Stanek K.Z. et al., 2003, *ApJ*, 591, L17.

[134] Strong I.B. and Klebesadel R.W., 1976, *Sci. Am.* (October Issue, p.66).

[135] Taub A.H., 1948, *Phys. Rev.*, 74, 328.

[136] Tiengo A., Mereghetti S., Ghisellini G., Rossi E., Ghirlanda G. and Schartel N., 2003, *A&A*, 409, 983.

[137] Tavani M., 1998, *ApJ*, 497, L21.

[138] Usov V.V., 1992, *Nature*, 357, 472.

[139] van Paradijs J. et al., 1997, *Nature*, 386, 686.

[140] van Paradijs J., Kouveliotou C. and Wijers R.A.M.J., 2000, *Annu. Rev. A&A*, 38, 379.

[141] *"Vela Satellites Still Viewing Space"*, LANL Newsbulletin (18 Novembre 1983), p. 8.

[142] Vietri M. and Stella L., 1998, *ApJ*, 507, L45.

[143] Vietri M., 1998, *Phys. Rev. Lett.*, 80, 3690.

[144] Waxman E., 1995, *Phys. Rev. Lett.*, 75, 386.

[145] Waxman E., 1997, *ApJ*, 491, L19.

[146] Weinberg S., 1972, *"Gravitation and Cosmology"*, John Wiley & Sons, Inc., USA.

[147] Wheaton Wm.A. et al., 1973, *ApJ*, 185, L57.

[148] Wilson J.R., Mathews G.J., Marronetti P., 1996, *Phys. Rev. D*, 54, 1317.

[149] Woosley S.E., 1993, *ApJ*, 405, 273.

[150] Zel'dovich Ya.B. and Rayzer Yu.R., 1966, *Physics of shock waves and high-temperature hydrodynamic phenomena*, Ed. by Wallace D. Hayes and Ronald F. Probstein, Academic press (New York and London).

8 Appendix 1

THE ASTROPHYSICAL JOURNAL, 555:L107–L111, 2001 July 10

RELATIVE SPACETIME TRANSFORMATIONS IN GAMMA-RAY BURSTS

REMO RUFFINI, CARLO LUCIANO BIANCO, FEDERICO FRASCHETTI, AND SHE-SHENG XUE
International Center for Relativistic Astrophysics, Dipartimento di Fisica, Universita degli Studi di Roma "La Sapienza," Piazzale Aldo Moro 5, I-00185 Rome, Italy; ruffini@icra.it
AND
PASCAL CHARDONNET
Université de Savoie, Laboratoire d'Annecy-le-Vieux de Physique Théorique, Laboratoire d'Annecy-le-Vieux de Physique des Particules, BP 110, F-74941 Annecy-le-Vieux Cedex, France
Received 2000 November 28; accepted 2001 June 1; published 2001 June 29

ABSTRACT

GRB 991216 and its relevant data acquired from the BATSE and the *Rossi X-Ray Timing Explorer* and *Chandra* satellites are used as a prototypical case to test the theory linking the origin of gamma-ray bursts (GRBs) to the process of vacuum polarization occurring during the formation phase of a black hole endowed with electromagnetic structure. The relative spacetime transformation paradigm is presented. It relates the observed signals of GRBs to their past light cones, defining the events on the worldline of the source that is essential for the interpretation of the data. Since GRBs present regimes with unprecedentedly large Lorentz factors, and also sharply varying with time, particular attention is given to the constitutive equations relating the four time variables: the comoving time, the laboratory time, the arrival time, and the arrival time at the detector corrected by the cosmological effects. This paradigm is at the very foundation of any possible interpretation of the data of GRBs.

Subject headings: black hole physics — gamma rays: bursts — supernovae: general

In recent years, a large variety of very accurate experimental data, ranging from gamma rays all the way to the radio band, has been obtained for the afterglows of gamma-ray bursts (GRBs), following their first discovery by the *BeppoSAX* satellite (see, e.g., Costa 2001 and references therein). In the theoretical models of GRBs, there are currently three topics under debate:

1. The "internal shock model," introduced by Rees & Mészáros (1994), has many aspects that have been developed by Paczyński & Xu (1994), Sari & Piran (1997), Fenimore (1999), and Fenimore et al. (1999). The underlying assumption of this model is that all the variations of GRBs in the range $\Delta t \sim 1$ ms up to the overall duration T on the order of 50 s are determined by the "inner engine." The difficulties of explaining the long timescale bursts by a single explosive model have led us to create a class of models assuming an inner engine with prolonged activity (see, e.g., Piran 2001 and references therein).
2. The "external shock model," also introduced by Mészáros & Rees (1993), is less popular today. It relates the GRBs' light curves and time variations to interactions of a single, thin blast wave with clouds in the external medium. There is the distinct possibility, within this model, that the "GRBs' light curves are tomographic images of the density distribution of the medium surrounding the sources of GRBs" (Dermer & Mitman 1999; see also Dermer, Chiang, & Böttcher 1999, Dermer 2000, and references therein). In this case, the structure of the burst does not come directly from the inner engine.
3. In order to decrease the energy requirements of GRBs, the effect of beaming has been advocated (see, e.g., Mao & Yi 1994 and Davies et al. 1994). The possibility of inferring its existence from changes in the power-law index of the afterglow is generally considered attractive (see, e.g., Mészáros & Rees 1997a; Rhoads 1997, 1999; Mészáros, Rees, & Wijers 1998; Panaitescu, Mészáros, & Rees 1998; Dermer & Chiang 1999; Sari, Piran, & Halpern 1999; Panaitescu & Mészáros 1999; Halpern et al. 2000; Gou et al. 2001).

For the astrophysical nature of the system originating GRBs, a binary system of merging neutron stars has been proposed (see, e.g., Eichler et al. 1989; Narayan, Paczyński, & Piran 1992; Mészáros & Rees 1992a, 1992b). Problems occur (1) in the general energetics that cannot exceed $\sim 3 \times 10^{52}$ ergs, (2) in explaining the longer bursts (see Salmonson, Wilson, & Mathews 2001 and Wilson, Mathews, & Marronetti 1996), and (3) in the observed location of the GRBs' sources in star-forming regions (see Bloom, Kulkarni, & Djorgovski 2000). Alternatively, novel classes of astrophysical systems have been postulated, including black hole–white dwarf (Fryer et al. 1999) and black hole–neutron star binaries (Paczyński 1991; Mészáros & Rees 1997b) as well as hypernovae (see Paczyński 1998), failed supernovae and collapsars (see Woosley 1993 and MacFadyen & Woosley 1999), and supranovae (see Vietri & Stella 1998, 1999).

We take a somewhat intermediate approach by studying the GRBs emitted by the process of vacuum polarization around a black hole endowed with electromagnetic structure: the EMBH model. Such a model has the advantage that all of its basic intermediate theoretical background, starting with the process of gravitational collapse itself, has been developed. The model can therefore make precise predictions that can be compared with the observations.

In order to create a new interpretative paradigm, we consider a "prototypical" GRB case, which we then apply to the observations of other GRBs. Since some of the best data, from BATSE[1] to the *Rossi X-Ray Timing Explorer* (*RXTE*; Corbet & Smith 2000), as well as the remarkable accuracy of the *Chandra* (Piro et al. 2000) satellite, are available for GRB 991216, we use it as our prototype. In addition, (1) it is one of the strongest observed GRBs; (2) it radiates mainly in X-rays and gamma rays, and less than 3% is emitted in optical and radio bands; and (3) a precise value of the slope of the energy emission during the afterglow as a function of time,

[1] See http://gammaray.msfc.nasa.gov/~kippen/batserbr.

$n = -1.64$ (Takeshima et al. 1999) and $n = -1.616 \pm 0.067$ (Halpern et al. 2000), has been obtained.

The EMBH model relates the origin of the energy of GRBs to the extractable electromagnetic energy of an EMBH (Christodoulou & Ruffini 1971) via the vacuum polarization process occurring during the gravitational collapse leading to the formation of an EMBH (Damour & Ruffini 1975). The first step in this theory is the definition of the dyadosphere (Ruffini 1998; Preparata, Ruffini, & Xue 1998), which is an extended region outside the EMBH horizon formed of an optically thick plasma of electron-positron pairs and radiation whose energy $E_{\rm dya}$ is related to the mass $\mu = M/M_{\odot}$ and the electromagnetic parameter $\xi = Q/(M\sqrt{G})$ of the EMBH by the relation

$$E_{\rm dya} = \frac{Q^2}{2r_+}\left(1 - \frac{r_+}{r_{\rm ds}}\right)\left[1 - \left(\frac{r_+}{r_{\rm ds}}\right)^2\right], \quad (1)$$

where $r_+ = 1.47 \times 10^5 \mu\,[1 + (1 - \xi^2)^{1/2}]$ is the horizon radius and $r_{\rm ds} = 1.12 \times 10^8\,(\mu\xi)^{1/2}$ is the dyadosphere radius; as usual, M and Q are the mass energy and charge of the EMBH, and G is the Newton constant of gravity.

The evolution of this pair-electromagnetic (PEM) plasma leads to the formation of a sharp pulse (the PEM pulse) that very rapidly reaches a Lorentz factor of 10^2 and higher. The subsequent interaction of this pulse with the baryonic matter of the remnant, left over from the gravitational collapse of the protostar, and with the interstellar medium (ISM) leads to the different eras of the GRBs. It is useful to parameterize the baryonic mass M_B of the remnant by introducing the dimensionless parameter B:

$$M_B c^2 = BE_{\rm dya}. \quad (2)$$

The confrontation of the theoretical model with the observational data allows us to estimate the values of the EMBH parameters. It also allows us to probe the density of the baryonic material in the remnant, in the ISM, as well as in the stellar distribution within a few parsecs of the EMBH (see Ruffini et al. 2001b, 2001c).

The first step in this process is the establishment of the first set of constitutive equations relating (1) the comoving time of the pulse (τ), which is the time used to compute the evolution of the thermodynamical quantities (density, temperature); (2) the laboratory time (t), which is defined by an inertial reference frame in which the EMBH is at rest; (3) the arrival time (t_a), which is the laboratory time at which light signals from the source reach a distant observer at rest in the laboratory frame (the zero of the arrival time has been chosen to coincide with the arrival of the light signals from the moment of formation of the EMBH); and (4) the arrival time at the detector (t_a^d), which is the arrival time that takes into account the cosmological redshift of the GRB source.

We have

$$t_a^d = t_a(1 + z), \quad (3)$$

where z is the cosmological redshift of the GRB source (Ruffini et al. 2001a; C. L. Bianco, P. Chardonnet, F. Fraschetti, R. Jantzen, R. Ruffini, & S.-S. Xue 2001, in preparation). In the case of GRB 991216, we have $z \simeq 1.00$. The mutual relations of these four times with the radial coordinate in the laboratory frame is the subject of this Letter. We first give emphasis to a basic feature of the arrival time determination. For signals emitted by a pulse moving with velocity v in the laboratory frame, we have

$$\Delta t_a = \left(t_0 + \Delta t + \frac{R_0 - r}{c}\right) - \left(t_0 + \frac{R_0}{c}\right) = \Delta t - \frac{r}{c}, \quad (4)$$

where Δt_a (Δt) is the time interval in arrival (laboratory) time, R_0 is the distance of the observer from the EMBH, t_0 is the laboratory time corresponding to the gravitational collapse, and r is the radius of the expanding pulse at the time $t = t_0 + \Delta t$.

For simplicity, we abbreviate the interval notation Δt_a (Δt) by t_a (t). Equation (4) can then be rewritten as

$$t_a = t - \frac{r}{c} = t - \frac{\int_0^t v(t')dt' + r_{\rm ds}}{c}, \quad (5)$$

where the dyadosphere radius $r_{\rm ds}$ is the value of $r\,(t = 0)$. We consider only the photons emitted along the line of sight since the spreading due to the angular dependence and to the thickness of the pulse is negligible (C. L. Bianco, R. Ruffini, & S.-S. Xue 2001, in preparation). Neglecting $r_{\rm ds}$, the solution of equation (5),

$$t_a = t - \frac{v_0}{c}t - \frac{1}{2}\frac{a}{c}t^2 - \dots, \quad (6)$$

is in general highly nonlinear.

If and only if v is constant and $v \simeq c$, can equation (5) be rewritten, neglecting $r_{\rm ds}$, as

$$t_a \simeq t\left(1 - \frac{v}{c}\right) = t\frac{(1 - v/c)(1 + v/c)}{(1 + v/c)} \simeq \frac{t}{2\gamma^2}. \quad (7)$$

It is clear that the knowledge of t_a, which is indeed essential for any physical interpretation of GRB data, depends on a definite integral whose integration limits extend from the gravitational collapse to the time t relevant for the observations (see eq. [5]). Such an integral is *not* generally expressible as a simple linear relation or even by any explicit analytic relation since we are dealing with processes with variable Lorentz factors of unprecedented magnitude and time variability. Most studies have adopted an approximation of the kind given in equation (7) (see, e.g., Fenimore, Madras, & Nayakshin 1996). We instead use equation (5). The adoption of equation (7) misses a crucial feature of the GRB process and leads to a subversion of the spacetime relations in GRBs, with a wide range of consequences: all theoretical computations on the power-law indices of the afterglow are affected. Specific illustrative examples pointing out these differences are shown in the following paragraphs (see Ruffini et al. 2001a for details).

The bookkeeping of the four different times and the corresponding space variables must be done carefully in order to keep the correct causal relation in the time sequence of the events involved. This will also have important consequences in the supernova-GRB correlation (see Ruffini et al. 2001c).

The second set of constitutive equations are the full nonlinear relativistic hydrodynamic equations of energy and momentum conservation, which are to be solved together with the rate equation for the $e^{\pm}$ plasma. The computations carried out semianalytically in Rome have been validated by the full numerical computations performed using Wilson's codes at Livermore (see Ruffini et al. 1999a, 1999b, 2000, 2001a).

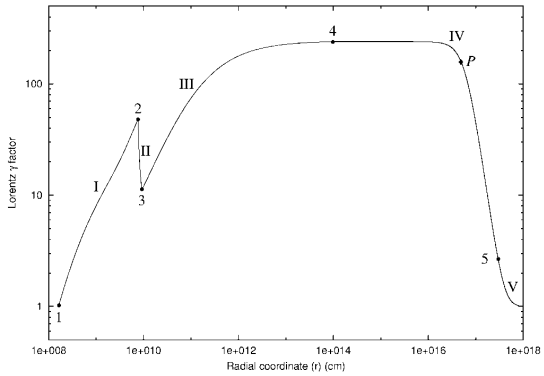

FIG. 1.—Theoretically computed Lorentz factor for the parameter values $E_{\rm dya} = 9.57 \times 10^{52}$ ergs and $B = 4 \times 10^{-3}$ given as a function of the radial coordinate in the laboratory frame. The corresponding values in the comoving time, laboratory time, and arrival time are given in Table 1. The different eras, indicated by roman numerals, are illustrated in the text, while the points 1, 2, 3, 4, and 5 mark the beginning and end of each of these eras. The point P marks the maximum of the afterglow flux (see Ruffini et al. 2001b). At point 4, the transparency condition is reached.

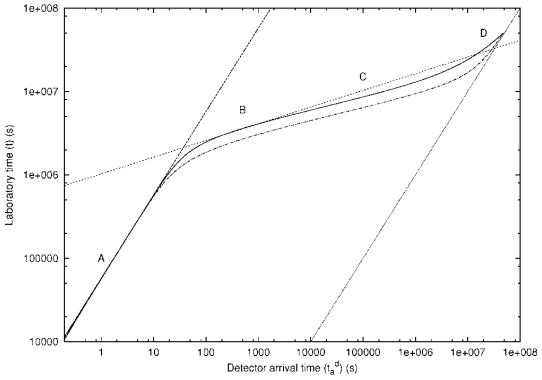

FIG. 2.—Relation between the arrival time (t_a^d) measured at the detector and the laboratory time (t) measured by an observer at rest in an inertial frame that is also at rest with the GRB source. The solid curve is computed using the exact formula given in eq. (5), incorporating as well the cosmological effects given in eq. (3), while the dash-dotted curve is the corresponding line obtained using the approximate formula given in eq. (7), computed with the time-varying γ given in Fig. 1. This is the approximation used by *all* recent works on GRBs. The difference is very conspicous, if one takes into account that the diagram is in logarithmic scale, and has basic consequences for the astrophysical scenario (see, e.g., Ruffini et al. 2001b, 2001c). We distinguish four different phases. In phase A, there is a linear relation between t and t_a^d. In phase B, there is an "effective" power-law relation between t and t_a^d (*dotted line*). In phase C, no single analytic formula holds; the relation between t and t_a^d can only be analyzed patchwise and has to be directly computed by the integration of the complete equations of energy and momentum conservation. In phase D, as the Lorentz factor approaches $\gamma = 1$, the relation between t and t_a^d asymptotically goes to $t = t_a^d$. Details are given in Ruffini et al. (2001a).

We have integrated both sets of constitutive field equations given in Ruffini et al. (1999a, 1999b, 2000) and Bianco, Ruffini, & Xue (2001) for the source GRB 991216. Correspondingly, we have obtained the parameter values presented in Ruffini et al. (2001b): $E_{\rm dya} \simeq 10^{53}$ ergs and $B = 4 \times 10^{-3}$. These values correspond to any of the following pairs of values for the EMBH mass and charge-to-mass ratio $(\mu, \xi) = (22.3, 0.1)$, (10.0, 0.15), and (5.5, 0.2).

Crucial to any GRB data interpretation is the relation of the Lorentz factor to the radial coordinate of the source in the laboratory frame and the corresponding values of the above four time parameters. In Figure 1, the γ factors for the different eras are given as a function of the radial coordinate of the source in the laboratory frame. Correspondingly, we present in Figure 2 the relation between the laboratory time and the detector arrival time for the source GRB 991216. The highly nonlinear behavior is obvious, and the different results obtained from the use of equations (6) and (7) are clearly visible. Details are given in Ruffini et al. (2001a).

In Table 1, for each successive "era" and for one very significant event, we give the initial and final values of the Lorentz factor, the four time parameters mentioned above, as well as the radial coordinates in the laboratory frame. We then have the following:

Era I.—The pair-electromagnetic plasma, initially at $\gamma = 1$, expands away from the EMBH horizon and from the dyadosphere as a pulse (the PEM pulse). In the comoving frame, the thickness of the pulse increases during the expansion, but the Lorentz contraction in the laboratory frame exactly balances this expansion so that, in the laboratory frame, a constant thickness approximation can be adopted for the burst (Ruffini et al. 1999a, 1999b). The expansion of the PEM pulse occurs in a region of very low baryonic contamination with density $\rho_B \ll 10^{-9}$ g cm^{-3} (Ruffini 2001). The final Lorentz factor and spacetime parameters are given for point 2 in Table 1.

Era II.—While the PEM pulse is still optically thick, it reaches the remnants left over by the gravitational collapse of the progenitor star. The engulfment of this baryonic material induces by conservation of energy and momentum a drastic reduction in the γ factor (Ruffini et al. 2000). The amount of baryonic matter in the remnant has been fixed by the determination of parameter B in the fitting of the afterglow data (see Ruffini et al. 2001b). Since these data contain important direct information on the progenitor star, we report in Table 2 some specific values of the parameters corresponding to selected values of the EMBH masses: they include the radius and thickness of the remnant as well as the density of baryonic matter. The

TABLE 1
LORENTZ FACTORS FOR SELECTED EVENTS AND THEIR SPACETIME COORDINATES

Point	r (cm)	τ (s)	t (s)	t_a (s)	t_a^d (s)	γ
1	1.610×10^{8}	0.0	0.0	0.0	0.0	1.00
2	7.659×10^{9}	1.985×10^{-2}	2.580×10^{-1}	1.846×10^{-3}	3.692×10^{-3}	48.38
3	9.153×10^{9}	2.292×10^{-2}	3.089×10^{-1}	2.780×10^{-3}	5.559×10^{-3}	11.38
4	9.692×10^{13}	14.23	3.295×10^{3}	6.805×10^{-2}	1.361×10^{-1}	239.6
P	4.863×10^{16}	7.784×10^{3}	1.653×10^{6}	11.86	23.72	160.2
5	2.958×10^{17}	1.082×10^{6}	9.989×10^{6}	1.2195×10^{5}	2.439×10^{5}	2.7

TABLE 2
BARYONIC MATTER OF THE REMNANT

M ($M_\odot$)	ξ	r_{ds}[a] ($\times 10^8$ cm)	r_{shell}[a] ($\times 10^9$ cm)	Δ_{shell}[a] ($\times 10^9$ cm)	ρ (g cm^{-3})
22.3	0.10	1.67	8.36	1.67	0.30
10.0	0.15	1.37	6.86	1.37	0.55
5.5	0.20	1.17	5.8	1.17	0.90

[a] In the laboratory frame.

results are largely independent of the thickness Δ of the remnants (Ruffini et al. 2000); they depend crucially only on the value B. The final Lorentz factor and spacetime parameters are given for point 3 in Table 1.

Era III.—A new pair-electromagnetic-baryonic (PEMB) pulse is formed that is composed of electron-positron pairs and baryons and electrons of the remnant material (a PEMB pulse). Since the opacity from Thomson scattering consequently increases, the process of the self-acceleration of the burst continues to even larger values of the Lorentz factor, which may reach values up to 10^3–10^4 in some sources (Ruffini et al. 2000). In the present case of GRB 991216, the maximum value reached is 239.6. It is remarkable that the constant thickness approximation for the pulse is still valid (Ruffini et al. 1999a, 1999b, 2000). This era ends at point 4 as the condition of transparency is reached. At that point, what we define here as the proper gamma-ray burst (P-GRB) is emitted (Ruffini et al. 1999a, 1999b, 2000; Bianco et al. 2001). This definition is assumed in order to distinguish the overall GRB phenomena from the specific emission occurring as the moment of transparency is reached. The shape, the intensity, and the duration of this P-GRB, also called in the literature the elementary spike (Bianco et al. 2001), strongly depend on the baryonic matter content (C. L. Bianco, R. Ruffini, & S.-S. Xue 2001, in preparation; Ruffini et al. 2001a). The final Lorentz factor and spacetime parameters are given for point 4 in Table 1.

These first three eras have no counterparts in earlier models since no detailed description of the early phases of GRB has been attempted.

Era IV.—The accelerated baryonic matter (ABM) expands still as a constant thickness pulse (the ABM pulse) at ultrarelativistic velocities and engulfs baryons and electrons from the ISM, which is assumed to have a constant number density n_{ism} of 1 proton cm^{-3}. We have assumed that all the internal energy made available by the relativistic conservation of energy and momentum is radiated away in the afterglow, mainly in gamma rays (~90%) and X-rays (~10%) and a few percent in the optical and radio emission (see Halpern et al. 2000). We have used the "fully radiative case" condition (see, e.g., Piran 1999), considering only the leading contribution of the head-on flux. We have neglected the spreading due to off-axis emission considered, e.g., in Fenimore et al. (1999) and have given physical reasons for neglecting such contributions (Ruffini et al. 2001a). At any specific time, the total flux, and consequently the bolometric luminosity of the afterglow, is fixed by the above requirements. The detailed spectral distribution depends on the dominant radiative processes of the internal energy. A variety of such processes have been considered in the literature, and their results within the context of our model are given in Ruffini et al. (2001a). In Figure 1, we show how, during this era, the Lorentz factor first coasts to a constant value and then rapidly decreases, going from $\gamma = 239.6$ to $\gamma = 2.7$. Most important is the point P where $\gamma \simeq 160.2$ corresponds to the peak of the afterglow (see Ruffini et al. 2001b). Beyond this point P, the slope of the afterglow flux, as a function of arrival time, approaches the power-law index $n = -1.6$ in perfect agreement with the observations of *RXTE* and *Chandra* (see Ruffini et al. 2001b). The final Lorentz factor and spacetime parameters are given for point 5 in Table 1. It is important to emphasize that this power-law index results from the combination of three critical assumptions: (1) the emission occurring in a "fully radiative" regime, (2) the condition of spherical symmetry, and (3) the constancy of the ISM density. Earlier results relevant to this treatment can be found in Sari (1997) and in Dermer et al. (1999) (see, for comparison and contrast, Ruffini et al. 2001a).

Era V.—This is the transition to the relativistic and nonrelativistic regimes. This era is more complex. It contains two successive suberas, one with a power-law index of the energy emitted in the afterglow as a function of the detector arrival time $n = -1.36$, corresponding to a still relativistic era ($1.1 \leq \gamma \leq 2.7$), and a final one approaching the pure Newtonian regime, with $n = -1.45$ and $\gamma < 1.1$. A contrast with existing slopes in the literature (see, e.g., Vietri 1997) are presented in Ruffini et al. (2001a). No data of GRB 991216 are available for checking the theoretical predictions of this last era.

In conclusion, we see from Table 1 and Figure 1 the remarkable and perfectly reasonable results that a motion of the pulse corresponding to a displacement of 9.692×10^{13} cm will correspond to an arrival time interval of 1.360×10^{-1} s, leading to what has been called apparent superluminal behavior. Similarly, on a larger scale, a displacement of the pulse by 2.958×10^{17} cm will correspond to an increment of 2.439×10^5 s in arrival time, leading again to apparently superluminal behavior.

From the above results, we are ready to express the relative spacetime transformation (RSTT) paradigm: the necessary condition for interpreting the GRB data, given in terms of the arrival time at the detector, is the knowledge of the *entire* worldline of the source from the gravitational collapse. In order to meet this condition, given a proper theoretical description and the correct constitutive equations, it is sufficient to know the energy of the dyadosphere and the mass of the remnant of the progenitor star (see Ruffini et al. 2001b). The application of this RSTT paradigm will have important consequences for the interpretation of the burst structure (IBS), leading to a new paradigm (the IBS paradigm; see Ruffini et al. 2001b), as well as for the GRB-supernova correlation (Ruffini et al. 2001c).

We thank three anonymous referees for their remarks, which have improved the presentation of this Letter.

REFERENCES

Bianco, C. L., Ruffini, R., & Xue, S.-S. 2001, A&A, 368, 377
Bloom, J. S., Kulkarni, S. R., & Djorgovski, S. G. 2000, ApJ, submitted (astro-ph/0010176)
Christodoulou, D., & Ruffini, R. 1971, Phys. Rev. D, 4, 3552
Corbet, R., & Smith, D. A. 2000, in Rossi2000: Astrophysics with the *Rossi X-Ray Timing Explorer* (Greenbelt: NASA), E97
Costa, E. 2001, in IX Marcel Grossmann Meeting on General Relativity, ed. V. Gurzadyan, R. Jantzen, & R. Ruffini (Singapore: World Scientific), in press
Damour, T., & Ruffini, R. 1975, Phys. Rev. Lett., 35, 463
Davies, M. B., Benz, W., Piran, T., & Thielemann, F. K. 1994, ApJ, 431, 742
Dermer, C. D. 2000, preprint (astro-ph/0005440)

Dermer, C. D., & Chiang, J. 1999, in ASP Conf. Ser. 161, High Energy Processes in Accreting Black Holes, ed. J. Poutanen & R. Svensson (San Francisco: ASP), 264
Dermer, C. D., Chiang, J., & Böttcher, M. 1999, ApJ, 513, 656
Dermer, C. D., & Mitman, K. E. 1999, ApJ, 513, L5
Eichler, D., Livio, M., Piran, T., & Schramm, D. N. 1989, Nature, 340, 126
Fenimore, E. E. 1999, ApJ, 518, 375
Fenimore, E. E., Cooper, C., Ramirez-Ruiz, E., Sumner, M. C., Yoshida, A., & Namiki, M. 1999, ApJ, 512, 683
Fenimore, E. E., Madras, C. D., & Nayakshin, S. 1996, ApJ, 473, 998
Fryer, C. L., Woosley, S. E., Herant, M., & Davies, M. B. 1999, ApJ, 520, 650
Gou, L. J., Dai, Z. G., Huang, Y. F., & Lu, T. 2001, A&A, 368, 464
Halpern, J. P., et al. 2000, ApJ, 543, 697
MacFadyen, A. I., & Woosley, S. E. 1999, ApJ, 524, 262
Mao, S., & Yi, I. 1994, ApJ, 424, L131
Mészáros, P., & Rees, M. J. 1992a, MNRAS, 257, 29P
———. 1992b, ApJ, 397, 570
———. 1993, ApJ, 405, 278
———. 1997a, ApJ, 476, 232
———. 1997b, ApJ, 482, L29
Mészáros, P., Rees, M. J., & Wijers, R. A. M. J. 1998, ApJ, 499, 301
Narayan, R., Paczyński, B., & Piran, T. 1992, ApJ, 395, L83
Paczyński, B. 1991, Acta Astron., 41, 257
———. 1998, ApJ, 494, L45
Paczyński, B., & Xu, G. 1994, ApJ, 427, 708
Panaitescu, A., & Mészáros, P. 1999, ApJ, 526, 707
Panaitescu, A., Mészáros, P., & Rees, M. J. 1998, ApJ, 503, 314
Piran, T. 1999, Phys. Rep., 314, 575
———. 2001, preprint (astro-ph/0104134)
Piro, L., et al. 2000, Science, 290, 955
Preparata, G., Ruffini, R., & Xue, S.-S. 1998, A&A, 338, L87
Rees, M. J., & Mészáros, P. 1994, ApJ, 430, L93
Rhoads, J. E. 1997, ApJ, 487, L1
———. 1999, ApJ, 525, 737
Ruffini, R. 1998, in Proc. 49th Yamada Conf., Black Holes and High Energy Astrophysics, ed. H. Sato & N. Sugiyama (Tokyo: Universal Academy Press), 167
———. 2001, in Proc. Joint CNR/ESO Meeting, Gamma-Ray Bursts in the Afterglow Era: Second Workshop, ed. E. Costa, F. Frontera, & J. Hjorth (Berlin: Springer), in press
Ruffini, R., Bianco, C. L., Chardonnet, P., Fraschetti, F., & Xue, S.-S. 2001a, A&A, submitted
Ruffini, R., Bianco, C. L., Fraschetti, F., Xue, S.-S., & Chardonnet, P. 2001b, ApJ, 555, L113
———. 2001c, ApJ, 555, L117
Ruffini, R., Salmonson, J. D., Wilson, J. R., & Xue, S.-S. 1999a, A&A, 350, 334
———. 1999b, A&AS, 138, 511
———. 2000, A&A, 359, 855
Salmonson, J. D., Wilson, J. R., & Mathews, G. J. 2001, ApJ, 553, 471
Sari, R. 1997, ApJ, 489, L37
Sari, R., & Piran, T. 1997, ApJ, 485, 270
Sari, R., Piran, T., & Halpern, J. P. 1999, ApJ, 519, L17
Takeshima, T., Markwardt, C., Marshall, F., Giblin, T., & Kippen, R. M. 1999, GCN Circ. 478 (http://gcn.gsfc.nasa.gov/gcn/gcn3/478.gcn3)
Vietri, M. 1997, ApJ, 478, L9
Vietri, M., & Stella, L. 1998, ApJ, 507, L45
———. 1999, ApJ, 527, L43
Wilson, J. R., Mathews, G. J., & Marronetti, P. 1996, Phys. Rev. D, 54, 1317
Woosley, S. E. 1993, ApJ, 405, 273

9 Appendix 2

THE ASTROPHYSICAL JOURNAL, 555:L113–L116, 2001 July 10

ON THE INTERPRETATION OF THE BURST STRUCTURE OF GAMMA-RAY BURSTS

REMO RUFFINI, CARLO LUCIANO BIANCO, FEDERICO FRASCHETTI, AND SHE-SHENG XUE
International Center for Relativistic Astrophysics, Dipartimento di Fisica, Universita degli Studi di Roma "La Sapienza," Piazzale Aldo Moro 5, I-00185 Rome, Italy; ruffini@icra.it
AND
PASCAL CHARDONNET
Université de Savoie, Laboratoire d'Annecy-le-Vieux de Physique Théorique, Laboratoire d'Annecy-le-Vieux de Physique des Particules, BP 110, F-74941 Annecy-le-Vieux Cedex, France
Received 2000 November 28; accepted 2001 June 1; published 2001 June 29

ABSTRACT

Given the very accurate data from the BATSE and the *Rossi X-Ray Timing Explorer* and *Chandra* satellites, we use GRB 991216 as a prototypical case to test the theory that links the origin of the energy of gamma-ray bursts (GRBs) to the extractable energy of electromagnetic black holes (EMBHs). The fit of the afterglow fixes the only two free parameters of the model and leads to a new paradigm for the interpretation of the burst structure (the IBS paradigm). It leads as well to a reconsideration of the relative roles of the afterglow and burst in GRBs by defining two new phases in this complex phenomenon: (1) the injector phase, giving rise to the proper GRB, and (2) the beam-target phase, giving rise to the extended afterglow peak emission and to the afterglow. Such differentiation leads to a natural possible explanation of the bimodal distribution of GRBs observed by BATSE. The agreement with the observational data in regions extending from the horizon of the EMBH all the way out to the distant observer confirms the uniqueness of the model.

Subject headings: black hole physics — gamma rays: bursts — supernovae: general

The most decisive tool in the identification of the energetics of gamma-ray bursts (GRBs) has been the discovery by *BeppoSAX* of the afterglow phenomenon. In this Letter, we show how the afterglow data can be fitted using the theory that relates the GRB energy to the extraction process of the electromagnetic energy of a black hole endowed with electromagnetic structure (the EMBH model). This energy extraction process occurs via vacuum polarization pair creation and approaches almost perfect reversibility in the sense of black hole physics (Christodoulou & Ruffini 1971; Damour & Ruffini 1975; Preparata, Ruffini, & Xue 1998).

In addition to yielding excellent agreement between the theory and the data, a new paradigm will be introduced here for the interpretation of the burst structure that we call the IBS paradigm. Because of the unique accuracy of its data, we use GRB 991216 as a prototype for a description that may then be generalized to other GRBs. The relevant data for GRB 991216 are reproduced in Figure 1, namely, the data on the burst as recorded by BATSE[1] and the data on the afterglow from the *Rossi X-Ray Timing Explorer* (*RXTE*; Corbet & Smith 2000) and *Chandra* satellites (Piro et al. 2000; see also Halpern et al. 2000). We have modeled the afterglow by assuming that, after reaching transparency, the ultra–high-energy baryons (the accelerated baryonic matter [ABM] pulse of Ruffini et al. 2001c), accelerated in the pair-electromagnetic-baryonic (PEMB) pulse following a black hole collapse process (see Ruffini et al. 2001c), interact with the interstellar medium (ISM), which is assumed to have an average density $n_{\rm ism}$ of 1 proton cm^{-3}. All of the internal energy that developed in the collision is assumed to be radiated away in a "fully radiative" regime (Bianco et al. 2001a).

In our model, there are only two free parameters characterizing the EMBH: the mass M in units of solar mass ($\mu = M/M_\odot$) and the charge-to-mass ratio $\xi = Q/(M\sqrt{G})$, where M and Q are the mass energy and charge of the EMBH and G is Newton's gravitational constant. These two quantities are related to the total energy of the dyadosphere ($E_{\rm dya}$) through the EMBH mass-energy formula (Christodoulou & Ruffini 1971; Preparata et al. 1998) as follows:

$$E_{\rm dya} = \frac{Q^2}{2r_+}\left(1-\frac{r_+}{r_{\rm ds}}\right)\left[1-\left(\frac{r_+}{r_{\rm ds}}\right)^2\right], \quad (1)$$

where $r_+ = 1.47 \times 10^5 \mu\,[1 + (1 - \xi^2)^{1/2}]$ is the horizon radius and $r_{\rm ds} = 1.12 \times 10^8\,(\mu\xi)^{1/2}$ is the dyadosphere radius. This energy is the source of the burst ($E_{\rm burst}$) and afterglow ($E_{\rm aft}$) energies

$$E_{\rm dya} = E_{\rm burst} + E_{\rm aft}. \quad (2)$$

The only remaining free parameters describe the amount and location of the baryonic matter left over in the collapse process of the precursor star of initial radius $\sim 10^{10}$ cm that forms the EMBH (see Ruffini et al. 2000). The amount of baryonic matter can be parameterized by the dimensionless parameter $B = (M_B c^2)/E_{\rm dya}$. As discussed in Ruffini et al. (2001c), the results are quite insensitive to the actual density of the baryonic component, but they are very sensitive to the value of B (Ruffini et al. 2000).

In Figure 2, we present some of the results of fitting the data from the *RXTE* and *Chandra* satellites; these results correspond to an EMBH mass of 22.3 $M_\odot$ and are for selected values of the parameters ξ and B. The main conclusions from our model are as follows:

1. The slope of the afterglow, $n = -1.6$, is rather insensitive to the values of the parameters μ, ξ, and B and is in perfect agreement with the observational data. The physical reason for this universality of the slope is essentially related to the ultrarelativistic energy of the baryons in the ABM pulse, the

[1] See http://gammaray.msfc.nasa.gov/~kippen/batserbr.

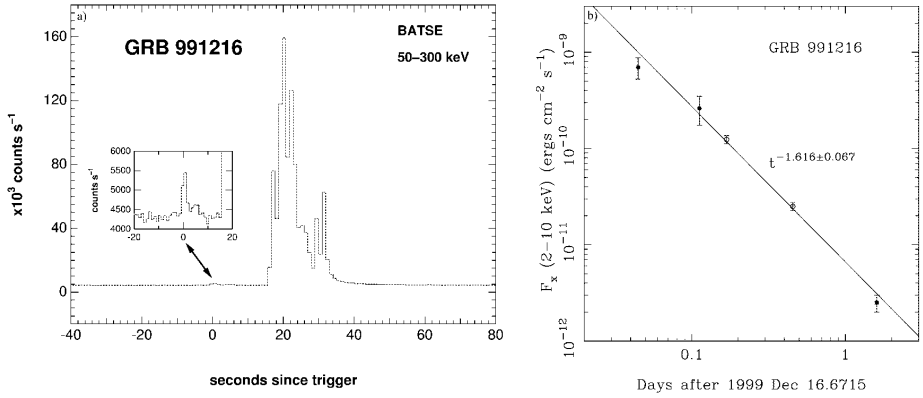

FIG. 1.—(*a*) Data on GRB 991216 obtained by BATSE (reproduced from BATSE Rapid Burst Response; see footnote 1) and (*b*) the corresponding data for the afterglow from both *RXTE* and *Chandra* (the last point after 10^5 s) given as a function of the detector arrival time (reproduced from Halpern et al. 2000).

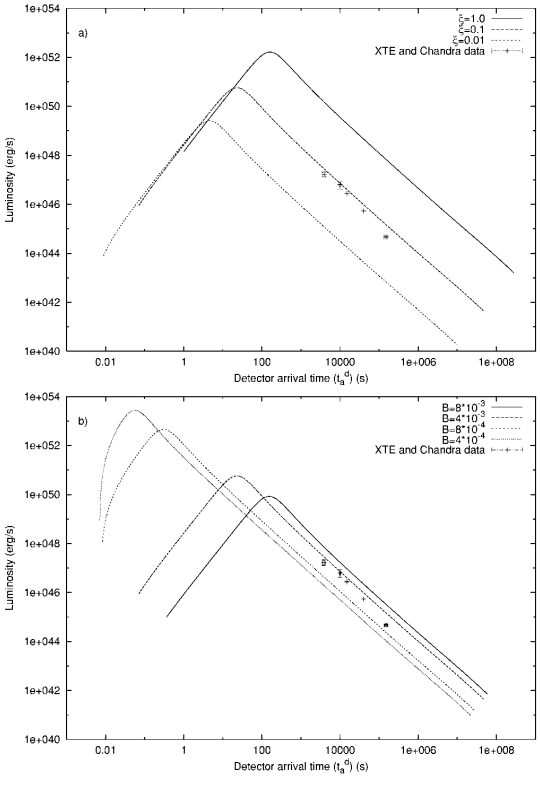

FIG. 2.—(*a*) Afterglow luminosity computed for an EMBH of 22.3 $M_\odot$ and $B = 4 \times 10^{-3}$ for three selected values of the electromagnetic parameter: $\xi = 0.01$, 0.1, and 1.0. (*b*) For the same EMBH mass and $\xi = 0.1$, we give the afterglow luminosities corresponding, respectively, to $B = 4 \times 10^{-4}$, 8×10^{-4}, 4×10^{-3}, and 8×10^{-3}.

assumption of a constant average density in the ISM, the fully radiative conditions leading predominantly to the X-ray emission, as well as all the different relativistic effects presented in the relative spacetime transformation (RSTT) paradigm (for details, see Ruffini et al. 2001b).

2. The afterglow fit does not depend on all three parameters μ, ξ and B but only on the combinations $E_{\rm dya}$ and B. Thus, there is a one-parameter family of values of the pair (μ, ξ) allowed by a given viable value of $E_{\rm dya}$.

3. It is clear from studying both the profiles and the time dependence of the afterglow that by suitably modifying the values of B and ξ, the average flux of the main burst observed by BATSE can also be fitted by the afterglow curve, up to the degeneracy in (μ, ξ), leading to (see Fig. 3)

$$E_{\rm dya} = 9.57 \times 10^{52} \text{ ergs}, \quad B = 4 \times 10^{-3}. \tag{3}$$

The peak of the average afterglow emission occurs at ~23.7 s, and its intensity and timescale are in excellent agreement with the BATSE observations, which is an important result (see also Ruffini et al. 2001a). In addition to the BATSE data, there is clearly also perfect agreement with the decaying part of the afterglow data from the *RXTE* and *Chandra* satellites. It is clear that such an extended afterglow peak emission (E-APE) is *not* a burst, but it is seen as such by BATSE because of the background noise level in this observation (see also Ruffini et al. 2001a). Thus, the long-standing unsolved problem of explaining the long GRBs (see, e.g., Wilson, Mathews, & Marronetti 1996; Salmonson, Wilson, & Mathews 2001; Piran 2001) is radically resolved. After we fix the free parameters of the EMBH theory, modulo the mass-charge relationship that fixes $E_{\rm dya}$, all other features of the observations must be explained by the theory.

A natural question can be asked: Where does one find the burst that is emitted when the condition of transparency against Thomson scattering is reached? We refer to this as the proper gamma-ray burst (P-GRB) in order to distinguish it from the

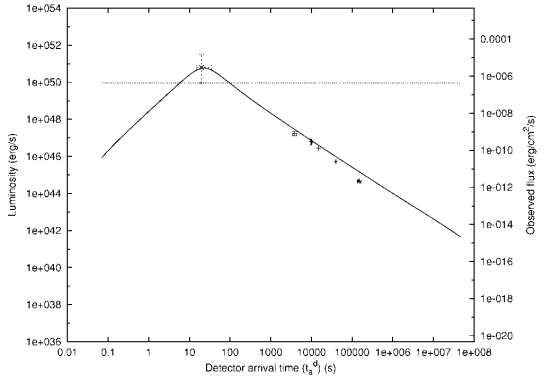

FIG. 3.—Best fit of the afterglow data of *Chandra* and *RXTE* as well as of the range of variability of the BATSE data on the major burst by a unique afterglow curve leading to the parameter values $E_{\rm dya} = 9.57 \times 10^{52}$ ergs and $B = 4 \times 10^{-3}$. The horizontal dotted line indicates the background noise of this observation. On the left axis, the luminosity is given in units of the energy emitted at the source, while the right axis gives the flux as received by the detectors.

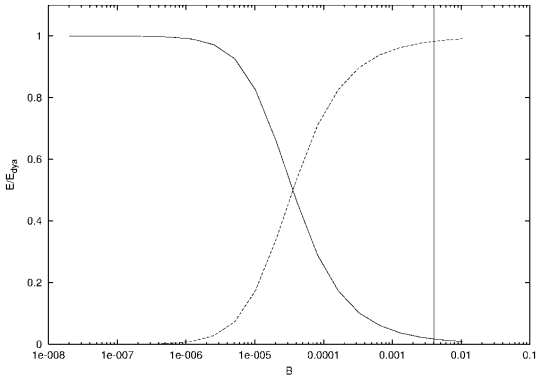

FIG. 4.—Relative intensities of the afterglow (*dashed line*) and the P-GRB (*solid line*), as predicted by the EMBH model corresponding to the values of the parameters determined in Fig. 3, as a function of *B*. Details are given in (Bianco et al. 2001a). The vertical line corresponds to the value $B = 4 \times 10^{-3}$.

global GRB phenomena (see Ruffini et al. 2001c and Bianco, Ruffini, & Xue 2001b). Ruffini et al. (2000) show that, for a fixed value of $E_{\rm dya}$, a value of B uniquely determines the energy of the P-GRB, which we indicate by $E_{\rm burst}$, and the energy of the afterglow $E_{\rm aft}$ (see Fig. 4). For the particular values of the parameters given in equation (3), we then predict that

$$\frac{E_{\rm burst}}{E_{\rm dya}} = 1.45 \times 10^{-2};$$
$$E_{\rm burst} = 1.39 \times 10^{51} \text{ ergs}; \quad (4)$$
$$E_{\rm dya} = 9.57 \times 10^{52} \text{ ergs}.$$

Is there any evidence of such a signal in the BATSE data? From the RSTT paradigm presented in Ruffini et al. (2001c), we can retrace such a P-GRB by reading off the time parameters of point 4 in Figure 1 from Table 1, both of which are found in Ruffini et al. (2001c). The transparency is reached at 14.23 s in comoving time, at a radial coordinate $r = 9.692 \times 10^{13}$ cm in the laboratory frame and at 1.361×10^{-1} s in arrival time at the detector. All this, namely, the energy predicted in equation (4) for the intensity of the burst and its time of arrival, leads to the unequivocal identification of the P-GRB with the apparently inconspicuous initial burst in the BATSE data. We have estimated the ratio of the first peak (the P-GRB) to the E-APE over the background noise level of the BATSE data to be $\sim 10^{-2}$, in very good agreement with the first entry in equation (4).

In summary, the observational data agree with the predictions of the model on (1) the intensity ratio, 1.45×10^{-2}, between the P-GRB and the E-APE, which strongly depends on the parameter B; (2) the absolute intensity of 1.39×10^{51} and 9.43×10^{52} ergs for the P-GRB and the E-APE, respectively, which depends on $E_{\rm dya}$; and (3) the arrival time of 1.361×10^{-1} and 23.7 s for the P-GRB and the peak of the E-APE, respectively. Without the introduction of any new parameter, the model offers additional information on the detailed structure of both the P-GRB and the E-APE.

Regarding the P-GRB spectrum, the initial energy of the electron-positron pairs and photons in the dyadosphere for given values of the parameters can be easily computed following the work of Preparata et al. (1998). We obtain $T = 1.95$ and $T = 29.4$ MeV, respectively, in the two approximations that we have used (Bianco et al. 2001a): for a given $E_{\rm dya}$, we have assumed either a constant average energy density over the entire dyadosphere volume or a more compact configuration with an energy density equal to the peak value. It is then possible to follow, in the laboratory frame, the time evolution of the temperature of the electron-positron pairs and photons through the different eras presented in Ruffini et al. 2001c (see Fig. 5). The condition of transparency is reached at temperatures in the range of ~15–55 keV at the detector, in agreement with the BATSE results.

Regarding the E-APE, all of the above considerations refer to the smoothed average emission. It is interesting to note that the detailed structure of the E-APE observed by BATSE can

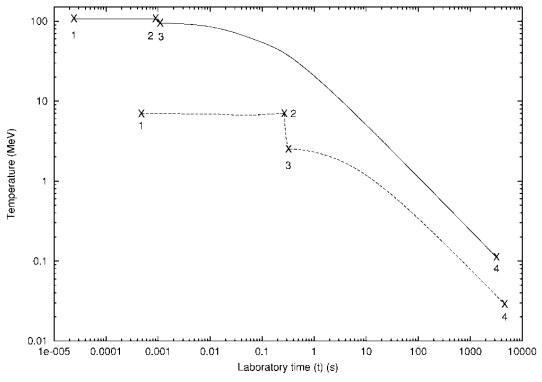

FIG. 5.—Temperature of the pulse in the laboratory frame for the first three eras of Fig. 1 of Ruffini et al. (2001c) given as a function of the laboratory time. The numbers 1, 2, 3, and 4 represent the beginning and end of each era. The two curves refer to two extreme approximations adopted in the description of the dyadosphere. Details are given in Ruffini et al. (2000) and Bianco et al. (2001a).

also be reproduced in the model in terms of relativistic effects and deviations from the average value of the ISM density due to inhomogeneities (Ruffini et al. 2001a, 2001b; R. Ruffini, C. Cherubini, L. Vitagliano, & S.-S. Xue 2001, in preparation).

We can now proceed to the formulation of the IBS paradigm: in GRBs, we can distinguish an *injector phase* and a *beam-target phase*. The injector phase includes the process of the gravitational collapse of a progenitor star into an EMBH, the formation of the dyadosphere and the associated phenomena of vacuum polarization, as well as the different eras presented in Ruffini et al. (2001c): era I corresponds to the pair-electromagnetic pulse, era II to the engulfment of the baryonic matter of the remnant, and era III to the PEMB pulse. The injector phase terminates at the point where the plasma transparency condition is reached and the P-GRB is emitted. The beam-target phase addresses the interaction of the ABM pulse, namely, the beam generated during the injection phase, with the ISM as the target. It gives rise to the E-APE and the decaying part of the afterglow.

We advance the possibility, to be verified on the basis of the time variabilities and spectral information mentioned above (Bianco et al. 2001b; R. Ruffini, C. Cherubini, L. Vitagliano, L., & S.-S. Xue 2001, in preparation), that the P-GRBs coincide with the class of short events (<2 s) discovered in the bimodal distribution of GRBs in the BATSE catalog (Kouveliotou et al. 1993), while the E-APEs coincide with the class of longer events (>2 s).

It is interesting to note that, even in this very energetic case of GRB 991216, the general energetic requirement can be easily fulfilled by an EMBH with $M = 22.3\ M_{\odot}$ and $\xi = 0.1$. No beaming is needed, and no evidence of beaming is obtained by the fitting of the theory and the observational data, contrary to views expressed by, e.g., Halpern et al. (2000). See Ruffini et al. (2001b) for details.

As the EMBH model is confirmed by additional sources, the GRBs will be used to scan the regions around the newly formed EMBHs, to infer their physical and astrophysical composition as well as to acquire information on the process of gravitational collapse leading to the EMBH and on the astrophysical structures in the high-redshift universe. The first clear intuition of such a possibility has been expressed by Dermer & Mitman (1999). We will give a first application of such a "tomographic" imaging technique in Ruffini et al. (2001d).

We conclude as follows:

1. In the range of distances (see Ruffini et al. 2001c, Table 1) $r \simeq 10^{14}$–10^{17} cm from the EMBH, information on the ISM, $\bar{\rho} \simeq 10^{-24}$ g cm^{-3}, and on the surrounding additional astrophysical systems can be inferred from the E-APE and from the afterglow (see Ruffini et al. 2001a, 2001b, 2001d).

2. At a distance $r \simeq 10^{10}$ cm, where $\bar{\rho} \simeq 1$ g cm^{-3} (see Ruffini et al. 2001c, Table 2), we can evaluate the percentage of mass of the progenitor star left in the remnant by the process of gravitational collapse. In fact, we have (see Bianco et al. 2001a)

$$M_B c^2 = BE_{\rm dya} \simeq \frac{1}{4} B\xi^2 c^2 M_{\rm BH}, \tag{5}$$

which, in the case of GRB 991216, implies that up to 99.9% of the matter of the progenitor star collapses into the EMBH. This indicates that the gravitational collapse into a black hole differs markedly from the corresponding process occurring in the formation of neutron stars (Bianco et al. 2001a).

3. At $r < r_{\rm ds} \simeq 10^{8}$ cm, the electrodynamical constraints imply that $\bar{\rho} < 10^{-9}$ g cm^{-3}, thus avoiding baryonic contamination in the dyadosphere. This condition can be easily satisfied during the gravitational collapse into an EMBH as the horizon is approached. The details of such a process, with all its general relativistic effects, can be followed through the structure of the P-GRB (R. Ruffini, C. Cherubini, L. Vitagliano, & S.-S. Xue 2001, in preparation).

The IBS paradigm that we have introduced is common to a number of models based on a single process of gravitational collapse, leading to GRBs. The uniqueness of the EMBH model resides (1) in the energetics (Ruffini 1998), (2) in the time structure of the P-GRB (R. Ruffini, C. Cherubini, L. Vitagliano, & S.-S. Xue 2001, in preparation; R. Ruffini, L. Vitagliano, & Xue, S.-S. 2001, in preparation), and (3) in the spectral information of the P-GRB (Bianco et al. 2001a).

The fact that the model is testable from the ISM all the way down to the horizon of the EMBH offers an unprecedented tool for proving its uniqueness, confirming that we are witnessing the formation of EMBHs and the extraction of their electromagnetic energy through the resulting GRBs. The intrinsic simplicity of the EMBH model of GRBs, which is shown here to depend on only two parameters, offers an unique opportunity to use GRBs as "standard candles" in cosmology.

We thank three anonymous referees for their remarks, which have improved the presentation of this Letter.

REFERENCES

Bianco, C. L., Chardonnet, P., Fraschetti, F., Ruffini, R., & Xue, S.-S. 2001a, A&A, submitted
Bianco, C. L., Ruffini, R., & Xue, S.-S. 2001b, A&A, 368, 377
Christodoulou, D., & Ruffini, R. 1971, Phys. Rev. D, 4, 3552
Corbet, R., & Smith, D. A. 2000, in Rossi2000: Astrophysics with the *Rossi X-Ray Timing Explorer* (Greenbelt: NASA), E97
Damour, T., & Ruffini, R. 1975, Phys. Rev. Lett., 35, 463
Dermer, C. D., & Mitman, K. E. 1999, ApJ, 513, L5
Halpern, J. P., et al. 2000, ApJ, 543, 697
Kouveliotou, C., Meegan, C. A., Fishman, G. J., Bhat, N. P., Briggs, M. S., Koshut, T. M., Paciesas, W. S., & Pendleton, G. N. 1993, ApJ, 413, L101
Piran, T. 2001, preprint (astro-ph/0104134)
Piro, L., et al. 2000, Science, 290, 955
Preparata, G., Ruffini, R., & Xue, S.-S. 1998, A&A, 338, L87
Ruffini, R. 1998, in Proc. 49th Yamada Conf., Black Holes and High Energy Astrophysics, ed. H. Sato & N. Sugiyama (Tokyo: Universal Academy Press), 167
Ruffini, R., Bianco, C. L., Chardonnet, P., Fraschetti, F., & Xue, S.-S. 2001a, Nuovo Cimento B, 116, 99
———. 2001b, A&A, submitted
Ruffini, R., Bianco, C. L., Fraschetti, F., Xue, S.-S., & Chardonnet, P. 2001c, ApJ, 555, L107
———. 2001d, ApJ, 555, L117
Ruffini, R., Salmonson, J. D., Wilson, J. R., & Xue, S.-S. 2000, A&A, 359, 855
Salmonson, J. D., Wilson, J. R., & Mathews, G. J. 2001, ApJ, 553, 471
Wilson, J. R., Mathews, G. J., & Marronetti, P. 1996, Phys. Rev. D, 54, 1317

10 Appendix 3

THE ASTROPHYSICAL JOURNAL, 555:L117–L120, 2001 July 10

ON A POSSIBLE GAMMA-RAY BURST–SUPERNOVA TIME SEQUENCE

REMO RUFFINI, CARLO LUCIANO BIANCO, FEDERICO FRASCHETTI, AND SHE-SHENG XUE
International Center for Relativistic Astrophysics, Dipartimento di Fisica, Universita degli Studi di Roma "La Sapienza," Piazzale Aldo Moro 5, I-00185 Rome, Italy; ruffini@icra.it

AND

PASCAL CHARDONNET
Université de Savoie, Laboratoire d'Annecy-le-Vieux de Physique Théorique, Laboratoire d'Annecy-le-Vieux de Physique des Particules, BP 110, F-74941 Annecy-le-Vieux Cedex, France
Received 2000 November 28; accepted 2001 June 1; published 2001 June 29

ABSTRACT

The data from the *Chandra* satellite on the iron emission lines in the afterglow of GRB 991216 are used to give further support to the theory that links the origin of the energy of gamma-ray bursts (GRBs) to the extractable energy of electromagnetic black holes (EMBHs), leading to an interpretation of the GRB-supernova correlation. Following the relative spacetime transformation paradigm and the interpretation of the burst structure paradigm, we introduce a paradigm for the correlation between GRBs and supernovae. The following sequence of events is shown as kinematically possible and consistent with the available data: (1) the GRB-progenitor star P_1 first collapses into an EMBH; (2) the proper GRB and the peak of the afterglow (the extended afterglow peak emission) propagate in interstellar space until the impact on a supernova-progenitor star P_2 at a distance $\leq 2.69 \times 10^{17}$ cm, and they induce the supernova explosion; and (3) the accelerated baryonic matter pulse, originating the afterglow, reaches the supernova remnants 18.5 hr after the supernova explosion and gives rise to the iron emission lines. Some considerations of the dynamical implementation of the paradigm are presented. The concept of an induced supernova explosion, introduced here specifically for the GRB-supernova correlation, may have a more general application in relativistic astrophysics.

Subject headings: black hole physics — gamma rays: bursts — supernovae: general

We have seen in the previous two Letters how the fit of the data from the *Rossi X-Ray Timing Explorer* (Corbet & Smith 2000) and *Chandra* (Piro et al. 2000) satellites on the afterglow of GRB 991216 offers a tool for determining the only two free parameters of the electromagnetic black hole (EMBH) theory. This theory links the energy source of gamma-ray bursts (GRBs) to the electromagnetic mass energy of black holes (Christodoulou & Ruffini 1971). We have also seen how this theory has consequences for the interpretation of the structure of GRBs (the interpretation of the burst structure [IBS] paradigm; see Ruffini et al. 2001d). The same analysis also yields information about the density and overall distribution of the baryonic matter in the remnant left over from the gravitational collapse of the GRB-progenitor star into an EMBH (see Ruffini et al. 2001c, 2001d; see also R. Ruffini, C. Cherubini, & L. Vitagliano, & S.-S. Xue 2001, in preparation). Similarly, it allows one to probe the density distribution of the interstellar matter around the newly formed EMBH (see, e.g., Ruffini 2001 and Ruffini et al. 2001a).

The aim of this Letter is to point out that the data on the iron lines of GRB 991216 from the *Chandra* satellite (Piro et al. 2000) and similar observations from other sources (Piro et al. 1999, 2000; Amati et al. 2000) make it possible to extend this analysis to a larger distance scale, possibly all the way out to a few light years, and consequently probe the distribution of stars in the surroundings of the newly formed EMBH. These considerations lead to a new paradigm for the interpretation of the supernova-GRB correlation.

That indeed a correlation between the occurrence of GRBs and supernova events exists has been established by the works of Bloom et al. (1999), Galama et al. (1998a, 1998b, 2000), Kulkarni et al. (1998), Piro et al. (1998), Pian et al. (1999), Reichart (1999), and van Paradijs, Kouveliotou, & Wijers (2000). Such an association has been assumed to indicate that GRBs are generated by supernovae explosions (see, e.g., Kulkarni et al. 1998).

We propose that, if relativistic effects are properly taken into account, then an alternative, kinematically viable explanation can be given of the supernova-GRB association. We again use GRB 991216 as a prototypical case. The same theoretical considerations have also been applied to other cases, including GRB 980425 and SN 1998BW (R. Ruffini, C. L. Bianco, P. Chardonnet, F. Fraschetti, & S.-S. Xue 2001, in preparation).

We focus on the detailed kinematical description of this GRB-supernova time-sequence process and outline a possible dynamical scenario. We introduce a process by which a massive GRB-progenitor star P_1 of mass M_1 undergoes gravitational collapse into an EMBH. During this process, a dyadosphere is formed, and subsequently the proper gamma-ray burst (P-GRB) and the extended afterglow peak emission (E-APE) of Ruffini et al. (2001d) are generated in sequence (see also Ruffini et al. 2001c). They propagate and impact, with their photon and neutrino components, on a second supernova-progenitor star P_2 of mass M_2. Assuming that both stars were generated approximately at the same time, we expect to have $M_2 < M_1$. For a wide range of parameters, such a collision will not affect the star M_2 (P. Chardonnet & R. Ruffini 2001, in preparation). Under some special conditions of the thermonuclear evolution of the supernova-progenitor star P_2, the collision can *induce a supernova explosion.*

We assume that the star P_2 is close to the line of sight of the EMBH. We will see in the following that this gives an upper limit to the distance $D_{P_2} = 2.69 \times 10^{17}$ cm of the supernova-progenitor star P_2 from the EMBH. The location of the star P_2 will then be constrained between the transparency point of the P-GRB, 9.692×10^{13} cm (see Ruffini et al. 2001c), and

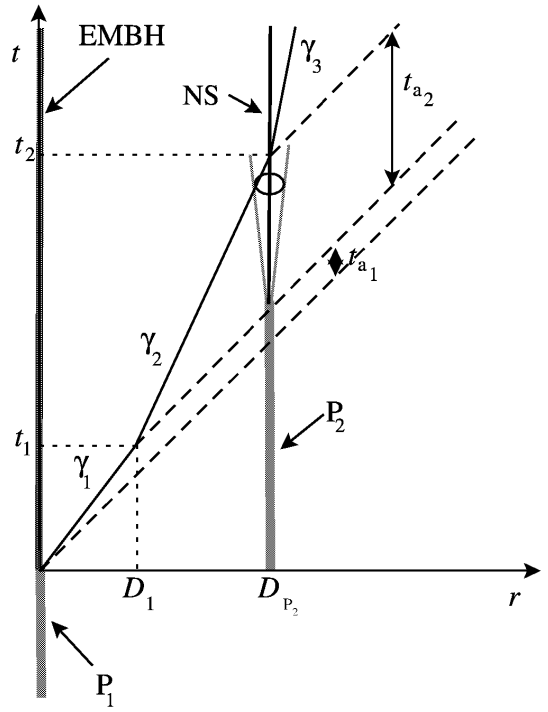

FIG. 1.—Qualitative simplified spacetime diagram (in arbitrary units) illustrating the GSTS paradigm. The EMBH, originating from the gravitational collapse of a massive GRB-progenitor star P_1, and the massive supernova-progenitor star P_2–neutron star (P_2-NS) system, separated by a radial distance D_{P_2}, are assumed to be at rest in the laboratory frame. Their worldlines are represented by two parallel vertical lines. The supernova shell, moving at $0.1c$ and generated by the P_2-NS transition, is represented by the dotted line cone. The solid line represents the motion of the pulse, as if it would move with an effective Lorentz factor $\gamma_1 \simeq 110.0$ during the eras reaching the condition of transparency. Similarly, the effective Lorentz factor $\gamma_2 \simeq 5.82$ applies during era IV up to the collision with the P_2-NS system. An effective Lorentz factor $\gamma_3 < 2$ occurs during era V after the collision as the nonrelativistic regime of expansion is reached (see Ruffini et al. 2001b). The dashed lines at 45° represent signals propagating at the speed of light.

the above upper limit, and will be a function of the angle subtended by the line of sight and the star P_2, as seen from the EMBH. The energy momentum deposited by the GRB in the collision with the star is in the range of 10^{39}–10^{45} ergs (R. Ruffini, C. L. Bianco, P. Chardonnet, F. Fraschetti, & S.-S. Xue 2001, in preparation).

Especially relevant to our model are the following data from the *Chandra* satellite (see Piro et al. 2000):

1. At the arrival time of 37 hr after the initial burst, there is evidence of iron emission lines for GRB 991216.

2. The emission lines are present during the entire observation period of 10^4 s. The iron lines could also have been produced earlier, before *Chandra* was observing. Thus, the times used in these calculations are not unique: they do serve to provide an example of the scenario.

3. The emission lines appear to have a peak at an energy of 3.49 ± 0.06 keV that, at a redshift $z = 1.00 \pm 0.02$, corresponds to a hydrogen-like iron line at 6.97 keV at rest. This source does not appear to have any significant motion departing from the cosmological flow. The iron lines have a width of 0.23 keV consistent with a radial velocity field of $0.1c$.

From the theoretical slope of the afterglow, presented in Ruffini et al. (2001d), we see that the flux of the afterglow observed by *Chandra* is in excellent agreement with the general afterglow slopes. Clearly, the iron lines are only a small fraction of the observed flux.

We assume that the laboratory frame is an inertial system of reference in which both stars P_1 and P_2 are at rest. A second asymptotic inertial reference frame is assumed in which the detector is at rest. Therefore, a detector arrival time t_a^d is defined that is related to the laboratory time t by

$$t_a^d = (1+z)t_a = (1+z)\left[t - \frac{r(t)}{c}\right], \qquad (1)$$

where z is the cosmological redshift, which, in the case of GRB 991216, is equal to $z = 1.0$, and $r(t)$ is the radius of the expanding pulse at laboratory time t.

To explain the above observations, we propose that the expansion of the accelerated baryonic matter (ABM; see Ruffini et al. 2001c), relativistically expanding away from a newly formed EMBH, reaches P_2 with a delay in arrival time of 18.5 hr (the details of the computation are given in Bianco et al. 2001a). The associated afterglow then illuminates the expanding supernova shell, producing the observed iron emission lines. The *Chandra* satellite observations then offer the first data on such an induced supernova explosion (Piro et al. 2000).

On the basis of the explicit computations of the different eras presented in Ruffini et al. (2001c), we make three key points:

1. An arrival time of 37 hr in the detector frame corresponds to a radial distance from the EMBH traveled by the ABM pulse of 2.69×10^{17} cm in the laboratory frame (see Ruffini et al. 2001c).

2. It is likely that a few stars are present within that radius as members of a cluster. It has become evident from observations of dense clusters of star-forming regions that a stellar average density of typically 10^2 pc^{-3} (Beck, Turner, & Kovo 2000) should be expected. There is also the distinct possibility for this case and other systems that the stars P_1 and P_2 are members of a detached binary system.

3. The possible observations at different wavelengths (R. Ruffini, C. L. Bianco, P. Chardonnet, F. Fraschetti, & S.-S. Xue 2001, in preparation) crucially depend on the relative intensities between the GRB and the supernova as well as on the value of the distance and the redshift of the source.

In order to reach an intuitive understanding of these complex computations, we present a very simplified schematic diagram (not to scale) in Figure 1. We now describe the specific data of this GRB-supernova time-sequence (GSTS) paradigm:

1. The two stars P_1 and P_2 are separated by a distance $D_{P_2} = 2.69 \times 10^{17}$ cm in the laboratory frame (see Fig. 1). Both stars are at rest in the inertial laboratory frame. At laboratory time $t = 0$ and at comoving time $\tau = 0$, the gravitational collapse of the GRB-progenitor star P_1 occurs. The initial emission of gravitational radiation or a neutrino burst from the event then synchronizes the arrival times $t_a = 0$ for the supernova-progenitor star P_2 and $t_a^d = 0$ for the distant observer at rest with the detector. The electromagnetic radiation emitted by the gravitational collapse process is instead practically zero, by comparison,

because of the optical thickness of the material at this stage (Bianco, Ruffini, & Xue 2001b).

2. From the determination of the parameters obtained in Ruffini et al. (2001d) and the computations in Ruffini et al. (1999a, 1999b, 2000) at laboratory time $t_1 = 3.295 \times 10^3$ s and at a distance from the EMBH of $D_1 = 9.692 \times 10^{13}$ cm, the condition of transparency for the pair-electromagnetic-baryon (PEMB) pulse is reached, and the P-GRB is emitted (see Fig. 1 and Ruffini et al. 2001c, 2001d). This time is recorded in the arrival time at the detector $t^d_{a_1} = 0.1361$ s and, at P_2, at $t_{a_1} = 6.805 \times 10^{-2}$ s.

The fact that the PEMB pulse in an arrival time of 0.1361 s covers a distance of 9.692×10^{13} cm gives rise to an apparent superluminal effect. In order to clarify this apparent inconsistency, we have introduced, from the computed values of t_1 and $t^d_{a_1}$, an "effective" Lorentz factor

$$\gamma \equiv \sqrt{\frac{t}{2t^d_a}}, \tag{2}$$

which gives $\gamma_1 \simeq 110.0$. Then we can straightforwardly explain the difference between the two times as $t^d_a = t/(2\gamma^2)$ (see Fig. 1).

This introduction of an effective Lorentz factor has no predictive power; it can only be introduced a posteriori as an heuristic tool in order to draw the qualitative diagram in Figure 1. In practice, the entire integration of the equations must be accomplished by taking into account all changes of the time-varying Lorentz factors and the corresponding space and time variables throughout each era (for details, see Bianco et al. 2001a and Ruffini et al. 2001b).

3. At laboratory time $t = 1.653 \times 10^6$ s and at a distance from the EMBH of 4.863×10^{16} cm in the laboratory frame, the peak of the E-APE is reached that is recorded at the arrival time $t_a = 11.86$ s at P_2 and $t^d_a = 23.72$ s at the detector. This also gives rise to an apparent superluminal effect that can also be explained by following the same arguments given above in point 2. This event has not been represented in Figure 1 so as not to confuse the image.

4. At a distance $D_{P_2} = 2.69 \times 10^{17}$ cm, the two bursts described in the above points 2 and 3 collide with the supernova-progenitor star P_2 at arrival times $t_{a_1} = 6.805 \times 10^{-2}$ s and $t_a = 11.86$ s, respectively. They can then induce the supernova explosion of the massive star P_2.

5. The associated supernova shell expands with velocity $0.1c$.

6. The expanding supernova shell is reached by the ABM pulse generating the afterglow with a delay of $t_{a_2} = 18.5$ hr in arrival time following the arrival of the P-GRB and the E-APE. This time delay coincides with the interval of laboratory time separating the two events since the P_2 is at rest in the inertial laboratory frame (see Fig. 2).

Again, as explained above in point 2, this time delay can be interpreted a posteriori by introducing (Bianco et al. 2001a) an effective Lorentz factor defined by

$$\gamma \equiv \sqrt{\frac{D_{P_2}}{2ct_{a_2}}}, \tag{3}$$

which gives $\gamma \simeq 8.21$. Then we can heuristically visualize the time delay as $t^d_{a_2} = D_{P_2}/(2c\gamma^2)$. Clearly, the results presented in Figure 2 do follow the complete integration of the equations of motion of the system through each different era defined in Ruffini et al. (2001c). The ABM pulse will have travelled in the laboratory frame a distance $D_{P_2} - D_1 \simeq D_{P_2} = 2.69 \times 10^{17}$ cm in a laboratory time $t_2 - t_1 \simeq t_2 = 9.02 \times 10^6$ s (neglecting the supernova expansion).

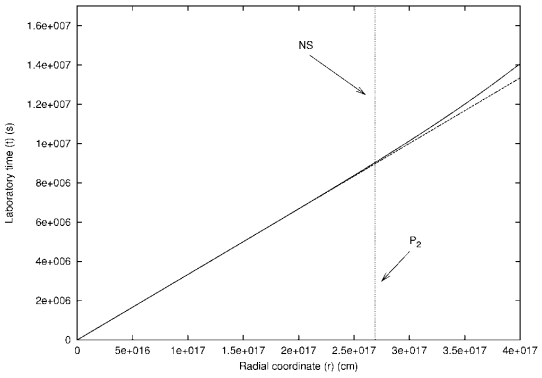

FIG. 2.—The spatial radial coordinates of the P-GRB and the peak of the afterglow radiation flux (represented by a single dotted line in this approximation), and of the pulse (represented by the solid line), as computed through the different eras presented in Ruffini et al. (2001c), using the results of Ruffini et al. (1999a, 2000) and Bianco et al. (2001a), are given as a function of the time in the laboratory frame. The vertical dotted line corresponds to the radial position of the supernova-progenitor massive star P_2, $D_{P_2} = 2.69 \times 10^{17}$ cm, which undergoes a supernova explosion after the collision with the P-GRB and the peak of the afterglow. The delay between the arrival time of the P-GRB, traveling at the speed of light, and the pulse, traveling with a Lorentz factor $\gamma \simeq 3.38$ (see Ruffini et al. 2001c) at the moment of collision with the supernova-progenitor star P_2, is $t_{a_2} = 18.5$ hr, namely, $t^d_{a_2} = 37$ hr.

This again gives rise to an apparent superluminal effect that can be interpreted heuristically, as in point 2, as a relativistic motion of the ABM pulse with an effective Lorentz factor of $\gamma_2 \simeq 5.82$ (see Fig. 1). The era IV extends from the point of transparency (point 4 in Fig. 1 of Ruffini et al. 2001c) all the way to the collision of the pulse with the supernova shell, which occurs at $\gamma \simeq 3.38$. By this time, the supernova shell has reached a dimension of 1.997×10^{14} cm, which is consistent with the observations from the *Chandra* satellite.

In the above considerations of GRB 991216, the supernova remnant has been assumed to be close to, but not exactly along, the line of sight extending from the EMBH to the distant observer. However, such a case should exist for other GRBs and would lead to an observation of iron absorption lines as well as to an increase in the radiation observed in the afterglow corresponding to the crossing of the supernova shell by the ABM pulse. In fact, as the ABM pulse engulfs the baryonic matter of the remnant, above and beyond the normal interstellar medium baryonic matter, the conservation of energy and momentum implies that a larger amount of internal energy is available and radiated in the process (Ruffini et al. 2001a). This increased energy momentum loss will generally affect the slope of the afterglow decay, approaching more rapidly a nonrelativistic expansion phase (details are give in Ruffini et al. 2001b).

If we now turn to the possibility of dynamically implementing the scenario, there are at least three different possibilities:

1. Particularly attractive is the possibility that a massive star P_2 has rapidly evolved during its thermonuclear evolution to a white dwarf (see, e.g., Chandrasekhar 1978). It is then sufficient

that the P-GRB and the E-APE implode the star sufficiently so as to reach a central density above the critical density for the ignition of thermonuclear burning. Consequently, the explosion of the star P_2 occurs, and a significant fraction of a solar mass of iron is generated. These configurations are currently generally considered precursors of some Type I supernovae (see, e.g., Filippenko 1997 and references therein).

2. Alternatively, the massive star P_2 could have evolved into a condition where it was close to the point of gravitational collapse, having developed the formation of an iron-silicon core, Type II supernova. The above transfer of energy momentum from the P-GRB and the E-APE may enhance the capture of the electrons on the iron nuclei and consequently decrease the Fermi energy of the core, leading to the onset of gravitational instability (see, e.g., Bethe 1991, p. 270). Since the time for the final evolution of a massive star with an iron-silicon core is short, this event will perhaps require an unlikely coincidence.

3. The pressure wave may trigger a massive and instantaneous nuclear-burning process, with corresponding changes in the chemical composition of the star, leading to the collapse.

The GSTS paradigm has been applied to the case of the correlation between SN 1998bw and GRB 980425, which, with a redshift of 0.0083, is one of the closest and weakest GRBs observed. In this case, the EMBH appears to have a significantly lower value of the parameter ξ, but the validity of the GSTS paradigm presented here is fully confirmed (R. Ruffini, C. L. Bianco, P. Chardonnet, F. Fraschetti, & S.-S. Xue 2001, in preparation).

The GSTS paradigm and the concept of *induced supernova explosion*, which we have introduced for the collapse into an EMBH, may also play a role in the case of a collapse of a white dwarf core into a neutron star in a binary system. It may solve the long-standing problem of the approximate equality of neutron star masses observed in some binary pulsars (see, e.g., Taylor & Weisberg 1989).

We thank three anonymous referees and J. Wilson for their remarks, which have improved the presentation of this Letter.

REFERENCES

Amati, L., et al. 2000, Science, 290, 953
Beck, S. C., Turner, J. L., & Kovo, O. 2000, AJ, 120, 244
Bethe, H. A. 1991, The Road from Los Alamos (New York: AIP)
Bianco, C. L., Chardonnet, P., Fraschetti, F., Ruffini, R., & Xue, S.-S. 2001a, A&A, submitted
Bianco, C. L., Ruffini, R., & Xue, S.-S. 2001b, A&A, 368, 377
Bloom, J. S., et al. 1999, Nature, 401, 453
Chandrasekhar, S. 1978, in Physics and Astrophysics of Neutron Stars and Black Holes, ed. R. Giacconi & R. Ruffini (Amsterdam: North-Holland), 1
Christodoulou, D., & Ruffini, R. 1971, Phys. Rev. D, 4, 3552
Corbet, R., & Smith, D. A. 2000, in Rossi2000: Astrophysics with the *Rossi X-Ray Timing Explorer* (Greenbelt: NASA), E97
Filippenko, A. V. 1997, ARA&A, 35, 309
Galama, T. J., et al. 2000, ApJ, 536, 185
———. 1998a, IAU Circ. 6895
———. 1998b, Nature, 395, 670
Kulkarni, S. R., et al. 1998, Nature, 395, 663
Pian, E., et al. 1999, A&AS, 138, 463
Piro, L., Butler, R. C., Fiore, F., Antonelli, A., & Pian, E. 1998, GCN Circ. 155 (http://gcn.gsfc.nasa.gov/gcn/gcn3/155.gcn3)
Piro, L., et al. 1999, ApJ, 514, L73
———. 2000, Science, 290, 955
Reichart, D. E. 1999, ApJ, 521, L111
Ruffini, R. 2001, in Proc. Joint CNR/ESO Meeting, Gamma-Ray Bursts in the Afterglow Era: Second Workshop, ed. E. Costa, F. Frontera, & J. Hjorth (Berlin: Springer), in press
Ruffini, R., Bianco, C. L., Chardonnet, P., Fraschetti, F., & Xue, S.-S. 2001a, Nuovo Cimento B, 116, 99
———. 2001b, A&A, submitted
Ruffini, R., Bianco, C. L., Fraschetti, F., Xue, S.-S., & Chardonnet, P. 2001c, ApJ, 555, L107
———. 2001d, ApJ, 555, L113
Ruffini, R., Salmonson, J. D., Wilson, J. R., & Xue, S.-S. 1999a, A&A, 350, 334
———. 1999b, A&AS, 138, 511
———. 2000, A&A, 359, 855
Taylor, J. H., & Weisberg, J. M. 1989, ApJ, 345, 434
van Paradijs, J., Kouveliotou, C., & Wijers, R. A. M. J. 2000, ARA&A, 38, 379

11 Appendix 4

IL NUOVO CIMENTO Vol. 116 B, N. 1 Gennaio 2001

On the physical processes which lie at the bases of time variability of GRBs

R. Ruffini([1])(*), C. L. Bianco([1]), P. Chardonnet([2])([1])
F. Fraschetti([1]) and She-Sheng Xue([1])

([1]) *ICRA - International Center for Relativistic Astrophysic and Physics Department Università di Roma "La Sapienza" - P.le Aldo Moro 5, I-00185 Roma, Italy*
([2]) *Université de Savoie, LAPTH LAPP - BP110, 74941 Annecy-le-Vieux Cedex, France*

(ricevuto il 9 Febbraio 2001; approvato il 26 Febbraio 2001)

Summary. — The relative-space-time-transformation (RSTT) paradigm and the interpretation of the burst-structure (IBS) paradigm are applied to probe the origin of the time variability of GRBs. Again GRB 991216 is used as a prototypical case, thanks to the precise data from the CGRO, RXTE and Chandra satellites. It is found that with the exception of the relatively inconspicuous but scientifically very important signal originating from the initial "proper gamma ray burst" (P-GRB), all the other spikes and time variabilities can be explained by the interaction of the accelerated-baryonic-matter pulse with inhomogeneities in the interstellar matter. This can be demonstrated by using the RSTT paradigm as well as the IBS paradigm, to trace a typical spike observed in arrival time back to the corresponding one in the laboratory time. Using these paradigms, the identification of the physical nature of the time variablity of the GRBs can be made most convincingly. It is made explicit the dependence of a) the intensities of the afterglow, b) the spikes amplitude and c) the actual time structure on the Lorentz gamma factor of the accelerated-baryonic-matter pulse. In principle it is possible to read off from the spike structure the detailed density contrast of the interstellar medium in the host galaxy, even at very high redshift.

PACS 04.70 – Physics of black holes.
PACS 04.62 – Quantum field theory in closed space time.
PACS 12.20 – Quantum electrodynamics.
PACS 95.30 – Fundamental aspects of astrophysics.
PACS 98.38 – Interstellar medium (ISM) and nebulae in Milky Way.

It is well known that one of the most successful cognitive tools in relativistic astrophysics has been the analysis of the time structure of signals received at a variety of wavelengths. Time variabilities, however, have not always been of significance in relativistic astrophysics. In the case of pulsars, for example, only the period of the average

(*) E-mail: ruffini@icra.it

pulsar signal and its monotonic lengthening with time have been essential in identifying pulsars as rotating neutron stars (Hewish, Bell, *et al.* (1977) [9]). Furthermore, the modulations of the pulsar signal, periodic in time, have been essential for the identification of binary pulsars and to give the first evidence for gravitational waves (Hulse and Taylor (1975) [11]). The secular variation of the shape of the pulse yields information relating the role of the spin of the neutron star and its angular momentum to additional general relativistic effects (Damour and Ruffini (1974) [7], Kramer (2001) [12]). Even in this very successful example, there is a broad range of effects connected to pulsars whose role in relativistic astrophysics and fundamental physics is null. We quote, as an example, the well known time delay in the arrival time of pulsar signals, inversely proportional to the square of the radiation frequency of observation, see, *e.g.* Rees *et al.* (1975) [17] page 26. Such an effect is *not* due to the mass of the photon, as one might have hoped for fundamental physics reasons (see, *e.g.*, Ohanian and Ruffini (1994) [10], page 117), but simply due to the dispersion by the electrons in interstellar plasma.

In approaching the analysis of GRB signals it is similarly essential to untangle information about the astrophysical system producing the GRBs, which is certainly in the realm of relativistic astrophysics, from other parts of the signal, also of similar magnitude and structure, which can instead be traced back to the environment in which the astrophysical process occurs and in that sense may very well belong to the domain of classical astronomy.

In the last decade an enormous number of papers have been written trying to link all the structures observed by the BATSE experiment on the CGRO satellite to the intrinsic properties of an unknown GRB source, whose properties should be determined, hopefully, by those observations. In the "internal shock models" of GRBs, which are currently very popular, it is assumed that *every spike* in the burst in the range $\Delta t \sim 1$ s to ~ 50 s is directly related to the physical properties of the "inner engine" (see, *e.g.*, Piran (2001) [13] and references therein). The fact that it is difficult to explain the long bursts has led the theorists working on the "internal shock model" to introduce a new family of models, in which the source of GRBs has a prolongued action in time. We shall see below that a simpler and very different explanation can be found.

The electromagnetic black hole (EMBH) model (Ruffini (1998) [18], Preparata, *et al.* (1998a) [15], Preparata, *et al.* (1998b) [16]) relates the origin of the energy of GRBs to the extractable electromagnetic energy of an EMBH [5] via the vacuum polarization process occurring during the gravitational collapse leading to the formation of an EMBH [8]. The first step in this theory is the definition of the dyadosphere [18, 15], an extended region outside the EMBH horizon formed of an optically thick plasma of electron-positron pairs and radiation whose energy $E_{\rm dya}$ is related to the mass $\mu = M/M_\odot$ and electromagnetic parameter $\xi = Q/\left(M\sqrt{G}\right)$ of the EMBH by the relation:

$$E_{\rm dya} = \frac{Q^2}{2\,r_+}\left(1 - \frac{r_+}{r_{\rm ds}}\right)\left[1 - \left(\frac{r_+}{r_{\rm ds}}\right)^2\right], \tag{1}$$

where $r_+ = 1.47 \times 10^5 \mu(1 + \sqrt{1-\xi^2})$ is the horizon radius and $r_{\rm ds} = 1.12 \times 10^8 \sqrt{\mu\xi}$ is the dyadosphere radius and, as usual, M and Q are the mass-energy and charge of the EMBH and G is the Newton constant of gravity.

The evolution of this pair-electromagnetic plasma leads to the formation of a sharp pulse (the PEM pulse) that very rapidly reaches a Lorentz gamma factor of 10^2 and

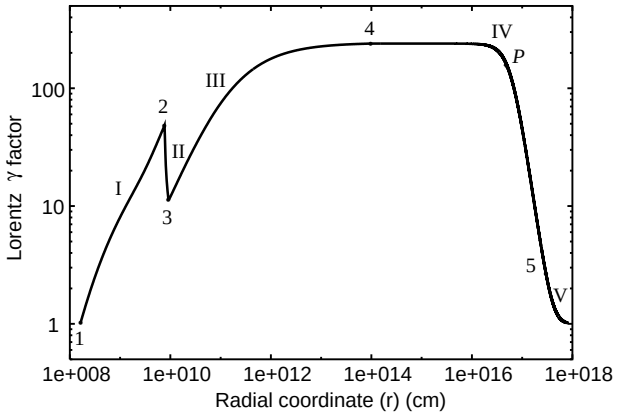

Fig. 1. – The Lorentz gamma factor corresponding to the different eras of GRB991216 is given as a function of the radial distance from the EMBH. Details in Letter 1.

higher. The subsequent interaction of this pulse with the baryonic matter of the remnant, left over from the gravitational collapse of the protostar, and with the interstellar medium (ISM) leads to the different eras of the GRBs. It is useful to parametrize the baryonic mass M_B of the remnant by introducing the dimensionless parameter B:

$$M_B c^2 = B E_{\rm dya} \ . \tag{2}$$

The confrontation of the theoretical model with the observational data allows an estimate for the values of the EMBH parameters. It also allows us to probe the density of the baryonic material in the remnant, in the ISM as well as in the stellar distribution within a few parsecs of the EMBH (see [22, 23]).

In Ruffini, *et al.* (2001a) [21] we presented the relative-space-time-transformation (RSTT) paradigm, leading to the diagram relating the Lorentz gamma factor of the pulse to the space and time parametrization both in the comoving and in the laboratory frame for the case of GRB 991216 (see fig. 1). In Ruffini, *et al.* (2001b) [22] we introduced the interpretation of the burst-structure (IBS) paradigm, presenting a drastic separation between the proper-gamma-ray burst (P-GRB) and the E-APE, the "not burst component of the GRB", see fig. 2.

It is important to stress that the results obtained in the IBS paradigm are of general validity for a variety of GRB sources based on a single gravitational collapse event. What makes the EMBH model uniqueness testable are:

– the energetics [18],

– the time structure of the P-GRB [25],

– the spectral information of the P-GRB [3].

Once again we use GRB 991216 as a prototypical case due to the excellent data from the BATSE (BATSE Rapid Burst Response (1999) [1]), RXTE (Corbet and Smith (2000)

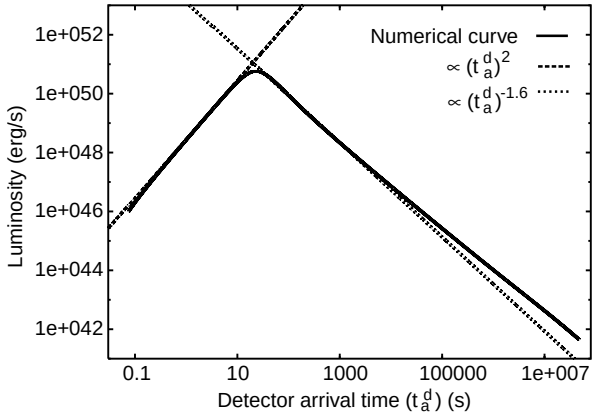

Fig. 2. – The flux of the afterglow of GRB991216, as computed using the best fit of the data obtained in Letter 2, is given as a function of the arrival time. The dashed (dotted) line corresponds to eq. (6) (eq. (9)) in the text.

[6]) and CHANDRA (Piro, *et al.* (2000) [14]) satellites, although the conclusions will be applicable to all GRBs. In a certain sense, in this paradigm all the features of a GRB are divided in two very distinct phases:

– the first, prior to decoupling and ending with emission of the P-GRB, which we shall call the "injector phase";

– the second, the "beam-target" phase, in which the accelerated-baryonic-matter (ABM) pulse (the beam) interacts with the interstellar medium (the target).

The P-GRB, which is clearly identifiable in the enlargement in fig. 3a, is emitted when the condition of transparency is reached by the pair-electromagnetic-baryonic matter-pulse, the PEMB pulse. As already stressed Ruffini, *et al.* (2001b) [22], the properties of the P-GRB are directly linked (Ruffini, *et al.* (1999) [19], Ruffini, *et al.* (2000) [20], Bianco, *et al.* (2001) [2], Ruffini, *et al.* (2001g) [25]) to the internal properties of the GRB source and to the detailed structure and energy distribution in the dyadosphere of the EMBH (Ruffini (1998) [18], Preparata, *et al.* (1998a) [15], Preparata, *et al.* (1998b) [16]). These results are essential in identifying the extractable energy of the EMBH, introduced in Christodoulou and Ruffini (1971) [5], as the GRB energy source. The operational tool of the energy extraction process is the vacuum polarization process introduced in Damour and Ruffini (1975) [8]. Similarly the intensity ratio of the P-GRB to the afterglow gives a precise measurement of the matter left in the remnant during the process of gravitational collapse of the progenitor star to the EMBH, see Ruffini, *et al.* (2000) [20] and Ruffini, *et al.* (2001b) [22] and references therein.

All the above results clearly involve relativistic astrophysics. Let us now turn to the afterglow and apply the RSTT and IBS paradigms in order to understand its detailed time structure.

The afterglow is emitted as the ABM pulse plows through the interstellar matter engulfing new baryonic material (Ruffini, *et al.* (2001f) [24]). In our previous works we

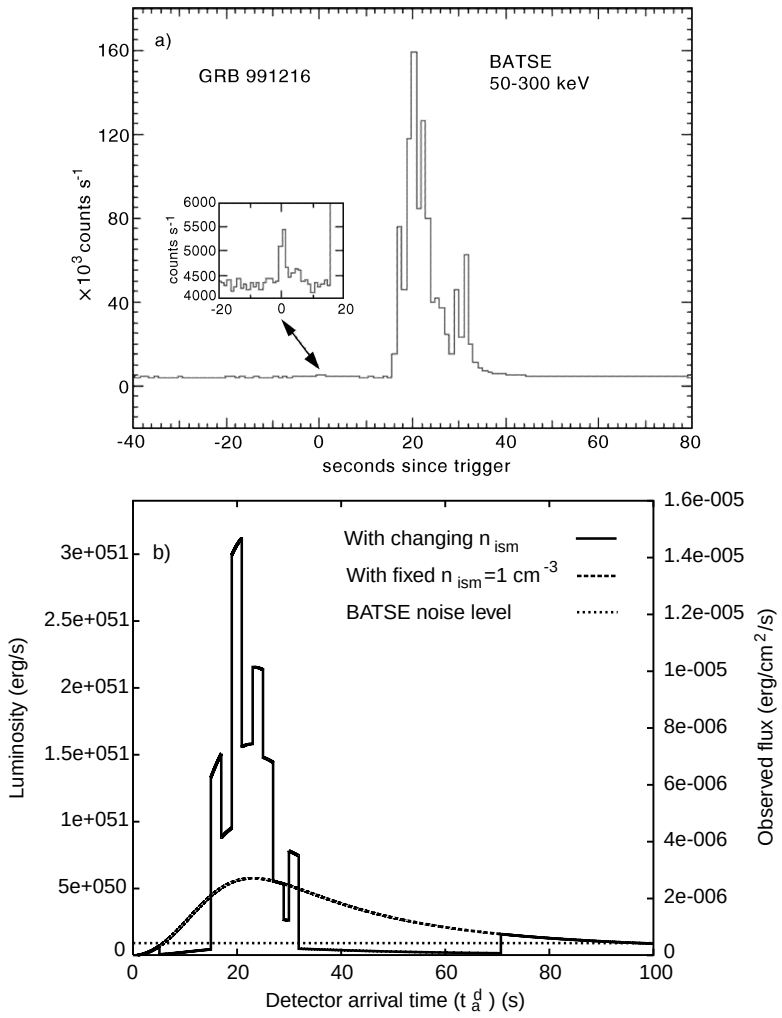

Fig. 3. – a) Flux of GRB 991216 observed by BATSE. The enlargement clearly shows the P-GRB (see Letter 2). b) Flux computed in the collision of the ABM pulse with an ISM cloud with the density profile given in fig. 4. The dashed line indicates the emission from an uniform ISM with $n = 1$ cm^{-3}. The dotted line indicates the BATSE noise level.

were interested in explaining the overall energetics of the GRB phenomena and in this sense, we have adopted the very simplified assumption that the interstellar medium is a constant density medium with $n_{\rm ism} = 1/$ cm^3. Consequently, the afterglow emission obtained is very smooth in time. We are now interested in seeing if in this frameowrk we

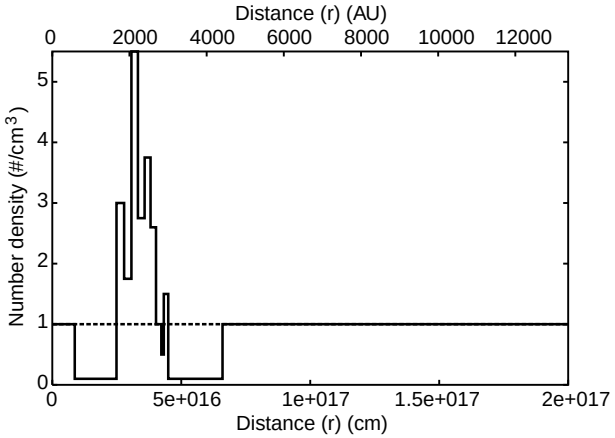

Fig. 4. – The density contrast of the ISM cloud profile introduced in order to fit the observation of the burst of GRB991216. The dashed line indicates the average uniform density $n = 1\ \mathrm{cm}^{-3}$.

can also explain most of the time variability observed by BATSE, all of which, except for the P-GRB, should correspond to the beam-target phase in the above paradigm.

We first recall the constitutive equations (Ruffini, *et al.* (1999,2000) [19, 20], Bianco, *et al.* (2001) [2]):

$$(3a)\ \Delta E_{\mathrm{int}} = \rho_{B_1} V_1 \sqrt{1 + 2\gamma_1 \frac{\Delta M_{\mathrm{ism}} c^2}{\rho_{B_1} V_1} + \left(\frac{\Delta M_{\mathrm{ism}} c^2}{\rho_{B_1} V_1}\right)^2} - \rho_{B_1} V_1 \left(1 + \frac{\Delta M_{\mathrm{ism}} c^2}{\rho_{B_1} V_1}\right),$$

$$(3b) \qquad \gamma_2 = \frac{\gamma_1 + \frac{\Delta M_{\mathrm{ism}} c^2}{\rho_{B_1} V_1}}{\sqrt{1 + 2\gamma_1 \frac{\Delta M_{\mathrm{ism}} c^2}{\rho_{B_1} V_1} + \left(\frac{\Delta M_{\mathrm{ism}} c^2}{\rho_{B_1} V_1}\right)^2}},$$

$$(4) \qquad t_a^d = (1+z)\left(t - \frac{r}{c}\right) = (1+z)\left(t - \frac{\int_0^t v\,(t')\,\mathrm{d}t' + r_{\mathrm{ds}}}{c}\right),$$

where the quantities with the index "1" are calculated before the collision of the ABM-pulse with an elementary ISM shell of thickness Δr and the quantities with "2" after the collision. We indicate by ΔE_{int} the increase in the proper internal energy due to the collision with a single shell and by ρ_B the proper energy density of the swept up baryonic matter, by V the ABM pulse volume in the comoving frame, by M_{ism} the ISM mass swept up until radius r in laboratory frame and by γ the Lorentz factor of the expanding ABM pulse. t_a^d is the arrival time of the signals on the detector, counting from the arrival of the first photon, z is the cosmological redshift of the source and t is

the emission time of the signal, counting from the dyadosphere formation. Details are given in Ruffini, *et al.* (2001f) [24].

In order to proceed, we first distinguish two different regimes in the afterglow (see fig. 2): in the first the intensity of the afterglow increases with time, in the second it decreases. The first regime goes from point 4, corresponding to the emission of the P-GRB (see fig. 1), to the point P, where the peak of the radiation of the afterglow is reached. During this regime, the amount of material engulfed from the interstellar medium is too small compared to the initial kinetic energy of the ABM pulse and the Lorentz gamma factor is slowly decreasing with time, so much so that we can assume γ is constant in this regime. The flux emitted by the afterglow is given (Ruffini, *et al.* (2001f) [24]), as a function of the laboratory time t by

$$F \propto {\gamma_0}^4 n_{\rm ism} t^2, \tag{5}$$

where γ_0 is the value of the Lorentz gamma factor at the moment of transparency. This expression can be simply expressed in terms of the arrival time t_a (Ruffini, *et al.* (2001f) [24])

$$F \propto {\gamma_0}^8 n_{\rm ism} \left(t_a^d\right)^2. \tag{6}$$

The second regime occurs as soon as the mass-energy accreted from the interstellar material is no longer negligible with respect to the initial kinetic energy of the ABM pulse (Ruffini, *et al.* (2001f) [24]). The flux emitted by the afterglow decreases now with the laboratory time following the law

$$F \propto {\gamma_P}^2 {t_P}^6 n_{\rm ism} t^{-4}, \tag{7}$$

where γ_P is the value of the Lorentz gamma factor at the point P and t_P is the value of the laboratory time when the point P is reached. There are actually two different peaks in the radiation flux, if the phenomenon is the spike in the laboratory frame or in the frame of an asymptotic observer comoving with the detector (see Ruffini, *et al.* (2001f) [24] for details). Here we consider the peak in the laboratory time. The peak of the radiation occurs at a value of γ given by (Ruffini, *et al.* (2001f) [24]): $(M_{\rm ism}/M_B) \simeq 10^{-3}$ and

$$\gamma_P \simeq 0.67 \gamma_0, \tag{8}$$

where M_B is the initial baryonic mass of the ABM pulse and $M_{\rm ism}$ is the mass of the ISM engulfed by the ABM pulse at the time t_P. Again we can express the energy flux given in eq. (7) as a function of the arrival time as (Ruffini, *et al.* (2001f) [24])

$$F \propto n_{\rm ism} \left(t_a^d\right)^{-1.6}, \tag{9}$$

in very good agreement with the results of the BATSE, RXTE and Chandra satellites (see Letter 2). The corresponding diagrams are summarized in fig. 2.

Once the two results presented in fig. 1 and fig. 2 have been understood, we can proceed to attack the specific problem of the time variability observed by BATSE.

The fundamental point is that in both regimes *the flux observed in the arrival time is proportional to the interstellar matter density*: any inhomogeneity in the interstellar

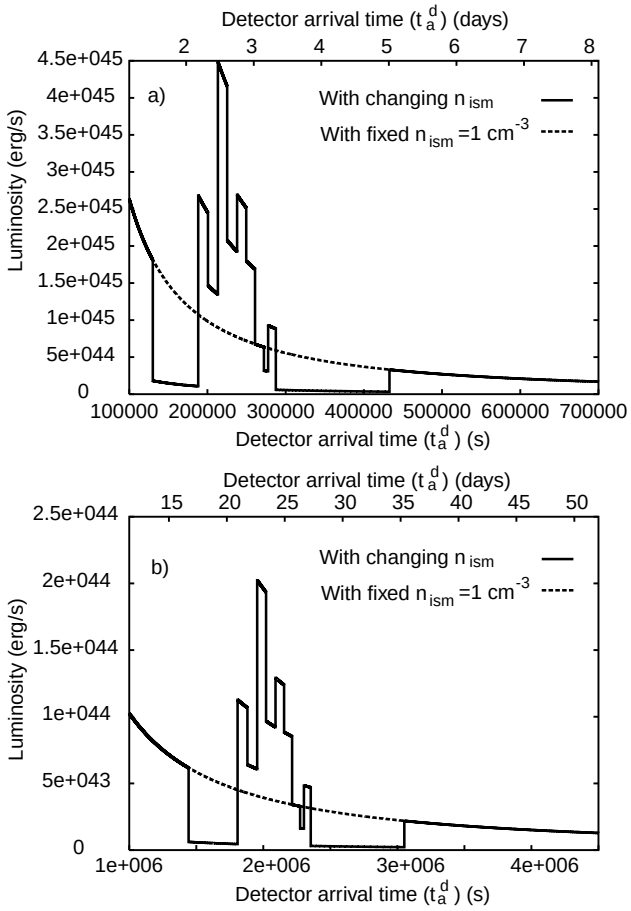

Fig. 5. – a) Same as fig. 3b with the ISM cloud located at a distance of 3.17×10^{17} cm from the EMBH, the time scale of the burst now extends to $\sim 1.58 \times 10^5$ s. b) Same as a) with the ISM cloud at a distance of 4.71×10^{17} cm from the EMBH, the time scale of the burst now extends to $\sim 1.79 \times 10^6$ s.

medium $\Delta n_{\rm ism}/\overline{n}_{\rm ism}$ will lead correspondingly to a proportional variation in the intensity $\Delta I/\overline{I}$ of the afterglow, which can indeed be erroneously interpreted as a burst originating in the "inner engine".

There is a very significant signature of this kind of intensity contrasts: the $\Delta I/\overline{I}$ is independent of the special moment of observation during the afterglow era and is only function of the density contrast. In particular, for the main burst observed by BATSE

(see fig. 3a) we have

$$\left(\Delta I/\overline{I}\right) = (\Delta n_{\rm ism}/n_{\rm ism}) \sim 5. \tag{10}$$

There are still a variety of physical circumstances which may lead to such density inhomogeneities.

The additional crucial parameter in understanding the physical nature of such inhomogeneities is the time scale of the burst observed by BATSE. Such a burst lasts $\Delta t_a \simeq 20$ s and shows substructures on a time scale of ~ 1 s (see fig. 3a). In order to infer the nature of the structure emitting such a burst we must express these times scales in the laboratory time (see Letter 1). Since we are at the peak of the GRB we have $\gamma_P \sim 159$ (see eq. (8)) and Δt_a corresponds in the laboratory time to an interval

$$\Delta t = \gamma_P^2 \times \Delta t_a \sim 7.5 \times 10^5 \text{ s} , \tag{11}$$

which determines the characteristic size of the inhomogeneity creating the burst $\Delta L \sim 2.2 \times 10^{16}$ cm.

It is immediately clear from eq. (10) and eq. (11) that these are the typical dimensions and density contrasts corresponding to a small interstellar cloud. As an explicit example we have shown in fig. 4 the density contrasts and dimensions of an interstellar cloud with an *average density* $\langle n \rangle = 1/\text{ cm}^3$. Such a cloud is located at a distance of $\sim 8.7 \times 10^{15}$ cm from the EMBH, gives rise to a signal similar to the one observed by BATSE (see fig. 3b).

It is now interesting to see the burst that would be emitted by the interaction of the ABM pulse with the same ISM cloud if it were encountered at later times during the evolution of the afterglow. Figure 5a shows the structure of the burst at a distance 2.59×10^{17} cm, corresponding to an arrival time delay of ~ 2 days, where the Lorentz factor is now $\gamma_\star \sim 3.60$. Although the overall intensity is smaller, the intensity ratio of the burst relative to the average emission is consistent with eq. (10), but the time scales of the burst are longer by a factor $\left(\frac{\gamma_P}{\gamma_\star}\right)^2 \simeq 2 \times 10^3$. Figure 5b shows the corresponding quantities for the same ISM cloud located at a distance 3.9×10^{17} cm from the EMBH, corresponding to an arrival time delay of ~ 1 month, where the Lorentz gamma factor is ~ 1.598.

The approximations adopted in this paper in the solution of eqs. (3), (4) have been explicitly presented in all details in Ruffini, *et al.* (2001f) [24].

It is then clear that all the fundamental information on relativistic astrophysics about the EMBH dyadosphere as well as its formation during the process of gravitational collapse have to be inferred from the data on the properties of the P-GRB (Bianco, *et al.* (2001) [2], Ruffini, *et al.* (2001g) [25]).

The data on the E-APE appear to give mainly information on the structure of the ISM clouds in star-forming regions in far away galaxies.

It is then possible to carry out, very efficiently, the sort of problematic examined, within our own galaxy, by the BeppoSAX satellite (see Bocchino and Bykov (2000) [4] and references therein). In these works the interstellar clouds have been examined using as "the beam" the material ejected in supernova remnants, and as "the target" a variety of ISM clouds in our galaxy. By properly taking into account the results summarized in fig. 1 and fig. 2 it is in principle possible, using different GRBs, to map the interstellar matter distribution in star-forming regions in far away galaxies at arbitrary red shift.

This leads us into the domain of another science, of classical astronomy, into which the object of this work does not allow us to go today.

REFERENCES

[1] BATSE Rapid Burst Response, `http://www.batse.ksfc.nasa.gov/~kippen/batserbr/brbr.html`
[2] Bianco C. L., Ruffini R. and Xue S.-S., *Astron. Astrophys.*, **368** (2001) 377.
[3] Bianco C. L., Chardonnet P., Fraschetti F., Ruffini R. and Xue S.-S., 2001, submitted to *Astron. Astrophys.*
[4] Bocchino F. and Bikov A. M., *Astron. Astrophys.*, **362** (2000) 29.
[5] Christodoulou D. and Ruffini R., *Phys. Rev. D*, **4** (1971) 3552.
[6] Corbet R. and Smith D. A., in *Rossi2000: Astrophysics with the Rossi X-ray Timing Explorer* (Greenbelt, USA) 2000.
[7] Damour T. and Ruffini R., *C. R. Acad. Sci. Paris A*, **279** (1974) 971.
[8] Damour T. and Ruffini R., *Phys. Rev. Lett.*, **35** (1975) 463.
[9] Hewish A., Bell S. J. *et al.*, *Nature*, **217** (1967) 709.
[10] Ohanian H. C. and Ruffini R., in *Gravitation and Specetime* (W.W. Norton & Co., New York) 1994.
[11] Hulse R. A. and Taylor J. H., *Astrophys. J. Lett.*, **195** (1975) 51.
[12] Kramer M., in *Proceedings of Ninth Marcel Grossmann Meeting* (World Scientific, Singapore) 2001, in press.
[13] Piran T., talk at *2000 Texas Meeting*, see also astro-ph/0104134.
[14] Piro L. *et al.*, *Science*, **290** (2000) 955.
[15] Preparata G., Ruffini R. and Xue S.-S., 1998a, submitted to *Phys. Rev. Lett.*
[16] Preparata G., Ruffini R. and Xue S.-S., *Astron. Astrophys.*, **338** (1998) L87.
[17] Rees M. J., Ruffini R. and Wheeler J. A., *Black Holes, Gravitational Waves and Cosmology* (Gordon & Breach Science Pub., New York) 1975.
[18] Ruffini R., in *Black Holes and High Energy Astrophysics, Proceedings of the 49th Yamada Conference*, edited by H. Sato and N. Sugiyama (Universal Ac. Press, Tokyo) 1998.
[19] Ruffini R., Salmonson J. D., Wilson J. R. and Xue S.-S., *Astron. Astrophys.*, **350** (1999) 334; *Astron. Astrophys.*, **138** (1999) 511.
[20] Ruffini R., Salmonson J. D., Wilson J. R. and Xue S-.S., *Astron. Astrophys.*, **359** (2000) 855.
[21] Ruffini R., Bianco C. L., Chardonnet P., Fraschetti F. and Xue S.-S., 2001a, submitted to *Astrophys. J. Lett.*
[22] Ruffini R., Bianco C. L., Chardonnet P., Fraschetti F. and Xue S.-S., 2001b, submitted to *Astrophys. J. Lett.*
[23] Ruffini R., Bianco C. L., Chardonnet P., Fraschetti F. and Xue S.-S., 2001c, submitted to *Astrophys. J. Lett.*
[24] Ruffini R., Bianco C. L., Chardonnet P., Fraschetti F. and Xue S.-S., 2001, submitted to *Astron. Astrophys.*
[25] Ruffini R., Vitagliano L. and Xue S.-S., 2001, in preparation.

12 Appendix 5

are described within the fully radiative and radial approximations: the ultrarelativistic, the relativistic and the nonrelativistic regimes. The best fit of the theory leads to an unequivocal identification of the "long GRBs" as extended emission occurring at the afterglow peak (E-APE). The relative intensities, the time separation and the hardness ratio of the P-GRB and the E-APE are used as distinctive observational test of the EMBH theory and the excellent agreement between our theoretical predictions and the observations are documented. The afterglow power-law indexes in the EMBH theory are compared and contrasted with the ones in the literature, and no beaming process is found for GRB 991216. Finally, some preliminary results relating the observed time variability of the E-APE to the inhomogeneities in the interstellar medium are presented, as well as some general considerations on the EMBH formation. The issue of the GSTS paradigm will be the object of a forthcoming publication while the relevance of the iron-lines observed in GRB 991216 is shortly reviewed. The general conclusions are then presented based on the three fundamental parameters of the EMBH theory: the dyadosphere energy, the baryonic mass of the remnant, the interstellar medium density. An in depth discussion and comparison of the EMBH theory with alternative theories is presented as well as indications of further developments beyond the radial approximation, which will be the subject of paper II in this series. Future needs for specific GRB observations are outlined.

Keywords: Afterglow; electromagnetic black hole theory; gamma-ray bursts.

1. Introduction

1.1. *The physical and astrophysical background*

Gamma-ray bursts (GRBs) are rapidly fuelling one of the broadest scientific pursuit in the entire field of science, both in the observational and theoretical domains. Following the discovery of GRBs by the Vela satellites,[4] the observations from the Compton satellite and BATSE[a] had shown the isotropic distribution of the GRBs strongly suggesting a cosmological nature for their origin. It was still through the data of BATSE that the existence of two families of bursts, the "short bursts" and the "long bursts" was presented, opening an intense scientific dialogue on their origin which is still active today (see e.g. Schmidt[5] (2001) and Sec. 11).

An enormous momentum was gained in this field by the discovery of the afterglow phenomena by the BeppoSAX satellite and the optical identification of GRBs which have allowed the unequivocal identification of their sources at cosmological distances.[6] It has become apparent that fluxes of 10^{54} erg/s are reached: during the peak emission the energy of a single GRB equals the energy emitted by all the stars of the Universe.[7]

From an observational point of view, an unprecedented campaign of observations is at work using the largest deployment of observational techniques from space with the satellites CGRO-BATSE, Beppo-SAX,[b] Chandra,[c] R-XTE,[d] XMM-Newton,[e]

[a]See http://cossc.gsfc.nasa.gov/batse/
[b]See http://www.asdc.asi.it/bepposax/
[c]See http://chandra.harvard.edu/
[d]See http://heasarc.gsfc.nasa.gov/docs/xte/
[e]See http://xmm.vilspa.esa.es/

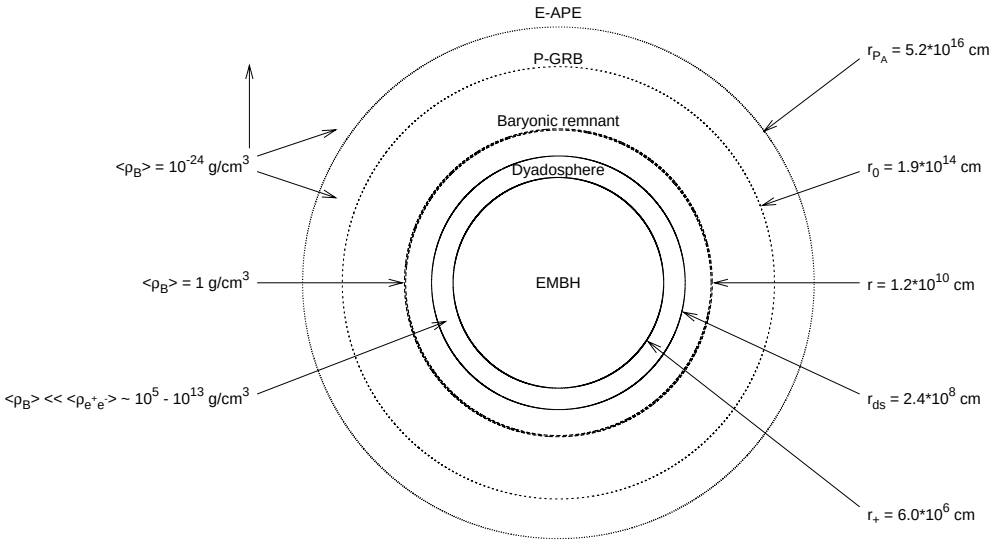

Fig. 1. Selected events in the EMBH theory are represented. For each one the values of the energy density of the medium and the distances from the EMBH, in the laboratory frame and in logarithmic scale, are given.

HETE-2,[f] as well as the HST,[g] and from the ground with optical (KECK,[h] VLT[i]) and radio (VLA[j]) observatories. The further possibility of examining correlations with the detection of ultra high energy cosmic rays (UHECR for short) and incidentally neutrinos should be reachable in the near future thanks to developments of AUGER[k] and AMANDA[l] (see also Halzen[8]).

From a theoretical point of view, GRBs offer comparable opportunities to develop entire new domains in yet untested directions of fundamental science. For the first time within the theory based on the vacuum polarization process occurring in an electromagnetic black hole, namely the EMBH theory (see Fig. 1), the opportunity to theoretically approach the following fundamental issues exists:

(1) The extremely relativistic hydrodynamic phenomena of an electron-positron plasma expanding with sharply varying gamma factors in the range 10^2 to 10^4 and the analysis of the very high energy collision of such an expanding plasma with baryonic matter reaching intensities 10^{38} larger than those usually obtained in Earth-based accelerators.

[f]See http://space.mit.edu/HETE/
[g]See http://www.stsci.edu/
[h]See http://www2.keck.hawaii.edu:3636/
[i]See http://www.eso.org/projects/vlt/
[j]See http://www.aoc.nrao.edu/vla/html/VLAhome.shtml
[k]See http://www.auger.org/
[l]See http://amanda.berkeley.edu/amanda/amanda.html

(2) The bulk process of vacuum polarization created by overcritical electromagnetic fields, in the sense of Heisenberg, Euler[9] and Schwinger.[10] This longly sought quantum ultrarelativistic effect has not yet been unequivocally observed in heavy ion collision on the Earth.[11−14] The difficulty of the heavy ion collision experiments appears to be that the overcritical field is reached only for time scales of the order $\hbar/m_p c^2$, which is much shorter than the characteristic time for the e^+e^- pair creation process which is of the order of $\hbar/m_e c^2$, where m_p and m_e are respectively the proton and the electron mass. It is therefore very possible that the first appearance of such an effect occurs in the strong electromagnetic fields developed in astrophysical conditions during the process of gravitational collapse to an EMBH, where no problem of confinement exists.
(3) A novel form of energy source: the extractable energy of a black hole. The enormous energy released almost instantly in the observed GRBs, points to the possibility that for the first time we are witnessing the release of the extractable energy of an EMBH, during the process of gravitational collapse itself. We can compute and have the opportunity to study all general relativistic as well as the associated ultrahigh energy quantum phenomena as the horizon of the EMBH is approached and is being formed.

It is clear that in approaching such a vast new field of research, implying previously unobserved relativistic regimes, it is not possible to proceed *as usual* with an uncritical comparison of observational data to theoretical models within the classical schemes of astronomy and astrophysics. Some insight to the new approach needed can be gained from past experience in the interpretation of relativistic effects in high energy particle physics as well as from the explanation of some observed relativistic effects in the astrophysical domain. Those relativistic regimes, both in physics and astrophysics, are however much less extreme than those encountered in GRBs.

There are three major new features in relativistic systems which have to be properly taken into account:

(1) Practically all data on astronomical and astrophysical systems is acquired using photon arrival times. It was Einstein[15] at the very initial steps of special relativity who cautioned about the use of such an arrival time analysis and stated that when dealing with objects in motion proper care should be taken in defining the time synchronization procedure in order to construct the correct space–time coordinate grid (see Fig. 2). It is not surprising that as soon as the first relativistic bulk motion effects were observed their interpretations within the classical framework of astrophysics led to the concept of "superluminal" motion. These were observations of extragalactic radio sources, with gamma factors[16] $\sim$10 and of microquasars in our own galaxy with gamma factor[17] $\sim$5. It has been recognized[18] that no "superluminal" motion exists if the prescriptions indicated by Einstein are used in order to establish the correct space–time

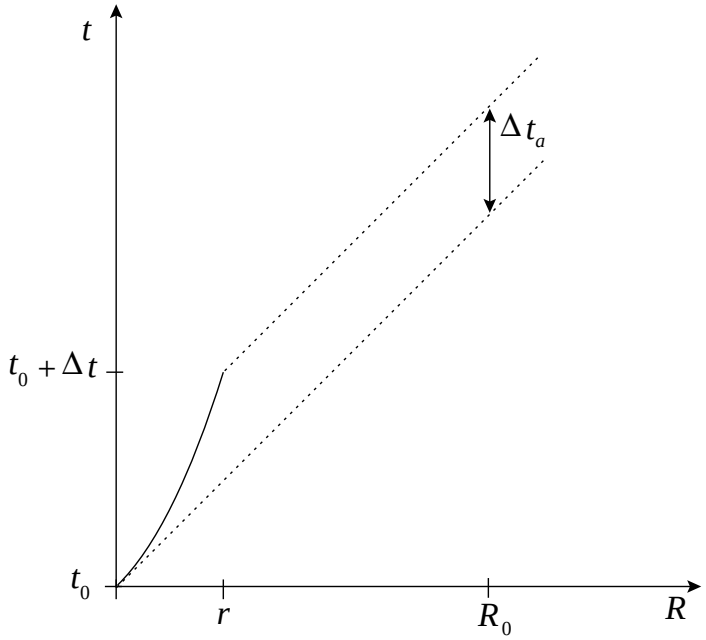

Fig. 2. This qualitative diagram illustrates the relation between the laboratory time interval Δt and the arrival time interval Δt_a for a pulse moving with velocity v in the laboratory time (solid line). We have indicated here the case where the motion of the source has a nonzero acceleration. The arrival time is measured using light signals emitted by the pulse (dotted lines). R_0 is the distance of the observer from the EMBH, t_0 is the laboratory time corresponding to the onset of the gravitational collapse, and r is the radius of the expanding pulse at a time $t = t_0 + \Delta t$.[1]

grid for the astrophysical systems. In the present context of GRBs, where the gamma factor can easily surpass 10^2, the direct application of classical concepts leads to enormous "superluminal" behaviours (see Table 1). An approach based on classical arrival time considerations, as sometimes done in the current literature, completely subverts the causal relation in the observed astrophysical phenomenon.

(2) One of the clear successes of relativistic field theories has been the understanding of the role of four-momentum conservation laws in multiparticle collisions and decays such as in the reaction: $n \to p + e^- + \bar{\nu}_e$. From the works of Pauli and Fermi it became clear how in such a process, contrary to the case of classical mechanics, it is impossible to analyze a single term of the decay, the electron or the proton or the neutrino or the neutron, out of the context of the global point of view of the relativistic conservation of the total four momentum of the system. This in turn involves the knowledge of the system during the entire decay process. These rules are routinely used by workers in high energy particle physics and have become part of their cultural background. If we apply these same rules to the case of the relativistic system of a GRB it is clear that it is just impossible to consider a part of the system, e.g. the afterglow, without

taking into account the general conservation laws and the whole relativistic history of the entire system. The description of the afterglow alone, as has been given at times in the literature, indeed possible within the framework of classical astronomy and astrophysics, is not viable in a relativistic astrophysics context where the space–time grid necessary for the description of the afterglow depends on the entire previous relativistic part of the worldline of the system (see also Sec. 14).

(3) The lifetime of a process does not has an absolute meaning as special and general relativity have shown. It depends both on the inertial reference frame of the laboratory and of the observer and on their relative motion. Such a phenomenon, generally expressed in the "twin paradox", has been extensively checked and confirmed to extremely high accuracy as a by-product of the elementary particle physics $(g-2)$ experiment.[19] This situation is much more extreme in GRBs due to the very large (in the range 10^2-10^4) and time varying (on time scales ranging from fractions of seconds to months) gamma factors between the comoving frame and the far away observer (see Fig. 9). Moreover in the GRB context such an observer is also affected by the cosmological recession velocities of its local Lorentz frame.

1.2. *The relative space–time transformations: The RSTT paradigm and current scientific literature*

Here are some of the reasons why we have recently presented a basic relative space–time transformation (RSTT) paradigm[1] to be applied prior to the interpretation of GRB data.

The first step is the establishment of the governing equations relating:

(a) The comoving time of the pulse (τ).
(b) The laboratory time (t).
(c) The arrival time at the detector (t_a).
(d) The arrival time at the detector corrected for cosmological expansion (t_a^d).

The book-keeping of the four different times and the corresponding space variables must be done carefully in order to keep the correct causal relation in the time sequence of the events involved.

As formulated the RSTT paradigm contains two parts: the first one is a necessary condition, the second one a sufficient condition. The first part reads: "The necessary condition in order to interpret the GRB data, given in terms of the arrival time at the detector, is the knowledge of the *entire* worldline of the source from the gravitational collapse".

Clearly such an approach is in contrast with articles in the current literature which emphasize either some qualitative description of the sources or some quantitative description of the afterglow era by itself.

In the current literature several attempts have addressed the issue of the sources of GRBs. They include scenarios of binary neutron stars mergers,[20–23] black hole/white dwarf[24] and black hole/neutron star binaries,[25,26] hypernovae,[27] failed supernovae or collapsars,[28,29] supranovae.[30,31] Only those based on binary neutron stars have reached the stage of a definite model and detailed quantitative estimates have been made. In this case, however, various problems have surfaced: in the general energetics which cannot be greater than $\sim 3 \times 10^{52}$ erg, in the explanation of "long bursts",[32,33] and in the observed location of the GRB sources in star forming regions.[34] In the remaining cases attention was directed to a qualitative analysis of the sources without addressing the overall problem from the source to the observations. The necessary details to formulate the equations of the dynamical evolution of the system are generally missing.

Other models in the literature have addressed the problem of only fitting the data of the afterglow observations by a phenomenological analysis. They are separated into two major classes:

The "internal shock model", first introduced by Rees & Mészáros[35] by far the most popular one, has been developed in many different aspects, e.g. by Paczyński & Xu,[36] Sari & Piran,[37] Fenimore[38] and Fenimore *et al.*[39] The underlying assumption is that all the variabilities of GRBs in the range $\Delta t \sim 1$ ms up to the overall duration T of the order of 50 s are determined by a yet undetermined "inner engine". The difficulties of explaining the long time scale bursts by a single explosive model has evolved into a subclass of approaches assuming an "inner engine" with extended activity (see e.g. Piran,[40] and references therein).

The "external shock model", also introduced by Mészáros & Rees,[41] is less popular today. It relates the GRB light curves and time variabilities to interactions of a single thin blast wave with clouds in the external medium. The interesting possibility has been recognized within this model, that GRB light curves "are tomographic images of the density distribution of the medium surrounding the sources of GRBs" (Dermer & Mitman[42]), see also Dermer, Chiang & Böttcher,[43] Dermer[44] and references therein. In this case, the structure of the burst is assumed not to depend directly on the "inner engine" (see e.g. Piran,[40] and references therein).

All these works encounter the above mentioned difficulty: they present either a purely qualitative or phenomenological or a piecewise description of the GRB phenomenon. By neglecting the earlier phases, their space–time grid is undefined and as we will explicitly show in the following, results are reached at variance from the ones obtained in a complete and unified description of the GRB phenomenon. We show in the following how such a unified description naturally leads to new characteristic features both in the burst and afterglow of GRBs.

1.3. *The EMBH theory*

In a series of papers, we have developed the EMBH theory[45] which has the advantage, despite its simplicity, that all eras following the process of gravitational

collapse are described by precise field equations which can then be numerically integrated.

Starting from the vacuum polarization process *à la* Heisenberg–Euler–Schwinger[9,10] in the overcritical field of an EMBH first computed in Damour & Ruffini,[46] we have developed the dyadosphere concept.[47]

The dynamics of the e^+e^--pairs and electromagnetic radiation of the plasma generated in the dyadosphere propagating away from the EMBH in a sharp pulse (PEM pulse) has been studied by the Rome group and validated by the numerical codes developed at Livermore Lab.[48]

The collision of the still optically thick e^+e^--pairs and electromagnetic radiation plasma with the baryonic matter of the remnant of the progenitor star has been again studied by the Rome group and validated by the Livermore Lab codes.[49] The further evolution of the sharp pulse of pairs, electromagnetic radiation and baryons (PEMB pulse) has been followed for increasing values of the gamma factor until the condition of transparency is reached.[50]

As this PEMB pulse reaches transparency the proper GRB (P-GRB) is emitted[2] and a pulse of accelerated baryonic matter (the ABM pulse) is injected into the interstellar medium (ISM) giving rise to the afterglow.

1.4. *The GRB 991216 as a prototypical source*

Until this stage, the EMBH theory has been done from first principles based on the exact solutions of the Einstein–Maxwell equations implied by the EMBH uniqueness theorem as well as on the quantum description of the vacuum polarization process in overcritical electromagnetic fields. Turning now to the afterglow, the variety of physical situations that can possibly be encountered are very large and far from unique: the description from first principles is just impossible. We have therefore proceeded to properly identify what we consider a prototypical GRB source and to develop a theoretical framework in close correspondence with the observational data.

We present the criteria which have guided us in the selection of the GRB source to be used as a prototype before proceeding to an uncritical comparison with the theory. It is now clear, since the observations of GRB 980425, GRB 991216, GRB 970514 and GRB 980326 that the afterglow phenomena can present, especially in the optical and radio wavelengths, features originating from phenomena spatially and causally distinct from the GRB phenomena. There is the distinct possibility that phenomena related to a supernova can be erroneously attributed to a GRB. This problem has been clearly addressed by the GRB supernova time sequence (GSTS) paradigm in which the time sequence of the events in the GRB supernova phenomena has been outlined.[3] This has led to the novel concept of an induced supernova.[3] This problem will be addressed in a forthcoming paper.[51]

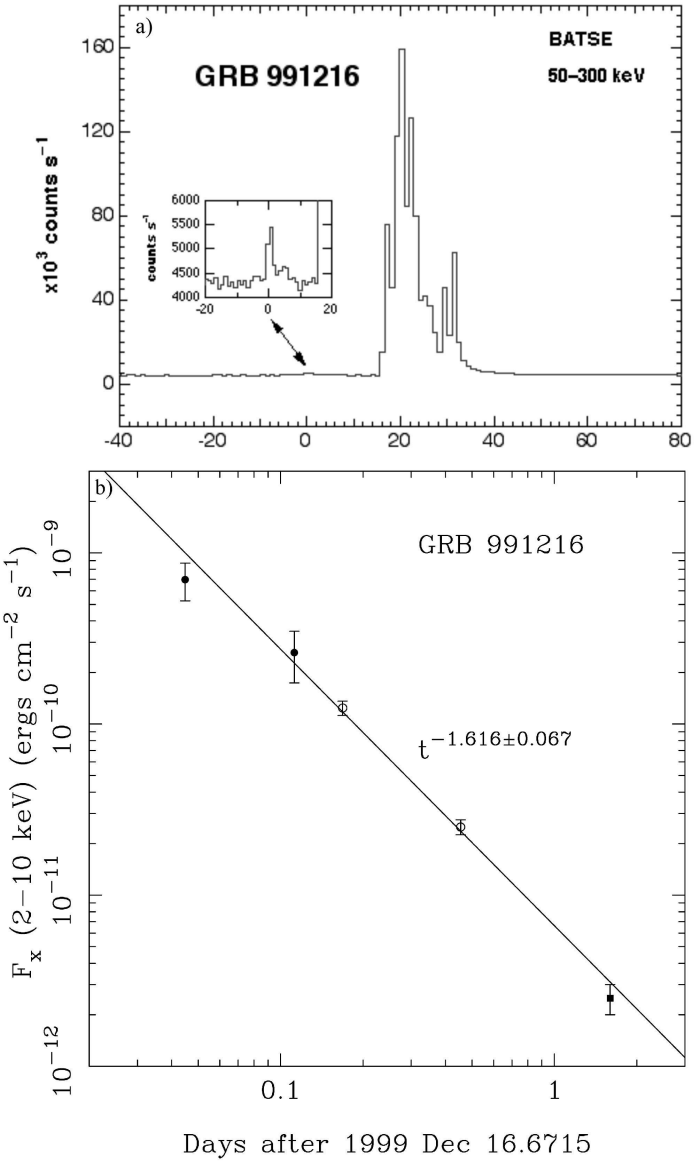

Fig. 3. (a) The peak emission of GRB 991216 as seen by BATSE (reproduced from BATSE Rapid Burst Response[52]). (b) The afterglow emission of GRB 991216 as seen by XTE and Chandra (reproduced from Halpern *et al.*[53]).

In view of these considerations we have selected GRB 991216 as a prototypical case (see Fig. 3) for the following reasons:

(1) GRB 991216 is one of the strongest GRBs in X-rays and is also quite general in the sense that it shows relevant cosmological effects. It radiates mainly in X-rays and in γ-rays and less than 3% is emitted in the optical and radio bands.[53]

(2) The excellent data obtained by BATSE on the burst[52] is complemented by the data on the afterglow acquired by Chandra[54] and RXTE.[55] Superb data have also been obtained from spectroscopy of the iron lines.[54]
(3) A value for the slope of the energy emission during the afterglow as a function of time has been obtained: $n = -1.64$ (Ref. 56) and $n = -1.616 \pm 0.067$.[53]

1.5. *The interpretation of the burst structure: The IBS paradigm and the different eras of the EMBH theory*

The comparison of the EMBH theory with the data of the GRB 991216 and its afterglow has naturally led to a new paradigm for the interpretation of the burst structures (IBS) paradigm of GRBs.[2] The IBS paradigm reads: "*In GRBs we can distinguish an injector phase and a beam-target phase. The injector phase includes the process of gravitational collapse, the formation of the dyadosphere, as well as Era I (the PEM pulse), Era II (the engulfment of the baryonic matter of the remnant) and Era III (the PEMB pulse). The injector phase terminates with the P-GRB emission. The beam-target phase addresses the interaction of the ABM pulse, namely the beam generated during the injection phase, with the ISM as the target. It gives rise to the E-APE and the decaying part of the afterglow.*" The detailed presentations of these results are the main topic of this article.

We recall that the **injector phase** starts from the moment of gravitational collapse and encompasses the following eras:

The zeroth Era: the formation of the dyadosphere. In Sec. 2 we review the basic scientific results which lie at the basis of the EMBH theory: the black hole uniqueness theorem, the mass formula of an EMBH, the process of vacuum polarization in the field of an EMBH. We also point out how after the discovery of the GRB afterglow the re-examination of these results has led to the novel concept of the dyadosphere of an EMBH. We have investigated this concept in the simplest possible case of an EMBH depending only on two parameters: the mass and charge, corresponding to the Reissner–Nordström space–time. We recall the definition of the energy $E_{\rm dya}$ of the dyadosphere as well as the spatial distribution and energetics of the e^+e^- pairs (see Fig. 4).

In order to analyse the time evolution of the dyadosphere we give in the three following sections the theoretical background for the needed equations.

In Sec. 3 we give the general relativistic equations governing the hydrodynamics and the rate equations for the plasma of e^+e^--pairs.

In Sec. 4 we give the governing equations relating the comoving time τ to the laboratory time t corresponding to an inertial reference frame in which the EMBH is at rest and finally to the time measured at the detector t_a which, to finally get t_a^d, must be corrected to take into account the cosmological expansion.

In Sec. 5 we describe the numerical integration of the hydrodynamical equations and the rate equation developed by the Rome and Livermore groups. This entire research program could never have materialized without the fortunate interaction

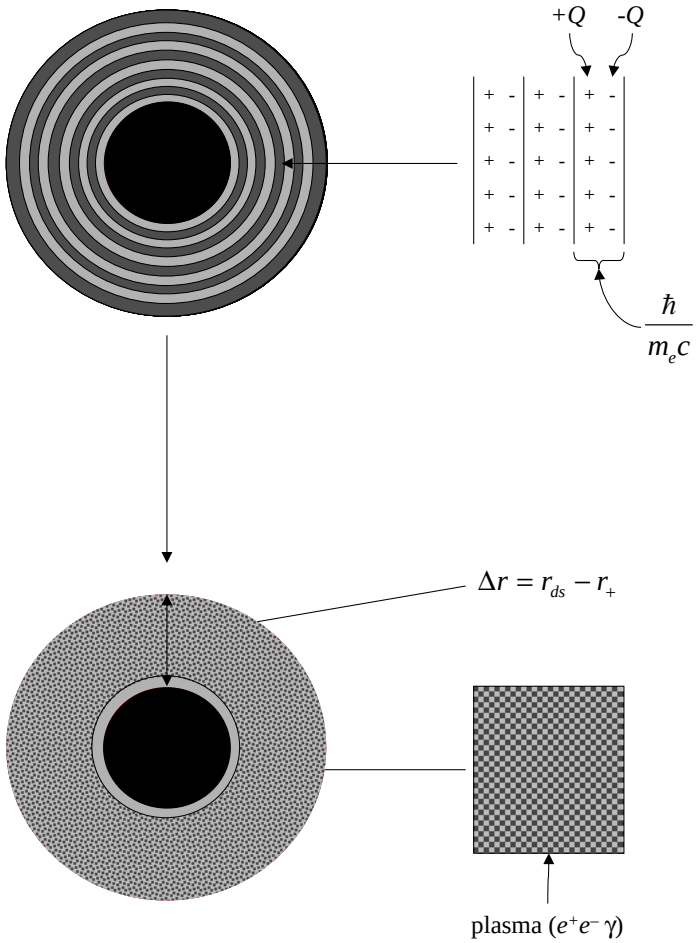

Fig. 4. The dyadosphere of a Reissner–Nordström black hole can be represented as constituted by a concentric set of shells of capacitors, each one of thickness $\hbar/m_e c$ and producing a number of e^+e^- pairs of the order of $\sim Q/e$ on a time scale of 10^{-21} s, where Q is the EMBH charge. The shells extend in a region Δr, from the horizon r_+ to the dyadosphere outer radius $r_{\rm ds}$ (see text). The system evolves to a thermalised plasma configuration.

between the complementary computational techniques developed by these two groups. The validation of the results of the Rome group by the fully general relativistic Livermore codes has been essential both from the point of view of the validity of the numerical results and the interpretation of the scientific content of the results.

The Era I: *the PEM pulse*. In Sec. 3, by direct comparison of the integrations performed with the Rome and Livermore codes we show that among all possible geometries the e^+e^- plasma moves outward from the EMBH reaching a very unique relativistic configuration: the plasma self-organizes in a sharp pulse which expands in the comoving frame exactly by the amount which compensates for the Lorentz contraction in the laboratory frame. The sharp pulse remains of constant thickness

in the laboratory frame and self-propels outwards reaching ultrarelativistic regimes, with gamma factors larger than 10^2, in a few dyadosphere crossing times. We recall that, in analogy with the electromagnetic (EM) pulse observed in a thermonuclear explosion on the Earth, we have defined this more energetic pulse formed of electron-positron pairs and electromagnetic radiation a pair-electromagnetic-pulse or PEM pulse.

The Era II: We describe the interaction of the PEM pulse with the baryonic remnant of mass M_B left over from the gravitational collapse of the progenitor star. We give the details of the decrease of the gamma factor and the corresponding increase in the internal energy during the collision. The dimensionless parameter $B = M_B c^2/E_{\rm dya}$ which measures the baryonic mass of the remnant in units of the $E_{\rm dya}$ is introduced. This is the second fundamental free parameter of the EMBH theory.

The Era III: We describe in Sec. 8 the further expansion of the e^+e^- plasma, after the engulfment of the baryonic remnant of the progenitor star. By direct comparison of the results of integration obtained with the Rome and the Livermore codes it is shown how the pair-electromagnetic-baryon (PEMB) plasma further expands and self organizes in a sharp pulse of constant length in the laboratory frame (see Fig. 5).

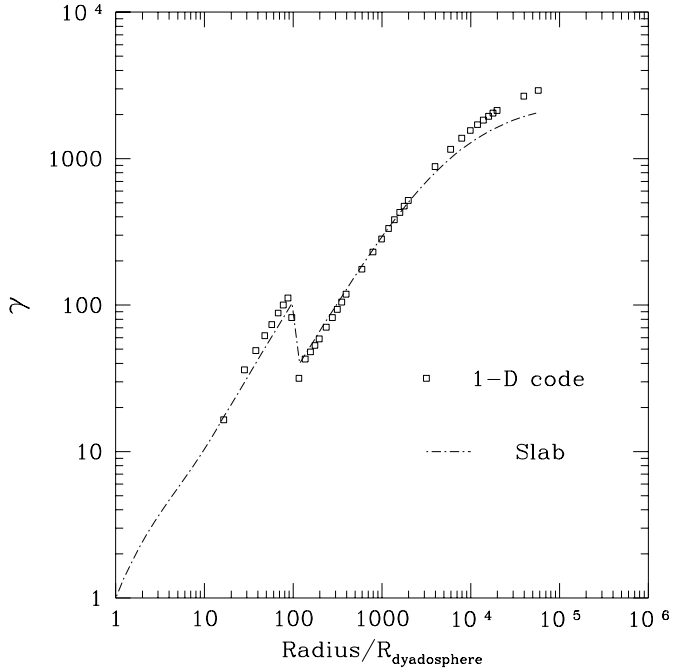

Fig. 5. Comparison of gamma factor for the one-dimensional (1-D) hydrodynamic calculations (Livermore code) and slab calculations (Rome code) as a function of the radial coordinate (in units of dyadosphere radius) in the laboratory frame. The calculations show an excellent agreement.

We have examined the formation of this PEMB pulse in a wide range of values $10^{-8} < B < 10^{-2}$ of the parameter B, the upper limit corresponding to the limit of validity of the theoretical framework developed.

In Sec. 9 it is shown how the effect of baryonic matter of the remnant, expressed by the parameter B, is to smear out all the detailed information on the EMBH parameters. The evolution of the PEMB pulse is shown to depend only on $E_{\rm dya}$ and B: the PEMB pulse is degenerate in the mass and charge parameters of the EMBH and rather independent of the exact location of the baryonic matter of the remnant.

In Sec. 10 the relevant thermodynamical quantities of the PEMB pulse, the temperature in the different frames and the e^+e^- pair densities, are given and the approach to the transparency condition is examined. Particular attention is given to the gradual transfer of the energy of the dyadosphere $E_{\rm dya}$ to the kinetic energy of the baryons $E_{\rm Baryons}$ during the optically thick part of the PEMB pulse.

In Sec. 11, as the condition of transparency is reached, the injector phase is concluded with the emission of a sharp burst of electromagnetic radiation and an accelerated beam of highly relativistic baryons. We recall that we have respectively defined the radiation burst (the proper GRB or for short P-GRB) and the accelerated-baryonic-matter (ABM) pulse. By computing for a fixed value of the EMBH different PEMB pulses corresponding to selected values of B in the range $10^{-8} - 10^{-2}$, it is possible to obtain a crucial universal diagram which is reproduced in Fig. 6. In the limit of $B \to 10^{-8}$ or smaller, almost all $E_{\rm dya}$ is emitted in the P-GRB and a negligible fraction is emitted in the kinetic energy $E_{\rm Baryons}$ of the baryonic matter and therefore in the afterglow. On the other hand in the limit $B \to 10^{-2}$ which is also the limit of validity of our theoretical framework, almost all $E_{\rm dya}$ is transferred to $E_{\rm Baryons}$, which gives origin to the afterglow and the intensity of the P-GRB correspondingly decreases. We have identified the limiting case of negligible values of B with the process of emission of the so called "short bursts". A complementary result reinforcing such an identification comes from the thermodynamical properties of the P-GRB: the hardness of the spectrum decreases for increasing values of B (see Fig. 7).

The injector phase is concluded by the emission of the P-GRB and the ABM pulse, as the condition of transparency is reached.

The **beam-target phase**, in which the accelerated baryonic matter (ABM) generated in the injector phase collides with the ISM, gives origin to the afterglow. Again for simplicity we have adopted a minimum set of assumptions:

(1) The ABM pulse is assumed to collide with a constant homogeneous interstellar medium of number density $n_{\rm ism} \sim 1$ cm^{-3}. The energy emitted in the collision is assumed to be instantaneously radiated away (fully radiative condition). The description of the collision and emission process is done using spherical symmetry, taking only the radial approximation neglecting all the delayed emission due to off-axis scattered radiation.

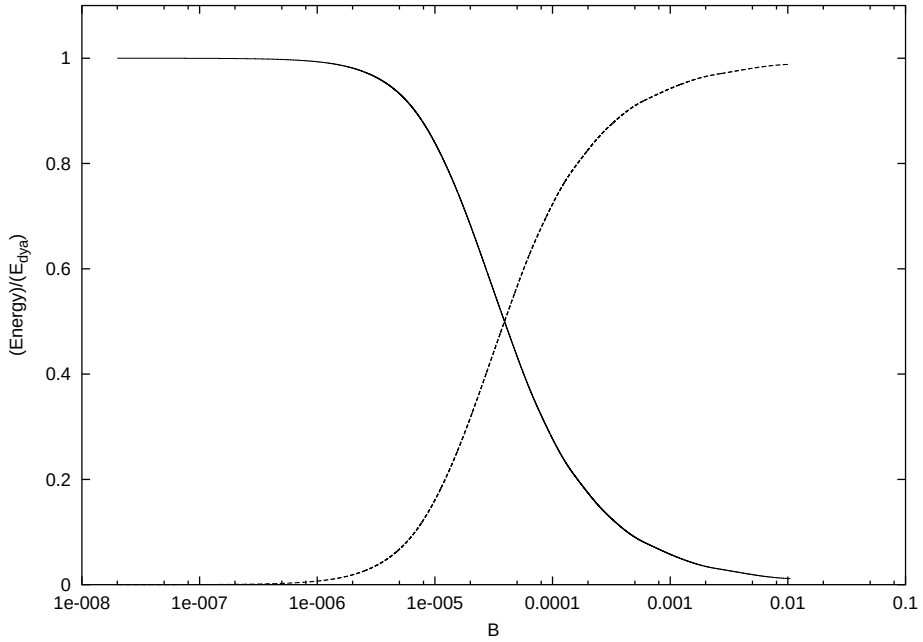

Fig. 6. At the transparent point, the energy radiated in the P-GRB (the solid line) and the final kinetic energy $E_{\rm Baryons}$, of baryonic matter (the dashed line) in units of the total energy of the dyadosphere ($E_{\rm dya}$), are plotted as functions of the B parameter.

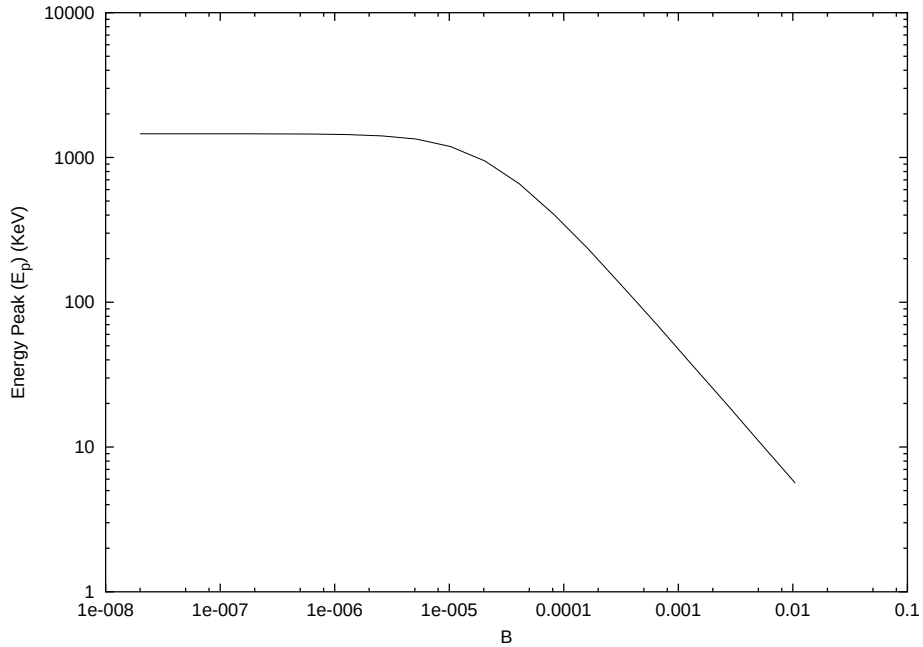

Fig. 7. The energy corresponding to the peak of the photon number spectrum in the P-GRB as measured in the laboratory frame is plotted as function of the B parameter.

(2) Special attention is given to numerically compute the power of the afterglow as a function of the arrival time using the correct governing equations for the space–time transformations in line with the RSTT paradigm.
(3) Finally some approximate solutions are adopted in order to determine the power law exponents of the afterglow flux and compare and contrast them with the observational results as well as with the alternative results in the literature.

In this paper we only consider the above mentioned radial approximation and a spherically symmetric distribution in order to concentrate on the role of the correct space–time transformations in the RSTT paradigm and illustrate their impact on the determination of the power law index of the afterglow. This topic has been seriously neglected in the literature. Details of the role of beaming and on the diffusion due to off-axis emission will be studied elsewhere.[57,58]

We can now turn to the two eras of the beam-target phase:

The Era IV: The ultrarelativistic and relativistic regimes in the afterglow. In Sec. 12 the hydrodynamic relativistic equations governing the collision of the ABM pulse with the interstellar matter are given in the form of a set of finite difference equations to be numerically integrated. Expressions for the internal energy developed in the collision as well as for the gamma factor are given as a function of the mass of the swept up interstellar materials and of the initial conditions. In Sec. 17 the infinitesimal limits of these equations are given, and so are the analytic power-law expansions in selected regimes.

The Era V: The approach to the nonrelativistic regimes in the afterglow. In Sec. 13 it is stressed that this last era often discussed in the current literature can be described by the same equations used for Era IV.

Having established all the governing equations for all the eras of the EMBH theory, we can proceed to compare and contrast the predictions of this theory with the observational data.

1.6. *The best fit of the EMBH theory to the GRB 991216*: *The global features of the solution*

As expressed in Sec. 14, we have proceeded to the identification of the only two free parameters of the EMBH theory, $E_{\rm dya}$ and B, by fitting the observational data from R-XTE and Chandra on the decaying part of the GRB 991216 afterglow. The afterglow appears to have three different parts: in the first part the luminosity increases as a function of the arrival time, it then reaches a maximum and finally monotonically decreases. In Fig. 8, we show how such a fit is actually made and how changing the two free parameters affects the intensity and the location in time of the peak of the afterglow. The best fit is obtained for $E_{\rm dya} = 4.83 \times 10^{53}$ erg and $B = 3 \times 10^{-3}$.

Having determined the two free parameters of the theory, we have integrated the governing equations corresponding to these values and then obtained for the first time the complete history of the gamma factor from the moment of gravitational

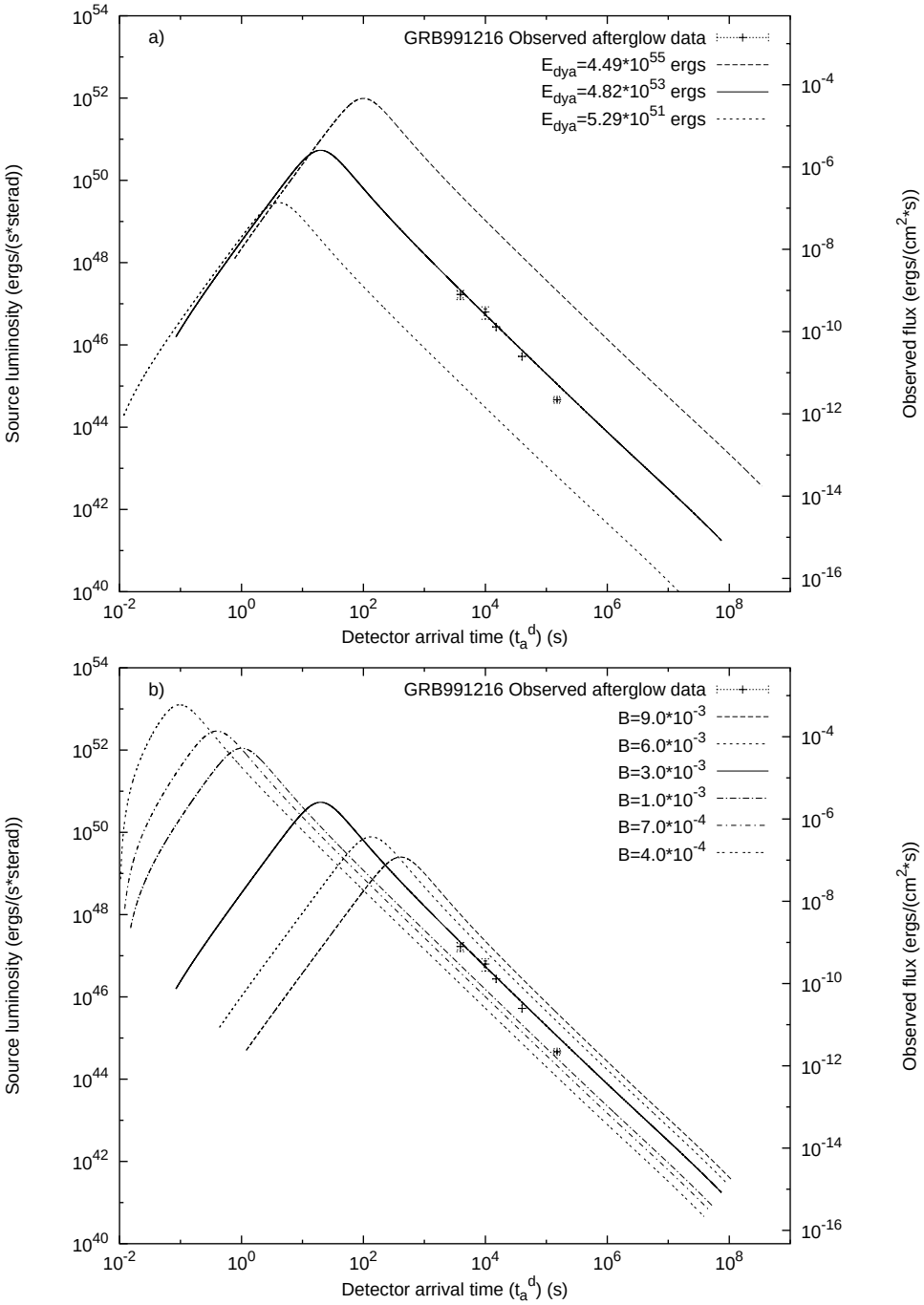

Fig. 8. (a) Afterglow luminosity computed for an EMBH of $E_{\rm dya} = 5.29 \times 10^{51}$ erg, $E_{\rm dya} = 4.83 \times 10^{53}$ erg, $E_{\rm dya} = 4.49 \times 10^{55}$ erg and $B = 3 \times 10^{-3}$. (b) For $E_{\rm dya} = 4.83 \times 10^{53}$, we give the afterglow luminosities corresponding respectively to $B = 9 \times 10^{-3}$, 6×10^{-3}, 3×10^{-3}, 1×10^{-3}, 7×10^{-4}, 4×10^{-4}.

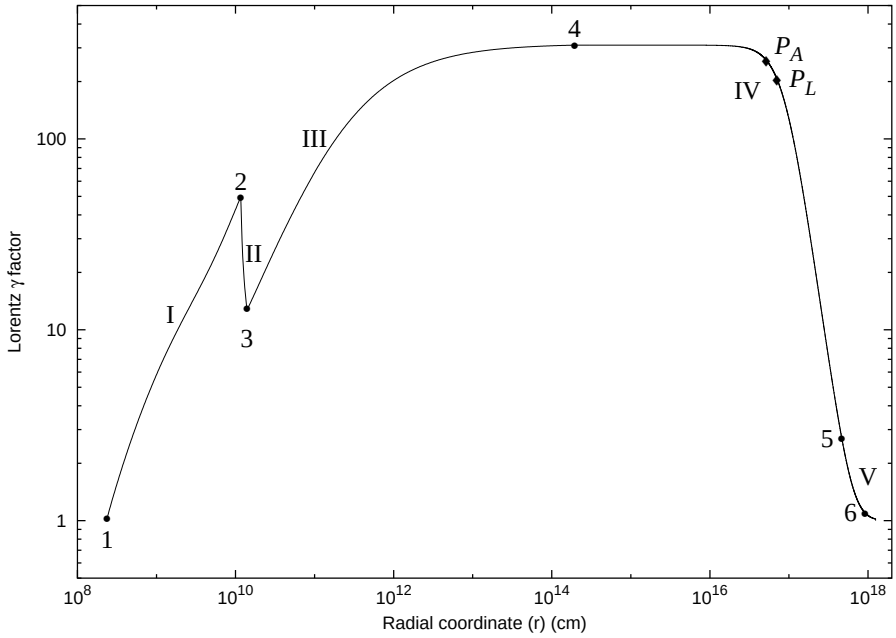

Fig. 9. The theoretically computed gamma factor for the parameter values $E_{\rm dya} = 4.83{\times}10^{53}$ erg, $B = 3 \times 10^{-3}$ is given as a function of the radial coordinate in the laboratory frame. The corresponding values in the comoving time, laboratory time and arrival time are given in Table 1. The different eras indicated by roman numerals are illustrated in the text (see Secs. 6–8, 12 and 13), while the points $1, 2, 3, 4, 5$ mark the beginning and end of each of these eras. The points P_L and P_A mark the maximum of the afterglow flux, respectively in emission time and in arrival time[2] (see Secs. 12 and 17). The point 6 is the beginning of Phase D in Era V (see Secs. 13 and 17). At point 4 the transparency condition is reached and the P-GRB is emitted.

collapse to the latest phases of the afterglow observations (see Fig. 9). We have also determined the different regimes encountered in the relation between the laboratory time and the detector arrival time within the RSTT paradigm (see Fig. 10). We have thus determined the entire space–time grid of the GRB 991216 by giving (see Table 1) the radial coordinate of the GRB phenomenon as a function of the four coordinate time variables. A quick glance to Table 1 shows how the extreme relativistic regimes at work leads to enormous superluminal behaviour (up to 10^5 c!) if the classical astrophysical concepts are adopted using the arrival time as the independent variable. In turn this implies that any causal relation based on classical astrophysics and the arrival time data, as often found in the current GRB literature, is incorrect!

1.7. *The explanation of the "long bursts" and the identification of the proper gamma ray burst (P-GRB)*

In Sec. 15, having determined the two free parameters of the EMBH theory, we analyze the theoretical predictions of this theory for the general structure of GRBs.

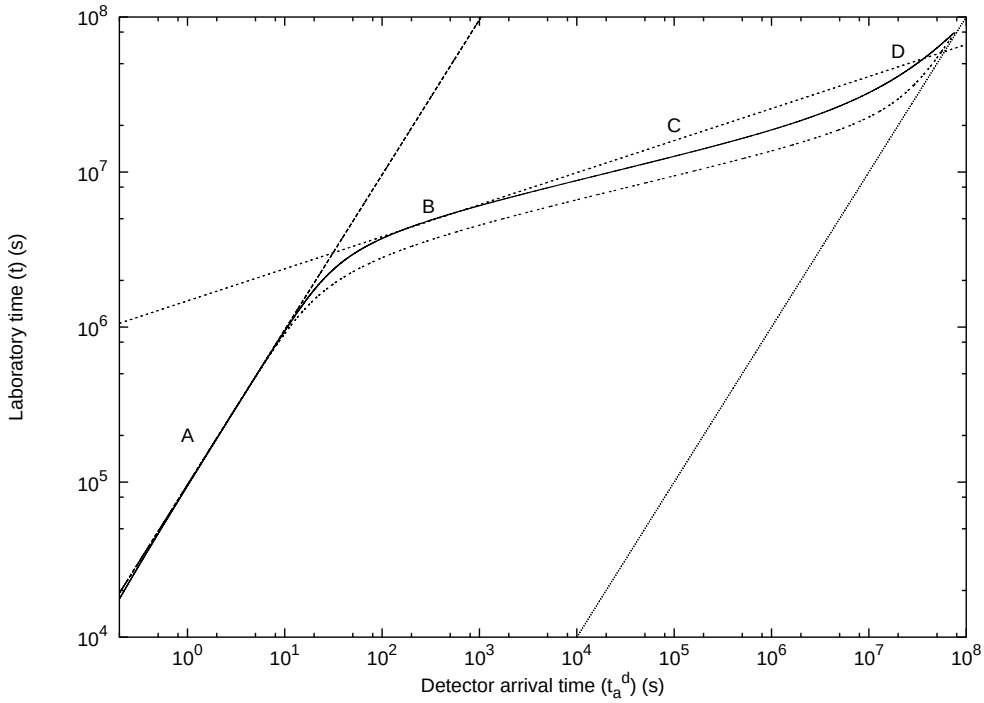

Fig. 10. Relation between the arrival time (t_a^d) measured at the detector and the laboratory time (t) measured at the GRB source. The solid curve is computed using the exact formula given in Eq. (37). The dashed-dotted curve is computed using the approximate formula given in Eq. (39) and often used in the current literature. We distinguish four different phases. **Phase A**: There is a linear relation between t and t_a^d, given by Eq. (134) in the text (dashed line). **Phase B**: There is an "effective" power-law relation between t and t_a^d, given by Eq. (139) (dotted line). **Phase C**: No analytic formula holds and the relation between t and t_a^d has to be directly computed by the integration of the complete equations of energy and momentum conservation (Eqs. (104) and (105)). **Phase D**: As the gamma factor approaches $\gamma = 1$, the relation between t and t_a^d asymptotically goes to $t = t_a^d$ (light gray line).[1]

The first striking result, illustrated in Fig. 11, shows that the peak of the afterglow emission coincides both in intensity and in arrival time (19.87 s) with the average emission of the long burst observed by BATSE. For this we have introduced the new concept of *extended afterglow peak emission* (*E-APE*). Once the proper space–time grid is given (see Table 1) it is immediately clear that the E-APE is generated at distances of 5×10^{16} cm from the EMBH. The long bursts are then identified with the E-APEs and are not bursts at all: they have been interpreted as bursts only because of the high threshold of the BATSE detectors (see Fig. 11). Thus the long standing unsolved problem of explaining the long GRBs[32,33,40] is radically resolved.

Still in Sec. 15, the search for the identification of the P-GRB in the BATSE data is described. This identification is made using the two fundamental diagrams shown in Fig. 12 and Fig. 13. Having established the value of $E_{\rm dya} = 4.83 \times 10^{53}$ erg

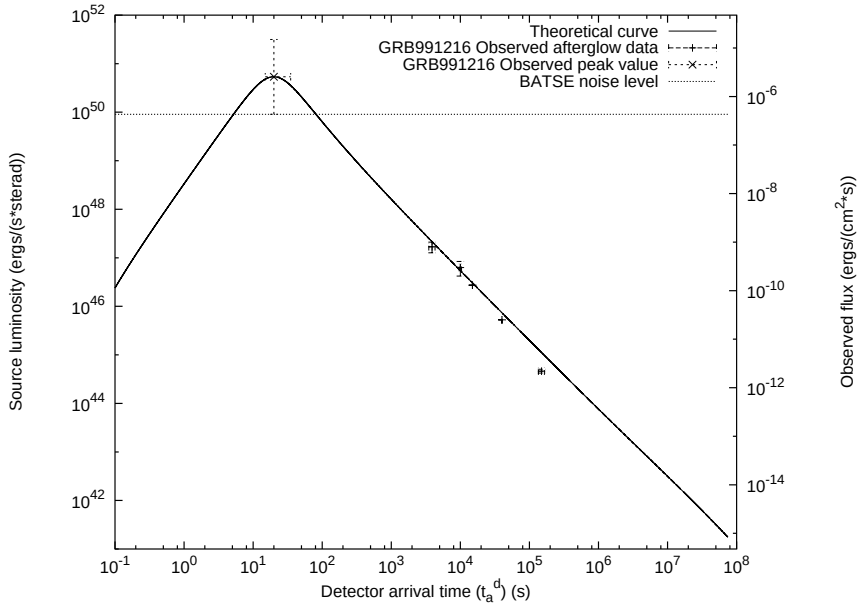

Fig. 11. Best fit of the afterglow data of Chandra, RXTE as well as of the range of variability of the BATSE data on the major burst, by a unique afterglow curve leading to the parameter values $E_{\rm dya} = 4.83 \times 10^{53}$ erg, $B = 3 \times 10^{-3}$. The horizontal dotted line indicates the BATSE noise threshold. On the left axis the luminosity is given in units of the energy emitted at the source, while the right axis gives the flux as received by the detectors.

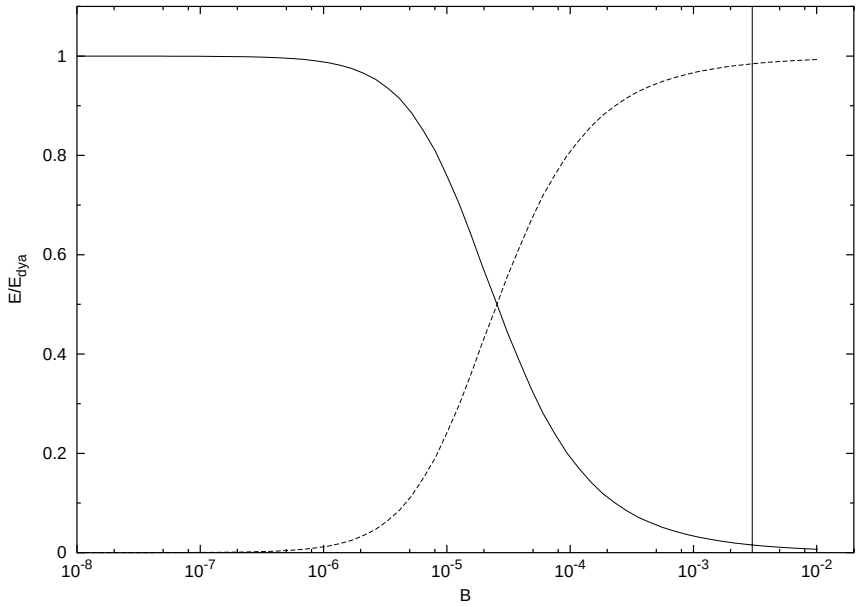

Fig. 12. Relative intensities of the E-APE (dashed line) and the P-GRB (solid line), as predicted by the EMBH theory corresponding to the values of the parameters determined in Fig. 11, as a function of B. Details are given in Sec. 15. The vertical line corresponds to the value $B = 3\times10^{-3}$.

Table 1. Gamma factors for selected events and their space–time coordinates. The points marked $1, 2, 3, 4, 5, 6$, P_L, P_A are the same reported in Fig. 9, while the point F is the endpoint of the simulation. It is particularly important to read the last column, where the apparent motion in the radial coordinate, evaluated in the arrival time at the detector, leads to an enormous "superluminal" behaviour, up to 9.55×10^4 c. This illustrates well the impossibility of using such a classical estimate in regimes with gamma factors up to 310.1.

Point	r (cm)	τ (s)	t (s)	t_a (s)	t_a^d (s)	γ	"Superluminal" $v \equiv \frac{r}{t_a^d}$
			The Injector Phase				
1	2.354×10^8	0.0	0.0	0.0	0.0	1.000	0
	1.871×10^9	1.550×10^{-2}	5.886×10^{-2}	4.312×10^{-3}	8.625×10^{-3}	10.08	$7.23c$
	4.486×10^9	2.141×10^{-2}	1.463×10^{-1}	4.523×10^{-4}	9.046×10^{-3}	20.26	$16.5c$
	7.080×10^9	2.485×10^{-2}	2.329×10^{-1}	4.594×10^{-3}	9.187×10^{-3}	30.46	$25.7c$
	9.533×10^9	2.715×10^{-2}	3.148×10^{-1}	4.627×10^{-3}	9.253×10^{-3}	40.74	$34.4c$
	1.162×10^{10}	2.868×10^{-2}	3.845×10^{-1}	4.644×10^{-3}	9.288×10^{-3}	49.70	$41.7c$
2	1.162×10^{10}	2.868×10^{-2}	3.845×10^{-1}	4.644×10^{-3}	9.288×10^{-3}	49.70	$41.7c$
	1.186×10^{10}	2.889×10^{-2}	3.923×10^{-1}	4.646×10^{-3}	9.292×10^{-3}	38.06	$42.6c$
	1.234×10^{10}	2.949×10^{-2}	4.083×10^{-1}	4.655×10^{-3}	9.311×10^{-3}	24.21	$44.2c$
	1.335×10^{10}	3.144×10^{-2}	4.423×10^{-1}	4.706×10^{-3}	9.413×10^{-3}	15.14	$47.3c$
	1.389×10^{10}	3.279×10^{-2}	4.603×10^{-1}	4.753×10^{-3}	9.506×10^{-3}	12.94	$48.7c$
3	1.389×10^{10}	3.279×10^{-2}	4.603×10^{-1}	4.753×10^{-3}	9.506×10^{-3}	12.94	$48.7c$
	2.326×10^{10}	5.208×10^{-2}	7.733×10^{-1}	5.369×10^{-3}	1.074×10^{-2}	20.09	$72.2c$
	6.913×10^{10}	9.694×10^{-2}	2.304	6.086×10^{-3}	1.217×10^{-2}	50.66	$1.89 \times 10^2 c$
	1.861×10^{11}	1.486×10^{-1}	6.206	6.446×10^{-3}	1.289×10^{-2}	100.1	$4.82 \times 10^2 c$
	9.629×10^{11}	3.112×10^{-1}	32.12	6.978×10^{-3}	1.396×10^{-2}	200.3	$2.30 \times 10^3 c$
	3.205×10^{13}	3.958	1.069×10^3	1.343×10^{-2}	2.685×10^{-2}	300.1	$3.98 \times 10^4 c$
	1.943×10^{14}	21.57	6.481×10^3	4.206×10^{-2}	8.413×10^{-2}	310.1	$7.70 \times 10^4 c$

Table 1 (*Continued*)

Point	r (cm)	τ (s)	t (s)	t_a (s)	t_a^d (s)	γ	"Superluminal" $v \equiv \frac{r}{t_a^d}$
			The Beam-Target Phase				
4	1.943×10^{14}	21.57	6.481×10^3	4.206×10^{-2}	8.413×10^{-2}	310.1	$7.70 \times 10^4 c$
	6.663×10^{15}	7.982×10^2	6.481×10^3	1.164	2.328	310.0	$9.55 \times 10^4 c$
	2.863×10^{16}	3.114×10^3	9.549×10^5	5.057	10.11	300.0	$9.45 \times 10^4 c$
	4.692×10^{16}	5.241×10^3	1.565×10^6	8.775	17.55	270.0	$8.92 \times 10^4 c$
P_A	5.177×10^{16}	5.853×10^3	1.727×10^6	9.933	19.87	258.5	$8.69 \times 10^4 c$
	5.878×10^{16}	6.791×10^3	1.961×10^6	11.82	23.63	240.0	$8.30 \times 10^4 c$
	6.580×10^{16}	7.811×10^3	2.195×10^6	14.03	28.06	220.0	$7.82 \times 10^4 c$
P_L	7.025×10^{16}	8.506×10^3	2.343×10^6	15.66	31.32	207.0	$7.48 \times 10^4 c$
	7.262×10^{16}	8.895×10^3	2.422×10^6	16.61	33.23	200.0	$7.29 \times 10^4 c$
	9.058×10^{16}	1.236×10^4	3.021×10^6	26.66	53.32	150.0	$5.67 \times 10^4 c$
	1.136×10^{17}	1.866×10^4	3.788×10^6	52.84	1.057×10^2	100.0	$3.58 \times 10^4 c$
	1.539×10^{17}	3.819×10^4	5.134×10^6	2.000×10^2	4.000×10^2	50.02	$1.28 \times 10^4 c$
	2.801×10^{17}	2.622×10^5	9.351×10^6	7.278×10^3	1.455×10^4	10.00	$6.42 \times 10^2 c$
	3.624×10^{17}	6.702×10^5	1.213×10^7	3.860×10^4	7.719×10^4	5.001	$1.57 \times 10^2 c$
	4.454×10^{17}	1.433×10^6	1.500×10^7	1.439×10^5	2.877×10^5	2.998	$51.6c$
5	4.454×10^{17}	1.433×10^6	1.500×10^7	1.439×10^5	2.877×10^5	2.998	$51.6c$
	4.830×10^{17}	1.928×10^6	1.635×10^7	2.381×10^5	4.762×10^5	2.500	$33.8c$
	5.390×10^{17}	2.873×10^6	1.844×10^7	4.643×10^5	9.285×10^5	2.000	$19.4c$
	6.422×10^{17}	5.387×10^6	2.271×10^7	1.291×10^6	2.581×10^6	1.500	$8.30c$
	1.034×10^{18}	2.903×10^7	5.002×10^7	1.552×10^7	3.103×10^7	1.054	$1.11c$
6	1.034×10^{18}	2.903×10^7	5.002×10^7	1.552×10^7	3.103×10^7	1.054	$1.11c$
	1.202×10^{18}	4.979×10^7	7.150×10^7	3.140×10^7	6.280×10^7	1.025	$6.38 \times 10^{-1} c$
F	1.248×10^{18}	5.706×10^7	7.894×10^7	3.731×10^7	7.461×10^7	1.000	$5.58 \times 10^{-1} c$

and of $B = 3 \times 10^{-3}$, it is possible from the dashed line and the solid line in Fig. 12 to evaluate the ratio of the energy $E_{\text{P-GRB}}$ emitted in the P-GRB to the energy E_{Baryons} emitted in the afterglow corresponding to the determined value of B (see the vertical line in Fig. 12). We obtain $E_{\text{P-GRB}}/E_{\text{Baryons}} = 1.58 \times 10^{-2}$, which gives $E_{\text{P-GRB}} = 7.54 \times 10^{51}$ erg. Having so determined the theoretically expected intensity of the P-GRB, a second fundamental observable parameter, which is also a function of E_{dya} and B, is the arrival time delay between the P-GRB and the peak E-APE, determined in Fig. 13. From Table 1, we have that the detector arrival time of the P-GRB occurs at 8.41×10^{-2} s, corresponding to a radial coordinate of 1.94×10^{14} cm, a comoving time of 21.57 s, a laboratory time of 6.48×10^{3} s and an arrival time of 4.21×10^{-2} s. At this point, the gamma factor is 310.1. The peak of the E-APE occurs at a detector arrival time of 19.87 s, corresponding to a radial coordinate of 5.18×10^{16} cm, a comoving time of 5.85×10^{3} s, a laboratory time of 1.73×10^{6} s and an arrival time of 9.93 s (see Table 1). The delay between the P-GRB and the peak of the E-APE is therefore 19.78 s (see Fig. 13). The theoretical prediction on the intensity and the arrival time uniquely identifies the P-GRB with the "precursor" in the GRB 991216 (see Fig. 3). Moreover, the hardness of the P-GRB spectra is also evaluated in this section. As pointed out in the conclusions, the fact that both the absolute and relative intensities of the P-GRB and E-APE

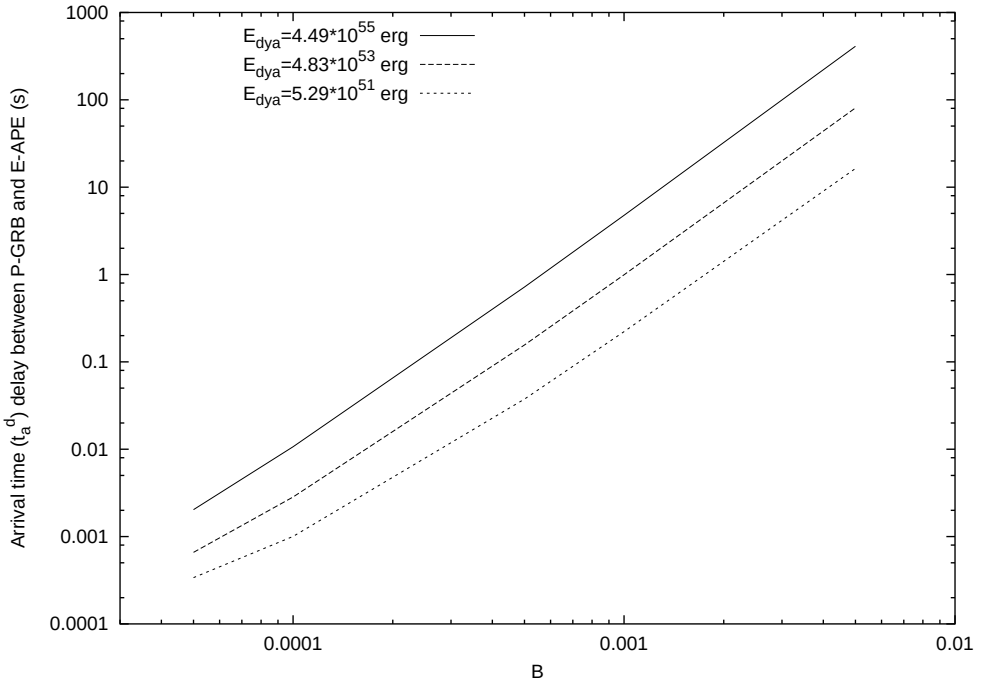

Fig. 13. The arrival time delay between the P-GRB and the peak of the E-APE is plotted as a function of the B parameter for three selected values of E_{dya}.

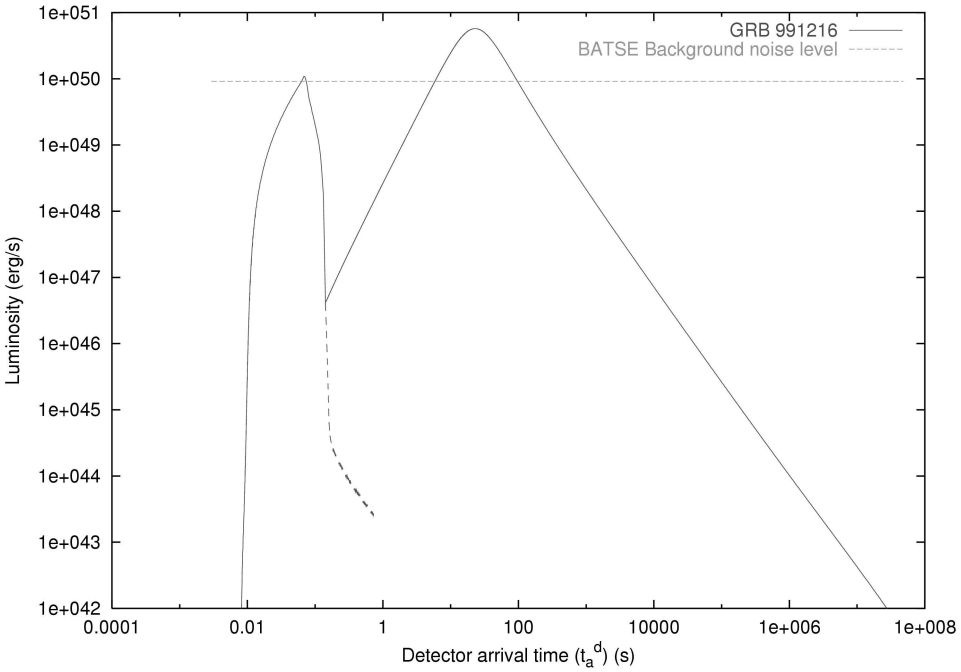

Fig. 14. A qualitative diagram showing the full picture of the model, with both P-GRB and E-APE.

have been predicted within a few percent accuracy as well as the fact that their arrival time has been computed with the precision of a few tenths of milliseconds (see Table 1 and Fig. 14), can be considered one of the major successes of the EMBH theory.

1.8. *On the power-laws, beaming and temporal structures in the afterglow of GRB 991216*

In Sec. 17 a piecewise description of the afterglow by the expansion of the fundamental hydrodynamical equations given by Taub[59] and Landau & Lifshitz[60] have allowed the determination of a power-law index for the dependence of the afterglow luminosity on the photon arrival time at the detector. It is evident that the determination of the power-law index is very sensitive to the basic assumptions made for the description of the afterglow, as well as to the relations between the different temporal coordinates which have been clarified by the RSTT paradigm.[1] The different power-law indices obtained are compared and contrasted with the ones in the current literature (see Table 2). As a byproduct of this analysis, see also the conclusions, there is a perfect agreement between the observational data and the theoretical predictions, implying that the assumptions adopted for the description of the afterglow are valid and therefore that there is no evidence for a beamed emission in GRB 991216.

In Sec. 19 the role of the inhomogeneities in the interstellar matter has been analysed in order to explain the observed temporal substructures in the BATSE data on GRB 991216. From the data of Table 1 and the highly "superluminal" behaviour of the source in the region of the E-APE, it is concluded that the observed time variability in the intensity of the emission $(\Delta I/\bar{I}) \sim 5$ can be traced to inhomogeneities in the interstellar matter: $(\Delta n_{\rm ism}/n_{\rm ism}) \sim 5$. The typical size of the scattering region is estimated to be 5×10^{16} cm, and these are the typical sizes and density contrasts found in interstellar clouds. Since the emission of the E-APE occurs at typical dimensions of the order of 5×10^{16} cm, the observed inhomogeneities are probing the structure of the interstellar medium, and have nothing to do with the "inner engine" of the source. These conclusions, reached in the radial approximation of the afterglow adopted in this article, have been proved to hold in the more general case when off-radial emission is taken into account.[57,58]

1.9. *The observation of the iron lines in GRB 991216*: *On a possible GRB-supernova time sequence*

In Sec. 20 the program of using GRBs to further explore the region surrounding the newly formed EMBH is carried one step further by using the observations of the emitted iron lines.[54] This gives us the opportunity to introduce the GRB-supernova time sequence (GSTS) paradigm and to introduce as well the novel concept of an *induced supernova explosion*. The GSTS paradigm reads: *A massive GRB-progenitor star P_1 of mass M_1 undergoes gravitational collapse to an EMBH. During this process a dyadosphere is formed and subsequently the P-GRB and the E-APE are generated in sequence. They propagate and impact, with their photon and neutrino components, on a second supernova-progenitor star P_2 of mass M_2. Assuming that both stars were generated approximately at the same time, we expect to have $M_2 < M_1$. Under some special conditions of the thermonuclear evolution of the supernova-progenitor star P_2, the collision of the P-GRB and the E-APE with the star P_2 can induce its supernova explosion.*

Using the result presented in Table 1 and in all preceding sections, the GSTS paradigm is illustrated in the case of GRB 991216. Some general considerations on the nature of the supernova progenitor star are also advanced.

Some general considerations on the EMBH formation are presented in Sec. 21. The general conclusions are presented in Sec. 22.

The understanding of all these points has led to the formulation of the second part, namely the sufficient condition of the RSTT paradigm which reads: "the necessary condition in order to interpret the GRB data, given in terms of the arrival time at the detector, is the knowledge of the *entire* worldline of the source from the gravitational collapse. In order to meet this condition, given a proper theoretical description and the correct governing equations, it is sufficient to know the energy of the dyadosphere and the mass of the remnant of the progenitor star".

2. The Zeroth Era: The Process of Gravitational Collapse and the Formation of the Dyadosphere

We first recall the three theoretical results which lie at the basis of the EMBH theory.

In 1971 in the article "*Introducing the Black Hole*",[61] the theorem was advanced that the most general black hole is characterized uniquely by three independent parameters: the mass-energy M, the angular momentum L and the charge Q making it an EMBH. Such an ansatz, which came to be known as the "uniqueness theorem" has turned out to be one of the most difficult theorems to be proven in all of physics and mathematics. The progress in the proof has been authoritatively summarized by Carter[62] in 1997. The situation can be considered satisfactory from the point of view of the physical and astrophysical considerations. Nevertheless some fundamental mathematical and physical issues concerning the most general perturbation analysis of an EMBH are still the topic of active scientific discussion.[63]

In 1971 it was shown that the energy extractable from an EMBH is governed by the mass-energy formula[64]

$$E_{\rm BH}^2 = M^2c^4 = \left(M_{\rm ir}c^2 + \frac{Q^2}{2\rho_+}\right)^2 + \frac{L^2c^2}{\rho_+^2} \tag{1}$$

with

$$\frac{1}{\rho_+^4}\left(\frac{G^2}{c^8}\right)(Q^4 + 4L^2c^2) \leq 1\,, \tag{2}$$

where

$$S = 4\pi\rho_+^2 = 4\pi(r_+^2 + \frac{L^2}{c^2M^2}) = 16\pi\left(\frac{G^2}{c^4}\right)M_{\rm ir}^2 \tag{3}$$

is the horizon surface area, $M_{\rm ir}$ is the irreducible mass, r_+ is the horizon radius and ρ_+ is the quasi-spheroidal cylindrical coordinate of the horizon evaluated at the equatorial plane. Extreme EMBHs satisfy the equality in Eq. (2). Up to 50% of the mass-energy of an extreme EMBH can in principle be extracted by a special set of transformations: the reversible transformations.[64]

In 1975, generalizing some previous results of Zaumen[65] and Gibbons,[66] Damour & Ruffini[46] showed in 1975 that the vacuum polarization process *à la* Heisenberg–Euler–Schwinger[9,10] created by an electric field of strength larger than

$$\mathcal{E}_c = \frac{m_e^2c^3}{\hbar e} \tag{4}$$

can indeed occur in the field of a Kerr–Newmann EMBH. Here m_e and e are respectively the mass and charge of the electron. There Damour and Ruffini considered an axially symmetric EMBH, due to the presence of rotation, and limited themselves to EMBH masses larger then the upper limit of a neutron star for astrophysical applications. They purposely avoided all complications of black holes with mass smaller then the dual electron mass of the electron $\left(m_e^\star = \frac{c\hbar}{Gm_e} = \frac{m_{\rm Planck}^2}{m_e}\right)$ which may lead to quantum evaporation processes.[67] They pointed out that:

(1) The vacuum polarization process can occur for an EMBH with mass larger than the maximum critical mass for neutron stars all the way up to $7.2 \times 10^6 M_\odot$.
(2) The process of pair creation occurs on very short time scales, typically $\hbar/m_e c^2$, and is an almost perfect reversible process, in the sense defined by Christodoulou–Ruffini, leading to a very efficient mechanism of extracting energy from an EMBH.
(3) The energy generated by the energy extraction process of an EMBH was found to be of the order of 10^{54} erg, released almost instantaneously. They concluded at the time "*this work naturally leads to a most simple model for the explanation of the recently discovered γ-ray bursts*".

After the discovery of the afterglow of GRBs and the determination of the cosmological distance of their sources we noticed the coincidence between the theoretically predicted energetics and the observed ones in Damour & Ruffini:[46] we returned to our theoretical results developing some new basic theoretical concepts,[45,47–49,68] which have led to the EMBH theory.

As a first simplifying assumption we have developed our considerations in the absence of rotation with spherically symmetric distributions. The space–time is then described by the Reissner–Nordström geometry, whose spherically symmetric metric is given by

$$d^2 s = g_{tt}(r) d^2 t + g_{rr}(r) d^2 r + r^2 d^2\theta + r^2 \sin^2\theta d^2\phi\,, \tag{5}$$

where

$$g_{tt}(r) = -\left[1 - \frac{2GM}{c^2 r} + \frac{Q^2 G}{c^4 r^2}\right] \equiv -\alpha^2(r) \text{ and } g_{rr}(r) = \alpha^{-2}(r)\,.$$

The first new result we obtained is that the pair creation process does not occur at the horizon of the EMBH: it extends over the entire region outside the horizon in which the electric field exceeds the critical value given by Eq. (4). Since the electric field in the Reissner–Nordström geometry has only a radial component given by[69]

$$\mathcal{E}(r) = \frac{Q}{r^2}\,, \tag{6}$$

this region extends from the horizon radius

$$r_+ = 1.47 \cdot 10^5 \mu (1 + \sqrt{1 - \xi^2}) \text{ cm} \tag{7}$$

out to an outer radius[45]

$$\begin{aligned} r^\star &= \left(\frac{\hbar}{mc}\right)^{\frac{1}{2}} \left(\frac{GM}{c^2}\right)^{\frac{1}{2}} \left(\frac{m_\mathrm{p}}{m}\right)^{\frac{1}{2}} \left(\frac{e}{q_\mathrm{p}}\right)^{\frac{1}{2}} \left(\frac{Q}{\sqrt{G}M}\right)^{\frac{1}{2}} \\ &= 1.12 \cdot 10^8 \sqrt{\mu\xi} \text{ cm}\,, \end{aligned} \tag{8}$$

where we have introduced the dimensionless mass and charge parameters $\mu = M/M_\odot$, $\xi = Q/(M\sqrt{G}) \leq 1$ (see Fig. 4).

The second new result has been to realize that the local number density of electron and positron pairs created in this region as a function of radius is given by

$$n_{e^+e^-}(r) = \frac{Q}{4\pi r^2(\hbar/mc)e}\left[1-\left(\frac{r}{r^\star}\right)^2\right], \tag{9}$$

and consequently the total number of electron and positron pairs in this region is

$$N^0_{e^+e^-} \simeq \frac{Q-Q_c}{e}\left[1+\frac{(r^\star - r_+)}{\hbar/mc}\right], \tag{10}$$

where $Q_c = \mathcal{E}_c r_+^2$.

The total number of pairs is larger by an enormous factor $r^\star/(\hbar/mc) > 10^{18}$ than the value Q/e which a naive estimate of the discharge of the EMBH would have predicted. Due to this enormous amplification factor in the number of pairs created, the region between the horizon and $r^\star$ is dominated by an essentially high density neutral plasma of electron-positron pairs. We have defined this region as the dyadosphere of the EMBH from the Greek duas, duadsos for pairs. Consequently we have called $r^\star$ the dyadosphere radius $r^\star \equiv r_{\rm ds}$.[45,47,68] The vacuum polarization process occurs as if the entire dyadosphere are subdivided into a concentric set of shells of capacitors each of thickness $\hbar/m_e c$ and each producing a number of e^+e^- pairs on the order of $\sim Q/e$ (see Fig. 4). The energy density of the electron-positron pairs is given by

$$\epsilon(r) = \frac{Q^2}{8\pi r^4}\left(1-\left(\frac{r}{r_{\rm ds}}\right)^4\right), \tag{11}$$

(see Figs. 2–3 of Preparata, Ruffini & Xue[68]). The total energy of pairs converted from the static electric energy and deposited within the dyadosphere is then

$$E_{\rm dya} = \frac{1}{2}\frac{Q^2}{r_+}\left(1-\frac{r_+}{r_{\rm ds}}\right)\left[1-\left(\frac{r_+}{r_{\rm ds}}\right)^2\right]. \tag{12}$$

As we will see in the following this is one of the two fundamental parameters of the EMBH theory (see Fig. 16). In the limit $r_+/r_{\rm ds} \to 0$, Eq. (12) leads to $E_{\rm dya} \to Q^2/2r_+$, which coincides with the energy extractable from EMBHs by reversible processes ($M_{\rm ir} = {\rm const}$), namely $E_{\rm BH} - M_{\rm ir} = Q^2/2r_+$ (see Fig. 15).[64] Due to the very large pair density given by Eq. (9) and to the sizes of the cross-sections for the process $e^+e^- \leftrightarrow \gamma+\gamma$, the system is expected to thermalize to a plasma configuration for which

$$n_{e^+} = n_{e^-} \sim n_\gamma \sim n^0_{e^+e^-}\,, \tag{13}$$

where $n^0_{e^+e^-}$ is the total number density of e^+e^--pairs created in the dyadosphere.[47,68]

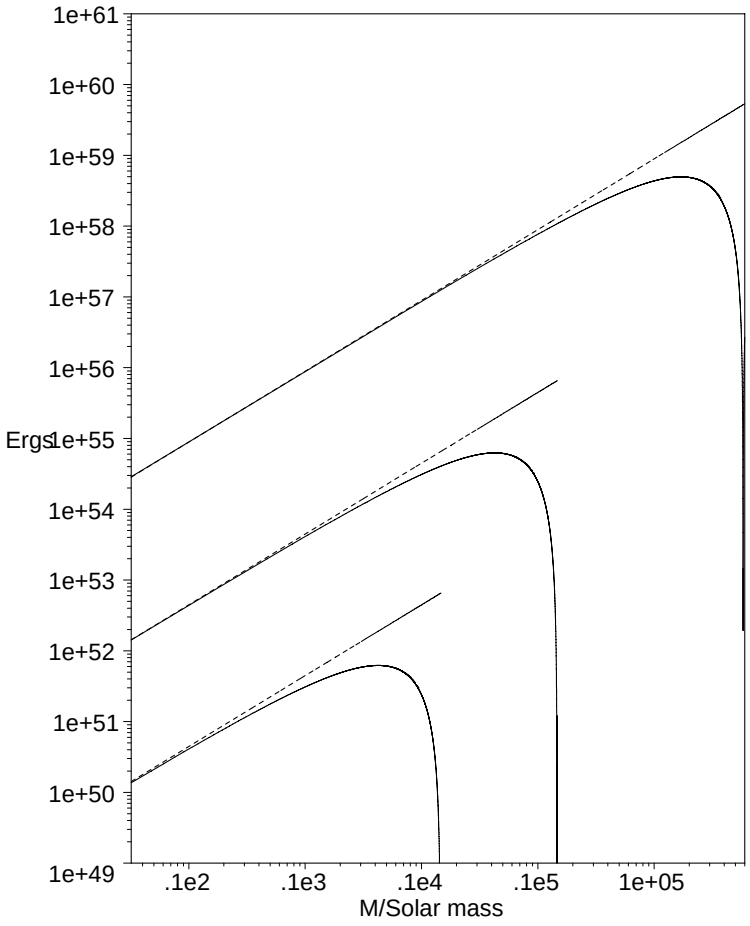

Fig. 15. The energy extracted by the process of vacuum polarization is plotted (solid lines) as a function of the mass M (in solar mass units) for selected values of the charge parameter $\xi = 1$, 0.1, 0.01 (from top to bottom) for an EMBH, the case $\xi = 1$ reachable only as a limiting process. For comparison we have also plotted the maximum energy extractable from an EMBH (dotted lines) given by Eq. (1). Details in Preparata, Ruffini & Xue.[70]

The third new result which we have introduced for simplicity is that for a given $E_{\rm dya}$ we have assumed either a constant average energy density over the entire dyadosphere volume, or a more compact configuration with energy density equal to the peak value. These are the two possible initial conditions for the evolution of the dyadosphere (see Fig. 17).

These three old and three new theoretical results permit a good estimate of the general energetics processes originating in the dyadosphere, assuming an already formed EMBH. In reality, if the data become accurate enough, the full dynamical description of the dyadosphere formation mentioned above will be needed in order to follow all the general relativistic effects and characteristic time scales of the approach to the EMBH horizon[71–74] (see also Sec. 21).

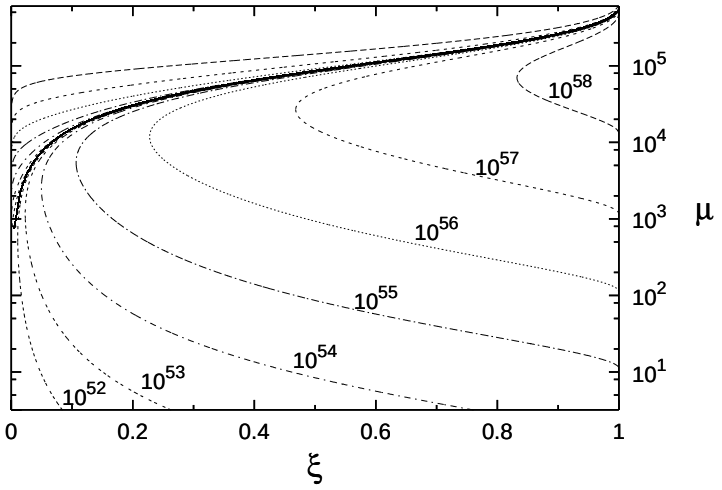

Fig. 16. Selected lines corresponding to fixed values of the $E_{\rm dya}$ are given as a function of the two parameters μ ξ, only the solutions below the continuous heavy line are physically relevant. The configurations above the continuous heavy lines correspond to unphysical solutions with $r_{\rm ds} < r_+$.

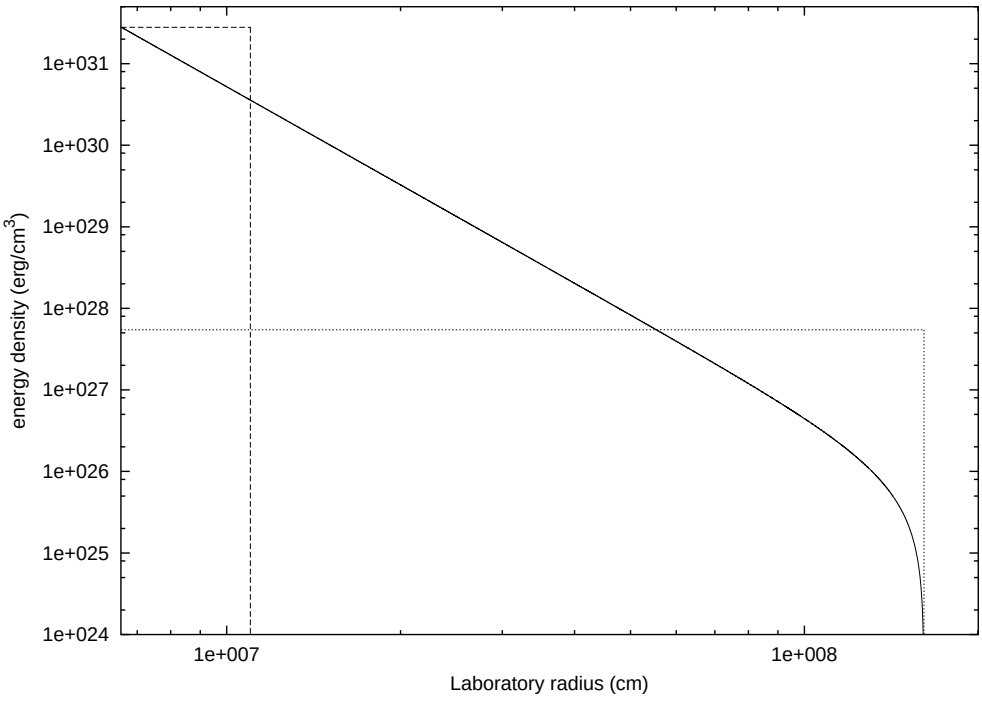

Fig. 17. Two different approximations for the energy density profile inside the dyadosphere. The first one (dashed line) fixes the energy density equal to its peak value, and computes an "effective" dyadosphere radius accordingly. The second one (dotted line) fixes the dyadosphere radius to its correct value, and assumes an uniform energy density over the dyadosphere volume. The total energy in the dyadosphere is of course the same in both cases. The solid curve represents the real energy density profile.

Below we shall concentrate on the dynamical evolution of the electron-positron plasma created in the dyadosphere. We shall first examine in the next three sections the governing equations necessary to approach such a dynamical description.

3. The Hydrodynamics and the Rate Equations for the Plasma of e^+e^--Pairs

The evolution of the e^+e^--pair plasma generated in the dyadosphere has been treated in two papers.[48,49] We recall here the basic governing equations in the most general case in which the plasma fluid is composed of e^+e^--pairs, photons and baryonic matter. The plasma is described by the stress-energy tensor

$$T^{\mu\nu} = pg^{\mu\nu} + (p+\rho)U^\mu U^\nu \,, \tag{14}$$

where ρ and p are respectively the total proper energy density and pressure in the comoving frame of the plasma fluid and U^μ is its four-velocity, satisfying

$$g_{tt}(U^t)^2 + g_{rr}(U^r)^2 = -1 \,, \tag{15}$$

where U^r and U^t are the radial and temporal contravariant components of the four-velocity.

The conservation law for baryon number can be expressed in terms of the proper baryon number density n_B:

$$\begin{aligned}(n_B U^\mu)_{;\mu} &= g^{-\frac{1}{2}}\left(g^{\frac{1}{2}} n_B U^\nu\right)_{,\nu} \\ &= (n_B U^t)_{,t} + \frac{1}{r^2}(r^2 n_B U^r)_{,r} = 0 \,.\end{aligned} \tag{16}$$

The radial component of the energy–momentum conservation law of the plasma fluid reduces to

$$\begin{aligned}&\frac{\partial p}{\partial r} + \frac{\partial}{\partial t}\left((p+\rho)U^t U_r\right) + \frac{1}{r^2}\frac{\partial}{\partial r}\left(r^2(p+\rho)U^r U_r\right) \\ &\quad - \frac{1}{2}(p+\rho)\left[\frac{\partial g_{tt}}{\partial r}(U^t)^2 + \frac{\partial g_{rr}}{\partial r}(U^r)^2\right] = 0 \,.\end{aligned} \tag{17}$$

The component of the energy–momentum conservation law of the plasma fluid equation along a flow line is

$$\begin{aligned}U_\mu (T^{\mu\nu})_{;\nu} &= -(\rho U^\nu)_{;\nu} - p(U^\nu)_{;\nu} \\ &= -g^{-\frac{1}{2}}\left(g^{\frac{1}{2}}\rho U^\nu\right)_{,\nu} - pg^{-\frac{1}{2}}\left(g^{\frac{1}{2}}U^\nu\right)_{,\nu} \\ &= (\rho U^t)_{,t} + \frac{1}{r^2}(r^2\rho U^r)_{,r} + p\left[(U^t)_{,t} + \frac{1}{r^2}(r^2 U^r)_{,r}\right] = 0 \,.\end{aligned} \tag{18}$$

Defining the total proper internal energy density ϵ and the baryonic mass density ρ_B in the comoving frame of the plasma fluid,

$$\epsilon \equiv \rho - \rho_B \,, \qquad \rho_B \equiv n_B m c^2 \,, \tag{19}$$

and using the law (16) of baryon-number conservation, we have from Eq. (18):

$$(\epsilon U^\nu)_{;\nu} + p(U^\nu)_{;\nu} = 0\,. \tag{20}$$

Recalling that $dV/d\tau = V(U^\mu)_{;\mu}$, where V is the comoving volume and τ is the proper time for the plasma fluid, we have along each flow line

$$\frac{d(V\epsilon)}{d\tau} + p\frac{dV}{d\tau} = \frac{dE}{d\tau} + p\frac{dV}{d\tau} = 0\,, \tag{21}$$

where $E = V\epsilon$ is the total proper internal energy of the plasma fluid. We express the equation of state by introducing a thermal index $\Gamma(\rho, T)$

$$\Gamma = 1 + \frac{p}{\epsilon}\,. \tag{22}$$

We now turn to the second set of governing equations describing the evolution of the e^+e^- pairs. Letting n_{e^-} and n_{e^+} be the proper number densities of electrons and positrons associated with pairs and $n^b_{e^-}$ the proper number densities of ionized electrons, we clearly have

$$n_{e^-} = n_{e^+} = n_{\rm pair}\,, \qquad n^b_{e^-} = \bar{Z} n_B\,, \tag{23}$$

where $n_{\rm pair}$ is the number of e^+e^- pairs and $\bar{Z}$ the average atomic number $\frac{1}{2} < \bar{Z} < 1$ ($\bar{Z} = 1$ for hydrogen atom and $\bar{Z} = \frac{1}{2}$ for general baryonic matter). The rate equation for electrons and positrons gives,

$$\begin{aligned}(n_{e^+}U^\mu)_{;\mu} &= (n_{e^+}U^t)_{,t} + \frac{1}{r^2}(r^2 n_{e^+}U^r)_{,r} \\ &= \overline{\sigma v}\big[\big(n_{e^-}(T) + n^b_{e^-}(T)\big)n_{e^+}(T) - (n_{e^-} + n^b_{e^-})n_{e^+}\big]\,, \end{aligned} \tag{24}$$

$$\begin{aligned}(n_{e^-}U^\mu)_{;\mu} &= (n_{e^-}U^t)_{,t} + \frac{1}{r^2}(r^2 n_{e^-}U^r)_{,r} \\ &= \overline{\sigma v}\big[n_{e^-}(T)n_{e^+}(T) - n_{e^-}n_{e^+}\big]\,, \end{aligned} \tag{25}$$

$$\begin{aligned}(n^b_{e^-}U^\mu)_{;\mu} &= (n^b_{e^-}U^t)_{,t} + \frac{1}{r^2}(r^2 n^b_{e^-}U^r)_{,r} \\ &= \overline{\sigma v}\big[n^b_{e^-}(T)n_{e^+}(T) - n^b_{e^-}n_{e^+}\big]\,, \end{aligned} \tag{26}$$

where $\overline{\sigma v}$ is the mean of the product of the annihilation cross-section and the thermal velocity of the electrons and positrons, $n_{e^\pm}(T)$ are the proper number densities of electrons and positrons associated with the pairs, given by the appropriate Fermi integrals with zero chemical potential, and $n^b_{e^-}(T)$ is the proper number density of ionized electrons, given by appropriate Fermi integrals with non-zero chemical potential μ_e at an appropriate equilibrium temperature T. These rate equations can be reduced to

$$\begin{aligned}(n_{e^\pm}U^\mu)_{;\mu} &= (n_{e^\pm}U^t)_{,t} + \frac{1}{r^2}(r^2 n_{e^\pm}U^r)_{,r} \\ &= \overline{\sigma v}\big[n_{e^-}(T)n_{e^+}(T) - n_{e^-}n_{e^+}\big]\,, \end{aligned} \tag{27}$$

$$(n^b_{e^-}U^\mu)_{;\mu} = (n^b_{e^-}U^t)_{,t} + \frac{1}{r^2}(r^2 n^b_{e^-}U^r)_{,r} = 0\,, \tag{28}$$

$$\mathrm{Frac} \equiv \frac{n_{e^\pm}}{n_{e^\pm}(T)} = \frac{n^b_{e^-}(T)}{n^b_{e^-}}\,. \tag{29}$$

Equation (28) is just the baryon-number conservation law (16) and (29) is a relationship satisfied by $n_{e^\pm}, n_{e^\pm}(T)$ and $n^b_{e^-}, n^b_{e^-}(T)$.

The equilibrium temperature T is determined by the thermalization processes occurring in the expanding plasma fluid with a total proper energy density ρ governed by the hydrodynamical equations (16)–(18). We have

$$\rho = \rho_\gamma + \rho_{e^+} + \rho_{e^-} + \rho^b_{e^-} + \rho_B\,, \tag{30}$$

where ρ_γ is the photon energy density, $\rho_B \simeq m_B c^2 n_B$ is the baryonic mass density which is considered to be nonrelativistic in the range of temperature T under consideration, and $\rho_{e^\pm}$ is the proper energy density of electrons and positrons pairs given by

$$\rho_{e^\pm} = \frac{n_{e^\pm}}{n_{e^\pm}(T)}\rho_{e^\pm}(T)\,, \tag{31}$$

where $n_{e^\pm}$ is obtained by integration of Eq. (27) and $\rho_{e^\pm}(T)$ is the proper energy density of electrons (positrons) obtained from zero chemical potential Fermi integrals at the equilibrium temperature T. On the other hand $\rho^b_{e^-}$ is the energy density of the ionized electrons coming from the ionization of baryonic matter

$$\rho^b_{e^-} = \frac{n^b_{e^-}}{n^b_{e^-}(T)}\rho^b_{e^-}(T)\,, \tag{32}$$

where $n^b_{e^-}$ is obtained by integration of Eq. (28) and $\rho_{e^-}(T)$ is the proper energy density of ionized electrons obtained from an appropriate Fermi integral of non-zero chemical potential μ_e at the equilibrium temperature T.

Having intrinsically defined the equilibrium temperature T in Eq. (30), we can also analogously evaluate the total pressure

$$p = p_\gamma + p_{e^+} + p_{e^-} + p^b_{e^-} + p_B\,, \tag{33}$$

where p_γ is the photon pressure, $p_{e^\pm}$ and $p^b_{e^-}$ are given by

$$p_{e^\pm} = \frac{n_{e^\pm}}{n_{e^\pm}(T)}p_{e^\pm}(T)\,, \tag{34}$$

$$p^b_{e^-} = \frac{n^b_{e^-}}{n^b_{e^-}(T)}p^b_{e^-}(T)\,. \tag{35}$$

The pressures $p_{e^\pm}(T)$ are determined by zero chemical potential Fermi integrals, and $p^b_{e^-}(T)$ is the pressure of the ionized electrons, evaluated by an appropriate Fermi integral of non-zero chemical potential μ_e at the equilibrium temperature T. In Eq. (33), the ion pressure p_B is negligible by comparison with the pressures $p_{\gamma,e^\pm,e^-}(T)$, since baryons and ions are expected to be nonrelativistic in the range

of temperature T under consideration. Finally using Eqs. (30) and (33) we compute the thermal factor Γ of the equation of state (22).

It is clear that the entire set of equations considered above, namely Eqs. (16)–(18) with equation of state given by Eq. (22) and the rate equation (27), have to be integrated satisfying the total energy conservation for the system. The boundary conditions adopted here are simply purely ingoing conditions at the horizon and purely outgoing conditions at radial infinity. The calculation is initiated by depositing a proper energy density (11) between the Reissner–Nordström horizon radius r_+ and the dyadosphere radius $r_{\rm ds}$, following the approximation presented in Fig. 15 The total energy deposited is given by Eq. (12).

4. The Equations Leading to the Relative Space–Time Transformations

In order to relate the above hydrodynamic and pair equations with the observations we need the governing equations relating the comoving time to the laboratory time corresponding to an inertial reference frame in which the EMBH is at rest and finally to the time measured at the detector, which must also include the effect of the cosmological expansion. These transformations have been the objective of the relative space–time transformations (RSTT) Paradigm.[1]

For signals emitted by a pulse moving with velocity v in the laboratory frame,[1] we have the following relation between the interval of arrival time Δt_a and the corresponding interval of laboratory time Δt (see Fig. 2):

$$\Delta t_a = \left(t_0 + \Delta t + \frac{R_0 - r}{c}\right) - \left(t_0 + \frac{R_0}{c}\right) = \Delta t - \frac{r}{c}\,. \tag{36}$$

For simplicity in what follows we indicate by t_a the interval of arrival time measured from the reception of a light signal emitted at the onset of the gravitational collapse. Analogously, t indicates the laboratory time interval measured from the time of the gravitational collapse. In this case, Eq. (36) can be written simply as

$$t_a = t - \frac{r}{c} = t - \frac{\int_0^t v(t')dt' + r_{\rm ds}}{c}\,, \tag{37}$$

where the dyadosphere radius $r_{\rm ds}$ is the value of r at $t = 0$. We consider here only the photons emitted along the line of sight from the external surface of the pulse. The arrival time spreading due to the angular dependence and that due to the thickness of the pulse will be considered elsewhere.[57,58] The solution of Eq. (37) has the expansion:

$$t_a = t - \frac{a_1}{c}t - \frac{1}{2}\frac{a_2}{c}t^2 - \cdots\,, \tag{38}$$

so the relation between t_a and t is in general highly nonlinear.

If and only if the expansion of the pulse is such that $r(t) = vt$ with $v \simeq c$, Eq. (37) can be written, neglecting $r_{\rm ds}$, in the following simplified form (see Fig. 10):

$$t_a \simeq t\left(1 - \frac{v}{c}\right) = t\frac{\left(1 - \frac{v}{c}\right)\left(1 + \frac{v}{c}\right)}{\left(1 + \frac{v}{c}\right)} \simeq \frac{t}{2\gamma^2}\,. \tag{39}$$

This formula has been uncritically and widely applied in all articles dealing with GRBs. It is clear, however, that the knowledge of t_a, which is indeed essential for any physical interpretation of GRB data, depends on the definite integral given in Eq. (37) whose integration limits in the laboratory time extend from the onset of the gravitational collapse to the time t relevant for the observations. Such an integral is not generally expressible as a simple linear relation or even by any explicit analytic relation since we are dealing with processes with variable gamma factor unprecedented in the entire realm of physics (see Figs. 9 and 10). Any linear approximation of the kind given in Eq. (39) with γ constant or changing with time[75] misses a crucial feature of the GRB process and is therefore erroneous in this context.

To relate the time in the laboratory frame to the time in the detector frame we have to do one additional step: the two frames are related by a transformation which is a function of the cosmological expansion. We recall that the geometry of the space–time of the universe is described by the Robertson–Walker metric:

$$ds^2 = dt^2 - \mathcal{R}^2(t)\left(\frac{dr^2}{1 - kr^2} + r^2 d\vartheta^2 + r^2 \sin^2\vartheta\, d\varphi^2\right), \tag{40}$$

where $\mathcal{R}\,(t)$ is the cosmic scale factor and k is a constant related to the curvature of the three-dimensional space ($k = 0$, $+1$, -1 corresponds to flat, close and open space respectively). The wavelength of an electromagnetic wave travelling from the point $P_1(t_1, r_1, \vartheta_1, \varphi_1)$ to the point $P_0(t_0, r_0, \vartheta_0, \varphi_0)$ where the observer is located is related to the red-shift parameter z by

$$z = \frac{\lambda_0 - \lambda_1}{\lambda_1}\,, \tag{41}$$

where λ_0 is the wavelength of the radiation for the observer and λ_1 for the emitter. We have the following general relation:

$$1 + z = (1 + z_u)(1 + z_o)(1 + z_s)\,, \tag{42}$$

where z is the total redshift due to the motion of the source z_s, the motion of the observer z_o and the cosmological redshift z_u. In the following we will assume $z_o \ll 1$ and $z_s \ll 1$ so that $z = z_u$. In terms of the scale factor $\mathcal{R}(t)$ the relation (41) gives

$$\frac{\lambda_0}{\lambda_1} = \frac{\mathcal{R}(t_0)}{\mathcal{R}(t_1)} = 1 + z = \frac{\omega_1}{\omega_0} \tag{43}$$

where ω_1 and ω_0 are the frequencies associated to λ_1 and λ_0 respectively. This frequency ratio then relates the time elapsing at the source with the time elapsing at the detector due to the cosmological expansion.

We can now define the corrected arrival time t_a^d measured at the detector, which is related to t_a by

$$t_a^d = t_a(1+z)\,, \tag{44}$$

where z is the cosmological redshift of the GRB source. In the case of GRB 991216 we have $z \simeq 1.00$.

The observed flux is the flux which crosses the surface $4\pi(\mathcal{R}(t_0)r)^2$ but this flux is lower by a factor $1+z$ due to the redshift energy of the photons and by another factor $1+z$ due to the fact that the number of photons at reception is less than the number at emission. Thus we can define a luminosity distance by

$$d_L^2 = \mathcal{R}_0^2 r^2 (1+z)^2\,. \tag{45}$$

Then the observed flux is related to the absolute luminosity of the GRB by the following relation

$$l = \frac{L}{4\pi d_L^2}\,, \tag{46}$$

where the luminosity distance d_L is simply related to the proper distance $d_p = \mathcal{R}_0 r$ by $d_L = d_p(1+z)$. The observed total fluence f is related to the total energy E of the GRB by the following relation:

$$f = \frac{E(1+z)}{4\pi d_L^2}\,. \tag{47}$$

Then the cosmological effect is taken into account by the definition of the proper distance $\mathcal{R}_0 r$ which depends on the cosmological parameters: the Hubble constant $H_0 = \dot{\mathcal{R}}\,(t_0)\,/\mathcal{R}\,(t_0)$ at time t_0 and the matter density ρ_0 or $\Omega_M = \rho_0/\rho_{\rm crit}$, where $\rho_{\rm crit} = 3H_0^2/8\pi G$.

The computation of the proper distance is then simply given by the relation:

$$d_p = \frac{c}{H_0}\int_0^z \frac{dz}{F(z)}\,, \tag{48}$$

where $F(z) = \sqrt{\Omega_M(1+z)^3}$.

In the case of the Friedman flat universe, $\Omega_M = 1$ and we have

$$d_p(z) = \frac{2c}{H_0}\left[1 - \frac{1}{\sqrt{1+z}}\right]\,. \tag{49}$$

So the measurement of the redshift gives us the luminosity distance via a cosmological scenario. With the measurement of the flux we can deduce the proper luminosity of the burst and from the measurement of the total fluence the total energy so we are then able to find the $E_{\rm dya}$.

5. The Numerical Integration of the Hydrodynamics and the Rate Equations

5.1. *The Livermore code*

A computer code[76,77] has been used to evolve the spherically symmetric general relativistic hydrodynamic equations starting from the dyadosphere.[48]

We define the generalized gamma factor γ and the radial 3-velocity in the laboratory frame V^r:

$$\gamma \equiv \sqrt{1 + U^r U_r}\,, \qquad V^r \equiv \frac{U^r}{U^t}\,. \tag{50}$$

From Eqs. (5) and (15), we then have

$$(U^t)^2 = -\frac{1}{g_{tt}}(1 + g_{rr}(U^r)^2) = \frac{1}{\alpha^2}\gamma^2\,. \tag{51}$$

Following Eq. (19), we also define

$$E \equiv \epsilon\gamma\,, \qquad D \equiv \rho_B\gamma\,, \quad \text{and} \quad \tilde{\rho} \equiv \rho\gamma\,, \tag{52}$$

so that the conservation law of baryon number (16) can then be written as

$$\frac{\partial D}{\partial t} = -\frac{\alpha}{r^2}\frac{\partial}{\partial r}\left(\frac{r^2}{\alpha}DV^r\right). \tag{53}$$

Equation (18) then takes the form

$$\frac{\partial E}{\partial t} = -\frac{\alpha}{r^2}\frac{\partial}{\partial r}\left(\frac{r^2}{\alpha}EV^r\right) - p\left[\frac{\partial\gamma}{\partial t} + \frac{\alpha}{r^2}\frac{\partial}{\partial r}\left(\frac{r^2}{\alpha}\gamma V^r\right)\right]. \tag{54}$$

Defining the radial momentum density in the laboratory frame as

$$S_r \equiv \alpha(p+\rho)U^t U_r = (D + \Gamma E)U_r\,, \tag{55}$$

we can express the radial component of the energy–momentum conservation law given in Eq. (17) by

$$\begin{aligned}\frac{\partial S_r}{\partial t} &= -\frac{\alpha}{r^2}\frac{\partial}{\partial r}\left(\frac{r^2}{\alpha}S_r V^r\right) - \alpha\frac{\partial p}{\partial r} \\ &\quad - \frac{\alpha}{2}(p+\rho)\left[\frac{\partial g_{tt}}{\partial r}(U^t)^2 + \frac{\partial g_{rr}}{\partial r}(U^r)^2\right] \\ &= -\frac{\alpha}{r^2}\frac{\partial}{\partial r}\left(\frac{r^2}{\alpha}S_r V^r\right) - \alpha\frac{\partial p}{\partial r} \\ &\quad - \alpha\left(\frac{M}{r^2} - \frac{Q^2}{r^3}\right)\left(\frac{D+\Gamma E}{\gamma}\right)\left[\left(\frac{\gamma}{\alpha}\right)^2 + \frac{(U^r)^2}{\alpha^4}\right].\end{aligned} \tag{56}$$

In order to determine the number-density of e^+e^--pairs, we turn to Eq. (27). Defining the e^+e^--pair density in the laboratory frame $N_{e^\pm} \equiv \gamma n_{e^\pm}$ and $N_{e^\pm}(T) \equiv \gamma n_{e^\pm}(T)$, where the equilibrium temperature T has been obtained from Eqs. (30)

and (31), and using Eq. (51), we rewrite the rate equation given by Eq. (27) in the form

$$\frac{\partial N_{e^\pm}}{\partial t} = -\frac{\alpha}{r^2}\frac{\partial}{\partial r}\left(\frac{r^2}{\alpha}N_{e^\pm}V^r\right) + \overline{\sigma v}(N^2_{e^\pm}(T) - N^2_{e^\pm})/\gamma^2\,. \tag{57}$$

These equations are integrated starting from the dyadosphere distributions given in Fig. 17 and assuming as usual ingoing boundary conditions on the horizon of the EMBH.

5.2. *The Rome code*

In the following we recall a zeroth order approximation of the fully relativistic equations of the previous section:[48]

(i) Since we are mainly interested in the expansion of the e^+e^--plasma away from the EMBH, we neglect the gravitational interaction.
(ii) We describe the expanding plasma by a special relativistic set of equations.
(iii) In contrast with the previous treatment where the evolution of the density profiles given in Fig. 17 are followed in their temporal evolution leading to a pulse-like structure, selected geometries of the pulse are *a priori* adopted and the correct one validated by the complete integration of the equations given by the Livermore codes.

In analogy to Eq. (21), from Eq. (16) we have along each flow line in the general case in which baryonic matter is present

$$\frac{d(n_B V)}{d\tau} = 0\,. \tag{58}$$

For the expansion of a shell from its initial volume ΔV_0 to the volume ΔV, we obtain

$$\frac{n_B^0}{n_B} = \frac{\Delta V}{\Delta V_0} = \frac{\Delta\mathcal{V}\gamma(r)}{\Delta\mathcal{V}_0\gamma_0(r)}\,, \tag{59}$$

where $\Delta\mathcal{V}$ is the volume of the shell in the laboratory frame, related to the proper volume ΔV in the comoving frame by $\Delta V = \gamma(r)\Delta\mathcal{V}$, and $\gamma(r)$ defined in Eq. (50) is the gamma factor of the shell at the radius r.

Similarly, from Eq. (21), using the equation of state (22), along the flow lines we obtain

$$d\ln\epsilon + \Gamma d\ln V = 0\,. \tag{60}$$

Correspondingly we obtain for the internal energy density ϵ along the flow lines

$$\frac{\epsilon_0}{\epsilon} = \left(\frac{\Delta V}{\Delta V_0}\right)^\Gamma = \left(\frac{\Delta\mathcal{V}}{\Delta\mathcal{V}_0}\right)^\Gamma\left(\frac{\gamma(r)}{\gamma_0(r)}\right)^\Gamma\,, \tag{61}$$

where the thermal index Γ given by Eq. (22) is a slowly-varying function with values around 4/3. It can be computed for each value of ϵ, p as a function of ΔV.

The overall energy conservation requires that the change of the internal proper energy of a shell be compensated by a change in its bulk kinetic energy. We then have[48]

$$dK = [\gamma(r) - 1](dE + \rho_B dV)\,. \tag{62}$$

In order to model the relativistic expansion of the plasma fluid, we assume that E and D, as defined by Eq. (52), are constant in space over the volume ΔV. As a consequence the total energy conservation for the shell implies[48]

$$(\epsilon_0 + \rho_B^0)\gamma_0^2(r)\Delta\mathcal{V}_0 = (\epsilon + \rho_B)\gamma^2(r)\Delta\mathcal{V}\,, \tag{63}$$

which leads to the solution

$$\gamma(r) = \gamma_0(r)\sqrt{\frac{(\epsilon_0 + \rho_B^0)\Delta\mathcal{V}_0}{(\epsilon + \rho_B)\Delta\mathcal{V}}}\,. \tag{64}$$

Corresponding to Eq. (57) we obtain the equation for the evolution of the $e^{\pm}$ number-density as seen by an observer in the laboratory frame

$$\frac{\partial}{\partial t}(N_{e^\pm}) = -N_{e^\pm}\frac{1}{\Delta\mathcal{V}}\frac{\partial\Delta\mathcal{V}}{\partial t} + \overline{\sigma v}\frac{1}{\gamma^2(r)}\left(N_{e^\pm}^2(T) - N_{e^\pm}^2\right). \tag{65}$$

Equations (59), (61), (64) and (65) are a complete set of equations describing the relativistic expansion of the shell. If we now turn from a single shell to a finite distribution of shells, we can introduce the average values of the proper internal-energy, baryon-mass, baryon-number and pair-number densities $(\bar{\epsilon}, \bar{\rho}_B, \bar{n}_B, \bar{n}_{e^\pm})$ and $\bar{E} \equiv \bar{\gamma}\bar{\epsilon}$, $\bar{D} \equiv \bar{\gamma}\bar{\rho}_B$, $\bar{N}_{e^\pm} \equiv \bar{\gamma}(r)\bar{n}_{e^\pm}$ for the PEM-pulse, where the average $\bar{\gamma}$-factor is defined by

$$\bar{\gamma} = \frac{1}{\mathcal{V}}\int_{\mathcal{V}}\gamma(r)d\mathcal{V}\,, \tag{66}$$

and $\mathcal{V}$ is the total volume of the shell in the laboratory frame. The corresponding equations are given by Ruffini, Salmonson, Wilson & Xue in 1999.[48] Having defined all its governing equations we can now return to the description of the different eras of the GRB phenomena.

6. The Era I: The PEM Pulse

We have assumed that, following the gravitational collapse process, a region of very low baryonic contamination exists in the dyadosphere all the way to the remnant of the progenitor star.

Recalling Eq. (9), the limit on such baryonic contamination, where ρ_{B_c} is the mass-energy density of baryons, is given by

$$\rho_{B_c} \ll m_p n_{e^+e^-}(r) = 3.2\cdot 10^8\left(\frac{r_{\rm ds}}{r}\right)^2\left[1 - \left(\frac{r}{r_{\rm ds}}\right)^2\right](\mathrm{g/cm^3})\,. \tag{67}$$

Near the horizon $r \simeq r_+$, this gives

$$\rho_{B_c} \ll m_p n_{e^+e^-}(r) = 1.86 \cdot 10^{14} \left(\frac{\xi}{\mu}\right) (\mathrm{g/cm^3}) \,, \tag{68}$$

and near the radius of the dyadosphere r_{ds}:

$$\rho_{B_c} \ll m_p n_{e^+e^-}(r) = 3.2 \cdot 10^8 \left[1 - \left(\frac{r}{r_{\mathrm{ds}}}\right)^2\right]_{r \to r_{\mathrm{ds}}} (\mathrm{g/cm^3}) \,. \tag{69}$$

Such conditions can be easily satisfied in the collapse to an EMBH, but not necessarily in a collapse to a neutron star.

Consequently we have solved the equations governing a plasma composed solely of e^+e^--pairs and electromagnetic radiation, starting at time zero from the dyadosphere configurations corresponding to constant density in Fig. 17. The Livermore code[48] has shown very clearly the self organization of the expanding plasma in a very sharp pulse which we have defined as the pair-electromagnetic pulse (PEM pulse), in analogy with the EM pulse observed in nuclear explosions. In order to further examine the structure of the PEM pulse with the simpler procedures of the Rome codes we have assumed[48] three alternative patterns of expansion of the PEM pulse on which to try the simplified special relativistic treatment and then compared the results with the fully general relativistic hydrodynamical results:

- Spherical model: We assume the radial component of the four-velocity $U_r(r) = Ur/\mathcal{R}$, where U is the radial component of the four-velocity at the moving outer surface $r = \mathcal{R}(t)$ of the PEM pulse and the $\bar{\gamma}$-factor and the velocity V_r are

  $$\bar{\gamma} = \frac{3}{8U^3}\left[2U(1+U^2)^{\frac{3}{2}} - U(1+U^2)^{\frac{1}{2}} - \ln(U + \sqrt{1+U^2})\right], \quad V_r = \frac{U_r}{\bar{\gamma}} \,. \tag{70}$$

  This distribution expands keeping a uniform density profile which decreases with time similar to a portion of a Friedmann Universe.
- Slab 1: We assume $U(r) = U_r = \mathrm{const}$, the constant width of the expanding slab $\mathcal{D} = R_0$ in the laboratory frame of the PEM pulse, while $\bar{\gamma}$ and V_r are

  $$\bar{\gamma} = \sqrt{1 + U_r^2} \,, \qquad V_r = \frac{U_r}{\bar{\gamma}} \,. \tag{71}$$

  This distribution does not need any averaging process.
- Slab 2: we assume a constant width $R_2 - R_1 = R_0$ of the expanding slab in the comoving frame of the PEM pulse, while $\bar{\gamma}$ and V_r are

  $$\bar{\gamma} = \sqrt{1 + U_r^2(\tilde{r})} \,, \qquad V_r = \frac{U_r}{\bar{\gamma}} \,, \tag{72}$$

  This distribution needs an averaging procedure and $R_1 < \tilde{r} < R_2$, i.e. $\tilde{r}$ is an intermediate radius in the slab.

These different assumptions lead to three different distinct slopes for the monotonically increasing $\bar{\gamma}$-factor as a function of the radius (or time) in the laboratory frame, having assumed for the energy of dyadosphere $E_{\mathrm{dya}} = 3.1 \times 10^{54}$ erg

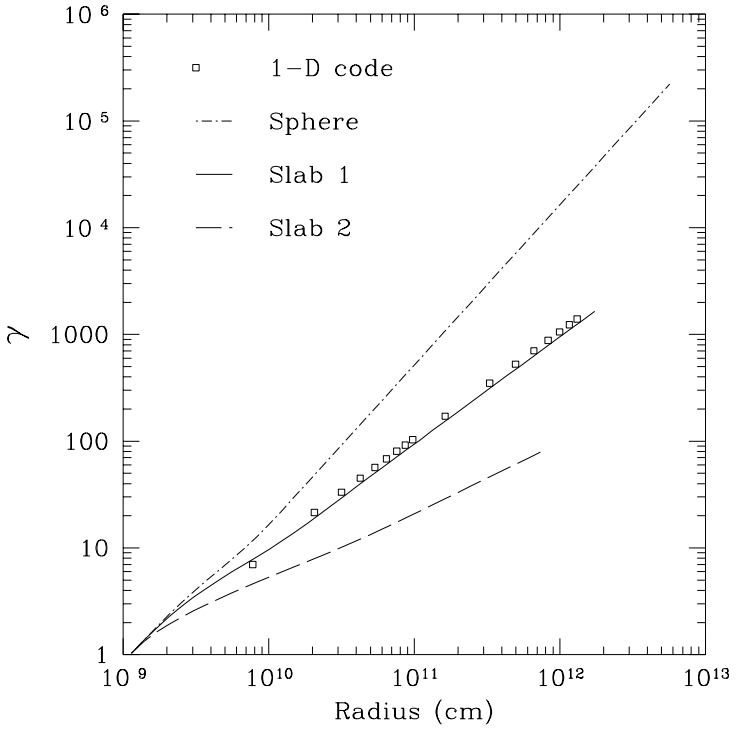

Fig. 18. Gamma factor as a function of radius. Three models for the expansion pattern of the PEM-pulse are compared with the results of the one-dimensional hydrodynamic code for an energy of dyadosphere $E_{\rm dya} = 3.1 \times 10^{54}$ erg. The 1-D code has an expansion pattern that strongly resembles that of a shell with constant thickness in the laboratory frame.

(see Fig. 18). In principle, we could have an infinite number of models by defining arbitrarily the geometry of the expanding fluid in the special relativistic treatment given above. To find out which expanding pattern of PEM pulses is the physically realistic one, we need to compare and contrast the results of our simplified models (performed in Rome) with the numerical results based on the hydrodynamic Eqs. (53), (54) and (56) (obtained at Livermore).[48] Details of the iterative method used to solve the special relativistic equation can be found in Ruffini, Salmonson, Wilson & Xue.[48]

It is manifest from the results (see Fig. 18) that the slab 1 approximation (constant thickness in the laboratory frame) is in excellent agreement with the Livermore results (open squares).

The remarkable validation of the special relativistic treatment of the PEM pulse,[48] allows us to easily estimate the related quantities of physical and astrophysical interest in the model, like the e^+e^--pair densities as a function of the laboratory time, the temperature of the plasma in the comoving and laboratory frames, the reheating ratio as a function of the e^+e^--pair annihilation for a variety of initial conditions.[48]

7. The Era II: The Interaction of the PEM Pulse with the Remnant of the Progenitor Star

The PEM pulse expands initially in a region of very low baryonic contamination created by the process of gravitational collapse. As it moves further out the baryonic remnant (see Fig. 1) of the progenitor star is encountered. As discussed in Sec. 21 below, the existence of such a remnant is necessary in order to guarantee the overall charge neutrality of the system: the collapsing core has the opposite charge of the remnant and the system as a whole is clearly neutral. The number of extra charges in the baryonic remnant negligibly affects the overall charge neutrality of the PEM pulse.[74,78]

The baryonic matter remnant is assumed to be distributed well outside the dyadosphere in a shell of thickness Δ between an inner radius $r_{\rm in}$ and an outer radius $r_{\rm out} = r_{\rm in} + \Delta$ at a distance from the EMBH at which the original PEM pulse expanding in vacuum has not yet reached transparency. For the sake of an example we choose

$$r_{\rm in} = 100 r_{\rm ds}\,, \qquad \Delta = 10 r_{\rm ds}\,. \tag{73}$$

The total baryonic mass $M_B = N_B m_p$ is assumed to be a fraction of the dyadosphere initial total energy ($E_{\rm dya}$). The total baryon-number N_B is then expressed as a function of the dimensionless parameter B given by

$$B = \frac{N_B m_p c^2}{E_{\rm dya}}\,, \tag{74}$$

where B is a parameter in the range $10^{-8} - 10^{-2}$ and m_p is the proton mass. We shall see below the paramount importance of B in the determination of the features of the GRBs. We will see in Sec. 9 the sense in which B and $E_{\rm dya}$ can be considered to be the only two free parameters of the EMBH theory for the entire GRB family, the so called "long bursts". We shall see in Sec. 11 that for the so called "short bursts" the EMBH theory depends on the two other parameters μ, ξ, since in that case $B = 0$. The baryon number density n_B^0 is assumed to be a constant

$$\bar{n}_B^0 = \frac{N_B}{V_B}\,, \qquad \bar{\rho}_B^0 = m_p \bar{n}_B^0 c^2\,. \tag{75}$$

As the PEM pulse reaches the region $r_{\rm in} < r < r_{\rm out}$, it interacts with the baryonic matter which is assumed to be at rest. In our simplified quasi-analytic model we make the following assumptions to describe this interaction:

- The PEM pulse does not change its geometry during the interaction.
- The collision between the PEM pulse and the baryonic matter is assumed to be inelastic.
- The baryonic matter reaches thermal equilibrium with the photons and pairs of the PEM pulse.

These assumptions are valid if: (i) the total energy of the PEM pulse is much larger than the total mass-energy of baryonic matter M_B, $10^{-8} < B < 10^{-2}$,

(ii) the ratio of the comoving number density of pairs and baryons at the moment of collision $n_{e^+e^-}/n_B^0$ is very high (e.g., $10^6 < n_{e^+e^-}/n_B^0 < 10^{12}$), and (iii) the PEM pulse has a large value for the gamma factor ($100 < \bar{\gamma}$).

In the collision between the PEM pulse and the baryonic matter at $r_{\rm out} > r > r_{\rm in}$, we impose total conservation of energy and momentum. We consider the collision process between two radii r_2, r_1 satisfying $r_{\rm out} > r_2 > r_1 > r_{\rm in}$ and $r_2 - r_1 \ll \Delta$. The amount of baryonic mass acquired by the PEM pulse is

$$\Delta M = \frac{M_B}{V_B}\frac{4\pi}{3}(r_2^3 - r_1^3)\,, \tag{76}$$

where M_B/V_B is the mean-density of baryonic matter at rest. The conservation of total energy leads to the estimate of the corresponding quantities before (with "0") and after such a collision

$$(\Gamma\bar{\epsilon}_0 + \bar{\rho}_B^0)\bar{\gamma}_0^2\mathcal{V}_0 + \Delta M = \left(\Gamma\bar{\epsilon} + \bar{\rho}_B + \frac{\Delta M}{V} + \Gamma\Delta\bar{\epsilon}\right)\bar{\gamma}^2\mathcal{V}\,, \tag{77}$$

where $\Delta\bar{\epsilon}$ is the corresponding increase of internal energy due to the collision. Similarly the momentum-conservation gives

$$(\Gamma\bar{\epsilon}_0 + \bar{\rho}_B^0)\bar{\gamma}_0 U_r^0\mathcal{V}_0 = \left(\Gamma\bar{\epsilon} + \bar{\rho}_B + \frac{\Delta M}{V} + \Gamma\Delta\bar{\epsilon}\right)\bar{\gamma}U_r\mathcal{V}\,, \tag{78}$$

where the radial component of the four-velocity of the PEM pulse is $U_r^0 = \sqrt{\bar{\gamma}_0^2 - 1}$ and Γ is the thermal index. We then find

$$\Delta\bar{\epsilon} = \frac{1}{\Gamma}\left[(\Gamma\bar{\epsilon}_0 + \bar{\rho}_B^0)\frac{\bar{\gamma}_0 U_r^0\mathcal{V}_0}{\bar{\gamma}U_r\mathcal{V}} - \left(\Gamma\bar{\epsilon} + \bar{\rho}_B + \frac{\Delta M}{V}\right)\right], \tag{79}$$

$$\bar{\gamma} = \frac{a}{\sqrt{a^2 - 1}}\,, \qquad a \equiv \frac{\bar{\gamma}_0}{U_r^0} + \frac{\Delta M}{(\Gamma\bar{\epsilon}_0 + \bar{\rho}_B^0)\bar{\gamma}_0 U_r^0\mathcal{V}_0}\,. \tag{80}$$

These equations determine the gamma factor $\bar{\gamma}$ and the internal energy density $\bar{\epsilon} = \bar{\epsilon}_0 + \Delta\bar{\epsilon}$ in the capture process of baryonic matter by the PEM pulse.

The effect of the collision of the PEM pulse with the remnant leads to the following results[49] as a function of the B parameter defined in Eq. (74):

(1) An abrupt decrease of the gamma factor given by

$$\gamma_{\rm coll} = \gamma_0\frac{1+B}{\sqrt{{\gamma_0}^2(2B+B^2)+1}}\,, \tag{81}$$

where γ_0 is the gamma factor of the PEM pulse prior to the collision and B is given by Eq. (74).

(2) An increase of the internal energy in the comoving frame $E_{\rm coll}$ developed in the collision given by

$$\frac{E_{\rm coll}}{E_{\rm dya}} = \frac{\sqrt{{\gamma_0}^2(2B+B^2)+1}}{\gamma_0} - \left(\frac{1}{\gamma_0} + B\right). \tag{82}$$

(3) A corresponding reheating of the plasma in the comoving frame but not in the laboratory frame, an increase of the number of e^+e^- pairs and correspondingly an overall increase of the opacity of the pulse. See details in Sec. 10.

8. The Era III: the PEMB Pulse

After the engulfment of the baryonic matter of the remnant the plasma formed of e^+e^--pairs, electromagnetic radiation and baryonic matter expands again as a sharp pulse, namely the PEMB pulse. The calculation is continued as the plasma fluid expands, cools and the e^+e^- pairs recombine until it becomes optically thin:

$$\int_R dr(n_{e^\pm} + \bar{Z}n_B)\sigma_T \simeq O(1)\,, \tag{83}$$

where $\sigma_T = 0.665 \cdot 10^{-24}$ cm^2 is the Thomson cross-section and the integration is over the radial interval of the PEMB pulse in the comoving frame. We have first explored the general problem of the PEMB pulse evolution by integrating the general relativistic hydrodynamical equations with the Livermore codes, for a total energy in the dyadosphere of 3.1×10^{54} erg and a baryonic shell of thickness $\Delta = 10 r_{\rm ds}$ at rest at a radius of $100 r_{\rm ds}$ and $B \simeq 1.3 \cdot 10^{-4}$.

In total analogy with the special relativistic treatment for the PEM pulse, presented in Sec. 6 (see also Ruffini, Salmonson, Wilson & Xue[48]), we obtain for the adiabatic expansion of the PEMB pulse, in the constant-slab approximation described by the Rome codes, the following hydrodynamical equations with $\rho_B \neq 0$:

$$\frac{\bar{n}_B^0}{\bar{n}_B} = \frac{V}{V_0} = \frac{\mathcal{V}\bar{\gamma}}{\mathcal{V}_0\bar{\gamma}_0}\,, \tag{84}$$

$$\frac{\bar{\epsilon}_0}{\bar{\epsilon}} = \left(\frac{V}{V_0}\right)^\Gamma = \left(\frac{\mathcal{V}}{\mathcal{V}_0}\right)^\Gamma \left(\frac{\bar{\gamma}}{\bar{\gamma}_0}\right)^\Gamma\,, \tag{85}$$

$$\bar{\gamma} = \bar{\gamma}_0 \sqrt{\frac{(\Gamma\bar{\epsilon}_0 + \bar{\rho}_B^0)\mathcal{V}_0}{(\Gamma\bar{\epsilon} + \bar{\rho}_B)\mathcal{V}}}\,, \tag{86}$$

$$\frac{\partial}{\partial t}(N_{e^\pm}) = -N_{e^\pm}\frac{1}{\mathcal{V}}\frac{\partial \mathcal{V}}{\partial t} + \overline{\sigma v}\frac{1}{\bar{\gamma}^2}(N_{e^\pm}^2(T) - N_{e^\pm}^2)\,. \tag{87}$$

In these equations ($r > r_{\rm out}$) the comoving baryonic mass and number densities are $\bar{\rho}_B = M_B/V$ and $\bar{n}_B = N_B/V$, where V is the comoving volume of the PEMB pulse.

We compare and contrast (see Fig. 5) the bulk gamma factor as computed from the Rome and Livermore codes, where excellent agreement has been found. This validates the constant-thickness approximation in the case of the PEMB pulse as well. On this basis we easily estimate a variety of physical quantities for an entire range of values of B.

For the same EMBH we have considered five different cases: a shell of baryonic mass with (1) $B \simeq 1.3{\cdot}10^{-4}$; (2) $B \simeq 3.8{\cdot}10^{-4}$; (3) $B \simeq 1.3{\cdot}10^{-3}$; (4) $B \simeq 3.8{\cdot}10^{-3}$; (5) $B \simeq 1.3{\cdot}10^{-3}$). The results of the integration, given in detail in 2000 by Ruffini, Salmonson, Wilson & Xue,[49] show that for the first parameter range the PEMB pulse propagates as a sharp pulse of constant thickness in the laboratory frame, but already for $B \simeq 1.3 \cdot 10^{-2}$ the expansion of the PEMB pulse becomes much more

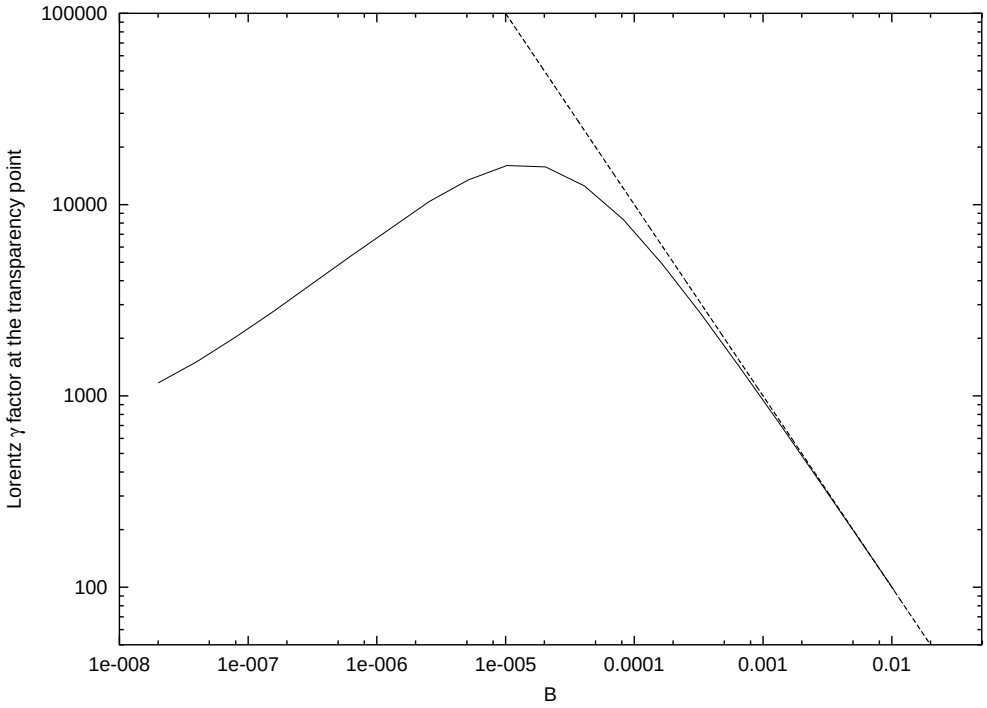

Fig. 19. The gamma factor (the solid line) at the transparent point is plotted as a function of the B parameter. The asymptotic value (the dashed line) $E_{\rm dya}/(M_B c^2)$ is also plotted.

complex and the constant-thickness approximation ceases to be valid (see Ruffini, Salmonson, Wilson & Xue[49] for details).

It is particularly interesting to evaluate the final value of the gamma factor of the PEMB pulse when the transparency condition given by Eq. (83) is reached as a function of B (see Fig. 19). For a given EMBH, there is a *maximum* value of the gamma factor at transparency. By further increasing the value of B the entire $E_{\rm dya}$ is transferred into the kinetic energy of the baryons (see also Sec. 11). Details are again given in Ruffini, Salmonson, Wilson & Xue.[49]

In Fig. 20 we plot the gamma factor of the PEMB pulse versus the radius for different amounts of baryonic matter. The diagram extends to values of the radial coordinate at which the transparency condition given by Eq. (83) is reached. The "asymptotic" gamma factor

$$\bar{\gamma}_{\rm asym} \equiv \frac{E_{\rm dya}}{M_B c^2} \tag{88}$$

is also shown for each curve. The closer the gamma value approaches the "asymptotic" value (88) at transparency, the smaller the intensity of the radiation emitted in the burst and the larger the amount of kinetic energy left in the baryonic matter.

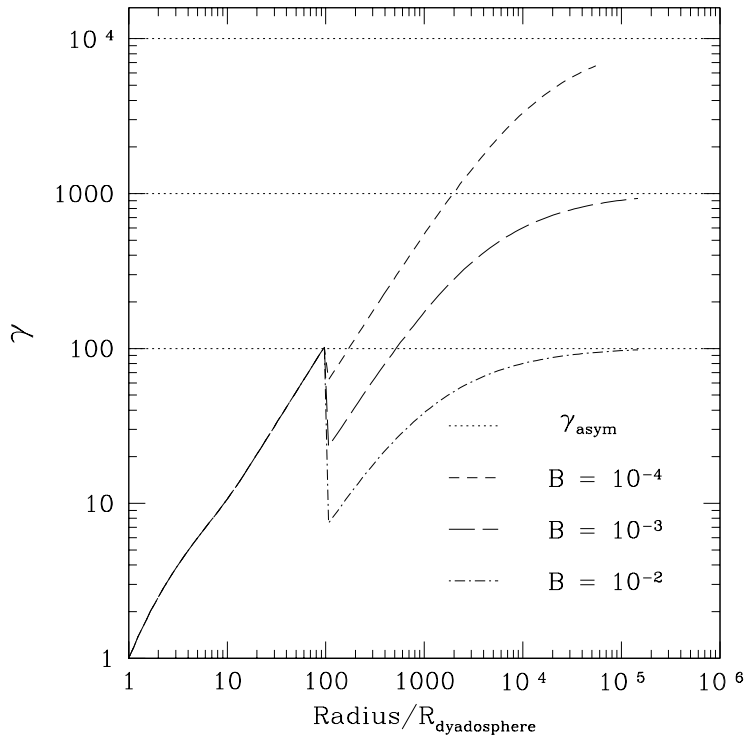

Fig. 20. The gamma factors are given as functions of the radius in units of the dyadosphere radius for selected values of B for the typical case $E_{\rm dya} = 3.1 \times 10^{54}$ erg. The asymptotic values $\gamma_{\rm asym} = E_{\rm dya}/(M_B c^2) = 10^4$, 10^3, 10^2 are also plotted. The collision of the PEM pulse with the baryonic remnant occurs at $r/r_{\rm ds} = 100$ where the jump occurs and the PEMB pulse starts.

9. The Identification of the Free Parameters of the EMBH Theory

Within the approximation presented in Sec. 2 the EMBH is characterized by two parameters: μ and ξ. The energy of the dyadosphere is expressed in terms of these two parameters by Eq. (12).

There is an entire family of EMBH solutions with different values of μ and ξ corresponding to the same value of $E_{\rm dya}$ (see Fig. 16). These solutions are physically different with respect to the density of electron-positron pair distributions given by Eq. (9), as well as to their energy density given by Eq. (11). A clear example of such a degeneracy is given in Fig. 21 where the two limiting energy density profiles approximating the dyadosphere as introduced in Fig. 17 are given for three different EMBH configurations corresponding to the same value of $E_{\rm dya} = 3.1 \times 10^{54}$ erg. The three configurations correspond respectively to the three different pairs (μ, ξ): $(10, 0.76)$, $(10^2, 0.27)$, $(10^3, 0.10)$.

The corresponding dynamical evolution of the PEM pulse introduced in Sec. 6 and in Ruffini, Salmonson, Wilson & Xue[48] is clearly different in the three cases. It is remarkable that when the collision with the remnant of the progenitor star

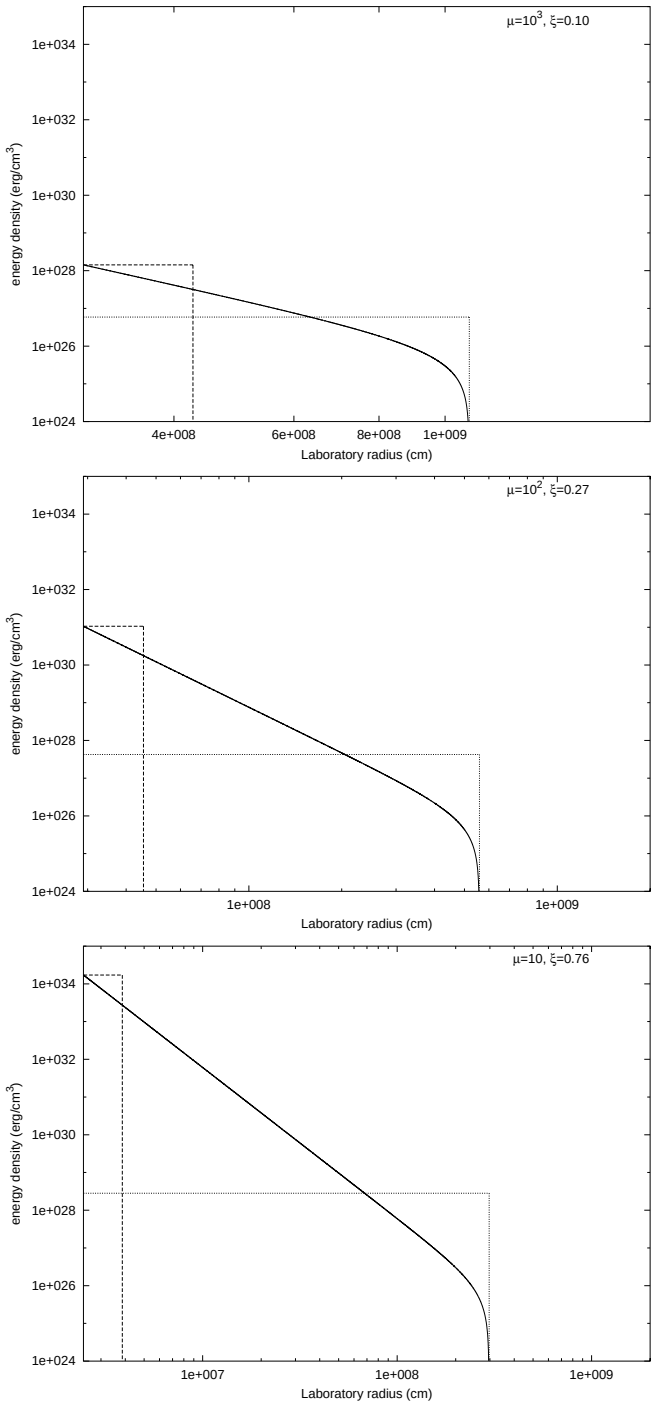

Fig. 21. Three different dyadospheres corresponding to the same value of $E_{\rm dya} = 3.1 \times 10^{54}$ erg and with different values of the two parameters μ and ξ are given. The three different configurations are markedly different in their spatial extent as well as in their energy-density distribution.

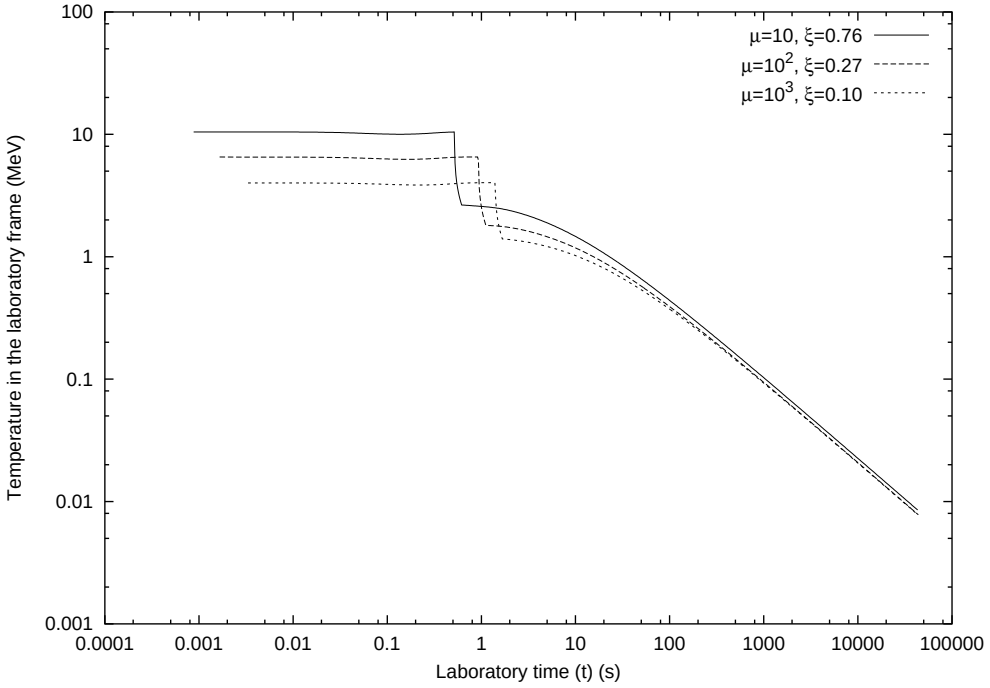

Fig. 22. The temperature of the plasma during the PEM pulse and PEMB pulse eras, measured in the laboratory frame, corresponding to the three configurations presented in Fig. 21 is given as a function of the laboratory time. The three different curves converge to a common one in the PEMB pulse era, which is therefore only a function of the $E_{\rm dya}$ and B. The difference among the three curves in the early part of the PEMB pulse follows from having located the baryonic matter at a distance of $50(r_{\rm ds} - r_+)$, which is different in the three cases. Such difference become negligible at large distances in the later phases of the evolution.

is considered all these differences disappear. As usual (see Sec. 7) we describe the baryonic content of the remnant by the parameter B. The PEMB pulse generated after the collision with the baryonic matter depends uniquely on the two parameters $E_{\rm dya}$ and B. In Fig. 22 the temperature in the laboratory frame is given for the PEM pulse and the PEMB pulse corresponding to the three configurations of Fig. 21 and $B = 4 \times 10^{-3}$. It is clear that while for the PEM pulse era the three configurations are markedly different, they do converge to a common behaviour in the PEMB pulse era.

If we turn now to the effect of the distance between the EMBH and the baryonic remnant, we see that this degeneracy is further extended: while the three PEM pulse eras are quite different, the common PEMB pulse era is largely insensitive to the location of the baryonic remnant (see Fig. 23). We have plotted the three gamma factors in the PEM pulse era corresponding to the different configurations of Fig. 21 and $B = 10^{-2}$, in the two cases the baryonic remnant is positioned at different distances from the EMBH.

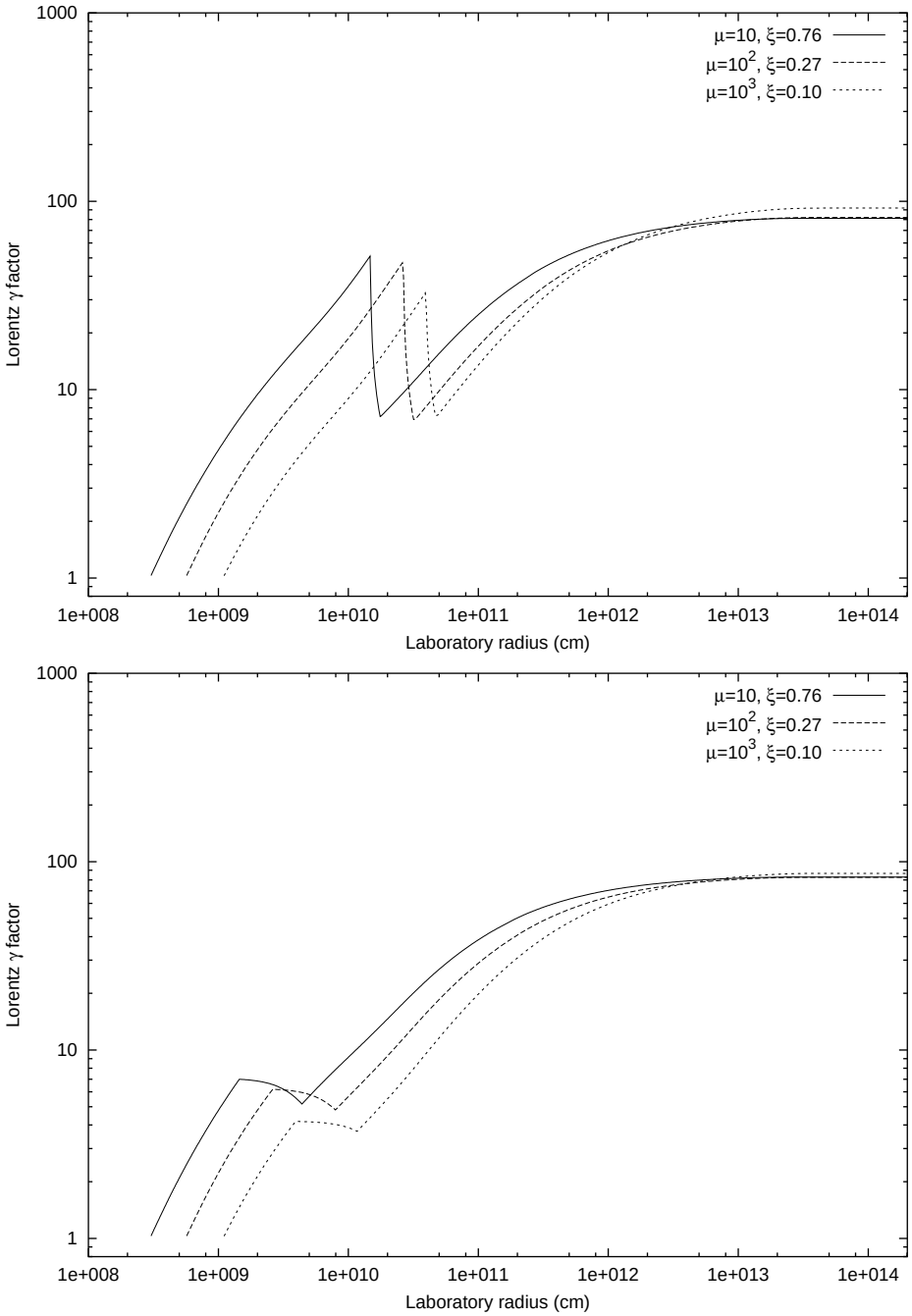

Fig. 23. The gamma factors for the three configurations considered in Fig. 21 are given as a function of the radial coordinate in the laboratory frame. The two figures correspond to a baryonic remnant positioned respectively at $r_{\rm in} = 50(r_{\rm ds} - r_+)$ (above) and at $r_{\rm in} = 5(r_{\rm ds} - r_+)$. Again the convergence to a common behaviour, uniquely a function of $E_{\rm dya}$ and B for the late stages of the PEMB pulse, is manifest.

If the PEM pulse has reached extreme relativistic regimes, the common value $\gamma_{\rm coll}$ to which the three gamma factors drop in the collision with the baryonic matter of the remnant can be simply expressed by the large gamma limit of Eq. (81):

$$\gamma_{\rm coll} = \frac{B+1}{\sqrt{B^2+2B}}\,, \tag{89}$$

while the internal energy $E_{\rm coll}$ developed in that collision is simply given by the corresponding limit of Eq. (82)

$$\frac{E_{\rm coll}}{E_{\rm dya}} = -B + \sqrt{B^2+2B}\,. \tag{90}$$

This approximation applies when the final gamma factor at the end of the PEM pulse era is larger than $\gamma_{\rm coll}$ (upper panel in Fig. 23).

Turning from these general considerations to the GRB data, this degeneracy in the PEMB pulse eras and their dependence on only two parameters $E_{\rm dya}$ and B have far reaching astrophysical implications for the identification of the source of GRBs. As we will see in the conclusions all the information obtainable from GRBs with a large value of the parameter B will lead to the determination of the above two parameters. An entire family of degenerate astrophysical solutions in the range of charges and masses given in Fig. 16 are possible. The direct knowledge of the mass and charge of the EMBH can only be gained from the PEM pulse or from GRBs with very small values of B — the so called "short bursts" (see Sec. 11 and the conclusions).

10. The Approach to Transparency: The Thermodynamical Quantities

As the condition of transparency expressed by Eq. (83) is reached the *injector phase* terminates. The electromagnetic energy of the PEMB pulse is released in the form of free-streaming photons — the proper GRB. The remaining energy of the PEMB pulse is released as an accelerated-baryonic-matter (ABM) pulse.

We now proceed to the analysis of the approach to the transparency condition. It is then necessary to turn from the pure dynamical description of the PEMB pulse described in the previous sections to the relevant thermodynamic parameters. Also such a description at the time of transparency needs the knowledge of the thermodynamical parameters in all previous eras of the GRB.

As above we shall consider as a typical case an EMBH of $E_{\rm dya} = 3.1 \times 10^{54}$ erg and $B = 10^{-2}$. We will refer to a dyadosphere configuration described by the two limiting approximations shown in Fig. 17.

One of the key thermodynamical parameters is represented by the temperature of the PEM and PEMB pulses. It is given as a function of the radius both in the comoving and in the laboratory frames in Fig. 24. Before the collision the PEM pulse expands keeping its temperature in the laboratory frame constant while its

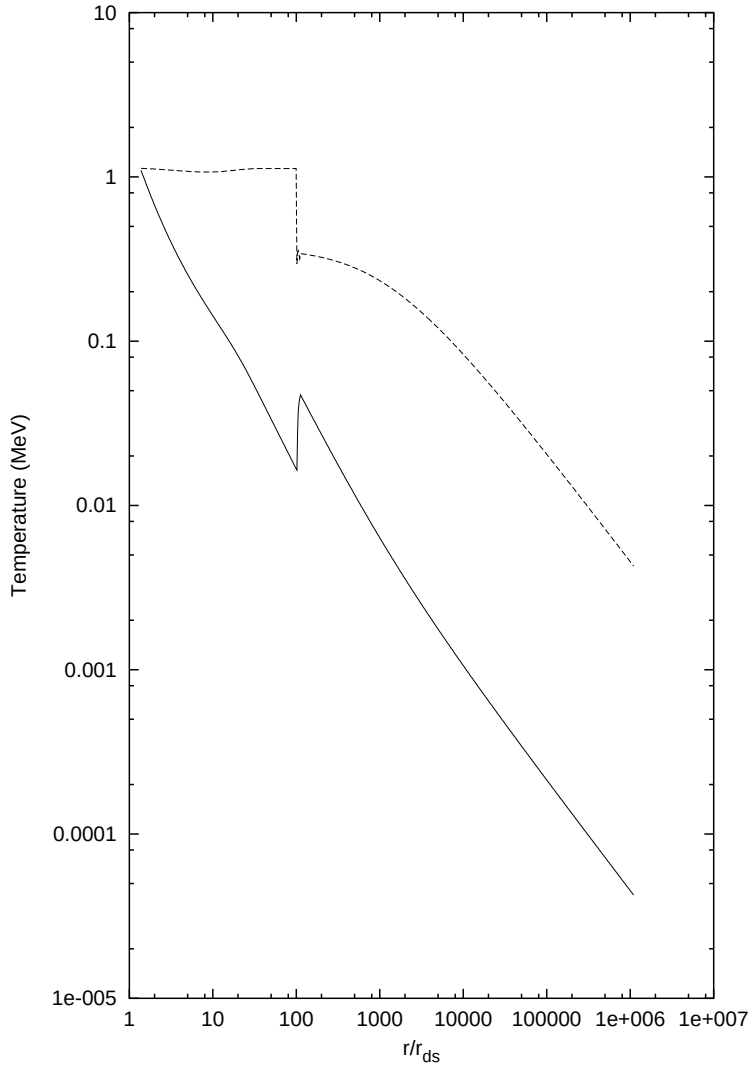

Fig. 24. The temperature of the plasma in the comoving frame T' (MeV) (the solid line) and in the laboratory frame $\bar{\gamma}T'$ (the dashed line) are plotted as functions of the radius in the unit of the dyadosphere radius $r_{\rm ds}$.

temperature in the comoving frame falls.[48] In fact Eqs. (63) and (64) are equivalent to

$$\frac{d(\epsilon\gamma^2\mathcal{V})}{dt} = 0\,, \tag{91}$$

where the baryon mass-density is $\rho_B = 0$ and the thermal energy-density of photons and e^+e^--pairs is $\epsilon = \sigma_B T^4(1 + f_{e^+e^-})$, σ_B is the Boltzmann constant and $f_{e^+e^-}$ is the Fermi-integral for e^+ and e^-. This leads to

$$\epsilon\gamma^2\mathcal{V} = E_{\rm dya}\,, \qquad T^4\gamma^2\mathcal{V} = \text{const.} \tag{92}$$

Since e^+ and e^- in the PEM pulse are extremely relativistic, we have the equation of state $p \simeq \epsilon/3$ and the thermal index (22) having the value $\Gamma \simeq 4/3$ in the evolution of PEM pulse. Equation (92) is thus equivalent to

$$T^3 \bar{\gamma} \mathcal{V} \simeq \text{const.} \tag{93}$$

These two equations (91) and (93) result in the constancy of the laboratory temperature $T\bar{\gamma}$ in the evolution of the PEM pulse.

It is interesting to note that Eqs. (92) and (93) hold as well in the cross-over region where $T \sim m_e c^2$ and e^+e^- annihilation takes place. In fact from conservation of entropy it follows that asymptotically we have

$$\frac{(VT^3)_{T<m_e c^2}}{(VT^3)_{T>m_e c^2}} = \frac{11}{4}\,, \tag{94}$$

exactly for the same reasons and physics scenario discussed in the cosmological framework by Weinberg, see e.g. Eq. (15.6.37) of Weinberg (1972). The same considerations when repeated for conservation of the total energy $\epsilon\gamma V = \epsilon\gamma^2\mathcal{V}$ following from Eq. (91) which then lead to

$$\frac{(VT^4\gamma)_{T<m_e c^2}}{(VT^4\gamma)_{T>m_e c^2}} = \frac{11}{4}\,. \tag{95}$$

The ratio of these last two quantities gives asymptotically

$$T_0 = (T\gamma)_{T>m_e c^2} = (T\gamma)_{T<m_e c^2}\,, \tag{96}$$

where T_0 is the initial average temperature of the dyadosphere at rest.

During the collision of the PEM pulse with the remnant we have an increase in the number density of e^+e^- pairs (see Fig. 25). This transition corresponds to an *increase* of the temperature in the comoving frame and a *decrease* of the temperature in the laboratory frame as a direct effect of the dropping of the gamma factor (see Fig. 20).

After the collision we have the further acceleration of the PEMB pulse (see Fig. 20). The temperature now decreases both in the laboratory and the comoving frame (see Fig. 24). Before the collision the total energy of the e^+e^- pairs and the photons is constant and equal to $E_{\rm dya}$. After the collision

$$E_{\rm dya} = E_{\rm Baryons} + E_{e^+e^-} + E_{\rm photons}\,, \tag{97}$$

which includes both the total energy $E_{e^+e^-} + E_{\rm photons}$ of the nonbaryonic components and the kinetic energy $E_{\rm Baryons}$ of the baryonic matter

$$E_{\rm Baryons} = \bar{\rho}_B V(\bar{\gamma} - 1)\,. \tag{98}$$

In Fig. 26 we plot both the total energy $E_{e^+e^-} + E_{\rm photons}$ of the nonbaryonic components and the kinetic energy $E_{\rm Baryons}$ of the baryonic matter as functions of the radius for the typical case $E_{\rm dya} = 3.1 \times 10^{54}$ erg and $B = 10^{-2}$. Further details are given in Ruffini, Salmonson, Wilson & Xue.[49]

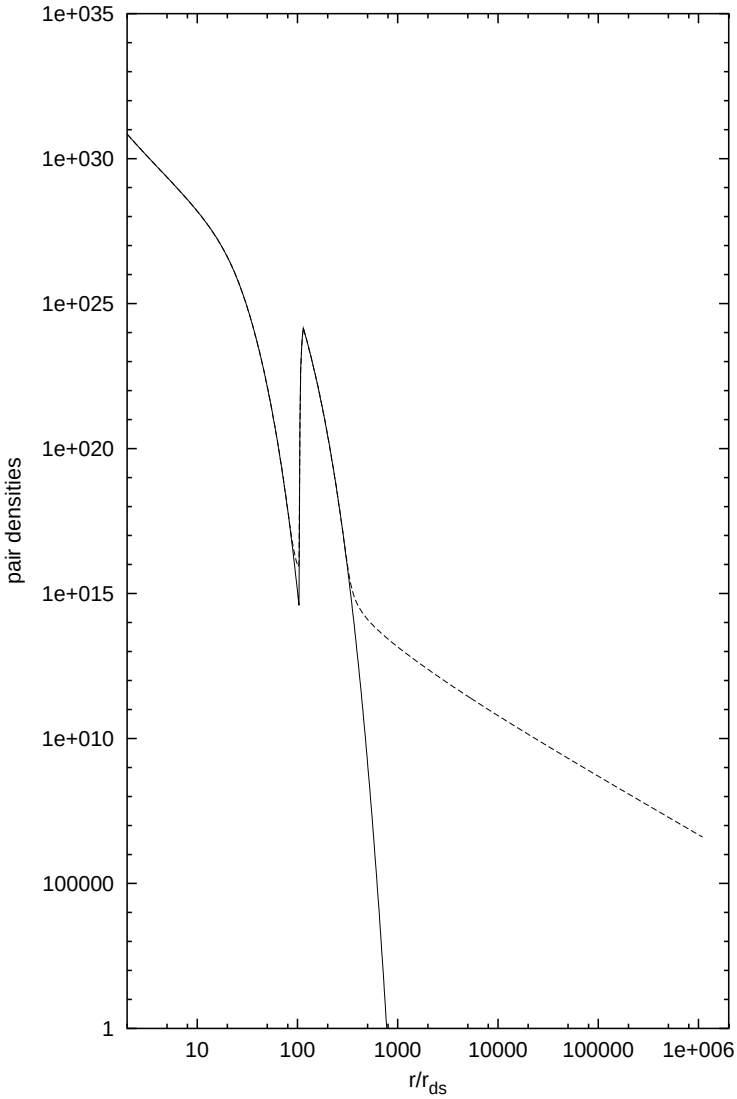

Fig. 25. The number densities $n_{e^+e^-}(T)$ (the solid line) computed by the Fermi integral and $n_{e^+e^-}$ (the dashed line) computed by the rate equation (see Sec. 3) are plotted as functions of the radius. $T' \ll m_e c^2$, two curves strongly divergent due to e^+e^--pairs frozen out of the thermal equilibrium. The peak at $r \simeq 100 r_{\rm ds}$ is due to the internal energy developed in the collision.

11. The P-GRBs and The "Short Bursts". The End of the Injector Phase

We now analyze the approach to the transparency condition given by Eq. (83). For selected values of B we give the energy $E_{\text{P-GRB}}$ of the P-GRB, and E_{Baryons} of the ABM pulse. We clearly have

$$E_{\rm dya} = E_{\text{P-GRB}} + E_{\text{Baryons}} \,. \tag{99}$$

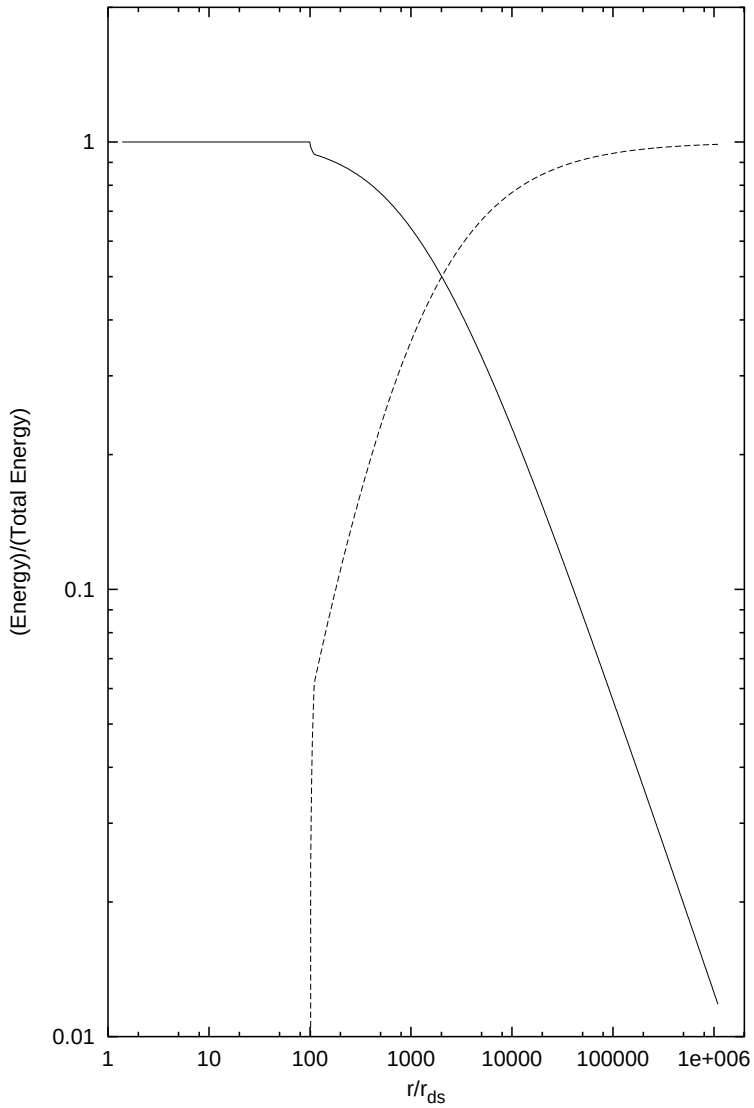

Fig. 26. The energy of the non-baryonic components of the PEMB pulse (the solid line) and the kinetic energy of the baryonic matter (the dashed line) in the unit of the total energy are plotted as functions of the radius in the unit of the dyadosphere radius $r_{\rm ds}$.

Taking into account the results shown in Figs. 24–26, we can repeat all the considerations for selected values of B. We shall examine values of B ranging from $B = 10^{-8}$ only up to $B = 10^{-2}$: for larger values of B our constant slab approximation breaks down. We will see in the following that this range does indeed cover the most relevant observational features of the GRBs.

As clearly shown in Fig. 20 both the final value of the gamma factor and the radial coordinate at which the transparency condition is reached depend very

strongly on B. Therefore a strong dependence on B is also found in the relative values of $E_{\text{P-GRB}}$ and E_{Baryons}.

We are now finally ready to give in Fig. 6 the crucial diagram representing the values of $E_{\text{P-GRB}}$ and E_{Baryons} in units of the E_{dya} as functions of B. This diagram, a universal one, is very important and is essential for the understanding of the GRB structure.

We find that for small values of B (around 10^{-8}) almost all the E_{dya} is emitted in the P-GRB (see also our previous paper Ruffini, Salmonson, Wilson & Xue[48]) and very little energy is left in the baryons. While for $B \simeq 10^{-2}$ roughly only 10^{-2} of the total initial energy of the dyadosphere is radiated away in the P-GRB and almost all energy is transferred to the baryons.

This behaviour is at the heart of the fundamental difference between the so called *short bursts* and *long bursts*. We have proposed[2] that the *short bursts* must be identified with the P-GRBs in the case of very small B. There are a variety of reasons supporting this identification:

(1) For small values of B, E_{Baryons} is negligible (see Fig. 6), and consequently the intensity of the afterglow is also negligible and the entire energy E_{dya} is released into the P-GRB. This is clearly consistent with the absence of observed afterglows in the short bursts.
(2) The temperature of the P-GRB in the laboratory frame $\bar{\gamma}T$ at the transparency point is a strongly decreasing function of B (see Fig. 7). $\bar{\gamma}T$ is related to the energy corresponding to the peak of the photon-number spectrum, as described in Ruffini, Salmonson, Wilson & Xue.[48] This is also in very good agreement with the observed decrease of the hardness ratio between the *short bursts* and the *long bursts*.[79]
(3) The time T_{90}, the duration where 90% of the energy emission as used in the current literature and discussed in Ruffini, Salmonson, Wilson & Xue[49] is plotted in Fig. 27 for selected values of E_{dya} and for different values of B.

Before concluding a word of caution is needed on how to use the above results: all these considerations are based on the drastic approximations in the description of the dyadosphere presented in Sec. 2 (see also Fig. 21). This treatment is very appropriate in estimating the general dependence of the energy of the P-GRB, the kinetic energy of the ABM pulse and consequently the intensity of the afterglow. Especially powerful is the establishment of the dependence of $E_{\text{P-GRB}}$ and E_{Baryons} on B (see Fig. 6). As we will see in the next sections, this approximation is similarly powerful in determining the overall time structure of the GRB and especially the time of the release of the P-GRB with respect to the moment of gravitational collapse and the afterglow.

If, however, we turn to the detailed temporal structure of the P-GRB and its detailed spectral distribution, it is clear that the approximations given in Sec. 2 is no longer valid. The detailed description of the formation of the dyadosphere as qualitatively expressed in Fig. 40 is now needed in all mathematical rigour with the

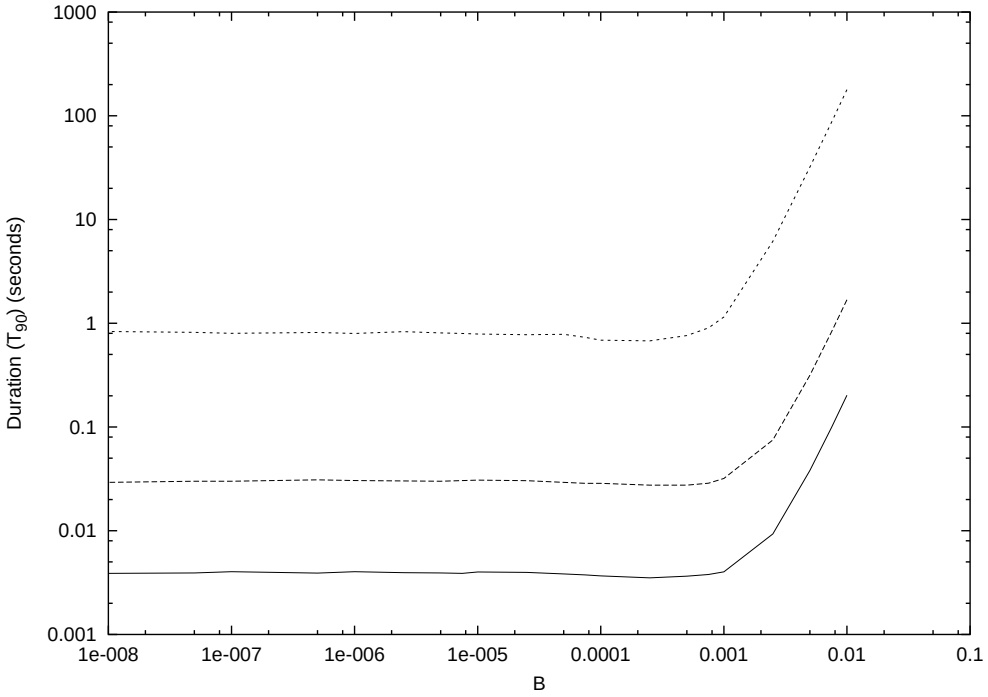

Fig. 27. The duration computed with the T_{90} criterion is represented as a function of the B parameter for three selected EMBH's respectively with $E_{\rm dya} = 4.4\times10^{52}$ erg, $E_{\rm dya} = 3.1\times10^{54}$ erg and $E_{\rm dya} = 4.1\times10^{58}$ erg, going from the lower curve to the upper one.

full development of all its governing equations. Progress in this direction is being made at this moment.[71−74] This situation, however, provides a unique opportunity to follow in real time the general relativistic effects of the approach to the EMBH horizon as it occurs. In other words all direct general relativistic effects of the GRBs are encoded in the fine structure of the P-GRB. For the reasons given in Sec. 9 the information on the EMBH mass and charge can only come from the short bursts.

This terminates the *injector phase*. We now turn to the *Beam-Target phase* in which the ABM pulse collides with the interstellar medium target and the afterglow is generated. We shall in the following sections review the basic theoretical treatment necessary for the description of these remaining eras and proceed then to the confrontation of the EMBH theory with the data.

12. The Era IV: The Ultrarelativistic and Relativistic Regimes in the Afterglow

In the introduction we have already expressed the basic assumptions which we have adopted for the description of the collision of the ABM pulse with the ISM. In analogy and by extension of the results obtained for the PEM and PEMB pulse

cases, we also assume that the expansion of the ABM pulse through the ISM occurs keeping its width constant in the laboratory frame, although the results are quite insensitive to this assumption. We assume then that this interaction can be represented by a sequence of inelastic collisions of the expanding ABM pulse with a large number of thin and cold ISM spherical shells at rest with respect to the central EMBH. Each of these swept up shells of thickness Δr has a mass $\Delta M_{\rm ism}$ and is assumed to be located between two radial distances r_1 and r_2 (where $r_2 - r_1 = \Delta r \ll r_1$) in the laboratory frame. These collisions create an internal energy $\Delta E_{\rm int}$.

We indicate by $\Delta\epsilon$ the increase in the proper internal energy density due to the collision with a single shell and by ρ_B the proper energy density of the swept up baryonic matter. This includes the baryonic matter composing the remnant around the central EMBH, already swept up in the PEMB pulse formation, and the baryonic matter from the ISM swept up by the ABM pulse:

$$\rho_B = \frac{(M_B + M_{\rm ism})c^2}{V}\,. \tag{100}$$

Here V is the ABM pulse volume in the comoving frame, M_B is the mass of the baryonic remnant and $M_{\rm ism}$ is the ISM mass swept up from the transparency point through the r in the laboratory frame:

$$M_{\rm ism} = m_p n_{\rm ism} \frac{4\pi}{3}\left(r^3 - {r_0}^3\right), \tag{101}$$

where m_p the proton mass and $n_{\rm ism}$ the number density of the ISM in the laboratory frame.

The energy conservation law in the laboratory frame at a generic step of the collision process is given by

$$\rho_{B_1}{\gamma_1}^2\mathcal{V}_1 + \Delta M_{\rm ism}c^2 = \left(\rho_{B_1}\frac{V_1}{V_2} + \frac{\Delta M_{\rm ism}c^2}{V_2} + \Delta\epsilon\right){\gamma_2}^2\mathcal{V}_2\,, \tag{102}$$

where the quantities with the index "1" are calculated before the collision of the ABM pulse with an elementary shell of thickness Δr and the quantities with "2" are calculated after the collision, γ is the gamma factor and $\mathcal{V}$ the volume of the ABM pulse in the laboratory frame so that $V = \gamma\mathcal{V}$.

The momentum conservation law in the laboratory frame is given by

$$\rho_{B_1}\gamma_1 U_{r_1}\mathcal{V}_1 = \left(\rho_{B_1}\frac{V_1}{V_2} + \frac{\Delta M_{\rm ism}c^2}{V_2} + \Delta\epsilon\right)\gamma_2 U_{r_2}\mathcal{V}_2\,, \tag{103}$$

where $U_r = \sqrt{\gamma^2 - 1}$ is the radial covariant component of the four-velocity vector[48,49] (see Eq. (50)).

We thus obtain

$$\Delta\epsilon = \rho_{B_1}\frac{\gamma_1 U_{r_1}\mathcal{V}_1}{\gamma_2 U_{r_2}\mathcal{V}_2} - \left(\rho_{B_1}\frac{V_1}{V_2} + \frac{\Delta M_{\rm ism}c^2}{V_2}\right), \tag{104}$$

$$\gamma_2 = \frac{a}{\sqrt{a^2 - 1}}\,, \qquad a \equiv \frac{\gamma_1}{U_{r_1}} + \frac{\Delta M_{\rm ism}c^2}{\rho_{B_1}\gamma_1 U_{r_1}\mathcal{V}_1}\,. \tag{105}$$

We can use for $\Delta\varepsilon$ the following expression

$$\Delta\varepsilon = \frac{E_{\mathrm{int}_2}}{V_2} - \frac{E_{\mathrm{int}_1}}{V_1} = \frac{E_{\mathrm{int}_1} + \Delta E_{\mathrm{int}}}{V_2} - \frac{E_{\mathrm{int}_1}}{V_1} = \frac{\Delta E_{\mathrm{int}}}{V_2} \tag{106}$$

because we have assumed a "fully radiative regime" and so $E_{\mathrm{int}_1} = 0$. Substituting Eq. (105) in Eq. (104) and applying Eq. (106), we obtain:

$$\Delta E_{\mathrm{int}} = \rho_{B_1} V_1 \sqrt{1 + 2\gamma_1 \frac{\Delta M_{\mathrm{ism}} c^2}{\rho_{B_1} V_1} + \left(\frac{\Delta M_{\mathrm{ism}} c^2}{\rho_{B_1} V_1}\right)^2} - \rho_{B_1} V_1 \left(1 + \frac{\Delta M_{\mathrm{ism}} c^2}{\rho_{B_1} V_1}\right), \tag{107}$$

$$\gamma_2 = \frac{\gamma_1 + \frac{\Delta M_{\mathrm{ism}} c^2}{\rho_{B_1} V_1}}{\sqrt{1 + 2\gamma_1 \frac{\Delta M_{\mathrm{ism}} c^2}{\rho_{B_1} V_1} + \left(\frac{\Delta M_{\mathrm{ism}} c^2}{\rho_{B_1} V_1}\right)^2}}. \tag{108}$$

These relativistic hydrodynamic (RH) equations have to be numerically integrated.

These are the actual set of equations we have integrated in the EMBH theory. In order to compare and contrast our results with the ones in the current literature, in Sec. 17 we have introduced the continuous limit of our equations and proceeded to have piecewise approximate power law solutions. We examine as well in Sec. 19 still under the above assumptions, the effects of a possible departure from homogeneity in the interstellar medium, still keeping the average density $n_{\mathrm{ism}} = \mathrm{const}$. Although these inhomogeneities are not relevant for the overall behaviour of the afterglow which we address here, they are indeed important for the actual observed flux and its temporal structures.[80] In addition these considerations are affected by the angular spreading.[57]

13. The Era V: The Approach to the Nonrelativistic Regimes in the Afterglow

The only reason for addressing this last era is that the issue of the approach to nonrelativistic behaviour has been extensively discussed in the literature. In our treatment these results do not show any particular problems and the relativistic equations of the previous section continue to hold. In the specific example of GRB 991216 we will present in Sec. 17 some analytic asymptotic expansions of these equations.

This concludes the exposition of the different eras of the EMBH theory. It goes without saying that for the description of each era, all the preceding eras must necessarily be known in order to determine the space–time grid in the laboratory frame and its relation to the arrival times as seen by a distant observer. This is the basic message expressed in the RSTT paradigm.

We can now turn to the comparison of the EMBH theory with the observational data.

14. The Best Fit of the EMBH Theory to the GRB 991216: The Global Features of the Solution

For reasons already explained in the introduction, we use the GRB 991216 as a prototype. We will then later apply the EMBH theory to other GRBs. The relevant data of GRB 991216 are reproduced in Fig. 3: the data on the burst as recorded by BATSE[52] and the data on the afterglow from the RXTE satellite[55] and the Chandra satellite[54] (see also Halpern *et al.*[53]).

The data fitting procedure relies on three basic assumption:

(1) In the E-APE region, the source luminosity is mainly in the energy band 50–300 KeV, so we consider the flux observed by BATSE a good approximation of the total flux.
(2) In the decaying part of the afterglow, we assume that during the R-XTE and Chandra observations the source luminosity is mainly in the energy band 2–10 KeV, so we can again assume that the flux observed by these satellites is a good approximation of the total one.
(3) We have neglected in this paper the optical and radio emissions, since they are always negligible with respect to the X-ray and γ-ray fluxes. In fact, even in the latest afterglow phases up to where the X-ray data are available, they are one order of magnitude smaller then the X-ray flux.

These assumptions were initially adopted for the sake of simplicity, but have now also been justified on the basis of the spectral description of the afterglow.[81]

As already emphasized in the previous sections, in the EMBH theory there are only two free parameters characterizing the afterglow: the energy of the dyadosphere $E_{\rm dya}$ and the baryonic matter in the remnant of the progenitor star, parametrized by the dimensionless parameter B. The location of the remnant has been assumed $\sim 10^{10}$ cm. As discussed in Ruffini *et al.*[1] and Sec. 9, the results are rather insensitive to the actual density and location of the baryonic component but they are very sensitive to the value of B.[49]

In Fig. 8 we present the actual first results of fitting our EMBH theory to the data from the R-XTE and Chandra satellites, corresponding to selected values of $E_{\rm dya}$ and B. There are three distinct features which are clearly evident as a function of the arrival time at the detector: an initial rising part in the afterglow luminosity which reaches a peak followed by a monotonically decreasing part.

We have then proceeded to fine tune the two parameters in Fig. 28. The main conclusions from our model are the following:

(1) The slope of the afterglow in the region where the experimental data are present is $n = -1.6$ and is in perfect agreement with the observational data. The index n in this region is rather insensitive to the values of the parameters $E_{\rm dya}$ and B. The physical reason for this universality of the slope is rather remarkable since it depends on a variety of factors including the ultrarelativistic energy of the baryons in the ABM pulse, the assumption of constant average density in the

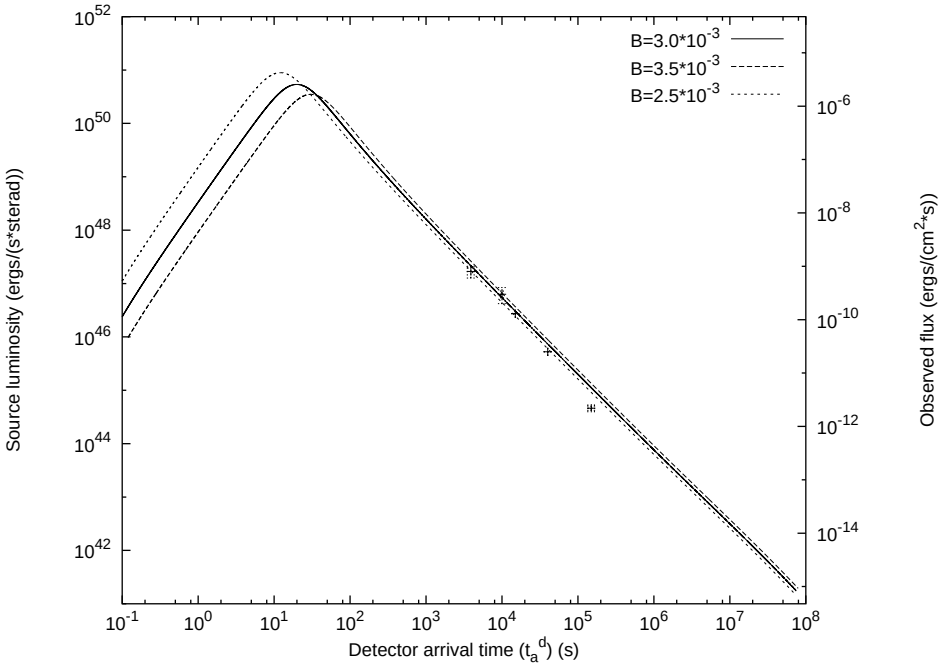

Fig. 28. Fine tuning of the best fit of the afterglow data of Chandra, RXTE as well as of the range of variability of the BATSE data on the major burst by a unique afterglow curve leading to the parameter values $E_{\rm dya} = 4.83 \times 10^{53}$ erg, $B = 3 \times 10^{-3}$.

ISM, the "fully radiative" conditions leading predominantly to X-ray emission, as well as all the different relativistic effects described in the RSTT paradigm (see also Sec. 17).

(2) The afterglow fit does not depend directly on the parameters μ, ξ but only through their combination $E_{\rm dya}$. Thus there is a 1-parameter family of values of the pair (μ, ξ) allowed by a given viable value of $E_{\rm dya}$ (see Fig 16 and Sec. 9).

(3) By fine tuning the parameters of the best fit of the luminosity profile and time evolution of the afterglow the following parameters have been found:

$$E_{\rm dya} = 4.83 \times 10^{53} \text{ erg}\,, \qquad B = 3 \times 10^{-3}\,. \tag{109}$$

After fixing in Eq. (109) the two free parameters of the EMBH theory, modulo the mass-charge relationship which fixes $E_{\rm dya}$, we can derive all the space–time parameters of the GRB 991216 (see Table 1) as well as the explicit dependence of the gamma factor as a function of the radial coordinate (see Fig. 9).

Of special interest is the fundamental diagram of Fig. 10. Its role is essential in interpreting all quantities measured in arrival time (the time of an observer in an inertial frame at the detector) and their relations to the ones measured in the laboratory time by an observer in an inertial frame at the GRB source. The two times are clearly related by light signals (see Fig. 2) and expressed by the integral Eq. (37) and are also affected by the cosmological expansion (see Sec. 4).

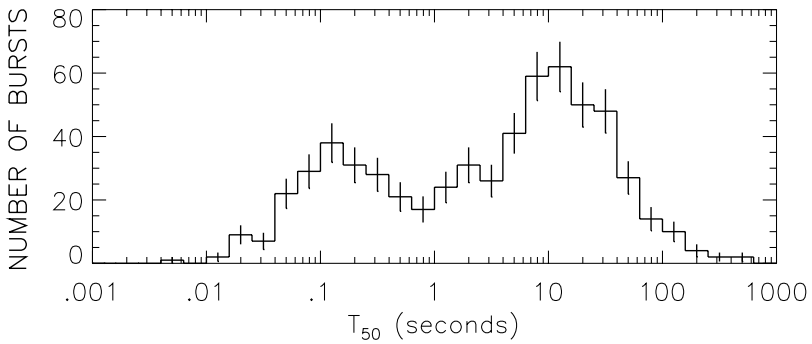

Fig. 29. The distribution of the burst durations clearly shows two different classes of events: the "short bursts" and the "long bursts" (reproduced from Paciesas *et al.*[82]).

15. The Explanation of the "Long Bursts" and the Identification of the Proper Gamma Ray Burst (P-GRB)

Having determined the two free parameters of the EMBH theory, any other feature is a new prediction. An unexpected result soon became apparent, namely that the average luminosity of the main burst observed by BATSE can be fitted by the afterglow curve (see Fig. 11). This led us to the identification of the long bursts observed by BATSE with the extended afterglow peak emission (E-APE). The peak of this E-APE occurs at ~ 19.87 s and its intensity and time scale are in excellent agreement with the BATSE observations.[80] It is clear that this E-APE is *not* a burst, but is seen as such by BATSE due to its high noise threshold.[80] Thus the outstanding unsolved problem of explaining the long GRBs[32,33,40] is radically resolved: the so called "long bursts" do not exist, they are just E-APEs (see Fig. 29).

We now turn to the most cogent question to be asked: where does one find the burst which is emitted when the condition of transparency against Thomson scattering is reached? We have referred to this as the proper gamma ray burst (P-GRB) in order to distinguish it from the global GRB phenomena.[1,50] We are guided in this search by two fundamental diagrams (see Figs. 12 and 13):

(1) In Ruffini, Salmonson, Wilson & Xue[49] it is shown that for a fixed value of $E_{\rm dya}$ the value of B uniquely determines the energy $E_{\rm P\text{-}GRB}$ of the P-GRB and the kinetic energy $E_{\rm Baryons}$ of the ABM pulse which gives origin to the afterglow (see Fig. 12). For the particular values of the parameters given in Eq. (109), we find

$$E_{\rm P\text{-}GRB} = 7.54 \times 10^{51}\ {\rm erg}\,, \qquad E_{\rm Baryons} = 9.43 \times 10^{52}\ {\rm erg} \tag{110}$$

and then:

$$\frac{E_{\rm P\text{-}GRB}}{E_{\rm Baryons}} = 1.58 \times 10^{-2}\,. \tag{111}$$

(2) One important additional piece of information comes from the differences in arrival time between the P-GRB and the peak of the E-APE (see Fig. 13). Using the results of this figure and the numerical values given in Table 1, we can retrace the P-GRB by reading off the time parameters of point 4 in Fig. 9. Transparency is reached at 21.57 s in comoving time at a radial coordinate $r = 1.94 \times 10^{14}$ cm in the laboratory frame and at 8.41×10^{-2} s in arrival time at the detector.

All this, namely the energy predicted in Eq. (110) for the intensity of the burst and its time of arrival, leads to the unequivocal identification of the P-GRB with the apparently inconspicuous initial burst in the BATSE data. We have estimated from the BATSE data the ratio of the P-GRB to the E-APE over the noise threshold to be $\sim 10^{-2}$, in excellent agreement with the result in Eq. (111) (see Fig. 14).

It is important to emphasize that the diagrams in Fig. 6 and Fig. 12 are not universal, but depend on the dyadosphere energy. The corresponding diagrams for three selected $E_{\rm dya}$ values ($E_{\rm dya} = 5.29 \times 10^{51}$ erg, $E_{\rm dya} = 4.83 \times 10^{53}$ erg and $E_{\rm dya} = 4.49 \times 10^{55}$ erg) are given in Fig. 30(a) where we have plotted the energy of the P-GRB and of the E-APE as a function of B. The crossing of the intensity of P-GRB and E-APE occurs respectively at $B_1 = 6.0 \times 10^{-5}$, $B_2 = 2.5 \times 10^{-5}$ and $B_3 = 1.2 \times 10^{-5}$ where $B_1 > B_2 > B_3$. In Fig. 30(b) the same quantities are plotted as a function of the baryon mass M_B in units of solar masses and the opposite dependence occurs: $M_1 < M_2 < M_3$.

The physical reasons beyond these results is the following. We recall that the kinetic energy $E_{\rm Baryons}$ and mass M_B of PEMB pulse are

$$E_{\rm Baryons} = (\gamma - 1) M_B \,, \qquad M_B \equiv B E_{\rm dya} \tag{112}$$

at the crossing point defined by

$$E_{\rm Baryons} = E_{\rm P\text{-}GRB} = \frac{1}{2} E_{\rm dya} \,. \tag{113}$$

From these two equations, we obtain

$$B = \frac{1}{2(\gamma_0 - 1)} \simeq \frac{1}{2\gamma_0} \,, \tag{114}$$

where γ_0 is the Lorentz gamma factor of the PEMB pulse at the transparency point, (see Sec. 10)

$$(n_{\rm pair} + n_B)\sigma_T \simeq n_B \sigma_T = 1 \,, \qquad n_B = \frac{M_B}{4\pi r_0^2 \Delta \gamma_0} \,, \tag{115}$$

Δ_t is the PEMB pulse thickness and r_0 the radial position at the transparency point. In addition, from the total energy conservation, we have

$$(\epsilon + n_B)\gamma_0^2 4\pi r_0^2 \Delta = {\rm const} \,, \tag{116}$$

where ϵ is the thermal energy of the PEMB pulse. In the regime $n_B \gg \epsilon$, we have

$$\gamma_0 \simeq \frac{E_{\rm dya}}{M_B} \,, \tag{117}$$

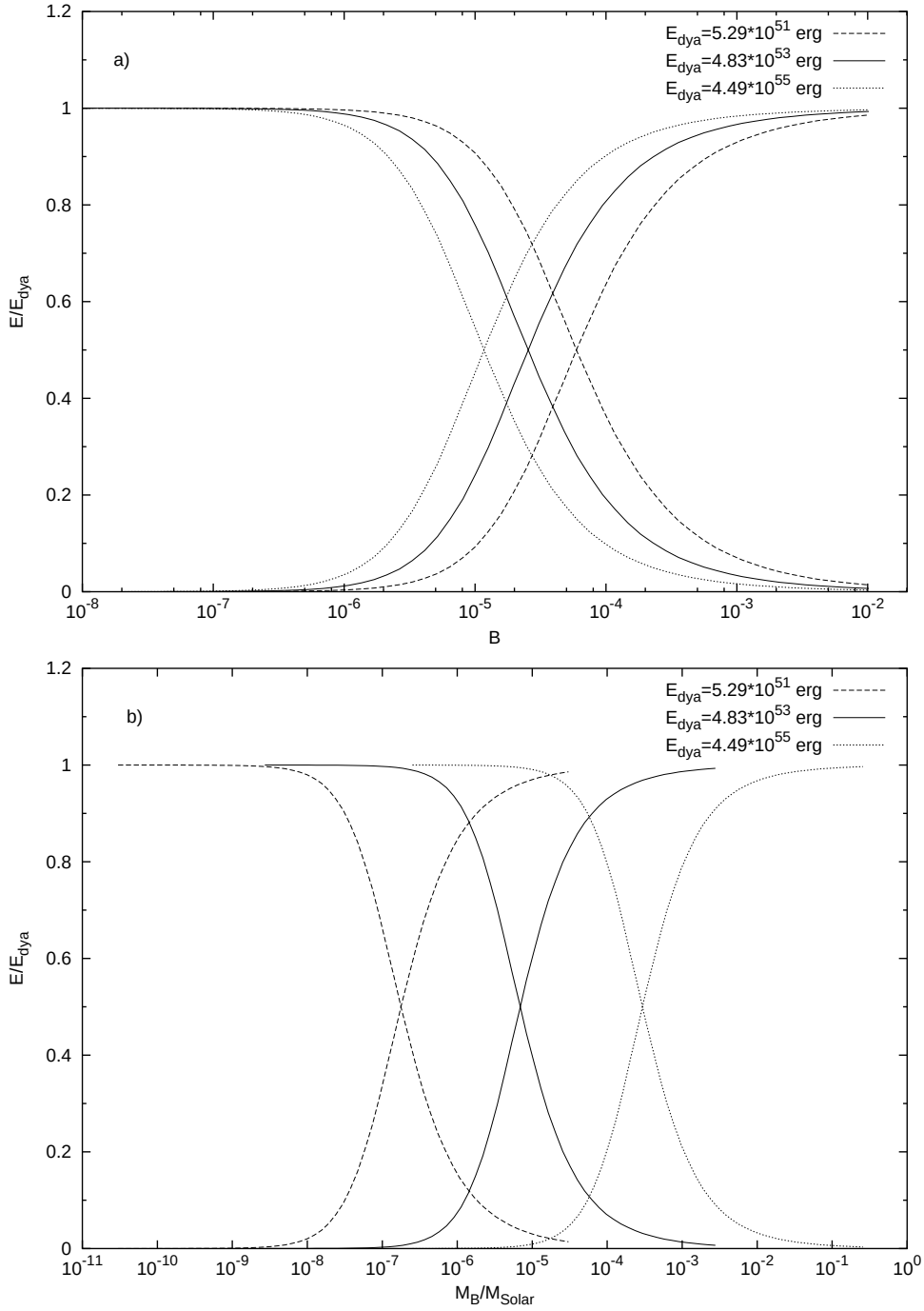

Fig. 30. (a) The same diagram of Fig. 6 is plotted for three different $E_{\rm dya}$ values: $E_{\rm dya} = 5.29 \times 10^{51}$ erg (dashed lines), $E_{\rm dya} = 4.83 \times 10^{53}$ erg (solid lines) and $E_{\rm dya} = 4.49 \times 10^{55}$ erg (dotted lines). (b) Same as in (a) but plotted as a function of the baryonic mass M_B in units of solar masses instead of B.

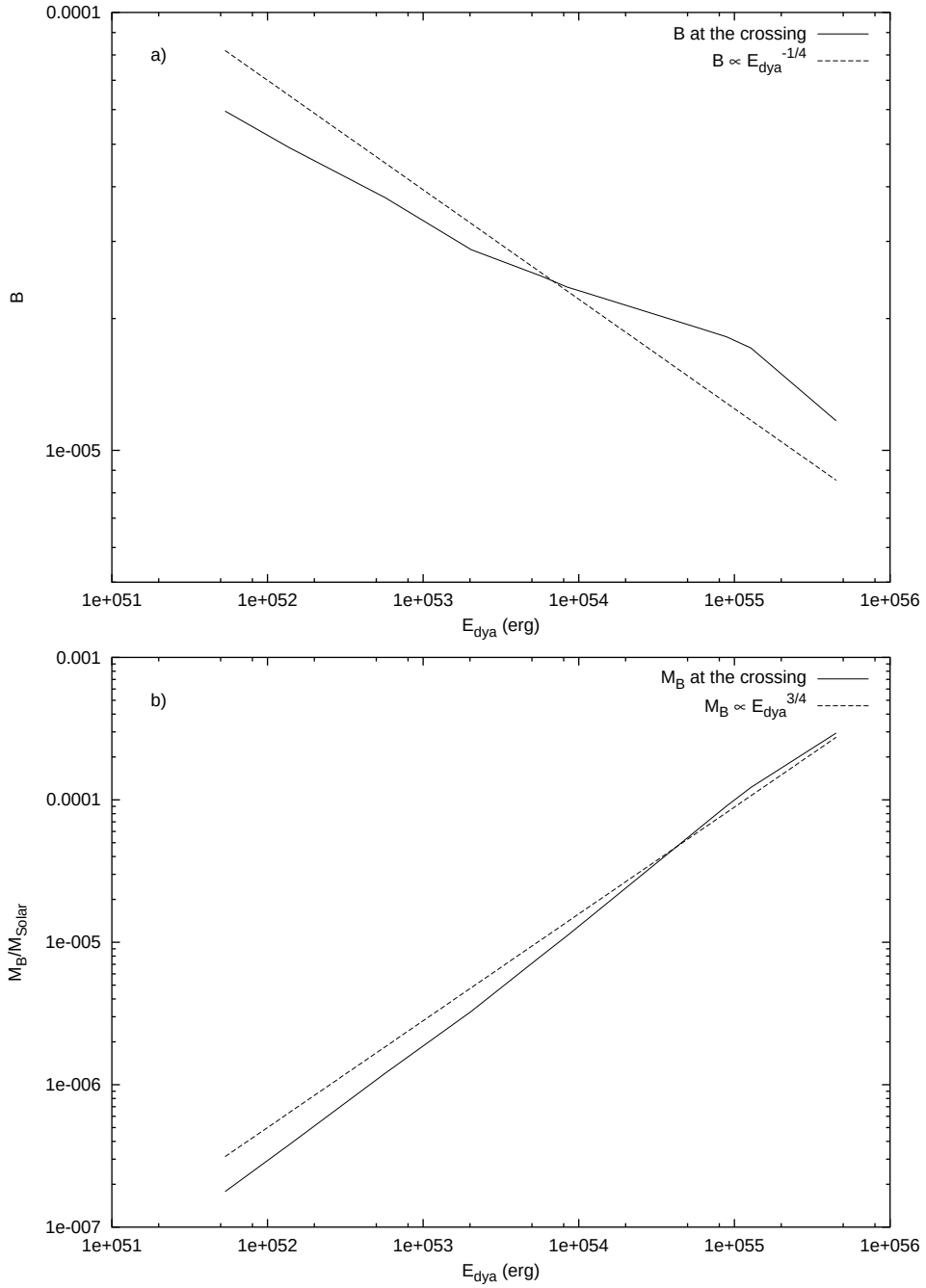

Fig. 31. (a) The B values corresponding to the crossings in Fig. 30(a) are plotted versus $E_{\rm dya}$ (solid line). The function $B \propto E_{\rm dya}^{-1/4}$ obtained from a qualitative theoretical estimate (see Eq. (119)) is also plotted (dashed line). (b) The M_B values corresponding to the crossings in Fig. 30(b) are plotted versus $E_{\rm dya}$ (solid line). The function $M_B \propto E_{\rm dya}^{3/4}$ obtained from a qualitative theoretical estimate (see Eq. (119)) is also plotted (dashed line).

and in the regime $n_B \ll \epsilon$, we have

$$\gamma_0 \sim r_0 \,. \tag{118}$$

Considering the crossing point to occur in the second regime, we obtain at the crossing point

$$B \sim (E_{\rm dya})^{-\frac{1}{4}} \,, \qquad M_B \sim (E_{\rm dya})^{\frac{3}{4}} \,. \tag{119}$$

These results are plotted in Figs. 31(a) and 31(b). The agreement with the computed results is quite satisfactory. The differences can be attributed to the approximation adopted in Eq. (118) which is modified for high B values.

The conclusion is that for increasing $E_{\rm dya}$ also the baryonic mass corresponding to the cross increases, but in percentage it increases less than $E_{\rm dya}$.

16. Considerations on the P-GRB Spectrum and the Hardness of the Short Bursts

Regarding the P-GRB spectrum, the initial energy of the electron-positron pairs and photons in the dyadosphere for given values of the parameters can be easily computed following the work of Preparata, Ruffini & Xue.[47] We obtain respectively $T = 1.95$ MeV and $T = 29.4$ MeV in the two approximations we have used for the average energy density of the dyadosphere (see Sec. 9). It is then possible to follow in the laboratory frame the time evolution of the temperature of the electron-positron pairs and photons through the different eras (see Fig. 32). The condition of transparency is reached at temperatures in the range of $\sim 15 - 55$ KeV at the detector, in agreement with the BATSE results. We emphasize that in the limit of B going to 10^{-8} in which the P-GRB coincides with the "short bursts" the spectrum of the P-GRB becomes harder, in agreement with the observational data[83–86] (see Fig. 7).

All the above are average values derived from the two approximations used in Fig. 17. If one wishes to compare the EMBH theoretical results with the fine temporal details of the observational data on the P-GRB, a departure from this average approach will be needed and the fully time varying relativistic analysis outlined in Fig. 40 applies will be further discussed in Sec. 21.

17. Approximations and Power Laws in the Description of the Afterglow

In addition to the BATSE data, there is clearly also a perfect agreement with the decaying part of the afterglow data from the RXTE and Chandra satellites.

We can also establish at this point a first set of conclusions on the luminosity power law index "n" which is a function depending strongly on the transformation $t \to t_a \to t_a^d$ (see Fig. 10). In the current literature such transformations and the corresponding n values are incorrect. Our theoretical value $n_{\rm theo} = -1.6$ obtained

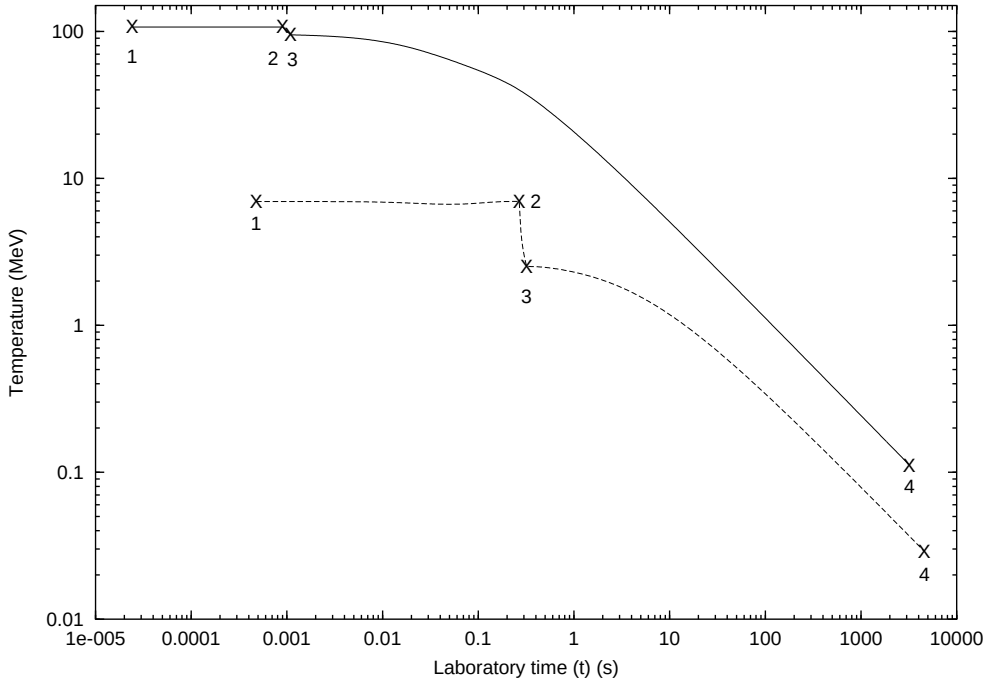

Fig. 32. The temperature of the pulse in the laboratory frame for the first three eras of Fig. 1 of Ruffini *et al.*[1] is given as a function of the laboratory time. The numbers 1, 2, 3, 4 represent the beginning and end of each era. The two curves refer to two extreme approximations adopted in the description of the dyadosphere. Details are given in Ruffini, Salmonson, Wilson & Xue[49] and in Sec. 9.

for spherical symmetry under fully radiative conditions and constant density of the ISM is in agreement with observed $n_{\rm obs} = -1.616 \pm 0.067$. No evidence of beaming is found in GRB 991216. We shall return to this point in the conclusions.

An extremely large number of papers in the literature deal with the power law index in the afterglow era. This issue has been particularly debated in connection with the aim of decreasing the energy requirements of GRBs by the effect of beaming.[87,88] It is currently very popular to infer the existence of beaming from the direct observations of breakings in the power-law index of the afterglow.[53,89–97] Our aim here is to underline an often neglected point that the power law index of the afterglow is the result of a variety of factors including the very different regimes in the relation between the laboratory time t and the detector arrival time t_a^d presented in Fig. 10. No meaningful statements on the values of the power-law index of the afterglow can be made having neglected these necessary considerations expressed in the RSTT paradigm. This becomes particularly transparent from the power law expansion in the semi-analytic treatments we present below. It is therefore not so surprising, as we will show in the next session, that the results obtained in the EMBH theory differ from the ones in the current literature.

17.1. *The approximate expression of the hydrodynamic equations*

We proceed to a first approximation and expand Eqs. (107) and (108) to second order in the quantity

$$\frac{\Delta M_{\rm ism} c^2}{\rho_{B_1} V_1} \ll 1 \,. \tag{120}$$

We obtain the following expressions:

$$\Delta E_{\rm int} = (\gamma_1 - 1)\Delta M_{\rm ism} c^2 - \frac{1}{2}\frac{\gamma_1^2 - 1}{M_B + M_{\rm ism}} (\Delta M_{\rm ism})^2 c^2 \,, \tag{121}$$

$$\Delta\gamma = -\frac{\gamma_1^2 - 1}{M_B + M_{\rm ism}} \Delta M_{\rm ism} + \frac{3}{2}\gamma_1 \frac{\gamma_1^2 - 1}{(M_B + M_{\rm ism})^2} (\Delta M_{\rm ism})^2 \,, \tag{122}$$

where we set $\Delta\gamma \equiv \gamma_2 - \gamma_1$ and have used the fact that $\rho_{B_1} V_1 \equiv (M_B + M_{\rm ism})c^2$. In the limit $\Delta E_{\rm int} \to dE_{\rm int}$, $\Delta\gamma \to d\gamma$, and $\Delta M_{\rm ism} \to dM_{\rm ism}$, in addition to neglecting second order terms, where

$$dM_{\rm ism} = 4\pi r^2 m_p n_{\rm ism} dr = 4\pi r^2 m_p n_{\rm ism} v dt \,, \qquad v = \frac{dr}{dt} \,, \tag{123}$$

and where the ISM number density $n_{\rm ism}$ is assumed for simplicity to be $n_{\rm ism} = 1\ {\rm cm}^{-3}$, we obtain:

$$dE_{\rm int} = (\gamma - 1) dM_{\rm ism} c^2 \,, \tag{124}$$

$$d\gamma = -\frac{\gamma^2 - 1}{M_B + M_{\rm ism}} dM_{\rm ism} \,. \tag{125}$$

Equations (124) and (125) are limiting cases of Taub's hydrodynamical equations.[59,60,98] They have been at times referred in the GRB literature as the Blandford–McKee equations.[99] It is clear that the application of these equations holds if Eq. (120) applies. The behaviour of $\Delta M_{\rm ism} c^2 / \rho_{B_1} V_1$ as a function of the radius, when $M_{\rm ism} \ll M_B$, is:

$$\frac{\Delta M_{\rm ism} c^2}{\rho_{B_1} V_1} \sim \frac{r^2 \Delta r}{M_B} \,. \tag{126}$$

The condition $M_{\rm ism} \ll M_B$ holds for GRB 991216 during the entire evolution of the system and so Eq. (120) is valid (see Fig. 33).

Equations (124) and (125) can be simply solved analytically (see e.g. Blandford and McKee[99]) we then have

$$\gamma = \frac{(M_B + M_{\rm ism})^2 + C}{(M_B + M_{\rm ism})^2 - C} \,, \tag{127}$$

where

$$C = {M_B}^2 \frac{\gamma_0 - 1}{\gamma_0 + 1} \,, \tag{128}$$

where we recall that r_0 and γ_0 are the radial coordinate and the gamma factor at the transparency point and M_B is the initial baryonic mass of the ABM pulse.

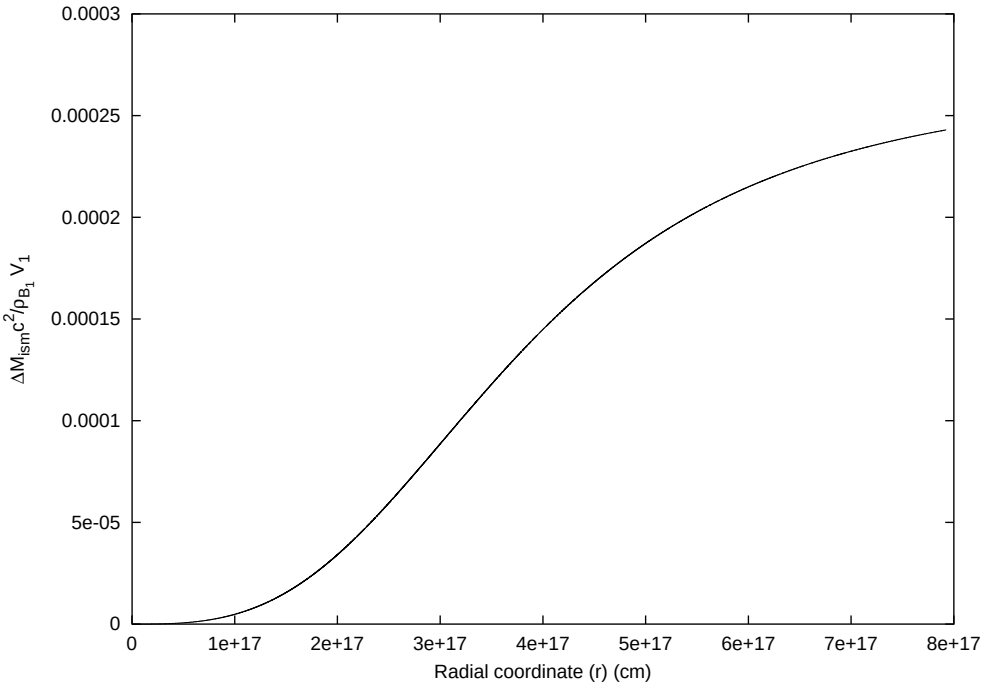

Fig. 33. The factor $\Delta M_{\rm ism}c^2/\rho_{B_1}V_1$ is represented as a function of the radial coordinate. It is manifestly an increasing function.

Equation (127) is a differential equation for $r\,(t)$, namely

$$1-\left(\frac{dr}{cdt}\right)^2=\left[\frac{(M_B+M_{\rm ism})^2+C}{(M_B+M_{\rm ism})^2-C}\right]^{-2}, \tag{129}$$

which can be integrated analytically with solution[100]

$$\begin{aligned}2c\sqrt{C}(t-t_0)=(M_B-m_i^0)(r-r_0)+\frac{1}{4}m_i^0r_0\left[\left(\frac{r}{r_0}\right)^4-1\right]\\ +\frac{Cr_0}{6m_i^0B^2}\ln\left[\frac{\left(B+\frac{r}{r_0}\right)^3}{B^3+\left(\frac{r}{r_0}\right)^3}\frac{B^3+1}{(B+1)^3}\right]\\ +\frac{Cr_0}{3m_i^0B^2}\left[\sqrt{3}\arctan\frac{2\frac{r}{r_0}-B}{B\sqrt{3}}-\sqrt{3}\arctan\frac{2-B}{B\sqrt{3}}\right],\end{aligned} \tag{130}$$

where $m_i^0=\frac{4}{3}\pi m_p n_{\rm ism}r_0^3$, $B=\sqrt[3]{(M_B-m_i^0)/m_i^0}$ and we recall that t_0 is the laboratory time at the transparency point. Clearly the fulfilment of Eq. (120) has to be checked to ensure the validity of this solution.

17.2. *The approximate expression of the emitted flux*

From Eqs. (124) and (125), it follows that the emitted flux in the laboratory frame is given by (see Fig. 34(a))

$$\frac{dE}{dt} = 4\pi r^2 n_{\rm ism} m_p v\gamma(\gamma-1)c^2\,, \tag{131}$$

and the corresponding flux in detector arrival time (see Fig. 34(b)) by

$$\begin{aligned}\frac{dE}{dt_a^d} &= \left[\frac{dt}{dt_a^d}\frac{dE}{dt}\right]_{t=t(t_a^d)} \\ &= 4\pi n_{\rm ism} m_p c^2 \left[vr^2\gamma(\gamma-1)\frac{dt}{dt_a^d}\right]_{t=t(t_a^d)}\,.\end{aligned} \tag{132}$$

For the solution of these equations we distinguish four different phases (A–D). The first two correspond to Era V.

Phase A

Just after the transparency condition is reached, the ISM matter involved is so small that we can approximately neglect the $M_{\rm ism}$ term in Eq. (127) and we have:

$$\gamma \simeq \gamma_0\,. \tag{133}$$

In the specific case of GRB 991216 we have $\gamma_0 = 310.1$, $r_0 = 1.94\times10^{14}$ cm, $t_0 = 6.48\times10^3$ s, $t_{a_0} \simeq 4.21\times10^{-2}$ s and $t^d_{a_0} \simeq 8.41\times10^{-2}$ s, where the index "0" refers to the quantities at the transparency point. We can then establish the following equation describing the ABM pulse motion in this phase: $r\,(t) = vt$ with $v \simeq c$. We can than use the following relation between laboratory time and arrival time:

$$t = 2{\gamma_0}^2 t_a = \frac{2{\gamma_0}^2}{1+z}t_a^d\,, \tag{134}$$

which is in perfect agreement with the full numerical computation (see Fig. 10).

We can substitute these equations into Eqs. (131) and (132), obtaining:

$$\frac{dE}{dt} \propto \gamma_0^2 n_{\rm ism} t^2 \tag{135}$$

in laboratory time and

$$\frac{dE}{dt_a^d} \propto \frac{\gamma_0^8 n_{\rm ism}}{(1+z)^3}\left(t_a^d\right)^2 \tag{136}$$

in arrival time, assuming $\gamma(\gamma-1) \simeq \gamma^2$. The results of the numerical integration of Eqs. (104) and (105) are in perfect agreement with these approximations (see Fig. 34).

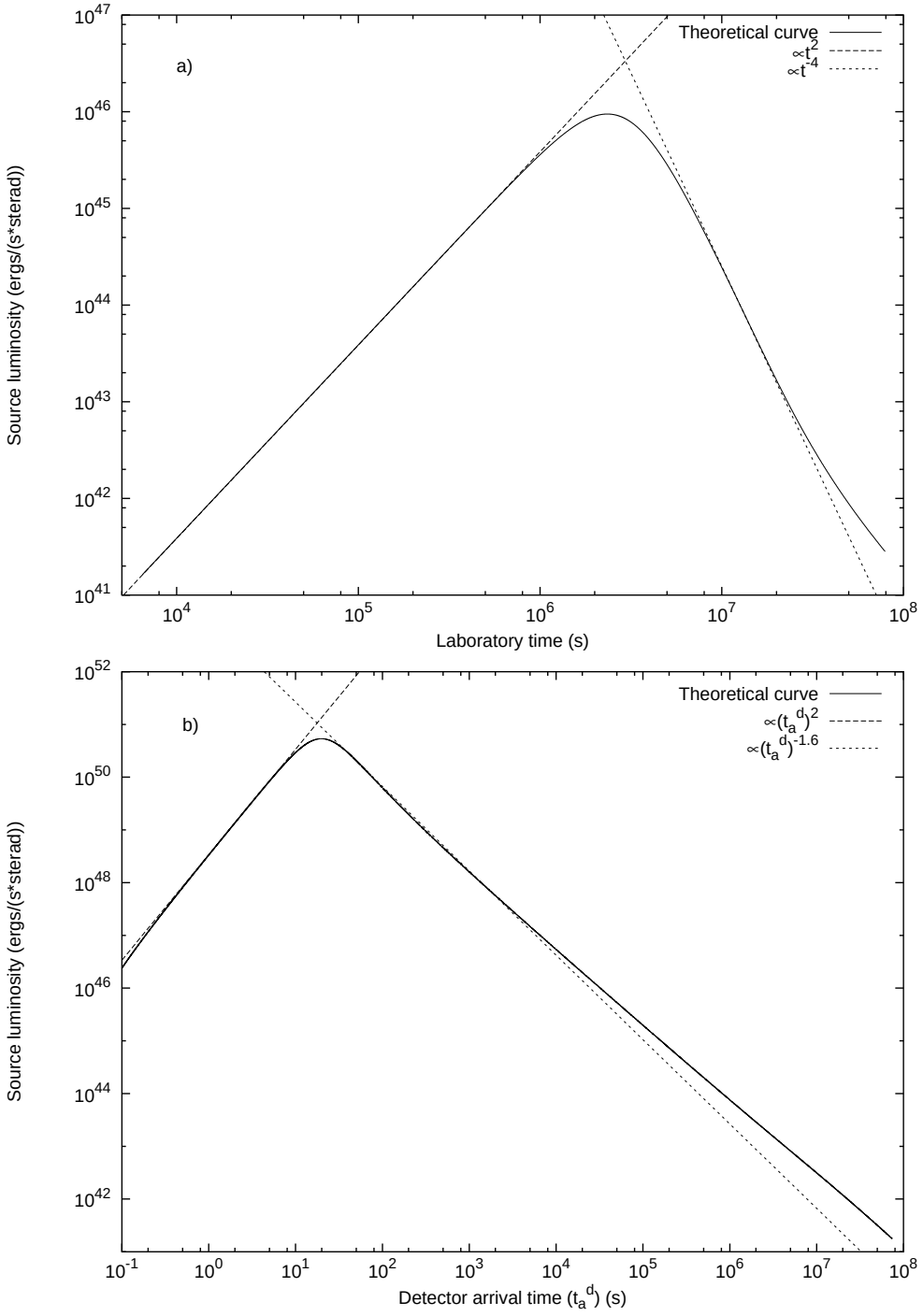

Fig. 34. (a) The GRB flux emitted in laboratory time. (b) The flux emitted in the arrival time, measured by an observer at rest with respect to the detector (see Sec. 17).

Points P — the two maxima of the energy flux

Since the contribution of the ISM mass in Eqs. (127) and (128) can no longer be neglected, the value of γ starts to significantly decrease (see Fig. 9) and the flux reaches a maximum value. We integrate Eqs. (131) and (132) using Eq. (127) for γ, assuming $r(t) = vt$ with $v \simeq c$ and Eq. (134) for the relation between the laboratory time and the arrival time (see Figs. 35–10). We can now obtain the point where the emitted flux reaches its maximum. In general, the location of the maximum of the flux, point P in the paper by Ruffini *et al.*,[1] will occur at different events, if considered in terms of the arrival time (P_A) or in the laboratory time (P_L). In this second case, the point P_L is determined by equating to zero the first derivative of Eq. (131), and we have:

$$\gamma_{P_L} \simeq \frac{2}{3}\gamma_0\,, \qquad \left.\frac{M_B}{M_{\rm ism}}\right|_{P_L} \simeq 2\gamma_0\,, \tag{137}$$

which in the case of GRB 991216 gives $\gamma_{P_L} = 206.7$ and $\left.\frac{M_B}{M_{\rm ism}}\right|_{P_L} \simeq 620.2$. The maximum of the observed flux is determined by equating to zero the first derivative of Eq. (132). We obtain:

$$\gamma_{P_A} \simeq \frac{5}{6}\gamma_0\,, \qquad \left.\frac{M_B}{M_{\rm ism}}\right|_{P_A} \simeq 5\gamma_0\,, \tag{138}$$

which in the case of GRB 991216 gives $\gamma_{P_A} \simeq 258.4$ and $\left.\frac{M_B}{M_{\rm ism}}\right|_{P_A} \simeq 1550.5$.

The results of the numerical integration of Eqs. (104) and (105) are in perfect agreement with these approximations (see Fig. 34).

Phase B — the "golden value" n = −1.6

In this phase γ can no longer be considered constant and strongly decreases (see Fig. 9). $M_{\rm ism}$ is increasing, but v is still almost constant, equal to c. As a consequence, we can still say that $r\,(t) = vt$ with $v = c$, but the relation between laboratory time and arrival time given in Eq. (134) is no longer valid, and also Eq. (39) is no longer applicable in this phase (see Fig. 10). We can instead write the following "effective" relation:

$$t \propto \left(t_a^d\right)^{0.20}\,, \tag{139}$$

which is a result of a best fit of the numerical data in this region. Expanding the squares in Eq. (127), neglecting $M_{\rm ism}^2$ with respect to M_B^2 but retaining the terms in $M_{\rm ism}$ and assuming $\gamma_0 \gg 1$ we obtain:

$$\gamma \sim \frac{M_B}{M_{\rm ism}} \sim \gamma_{P_L}\frac{r_{P_L}^3}{r^3} = \gamma_{P_L}\frac{t_{P_L}^3}{t^3}\,, \tag{140}$$

where r_{P_L} and t_{P_L} are the values of r and t at point P_L. Substituting this result into Eq. (131), we obtain the emitted flux in the laboratory frame, given by

$$\frac{dE}{dt} \propto \gamma_P^2 t_P^6 n_{\rm ism} t^{-4}\,, \tag{141}$$

and this is in good agreement with the full numerical computation (see Fig. 34).

To obtain an analytic formula for the observed flux on the detector, we can still try to use the approximate relation between t and t_a^d given by Eq. (39):

$$t = 2\gamma(t)^2 t_a = \frac{2\gamma(t)^2}{1+z} t_a^d\,, \tag{142}$$

where $\gamma(t)$ is given by Eq. (140). We obtain:

$$t = \left(\frac{2\gamma_{P_L}^2 t_{P_L}^6}{1+z} t_a^d\right)^{1/7}\,. \tag{143}$$

Using this formula in Eq. (132), we finally obtain:

$$\frac{dE}{dt_a^d} \propto \frac{\gamma_P^{\frac{8}{7}} t_P^{\frac{24}{7}} n_{\rm ism}}{(1+z)^{-\frac{17}{7}}} (t_a^d)^{-\frac{10}{7}} \tag{144}$$

where we have again assumed $\gamma(\gamma-1) \simeq \gamma^2$. This results are not in agreement with the observational data, because the power-law index for the observed flux is $-10/7 \simeq -1.43$, instead of the observed value -1.6.

This is a confirmation that Eq. (142) cannot be applied in this phase, which instead has been done by many authors in the current literature. We instead have to use Eq. (139). In fact, doing so we obtain the correct value:

$$\frac{dE}{dt_a^d} \propto n_{\rm ism} (t_a^d)^{-1.6}\,, \tag{145}$$

The results of the numerical integration of Eqs. (104) and (105) are in perfect agreement with these approximations (see Fig. 34). This implies that the approximate Eq. (124) and (125) can still be used in this regime, but not Eq. (39) which has to be replaced by an "effective" local power-law behaviour (see Eq. (139)).

Phase C

This new phase begins when γ has decreased so much that the approximation $r = ct$ is no longer valid (see Fig. 35). In the case of GRB 991216 this happens when $\gamma \simeq 3.0$, $t \simeq 1.5 \times 10^7$ s, $t_a^d \simeq 2.9 \times 10^5$ s and $r \simeq 4.4 \times 10^{17}$ cm. In this entire phase, $r(t)$ manifests the following behaviour typical of damped motion:

$$r(t) = \hat{r}\left(1 - e^{-\frac{t-t^\star}{\tau}}\right), \tag{146}$$

where $\hat{r}$, $t^\star$ and τ are constants that can be determined by the best fit of the numerical solution. In the present case of GRB 991216 we obtain:

$$\hat{r} \simeq 1.101 \times 10^{18}\ {\rm cm}\,, \qquad \tau \simeq 2.072 \times 10^7\ {\rm s}\,, \quad t^\star \simeq 4.52 \times 10^6\ {\rm s}\,. \tag{147}$$

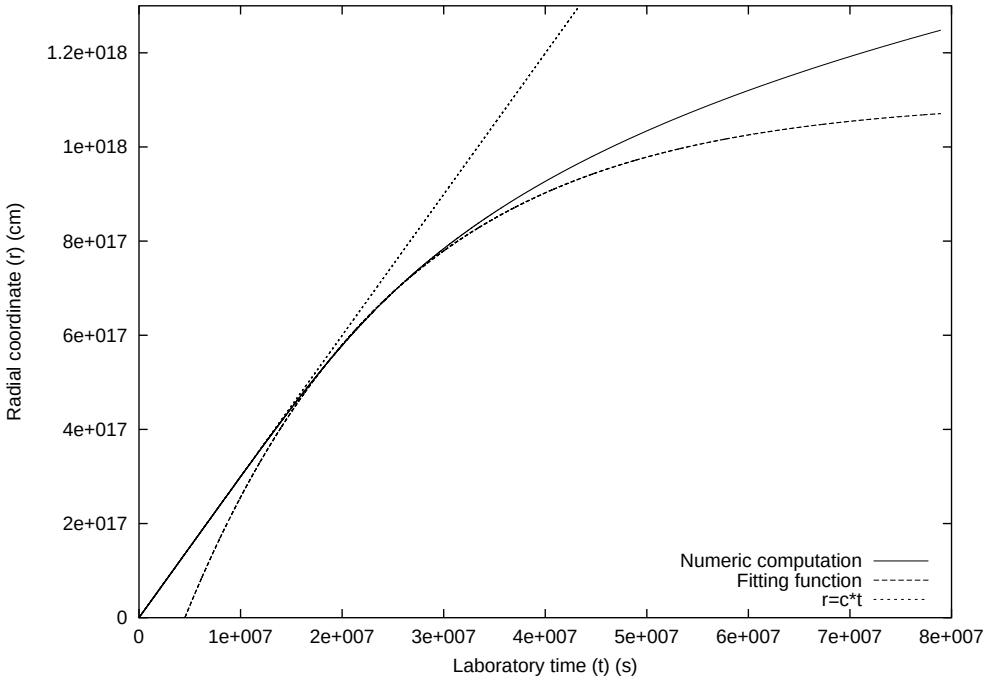

Fig. 35. The exact numerical solution for $r(t)$ (solid line), together with the line $r = ct$ (dotted line) and the fitting function given in Eq. (146) (dashed line).

It is important to note that this interesting behaviour, typical of a damped motion, does not lead to any power-law relationship for the emitted flux as a function of the laboratory time (see Fig. 34). However, if we look at the observed flux as a function of the detector arrival time, we see that a power-law relationship still can be established, fitting the numerical solution. The result is:

$$\frac{dE}{dt_a^d} \propto (t_a^d)^{-1.36}. \tag{148}$$

This quite unexpected result can be explained because the relation between t and t_a^d depends on $r\,(t)$ in a nonpower-law behaviour. This fact balances the complex behaviour of the emitted flux as a function of the laboratory time, leading finally again to a power-law behaviour arrival time.

In this last phase, however, the flux decreases markedly, and from the point of view of the GRB observations, the most relevant regions are phases A and B described above, as well as the peak separating them.

Phase D

This last phase starts when the system approaches a Newtonian regime. In the case of GRB 991216 this occurs when $\gamma \simeq 1.05$, $t \simeq 5.0 \times 10^7$ s, $t_a^d \simeq 3.1 \times 10^7$ s

and $r \simeq 1.0 \times 10^{18}$ cm. In this phase $r(t)$ is again approaching a linear behaviour, since the decrease in velocity is less steeply than in Phase C. The emitted flux as a function of the laboratory time still does not show a power-law behaviour, while the observed flux as a function of detector arrival time does, with an index $n = -1.45$ (see Fig. 34).

18. The Power-Law Index of the Afterglow and Inferences on Beaming in GRBs

The results obtained in the previous sections have emphasized the relevance of the proper application of the RSTT paradigm to the determination of the power-law index of the afterglow. Particularly interesting is the subtle interplay between the different regimes in the relation between the laboratory time and the arrival time at the detector clearly expressed by Fig. 10 and the corresponding different regimes encountered in the first order expansion of the relativistic hydrodynamic equations of Taub[59] (see Sec. 17). It is interesting to compare and contrast our treatment with selected results of the current literature, in order to illustrate some relevant points (see Table 2). We will consider the results in the literature only with reference to the limiting case which we address in our work: the condition of fully radiative emission.

The first line of Table 2 describes the ultrarelativistic regime, corresponding to an increasing energy flux of the afterglow as a function of the arrival time (phase A in previous section). Our treatment and the results in the literature by Dermer *et al.*[43,101,105] coincide. They agree as well with the results by Piran *et al.*[40,102,103]

The second line corresponds to the relativistic regime, in which the energy flux of the afterglow, after having reached the maximum (point P in previous section), monotonically decreases (phase B in previous section). The dependence we have found of the gamma factor on the radial coordinate of the expanding ABM pulse does coincide with the one given by Dermer *et al.* and Piran *et al.* Our power law index n in this regime, which perfectly fits the data, however, is markedly different from the others. Particularly interesting is the difference between our results and those of Dermer *et al.*: the two treatments coincide up to the last relation between the laboratory time and the arrival time at the detector. As explained in Eqs. (144) and (145), the two treatments differ in the approximation adopted in relating the laboratory time to the arrival time at the detector, illustrated in Fig. 10. Dermer *et al.* incorrectly adopted the approximation represented by the lower curve in Fig. 10 and consequently they do not find agreement with the observational data. We have not been able to retrace in the treatment by Piran *et al.* the steps which have led to their different results. Special mention must be made of a result stated by Halpern *et al.*,[53] the last entry in line 2, that an absolute lower limit for the power-law index $n - 1.47$ can be established on theoretical grounds. Such a result, clearly not correct also on the basis of our analysis, has

Table 2. We compare and contrast the results on the power-law index n of the afterglow in the EMBH theory with other treatments in the current literature, in the limit of high energy and fully radiative conditions. The differences between the values of $-10/7 \sim -1.43$ (Dermer) and the results -1.6 in the EMBH theory can be retraced to the use of the two different approximation in the arrival time versus the laboratory time given in Fig. 10. See details in Sec. 17.

	EMBH theory	Chiang & Dermer[101] Dermer, Chiang & Böttcher[43] Böttcher & Dermer[105]	Piran[102] Sari & Piran[103] Piran[40]	Vietri[104]	Halpern *et al.*[53]
Ultra-relativistic	$\gamma = \gamma_0$ $\gamma_0 = 310.1$ $n = 2$	$\gamma = \gamma_0$ $n = 2$	$\gamma = \gamma_0$ $n \simeq 2$		
Relativistic	$\gamma \simeq r^{-3}$ $3.0 < \gamma < 258.5$ $n = -1.6$	$\gamma \sim r^{-3}$ $n = -\frac{10}{7} = -1.43$	$\gamma \sim r^{-3}$ $n = -\frac{5.5}{4} = -1.375$		$n > -1.47$
Non-relativistic	$n = -1.36$ $1.05 < \gamma < 3.0$			$n = -1.7$	
Newtonian	$n = -1.45$ $1 < \gamma < 1.05$				

been erroneously used to support the existence of beaming in GRBs, as we will see below.

The third line in Table 2 is also interesting, treating the nonrelativistic limit (Phase C in previous section). This regime has been analysed by Vietri,[104] avoiding the exact integration of the equations and relying on simple qualitative arguments. These results are not confirmed by the integration of the equations we have performed. This is an interesting case to be examined for its pedagogical consequences. Having totally neglected the relation between the laboratory time and the time of arrival at the detector, which we have illustrated in Fig. 10, and identifying $t_a^d \equiv t$, Vietri reaches a very different power law from our. Moreover, his solution brings to an underestimation of the radial coordinate: he estimated a radial coordinate of 1.1×10^{15} cm at $t_a^d = 3.5 \times 10^4$ s, while the exact computation shows a result greater than 3.0×10^{17} cm (see Table 1). On the other hand if one assumes, from the above mentioned identity $t_a^d \equiv t$, $t = 3.5 \times 10^4$ s, one obtains a gamma factor of ~ 300 (see Table 1) in total disagreement with the nonrelativistic approximation adopted by Vietri. Quite apart from this pedagogical value, this nonrelativistic phase is of little interest from the observational point of view, due to the smallness of the flux emitted.

For completeness, we have also shown our estimates of the index n as the Newtonian phase is approached in the last line of Table 2.

The perfect agreement between our theoretically predicted value for the power-law index $n_{\rm theo}$ and the observed one $n_{\rm obs}$:

$$n_{\rm theo} = -1.6\,, \qquad n_{\rm obs} = -1.616 \pm 0.067\,, \tag{149}$$

confirms the validity of our major assumptions:

(1) The fully radiative regime.
(2) The constant average density of the ISM ($n_{\rm ism} = 1$ proton/cm^3).
(3) The spherical symmetry of the emission and the absence of beaming in GRB 991216.

After the work of Mao & Yi[87] which points to the possibility of introducing beaming to reduce the energetics of GRBs and after the discovery of the afterglow, many articles have appeared trying to obtain theoretical and observational evidence for beamed emission in GRBs. The observations have ranged from radio[106,107] to optical[53,108–110] all the way to X-rays. Particular attention has been devoted to relating the existence of beaming to possible breaks in the light curve slope, generally expected at a value of the gamma factor

$$\gamma = \frac{1}{\vartheta_0}\,, \tag{150}$$

where ϑ_0 is the beam opening angle. There are many articles on this subject; to mention only the most popular ones, we recall Refs. 90, 91, 94–96, 111. Far from

having reached a standard formulation, these approaches differ from each other in the expected time at which the break should take place up to a factor[94] of 20. They differ as well for the opening angle of the beam, up to a factor[94] of 3. Disagreement still exists on the number of breaking points: two in the case of Ref. 95, one in the case of Ref. 94, and again one each in the case of Refs. 90, 96 and 111 but differing in position from the one of Ref. 94. It has also been noticed that other authors have shown through numerical simulations that such a transition, if visible at all, is not very sharp.[53]

Ample observational data have been obtained for the GRB 991216 in the optical and radio, in addition to the X-ray band. For the reason mentioned at the beginning of Sec. 14, we only address in this article the problem of the γ- and the X-ray emission. In that respect, the main article addressing the issue of beaming in the X-rays for GRB 991216 is the one of Ref. 53. The key argument is based on the theoretical inequality claimed to exist for the power-law index $n > -1.47$ (see above). The fact that the observed X-ray decay rate is found to be $n_{\rm obs} = 1.616 \pm 0.067$ is interpreted by the authors as evidence for beaming. Moreover, the fact that the decay rate $n = -1.6$ has been observed before a steepening in the optical decay occurred at approximately 1 day of arrival time authorized an even more extreme proposal of a narrower beam in the X-rays within the optical beam.

It is clear from the entire treatment which we have presented and the results of the EMBH theory given by $n_{\rm theo} = -1.6$ that there is no evidence for such a beaming, as already stated above. The motivation by Halpern *et al.*[53] stems from the incorrect theoretical assumption of the existence of a lower limit in the afterglow power-law index $n > -1.47$. From our theoretical analysis the existence of $n = -1.6$ is a clear proof of isotropic emission in the GRB 991216 and a clear test of the complete relativistic treatment of the source. The fact that the break in the index should be "achromatic" and the absence of beaming in the X-rays imply an absence of beaming also in the optical and radio bands. The observed steepening in the optical decay has to find an alternative explanation. Although this is not the subject of our present work for the above mentioned reasons, we have found interesting the considerations by Panaitescu & Kumar,[112] which find that "there are some major difficulties to apply a jet model to GRB 991216". They have also stated, still for GRB 991216, that "the steepening of the optical decay of a few days is not due to a jet effect, as suggested by Halpern *et al.*,[53] but to the passage of a spectral break".

Concerning our own position on the possibility of beaming in GRBs, we would like just to remark that, from a preliminary analysis of beamed emission within the EMBH model, we have found some new features which are not encompassed by the results in the current literature, and they could become a distinctive signature for the discrimination of the existence or nonexistence of beaming.[58] The study of the steepening in the optical and radio decay is addressed within the EMBH theory in a forthcoming paper.[81]

19. Substructures in the E-APE Due to Inhomogeneities in the Interstellar Medium

The afterglow is emitted as the ABM pulse plows through the interstellar matter engulfing new baryonic material. In our previous articles we were interested in explaining the overall energetic processes of the GRB phenomena and in this sense, we have adopted the very simplified assumption that the interstellar medium is a constant density medium with $n_{\rm ism} = 1/{\rm cm}^3$. Consequently, the afterglow emission obtained is very smooth in time. We are now interested in seeing if in this framework we can also explain most of the time variability observed by BATSE, all of which except for the P-GRB should correspond to the beam-target phase in the IBS paradigm.

We pursue this treatment while still neglecting the angular spreading due to off-axis scattering in the radiation of the afterglow.

Our goal is to focus in this simplified model on the basic energetic parameters as well as on the drastic consequences of the space–time variables expressed in the RSTT paradigm.

Having obtained the two results presented in Figs. 9 and 34, we can proceed to attack the specific problem of the time variability observed by BATSE.

The fundamental point is that in both regimes *the flux observed in the arrival time is proportional to the interstellar matter density*: any inhomogeneity in the interstellar medium $\Delta n_{\rm ism}/\bar{n}_{\rm ism}$ will lead correspondingly to a proportional variation in the intensity $\Delta I/\bar{I}$ of the afterglow. This result has been erroneously interpreted in the current literature as a burst originating in an unspecified "inner engine".

In particular, for the main burst observed by BATSE (see Fig. 36(a)) we have

$$(\Delta I/\bar{I}) = (\Delta n_{\rm ism}/n_{\rm ism}) \sim 5\,. \tag{151}$$

There are still a variety of physical circumstances which may lead to such density inhomogeneities.

The additional crucial parameter in the understanding of the physical nature of such inhomogeneities is the time scale of the burst observed by BATSE. Such a burst lasts $\Delta t_a \simeq 20$ s and shows substructures on a time scale of ~ 1 s (see Fig. 36(a)). In order to infer the nature of the structure emitting such a burst we must express these time scales in the laboratory time.[1] Since we are at the peak of the GRB we have $\gamma_{P_A} \sim 258.5$ (see Eq. (138)) and Δt_a corresponds in the laboratory time to an interval

$$\Delta t \sim 1.0 \times 10^6 \text{ s}\,, \tag{152}$$

which determines the characteristic size of the inhomogeneity creating the burst $\Delta L \sim 5.0 \times 10^{16}$ cm (see Table 1 and Fig. 10).

It is immediately clear from Eqs. (151) and (152) that these are the typical dimensions and density contrasts corresponding to a small interstellar cloud. As an

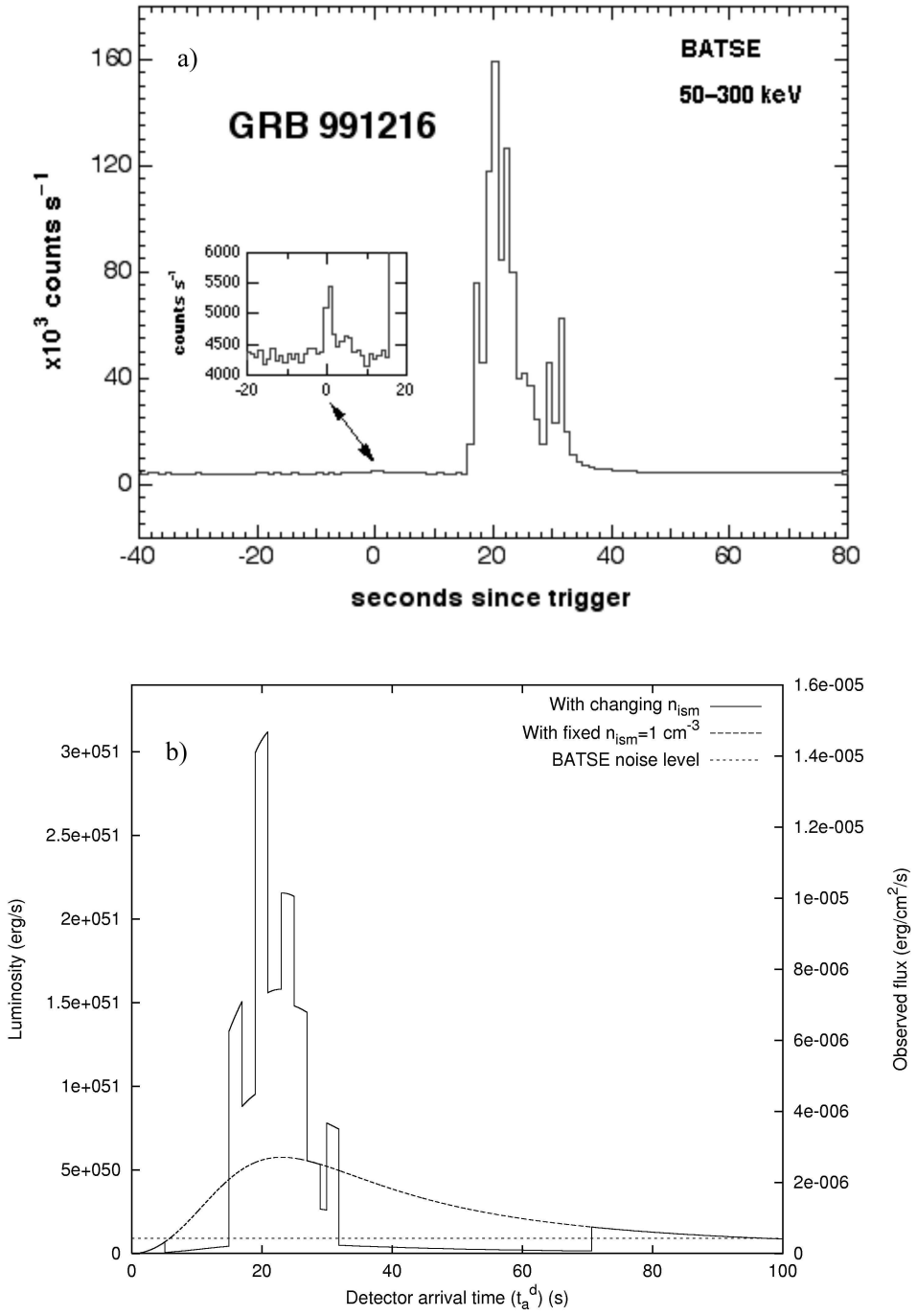

Fig. 36. (a) Flux of GRB 991216 observed by BATSE. The enlargement clearly shows the P-GRB.[2] (b) Flux computed in the collision of the ABM pulse with an ISM cloud with the density profile given in Fig. 37. The dashed line indicates the emission from an uniform ISM with $n = 1\ \mathrm{cm}^{-3}$. The dotted line indicates the BATSE noise level.

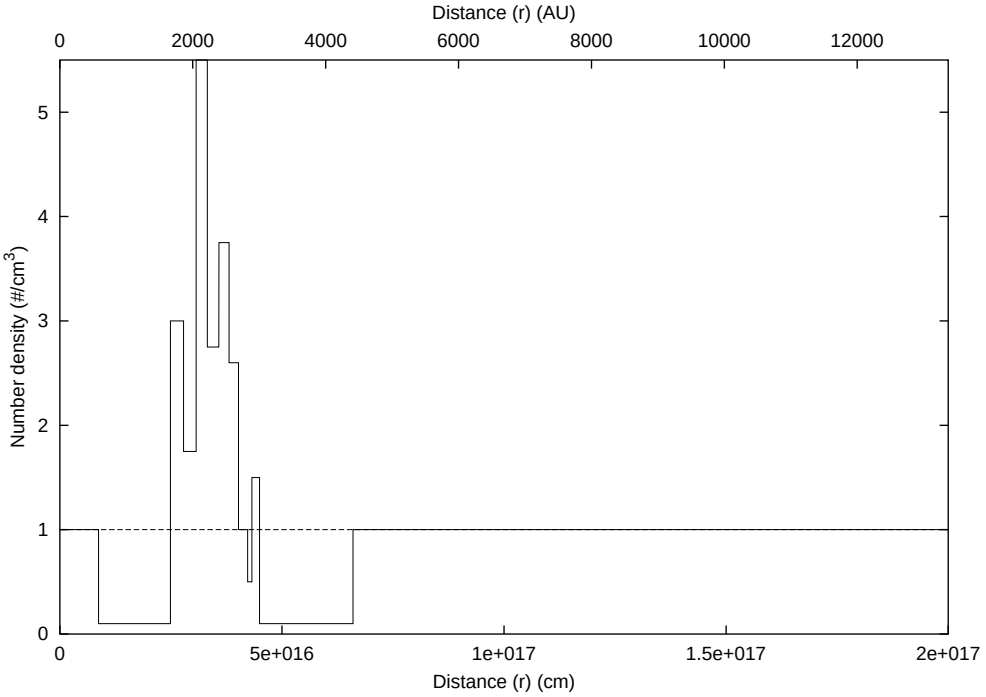

Fig. 37. The density contrast of the ISM cloud profile introduced in order to fit the observation of the burst of GRB991216. The dashed line indicates the average uniform density $n = 1$ cm^{-3}.

explicit example we have shown in Fig. 37 the density contrasts and dimensions of an interstellar cloud with an *average density* $\langle n \rangle = 1/\mathrm{cm}^3$. Such a cloud is located at a distance of $\sim 8.7 \times 10^{15}$ cm from the EMBH, gives rise to a signal similar to the one observed by BATSE (see Fig. 36(b)).

It is now interesting to see the burst that would be emitted, if our present approximation would still apply, by the interaction of the ABM pulse with the same ISM cloud encountered at later times during the evolution of the afterglow. Figure 38(a) shows the expected structure of the burst at a distance 4.1×10^{17} cm, corresponding to an arrival time delay of ~ 2 days, where the gamma factor is now $\gamma_\star \sim 3.6$. It is interesting that the overall intensity would be smaller, the intensity ratio of the burst relative to the average emission would remains consistent with Eq. (151), but the time scale of the burst would be longer by a factor $\left(\frac{\gamma_{P_A}}{\gamma_\star}\right)^2 \simeq 5 \times 10^3$. Figure 38(b) shows the corresponding quantities for the same ISM cloud located at a distance 6.4×10^{17} cm from the EMBH, corresponding to an arrival time delay of ~ 1 month, where the gamma factor is ~ 1.5.

We return in future work[57] to examine the angular spreading effects pointing out how they improve the results presented here: the explanation of the time variability observed in the so called "long bursts" in the BATSE classification of GRBs is confirmed. The smoothness, namely the absence of the above mentioned

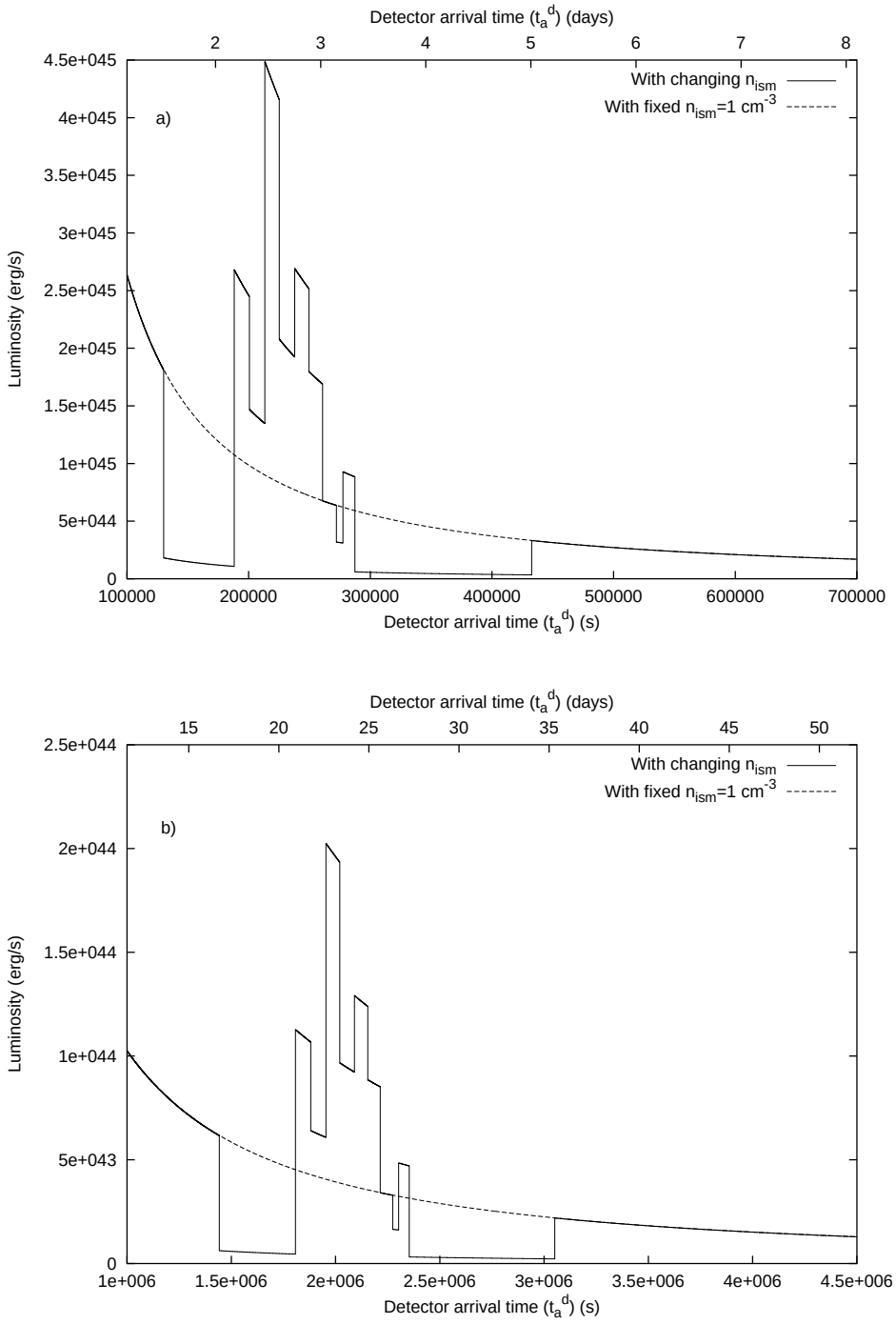

Fig. 38. (a) Same as Fig. 36(b) with the ISM cloud located at a distance of 3.17×10^{17} cm from the EMBH, the time scale of the burst now extends to $\sim 1.58 \times 10^5$ s. (b) Same as (a) with the ISM cloud at a distance of 4.71×10^{17} cm from the EMBH, the time scale of the burst now extends to $\sim 1.79 \times 10^6$ s.

substructures, observed in the latest phases of the afterglow finds as well a most natural explanation.

20. The Observation of the Iron Lines in GRB 991216: On a Possible GRB-Supernova Time Sequence

We have seen in the previous sections how the time structure of the E-APE gives information on the composition of the interstellar matter at distances of the order of 5×10^{16} cm from the source. We would like now to point out that the data on the iron lines from the Chandra satellite on the GRB 991216[54] and similar observations from other sources[54,113,114] make it possible to extend this analysis to a larger distance scale, possibly all the way out to a few light years, and consequently probe the distribution of stars in the surroundings of the newly formed EMBH.

Most importantly, these considerations lead to a new paradigm for the interpretation of the supernova-GRB correlation.[3] Indeed a correlation between the occurrence of GRBs and supernova events exists and has been established by the works.[96,102,115−121]

Such an association has been assumed to indicate that GRBs are generated by supernova explosions.[119] In turn, such a point of view has implied further consequences: the optical and radio data of the supernova have been attributed to the GRB afterglow, and many theorists have tried to encompass these data and explain them as a genuine component of the GRB scenario.

We propose instead an alternative point of view implying a very clear distinction between the GRB phenomenon and the supernova: if relativistic effects presented in the RSTT paradigm are properly taken into account, then a kinematically viable explanation can be given of the supernova-GRB association. We still use GRB 991216 as a prototypical case.

The GRB-Supernova Time Sequence paradigm, which we have indicated for short as GSTS paradigm,[3] states that: *A massive GRB-progenitor star P_1 of mass M_1 undergoes gravitational collapse to an EMBH. During this process a dyadosphere is formed and subsequently the P-GRB and the E-APE are generated in sequence. They propagate and impact, with their photon and neutrino components, on a second supernova-progenitor star P_2 of mass M_2. Assuming that both stars were generated approximately at the same time, we expect to have $M_2 < M_1$. Under some special conditions of the thermonuclear evolution of the supernova-progenitor star P_2, the collision of the P-GRB and the E-APE with the star P_2 can induce its supernova explosion.*

Especially relevant to our paradigm are the following data from the Chandra satellite:[54]

(1) At the arrival time of 37 hr after the initial burst there is evidence of iron emission lines for GRB 991216.
(2) The emission lines are present during the entire observation period of 10^4 s. The iron lines could also have been produced earlier, before Chandra was observing.

Thus the times used in these calculations are not unique: they do serve to provide an example of the scenario.

(3) The emission lines appear to have a peak at an energy of 3.49 ± 0.06 keV which, at a redshift $z = 1.00 \pm 0.02$ corresponds to an hydrogen-like iron line at 6.97 keV at rest. This source does not appear to have any significant motion departing from the cosmological flow. The iron lines have a width of 0.23 keV consistent with a radial velocity field of $0.1c$. The iron lines are only a small fraction of the observed flux.

On the basis of the explicit computations of the different eras presented in the above sections, we make three key points:

(1) An arrival time of 37 hr in the detector frame corresponds to a radial distance from the EMBH travelled by the ABM pulse of 3.94×10^{17} cm in the laboratory frame (see Table 1).
(2) It is likely that a few stars are present within that radius as members of a cluster. It has become evident from observations of dense clusters of star-forming regions that a stellar average density[122] of typically 10^2 pc^{-3} should be expected. There is also the distinct possibility for this case and other systems that the stars P_1 and P_2 are members of a binary system.
(3) The possible observations at different wavelengths of the supernova crucially depend on the relative intensities between the GRB and the supernova as well as on the value of the distance and the redshift of the source. In the present case of GRB 991216, the expected optical and radio emission from the supernova are many orders of magnitude smaller than the GRB intensity. The opposite situation will be encountered in GRB 980425.[51]

In order to reach an intuitive understanding of these complex computations we present a schematically very simplified diagram (not to scale) in Fig. 39.

We now describe the sequence of events and the specific data corresponding to the GSTS paradigm:

(1) The two stars P_1 and P_2 are separated by a distance $D_{P_2} = 3.94 \times 10^{17}$ cm in the laboratory frame, see Fig. 39. Both stars are at rest in the inertial laboratory frame. At laboratory time $t = 0$ and at comoving time $\tau = 0$, the gravitational collapse of the GRB-progenitor star P_1 occurs, and the initial emission of gravitational radiation or a neutrino burst from the event then synchronizes this event with the arrival times $t_a = 0$ at the supernova-progenitor star P_2 and $t_a^d = 0$ for the distant observer at rest with the detector. The electromagnetic radiation emitted by the gravitational collapse process is instead practically zero, due to the optical thickness of the material at this stage,[50] see Table 1.
(2) From Table 1, at laboratory time $t_1 = 6.48 \times 10^3$ s and at a distance of $D_1 = 1.94 \times 10^{14}$ cm from the EMBH, the condition of transparency for the PEMB pulse is reached and the P-GRB is emitted (see Sec. 8). This time is recorded as arrival time at the detector $t_{a_1}^d = 8.41 \times 10^{-2}$ s, and, at P_2, as $t_{a_1} = 4.20 \times 10^{-2}$ s.

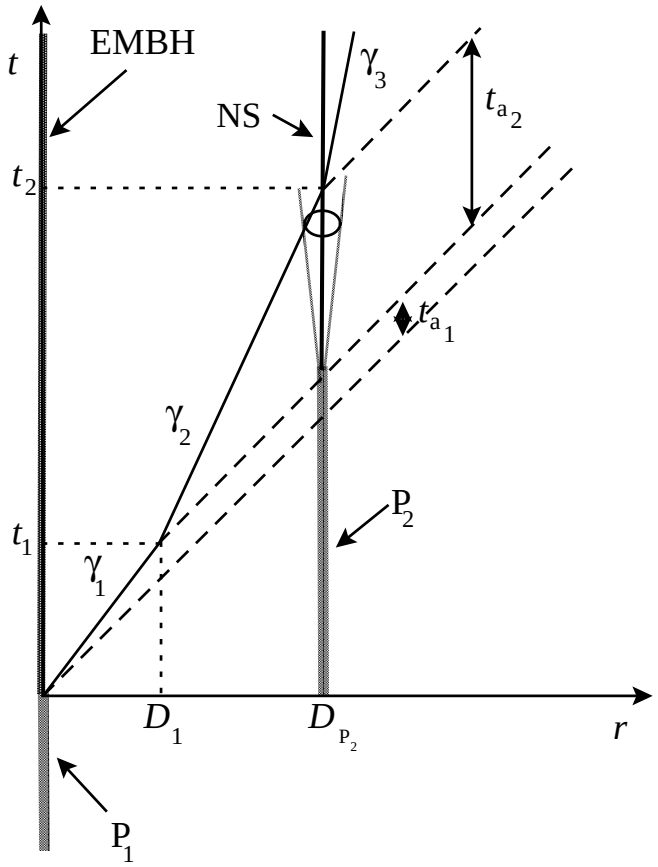

Fig. 39. A qualitative simplified space–time diagram (in arbitrary units) illustrating the GSTS paradigm. The EMBH, originating from the gravitational collapse of a massive GRB-progenitor star P_1, and the massive supernova-progenitor star P_2-neutron star (P_2-NS) system, separated by a radial distance D_{P_2}, are assumed to be at rest in in the laboratory frame. Their worldlines are represented by two parallel vertical lines. The supernova shell moving at $0.1c$ generated by the P_2-NS transition is represented by the dotted line cone. The solid line represents the motion of the pulse, as if it would move with an "effective" constant gamma factor γ_1 during the eras reaching the condition of transparency. Similarly, another "effective" constant gamma factor $\gamma_2 < \gamma_1$ applies during Era IV up to the collision with the P_2-NS system. A third "effective" constant gamma factor $\gamma_3 < \gamma_2$ occurs during Era V after the collision as the nonrelativistic regime of expansion is reached. The dashed lines at 45 degrees represent signals propagating at speed of light.

The fact that the PEMB pulse in an arrival time of 8.41×10^{-2} s covers a distance of 1.94×10^{14} cm gives rise to an apparent "superluminal" effect. This apparent paradox can be straightforwardly explained by introducing an "effective" gamma factor.[3]

(3) At laboratory time $t = 1.73 \times 10^6$ s and at a distance from the EMBH of 5.18×10^{16} cm in the laboratory frame, the peak of the E-APE is reached which is recorded at the arrival time $t_a = 9.93$ s at P_2 and $t_a^d = 19.87$ s at the detector. This also gives rise to an apparent "superluminal" effect.

(4) At a distance $D_{P_2} = 3.94 \times 10^{17}$ cm, the two bursts described in the above points (2) and (3) collide with the supernova-progenitor star P_2 at arrival times $t_{a_1} = 4.20 \times 10^{-2}$ s and $t_a = 9.93$ s respectively. They can then induce the supernova explosion of the massive star P_2.
(5) The associated supernova shell expands with velocity $0.1c$.
(6) The expanding supernova shell is reached by the ABM pulse generating the afterglow with a delay of $t_{a_2} = 18.5$ hr in arrival time following the arrival of the P-GRB and the E-APE. This time delay coincides with the interval of laboratory time separating the two events, since the P_2 is at rest in the inertial laboratory frame.[3] The ABM pulse has travelled in the laboratory frame a distance $D_{P_2} - D_1 \simeq D_{P_2} = 3.94 \times 10^{17}$ cm in a laboratory time $t_2 - t_1 \simeq t_2 = 1.32 \times 10^7$ s (neglecting the supernova expansion).

The collision of the pulse with the supernova shell occurs at $\gamma \simeq 4.0$. By this time the supernova shell has reached a dimension of 1.997×10^{14} cm, which is consistent with the observations from the Chandra satellite.

In these considerations on GRB 991216 the supernova remnant has been assumed to be close to but not exactly along the line of sight extending from the EMBH to the distant observer. If such an alignment should exist for other GRBs, it would lead to an observation of iron absorption lines as well as to an increase in the radiation observed in the afterglow corresponding to the crossing of the supernova shell by the ABM pulse. In fact, as the ABM pulse engulfs the baryonic matter of the remnant, above and beyond the normal interstellar medium baryonic matter, the conservation of energy and momentum implies that a larger amount of internal energy is available and radiated in the process (see Sec. 12). This increased energy-momentum loss will generally affect the slope of the afterglow decay, approaching more rapidly a nonrelativistic expansion phase (where details are given in Sec. 17).

It is quite clear that as soon as the relativistic transformations of the RSTT paradigm are duly taken into account, the sequence of events between the supernova and the GRB occurrences are exactly the opposite of the one postulated in the so-called "supranova" scenario.[30,31,123] This can be considered a very appropriate pedagogical example of how classical nonrelativistic considerations applied to ultra-relativistic regimes can indeed subvert the very causal relation between events.

If we now turn to the possibility of dynamically implementing the scenario, there are at least three different possibilities:

(1) Particularly attractive is the possibility that a massive star P_2 has rapidly evolved during its thermonuclear evolution to a white dwarf.[124] It it then sufficient that the P-GRB and the E-APE implode the star sufficiently as to reach a central density above the critical density for the ignition of thermonuclear burning. Consequently, the explosion of the star P_2 occurs, and a significant fraction of a solar mass of iron is generated. These configurations are currently generally considered precursors of some type I supernovae (see e.g. Filippenko,[125] and references therein).

(2) Alternatively, the massive star P_2 can have evolved to the condition of being close to the point of gravitational collapse, having developed the formation of an iron-silicon core, type II supernovae. The above transfer of energy momentum from the P-GRB and the E-APE may enhance the capture of the electrons on the iron nuclei and consequently decrease the Fermi energy of the core, leading to the onset of gravitational instability (see e.g. Bethe,[126] p. 270 and followings). Since the time for the final evolution of a massive star with an iron-silicon core is short, this event requires a well tuned coincidence.
(3) The pressure wave may trigger massive and instantaneous nuclear burning process, with corresponding changes in the chemical composition of the star, leading to the collapse.

The GSTS paradigm has been applied to the case of the GRB 980425 — SN1998bw which, with a red shift of 0.0083, is one of the closest and weaker GRBs observed. In this case, the radio and the optical emission of the supernova is distinctively observed. For this particular case, the EMBH appears to have a significantly lower value of the parameter ξ and the validity of the GSTS paradigm presented here is confirmed.[51]

21. General Considerations on the EMBH Formation

Before concluding let us consider the problem of the EMBH formation. Such a problem has been debated for many years since the earliest discussions in 1970 in Princeton and has been finally clarified and addressed in general terms to justify the plausibility of the hypothesis in Ref. 78. There has been a basic change of paradigm. All the considerations on the electric charge of stars were traditionally directed, following the classical work by Shvartsman[127] all the way to the fundamental book by Punsly,[128] to the presence of a net charge on the star surface in a steady state condition. The star can be endowed with rotation and magnetic field and surrounded by plasma, like in the case of Goldreich & Julian,[129] or, in the case of absence of both magnetic field and rotation, the electrostatic processes can be related to the depth of the gravitational well, like in the treatment of Shvartsman.[127] However, in neither cases is it possible to reach the condition of the overcritical field needed for pair creation nor has it the condition of no baryonic contamination discussed in Secs. 2, 6 and essential for the dyadosphere formation. The basic conceptual point is that GRBs are maybe the most violent transient phenomenon occurring in the universe and so the condition for the dyadosphere creation have to be searched in a transient phenomenon. The solution is related to the most transient phenomenon occurring in the life of a star: the process of gravitational collapse.

Having acquired such a fundamental understanding, the next step is to estimate the amount of polarization needed in order to reach the fully relativistic condition

$$\frac{Q}{M\sqrt{G}} = 1\,. \tag{153}$$

Recalling that the charge to mass ratio of a proton is $q_p/(m_p\sqrt{G}) = 1.1 \times 10^{18}$, it is enough to have an excess of one quantum of charge every 10^{18} nucleons in the core of the collapsing star to obtain an extreme EMBH after the occurrence of the gravitational collapse. Physically this means that we are dealing with a process of charge segregation between the core and the outer part of the star which has the opposite sign of net charge in order to enforce the overall charge neutrality condition. We here emphasize the name "charge segregation" instead of the name "charge separation" in order to contrast a very mild charge surplus created in different part of the star, keeping the overall charge neutrality, from the much more extreme condition of charge separation in which all the charges of the atomic component of the star are separated. It is indeed reassuring that such a core, endowed with charge segregation, is indeed stable with respect to the Fermi–Chandrasekhar criteria for the stability of self-gravitating stars duly extended from the magnetic to the electric case: the electric energy of such a core is consistently smaller than its gravitational energy.[98]

Such a condition of charge segregation between the core and the oppositely charged star surface layer can be reached under a very large number of physical conditions. We consider, for simplicity, one of the oldest example: the one of a star endowed with both a magnetic field and rotation. It is proved that a typical magnetic field expected for the ISM is $B_0 \sim 10^{-5}$ G.[130] We further assume, consistently with the data which we have acquired and verified in the present article (see Secs. 12 and 18), that also in the galaxy where GRB 991216 occurred the ISM has an average density of $n_{\rm ism} = 1$ proton/cm^3. From this value of density we have that an ISM cloud with mass $M \sim 10 M_\odot$ occupies a sphere of radius $R_0 \sim 1.4 \times 10^{19}$ cm. If this sphere collapse to a star with radius $R = R_\odot$, from the flux conservation we obtain that it is enough for this star to rotate with the most reasonable angular speed

$$\Omega \sim \frac{\xi M c \sqrt{G}}{R_\odot R_0^2 B_0} \tag{154}$$

to conclude that the progenitor star core is endowed of a charge to mass ratio equal to ξ. In the extreme case of Eq. (153) we have $\xi = 1$ and so the angular speed is $\Omega \sim 1.1 \times 10^{-3}$ rad/s — i.e. one round in 1.5 hr — and correspondingly we have smaller Ω values for $\xi < 1$.[98] Clearly the overall neutrality is guaranteed by the oppositely charged baryonic matter which is the one measured by the B parameter in the EMBH model (see Secs. 7 and 8). The smallness of the B value clearly points to the absence of an extended envelope of the progenitor star.

The formation process of such an electromagnetised progenitor star will be clearly affected by the presence of differential rotation, the consequent amplification of the magnetic field and a variety of magnetohydrodynamical problems which will affect somewhat the simplicity of the heuristic Eq. (154). Similarly the process of gravitational collapse of such a progenitor star endowed with rotation will lead to complex phenomena of "gravitationally induced electromagnetic radiation"[131]

and of "electromagnetically induced gravitational radiation"[132] which will tend to reduce both the eccentricity and the angular velocity of the collapsing core. The general outcome of gravitational collapse will be a Kerr–Newmann space–time. It is interesting that such a general case will break the degeneracy in (μ, ξ) described in Sec. 9.[133] In this article we have addressed the much simpler case of a solution in which $(cL) / \left(GM^2\right) \ll 1$ and the treatment can be well approximated by a collapse described by a Reissner–Nordström geometry.

In addition to this scenario, based on the role of magnetic field and rotation, we are also pursuing the possible generation of the charge segregation by quantum effects at the surface of the almost Fermi degenerate core. This most straightforward analysis also leads to a Reissner–Nordström geometry.

In both these cases the Reissner–Nordström geometry appears indeed to be the relevant model for GRB 991216 as discussed in the previous sections. We shall return to non-spherical configuration in forthcoming publications and/or when requested by observational evidence.[133]

Turning now from this general scenario to a more detailed analysis of a Reissner–Nordström geometry, some preliminary necessary steps have to be accomplished. In Cherubini, Ruffini & Vitagliano (2002)[71] we have considered the gravitational collapse of a charged spherical shell with selected boundary conditions: either starting from infinite distance with a null or non-null kinetic energy, or imploding from a finite distance initially at rest. A new analytic solution has been obtained for such a boundary condition, corresponding both to a collapse into an already formed EMBH or to a collapse in Minkowsky space. In both cases we have followed the process of gravitational collapse all the way to the self closure of the shell by the formation of an horizon.

Using this analytic solution it has been possible to clarify the independent physical components, contributing to the formation of the EMBH irreducible mass.[72] Surprisingly, the irreducible mass does not directly depend on the electromagnetic energy of the imploding shell: it is uniquely a function of the initial baryonic mass, of its gravitational energy and of the kinetic energy of the implosion. The electromagnetic energy is stored around the EMBH and can be extracted by two very different process as a function of the electromagnetic field strength. (a) When the electric field on the collapsing shell is smaller than $\mathcal{E}_c$, the process of energy extraction occurs in the effective EMBH ergosphere[134,135] by a sequence of discrete high energy events, with energy up to 10^{21}–10^{27} eV. Such sources can be of relevance for the explanation of the ultra high energy cosmic rays.[136] (b) When the electric field on the collapsing shell is larger than $\mathcal{E}_c$, the conditions relevant to the present article are fulfilled. The energy extraction process occurs in the dyadosphere and a much larger number of electron and positron pairs are created with typical energies of the order of 10 MeV which are relevant for the process considered in the present paper.

It is interesting that the clarification obtained by Ruffini & Vitagliano[72] has allowed a deeper understanding of the essential role of the gravitational and kinetic

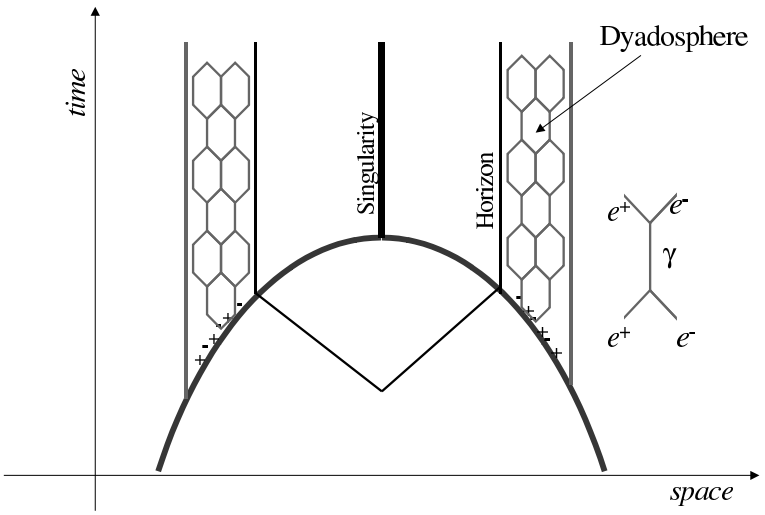

Fig. 40. Space–time diagram of the collapse process leading to the formation of the dyadosphere. As the collapsing core crosses the dyadosphere radius the pair creation process starts, and the pairs thermalize in a neutral plasma configuration. Then also the horizon is crossed and the singularity is formed.

implosion energies and the storage of the electromagnetic energy in the entire region surrounding the EMBH horizon. It has been shown by Ruffini & Vitagliano[73] that the central point can simply be summarized: the Coulomb repulsion of the collapsing matter reduces the kinetic energy of implosion leading to a smaller value of the irreducible mass and consequently to a larger value of the extractable energy.

Having so established and clarified the basic conceptual energetic processes of the EMBH, we are now ready to approach, using the new analytic solution obtained, the dynamical process of vacuum polarization occurring during the formation of an EMBH as qualitatively represented in Fig. 40. The study of the dyadosphere dynamical formation as well as of the electron-positron plasma dynamical evolution will lead to the first possibility of directly observing the general relativistic effects approaching the EMBH horizon.

Before closing we would like to emphasize once more a basic point: all the considerations presented in the description of the preceding eras are based on the approximations in the description of the dyadosphere presented in Sec. 2. This treatment is very appropriate in estimating the general dependence of the energy of the P-GRB, the kinetic energy of the ABM pulse and consequently the intensity of the afterglow, as well as the overall time structure of the GRB and especially the time of the release of the P-GRB with respect to the moment of gravitational collapse and its relative intensity with respect to the afterglow. If, however, ine is to address the issue of the detailed temporal structure of the P-GRB and its detailed spectral distribution, the above dynamical considerations on the dyadosphere formation are needed.[74] In turn, this detailed analysis is needed if the general relativistic effects

close to the horizon formation have to be followed. As expressed already in Sec. 11, all general relativistic quantum field theory effects are encoded in the fine structure of the P-GRB. As emphasized in Sec. 9, the only way to differentiate between solutions with same $E_{\rm dya}$ but different EMBH mass and charge is to observe the P-GRBs in the limit $B \to 0$, namely, to observe the short GRBs.

22. Conclusions

This paper is a consequence of a process of revision, reanalysis and further expansion of all the results presented in the previous articles.[1–3,47–49] In this process all the numerical estimates have been reanalysed for consistency. Most noticeably we have found a missing factor of 2π in the values of the experimental data on GRB 991216 we had used in our previous works which led to an underestimate of the total energy of the source.

This process of revision, far from being just a detailed computational verification, has given us the opportunity to rethink the entire GRB process in an unitary description starting from the moment of gravitational collapse all the way up to the latest phases of the afterglow and in identifying the three fundamental actors of the GRB phenomenon:

(1) $E_{\rm dya}$. Having reanalysed in Sec. 2 the physics of the dyadosphere we have pointed out in Fig. 16 that the same value of $E_{\rm dya}$ can be obtained from an entire family of (μ, ξ) parameters (i.e. $E_{\rm dya}$ is degenerate in (μ, ξ)). We have then shown in the reexamination of all the GRB eras that all the results depend only on the value of $E_{\rm dya}$ and not on the particular value of (μ, ξ) (see Secs. 7, 8, 12 and 13). The only exception to this occurs in the Era I (see Sec. 6) which is the only one relevant for short GRBs.
(2) B. The crucial role played by the baryonic remnant of the progenitor star in determining the relative intensity ratio and the time delay between the P-GRB and the E-APE has been summarized already in Figs. 12 and 13 in the introduction.
(3) ISM. The density $n_{\rm ism}$ of the interstellar medium and its inhomogeneities appears to have a fundamental role in the intensity and the temporal substructures of the E-APE and the afterglow. In order to identify such a crucial role, however, the correct relativistic space–time relations expressed by the RSTT paradigm are needed as amply exemplified in Secs. 17–19.

The observational data agree with the predictions of the model on:

(1) The intensity ratio, 1.58×10^{-2}, between the P-GRB and the E-APE, which strongly depends on the parameter B.
(2) The absolute intensities for both the P-GRB and the E-APE, respectively 7.54×10^{51} erg and 4.75×10^{53}.
(3) The arrival time of the P-GRB and the peak of the E-APE, respectively 8.41×10^{-2} s and 19.87 s.

These results can certainly be considered the greatest success of the EMBH theory.

Before closing, we like to draw some specific conclusions based on the first fundamental parameter of the EMBH theory: $E_{\rm dya}$. It is clear that $E_{\rm dya}$ is the fundamental parameter which determine the general energetic requirements of the GRB 991216. This energetics strongly depends on the possible existence or absence of beaming in the radiation process. In turn, as expressed in Secs. 17 and 18, the presence of beaming is led back to the power-law index n of the afterglow. The general conclusions reached on $E_{\rm dya}$ can be summarized as follow:

1.1 The value of n is a function of the transformation between $t \to t_a \to t_a^d$ (see Sec. 17). These transformations are a function of the entire relativistic regime of the world line of the source (see Sec. 4). By systematically neglecting this information the current works in the GRBs literature have obtained incorrect n values (see Table 2 and Sec. 18).

1.2 The value $n_{\rm theo} = -1.6$, which we have obtained within the EMBH theory, in the region of interest for the observations, based on the assumptions of spherical symmetry, fully radiative condition in the emission process and constant density of ISM, is in agreement with observed $n_{\rm obs} = -1.616 \pm 0.067$ (see Secs. 17 and 18). No evidence of beaming is therefore found is GRB 991216 (see Sec. 18).

1.3 For GRB 991216 $E_{\rm dya} = 4.83 \times 10^{53}$ erg is found in the EMBH theory. This value is systematically larger than the ones quoted in the current literature by Panaitescu & Kumar[112] and by Halpern *et al.*[53] due to the fact that they respectively consider beaming angles of $3^\circ - 4^\circ$ and 6°. These considerations have been shown to be untenable in Sec. 18. There is still a difference of $\sim 28\%$ between the total energy implied by the EMBH theory (4.83×10^{53} erg) and the value quoted by Halpern ($E_{\rm dya} = 6.7 \times 10^{53}$ erg) in the case of spherical emission. We trust that this is a consequence of the underlying assumption of the spectral distribution of the radiation assumed by Halpern *et al.*[53] (see e.g. Frail *et al.*[137]), which should be reassessed on the ground of our theoretical results. See also Ref. 133.

We turn now to the second fundamental parameter of the EMBH theory: B. It is essential in explaining the difference between the so called "long bursts" and "short bursts" (see Secs. 11 and 15). The general conclusions reached on B can be summarized as follows:

2.1 The most general GRB contains three different components: the P-GRB, the E-APE and the rest of the afterglow. The ratio between the P-GRB and the E-APE intensity and their temporal separation is a function of the B parameter (see Figs. 12 and 13). The best fit is obtained for $B = 3.0 \times 10^{-3}$ (see Sec. 14). We recall that in the present case for $B < 2.5 \times 10^{-5}$ the energy of the P-GRB would be larger than the one of the E-APE and the energy of the dyadosphere would be mainly

emitted in what have been called the "short bursts", while for $B > 2.5 \times 10^{-5}$ the energy of the E-APE would predominate and the energy of the dyadosphere would be mainly carried by the ABM pulse and emitted in the afterglow.

2.2 The difficulties encountered by *all* theoretical models, through the years, in order to explain the so called "long bursts" are resolved in a drastic way (see Sec. 15). The so called "long bursts" are *not* bursts at all. They represent just the E-APE which was interpreted as a burst only due to the noise threshold in the BATSE observations (see Fig. 11). The E-APE is emitted at distances from the EMBH in the range $1.0 \times 10^{16} \sim 1.0 \times 10^{17}$ cm, see Table 1, namely well outside the size of the progenitor star and already deep in interstellar space. The fact that the crossing of such distance, which is a typical dimension of an interstellar cloud, appears to occur in arrival time in only ~ 100 seconds is perfectly explained by the relativistic transformations encoded in the RSTT paradigm corresponding to a gamma factor between 100 and 300 (see Sec. 4 and Table 1). This effect would be interpreted within a classical and incorrect astronomical picture by a "superluminal" behaviour propagating at $\sim 3.6 \times 10^4 c$ (see Table 1).

2.3 In the limit $B \to 0$ the entire dyadosphere energy is emitted in the P-GRB. These events represents the "short bursts" class, for which the afterglow intensity is smaller than the P-GRB emission and below the actual observational limits (see Sec. 11). It is interesting that the proposed differentiation between the "short bursts" and "long bursts" within the EMBH theory is merely due to the amount of baryonic matter in the remnant, described by the B parameter, and totally independent from the process of gravitational collapse which is clearly identical in both cases. This explains at once the recently found conclusion that the distribution of short and long GRBs have essentially the same characteristic peak luminosity.[5] Also the result expressed in Fig. 7 that the average temperature corresponding to the P-GRB emission does increase for decreasing values of the B parameter can explain the observed fact that the "short bursts", which are obtained in the limit $B \to 0$, are systematically harder than "long bursts".[79]

Finally, the EMBH theory offers an unprecedented tool in order to map with great accuracy all the matter distribution around the newly formed EMBH from the horizon all the way to the ISM. This concept was pioneered by Dermer & Mitman[42] who proposed to use GRB sources as "tomographic images of the density distributions of the medium surrounding the sources of GRBs". It is important to emphasize that the very precise reading of the matter distribution encoded in the data of the P-GRB, the E-APE and the afterglow in GRB 991216 is in marked disagreement with the matter distribution postulated by the "collapsar" scenario.[27–29] This conclusion is evidenced not only by the absence of beaming already mentioned above, but also for the paucity of the baryonic matter encountered by the PEM pulse in its way out from the EMBH. There is no evidence for the presence either of a baryonic disk component nor of a conspicuous baryonic remnant. We actually

have $B = 3.0 \times 10^{-3}$. The general conclusions reached on this topic can then be summarized as follow:

3.1 Starting from the inside out we have, from the electrodynamics of the dyadosphere, that the baryonic contamination in that region has to be much smaller than 10^8 g/cm^3 (see Sec. 6). This condition can be achieved in the formation of an EMBH. The same electrodynamical process would be hampered in the formation of a neutron star due to the high density and baryonic contamination. Among all process of discharge of the overcritical electromagnetic field the pair creation is the most effective one due to the very short time scale of the order of $\hbar/m_e c^c \alpha \sim 10^{-19}$ seconds (see Sec. 2).

3.2 Unlike the case of formation of a neutron star, the mass of the remnant of the progenitor star is very small indeed. This mass, determined by B, is very accurately inferable from the relative intensity and temporal distance between the P-GRB and the E-APE (see above). In the present case we have $M_B \sim 8.1 \times 10^{-4} M_\odot$. The presence of the remnant is also important for guaranteeing the overall charge neutrality of the system formed by the oppositely charged collapsing core and the remnant. It has been pointed out in Sec. 21 that this condition of charge separation between the collapsing core and the remnant occurs only during the relevant part of the gravitational collapse process which, we recall, for a $10M_\odot$ is of the order of 30 seconds.

3.3 The structure of the E-APE and the afterglow gives as well an unprecedented tool in order to estimate the average density and filamentary structure in the ISM: the structures down to a fraction of seconds observed in the E-APEs, the so called "long bursts" of the current literature (see Fig. 3), can be used in order to map the filamentary structure as well as the size of interstellar clouds surrounding the EMBH (see Sec. 19). When all the geometrical and relativistic effects are duly taken into account the intensity and the average profile of the E-APE and of the afterglow point to an average value of the ISM density $n_{\rm ism} \sim 1$ proton/cm^3 in very good agreement with a large variety of independent estimates. The very late phases of the afterglow gives information of the induced supernova collapse (see Sec. 20 and Ruffini *et al.*,[3]) which will be addressed in a forthcoming publication. Since now we can assert that the correct space–time sequence based on the RSTT paradigm is in contrast with the "supranova" scenario[30,31,123] which was based on a nonrelativistic consideration in ultrarelativistic regimes (see Sec. 20).

This concludes the presentation of the basic model which is now ready to be applied to additional sources. If we look to the future we can see three main topics to be addressed with special attention:

(1) We have performed a more detailed description of beaming, of the angular spreading and of the spectral properties which is going to be the subject of

paper II. Since now, we can assert that this more detailed treatment supports all general conclusions obtained in the present paper.

(2) If one is interested in the detailed effects of general relativity and relativistic field theory, all the attention should be directed to the structure of the short bursts. This needs the development of detailed theoretical works on the approach of the horizon of the black hole and the associated electrodynamical process. From the description presented in this paper of an already formed and averaged dyadosphere (see Fig. 17) we have to move to the treatment of its dynamical formation (see Fig. 40). Such an analysis describing the approach to the formation of the horizon of the EMBH, within the EMBH theory, is in advanced phase of development[71–74] (see Fig. 40). Some preliminary results have appeared in Bianco, Ruffini & Xue.[50]

(3) From the observational point of view, the detailed observations of the yet unexplored region in the range up to 10^2 seconds in Fig. 14 and the corresponding observations of the "short bursts" by a new class of space missions with higher sensitivity than the BATSE instrument appear to be of great importance. Such observations should allow one to directly observe for the first time the general relativistic and extreme quantum field theory effects connected to the process of formation of the EMBH. It can be of some interest to explore the possibility of observing in these regimes the "gravitationally induced electromagnetic radiation"[131] and the "electromagnetically induced gravitational radiation"[132] phenomena.

References

1. R. Ruffini, C. L. Bianco, P. Chardonnet, F. Fraschetti and S.-S. Xue, *Astrophys. J.* **555**, L107 (2001a).
2. R. Ruffini, C. L. Bianco, P. Chardonnet, F. Fraschetti and S.-S. Xue, *Astrophys. J.* **555**, L113 (2001b).
3. R. Ruffini, C. L. Bianco, P. Chardonnet, F. Fraschetti and S.-S. Xue, *Astrophys. J.* **555**, L117 (2001c).
4. I. B. Strong, in *Neutron Stars, Black Holes and Binary X-Ray Sources*, eds. H. Gursky and R. Ruffini (D. Reidel Publishing Company, 1975).
5. M. Schmidt, *Astrophys. J.* **559**, L79 (2001).
6. E. Costa, invited talk in *IX Marcel Grossmann Meeting on General Relativity*, eds. V. Gurzadyan, R. Jantzen and R. Ruffini (World Scientific, 2002), in press.
7. R. Ruffini, in *Fluctuating Paths and Fields* — Dedicated to Hagen Kleinert on the occasion of his 60th Birthday," eds. W. Janke, A. Pelster, H.-J. Schmidt and M. Bachmann (World Scientific, Singapore, 2001), p. 771.
8. F. Halzen, "High energy neutrino astronomy," in *Weak Interactions and Neutrinos, Proceedings of the 17th International Workship*, Cape Town, South Africa, eds. C. A. Dominguez and R. D. Viollier (World Scientific, Singapore, 2000), p. 123.
9. W. Heisenberg and H. Euler, *Z. Phys.* **98**, 714 (1935).
10. J. Schwinger, *Phys. Rev.* **98**, 714 (1951).
11. R. Ganz *et al.*, *Phys. Lett.* **B389**, 4 (1996).
12. U. Leinberger *et al.*, *Phys. Lett.* **B394**, 16 (1997).

13. U. Leinberger *et al.*, *Eur. Phys. J.* **A1**, 249 (1998).
14. S. Heinz *et al.*, *Eur. Phys. J.* **A1**, 27 (1998).
15. A. Einstein, *Ann. Phys.* (*Germany*) **17**, 891 (1905).
16. J. A. Biretta, W. B. Sparks and F. Macchetto, *Astrophys. J.* **520**, 621 (1999).
17. I. F. Mirabel and L. F. Rodriguez, *Annu. Rev. Astron. Astrophys.* **37**, 409 (1999).
18. M. J. Rees, *Nature* **211**, 468 (1966)
19. R. S. van Dick, P. B. Schwinberg and H. G. Dehmelt, *Phys. Rev. Lett.* **38**, 310 (1977).
20. D. Eichler, M. Livio, T. Piran and D. N. Schramm, *Nature* **340**, 126 (1989).
21. R. Narayan, B. Paczyński and T. Piran, *Astrophys. J.* **395**, L83 (1992).
22. P. Mészáros and M. J. Rees, *Mon. Not. R. Astron. Soc.* **257**, 29 (1992a).
23. P. Mészáros and M. J. Rees, *Astrophys. J.* **397**, 570 (1992b).
24. C. L. Fryer, S. E. Woosley, M. Herant and M. B. Davies, *Astrophys. J.* **520**, 650 (1999).
25. B. Paczyński, *Acta Astronomica* **41**, 257 (1991).
26. P. Mészáros and M. J. Rees, *Astrophys. J.* **482**, L29 (1997b).
27. B. Paczyński, *Astrophys. J.* **494**, L45 (1998).
28. S. E. Woosley, *Astrophys. J.* **405**, 273 (1993).
29. A. I. MacFadyen and S. E. Woosley, *Astrophys. J.* **524**, 262 (1999).
30. M. Vietri and L. Stella, *Astrophys. J.* **507**, L45 (1998).
31. M. Vietri and L. Stella, *Astrophys. J.* **527**, L43 (1999).
32. J. D. Salmonson, J. R. Wilson and G. J. Mathews, to appear in *Astrophys. J.* (2001), astro-ph/0002312.
33. J. R. Wilson, G. J. Mathews and P. Marronetti, *Phys. Rev.* **D54**, 1317 (1996).
34. J. S. Bloom, S. R. Kulkarni and S. G. Djorgowski, *Astron. J.* **123**, 1111 (2002).
35. M. J. Rees and P. Mészáros, *Astrophys. J.* **430**, L93 (1994).
36. B. Paczyński and G. Xu, *Astrophys. J.* **427**, 708 (1994).
37. R. Sari and T. Piran, *Astrophys. J.* **485**, 270 (1997).
38. E. E. Fenimore, *Astrophys. J.* **518**, 375 (1999).
39. E. E. Fenimore, C. Cooper, E. Ramirez-Ruiz, M. C. Sumner, A. Yoshida and M. Namiki, *Astrophys. J.* **512**, 683 (1999).
40. T. Piran, talk at 2000 Texas Meeting, see also astro-ph/0104134.
41. P. Mészáros and M. J. Rees, *Astrophys. J.* **405**, 278 (1993).
42. C. D. Dermer and K. E. Mitman, *Astrophys. J.* **513**, L5 (1999).
43. C. D. Dermer, J. Chiang and M. Böttcher, *Astrophys. J.* **513**, 656 (1999b).
44. C. D. Dermer, *Astrophys. J.* **574**, 65 (2002).
45. R. Ruffini, in *Black Holes and High Energy Astrophysics*, Proceedings of the 49th Yamada Conference, eds. H. Sato and N. Sugiyama (Universal Academic Press, Tokyo, 1998).
46. T. Damour and R. Ruffini, *Phys. Rev. Lett.* **35**, 463 (1975).
47. G. Preparata, R. Ruffini and S.-S. Xue, *Astron. Astrophys.* **338**, L87 (1998b).
48. R. Ruffini, J. D. Salmonson, J. R. Wilson and S. S. Xue, *Astron. Astrophys.* **350**, 334 (1999); *Astron. Astrophys. Supplement Series* **138**, 511 (1999).
49. R. Ruffini, J. D. Salmonson, J. R. Wilson and S. S. Xue, *Astron. Astrophys.* **359**, 855 (2000).
50. C. L. Bianco, R. Ruffini and S.-S. Xue, *Astron. Astrophys.* **368**, 377 (2001a).
51. R. Ruffini, C.L. Bianco, P. Chardonnet, F. Fraschetti and S.-S. Xue, (2002d), in preparation.
52. BATSE Rapid Burst Response, (1999)
http://gammaray.msfc.nasa.gov/∼kippen/batserbr/

53. J. P. Halpern, R. Uglesich, N. Mirabal, S. Kassin, J. Thorstensen, W. C. Keel, A. Diercks, J. S. Bloom, F. Harrison, J. Mattox and M. Eracleous, *Astrophys. J.* **543**, 697 (2000).
54. L. Piro *et al.*, *Science* **290**, 955 (2000).
55. R. Corbet and D. A. Smith, in *Rossi2000*: *Astrophysics with the Rossi X-ray Timing Explorer* (Greenbelt, USA, 2000).
56. T. Takeshima, C. Markwardt, F. Marshall, T. Giblin and R. M. Kippen, GCN Circ. 478 (http://gcn.gsfc.nasa.gov/gcn/gcn3/478.gcn3), (1999).
57. R. Ruffini, C. L. Bianco, P. Chardonnet, F. Fraschetti and S.-S. Xue, (2002a), in preparation.
58. R. Ruffini, C. L. Bianco, P. Chardonnet, F. Fraschetti and S.-S. Xue, (2002b), in preparation.
59. A. H. Taub, *Phys. Rev.* **74**, 328 (1948).
60. L. D. Landau and E. M. Lifshitz, *Course of Theoretical Physics*, Vol. 6: *Fluid Mechanics*, 2nd edn., paperback (Butterworth Heinemann, 1995) Sec. 135, p. 510.
61. R. Ruffini and J. A. Wheeler, *Physics Today* **24**(1), 30 (1971).
62. B. Carter, *Proceedings of the Eighth Marcel Grossmann Meeting on General Relativity*, eds. T. Piran and R. Ruffini (World Scientific, Singapore, 1997), p. 136.
63. D. Bini, C. Cherubini, R. Jantzen and R. Ruffini, *Prog. Theor. Phys.* **107**(5), 000 (2002), in press.
64. D. Christodoulou and R. Ruffini, *Phys. Rev.* **D4**, 3552 (1971).
65. W. T. Zaumen, *Nature* **247**, 530 (1974).
66. G. W. Gibbons, *Commun. Math. Phys.* **44**, 245 (1975).
67. S. W. Hawking, *Nature* **248**, 30 (1974).
68. G. Preparata, R. Ruffini and S.-S. Xue, in *Proceedings of the VII Italian-Korean Meeting* (Korean Phys. Soc., 2003).
69. R. Ruffini, in *Physics and Astrophysics of Neutron Stars and Black Holes*, eds. R. Giacconi, R. Ruffini and coauthors (North Holland, Amsterdam, 1978).
70. G. Preparata, R. Ruffini and S.-S. Xue, in *Proceedings of the Italo Korean Meeting* (SIF, 2001).
71. C. Cherubini, R. Ruffini and L. Vitagliano, (2002), in preparation.
72. R. Ruffini and L. Vitagliano, (2002a), in preparation.
73. R. Ruffini and L. Vitagliano, (2002b), in preparation.
74. R. Ruffini, L. Vitagliano and S.-S. Xue, (2002f), in preparation.
75. E. E. Fenimore, C. D. Madras and S. Nayakshin, *Astrophys. J.* **473**, 998 (1996).
76. J. R. Wilson, J. D. Salmonson and G. J. Mathews, in *Gamma-Ray Bursts*: *4th Huntsville Symposium*, eds. C. A. Meegan, R. D. Preece and T. M. Koshut (American Institute of Physics, 1997).
77. J. R. Wilson, J. D. Salmonson and G. J. Mathews, in *2nd Oak Ridge Symposium on Atomic and Nuclear Astrophysics* (IOP Publishing, 1998).
78. R. Ruffini, *Proceedings of the Ninth Marcel Grossmann Meeting on General Relativity* (World Scientific, Singapore, 2002), in press.
79. C. Kouveliotou, C. A. Meegan, G. J. Fishman, N. P. Bath, M. S. Briggs, T. M. Koshut, W. S. Paciesas and G. N. Pendleton, *Astrophys. J.* **413**, L101 (1993).
80. R. Ruffini, C. L. Bianco, P. Chardonnet, F. Fraschetti and S.-S. Xue, *Nuovo Cimento* **116**, 99 (2001e).
81. R. Ruffini, C. L. Bianco, P. Chardonnet, F. Fraschetti and S.-S. Xue, (2002c), in preparation.
82. W. S. Paciesas *et al.*, *Astrophys. J. Supplement Series* **122**, 465 (1999).
83. J. P. Norris, *et al.*, *Astrophys. J.* **301**, 213 (1986).

84. D. Band, *et al.*, *Astrophys. J.* **413**, 281 (1993).
85. C. D. Dermer, M. Böttcher and J. Chiang, *Astrophys. J.* **515**, L49 (1999a).
86. F. Frontera, *et al.*, *Astrophys. J. Supplement Series* **127**, 59 (2000).
87. S. Mao and I. Yi, *Astrophys. J.* **424**, L131 (1994).
88. M. B. Davies, W. Benz, T. Piran and F. K. Thielemann, *Astrophys. J.* **431**, 742 (1994).
89. P. Mészáros and M. J. Rees, *Astrophys. J.* **476**, 232 (1997a).
90. J. E. Rhoads, *Astrophys. J.* **487**, L1 (1997a).
91. P. Mészáros, M. J. Rees and R. A. M. J. Wijers, *Astrophys. J.* **499**, 301 (1998).
92. A. Panaitescu, P. Mészáros and M. J. Rees, *Astrophys. J.* **503**, 314 (1998).
93. C. D. Dermer and J. Chiang, in *Proceedings of High Energy Processes in Accreting Black Holes*, held in Graftavallen, Sweden, June 29–July 4, 1998, eds. J. Poutanen and R. Svensson, astro-ph/9810222.
94. R. Sari, T. Piran and J. P. Halpern, *Astrophys. J.* **519**, L17 (1999).
95. A. Panaitescu and P. Mészáros, *Astrophys. J.* **526**, 707 (1999).
96. J. E. Rhoads, *Astrophys. J.* **525**, 737 (1999).
97. L. J. Gou, Z. G. Dai, Y. F. Huang and T. Lu, *Astron. Astrophys.* **368**, 464 (2001).
98. D. Boccaletti, H. C. Ohanian and R. Ruffini, (2002), in preparation.
99. R. D. Blandford and C. F. McKee, *Phys. Fluids* **19**, 1130 (1976).
100. M. Abramowitz and I. A. Stegun (eds.), *Handbook of Mathematical Functions*, (National Bureau of Standards, Washington D.C., 1970).
101. J. Chiang and C. D. Dermer, *Astrophys. J.* **512**, 699 (1999).
102. T. Piran, *Phys. Rep.* **314**, 575 (1999).
103. R. Sari and T. Piran, *Astrophys. J.* **520**, 641 (1999).
104. M. Vietri, *Astrophys. J.* **478**, L9 (1997).
105. M. Böttcher and C. D. Dermer, *Astrophys. J.* **532**, 281 (2000).
106. E. Rol *et al.*, (1999), GCN Circ. 491 (http://gcn.gsfc.nasa.gov/gcn/gcn3/491.gcn3).
107. D. Frail *et al.*, *Astrophys. J.* **538**, L129 (2000).
108. P. Garnavich *et al.*, *Astrophys. J.* **543**, 61 (2000).
109. R. Sagar *et al.*, *Bull Astron. Soc. India* **28**, 15 (2000).
110. B. Schaefer, (2000), GCN Circ. 517 (http://gcn.gsfc.nasa.gov/gcn/gcn3/517.gcn3).
111. J. E. Rhoads, in *AIP Conf. Proc. 428*, *Gamma-Ray Bursts*: *Fourth Huntsville Symposium*, eds. C. Meegan, R. Preece and T. Koshut (AIP, New York, 1997b), p. 699.
112. A. Panaitescu and P. Kumar, *Astrophys. J.* **554**, 667 (2001).
113. L. Piro *et al.*, *Astrophys. J.* **514**, L73 (1999).
114. L. Amati *et al.*, *Science* **290**, 953 (2000).
115. L. Bloom *et al.*, *Nature* **401**, 453 (1999).
116. T. J. Galama *et al.*, (1998a), IAU Circ., 6895.
117. T. J. Galama *et al.*, *Nature* **395**, 670 (1998b).
118. T. J. Galama *et al.*, *Astrophys. J.* **536**, 185 (2000).
119. S. R. Kulkarni *et al.*, *Nature* **395**, 663 (1998).
120. L. Piro *et al.*, (1998), GCN 155.
121. J. van Paradijs, C. Kouveliotou and R. A. M. J. Wijers, *Annu. Rev. Astron. Astrophys.* **38**, 379 (2000).
122. S. C. Beck, J. L. Turner and O. Kovo, *Astron. J.* **120**, 244 (2000).
123. M. Vietri, C. Perola, L. Piro and L. Stella, *Mon. Not. R. Astron. Soc.* **308**, L29 (1999).
124. S. Chandrasekhar, "Why are the stars as they are," in *Physics and Astrophysics of Neutron Stars and Black Holes*, eds. R. Giacconi and R. Ruffini (Elsevier, North Holland, 1978).

125. A. V. Filippenko, *Annu. Rev. Astron. Astrophys.* **35**, 309 (1997).
126. H. A. Bethe, *The Road from Los Alamos* (Touchstone, American Institute of Physics, New York, 1991).
127. V. F. Shvartsman, *Soviet Physics JETP* **33**, 475 (1097).
128. B. Punsly, *Black Hole Gravitohydromagnetics* (Springer, 2001).
129. P. Goldreich and W. H. Julian, *Astrophys. J.* **157**, 869 (1969).
130. K. M. Ferrière, *Rev. Mod. Phys.* **73**, 1031 (2001).
131. M. Johnston, R. Ruffini and F. Zerilli, *Phys. Rev. Lett.* **31**, 1317 (1973).
132. M. Johnston, R. Ruffini and F. Zerilli, *Phys. Lett.* **B49**, 185 (1974).
133. R. Ruffini, C. L. Bianco, P. Chardonnet, F. Fraschetti and S.-S. Xue, (2002e), in preparation.
134. G. Denardo and R. Ruffini, *Phys. Lett.* **B45**, 259 (1973).
135. G. Denardo, L. Hively and R. Ruffini, *Phys. Lett.* **B50**, 270 (1974).
136. C. L. Bianco, P. Chardonnet, R. Ruffini and S.-S. Xue, (2002), in preparation.
137. D. Frail *et al.*, *Astrophys. J.* **562**, L55 (2001).

13 Appendix 6

The Astrophysical Journal, 581:L19–L22, 2002 December 10

ON THE STRUCTURES IN THE AFTERGLOW PEAK EMISSION OF GAMMA-RAY BURSTS

Remo Ruffini,[1,2] Carlo Luciano Bianco,[1,2] Pascal Chardonnet,[1,3]
Federico Fraschetti,[1,4] and She-Sheng Xue[1,2]

Received 2002 October 7; accepted 2002 October 29; published 2002 November 11

ABSTRACT

Using GRB 991216 as a prototype, we show that the intensity substructures observed in what is generally called the "prompt emission" in gamma-ray bursts (GRBs) do originate in the collision between the accelerated baryonic matter pulse with inhomogeneities in the interstellar medium (ISM). The initial phase of such process occurs at a Lorentz factor $\gamma \sim 310$. The crossing of ISM inhomogeneities of sizes $\Delta R \sim 10^{15}$ cm occurs in a detector arrival time interval of ~0.4 s, implying an apparent superluminal behavior of $\sim 10^5 c$. The long-lasting debate between the validity of the external shock model versus the internal shock model for GRBs is solved in favor of the first.

Subject headings: black hole physics — gamma rays: bursts — gamma rays: observations — gamma rays: theory — ISM: clouds — ISM: structure

To reproduce the observed light curve of GRB 991216, we have adopted, as initial conditions (Ruffini et al. 2002a) at $t = 10^{-21}$ s ~ 0 s, a spherical shell of electron-positron-photon neutral plasma lying between the radii $r_0 = 6.03 \times 10^6$ cm and $r_1 = 2.35 \times 10^8$ cm: the temperature of such a plasma is 2.2 MeV, the total energy $E_{\rm tot} = 4.83 \times 10^{53}$ ergs, and the total number of pairs $N_{e^+e^-} = 1.99 \times 10^{58}$.

Such initial conditions follow from the electromagnetic black hole (EMBH) theory we have recently developed based on energy extraction from a black hole endowed with electromagnetic structure (Ruffini 1998; Preparata, Ruffini, & Xue 1998; Ruffini et al. 1999a, 1999b, 2000, 2001a, 2001b, 2001c, 2002a; Bianco, Ruffini, & Xue 2001), r_0 being the horizon radius, r_1 being the dyadosphere radius, and $E_{\rm tot}$ coinciding with the dyadosphere energy $E_{\rm dya}$. The above set of parameters is uniquely determined by the value of $E_{\rm dya}$. The EMBH energy (Christodoulou & Ruffini 1971) is carried away by a plasma of electron-positron pairs created by the vacuum polarization process (Damour & Ruffini 1975) occurring during the gravitational collapse leading to the EMBH (Cherubini, Ruffini, & Vitagliano 2002; Ruffini & Vitagliano 2002). Such an optically thick electron-positron plasma self-propels itself outward reaching ultrarelativistic velocities (Ruffini et al. 1999a, 1999b), interacts with the remnant of the progenitor star, and by further expansion becomes optically thin (Ruffini et al. 2000). The physical reason for such an extraordinary process of self-acceleration, achieving in a tenth of a second in arrival time an increase in the Lorentz gamma factor from $\gamma = 1$ to $\gamma \sim 300$, has been shown to be critically dependent on $E_{\rm dya}$ and on the amount of baryonic matter engulfed by the plasma in its expansion (see Ruffini et al. 1999a, 1999b, 2000). It is interesting that this process is extremely efficient even in the present case, regardless of the relatively slow random thermal motion of the 2.2 MeV e^+e^- plasma (see Ruffini et al. 2002a). As the transparency condition is reached, a proper gamma-ray burst (P-GRB) is emitted as well as an extremely relativistic shell of accelerated baryonic matter (ABM). It is this ABM pulse that, interacting with the interstellar medium (ISM), gives origin to the afterglow (see Ruffini et al. 2001b, 2002a).

One of the most novel results of the EMBH model has been the identification of what is generally called the "prompt emission" (see, e.g., Piran 1999 and references therein) as an integral part of the afterglow: the extended afterglow peak emission (E-APE; Ruffini et al. 2001a, 2001b, 2002a). This result is clearly at variance with the models explaining the prompt emission with ad hoc mechanisms distinct from the afterglow process (see, e.g., Rees & Mészáros 1994, 1998, 2000; Mészáros & Rees 1997, 2001; Kobayashi, Piran, & Sari 1997; Kumar & Piran 2000; Mészáros 2002). The fact that the EMBH model, using GRB 991216 as a prototype, has allowed the computation of the temporal separation of the P-GRB and the E-APE to an accuracy of a few milliseconds and also to predict their relative intensities within a few percent can certainly be considered a major success of the model (see Ruffini et al. 2001a, 2001b, 2002a).

The aim of this Letter is to report a further extension of the EMBH model in order to identify the physical processes giving origin to the intensity variability observed in the E-APE on timescales as short as a fraction of a second (Fishman & Meegan 1995), which contrasts with the smoother emission in the last phases of the afterglow (see, e.g., Costa, Frontera, & Hjorth 2001).

In our former work on the EMBH model (Ruffini et al. 2001b, 2002a), we have assumed a homogeneous ISM with a density $n_{\rm ism} = \langle n_{\rm ism} \rangle = 1$ particle cm^{-3} and we have also assumed that during the collision of the ABM pulse with the ISM the "fully radiative condition" applies. These assumptions have led to the theoretical prediction of the power-law index of the afterglow slope $n = -1.6$, in excellent agreement with the observational data $n = -1.616 \pm 0.067$ (Halpern et al. 2000). Our goal here is to show that the variability in the E-APE can indeed be traced back to inhomogeneities in the ISM. We again consider, as in the previous work, the case of an ABM pulse expanding with spherical symmetry (i.e., no beaming), and for simplicity we describe the ISM inhomogeneities as spherical shells concentric to the ABM pulse. Each shell has a selected density and a constant thickness $\Delta R = 1.0 \times 10^{15}$ cm.

We recall now the relation between the relativistic beaming angle and the arrival time of the emitted photon on the detector. The visible part of the ABM pulse spherical surface is con-

[1] International Center for Relativistic Astrophysics, Università di Roma "La Sapienza," Piazzale Aldo Moro 5, I-00185 Rome, Italy; ruffini@icra.it, xue@icra.it, bianco@icra.it, fraschetti@icra.it.
[2] Dipartimento di Fisica, Università di Roma "La Sapienza," Piazzale Aldo Moro 5, I-00185 Rome, Italy.
[3] Université de Savoie, LAPTH-LAPP, BP 110, F-74941 Annecy-le-Vieux Cedex, France; chardon@lapp.in2p3.fr.
[4] Università di Trento, via Sommarive 14, I-38050 Povo (Trento), Italy.

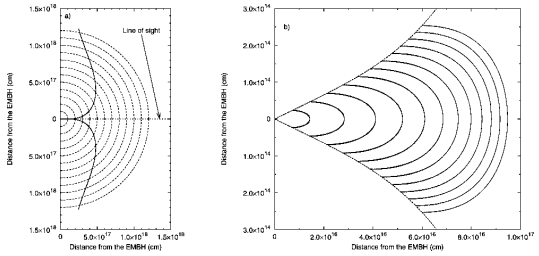

FIG. 1.—(*a*) Temporal evolution of the ABM pulse visible area. The dashed half-circles are the expanding ABM pulse at selected values of its radius corresponding to different laboratory times. The solid curve marks the boundary of the visible region. The EMBH is located at position (0, 0). The *X*- (*Y*-)axis is directed along (orthogonal to) the line of sight. In the earliest GRB phases, the visible region is squeezed on the line of sight, while in the latest afterglow phases almost all the emitted photons reach the observer. (*b*) In the same coordinate system used in (*a*), we represent the EQTSs (*solid lines*; see text). They correspond to values of the arrival time ranging from 5 s (the smallest surface on the left of the plot) to 60 s (the largest one on the right) in steps of 5 s. The dashed lines are the boundaries of the ABM pulse visible area. Note the different scale on the two axes, indicating the very high EQTS "effective eccentricity." The arrival time interval has been chosen to encompass the E-APE emission, occurring between ~15 and ~40 s (see Figs. 4 and 5 and Table 1).

strained by

$$\cos\vartheta \geq \frac{v}{c}, \tag{1}$$

where ϑ is the angle in the laboratory frame between the radial direction of each point on the ABM pulse surface and the line of sight and v is the expansion speed (Ruffini et al. 2002b). This follows from the requirement that in the comoving frame the component of the photon momentum along the radial expansion velocity direction be positive, in order to escape. There exists then a maximum allowed ϑ-value $\vartheta_{\rm max}$ defined by $\cos\vartheta_{\rm max} = v/c$ (see Fig. 1*a*).

Owing to the high value of the Lorentz γ factor (~310) for the bulk motion of the ABM pulse, the spherical waves emitted from its external surface do appear extremely distorted to a distant observer. To show this, we need to express the photon arrival time at the detector t_a^d as a function of its emission time t and angle ϑ. We set $t = 0$ when the plasma starts to expand, so that $r(0) = r_{\rm ds}$. We then have (see Ruffini et al. 2002b)

$$t_a^d = (1+z)\left[t - \frac{\int_0^t v(t')dt' + r_{\rm ds}}{c}\cos\vartheta + \frac{r_{\rm ds}}{c}\right], \tag{2}$$

where z is the redshift of the source. Then, in order to compute the arrival time of the emitted radiation, we must know *all* the previous values of the source velocity starting from $t = 0$. The great advantage of the EMBH model is that for the first time we have been able to obtain the precise values of the gamma Lorentz factor as a function of the radial coordinate or equivalently of the laboratory time (see Fig. 2). This allows us, for the first time, to evaluate equation (2) and correspondingly determine the surfaces that emit the photons detected at a fixed arrival time t_a^d, which we will call in the following "equitemporal surfaces" (EQTSs). The profiles of such surfaces are reported in Figure 1*b*. We emphasize once again the direct connection between the evaluation of the EQTSs and the *entire* past history of the source.

We have created an ISM inhomogeneity "mask" (see Fig. 3 and Table 1) with the main criteria that the density inhomogeneities and their spatial distribution still fulfill $\langle n_{\rm ism}\rangle = 1$ particle cm^{-3}.

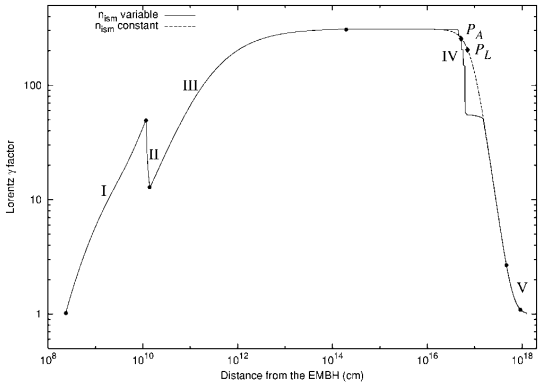

FIG. 2.—Theoretically computed gamma factors of the expanding pulse given as a function of its distance from the EMBH. The dashed line corresponds to $n_{\rm ism} = 1$ particle cm^{-3}, while the solid line corresponds to the density profile given in Fig. 3. The roman numerals correspond to the different eras of the EMBH theory (see Ruffini et al. 2002a). Near the E-APE (namely, around P_A and P_L), the two curves differ markedly owing to the impact on the high-density ISM regions, which brake the ABM pulse more efficiently. When the ABM pulse overcomes the ISM cloud, the two curves coincide again, since the average density of the cloud is ~1 particle cm^{-3}.

The source luminosity in a detector arrival time t_a^d and per unit solid angle $d\Omega$ is given by (details in Ruffini et al. 2002b)

$$\frac{dE_\gamma}{dt_a^d\, d\Omega} = \int_{\rm EQTS} \frac{\Delta\epsilon}{4\pi} v\cos\vartheta\Lambda^{-4}\frac{dt}{dt_a^d}\, d\Sigma, \tag{3}$$

where $\Delta\epsilon$ is the energy density released in the interaction of the ABM pulse with the ISM inhomogeneities measured in the comoving frame, $\Lambda = \gamma[1 - (v/c)\cos\vartheta]$ is the Doppler factor, and $d\Sigma$ is the surface element of the EQTS at detector arrival time t_a^d on which the integration is performed. In the present case, the Doppler factor Λ^{-4} in equation (3) enhances the apparent luminosity of the burst, as compared to the intrinsic

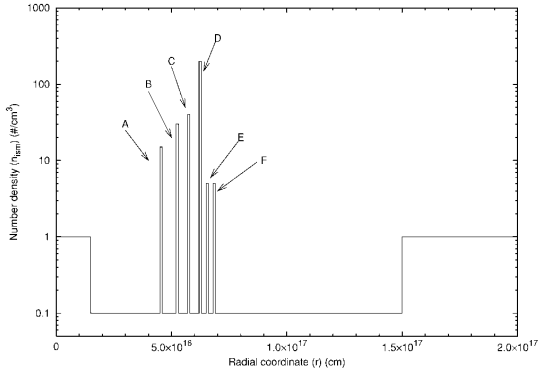

FIG. 3.—Density profile (mask) of an ISM cloud used to reproduce the GRB 991216 temporal structure. As before, the radial coordinate is measured from the black hole. In this cloud, we have six "spikes" with overdensity separated by low-density regions. Each spike has the same spatial extension of 10^{15} cm. The cloud average density is $\langle n_{\rm ism}\rangle = 1$ particle cm^{-3}.

TABLE 1
ISM Density Mask Parameters

Peak	r ($\times 10^{16}$ cm)	τ (s)	t ($\times 10^{6}$ s)	t_a^d (s)	d_v (cm)	Δt_a^d (s)	γ	Superluminal $v \equiv r/t_a^d$ ($\times 10^4 c$)
A	4.50	4.88×10^3	1.50	15.8	2.95×10^{14}	0.400	303.8	9.5
B	5.20	5.74×10^3	1.73	19.0	3.89×10^{14}	0.622	265.4	9.1
C	5.70	6.54×10^3	1.90	22.9	5.83×10^{14}	1.13	200.5	8.3
D	6.20	7.64×10^3	2.07	30.1	9.03×10^{14}	5.16	139.9	6.9
E	6.50	9.22×10^3	2.17	55.9	2.27×10^{15}	10.2	57.23	3.9
F	6.80	1.10×10^4	2.27	87.4	2.42×10^{15}	10.6	56.24	2.6

NOTE.—For each ISM density peak represented in Fig. 3, we give the initial radius r, the corresponding comoving time τ, laboratory time t, arrival time at the detector t_a^d, diameter of the ABM pulse visible area d_v, Lorentz factor γ, and observed duration Δt_a^d of the afterglow luminosity peaks generated by each density peak. In the last column, the apparent motion in the radial coordinate, evaluated in the arrival time at the detector, leads to an enormous superluminal behavior, up to $9.5 \times 10^4 c$.

luminosity, by a factor that at the E-APE is in the range between 10^{10} and 10^{12}!

The results are given in Figure 5. We obtain, in perfect agreement with the observations (see Fig. 4):

1. the theoretically computed intensity of the A, B, and C peaks as a function of the ISM inhomogneities;
2. the fast rise and exponential decay shape for each peak;
3. a continuous and smooth emission between the peaks.

Interestingly, the signals from shells E and F, which have a density inhomogeneity comparable to A, are undetectable. The reason is due to a variety of relativistic effects and partly to the spreading in the arrival time, which for A, corresponding to $\gamma = 303.8$, is 0.4 s, while for E (F), corresponding to $\gamma = 57.23$ (56.24), is 10.2 s (10.6 s) (see Table 1 and Ruffini et al. 2002b).

In the case of D, the agreement with the arrival time is reached, but we do not obtain the double-peaked structure. The ABM pulse visible area diameter at the moment of interaction with the D shell is $\sim 1.0 \times 10^{15}$ cm, equal to the extension of the ISM shell (see Table 1 and Ruffini et al. 2002b). Under these conditions, the concentric shell approximation does not hold anymore: the disagreement with the observations simply makes manifest the need for a more detailed description of the three-dimensional nature of the ISM cloud.

The physical reasons for these results can be simply summarized: we can distinguish two different regimes corresponding in the afterglow of GRB 991216, respectively, to $\gamma > 150$ and to $\gamma < 150$. For different sources, this value may be slightly different. In the E-APE region ($\gamma > 150$), the GRB substructure intensities indeed correlate with the ISM inhomogeneities. In this limited region (see peaks A, B, and C), the Lorentz gamma factor of the ABM pulse ranges from $\gamma \sim 304$ to $\gamma \sim 200$. The boundary of the visible region is smaller than the thickness ΔR of the inhomogeneities (see Fig. 1 and Table 1). Under this condition, the adopted spherical approximation is not only mathematically simpler but also fully jus-

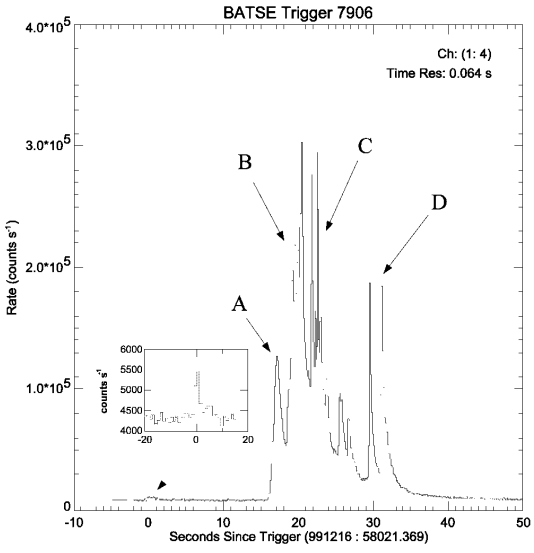

FIG. 4.—BATSE data on the E-APE of GRB 991216 (source: BATSE GRB light curves; see http://gammaray.msfc.nasa.gov/batse/grb/lightcurve) together with an enlargement of the P-GRB data (source: BATSE rapid burst response; see http://gammaray.msfc.nasa.gov/~kippen/batserbr). For convenience, each E-APE peak has been labeled by a different uppercase Latin letter.

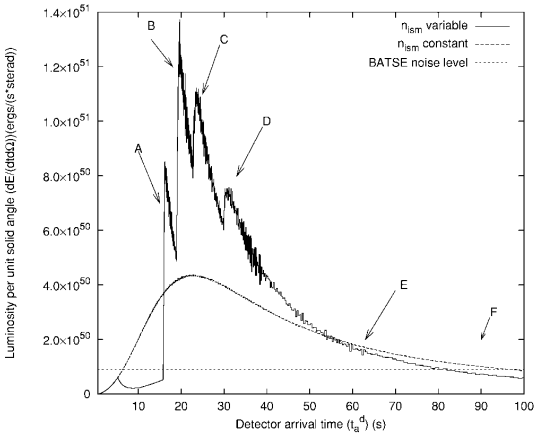

FIG. 5.—Source luminosity connected to the mask in Fig. 3 given as a function of the detector arrival time (*solid "spiky" line*), with the corresponding curve for the case of constant $n_{\rm ism} = 1$ particle cm^{-3} (*smooth dashed line*) and the BATSE noise level (*horizontal dotted line*). The "noise" observed in the theoretical curves is due to the discretization process adopted, described in Ruffini et al. (2002b), for the description of the angular spreading of the scattered radiation. For each fixed value of the laboratory time, we have summed 500 different contributions from different angles. The integration of the equation of motion of this system is performed in 22,314,500 contributions to be considered. An increase in the number of steps and in the precision of the numerical computation would lead to a smoother curve.

tified. The angular spreading is not strong enough to wipe out the signal from the inhomogeneity spike.

As we descend in the afterglow ($\gamma < 150$), the Lorentz gamma factor decreases markedly. In the borderline case of peak D, we have $\gamma \sim 140$. For peaks E and F, we have $\gamma \sim 50$, and, under these circumstances, the boundary of the visible region becomes much larger than the thickness ΔR of the inhomogeneities (see Fig. 1 and Table 1). A three-dimensional description would be necessary, breaking the spherical symmetry and making the computation more difficult. However, we do not need to perform this more complex analysis for peaks E and F: any three-dimensional description would a fortiori augment the smoothing of the observed flux. The spherically symmetric description of the inhomogeneities is already enough to prove the overwhelming effect of the angular spreading (Ruffini et al. 2002b).

On this general issue of the possible explanation of the observed substructures with the ISM inhomogeneities, there exists in the literature two extreme points of view: the one by Fenimore and collaborators (see, e.g., Fenimore, Madras, & Nayakshin 1996; Fenimore et al. 1999; Fenimore 1999) and Piran and collaborators (see, e.g., Sari & Piran 1997; Piran 1999, 2000, 2001) on one side and the one by Dermer and collaborators (Dermer 1998; Dermer, Böttcher, & Chiang 1999; Dermer & Mitman 1999) on the other.

Fenimore and collaborators have emphasized the relevance of a specific signature to be expected in the collision of a relativistic expanding shell with the ISM, what they call a fast rise and exponential decay shape. This feature is confirmed by our analysis (see peaks A, B, and C in Fig. 5). However, they also conclude, sharing the opinion by Piran and collaborators, that the variability observed in GRBs is inconsistent with causally connected variations in a single, symmetric, relativistic shell interacting with the ambient material ("external shocks"; Fenimore et al. 1999). In their opinion, the solution of the short time variability has to be envisioned within the protracted activity of an unspecified "inner engine" (Sari & Piran 1997; see as well Rees & Mészáros 1994; Panaitescu & Mészáros 1998; Mészáros & Rees 2000, 2001; Mészáros 2002).

On the other hand, Dermer and collaborators, by considering an idealized process occurring at a fixed $\gamma = 300$, have reached the opposite conclusions, and they purport that GRB light curves are tomographic images of the density distributions of the medium surrounding the sources of GRBs (Dermer & Mitman 1999).

From our analysis, we can conclude that Dermer's conclusions are correct for $\gamma \sim 300$ and do indeed hold for $\gamma > 150$. However, as the gamma factor drops from $\gamma \sim 150$ to $\gamma \sim 1$ (see Fig. 2), the intensity due to the inhomogeneities markedly decreases also due to the angular spreading (events E and F). The initial Lorentz factor of the ABM pulse $\gamma \sim 310$ decreases very rapidly to $\gamma \sim 150$ as soon as a fraction of a typical ISM cloud is engulfed (see Fig. 2 and Table 1). We conclude that the "tomography" is indeed effective but uniquely in the first ISM region close to the source and for GRBs with $\gamma > 150$.

One of the most striking features in our analysis is clearly represented by the fact that the inhomogeneities of a mask of radial dimension of the order of 10^{17} cm give rise to arrival time signals of the order of 20 s. This outstanding result implies an apparent "superluminal velocity" of $\sim 10^5 c$ (see Table 1). The superluminal velocity here considered, first introduced in Ruffini et al. (2001a), refers to the motion along the line of sight. This effect is proportional to γ^2. It is much larger than the one usually considered in the literature, within the context of radio sources and microquasars (see, e.g., Mirabel & Rodriguez 1994), referring to the component of the velocity at right angles to the line of sight (see details in Ruffini et al. 2002b). This second effect is in fact proportional to γ (see Rees 1966). We recall that this superluminal velocity was the starting point for the enunciation of the relative spacetime transformation paradigm (Ruffini et al. 2001a), emphasizing the need of the knowledge of the *entire* past worldlines of the source. This need has been further clarified here in the determination of the EQTSs (see Fig. 1*b*), which indeed depend on an integral of the Lorentz gamma factor extended over the *entire* past worldlines of the source. In turn, therefore, the agreement between the observed structures and the theoretical predicted ones (see Figs. 4 and 5) is also an extremely stringent additional test on the values of the Lorentz gamma factor determined as a function of the radial coordinate within the EMBH theory (see Fig. 2).

We thank R. Giacconi for suggestions on the wording of the manuscript, an anonymous referee for excellent advice, and M. Rees for convincing us of the necessity of presenting our results.

REFERENCES

Bianco, C. L., Ruffini, R., & Xue, S.-S. 2001, A&A, 368, 377
Cherubini, C., Ruffini, R., & Vitagliano, L. 2002, Phys. Lett. B, 545, 226
Christodoulou, D., & Ruffini, R. 1971, Phys. Rev. D, 4, 3552
Costa, E., Frontera, F., & Hjorth, J., eds. 2001, Gamma-Ray Bursts in the Afterglow Era (Berlin: Springer)
Damour, T., & Ruffini, R. 1975, Phys. Rev. Lett., 35, 463
Dermer, C. D. 1998, ApJ, 501, L157
Dermer, C. D., Böttcher, M., & Chiang, J. 1999, ApJ, 515, L49
Dermer, C. D., & Mitman, K. E. 1999, ApJ, 513, L5
Fenimore, E. E. 1999, ApJ, 518, 375
Fenimore, E. E., Cooper, C., Ramirez-Ruiz, E., Sumner, M. C., Yoshida, A., & Namiki, M. 1999, ApJ, 512, 683
Fenimore, E. E., Madras, C. D., & Nayakshin, S. 1996, ApJ, 473, 998
Fishman, G., & Meegan, C. 1995, ARA&A, 33, 415
Halpern, J. P., et al. 2000, ApJ, 543, 697
Kobayashi, S., Piran, T., & Sari, R. 1997, ApJ, 490, 92
Kumar, P., & Piran, T. 2000, ApJ, 532, 286
Mészáros, P. 2002, ARA&A, 40, 137
Mészáros, P., & Rees, M. J. 1997, ApJ, 482, L29
———. 2000, ApJ, 530, 292
———. 2001, ApJ, 556, L37
Mirabel, I. F., & Rodriguez, L. F. 1994, Nature, 371, 46
Panaitescu, A., & Mészáros, P. 1998, ApJ, 492, 683
Piran, T. 1999, Phys. Rep., 314, 575
———. 2000, Phys. Rep., 333, 529
———. 2001, preprint (astro-ph/0104134)
Preparata, G., Ruffini, R., & Xue, S.-S. 1998, A&A, 338, L87
Rees, M. J. 1966, Nature, 211, 468
Rees, M. J., & Mészáros, P. 1994, ApJ, 430, L93
———. 1998, ApJ, 496, L1
———. 2000, ApJ, 545, L73
Ruffini, R. 1998, in Black Holes and High Energy Astrophysics, ed. H. Sato & N. Sugiyama (Tokyo: Universal Academy), 167
Ruffini, R., Bianco, C. L., Chardonnet, P., Fraschetti, F., & Xue, S.-S. 2001a, ApJ, 555, L107
———. 2001b, ApJ, 555, L113
———. 2001c, ApJ, 555, L117
———. 2002a, A&A, submitted
———. 2002b, A&A, submitted
Ruffini, R., Salmonson, J. D., Wilson, J. R., & Xue, S.-S. 1999a, A&A, 350, 334
———. 1999b, A&AS, 138, 511
———. 2000, A&A, 359, 855
Ruffini, R., & Vitagliano, L. 2002, Phys. Lett. B, 545, 233
Sari, R., & Piran, T. 1997, ApJ, 485, 270

14 Appendix 7

New perspectives in physics and astrophysics from the theoretical understanding of Gamma-Ray Bursts

Remo Ruffini,[1,2,*] Carlo Luciano Bianco,[1,2,†] Pascal Chardonnet,[1,3,‡]
Federico Fraschetti,[1,4,§] Luca Vitagliano,[1,2,¶] and She-Sheng Xue[1,2,**]

[1] *ICRA — International Center for Relativistic Astrophysics.*
[2] *Dipartimento di Fisica, Università di Roma "La Sapienza", Piazzale Aldo Moro 5, I-00185 Roma, Italy.*
[3] *Université de Savoie, LAPTH - LAPP, BP 110, F74941 Annecy-le-Vieux Cedex, France.*
[4] *Università di Trento, Via Sommarive 14, I-38050 Povo (Trento), Italy.*

If due attention is given in formulating the basic equations for the Gamma-Ray Burst (GRB) phenomenon and in performing the corresponding quantitative analysis, GRBs open a main avenue of inquiring on totally new physical and astrophysical regimes. This program is very likely one of the greatest computational efforts in physics and astrophysics and cannot be actuated using shortcuts. A systematic approach is needed which has been highlighted in three basic new paradigms: the relative space-time transformation (RSTT) paradigm (Ruffini et al. [144]), the interpretation of the burst structure (IBS) paradigm (Ruffini et al. [145]), the GRB-supernova time sequence (GSTS) paradigm (Ruffini et al. [146]). From the point of view of fundamental physics new regimes are explored: (1) the process of energy extraction from black holes; (2) the quantum and general relativistic effects of matter-antimatter creation near the black hole horizon; (3) the physics of ultrarelativisitc shock waves with Lorentz gamma factor $\gamma > 100$. From the point of view of astronomy and astrophysics also new regimes are explored: (i) the occurrence of gravitational collapse to a black hole from a critical mass core of mass $M \gtrsim 10 M_\odot$, which clearly differs from the values of the critical mass encountered in the study of stars "catalyzed at the endpoint of thermonuclear evolution" (white dwarfs and neutron stars); (ii) the extremely high efficiency of the spherical collapse to a black hole, where almost 99.99% of the core mass collapses leaving negligible remnant; (iii) the necessity of developing a fine tuning in the final phases of thermonuclear evolution of the stars, both for the star collapsing to the black hole and the surrounding ones, in order to explain the possible occurrence of the "induced gravitational collapse". New regimes are as well encountered from the point of view of nature of GRBs: (I) the basic structure of GRBs is uniquely composed by a proper-GRB (P-GRB) and the afterglow; (II) the long bursts are then simply explained as the peak of the afterglow (the E-APE) and their observed time variability is explained in terms of inhomogeneities in the interstellar medium (ISM); (III) the short bursts are identified with the P-GRBs and the crucial information on general relativistic and vacuum polarization effects are encoded in their spectra and intensity time variability. A new class of space missions to acquire information on such extreme new regimes are urgently needed.

Keywords: black holes physics – gamma rays: bursts – gamma rays: theory – gamma rays: observations

Contents

*Electronic address: ruffini@icra.it
†Electronic address: bianco@icra.it
‡Electronic address: chardonnet@icra.it
§Electronic address: fraschetti@icra.it
¶Electronic address: vitagliano@icra.it
**Electronic address: xue@icra.it

I. INTRODUCTION

In understanding new astrophysical phenomena, the solution has been found as soon as the energy source of the phenomena has been identified. This has been the case for pulsars (see Hewish et al. [79]) where the rotational energy of the neutron star was identified as the energy source (see e.g. Gold [68, 69]). Similarly, in binary X-ray sources the accretion process from a normal companion star in the deep potential well of a neutron star or a black hole has clearly pointed to the gravitational energy of the accreting matter as the basic energy source and all the main features of the light curves of the sources have been clearly understood (Giacconi & Ruffini [66]). In this spirit, our work in the field of Gamma-Ray Bursts (GRBs) has focused to identify the energy extraction process from the black hole (Christodoulou & Ruffini [30]) as the basic energy sources for the GRB phenomenon: a distinguishing feature of this process is a theoretically predicted energetics of the source all the way up to $1.8 \times 10^{54}\,(M_{BH}/M_\odot)$ ergs for $3.2M_\odot \leq M_{BH} \leq 7.2 \times 10^6 M_\odot$ (Damour & Ruffini [33]). In particular, the very specific process of the formation of a "dyadosphere", during the process of gravitational collapse leading to a black hole endowed with electromagnetic structure (EMBH), has been indicated as originating and giving the initial boundary conditions of the onset of the GRB process (Preparata et al. [124], Ruffini [137]). Our model has been referred as "the EMBH model for GRBs", although the EMBH physics only determines the initial boundary conditions of the GRB process by specifying the physical parameters and spatial extension of the neutral electron positron plasma originating the phenomenon.

Traditionally, following the observations of the *Vela* (Strong [175]) and *CGRO*[1] satellites, GRBs have been characterized by few parameters such as the fluence, the characteristic duration (T_{90} or T_{50}) and the global time averaged spectral distribution (Band et al. [7]). With the observations of *BeppoSAX*[2] and the discovery of the afterglow, and the consequent optical identification, the distance of the GRB source has been determined and consequently the total energetics of the source has been added as a crucial parameter.

The observed energetics of GRBs, coinciding for spherically symmetric explosions with the ones theoretically predicted in (Damour & Ruffini [33]), has convinced us to develop in full details the EMBH model. For simplicity, we have considered the vacuum polarization process occurring in an already formed Riessner-Nordström black hole (Preparata et al. [124], Ruffini [137]), whose dyadosphere has an energy E_{dya}. It is clear, however, that this is only an approximation to the real dynamical description of the process of gravitational collapse to an EMBH. In order to prepare the background for attacking this extremely complex dynamical process, we have clarified some basic theoretical issues, necessary to be implemented prior to the description of the fully dynamical process of gravitational collapse to an EMBH (Cherubini et al. [28], Ruffini & Vitagliano [156, 157], see section XXVII). We have then described the following five eras in our model. *Era I*: the e^+e^- pairs plasma, initially at $\gamma = 1$, expands away from the dyadosphere as a sharp pulse (the PEM pulse), reaching Lorentz gamma factor of the order of 100 (Ruffini et al. [142]). *Era II*: the PEM pulse, still optically thick, engulfs the remnant left over in the process of gravitational collapse of the progenitor star with a drastic reduction of the gamma factor; the mass M_B of this engulfed baryonic material is expressed by the dimensionless parameter $B = M_B c^2/E_{dya}$ (Ruffini et al. [143]). *Era III*: the newly formed pair-electromagnetic-baryonic (PEMB) pulse, composed of e^+e^- pair and of the electrons and baryons of the engulfed

[1] see http://cossc.gsfc.nasa.gov/batse/
[2] see http://www.asdc.asi.it/bepposax/

material, self-propels itself outward reaching in some sources Lorentz gamma factors of 10^3–10^4; this era stops when the transparency condition is reached and the emission of the proper-GRB (P-GRB) occurs (Bianco et al. [13]). *Era IV*: the resulting accelerated baryonic matter (ABM) pulse, ballistically expanding after the transparency condition has been reached, collides at ultrarelativistic velocities with the baryons and electrons of the interstellar matter (ISM) which is assumed to have a average constant number density, giving origin to the afterglow. *Era V*: this era represents the transition from the ultrarelativistic regime to the relativistic and then to the non relativistic ones (Ruffini et al. [149]).

Our approach differs in many respect from the ones in the current literature. The major difference consists in the appropriate theoretical description of all the above five eras, as well as in the evaluation of the process of vacuum polarization originating the dyadosphere. The dynamical equations as well as the description of the phenomenon in the laboratory time and the time sequence carried by light signals recorded at the detector have been explicitly integrated (see e.g. Tab. I and Ruffini et al. [149, 153]). In doing so we have also corrected a basic conceptual mistake, common to all the current works on GRBs, which led to the wrong spacetime parametrization of the GRB phenomenon, preempting all these theoretical works from their predictive power. The description of the inner engine originating the GRBs has never been addressed in the necessary details in the literature. In this sense neither the specific boundary conditions originating in the dyadosphere nor the needed solutions of the relativistic hydrodynamic and pair equations for the first three eras described above have been considered. Only the treatment of the afterglow has been widely considered in the literature by the so-called "fireball model" (see e.g. Mészáros & Rees [92, 94], Piran [116], Rees & Mészáros [128] and references therein).

However, also in the description of the afterglow, which is represented by the two conceptually and technically simplest eras in our model, there are major differences between the works in the literature and our approach:
a) Processes of synchrotron radiation and inverse Compton as well as an adiabatic expansion in the source generating the afterglow are usually adopted in the current literature. On the contrary, in our approach a "fully radiative" condition is systematically adopted in the description of the X-ray and γ-ray emission of the afterglow. The basic microphysical emission process is traced back to the physics of shock waves as considered by Zel'dovich & Rayzer [193]. A special attention is given to identify such processes in the comoving frame of the shock front generating the observed spectra of the afterglow (see Ruffini et al. [150]).
b) In the literature the variation of the gamma Lorentz factor during the afterglow is expressed by a unique power-law of the radial co-ordinate of the source and a similar power-law relation is assumed also between the radial coordinate of the source and the asymptotic observer frame time. Such simple approximations appear to be quite inadequate and do contrast with the almost hundred pages summarizing the needed computations which we recall in the rest of this article. In our approach the dynamical equations of the source are integrated self-consistently with the constitutive equations relating the observer frame time to the laboratory time and the boundary conditions are adopted and uniquely determined by each previous era of the GRB source (see e.g. Ruffini et al. [148, 149, 150, 153]).
c) At variance with the many power-laws for the observed afterglow flux found in the literature, our treatment naturally leads to a "golden value" for the power-law index $n = -1.6$. The fit of the EMBH model to the observed afterglow data fixes the only two free parameters of our theory: the E_{dya} and the B parameter, measuring the remnant mass left over by the gravitational collapse of the progenitor star (Ruffini et al. [148, 149, 150, 153]).

It is not surprising that such large differences in the theoretical treatment have led to a different interpretation of the GRB phenomenon as well as to the identification of new fundamental physical regimes. The introduction of new interpretative paradigms has been necessary and the theory has been confirmed by the observation to extremely high accuracy.

In particular from the definition of the complete space-time coordinates of the GRB phenomenon as a function of the radial coordinate, the comoving time, the laboratory time, the arrival time and the arrival time at the detector, expressed in Tab. I, it has been concluded that in no way a description of a given era is possible in the GRB phenomena without the knowledge of the previous ones. Therefore the afterglow as such cannot be interpreted unless all the previous eras have been correctly computed and estimated. It has also become clear that a great accuracy in the analysis of each era is necessary in order to identify the theoretically predicted features with the observed ones. If this is done, the GRB phenomena presents an extraordinary and extremely precise correspondence between the theoretically predicted features and the observations leading to the exploration of totally new physical and astrophysical process with unprecedented accuracy. This has been expressed in the relative space-time transformation (RSTT) paradigm: "the necessary condition in order to interpret the GRB data, given in terms of the arrival time at the detector, is the knowledge of the *entire* worldline of the source from the gravitational collapse. In order to meet this condition, given a proper theoretical description and the correct constitutive equations, it is sufficient to know the energy of the dyadosphere and the mass of the remnant of the progenitor star" (Ruffini et al. [144]).

Having determined the two independent parameters of the EMBH model, namely E_{dya} and B, by the fit of the afterglow we have introduced a new interpretative paradigm for the burst structure: the IBS paradigm (Ruffini et al. [145]). In it we reconsider the relative roles of the afterglow and the burst in the GRBs by defining in this complex

phenomenon two new phases:
1) the *injector phase* starting with the process of gravitational collapse, encompassing the above Eras I, II, III and ending with the emission of the Proper-GRB (P-GRB);
2) the *beam-target phase* encompassing the above Eras IV and V giving rise to the afterglow. In particular in the afterglow three different regimes are present for the average bolometric intensity : one increasing with arrival time, a second one with an Extended Afterglow Peak Emission (E-APE) and finally one decreasing as a function of the arrival time. Only this last one appears to have been considered in the current literature (Ruffini et al. [145]).

The EMBH model allows, in the case of GRB 991216, to compute the intensity ratio of the afterglow to the P-GRB ($1.45 \cdot 10^{-2}$), and the arrival time of the P-GRB ($8.413 \cdot 10^{-2}$s) as well as the arrival time of the peak of the afterglow (19.87s) (see Figs. 12,6,11). The fact that the theoretically predicted intensities coincide within a few percent with the observed ones and that the arrival time of the P-GRB and the peak of the afterglow also do coincide within a tenth of millisecond with the observed one can be certainly considered a clear success of the predictive power of the EMBH model.

As a by-product of this successful analysis, we have reached the following conclusions:
a) The most general GRB is composed by a P-GRB, an E-APE and the rest of the afterglow. The ratio between the P-GRB and the E-APE intensities is a function of the B parameter.
b) In the limit B=0 all the energy is emitted in the P-GRB. These events represent the "short burst" class, for which no afterglows has been observed.
c) The "long bursts" do not exist, they are just part of the afterglow, the E-APEs.

We are currently verifying these theoretical predictions on the following GRBs: GRB 991216, GRB 980425, GRB 970228, GRB 980519. It is very remarkable that, although the energetics of GRB 980425 (see Fig. 12) differs from the one of GRB 991216 by roughly five orders of magnitude, the model applies also to this case with success. Furthermore from these analysis we can claim that both in the case of GRB 991216 and in the case of GRB 980425 there is not significant departure from spherical symmetry.

While this analysis of the average bolometric intensity of GRB was going on in the radial approximation, we have proceeded to the full non-radial approximation, taking into account all the relativistic corrections for the off-axis emission from the spherically symmetric expansion of the ABM pulse (Ruffini et al. [148, 153]). We have so defined the temporal evolution of the ABM pulse visible area (see Fig. 13), as well as the equitemporal surfaces (see Fig. 13) (Ruffini et al. [148, 153]).

We have then addressed the issue whether the fast temporal variations observed in the so-called long bursts, on time scales as short as fraction of a second (Ruffini et al. [148]), can indeed be explained as an effect of inhomogeneities in the interstellar medium.

We are making further progress in identifying the basic mechanisms of energy release in the afterglow by presenting a new theoretical formalism which as a function of only one parameter fits the entire spectral distribution of the X-ray and γ-ray radiation in GRB 991216 (Ruffini et al. [150]).

Finally the GRB-supernova time sequence (GSTS) paradigm introduces the concept of *induced supernova explosion* in the supernovae-GRB association (Ruffini et al. [146]) leading to the very novel possibility of a process of gravitational collapse induced on a companion star in a very special evolution phase by the GRB explosion.

Before concluding, we also present some theoretical developments which have been motivated by preparing the analysis of the general relativistic effects during the process of gravitational collapse itself and we also show how such results motivated by GRB studies have already generated new results in the fundamental understanding of black hole physics.

In the next section we briefly summarize the main results and we will then give the summary of the treatment in the following sections. For the complete details we refer to the quoted papers.

II. SUMMARY OF THE MAIN RESULTS

A. The physical and astrophysical background

Gamma-ray bursts (GRBs) are rapidly fueling one of the broadest scientific pursuit in the entire field of science, both in the observational and theoretical domains. Following the discovery of GRBs by the Vela satellites (Strong [175]), the observations from the Compton satellite and BATSE had shown the isotropic distribution of the GRBs strongly suggesting a cosmological nature for their origin. It was still through the data of BATSE that the existence of two families of bursts, the "short bursts" and the "long bursts" was presented, opening an intense scientific dialogue on their origin still active today, see e.g. Schmidt [170] and section XII.

An enormous momentum was gained in this field by the discovery of the afterglow phenomena by the BeppoSAX satellite and the optical identification of GRBs which have allowed the unequivocal identification of their sources at

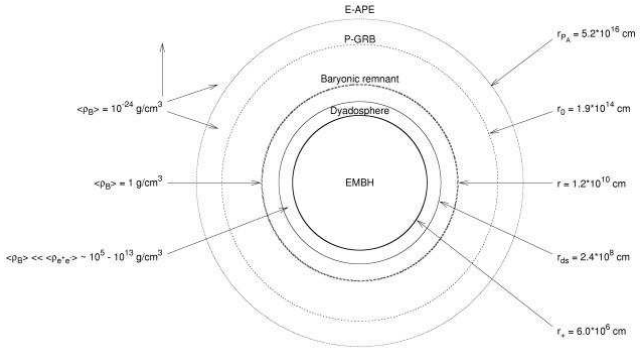

Figure 1: Selected events in the EMBH theory are represented. For each one the values of the energy density of the medium and the distances from the EMBH, in the laboratory frame and in logarithmic scale, are given.

cosmological distances (see e.g. Costa [32]). It has become apparent that fluxes of 10^{54} erg/s are reached: during the peak emission the energy of a single GRB equals the energy emitted by all the stars of the Universe (see e.g. Ruffini [138]).

From an observational point of view, an unprecedented campaign of observations is at work using the largest deployment of observational techniques from space with the satellites CGRO-BATSE, Beppo-SAX, Chandra[3], R-XTE[4], XMM-Newton[5], HETE-2[6], as well as the HST[7], and from the ground with optical (KECK[8], VLT[9]) and radio (VLA[10]) observatories. The further possibility of examining correlations with the detection of ultra high energy cosmic rays, UHECR for short, and in coincidence neutrinos should be reachable in the near future thanks to developments of AUGER[11] and AMANDA[12] (see also Halzen [74]).

From a theoretical point of view, GRBs offer comparable opportunities to develop entire new domains in yet untested directions of fundamental science. For the first time within the theory based on the vacuum polarization process occurring in an electromagnetic black hole, the EMBH theory, see Fig. 1, the opportunity exists to theoretically approach the following fundamental issues:

1. The extremely relativistic hydrodynamic phenomena of an electron-positron plasma expanding with sharply varying gamma factors in the range 10^2 to 10^4 and the analysis of the very high energy collision of such an expanding plasma with baryonic matter reaching intensities 10^{38} larger than the ones usually obtained in Earth-based accelerators.

2. The bulk process of vacuum polarization created by overcritical electromagnetic fields, in the sense of Heisenberg, Euler (Heisenberg & Euler [78]) and Schwinger (Schwinger [172]). This longly sought quantum ultrarelativistic effect has not been yet unequivocally observed in heavy ion collision on the Earth (see e.g. Ganz et al. [62], Heinz et al. [77], Leinberger et al. [88, 89]). The difficulty of the heavy ion collision experiments appears to be that the overcritical field is reached only for time scales of the order $\hbar/m_pc^2$, which is much shorter than the characteristic time for the e^+e^- pair creation process which is of the order of $\hbar/m_ec^2$, where m_p and m_e are respectively the proton and the electron mass. It is therefore very possible that the first appearance of such an effect occurs in the present general relativistic context: in the strong electromagnetic fields developed in astrophysical conditions during the process of gravitational collapse to an EMBH, where no problem of confinement exists.

---

[3] see http://chandra.harvard.edu/
[4] see http://heasarc.gsfc.nasa.gov/docs/xte/
[5] see http://xmm.vilspa.esa.es/
[6] see http://space.mit.edu/HETE/
[7] see http://www.stsci.edu/
[8] see http://www2.keck.hawaii.edu:3636/
[9] see http://www.eso.org/projects/vlt/
[10] see http://www.aoc.nrao.edu/vla/html/VLAhome.shtml
[11] see http://www.auger.org/
[12] see http://amanda.berkeley.edu/amanda/amanda.html

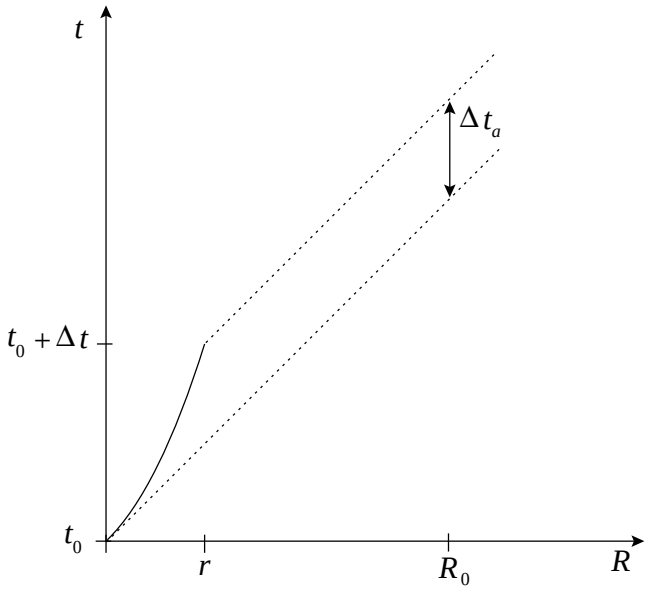

Figure 2: This qualitative diagram illustrates the relation between the laboratory time interval Δt and the arrival time interval Δt_a for a pulse moving with velocity v in the laboratory time (solid line). We have indicated here the case where the motion of the source has a nonzero acceleration. The arrival time is measured using light signals emitted by the pulse (dotted lines). R_0 is the distance of the observer from the EMBH, t_0 is the laboratory time corresponding to the onset of the gravitational collapse, and r is the radius of the expanding pulse at a time $t = t_0 + \Delta t$. See also Ruffini et al. [144].

3. A novel form of energy source: the extractable energy of a black hole. The enormous energies released almost instantly in the observed GRBs, points to the possibility that for the first time we are witnessing the release of the extractable energy of an EMBH, during the process of gravitational collapse itself. This problem presents still some outstanding theoretical issues in black hole physics. Having progressed in some of these issues (see Cherubini et al. [28], Ruffini & Vitagliano [156, 157], Ruffini et al. [159]) we can now compute and have the opportunity to study all general relativistic as well as the associated ultrahigh energy quantum phenomena as the horizon of the EMBH is approached and is being formed (see section XXVII).

It is clear that in approaching such a vast new field of research, implying previously unobserved relativistic and quantum regimes, it is not possible to proceed *as usual* with an uncritical comparison of observational data to theoretical models within the classical schemes of astronomy and astrophysics. Some insight to the new approach needed can be gained from past experience in the interpretation of relativistic effects in high energy particle physics as well as from the explanation of some observed relativistic effects in the astrophysical domain. Those relativistic regimes, both in physics and astrophysics, are however much less extreme than those encountered now in GRBs.

There are three major new features in relativistic systems which have to be properly taken into account:

1. Practically all data on astronomical and astrophysical systems is acquired by using photon arrival times. It was Einstein [47] at the very initial steps of special relativity who cautioned about the use of such an arrival time analysis and stated that when dealing with objects in motion proper care should be taken in defining the time synchronization procedure in order to construct the correct space-time coordinate grid (see Fig. 2). It is not surprising that as soon as the first relativistic bulk motion effects were observed their interpretations within the classical framework of astrophysics led to the concept of "superluminal" motion. These were observations of extragalactic radio sources, with gamma factors ~ 10 (Biretta et al. [16]) and of microquasars in our own galaxy with gamma factor ~ 5 (Mirabel & Rodriguez [102]). It has been recognized (Rees [127]) that no "superluminal" motion exists if the prescriptions indicated by Einstein are used in order to establish the correct space-time grid for the astrophysical systems. In the present context of GRBs, where the gamma factor can easily surpass 10^2 and is very highly varying, this approximation breaks down (Bianco et al. [13], Ruffini et al. [144, 153]). The direct application of classical concepts in this context would lead to enormous "superluminal" behaviors (see e.g.

Tab. I). An approach based on classical arrival time considerations as sometimes done in the current literature completely subverts the causal relation in the observed astrophysical phenomenon.

2. One of the clear successes of relativistic field theories has been the understanding of the role of four-momentum conservation laws in multiparticle collisions and decays such as in the reaction: $n \rightarrow p + e^- + \bar{\nu}_e$. From the works of Pauli and Fermi it became clear how in such a process, contrary to the case of classical mechanics, it is impossible to analyze a single term of the decay, the electron or the proton or the neutrino or the neutron, out of the context of the global point of view of the relativistic conservation of the total four momentum of the system. This in turn involves the knowledge of the system during the entire decay process. These rules are routinely used by workers in high energy particle physics and have become part of their cultural background. If we apply these same rules to the case of the relativistic system of a GRB it is clear that it is just impossible to consider a part of the system, e.g. the afterglow, without taking into account the general conservation laws and whole relativistic history of the entire system. Especially since in astrophysics the "somewhat pathological" arrival time coordinate is basically used (see Fig. 2). The description of the afterglow alone, as has been given at times in the literature, indeed possible within the framework of classical astronomy and astrophysics, is not viable in a relativistic astrophysics context where the space-time grid necessary for the description of the afterglow depends on the entire previous relativistic part of the worldline of the system (see also section XV).

3. The lifetime of a process has not an absolute meaning as special and general relativity have shown. It depends both on the inertial reference frame of the laboratory and of the observer and on their relative motion. Such a phenomenon, generally expressed in the "twin paradox", has been extensively checked and confirmed to extremely high accuracy as a byproduct of the elementary particle physics (g-2) experiment (see e.g. van Dick [178]). This situation is much more extreme in GRBs due to the very large (in the range 10^2–10^4) and time varying (on time scales ranging from fractions of seconds to months) gamma factors between the comoving frame and the far away observer (see Fig. 8). Moreover in the GRB context such an observer is also affected by the cosmological recession velocities of its local Lorentz frame.

B. The Relative Space-Time Transformations: the RSTT paradigm and current scientific literature

Here are some of the reasons why we have presented a basic relative space-time transformation (RSTT) paradigm (Ruffini et al. [144]) to be applied prior to the interpretation of GRB data.

The first step is the establishment of the governing equations relating:
a) The comoving time of the pulse (τ)
b) The laboratory time (t)
c) The arrival time at the detector (t_a)
d) The arrival time at the detector corrected for cosmological expansion (t_a^d)
The book-keeping of the four different times and corresponding space variables must be done carefully in order to keep the correct causal relation in the time sequence of the events involved.

As formulated the RSTT paradigm contains two parts: the first one is a necessary condition, the second one a sufficient condition. The first part reads: "the necessary condition in order to interpret the GRB data, given in terms of the arrival time at the detector, is the knowledge of the *entire* worldline of the source from the gravitational collapse".

Clearly such an approach is in contrast with articles in the current literature which emphasize either some too qualitative description of the sources and the quantitative description of the sole afterglow era. In this quantitative description they oversimplify the relations between the radial coordinate of the source and its gamma Lorentz factor as well as the relation between the radial coordinate and the arrival time using power-law relations which do not correctly take into account the complexity of the problem.

In the current literature several attempts have addressed the issue of the sources of GRBs. They include scenarios of binary neutron stars mergers (see e.g. Eichler et al. [46], Mészáros & Rees [92, 93], Narayan et al. [104]), black hole / white dwarf (Fryer et al. [57]) and black hole / neutron star binaries (Mészáros & Rees [96], Paczyński [108]), hypernovae (see Paczyński [110]), failed supernovae or collapsars (see MacFadyen & Woosley [90], Woosley [190]), supranovae (see Vietri & Stella [181, 182]). Only those based on binary neutron stars have reached the stage of a definite model and detailed quantitative estimates have been made. In this case, however, various problems have surfaced: in the general energetics which cannot be greater than $\sim 3 \times 10^{52}$ erg, in the explanation of "long bursts" (see Salmonson et al. [162], Wilson et al. [187]), and in the observed location of the GRB sources in star forming regions (see Bloom et al. [21]). In the remaining cases attention was directed to a qualitative analysis of the sources without addressing the overall problem from the source to the observations. Also generally missing are the necessary

details to formulate the equations of the dynamical evolution of the system and to develop a complete theory to be compared with the observations.

Other models in the literature have addressed the problem of only fitting the data of the afterglow observations by simple power-laws. They are separated into two major classes:

The "internal shock model", introduced by Rees & Mészáros [128], by far the most popular one, has been developed in many different aspects, e.g. by Fenimore [49], Fenimore et al. [50], Paczyński & Xu [109], Sari & Piran [165]. The underlying assumption is that all the variabilities of GRBs in the range $\Delta t \sim 1\,\mathrm{ms}$ up to the overall duration T of the order of 50 s are determined by a yet undetermined "inner engine". The difficulties of explaining the long time scale bursts by a single explosive model has evolved into a subclass of approaches assuming an "inner engine" with extended activity (see e.g. Piran [117] and references therein).

The "external shock model", see e.g. Cavallo & Rees [25], Mészáros & Rees [94], Shemi & Piran [173], is less popular today. Paradoxically, some of the authors who have qualitatively highlighted distinctive features of this model have later disclaimed its validity (see e.g. Mészáros & Rees [98], Piran [116], Rees & Mészáros [128] and references therein). Possibly they were carried to this extreme conclusion by an impressive sequence of mistakes they made in implementing the basic physical processes of the model. This model relates the GRB light curves and time variabilities to interactions of a single thin blast wave with clouds in the external medium. The interesting possibility has been also recognized within this model, that GRB light curves "are tomographic images of the density distribution of the medium surrounding the sources of GRBs" (Dermer & Mitman [42]), see also Dermer et al. [41], Dermer [43] and references therein. In this case, the structure of the burst is assumed not to depend directly on the "inner engine" (see e.g. Piran [117] and references therein).

All these works encounter the above mentioned difficulty: they present either a purely qualitative or phenomenological or a piecewise description of the GRB phenomenon. By neglecting the earlier phases, the relation of the space-time grid to the photon arrival time is not properly estimated. To tell more explicitly, their clocks are out of the proper synchronization and the theory is emptied of any predictive power!

We will explicitly show in the following how an unified description naturally leads to the identification of new characteristic features both in the burst and afterglow of GRBs. Our theory, in respect to the afterglow description, can be generally considered an "external shock model" and fits most satisfactorily all the observations.

C. The EMBH Theory

In a series of papers, we have developed the EMBH theory (Ruffini [137]) which has the advantage, despite its simplicity, that all eras following the process of gravitational collapse are described by precise field equations which can then be numerically integrated.

Starting from the vacuum polarization process *à la* Heisenberg-Euler-Schwinger (Heisenberg & Euler [78], Schwinger [172]) in the overcritical field of an EMBH first computed in Damour & Ruffini [33], we have developed the dyadosphere concept (Preparata et al. [124]).

The dynamics of the e^+e^--pairs and electromagnetic radiation of the plasma generated in the dyadosphere propagating away from the EMBH in a sharp pulse (PEM pulse) has been studied by the Rome group and validated by the numerical codes developed at Livermore Lab (Ruffini et al. [142]).

The collision of the still optically thick e^+e^--pairs and electromagnetic radiation plasma with the baryonic matter of the remnant of the progenitor star has been again studied by the Rome group and validated by the Livermore Lab codes (Ruffini et al. [143]). The further evolution of the sharp pulse of pairs, electromagnetic radiation and baryons (PEMB pulse) has been followed for increasing values of the gamma factor until the condition of transparency is reached (Bianco et al. [13]).

As this PEMB pulse reaches transparency the proper GRB (P-GRB) is emitted (Ruffini et al. [145]) and a pulse of accelerated baryonic matter (the ABM pulse) is injected into the interstellar medium (ISM) giving rise to the afterglow.

D. The GRB 991216 as a prototypical source

In the early phases of development of our model, the EMBH theory was developed from first principles by the EMBH uniqueness theorem (Ruffini & Wheeler [141]), the energetics of black hole (Christodoulou & Ruffini [30]) as well as the quantum description of the vacuum polarization process in overcritical electromagnetic fields (Damour & Ruffini [33]). Turning now to the afterglow, the variety of physical situations that can possibly be encountered are very large and far from unique: the description from first principles is just impossible. We have therefore proceeded

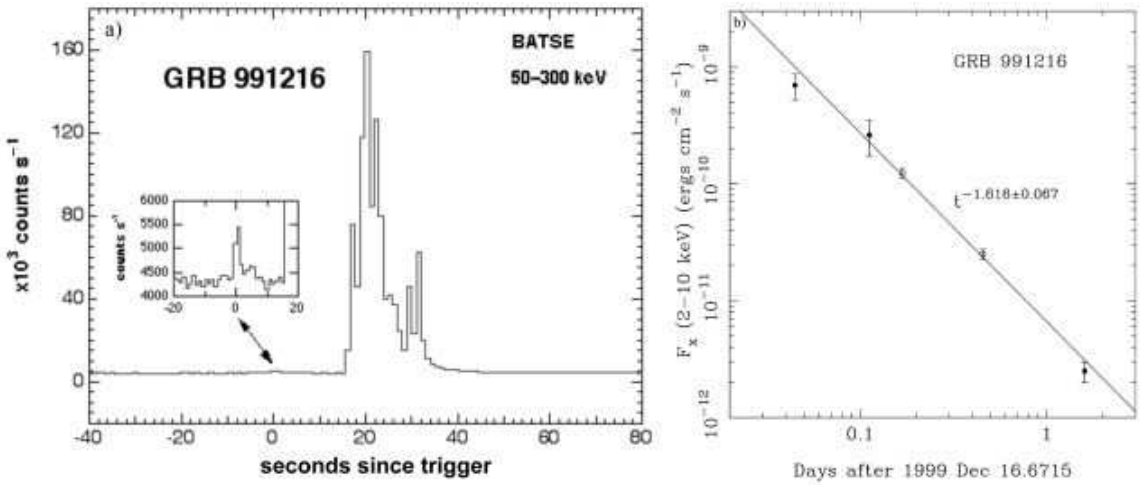

Figure 3: **a)** The peak emission of GRB 991216 as seen by BATSE (reproduced from BATSE Rapid Burst Response [6]); **b)** The afterglow emission of GRB 991216 as seen by XTE and Chandra (reproduced from Halpern et al. [73]).

to properly identify what we consider a prototypical GRB source and to develop a theoretical framework in close correspondence with the observational data.

The criteria which have guided us in the selection of the GRB source to be used as a prototype before proceeding to an uncritical comparison with the theory are expressed in the following. It is now clear, since the observations of GRB 980425, GRB 991216, GRB 970514 and GRB 980326 that the afterglow phenomena can present, especially in the optical and radio wavelengths, features originating from phenomena spatially and causally distinct from the GRB phenomena. There is also the distinct possibility that phenomena related to a supernova can be erroneously attributed to a GRB. This problem has been clearly addressed by the GRB supernova time sequence (GSTS) paradigm in which the time sequence of the events in the GRB supernova phenomena has been outlined (Ruffini et al. [146]). This has led to the novel concept of an induced supernova (Ruffini et al. [146]). This problem will be addressed in a forthcoming paper (Ruffini et al. [152]).

In view of these considerations we have selected GRB 991216 as a prototypical case (see Fig. 3) for the following reasons:

1. GRB 991216 is one of the strongest GRBs in X-rays and is also quite general in the sense that it shows relevant cosmological effects. It radiates mainly in X-rays and in γ-rays and less than 3% is emitted in the optical and radio bands (see Halpern et al. [73]).

2. The excellent data obtained by BATSE on the burst (BATSE Rapid Burst Response [6]) is complemented by the data on the afterglow acquired by Chandra (Piro et al., [120]) and RXTE (Corbet & Smith [31]). Also superb data have been obtained from spectroscopy of the iron lines (Piro et al., [120]).

3. A value for the slope of the energy emission during the afterglow as a function of time has been obtained: $n = -1.64$ (Takeshima et al. [176]) and $n = -1.616 \pm 0.067$ (Halpern et al. [73]).

E. The interpretation of the burst structure: the IBS paradigm and the different eras of the EMBH theory

The comparison of the EMBH theory with the data of the GRB 991216 and its afterglow has naturally led to a new paradigm for the interpretation of the burst structures (IBS paradigm)) of GRBs (Ruffini et al. [145]). The IBS paradigm reads: *"In GRBs we can distinguish an injector phase and a beam-target phase. The injector phase includes the process of gravitational collapse, the formation of the dyadosphere, as well as Era I (the PEM pulse), Era II (the engulfment of the baryonic matter of the remnant) and Era III (the PEMB pulse). The injector phase terminates with the P-GRB emission. The beam-target phase addresses the interaction of the ABM pulse, namely the beam generated during the injection phase, with the ISM as the target. It gives rise to the E-APE and the decaying part of the afterglow"*. The detailed presentations of these results are a major topic in this article.

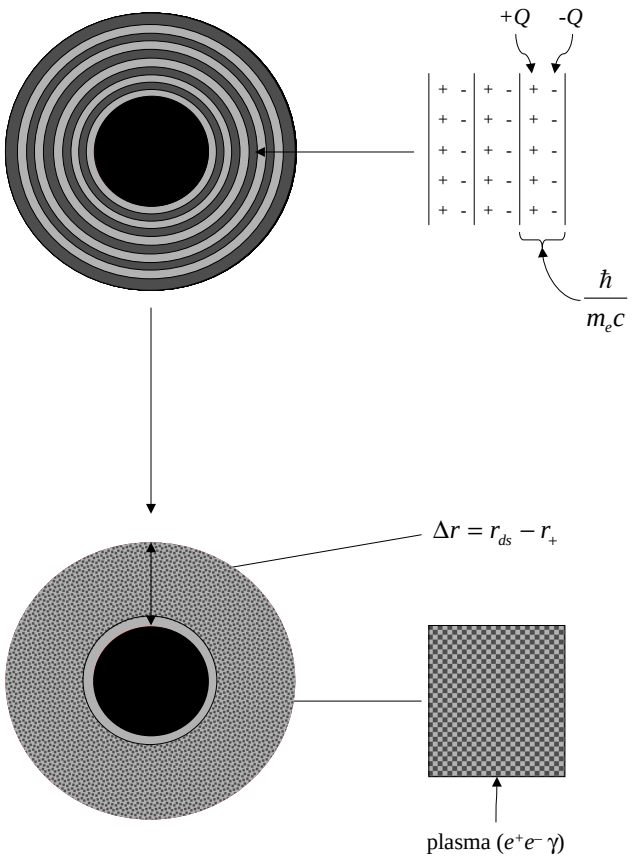

Figure 4: The dyadosphere of a Reissner-Nordström black hole can be represented as constituted by a concentric set of shells of capacitors, each one of thickness $\hbar/m_e c$ and producing a number of e^+e^- pairs of the order of $\sim Q/e$ on a time scale of 10^{-21} s, where Q is the EMBH charge. The shells extend in a region Δr, from the horizon r_+ to the dyadosphere outer radius $r_{\rm ds}$ (see text). The system evolves to a thermalised plasma configuration.

We recall that the **injector phase** starts from the moment of gravitational collapse and encompasses the following eras:

The zeroth Era: the formation of the dyadosphere. In section III we review the basic scientific results which lie at the basis of the EMBH theory: the black hole uniqueness theorem, the mass formula of an EMBH, the process of vacuum polarization in the field of an EMBH. We also point out how after the discovery of the GRB afterglow the reexamination of these results has led to the novel concept of the dyadosphere of an EMBH. We have investigated this concept in the simplest possible case of an EMBH depending only on two parameters: the mass and charge, corresponding to the Reissner-Nordström spacetime. We recall the definition of the energy E_{dya} of the dyadosphere as well as the spatial distribution and energetics of the e^+e^- pairs. See Fig. 4. We return in section XXVII to the theoretical development of the time varying process lasting less than a second in the process of a realistic gravitational collapse. In reality the vacuum polarization process will lead to a final uncharged black hole, but the analysis based on a Reissner-Nordström black hole is an excellent approximation to the description of this phenomenon (Ruffini et al. [160]).

In order to analyse the time evolution of the dyadosphere we give in the three following sections the theoretical background for the needed equations.

In section IV we give the general relativistic equations governing the hydrodynamics and the rate equations for the plasma of e^+e^--pairs.

In section V we give the governing equations relating the comoving time τ to the laboratory time t corresponding

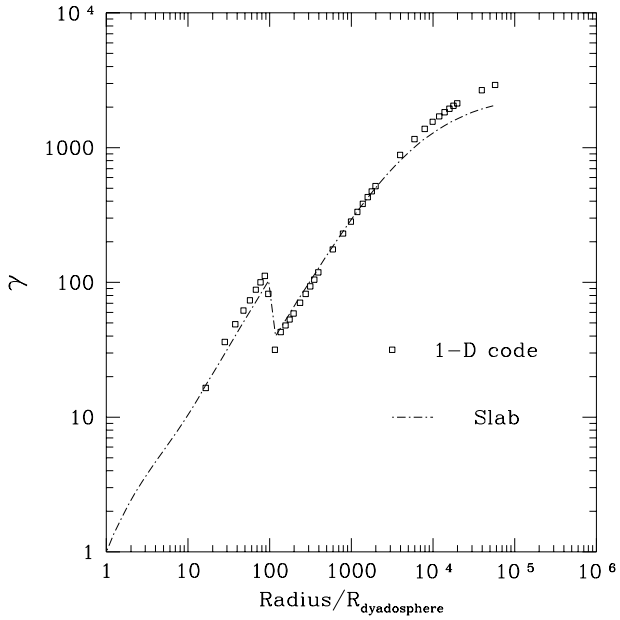

Figure 5: Comparison of gamma factor for the one-dimensional (1-D) hydrodynamic calculations (Livermore code) and slab calculations (Rome code) as a function of the radial coordinate (in units of dyadosphere radius) in the laboratory frame. The calculations show an excellent agreement.

to an inertial reference frame in which the EMBH is at rest and finally to the time measured at the detector t_a which, to finally get t_a^d, must be corrected to take into account the cosmological expansion.

In section VI we describe the numerical integration of the hydrodynamical equations and the rate equation developed by the Rome and Livermore groups. This entire research program could never have materialized without the fortunate interaction between the complementary computational techniques developed by these two groups. The validation of the results of the Rome group by the fully general relativistic Livermore codes has been essential both from the point of view of the validity of the numerical results and the interpretation of the scientific content of the results.

The Era I: the PEM pulse. In section IV by the direct comparison of the integrations performed with the Rome and Livermore codes we show that among all possible geometries the e^+e^- plasma moves outward from the EMBH reaching a very unique relativistic configuration: the plasma self-organizes in a sharp pulse which expands in the comoving frame exactly by the amount which compensates for the Lorentz contraction in the laboratory frame. The sharp pulse remains of constant thickness in the laboratory frame and self-propels outwards reaching ultrarelativistic regimes, with gamma factors larger than 10^2, in a few dyadosphere crossing times. We recall that, in analogy with the electromagnetic (EM) pulse observed in a thermonuclear explosion on the Earth, we have defined this more energetic pulse formed of electron-positron pairs and electromagnetic radiation a pair-electromagnetic-pulse or PEM pulse.

The Era II: We describe the interaction of the PEM pulse with the baryonic remnant of mass M_B left over from the gravitational collapse of the progenitor star. We give the details of the decrease of the gamma factor and the corresponding increase in the internal energy during the collision. The dimensionless parameter $B = M_B c^2/E_{dya}$ which measures the baryonic mass of the remnant in units of the E_{dya} is introduced. This is the second fundamental free parameter of the EMBH theory.

The Era III: We describe in section IX the further expansion of the e^+e^- plasma, after the engulfment of the baryonic remnant of the progenitor star. By direct comparison of the results of integration obtained with the Rome and the Livermore codes it is shown how the pair-electromagnetic-baryon (PEMB) plasma further expands and self organizes in a sharp pulse of constant length in the laboratory frame (see Fig. 5). We have examined the formation of this PEMB pulse in a wide range of values $10^{-8} < B < 10^{-2}$ of the parameter B, the upper limit corresponding to the limit of validity of the theoretical framework developed.

In section X it is shown how the effect of baryonic matter of the remnant, expressed by the parameter B, is to smear out all the detailed information on the EMBH parameters. The evolution of the PEMB pulse is shown to

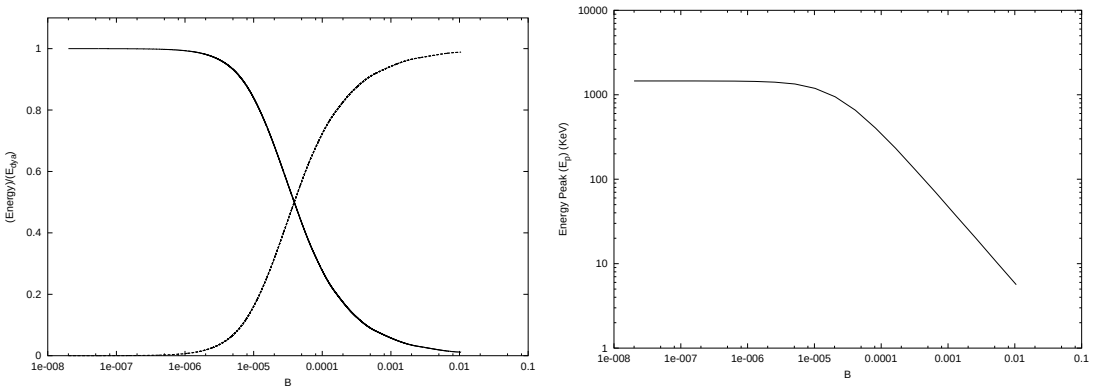

Figure 6: **Left)** At the transparent point, the energy radiated in the P-GRB (the solid line) and (the dashed line) the final kinetic energy of baryonic matter, $E_{Baryons}$, in units of the total energy of the dyadosphere (E_{dya}), are plotted as functions of the B parameter. **Right)** The energy corresponding to the peak of the photon number spectrum in the P-GRB as measured in the laboratory frame is plotted as function of the B parameter.

depend only on E_{dya} and B: the PEMB pulse is degenerate in the mass and charge parameters of the EMBH and rather independent of the exact location of the baryonic matter of the remnant.

In section XI the relevant thermodynamical quantities of the PEMB pulse, the temperature in the different frames and the e^+e^- pair densities, are given and the approach to the transparency condition is examined. Particular attention is given to the gradual transfer of the energy of the dyadosphere E_{dya} to the kinetic energy of the baryons $E_{Baryons}$ during the optically thick part of the PEMB pulse.

In section XII, as the condition of transparency is reached, the injector phase is concluded with the emission of a sharp burst of electromagnetic radiation and an accelerated beam of highly relativistic baryons. We recall that we have respectively defined the radiation burst (the proper GRB or for short P-GRB) and the accelerated-baryonic-matter (ABM) pulse. By computing for a fixed value of the EMBH different PEMB pulses corresponding to selected values of B in the range $\left[10^{-8}–10^{-2}\right]$, it has been possible to obtain a crucial universal diagram which is reproduced in Fig.6. In the limit of $B \to 10^{-8}$ or smaller almost all E_{dya} is emitted in the P-GRB and a negligible fraction is emitted in the kinetic energy $E_{Baryons}$ of the baryonic matter and therefore in the afterglow. On the other hand in the limit $B \to 10^{-2}$ which is also the limit of validity of our theoretical framework, almost all E_{dya} is transferred to $E_{Baryons}$ and gives origin to the afterglow and the intensity of the P-GRB correspondingly decreases. We have identified the limiting case of negligible values of B with the process of emission of the so called "short bursts". A complementary result reinforcing such an identification comes from the thermodynamical properties of the P-GRB: the hardness of the spectrum decreases for increasing values of B, see Fig. 6.

The injector phase is concluded by the emission of the P-GRB and the ABM pulse, as the condition of transparency is reached.

The **beam-target phase**, in which the accelerated baryonic matter (ABM) generated in the injector phase collides with the ISM, gives origin to the afterglow. Again for simplicity we have adopted a minimum set of assumptions:

1. The ABM pulse is assumed to collide with a constant homogeneous interstellar medium of number density $n_{\rm ism} \sim 1cm^{-3}$. The energy emitted in the collision is assumed to be instantaneously radiated away (fully radiative condition). The description of the collision and emission process is done using spherical symmetry, taking only the radial approximation neglecting all the delayed emission due to off-axis scattered radiation.

2. Special attention is given to numerically compute the power of the afterglow as a function of the arrival time using the correct governing equations for the space-time transformations in line with the RSTT paradigm.

3. Finally some approximate solutions are adopted in order to obtain the determination of the power law exponents of the afterglow flux and compare and contrast them with the observational results as well as with the alternative results in the literature.

We first consider the above mentioned radial approximation and a spherically symmetric distribution in order to concentrate on the role of the correct space-time transformations in the RSTT paradigm and illustrate their impact on the determination of the power law index of the afterglow. This topic has been seriously neglected in the literature.

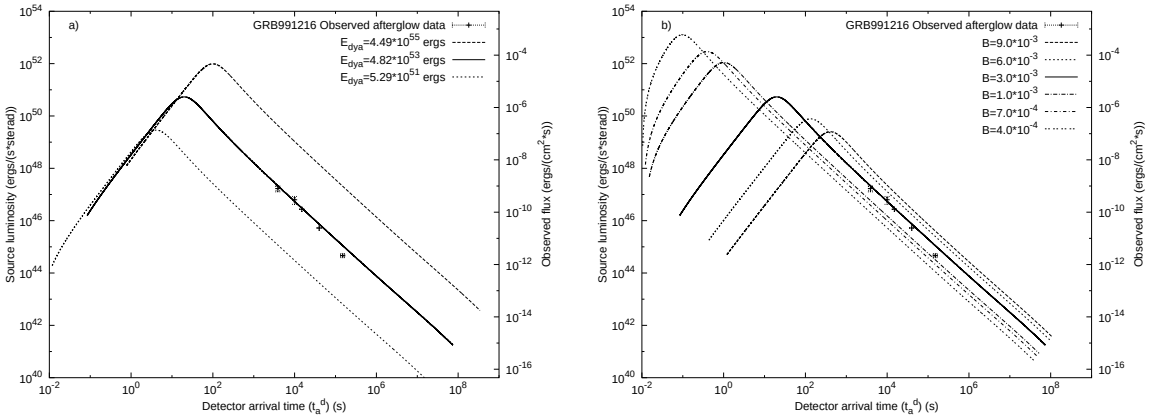

Figure 7: a) Afterglow luminosity computed for an EMBH of $E_{dya} = 5.29 \times 10^{51}$ erg, $E_{dya} = 4.83 \times 10^{53}$ erg, $E_{dya} = 4.49 \times 10^{55}$ erg and $B = 3 \times 10^{-3}$. b) for the $E_{dya} = 4.83 \times 10^{53}$, we give the afterglow luminosities corresponding respectively to $B = 9 \times 10^{-3}$, 6×10^{-3}, 3×10^{-3}, 1×10^{-3}, 7×10^{-4}, 4×10^{-4}.

We then turn to the fully relativistic analysis of the off-axis emission and of the temporal structure in the long bursts (see also Ruffini et al. [148] and sections XXI–XXII) and of their spectral distribution (see also Ruffini et al. [150] and section XXIV). Details of the role of beaming are going to be discussed elsewhere (Ruffini et al. [151]).

We can now turn to the two eras of the beam-target phase:

The Era IV: the ultrarelativistic and relativistic regimes in the afterglow. In section XIII the hydrodynamic relativistic equations governing the collision of the ABM pulse with the interstellar matter are given in the form of a set of finite difference equations to be numerically integrated. Expressions for the internal energy developed in the collision as well as for the gamma factor are given as a function of the mass of the swept up interstellar material and of the initial conditions. In section XVIII the infinitesimal limit of these equations is given as well as analytic power-law expansions in selected regimes.

The Era V: the approach to the nonrelativistic regimes in the afterglow. In section XIV it is stressed that this last era often discussed in the current literature can be described by the same equations used for era IV.

Having established all the governing equations for all the eras of the EMBH theory, we can proceed to compare and contrast the predictions of this theory with the observational data.

F. The Best fit of the EMBH theory to the GRB 991216: the global features of the solution

As expressed in section XV, we have proceeded to the identification of the only two free parameters of the EMBH theory, E_{dya} and B, by fitting the observational data from R-XTE and Chandra on the decaying part of the GRB 991216 afterglow. The afterglow appears to have three different parts: in the first part the luminosity increases as a function of the arrival time, it then reaches a maximum and finally monotonically decreases. In Fig. 7, we show how such a fit is actually made and how changing the two free parameters affects the intensity and the location in time of the peak of the afterglow. The best fit is obtained for $E_{dya} = 4.83 \times 10^{53}\, erg$ and $B = 3 \times 10^{-3}$.

Having determined the two free parameters of the theory, we have integrated the governing equations corresponding to these values and then obtained for the first time the complete history of the gamma factor from the moment of gravitational collapse to the latest phases of the afterglow observations (see Fig. 8). This diagram clearly shows the inadequacy of considering a simple power-law relation $\gamma \propto r^{-3/2}$ for the relation between the radius of the source and its Lorentz gamma factor as assumed in the large majority of current papers on GRBs (see e.g. Panaitescu & Mészáros [114], Piran [116], Sari [163, 164], Sari et al. [166], Waxman [186] and references therein). Actually, such a power-law behaviour is never found to exist.

We have also determined the different regimes encountered in the relation between the laboratory time and the detector arrival time within the RSTT paradigm compared and contrasted with the ones in the current literature (see Fig. 9). The solid curve is computed using the exact formula prescribed by the RSTT paradigm (see Eq.(37) in

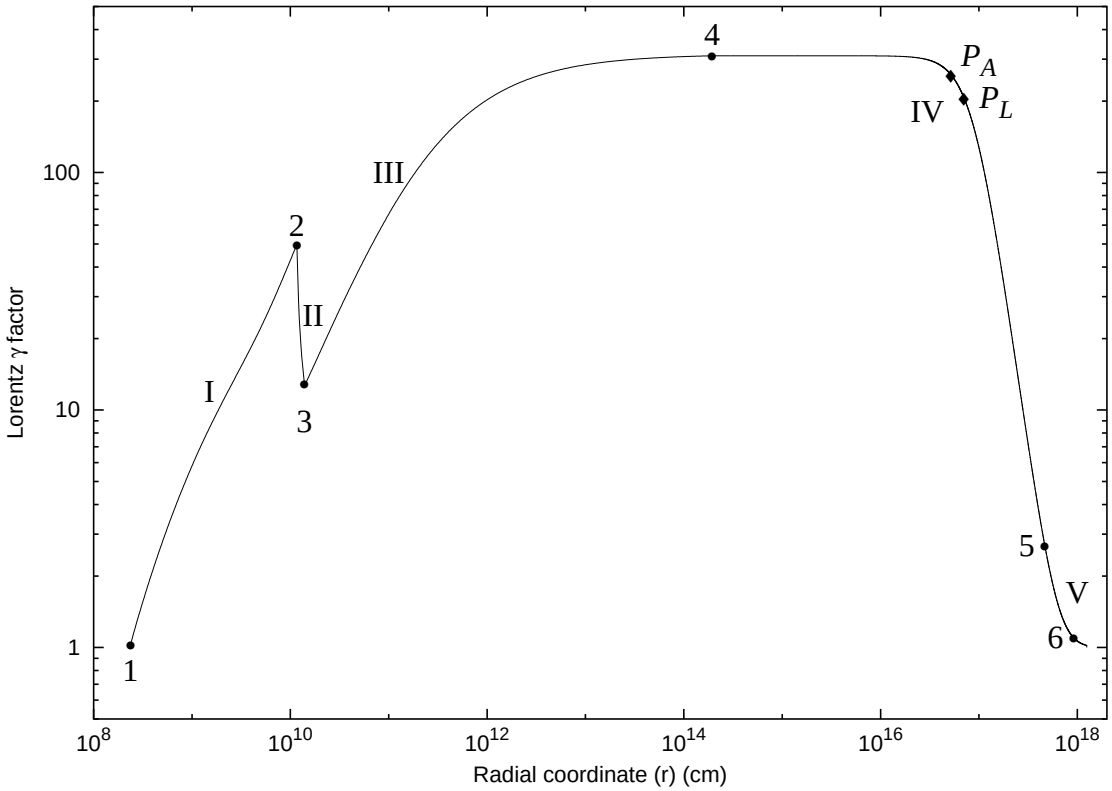

Figure 8: The theoretically computed gamma factor for the parameter values $E_{dya} = 4.83 \times 10^{53}$ erg, $B = 3 \times 10^{-3}$ is given as a function of the radial coordinate in the laboratory frame. The corresponding values in the comoving time, laboratory time and arrival time are given in Tab. I. The different eras indicated by roman numerals are illustrated in the text (see sections VII,VIII,IX,XIII,XIV), while the points 1,2,3,4,5 mark the beginning and end of each of these eras. The points P_L and P_A mark the maximum of the afterglow flux, respectively in emission time and in arrival time (see Ruffini et al. [145] and sections XIII,XVIII). The point 6 is the beginning of Phase D in Era V (see sections XIV,XVIII). At point 4 the transparency condition is reached and the P-GRB is emitted. This diagram clearly shows the inadequacy of considering a simple power-law relation $\gamma \propto r^{-3/2}$ for the relation between the radius of the source and its Lorentz gamma factor as assumed in the large majority of current papers on GRBs (see e.g. Panaitescu & Mészáros [114], Piran [116], Sari [163, 164], Sari et al. [166], Waxman [186] and references therein). Actually, such a power-law behaviour is never found to exist.

section V)

$$t_a^d = (1+z)\left(t - \int_0^t \frac{\sqrt{\gamma^2(t')-1}}{\gamma(t')}dt' - \frac{r_{ds}}{c}\right).$$

The dashed-dotted curve is computed using the approximate formula (see Eq.(41))

$$t_a^d = (1+z)\,\frac{t}{2\gamma^2(t)},$$

often used in the current literature (see e.g. Fenimore et al. [48], Piran [116], Sari [163, 164], Waxman [186] and references therein). The difference between the solid line and the dashed-dotted line clearly shows the inadequacy of using such an approximate relation. We like to stress that the difference between the above two curves is especially marked in the afterglow region. Note that this difference as been estimated assuming in both curves the correct relation between the Lorentz gamma factor and the radial coordinated of the source given in Fig. 8. In the case that the wrong relation $\gamma \propto r^{-3/2}$ is adopted as done in the literature (see e.g. Panaitescu & Mészáros [114], Piran [116], Sari

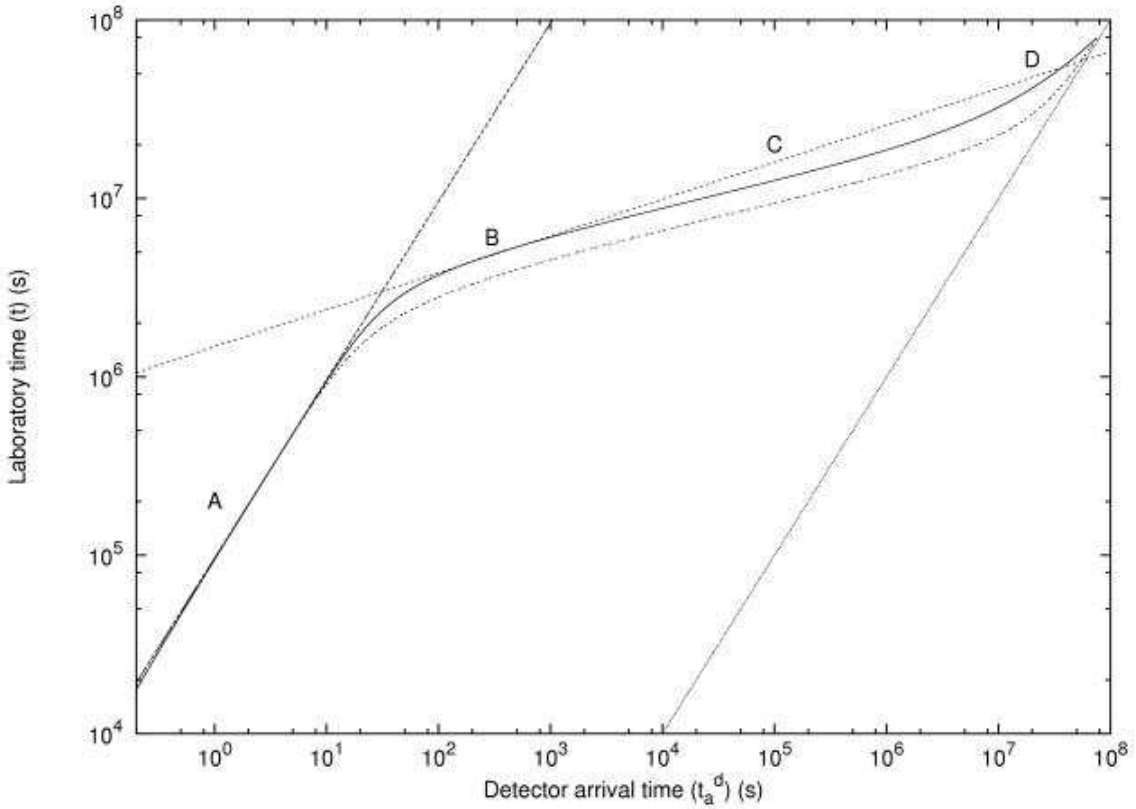

Figure 9: Relation between the arrival time (t_a^d) measured at the detector and the laboratory time (t) measured at the GRB source. The solid curve is computed using the exact formula prescribed by the RSTT paradigm $t_a^d = (1+z)\left(t - \int_0^t \frac{\sqrt{\gamma^2(t')-1}}{\gamma(t')}dt' - \frac{r_{ds}}{c}\right)$ (see Eq.(37) in section V). The dashed-dotted curve is computed using the approximate formula $t_a^d = (1+z)\left(t/2\gamma^2(t)\right)$ (see Eq.(41)) often used in the current literature (see e.g. Fenimore et al. [48], Piran [116], Sari [163, 164], Waxman [186] and references therein). The difference between the solid line and the dashed-dotted line clearly shows the inadequacy of using such an approximate relation. We like to stress that the difference between the above two curves is especially marked in the afterglow region. Note that this difference as been estimated assuming in both curves the correct relation between the Lorentz gamma factor and the radial coordinated of the source given in Fig. 8. In the case that the wrong relation $\gamma \propto r^{-3/2}$ is adopted as done in the literature (see e.g. Panaitescu & Mészáros [114], Piran [116], Sari [163, 164], Sari et al. [166], Waxman [186] and references therein) the discrepancy between the two curves will be much larger. It is anyway clear that, even knowing quantitatively the exact Lorentz gamma factor curve reported in Fig. 8, the use of the approximate relation given in Eq.(41) is enough to miss the correct clock synchronization and to obtain a wrong value for the power-law index n in the decaying phases of the afterglow (see sections XVIII–XIX and Tab. II). We distinguish four different phases. **Phase A**: There is a linear relation between t and t_a^d, given by Eq.(137) in the text (dashed line). **Phase B**: There is an "effective" power-law relation between t and t_a^d, given by Eq.(142) (dotted line). **Phase C**: No analytic formula holds and the relation between t and t_a^d has to be directly computed by the integration of the complete equations of energy and momentum conservation (Eqs.(107,108)). **Phase D**: As the gamma factor approaches $\gamma = 1$, the relation between t and t_a^d asymptotically goes to $t = t_a^d$ (light gray line). See also Ruffini et al. [144].

[163, 164], Sari et al. [166], Waxman [186] and references therein) the discrepancy between the two curves will be much larger. It is anyway clear that, even knowing quantitatively the exact Lorentz gamma factor curve reported in Fig. 8, the use of the approximate relation given in Eq.(41) is enough to miss the correct clock synchronization and to obtain a wrong value for the power-law index n in the decaying phases of the afterglow (see sections XVIII–XIX and Tab. II).

To be more explicit, from the result given in Figs. 8–9 follows that all existing GRB models, with the exception of

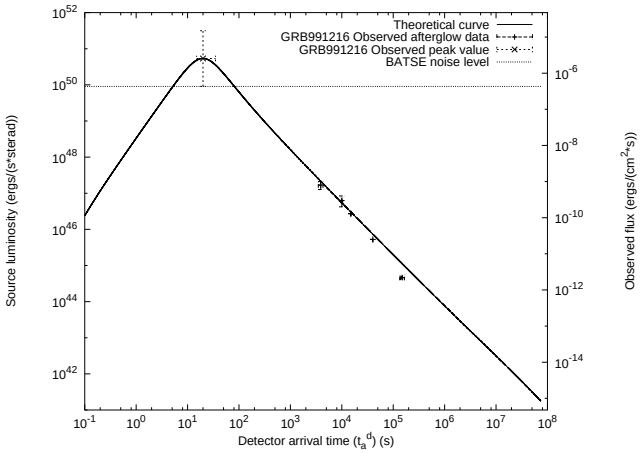

Figure 10: Best fit of the afterglow data of Chandra, RXTE as well as of the range of variability of the BATSE data on the major burst, by a unique afterglow curve leading to the parameter values $E_{dya} = 4.83 \times 10^{53} erg, B = 3 \times 10^{-3}$. The horizontal dotted line indicates the BATSE noise threshold. On the left axis the luminosity is given in units of the energy emitted at the source, while the right axis gives the flux as received by the detectors.

ours, have the wrong spacetime coordinatization of the GRB phenomenon and they therefore lack the fundamental toola to compare the theoretical prediction in the laboratory time to the observations carried out in the asymptotic photon arrival time. This extreme situation affects all considerations on GRBs: as an example, all the considerations on the afterglow slopes, which drastically depend on the functional dependence between the laboratory time and the photon arrival time, are drastically affected (see subsection II H below and Tab. II). In turn, all the considerations about the possible existence of beaming in GRBs inferred from the afterglow slopes are in this circumstance deprived of any meaning.

We have thus determined the entire space-time grid of the GRB 991216 by giving (see Tab. I) the radial coordinate of the GRB phenomenon as a function of the four coordinate time variables. A quick glance to Tab. I shows how the extreme relativistic regimes at work lead to enormous superluminal behaviour (up to $10^5 c$!) if the classical astrophysical concepts are adopted using the arrival time as the independent variable. In turn this implies that any causal relation based on classical astrophysics and the arrival time data, as at times found in the current GRB literature, is incorrect.

G. The explanation of the "long bursts" and the identification of the proper gamma ray burst(P-GRB)

In section XVI, having determined the two free parameters of the EMBH theory, we analyze the theoretical predictions of this theory for the general structure of GRBs. The first striking result, illustrated in Fig. 10, shows that the peak of the afterglow emission coincides both in intensity and in arrival time ($19.87\,s$) with the average emission of the long burst observed by BATSE. For this we have introduced the new concept of *extended afterglow peak emission (E-APE)*. Once the proper space-time grid is given (see Tab. I) it is immediately clear that the E-APE is generated at distances of 5×10^{16} cm from the EMBH. The long bursts are then identified with the E-APEs and are not bursts at all: they have been interpreted as bursts only because of the high threshold of the BATSE detectors (see Fig. 10). Thus the long standing unsolved problem of explaining the long GRBs (see e.g. Piran [117], Salmonson et al. [162], Wilson et al. [187]) is radically resolved.

Still in section XVI, the search for the identification of the P-GRB in the BATSE data is described. This identification is made using the two fundamental diagrams shown in Fig. 11. Having established the value of $E_{dya} = 4.83 \times 10^{53}\, erg$ and of $B = 3 \times 10^{-3}$, it is possible from the dashed line and the solid line in Fig. 11 to evaluate the ratio of the energy $E_{P\text{-}GRB}$ emitted in the P-GRB to the energy $E_{Baryons}$ emitted in the afterglow corresponding to the determined value of B, see the vertical line in Fig. 11. We obtain $E_{P\text{-}GRB}/E_{Baryons} = 1.58 \times 10^{-2}$, which gives $E_{P\text{-}GRB} = 7.54 \times 10^{51}\, erg$. Having so determined the theoretically expected intensity of the P-GRB, a second fundamental observable parameter, which is also a function of E_{dya} and B, is the arrival time delay between the P-GRB and the peak E-APE, determined in Fig. 11. From Tab. I, we have that the detector arrival time of the

Table I: Gamma factors for selected events and their space-time coordinates. The points marked 1,2,3,4,5,6,P_L,P_A are the same reported in Fig. 8, while the point F is the endpoint of the simulation. It is particularly important to read the last column, where the apparent motion in the radial coordinate, evaluated in the arrival time at the detector, leads to an enormous "superluminal" behaviour, up to $9.55 \times 10^4\ c$. This illustrates well the impossibility of using such a classical estimate in regimes with gamma factors up to 310.1.

Point	$r(cm)$	$\tau(s)$	$t(s)$	$t_a(s)$	$t_a^d(s)$	γ	"Superluminal" $v \equiv \frac{r}{t_a^d}$
			The Injector Phase				
1	2.354×10^8	0.0	0.0	0.0	0.0	1.000	0
	1.871×10^9	1.550×10^{-2}	5.886×10^{-2}	4.312×10^{-3}	8.625×10^{-3}	10.08	$7.23c$
	4.486×10^9	2.141×10^{-2}	1.463×10^{-1}	4.523×10^{-4}	9.046×10^{-3}	20.26	$16.5c$
	7.080×10^9	2.485×10^{-2}	2.329×10^{-1}	4.594×10^{-3}	9.187×10^{-3}	30.46	$25.7c$
	9.533×10^9	2.715×10^{-2}	3.148×10^{-1}	4.627×10^{-3}	9.253×10^{-3}	40.74	$34.4c$
	1.162×10^{10}	2.868×10^{-2}	3.845×10^{-1}	4.644×10^{-3}	9.288×10^{-3}	49.70	$41.7c$
2	1.162×10^{10}	2.868×10^{-2}	3.845×10^{-1}	4.644×10^{-3}	9.288×10^{-3}	49.70	$41.7c$
	1.186×10^{10}	2.889×10^{-2}	3.923×10^{-1}	4.646×10^{-3}	9.292×10^{-3}	38.06	$42.6c$
	1.234×10^{10}	2.949×10^{-2}	4.083×10^{-1}	4.655×10^{-3}	9.311×10^{-3}	24.21	$44.2c$
	1.335×10^{10}	3.144×10^{-2}	4.423×10^{-1}	4.706×10^{-3}	9.413×10^{-3}	15.14	$47.3c$
	1.389×10^{10}	3.279×10^{-2}	4.603×10^{-1}	4.753×10^{-3}	9.506×10^{-3}	12.94	$48.7c$
3	1.389×10^{10}	3.279×10^{-2}	4.603×10^{-1}	4.753×10^{-3}	9.506×10^{-3}	12.94	$48.7c$
	2.326×10^{10}	5.208×10^{-2}	7.733×10^{-1}	5.369×10^{-3}	1.074×10^{-2}	20.09	$72.2c$
	6.913×10^{10}	9.694×10^{-2}	2.304	6.086×10^{-3}	1.217×10^{-2}	50.66	$1.89 \times 10^2 c$
	1.861×10^{11}	1.486×10^{-1}	6.206	6.446×10^{-3}	1.289×10^{-2}	100.1	$4.82 \times 10^2 c$
	9.629×10^{11}	3.112×10^{-1}	32.12	6.978×10^{-3}	1.396×10^{-2}	200.3	$2.30 \times 10^3 c$
	3.205×10^{13}	3.958	1.069×10^3	1.343×10^{-2}	2.685×10^{-2}	300.1	$3.98 \times 10^4 c$
	1.943×10^{14}	21.57	6.481×10^3	4.206×10^{-2}	8.413×10^{-2}	310.1	$7.70 \times 10^4 c$
			The Beam-Target Phase				
4	1.943×10^{14}	21.57	6.481×10^3	4.206×10^{-2}	8.413×10^{-2}	310.1	$7.70 \times 10^4 c$
	6.663×10^{15}	7.982×10^2	6.481×10^3	1.164	2.328	310.0	$9.55 \times 10^4 c$
	2.863×10^{16}	3.114×10^3	9.549×10^5	5.057	10.11	300.0	$9.45 \times 10^4 c$
	4.692×10^{16}	5.241×10^3	1.565×10^6	8.775	17.55	270.0	$8.92 \times 10^4 c$
P_A	5.177×10^{16}	5.853×10^3	1.727×10^6	9.933	19.87	258.5	$8.69 \times 10^4 c$
	5.878×10^{16}	6.791×10^3	1.961×10^6	11.82	23.63	240.0	$8.30 \times 10^4 c$
	6.580×10^{16}	7.811×10^3	2.195×10^6	14.03	28.06	220.0	$7.82 \times 10^4 c$
P_L	7.025×10^{16}	8.506×10^3	2.343×10^6	15.66	31.32	207.0	$7.48 \times 10^4 c$
	7.262×10^{16}	8.895×10^3	2.422×10^6	16.61	33.23	200.0	$7.29 \times 10^4 c$
	9.058×10^{16}	1.236×10^4	3.021×10^6	26.66	53.32	150.0	$5.67 \times 10^4 c$
	1.136×10^{17}	1.866×10^4	3.788×10^6	52.84	1.057×10^2	100.0	$3.58 \times 10^4 c$
	1.539×10^{17}	3.819×10^4	5.134×10^6	2.000×10^2	4.000×10^2	50.02	$1.28 \times 10^4 c$
	2.801×10^{17}	2.622×10^5	9.351×10^6	7.278×10^3	1.455×10^4	10.00	$6.42 \times 10^2 c$
	3.624×10^{17}	6.702×10^5	1.213×10^7	3.860×10^4	7.719×10^4	5.001	$1.57 \times 10^2 c$
	4.454×10^{17}	1.433×10^6	1.500×10^7	1.439×10^5	2.877×10^5	2.998	$51.6c$
5	4.454×10^{17}	1.433×10^6	1.500×10^7	1.439×10^5	2.877×10^5	2.998	$51.6c$
	4.830×10^{17}	1.928×10^6	1.635×10^7	2.381×10^5	4.762×10^5	2.500	$33.8c$
	5.390×10^{17}	2.873×10^6	1.844×10^7	4.643×10^5	9.285×10^5	2.000	$19.4c$
	6.422×10^{17}	5.387×10^6	2.271×10^7	1.291×10^6	2.581×10^6	1.500	$8.30c$
	1.034×10^{18}	2.903×10^7	5.002×10^7	1.552×10^7	3.103×10^7	1.054	$1.11c$
6	1.034×10^{18}	2.903×10^7	5.002×10^7	1.552×10^7	3.103×10^7	1.054	$1.11c$
	1.202×10^{18}	4.979×10^7	7.150×10^7	3.140×10^7	6.280×10^7	1.025	$6.38 \times 10^{-1} c$
F	1.248×10^{18}	5.706×10^7	7.894×10^7	3.731×10^7	7.461×10^7	1.000	$5.58 \times 10^{-1} c$

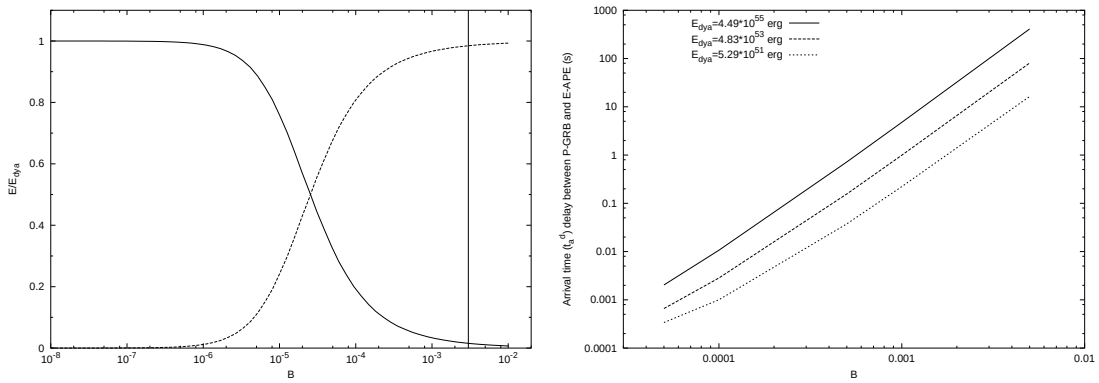

Figure 11: **Left)** Relative intensities of the E-APE (dashed line) and the P-GRB (solid line), as predicted by the EMBH theory corresponding to the values of the parameters determined in Fig. 10, as a function of B. Details are given in section XVI. The vertical line corresponds to the value $B = 3 \times 10^{-3}$. **Right)** The arrival time delay between the P-GRB and the peak of the E-APE is plotted as a function of the B parameter for three selected values of E_{dya}.

P-GRB occurs at $8.41 \times 10^{-2}\, s$, corresponding to a radial coordinate of $1.94 \times 10^{14}\, cm$, a comoving time of $21.57\, s$, a laboratory time of $6.48 \times 10^{3}\, s$ and an arrival time of $4.21 \times 10^{-2}\, s$. At this point, the gamma factor is 310.1. The peak of the E-APE occurs at a detector arrival time of $19.87\, s$, corresponding to a radial coordinate of $5.18 \times 10^{16}\, cm$, a comoving time of $5.85 \times 10^{3}\, s$, a laboratory time of $1.73 \times 10^{6}\, s$ and an arrival time of $9.93\, s$ (see Tab. I). The delay between the P-GRB and the peak of the E-APE is therefore $19.78\, s$, see Fig. 11. The theoretical prediction on the intensity and the arrival time uniquely identifies the P-GRB with the "precursor" in the GRB 991216 (see Fig. 3). Moreover, the hardness of the P-GRB spectra is also evaluated in this section. As pointed out in the conclusions, the fact that both the absolute and relative intensities of the P-GRB and E-APE have been predicted within a few percent accuracy as well as the fact that their arrival time has been computed with the precision of a few tenths of milliseconds, see Tab. I and Fig. 12, can be considered one of the major successes of the EMBH theory.

H. On the power-laws and beaming in the afterglow of GRB 991216.

In section XVIII a piecewise description of the afterglow by the expansion of the fundamental hydrodynamical equations given by Taub [177] and Landau & Lifshitz [87] have allowed the determination of a power-law index for the dependence of the afterglow luminosity on the photon arrival time at the detector. It is evident that the determination of the power-law index is very sensitive to the basic assumptions made for the description of the afterglow, as well as to the relations between the different temporal coordinates which have been clarified by the RSTT paradigm (see Ruffini et al. [144]). The different power-law indexes obtained are compared and contrasted with the ones in the current literature (see Tab. II and section. XIX). As a byproduct of this analysis, see also the conclusions, there is a perfect agreement between the observational data and the theoretical predictions, implying that the assumptions we have adopted for the description of the afterglow (see section XIII) must be necessarily all valid and therefore, in particular, there is no evidence for a beamed emission in GRB 991216.

We then summarize in Fig. 12 the results for the average bolometric luminosity of GRB 991216 with particular attention to the striking agreement, both in arrival time and in intensity, for the theoretically predicted structure of the P-GRB and the E-APE with the observational data. To show the generality of application of the EMBH theory, we have applied it also to GRB 980425 (see Ruffini [140]) and the excellent results are also shown, for comparsion, in Fig. 12.

I. Substructures in the E-APE due to inhomogeneities in the Interstellar medium

In section XX the role of the inhomogeneities in the interstellar matter has been analyzed in order to explain the observed temporal substructures in the BATSE data on GRB 991216. Having satisfactorily identified the average intensity distribution of the afterglow and the relative position of the P-GRB, in Ruffini et al. [147] we have addressed the issue whether the fast temporal variation observed in the so-called long bursts, on time scales as short as fraction of

Table II: We compare and contrast the results on the power-law index n of the afterglow in the EMBH theory with other treatments in the current literature, in the limit of high energy and fully radiative conditions. The differences between the values of $-10/7 \sim -1.43$ (Dermer) and the results -1.6 in the EMBH theory can be retraced to the use of the two different approximation in the arrival time versus the laboratory time given in Fig. 9. See details in section XVIII.

	EMBH theory	Chiang & Dermer [29] Dermer et al. [41] Böttcher & Dermer [20]	Piran [116] Sari & Piran [168] Piran [117]	Vietri [180]	Halpern et al. [73]
Ultra-relativistic	$\gamma = \gamma_\circ$ $\gamma_\circ = 310.1$ $n = 2$	$\gamma = \gamma_\circ$ $n = 2$	$\gamma = \gamma_\circ$ $n \simeq 2$		
Relativistic	$\gamma \simeq r^{-3}$ $3.0 < \gamma < 258.5$ $n = -1.6$	$\gamma \sim r^{-3}$ $n = -\frac{10}{7} = -1.43$	$\gamma \sim r^{-3}$ $n = -\frac{5.5}{4} = -1.375$		$n > -1.47$
Non-relativistic	$n = -1.36$ $1.05 < \gamma < 3.0$			$n = -1.7$	
Newtonian	$n = -1.45$ $1 < \gamma < 1.05$				

a second (see e.g. Fishman & Meegan [53]), can indeed be explained as an effect of inhomogeneities in the interstellar medium. Such a possibility was pioneered in the work by Dermer & Mitman [42], purporting that such a time variability corresponds to a tomographic analysis of the ISM. In order to probe the validity of such an explanation, we have first considered the simplified case of the radial approximation (Ruffini et al. [147]). The aim has been to explore the possibility of explaining the observed fluctuation in intensity on a fraction of a second as originated from inhomogeneities in ISM, typically of the order of 10^{16} due to apparent superluminal behaviour of roughly 10^5c. We have shown there that this approach is indeed viable: both the intensity variation and the time scale of the variability in the E-APE region can be explained by the interaction of the ABM pulse with inhomogeneities in the ISM, taking into due account the apparent superluminal effects. These effects, in turn, can be derived and computed self consistently from the dynamics of the source. We have then described the inhomogeneities of the ISM by an appropriate density profile (mask) of an ISM cloud. Of course at this stage, for simplicity, only the case of spherically symmetric "spikes" with over-density separated by low-energy regions, has been considered. Each spike has been assumed to have the spatial extension of 10^{15}cm. The cloud average density is $< n_{ism} >= 1\,\text{particle/cm}^3$. In conclusion, from the data of Tab. I and the highly "superluminal" behaviour of the source in the region of the E-APE, it is concluded that the observed time variability in the intensity of the emission $\left(\Delta I/\overline{I}\right) \sim 5$ can be traced to inhomogeneities in the interstellar matter: $(\Delta n_{ism}/n_{ism}) \sim 5$. The typical size of the scattering region is estimated to be $5 \times 10^{16}\,cm$, and these are the typical sizes and density contrasts found in interstellar clouds. Since the emission of the E-APE occurs at typical dimensions of the order of $5 \times 10^{16}\,cm$, the observed inhomogeneities are probing the structure of the interstellar medium, and have nothing to do with the "inner engine" of the source.

The big issue was then open if all these results, obtained in the radial approximation, would still be valid in the more general case when off-axis emission in the description of the afterglow is taken into account. This is the reason why we have proceeded to the topic summarized in the next subsections (see Ruffini et al. [148]).

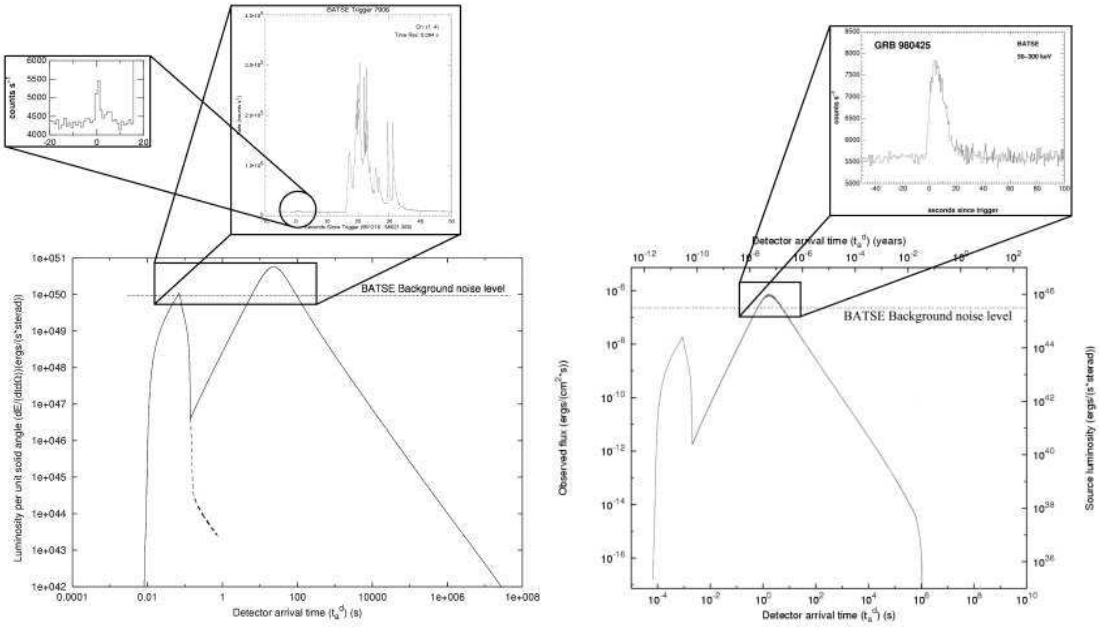

Figure 12: **Left)** The overall description of the EMBH theory applied to GRB 991216. The BATSE noise threshold is represented and the observations both of the P-GRB and of the E-APE are clearly shown in the subpanels. The continuos line in the picture represents the theoretical prediction of the EMBH model. **Right)** The same diagrams are represented for GRB 980425. Two aspects are especially important to be mentioned: a) in this source the theoretical prediction of the P-GRB intensity is lower than the BATSE noise treshold and is therefore unobservable and unobserved; b) the E-APE is especially smooth as a consequence of the low value of the gamma Lorentz factor (see also section XXIII and Ruffini [140]).

J. The definition of the equitemporal surfaces (EQTS) and the afterglow delayed intensity as a function of the viewing angle

While the analysis of the average bolometric intensity of GRB was going on in the radial approximation, we have proceeded to develop the full non-radial approximation, taking into account all the relativistic corrections for the off-axis emission from the spherically symmetric expansion of the ABM pulse (see Ruffini et al. [148, 153] and sections XXI–XXII). Photons emitted at the same time but at different angles of displacement from the line of sight reach the detector at very different arrival times. Correspondingly, photons detected at the same arrival time are emitted at very different times and angles. We have so defined the temporal evolution of the ABM pulse visible area as well as the equitemporal surfaces (EQTS), i.e. the locus of points on the ABM pulse emitting surface corresponding to a constant value of the photon arrival time at the detector.

The very same difficulties found in the current literature, relating the laboratory time to the photon arrival time at the detector (see Figs. 8–9), still exists in the present context and are even magnified in the definition of the EQTS. In a classical article, Rees [127] expressed the relation between the laboratory time and the arrival time at the detector in order to explain observations in radio sources with a constant expansion velocity v and Lorentz gamma factor $\gamma \sim 5$. He pointed out the EQTS are ellipsoids of constant eccentricity v/c. In the current literature, the Rees approach has been adapted to the analysis of GRBs (see e.g. Fenimore et al. [48], Piran [116], Sari [163, 164], Waxman [186] and references therein). In addition to the very crucial relation between the laboratory time and the photon arrival time, which has not been properly treated, there have been a variety of other approximation and averaging processes on which we do not agree. Instead of specifically criticizing each assumption which we consider not correct, such comparison will be made in a forthcoming paper (Ruffini et al. [155]), we just report here in the following the results of the EQTS surfaces (see Fig. 13) obtained in conformity with the RSTT paradigm. In the present case of GRBs, the gamma factor is not only much larger than the one observed in radio sources, but is also strongly time varying (see Fig. 8). The Rees treatment has to be significantly improved to take into account the huge time variations in the Lorentz gamma factor: this is not just a technical point of modifying a formula by the introduction of a new

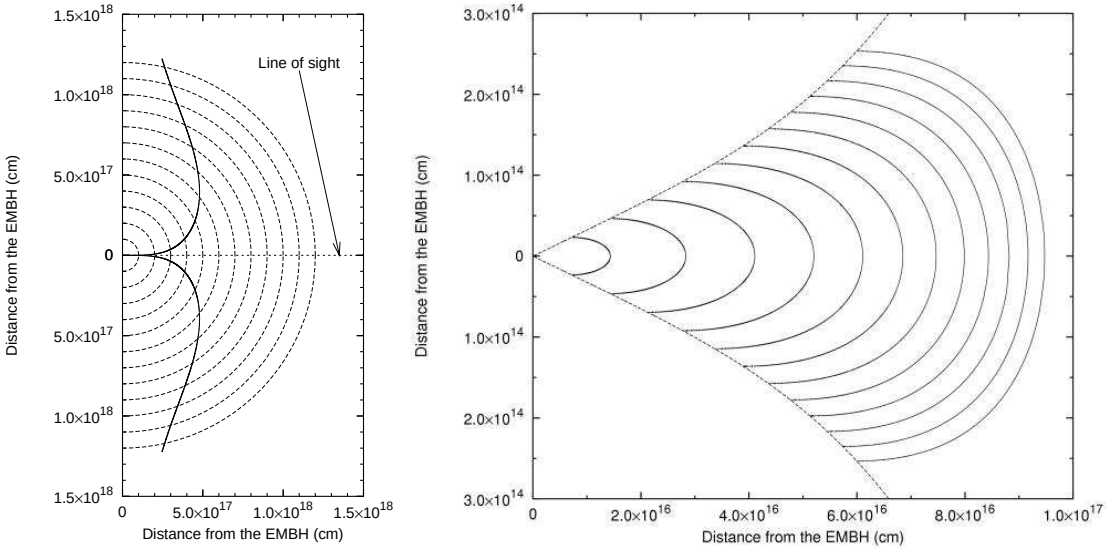

Figure 13: **Left)** This figure shows the temporal evolution of visible area of the ABM pulse. The dashed half-circles are the expanding ABM pulse at radii corresponding to different laboratory times. The black curve marks the boundary of the visible region. The EMBH is located at position (0,0) in this plot. Again, in the earliest GRB phases the visible region is squeezed along the line of sight, while in the final part of the afterglow phase almost all the emitted photons reach the observer. This time evolution of the visible area is crucial to the explanation of the GRB temporal structure. **Right)** Due to the extremely high and extremely varying Lorentz gamma factor, photons reaching the detector on the Earth at the same arrival time are actually emitted at very different times and positions. We represent here the surfaces of photon emission corresponding to selected values of the photon arrival time at the detector: the *equitemporal surfaces* (EQTS). Such surfaces differ from the ellipsoids described by Rees in the context of the expanding radio sources with typical Lorentz factor $\gamma \sim 4$ and constant. In fact, in GRB 991216 the Lorentz gamma factor ranges from 310 to 1. The EQTSes represented here (solid lines) correspond respectively to values of the arrival time ranging from $5\,s$ (the smallest surface on the left of the plot) to $60\,s$ (the largest one on the right). Each surface differs from the previous one by $5\,s$. To each EQTS contributes emission processes occurring at different values of the Lorentz gamma factor. The dashed lines are the boundaries of the visible area of the ABM pulse and the EMBH is located at position $(0, 0)$ in this plot. Note the different scale on the two axes, indicating the very high EQTS "effective eccentricity". The time interval from 5 s to 60 s has been chosen to encompass the E-APE emission, ranging from $\gamma = 308.8$ to $\gamma = 56.84$.

integral. There is in the present context the crucial point expressed in the RSTT paradigm that the relation between the laboratory time and the arrival time at the detector is a function of all the the previous Lorentz gamma factors in the history of the source since $\gamma = 1$ (see Fig. 9). In the definition of each EQTS, therefore, the entire previous past history of the source does concur and the EQTS surfaces become therefore a very refined and sensitive test of the correct description of the entire spacetime evolution of the source. In this case, we no longer have ellipsoids of constant eccentricity $\frac{v}{c}$. Since the velocity is strongly varying from point to point, we have more complicated surfaces like the profiles reported in Fig. 13 where at every point there will be a tangent ellipsoid of a given eccentricity, but such an ellipsoid varies in eccentricity from point to point (see Fig. 13 and section XXI). Any departure from the correct equation of motion strongly alters the EQTS surfaces and accordingly modifies all the results of the integrations based on the EQTS surfaces, e.g. the spectral distribution or the afterglow (Ruffini et al. [154]).

Having determined the EQTS surfaces we have computed the observed GRB flux at selected values of the photon arrival time at the detector, taking into due account the delayed contributions at different angles and we have presented the results in section XXII and Fig. 14.

We have then recomputed the afterglow emission of GRB 991216 taking into account all the effects due to this temporal spreading in the arrival time as well as the ones due to the dependency of the photon Doppler shift on the angle of displacement from the line of sight of the emission location (see section XXII). The result is reported in Fig. 14.

From now on all the afterglow intensities are estimated using this very complex and extensive numerical program

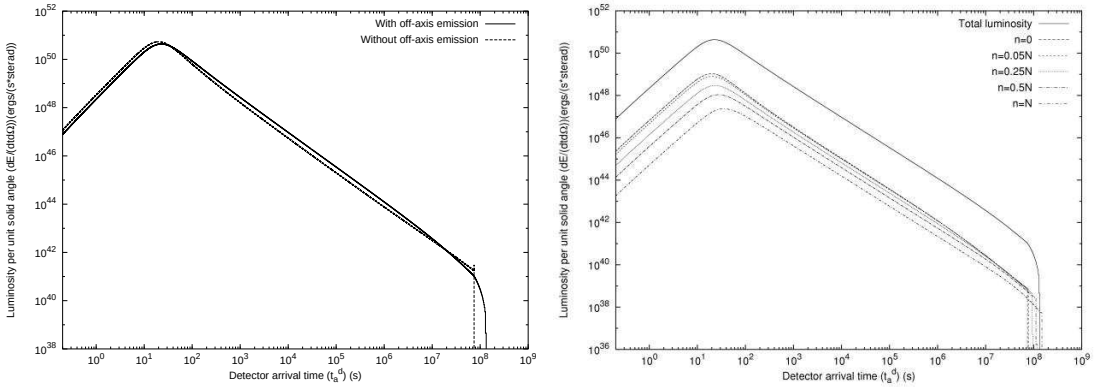

Figure 14: **Left)** The predicted afterglow curve for GRB 991216 assuming a constant ISM density equal to 1 particle/cm^3 and taking into account all the effects due to off-axis emission (solid line). For comparison we plot also the corresponding curve obtained in the simple radial approximation (dashed line). We see that this last curve falls sharply to zero when the ABM pulse reaches $\gamma = 1$, while the first one has a much smoother behavior due to the time delay in the arrival of the photons emitted at large ϑ. Recall that when γ tends to 1, the maximum allowed values of ϑ tend to 90°. **Right)** This figure shows how the radiation emitted from different angles contributes to the afterglow luminosity. The solid line on the top of the picture is the total luminosity as in the previous plots. The other dashed and dotted curves represent the radiation components corresponding to selected values of n in Eq.(181). From the upper to the lower one they corresponds respectively to $n = 0$, $n = 0.05N$, $n = 0.25N$, $n = 0.5N$, $n = N$, where in this plot $N = 200$. We can easily see that the radiation emitted at large angles ($n = N$) is time shifted with respect to that emitted near the line of sight ($n = 0$).

which is rooted in all previous history of the source: the general considerations on simple analytic expansion expressed in section XVIII are kept only as an heuristic procedure as a guideline to comprehend these more complex results.

K. The E-APE temporal substructures taking into account the off-axis emission

Having determined the EQTS surfaces, we have reconsidered the E-APE temporal substructure taking into due account the off-axis emission contribution (see Fig. 15 and section XXIII).

We can distinguish two different regimes corresponding respectively to $\gamma > 150$ and to $\gamma < 150$. In the E-APE region ($\gamma > 150$) the GRB substructure intensities indeed correlate with the ISM inhomogeneities. In this limited region (see peaks A, B, C) the Lorentz gamma factor of the ABM pulse ranges from $\gamma \sim 304$ to $\gamma \sim 200$. The boundary of the visible region is smaller than the thickness ΔR of the inhomogeneities (see Figs. 15,13, Tab. IV and Ruffini et al. [148, 153]). Under these conditions the adopted spherical symmetry for the density spikes is not only mathematically simpler but also fully justified. The angular spreading is not strong enough to wipe out the signal from the inhomogeneity spike.

As we descend in the afterglow ($\gamma < 150$), a border-line case occurs at peak D where $\gamma \sim 140$. There the visible region is comparable to the thickness ΔR: to fit the observed data a three dimensional description would be necessary, breaking the spherical symmetry and making the computation more difficult, but we do not foresee any conceptual difficulty. For the peaks E and F we have $\gamma \sim 50$: under these circumstances the boundary of the visible region becomes much larger than the thickness ΔR. The spherically symmetric description of the inhomogeneities is already enough to prove the overwhelming effect of the angular spreading and no three dimensional description is needed (Ruffini et al. [148, 153]).

From our analysis we can conclude that Dermer's expectations do indeed hold for $\gamma > 150$. However, as the gamma factor drops from $\gamma \sim 150$ to $\gamma \sim 1$ the intensity due to the inhomogeneities markedly decreases due to the angular spreading (events E and F). The initial Lorentz factor of the ABM pulse $\gamma \sim 310$ decreases very rapidly to $\gamma \sim 150$ as soon as a fraction of a typical ISM cloud is engulfed (see Figs. 15,8, Tab. IV and Ruffini et al. [148, 153]). We conclude that the "tomography" is indeed effective, but uniquely in the first ISM region close to the source and for GRBs with $\gamma > 150$.

It is then clear that no information on the nature of the GRB source can be inferred by the analysis of the T_{90}, nor by the intensity variability structure of the so-called "long burts": the only indirect information can be obtained

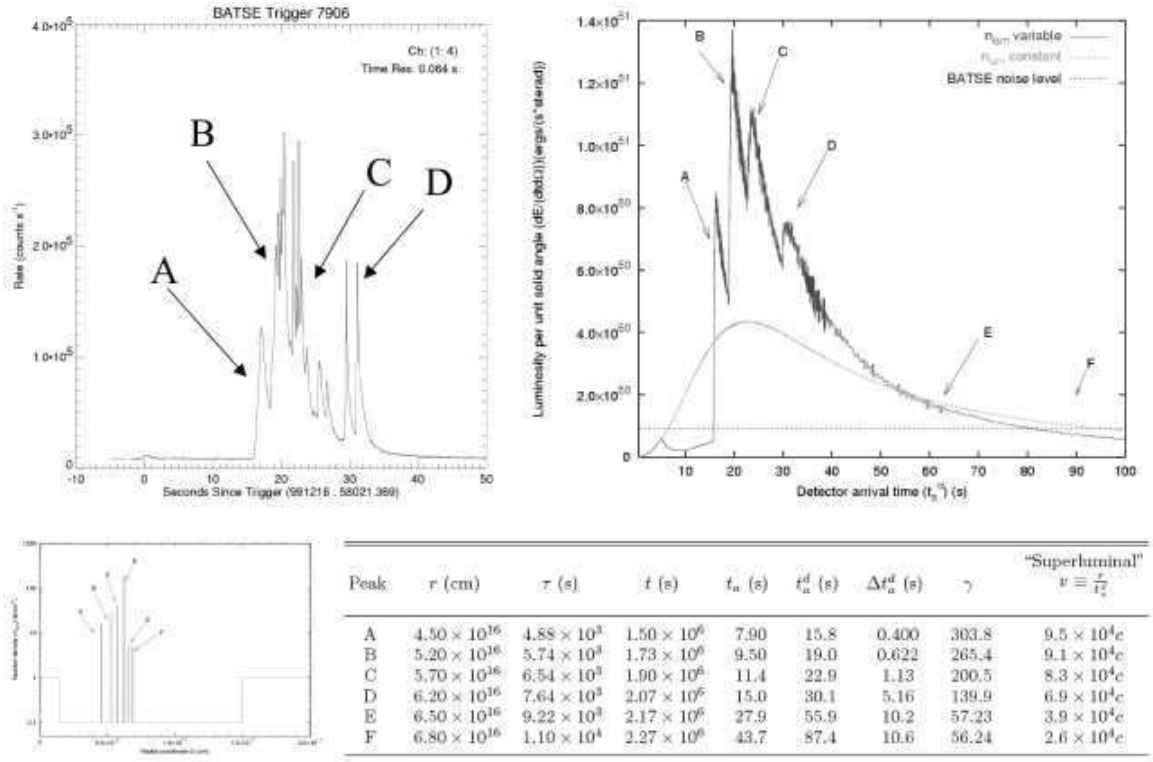

Peak	r (cm)	τ (s)	t (s)	t_a (s)	t_a^d (s)	Δt_a^d (s)	γ	"Superluminal" $v \equiv \frac{r}{t_a^d}$
A	4.50×10^{16}	4.88×10^{3}	1.50×10^{6}	7.90	15.8	0.400	303.8	$9.5 \times 10^{4}c$
B	5.20×10^{16}	5.74×10^{3}	1.73×10^{6}	9.50	19.0	0.622	265.4	$9.1 \times 10^{4}c$
C	5.70×10^{16}	6.54×10^{3}	1.90×10^{6}	11.4	22.9	1.13	200.5	$8.3 \times 10^{4}c$
D	6.20×10^{16}	7.64×10^{3}	2.07×10^{6}	15.0	30.1	5.16	139.9	$6.9 \times 10^{4}c$
E	6.50×10^{16}	9.22×10^{3}	2.17×10^{6}	27.9	55.9	10.2	57.23	$3.9 \times 10^{4}c$
F	6.80×10^{16}	1.10×10^{4}	2.27×10^{6}	43.7	87.4	10.6	56.24	$2.6 \times 10^{4}c$

Figure 15: In this figure we summarize the main results of the fit obtained by the EMBH model for the E-APE intensity in the case of GRB 991216 taking into account all off-axis contributions. The upper two diagrams represent respectively the observational data and the corresponding theoretically computed results. On the lower left the "mask" of the spherically symmetric density inhomogeneities with average $< n_{ism} >= 1\,\text{particle/cm}^3$ is represented. The table summarizes all the parameters corresponding to the inhomogeneities including the vary large apparent superluminal effect up to $\sim 10^5 c$. Details in section 23.

from the value of Lorentz gamma factor, which has to be $\gamma > 150$ in presence of significant observed substructure. In this sense compare and contrast the two cases of GRB 991216 and GRB 980425 where the γ value in the E-APE is found to be $\gamma \sim 120$ (see Ruffini [140]). The intensity substructures in the E-APE only carry information on the structure of the ISM clouds.

L. The observation of the iron lines in GRB 991216: on a possible GRB-supernova time sequence

In section XXV the program of using GRBs to further explore the region surrounding the newly formed EMBH is carried one step further by using the observations of the emitted iron lines (Piro et al., [120]). This gives us the opportunity to introduce the GRB-supernova time sequence (GSTS) paradigm and to introduce as well the novel concept of an *induced supernova explosion*. The GSTS paradigm reads: *A massive GRB-progenitor star P_1 of mass M_1 undergoes gravitational collapse to an EMBH. During this process a dyadosphere is formed and subsequently the P-GRB and the E-APE are generated in sequence. They propagate and impact, with their photon and neutrino components, on a second supernova-progenitor star P_2 of mass M_2. Assuming that both stars were generated approximately at the same time, we expect to have $M_2 < M_1$. Under some special conditions of the thermonuclear evolution of the supernova-progenitor star P_2, the collision of the P-GRB and the E-APE with the star P_2 can induce its supernova explosion.*

Using the result presented in Tab. I and in all preceding sections, the GSTS paradigm is illustrated in the case of

GRB 991216. Some general considerations on the nature of the supernova progenitor star are also advanced.

Some general considerations on the EMBH formation are presented in section XXVI. The general conclusions are presented in section XXIX.

We now proceed to a more detailed presentation of the results and we refer to the already published material for the complete details.

III. THE ZEROTH ERA: THE PROCESS OF GRAVITATIONAL COLLAPSE AND THE FORMATION OF THE DYADOSPHERE

We first recall the three theoretical results which lie at the basis of the EMBH theory.

In 1971 in the article *"Introducing the Black Hole"* (Ruffini & Wheeler [141]), the theorem was advanced that the most general black hole is characterized uniquely by three independent parameters: the mass-energy M, the angular momentum L and the charge Q making it an EMBH. Such an ansatz, which came to be known as the "uniqueness theorem" has turned out to be one of the most difficult theorems to be proven in all of physics and mathematics. The progress in the proof has been authoritatively summarized by Carter [24]. The situation can be considered satisfactory from the point of view of the physical and astrophysical considerations. Nevertheless some fundamental mathematical and physical issues concerning the most general perturbation analysis of an EMBH are still the topic of active scientific discussion (Bini et al. [15]).

In 1971 it was shown that the energy extractable from an EMBH is governed by the mass-energy formula (Christodoulou & Ruffini [30]),

$$E_{BH}^2 = M^2c^4 = \left(M_{\rm ir}c^2 + \frac{Q^2}{2\rho_+}\right)^2 + \frac{L^2c^2}{\rho_+^2}, \tag{1}$$

with

$$\frac{1}{\rho_+^4}\left(\frac{G^2}{c^8}\right)\left(Q^4 + 4L^2c^2\right) \leq 1, \tag{2}$$

where

$$S = 4\pi\rho_+^2 = 4\pi(r_+^2 + \frac{L^2}{c^2M^2}) = 16\pi\left(\frac{G^2}{c^4}\right)M_{\rm ir}^2, \tag{3}$$

is the horizon surface area, $M_{\rm ir}$ is the irreducible mass, r_+ is the horizon radius and ρ_+ is the quasi-spheroidal cylindrical coordinate of the horizon evaluated at the equatorial plane. Extreme EMBHs satisfy the equality in Eq.(2). Up to 50% of the mass-energy of an extreme EMBH can in principle be extracted by a special set of transformations: the reversible transformations (Christodoulou & Ruffini [30]).

In 1975, generalizing some previous results of Zaumen [191], and Gibbons [67], Damour & Ruffini [33] showed that the vacuum polarization process *à la* Heisenberg-Euler-Schwinger (Heisenberg & Euler [78], Schwinger [172]) created by an electric field of strength larger than

$$\mathcal{E}_c = \frac{m_e^2c^3}{\hbar e} \tag{4}$$

can indeed occur in the field of a Kerr-Newmann EMBH. Here m_e and e are respectively the mass and charge of the electron. There Damour and Ruffini considered an axially symmetric EMBH, due to the presence of rotation, and limited themselves to EMBH masses larger then the upper limit of a neutron star for astrophysical applications. They purposely avoided all complications of black holes with mass smaller then the dual electron mass of the electron $\left(m_e^\star = \frac{c\hbar}{Gm_e} = \frac{m_{Planck}^2}{m_e}\right)$ which may lead to quantum evaporation processes (Hawking [76]). They pointed out that:

1. The vacuum polarization process can occur for an EMBH mass larger than the maximum critical mass for neutron stars all the way up to $7.2 \times 10^6 M_\odot$.
2. The process of pair creation occurs on very short time scales, typically $\frac{\hbar}{m_ec^2}$, and is an almost perfect reversible process, in the sense defined by Christodoulou-Ruffini, leading to a very efficient mechanism of extracting energy from an EMBH.
3. The energy generated by the energy extraction process of an EMBH was found to be of the order of 10^{54} erg, released almost instantaneously. They concluded at the time *"this work naturally leads to a most simple model for the explanation of the recently discovered γ-ray bursts"*.

After the discovery of the afterglow of GRBs and the determination of the cosmological distance of their sources we noticed the coincidence between the theoretically predicted energetics and the observed ones in Damour & Ruffini [33]: we returned to our theoretical results developing some new basic theoretical concepts (Preparata et al. [123, 124], Ruffini [137], Ruffini et al. [142, 143]), which have led to the EMBH theory.

As a first simplifying assumption we have developed our considerations in the absence of rotation with spherically symmetric distributions. The space-time is then described by the Reissner-Nordström geometry, whose spherically symmetric metric is given by

$$d^2s = g_{tt}(r)d^2t + g_{rr}(r)d^2r + r^2d^2\theta + r^2\sin^2\theta d^2\phi \ , \tag{5}$$

where $g_{tt}(r) = -\left[1 - \frac{2GM}{c^2r} + \frac{Q^2G}{c^4r^2}\right] \equiv -\alpha^2(r)$ and $g_{rr}(r) = \alpha^{-2}(r)$.

The first new result we obtained is that the pair creation process does not occur at the horizon of the EMBH: it extends over the entire region outside the horizon in which the electric field exceeds the critical value given by Eq. 4. Since the electric field in the Reissner-Nordström geometry has only a radial component given by (see Ruffini [136])

$$\mathcal{E}\,(r) = \frac{Q}{r^2}\,, \tag{6}$$

this region extends from the horizon radius

$$r_+ \ = \ 1.47 \cdot 10^5 \mu (1 + \sqrt{1-\xi^2})\ \mathrm{cm} \tag{7}$$

out to an outer radius (Ruffini [137])

$$r^\star = \left(\frac{\hbar}{mc}\right)^{\frac{1}{2}} \left(\frac{GM}{c^2}\right)^{\frac{1}{2}} \left(\frac{m_{\rm p}}{m}\right)^{\frac{1}{2}} \left(\frac{e}{q_{\rm p}}\right)^{\frac{1}{2}} \left(\frac{Q}{\sqrt{G}M}\right)^{\frac{1}{2}} = 1.12 \cdot 10^8 \sqrt{\mu\xi}\ \mathrm{cm}, \tag{8}$$

where we have introduced the dimensionless mass and charge parameters $\mu = \frac{M}{M_\odot}$, $\xi = \frac{Q}{(M\sqrt{G})} \leq 1$, see Fig. 4.

The second new result has been to realize that the local number density of electron and positron pairs created in this region as a function of radius is given by

$$n_{e^+e^-}(r) = \frac{Q}{4\pi r^2 \left(\frac{\hbar}{mc}\right) e} \left[1 - \left(\frac{r}{r^\star}\right)^2\right] \ , \tag{9}$$

and consequently the total number of electron and positron pairs in this region is

$$N^\circ_{e^+e^-} \simeq \frac{Q - Q_c}{e} \left[1 + \frac{(r^\star - r_+)}{\frac{\hbar}{mc}}\right], \tag{10}$$

where $Q_c = \mathcal{E}_c r_+^2$.

The total number of pairs is larger by an enormous factor $r^\star/\left(\hbar/mc\right) > 10^{18}$ than the value Q/e which a naive estimate of the discharge of the EMBH would have predicted. Due to this enormous amplification factor in the number of pairs created, the region between the horizon and $r^\star$ is dominated by an essentially high density neutral plasma of electron-positron pairs. We have defined this region as the dyadosphere of the EMBH from the Greek duas, duadsos for pairs. Consequently we have called $r^\star$ the dyadosphere radius $r^\star \equiv r_{\rm ds}$ (Preparata et al. [123, 124], Ruffini [137]). The vacuum polarization process occurs as if the entire dyadosphere are subdivided into a concentric set of shells of capacitors each of thickness $\hbar/m_ec$ and each producing a number of e^+e^- pairs on the order of $\sim Q/e$ (see Fig. 4). The energy density of the electron-positron pairs is given by

$$\epsilon(r) = \frac{Q^2}{8\pi r^4}\left(1 - \left(\frac{r}{r_{\rm ds}}\right)^4\right) \ , \tag{11}$$

(see Figs. 2–3 of Preparata et al. [123]). The total energy of pairs converted from the static electric energy and deposited within the dyadosphere is then

$$E_{\rm dya} = \frac{1}{2}\frac{Q^2}{r_+}\left(1 - \frac{r_+}{r_{\rm ds}}\right)\left[1 - \left(\frac{r_+}{r_{\rm ds}}\right)^4\right] \ . \tag{12}$$

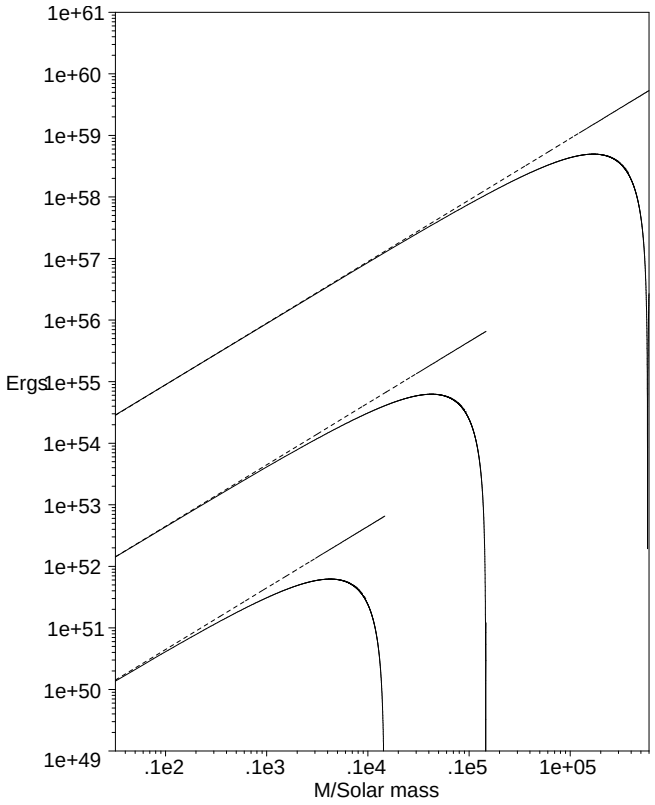

Figure 16: The energy extracted by the process of vacuum polarization is plotted (solid lines) as a function of the mass M in solar mass units for selected values of the charge parameter $\xi = 1, 0.1, 0.01$ (from top to bottom) for an EMBH, the case $\xi = 1$ reachable only as a limiting process. For comparison we have also plotted the maximum energy extractable from an EMBH (dotted lines) given by eq. (1). Details in Preparata et al. [125].

As we will see in the following this is one of the two fundamental parameters of the EMBH theory (see Fig. 17). In the limit $\frac{r_+}{r_{\rm ds}} \to 0$, Eq.(12) leads to $E_{\rm dya} \to \frac{1}{2}\frac{Q^2}{r_+}$, which coincides with the energy extractable from EMBHs by reversible processes ($M_{\rm ir} = {\rm const.}$), namely $E_{BH} - M_{\rm ir} = \frac{1}{2}\frac{Q^2}{r_+}$ (Christodoulou & Ruffini [30]), see Fig. 16. Due to the very large pair density given by Eq.(9) and to the sizes of the cross-sections for the process $e^+e^- \leftrightarrow \gamma + \gamma$, the system is expected to thermalize to a plasma configuration for which

$$n_{e^+} = n_{e^-} \sim n_\gamma \sim n^\circ_{e^+e^-}, \tag{13}$$

where $n^\circ_{e^+e^-}$ is the total number density of e^+e^--pairs created in the dyadosphere (see Preparata et al. [123, 124]).

The third new result which we have introduced for simplicity is that for a given E_{dya} we have assumed either a constant average energy density over the entire dyadosphere volume, or a more compact configuration with energy density equal to the peak value. These are the two possible initial conditions for the evolution of the dyadosphere (see Fig. 17).

These three old and three new theoretical results permit a good estimate of the general energetics processes originating in the dyadosphere, assuming an already formed EMBH. In reality, if the data become accurate enough, the full dynamical description of the dyadosphere formation mentioned above will be needed in order to follow all the general relativistic effects and characteristic time scales of the approach to the EMBH horizon (Cherubini et al. [28], Ruffini & Vitagliano [156, 157], Ruffini et al. [159] see also section XXVI).

Below we shall concentrate on the dynamical evolution of the electron-positron plasma created in the dyadosphere. We shall first examine in the next three sections the governing equations necessary to approach such a dynamical description.

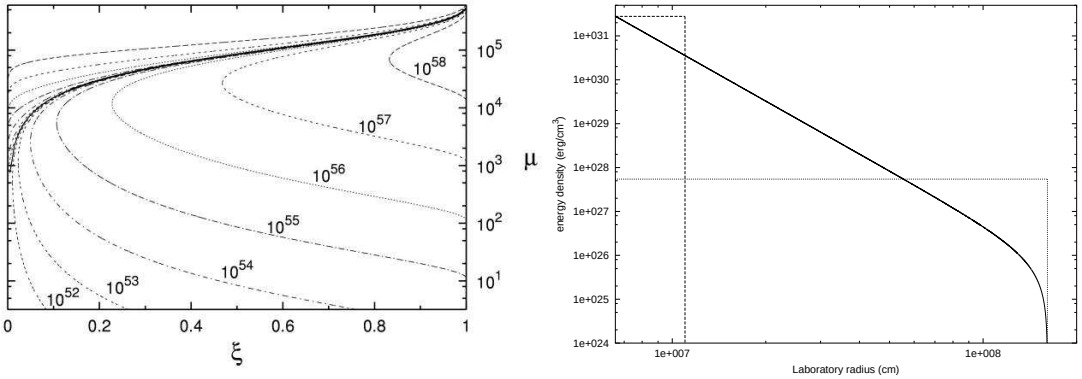

Figure 17: **Left)** Selected lines corresponding to fixed values of the E_{dya} are given as a function of the two parameters μ ξ, only the solutions below the continuous heavy line are physically relevant.The configurations above the continuous heavy lines correspond to unphysical solutions with $r_{\rm ds} < r_+$. **Right)** Two different approximations for the energy density profile inside the dyadosphere. The first one (dashed line) fixes the energy density equal to its peak value, and computes an "effective" dyadosphere radius accordingly. The second one (dotted line) fixes the dyadosphere radius to its correct value, and assumes an uniform energy density over the dyadosphere volume. The total energy in the dyadosphere is of course the same in both cases. The solid curve represents the real energy density profile.

IV. THE HYDRODYNAMICS AND THE RATE EQUATIONS FOR THE PLASMA OF e^+e^--PAIRS

The evolution of the e^+e^--pair plasma generated in the dyadosphere has been treated in two papers (Ruffini et al. [142, 143]). We recall here the basic governing equations in the most general case in which the plasma fluid is composed of e^+e^--pairs, photons and baryonic matter. The plasma is described by the stress-energy tensor

$$T^{\mu\nu} = pg^{\mu\nu} + (p+\rho)U^\mu U^\nu \,, \tag{14}$$

where ρ and p are respectively the total proper energy density and pressure in the comoving frame of the plasma fluid and U^μ is its four-velocity, satisfying

$$g_{tt}(U^t)^2 + g_{rr}(U^r)^2 = -1 \,, \tag{15}$$

where U^r and U^t are the radial and temporal contravariant components of the 4-velocity.

The conservation law for baryon number can be expressed in terms of the proper baryon number density n_B

$$\begin{aligned}(n_B U^\mu)_{;\mu} &= g^{-\frac{1}{2}}(g^{\frac{1}{2}} n_B U^\nu)_{,\nu} \\ &= (n_B U^t)_{,t} + \frac{1}{r^2}(r^2 n_B U^r)_{,r} = 0 \,.\end{aligned} \tag{16}$$

The radial component of the energy-momentum conservation law of the plasma fluid reduces to

$$\frac{\partial p}{\partial r} + \frac{\partial}{\partial t}\left((p+\rho)U^t U_r\right) + \frac{1}{r^2}\frac{\partial}{\partial r}\left(r^2(p+\rho)U^r U_r\right) - \frac{1}{2}(p+\rho)\left[\frac{\partial g_{tt}}{\partial r}(U^t)^2 + \frac{\partial g_{rr}}{\partial r}(U^r)^2\right] = 0 \,. \tag{17}$$

The component of the energy-momentum conservation law of the plasma fluid equation along a flow line is

$$\begin{aligned}U_\mu (T^{\mu\nu})_{;\nu} &= -(\rho U^\nu)_{;\nu} - p(U^\nu)_{;\nu}, \\ &= -g^{-\frac{1}{2}}(g^{\frac{1}{2}}\rho U^\nu)_{,\nu} - pg^{-\frac{1}{2}}(g^{\frac{1}{2}}U^\nu)_{,\nu} \\ &= (\rho U^t)_{,t} + \frac{1}{r^2}(r^2 \rho U^r)_{,r} \\ &+ p\left[(U^t)_{,t} + \frac{1}{r^2}(r^2 U^r)_{,r}\right] = 0 \,.\end{aligned} \tag{18}$$

Defining the total proper internal energy density ϵ and the baryonic mass density ρ_B in the comoving frame of the plasma fluid,

$$\epsilon \equiv \rho - \rho_B, \qquad \rho_B \equiv n_B m c^2 \,, \tag{19}$$

and using the law (16) of baryon-number conservation, from Eq. (18) we have

$$(\epsilon U^\nu)_{;\nu} + p(U^\nu)_{;\nu} = 0 \ . \tag{20}$$

Recalling that $\frac{dV}{d\tau} = V(U^\mu)_{;\mu}$, where V is the comoving volume and τ is the proper time for the plasma fluid, we have along each flow line

$$\frac{d(V\epsilon)}{d\tau} + p\frac{dV}{d\tau} = \frac{dE}{d\tau} + p\frac{dV}{d\tau} = 0 \ , \tag{21}$$

where $E = V\epsilon$ is the total proper internal energy of the plasma fluid. We express the equation of state by introducing a thermal index $\Gamma(\rho, T)$

$$\Gamma = 1 + \frac{p}{\epsilon} \ . \tag{22}$$

We now turn to the second set of governing equations describing the evolution of the e^+e^- pairs. Letting n_{e^-} and n_{e^+} be the proper number densities of electrons and positrons associated with pairs and $n^b_{e^-}$ the proper number densities of ionized electrons, we clearly have

$$n_{e^-} = n_{e^+} = n_{\rm pair}, \qquad n^b_{e^-} = \bar{Z} n_B, \tag{23}$$

where $n_{\rm pair}$ is the number of e^+e^- pairs and $\bar{Z}$ the average atomic number $\frac{1}{2} < \bar{Z} < 1$ ($\bar{Z} = 1$ for hydrogen atom and $\bar{Z} = \frac{1}{2}$ for general baryonic matter). The rate equation for electrons and positrons gives,

$$\begin{aligned}
(n_{e^+}U^\mu)_{;\mu} &= (n_{e^+}U^t)_{,t} + \frac{1}{r^2}(r^2 n_{e^+}U^r)_{,r} \\
&= \overline{\sigma v}\big[(n_{e^-}(T) + n^b_{e^-}(T))n_{e^+}(T) \\
&- (n_{e^-} + n^b_{e^-})n_{e^+}\big], \qquad (24) \\
(n_{e^-}U^\mu)_{;\mu} &= (n_{e^-}U^t)_{,t} + \frac{1}{r^2}(r^2 n_{e^-}U^r)_{,r} \\
&= \overline{\sigma v}\left[n_{e^-}(T)n_{e^+}(T) - n_{e^-}n_{e^+}\right], \qquad (25) \\
(n^b_{e^-}U^\mu)_{;\mu} &= (n^b_{e^-}U^t)_{,t} + \frac{1}{r^2}(r^2 n^b_{e^-}U^r)_{,r} \\
&= \overline{\sigma v}\left[n^b_{e^-}(T)n_{e^+}(T) - n^b_{e^-}n_{e^+}\right], \qquad (26)
\end{aligned}$$

where $\overline{\sigma v}$ is the mean of the product of the annihilation cross-section and the thermal velocity of the electrons and positrons, $n_{e^\pm}(T)$ are the proper number densities of electrons and positrons associated with the pairs, given by appropriate Fermi integrals with zero chemical potential, and $n^b_{e^-}(T)$ is the proper number density of ionized electrons, given by appropriate Fermi integrals with non-zero chemical potential μ_e at an appropriate equilibrium temperature T. These rate equations can be reduced to

$$\begin{aligned}
(n_{e^\pm}U^\mu)_{;\mu} &= (n_{e^\pm}U^t)_{,t} + \frac{1}{r^2}(r^2 n_{e^\pm}U^r)_{,r} \\
&= \overline{\sigma v}\big[n_{e^-}(T)n_{e^+}(T) - n_{e^-}n_{e^+}\big], \qquad (27) \\
(n^b_{e^-}U^\mu)_{;\mu} &= (n^b_{e^-}U^t)_{,t} + \frac{1}{r^2}(r^2 n^b_{e^-}U^r)_{,r} = 0, \qquad (28) \\
Frac &\equiv \frac{n_{e^\pm}}{n_{e^\pm}(T)} = \frac{n^b_{e^-}(T)}{n^b_{e^-}}. \qquad (29)
\end{aligned}$$

Equation (28) is just the baryon-number conservation law (16) and (29) is a relationship satisfied by $n_{e^\pm}, n_{e^\pm}(T)$ and $n^b_{e^-}, n^b_{e^-}(T)$.

The equilibrium temperature T is determined by the thermalization processes occurring in the expanding plasma fluid with a total proper energy density ρ governed by the hydrodynamical equations (16,17,18). We have

$$\rho = \rho_\gamma + \rho_{e^+} + \rho_{e^-} + \rho^b_{e^-} + \rho_B, \tag{30}$$

where ρ_γ is the photon energy density, $\rho_B \simeq m_B c^2 n_B$ is the baryonic mass density which is considered to be non-relativistic in the range of temperature T under consideration, and $\rho_{e^\pm}$ is the proper energy density of electrons and positrons pairs given by

$$\rho_{e^\pm} = \frac{n_{e^\pm}}{n_{e^\pm}(T)}\rho_{e^\pm}(T), \tag{31}$$

where $n_{e^\pm}$ is obtained by integration of Eq.(27) and $\rho_{e^\pm}(T)$ is the proper energy density of electrons(positrons) obtained from zero chemical potential Fermi integrals at the equilibrium temperature T. On the other hand $\rho^b_{e^-}$ is the energy density of the ionized electrons coming from the ionization of baryonic matter

$$\rho^b_{e^-} = \frac{n^b_{e^-}}{n^b_{e^-}(T)}\rho^b_{e^-}(T), \tag{32}$$

where $n^b_{e^-}$ is obtained by integration of Eq.(28) and $\rho_{e^-}(T)$ is the proper energy density of ionized electrons obtained from an appropriate Fermi integral of non-zero chemical potential μ_e at the equilibrium temperature T.

Having intrinsically defined the equilibrium temperature T in Eq.(30), we can also analogously evaluate the total pressure

$$p = p_\gamma + p_{e^+} + p_{e^-} + p^b_{e^-} + p_B, \tag{33}$$

where p_γ is the photon pressure, $p_{e^\pm}$ and $p^b_{e^-}$ are given by

$$p_{e^\pm} = \frac{n_{e^\pm}}{n_{e^\pm}(T)}p_{e^\pm}(T), \tag{34}$$

$$p^b_{e^-} = \frac{n^b_{e^-}}{n^b_{e^-}(T)}p^b_{e^-}(T), \tag{35}$$

the pressures $p_{e^\pm}(T)$ are determined by zero chemical potential Fermi integrals, and $p^b_{e^-}(T)$ is the pressure of the ionized electrons, evaluated by an appropriate Fermi integral of non-zero chemical potential μ_e at the equilibrium temperature T. In Eq.(33), the ion pressure p_B is negligible by comparison with the pressures $p_{\gamma,e^\pm,e^-}(T)$, since baryons and ions are expected to be nonrelativistic in the range of temperature T under consideration. Finally using Eqs.(30,33) we compute the thermal factor Γ of the equation of state (22).

It is clear that the entire set of equations considered above, namely Eqs.(16,17,18) with equation of state given by Eq.(22) and the rate equation (27), have to be integrated satisfying the total energy conservation for the system. The boundary conditions adopted here are simply purely ingoing conditions at the horizon and purely outgoing conditions at radial infinity. The calculation is initiated by depositing a proper energy density (11) between the Reissner-Nordström horizon radius r_+ and the dyadosphere radius r_{ds}, following the approximation presented in Fig.16 The total energy deposited is given by Eq.(12).

V. THE EQUATIONS LEADING TO THE RELATIVE SPACE-TIME TRANSFORMATIONS

In order to relate the above hydrodynamic and pair equations with the observations we need the governing equations relating the comoving time to the laboratory time corresponding to an inertial reference frame in which the EMBH is at rest and finally to the time measured at the detector, which must also include the effect of the cosmological expansion. These transformations have been the object of the Relative space-time Transformations (RSTT) Paradigm, (Ruffini et al. [144]).

For signals emitted by a pulse moving with velocity v in the laboratory frame (see also Ruffini et al. [144]), we have the following relation between the interval of arrival time Δt_a and the corresponding interval of laboratory time Δt (see Fig. 18):

$$\Delta t_a = \left(t_0 + \Delta t + \frac{R_0 - r}{c}\right) - \left(t_0 + \frac{R_0}{c}\right) = \Delta t - \frac{r}{c}\,. \tag{36}$$

For simplicity in what follows we indicate by t_a the interval of arrival time measured from the reception of a light signal emitted at the onset of the gravitational collapse. Analogously, t indicates the laboratory time interval measured from the time of the gravitational collapse. In this case, Eq.(36) can be written simply as:

$$t_a = t - \frac{r}{c} = t - \frac{\int_0^t v\,(t')\,dt' + r_{ds}}{c} = t - \int_0^t \frac{\sqrt{\gamma^2\,(t') - 1}}{\gamma\,(t')}dt' - \frac{r_{ds}}{c}\,, \tag{37}$$

where, as usual, $\gamma\,(t') = 1/\sqrt{1 - v^2\,(t')\,/c^2}$ and the dyadosphere radius r_{ds} is the value of r at $t = 0$. It is important to stress that, although there is the presence of the Lorentz gamma factor, Eq.(37) is not a Lorentz transformation,

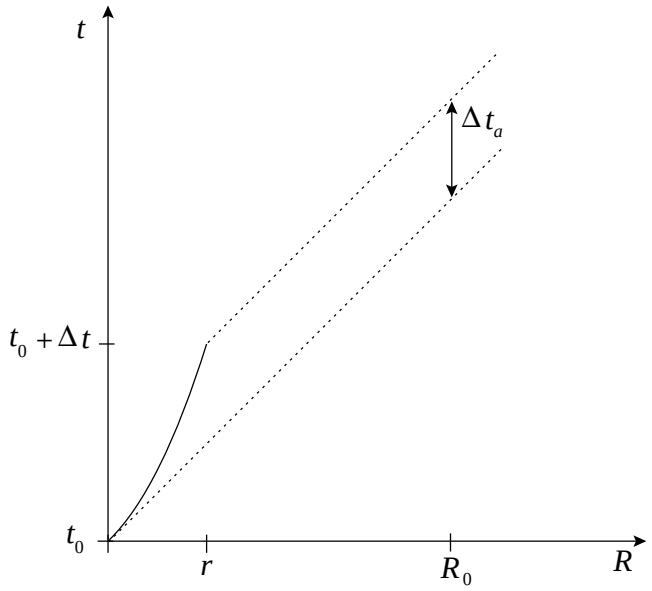

Figure 18: This qualitative diagram illustrates the relation between the laboratory time interval Δt and the arrival time interval Δt_a for a pulse moving with velocity v in the laboratory time (solid line). We have indicated here the case where the motion of the source has a nonzero acceleration. The arrival time is measured using light signals emitted by the pulse (dotted lines). R_0 is the distance of the observer from the EMBH, t_0 is the laboratory time corresponding to the onset of the gravitational collapse, and r is the radius of the expanding pulse at a time $t = t_0 + \Delta t$. See also Ruffini et al. [144].

which by its own nature is linear and refers to a specific value of the Lorentz gamma factor at a given laboratory time. The transformation in Eq.(37) is nonlinear in the Lorentz gamma factor and do depend on all the values of the gamma factor of the source from the time $t = 0$ to the laboratory time t. This transformation is the price to pay to relate the laboratory time t, relativistically correct, to the "highly pathological" time usually considered by the astronomers, even in the case of object moving close to the speed of light, against the correct synchronization procedures established by Einstein in his classical paper of 1905 (Einstein [47]). We consider here only the photons emitted along the line of sight from the external surface of the pulse. The arrival time spreading due to the angular dependence and that due to the thickness has also been given (see section XXI and Ruffini et al. [148, 151]). The solution of Eq.(37) has the expansion:

$$t_a = t - \frac{r_{ds}}{c} - \frac{v\,(0)}{c}t - \frac{1}{2}\frac{v'\,(0)}{c}t^2 - \frac{1}{3}\frac{v''\,(0)}{c}t^3 - \ldots, \tag{38}$$

so the relation between t_a and t in the specific case of GRBs is very highly nonlinear: it is sufficient to recall that in the early GRB phases we are witnessing the strongest acceleration ever recorded in the universe, since the PEM pulse goes from Lorentz factor $\gamma = 1$ to Lorentz factor $\gamma = 1000$ in 10^2 seconds in the laboratory time (see section VII). The series in Eq.(38) will definitely converge, but the number of terms needed to reach a good approximation will strongly depend on the variability of the functions around the initial values $\gamma = 1$. It is clear that the precise knowledge of t_a as a function of the laboratory time, which is indeed essential for any physical interpretation of GRB data, depends on the definite integral given in Eq.(37) whose limits in the laboratory time extend from the onset of the gravitational collapse to the time t relevant for the observations. Such an integral depends on all previous values of the Lorentz gamma factor in the history of the source and is not generally expressible by a simple linear relation or even by any explicit analytic relation since we are dealing with processes with variable gamma factor unprecedented in the entire realm of physics (see Figs. 8 and Fig. 9). This is the crucial point of the RSTT paradigm (Ruffini et al. [144]) and this is the reason why we have spent a very large amount of work to develop the exact equations of motion of all different eras of the GRB phenomenon, starting from the onset of gravitational collapse and the creation of dyadosphere (see the following sections). It is clear then that, in order to express the arrival time t_a and the radial coordinate of the source at the start of the afterglow phase, we need the explicit knowledge of all the previous eras of the GRB

phenomenon, starting from $\gamma = 1$ (Ruffini et al. [144]).

What has been currently done in the literature, is an extremely different approach. First they have assumed γ constant. Therefore Eq.(37) has been modified in:

$$t_a = t - \frac{\sqrt{\gamma^2 - 1}}{\gamma} \int_0^t dt' - \frac{r_{ds}}{c} \simeq t - \frac{\sqrt{\gamma^2 - 1}}{\gamma} t \,, \tag{39}$$

where in the last approximation the contribution of the initial size of the source has been neglected. Even the validity of this last approximation has to be actually carefully verified since it is only valid in the late phases of the GRB expansion. They have further assumed $\gamma \gg 1$ and obtained:

$$t_a \simeq t - \left(1 - \frac{1}{2\gamma^2}\right) t = \frac{t}{2\gamma^2} \,. \tag{40}$$

At this stage, they emphasize the existence of a linear relation between the arrival time t_a and the laboratory time t. After this they proceed in two different directions. One to assume (see e.g. Fenimore et al. [48], Fenimore [49], Fenimore et al. [50], Sari & Piran [165], Waxman [186])

$$t_a = t/\left(2\gamma^2\left(t\right)\right) \,, \tag{41}$$

concurrently advancing the belief that the relation between the arrival time and the laboratory time does not depend from an integral on all the previous values of the gamma Lorentz factor of the source but from the instantaneous value of the gamma Lorentz factor at the time t, much like in a Lorentz transformation. This claim is clearly absurd from a physical point of view.

They further assume (see e.g. Panaitescu & Mészáros [113], Piran [116], Sari [163, 164] and references therein)

$$\delta t_a = \delta t/\left(2\gamma^2\left(t\right)\right) \text{ or, alternatively, } dt_a = dt/\left(2\gamma^2\left(t\right)\right) \,, \tag{42}$$

and they proceed to develop all the observable quantities of the GRB phenomenon by integrating using the "differential" given in Eq.(42), reaching clearly meaningless results. As we show later, this also leads to the unfortunate attempt to obtain the gamma Lorentz factor and its time variability from the astrophysical data of the afterglow, neglecting all previous GRB source history what is clearly physically and astrophysically impossible.

Having established the correct relations between the laboratory time t and the arrival time t_a in Eq.(37), we now proceed to relate the time in the laboratory frame t to the time in the detector frame t_a^d. We have to do one additional step: the two frames are related by a transformation which is a function of the cosmological expansion. We recall that the geometry of the space-time of the universe is described by the Robertson-Walker metric:

$$ds^2 = dt^2 - \mathcal{R}^2(t) \left(\frac{dr^2}{1 - kr^2} + r^2 d\vartheta^2 + r^2 sin\vartheta^2 d\varphi^2\right), \tag{43}$$

where $\mathcal{R}\left(t\right)$ is the cosmic scale factor and k is a constant related to the curvature of the three-dimensional space ($k = 0, +1, -1$ corresponds to flat, close and open space respectively). The wavelength of an electromagnetic wave traveling from the point $P_1(t_1, r_1, \vartheta_1, \varphi_1)$ to the point $P_\circ(t_\circ, r_\circ, \vartheta_\circ, \varphi_\circ)$ where the observer is located is related to the red-shift parameter z by

$$z = \frac{\lambda_\circ - \lambda_1}{\lambda_1}, \tag{44}$$

where $\lambda_\circ$ is the wavelength of the radiation for the observer and λ_1 for the emitter. We have the following general relation:

$$1 + z = (1 + z_u)(1 + z_o)(1 + z_s) \,, \tag{45}$$

where z is the total redshift due to the motion of the source z_s, the motion of the observer z_o and the cosmological redshift z_u. In the following we will assume $z_o << 1$ and $z_s << 1$ so $z = z_u$. In terms of the scale factor $\mathcal{R}\left(t\right)$ the relation (44) gives

$$\frac{\lambda_\circ}{\lambda_1} = \frac{\mathcal{R}\left(t_o\right)}{\mathcal{R}\left(t_1\right)} = 1 + z = \frac{\omega_1}{\omega_0} \tag{46}$$

where ω_1 and ω_0 are the frequencies associated to λ_1 and λ_0 respectively. This frequency ratio then relates the time elapsing at the source with the time elapsing at the detector due to the cosmological expansion.

We can now define the corrected arrival time t_a^d measured at the detector, which is related to t_a, clearly defined by Eq.(37), by

$$t_a^d = t_a\,(1+z)\,, \tag{47}$$

where z is the cosmological redshift of the GRB source. In the case of GRB 991216 we have $z \simeq 1.00$.

The observed flux is the flux which crosses the surface $4\pi(\mathcal{R}\,(t_o)\,r)^2$ but this flux is lower by a factor $1+z$ due to the redshift energy of the photons and by another factor $1+z$ due to the fact that the number of photons at reception is less than the number at emission. Thus we can define a luminosity distance by:

$$d_L^2 = \mathcal{R}_o^2 r^2 (1+z)^2. \tag{48}$$

Then the observed flux is related to the absolute luminosity of the GRB by the following relation:

$$l = \frac{L}{4\pi d_L^2}\,, \tag{49}$$

where the luminosity distance d_L is simply related to the proper distance $d_p = \mathcal{R}_o r$ by $d_L = d_p(1+z)$. The observed total fluence f is related to the total energy E of the GRB by the following relation:

$$f = \frac{E(1+z)}{4\pi d_L^2} \tag{50}$$

Then the cosmological effect is taken into account by the definition of the proper distance $\mathcal{R}_o r$ which depends on the cosmological parameters: the Hubble constant $H_\circ = \dot{\mathcal{R}}\,(t_\circ)\,/\mathcal{R}\,(t_\circ)$ at time $t_\circ$ and the matter density $\rho_\circ$ or $\Omega_M = \rho_\circ/\rho_{crit}$, where $\rho_{crit} = \frac{3H_\circ^2}{8\pi G}$.

The computation of the proper distance is then simply given by the relation :

$$d_p = \frac{c}{H_o}\int_0^z \frac{dz}{F(z)}\,, \tag{51}$$

where $F(z) = \sqrt{\Omega_M(1+z)^3}$.

In the case of the Friedman flat universe, $\Omega_M = 1$ and we have:

$$d_p(z) = \frac{2c}{H_o}\left[1 - \frac{1}{\sqrt{1+z}}\right]. \tag{52}$$

So the measurement of the redshift gives us the luminosity distance via a cosmological scenario. With the measurement of the flux we can deduce the proper luminosity of the burst and from the measurement of the total fluence the total energy so we are then able to find the E_{dya}.

VI. THE NUMERICAL INTEGRATION OF THE HYDRODYNAMICS AND THE RATE EQUATIONS

A. The Livermore code

A computer code (Wilson et al. [188, 189]) has been used to evolve the spherically symmetric general relativistic hydrodynamic equations starting from the dyadosphere (Ruffini et al. [142]).

We define the generalized gamma factor γ and the radial 3-velocity in the laboratory frame V^r

$$\gamma \equiv \sqrt{1 + U^r U_r}, \qquad V^r \equiv \frac{U^r}{U^t}. \tag{53}$$

From Eqs.(5, 15), we then have

$$(U^t)^2 = -\frac{1}{g_{tt}}(1 + g_{rr}(U^r)^2) = \frac{1}{\alpha^2}\gamma^2. \tag{54}$$

Following Eq.(19), we also define

$$E \equiv \epsilon\gamma, \qquad D \equiv \rho_B\gamma, \quad \text{and} \quad \tilde{\rho} \equiv \rho\gamma \tag{55}$$

so that the conservation law of baryon number (16) can then be written as

$$\frac{\partial D}{\partial t} = -\frac{\alpha}{r^2}\frac{\partial}{\partial r}(\frac{r^2}{\alpha}DV^r). \tag{56}$$

Eq.(18) then takes the form,

$$\frac{\partial E}{\partial t} = -\frac{\alpha}{r^2}\frac{\partial}{\partial r}(\frac{r^2}{\alpha}EV^r) - p\Big[\frac{\partial \gamma}{\partial t} + \frac{\alpha}{r^2}\frac{\partial}{\partial r}(\frac{r^2}{\alpha}\gamma V^r)\Big]. \tag{57}$$

Defining the radial momentum density in the laboratory frame

$$S_r \equiv \alpha(p+\rho)U^t U_r = (D + \Gamma E)U_r, \tag{58}$$

we can express the radial component of the energy-momentum conservation law given in Eq.(17) by

$$\begin{aligned}\frac{\partial S_r}{\partial t} &= -\frac{\alpha}{r^2}\frac{\partial}{\partial r}(\frac{r^2}{\alpha}S_r V^r) - \alpha\frac{\partial p}{\partial r} \\ &- \frac{\alpha}{2}(p+\rho)\left[\frac{\partial g_{tt}}{\partial r}(U^t)^2 + \frac{\partial g_{rr}}{\partial r}(U^r)^2\right] \\ &= -\frac{\alpha}{r^2}\frac{\partial}{\partial r}(\frac{r^2}{\alpha}S_r V^r) - \alpha\frac{\partial p}{\partial r} \\ &- \alpha\left(\frac{M}{r^2} - \frac{Q^2}{r^3}\right)\left(\frac{D+\Gamma E}{\gamma}\right)\left[\Big(\frac{\gamma}{\alpha}\Big)^2 + \frac{(U^r)^2}{\alpha^4}\right].\end{aligned} \tag{59}$$

In order to determine the number-density of e^+e^- pairs, we turn to Eq.(27). Defining the e^+e^--pair density in the laboratory frame $N_{e^\pm} \equiv \gamma n_{e^\pm}$ and $N_{e^\pm}(T) \equiv \gamma n_{e^\pm}(T)$, where the equilibrium temperature T has been obtained from Eqs.(30) and (31), and using Eq.(54), we rewrite the rate equation given by Eq.(27) in the form

$$\frac{\partial N_{e^\pm}}{\partial t} = -\frac{\alpha}{r^2}\frac{\partial}{\partial r}(\frac{r^2}{\alpha}N_{e^\pm}V^r) + \overline{\sigma v}(N^2_{e^\pm}(T) - N^2_{e^\pm})/\gamma^2\ , \tag{60}$$

These equations are integrated starting from the dyadosphere distributions given in Fig. 17 and assuming as usual ingoing boundary conditions on the horizon of the EMBH.

B. The Rome code

In the following we recall a zeroth order approximation of the fully relativistic equations of the previous section (Ruffini et al. [142]):
(i) Since we are mainly interested in the expansion of the e^+e^- plasma away from the EMBH, we neglect the gravitational interaction.
(ii) We describe the expanding plasma by a special relativistic set of equations.
(iii) In contrast with the previous treatment where the evolution of the density profiles given in Fig. 17 are followed in their temporal evolution leading to a pulse-like structure, selected geometries of the pulse are a priori adopted and the correct one validated by the complete integration of the equations given by the Livermore codes.

Analogously to Eq.(21), from Eq.(16) we have along each flow line in the general case in which baryonic matter is present

$$\frac{d(n_B V)}{d\tau} = 0\,. \tag{61}$$

For the expansion of a shell from its initial volume $\Delta V_\circ$ to the volume ΔV, we obtain

$$\frac{n_B^\circ}{n_B} = \frac{\Delta V}{\Delta V_\circ} = \frac{\Delta\mathcal{V}\gamma(r)}{\Delta\mathcal{V}_\circ\gamma_\circ(r)}, \tag{62}$$

where $\Delta\mathcal{V}$ is the volume of the shell in the laboratory frame, related to the proper volume ΔV in the comoving frame by $\Delta V = \gamma(r)\Delta\mathcal{V}$, where $\gamma(r)$ defined in Eq.(53) is the gamma factor of the shell at the radius r.

Similarly from Eq.(21), using the equation of state (22), along the flow lines we obtain

$$d\ln\epsilon + \Gamma d\ln V = 0. \tag{63}$$

Correspondingly we obtain for the internal energy density ϵ along the flow lines

$$\frac{\epsilon_\circ}{\epsilon} = \left(\frac{\Delta V}{\Delta V_\circ}\right)^\Gamma = \left(\frac{\Delta \mathcal{V}}{\Delta \mathcal{V}_\circ}\right)^\Gamma \left(\frac{\gamma(r)}{\gamma_\circ(r)}\right)^\Gamma \ , \tag{64}$$

where the thermal index Γ given by (22) is a slowly-varying function with values around 4/3. It can be computed for each value of ϵ, p as a function of ΔV.

The overall energy conservation requires that the change of the internal proper energy of a shell is compensated by a change in its bulk kinetic energy. We then have (Ruffini et al. [142])

$$dK = [\gamma(r) - 1](dE + \rho_B dV). \tag{65}$$

In order to model the relativistic expansion of the plasma fluid, we assume that E and D as defined by Eq.(55) are constant in space over the volume ΔV. As a consequence the total energy conservation for the shell implies (Ruffini et al. [142])

$$(\epsilon_\circ + \rho_B^\circ)\gamma_\circ^2(r)\Delta\mathcal{V}_\circ = (\epsilon + \rho_B)\gamma^2(r)\Delta\mathcal{V}, \tag{66}$$

which leads the solution

$$\gamma(r) = \gamma_\circ(r)\sqrt{\frac{(\epsilon_\circ + \rho_B^\circ)\Delta\mathcal{V}_\circ}{(\epsilon + \rho_B)\Delta\mathcal{V}}}. \tag{67}$$

Corresponding to Eq.(60) we obtain the equation for the evolution of the $e^\pm$ number-density as seen by an observer in the laboratory frame

$$\frac{\partial}{\partial t}(N_{e^\pm}) = -N_{e^\pm}\frac{1}{\Delta\mathcal{V}}\frac{\partial\Delta\mathcal{V}}{\partial t} + \overline{\sigma v}\frac{1}{\gamma^2(r)}(N_{e^\pm}^2(T) - N_{e^\pm}^2) \ . \tag{68}$$

Eqs.(62), (64), (67) and (68) are a complete set of equations describing the relativistic expansion of the shell. If we now turn from a single shell to a finite distribution of shells, we can introduce the average values of the proper internal-energy, baryon-mass, baryon-number and pair-number densities $(\bar{\epsilon}, \bar{\rho}_B, \bar{n}_B, \bar{n}_{e^\pm})$ and $\bar{E} \equiv \bar{\gamma}\bar{\epsilon}$, $\bar{D} \equiv \bar{\gamma}\bar{\rho}_B$, $\bar{N}_{e^\pm} \equiv \bar{\gamma}(r)\bar{n}_{e^\pm}$ for the PEM-pulse, where the average $\bar{\gamma}$-factor is defined by

$$\bar{\gamma} = \frac{1}{\mathcal{V}}\int_{\mathcal{V}} \gamma(r) d\mathcal{V}, \tag{69}$$

and $\mathcal{V}$ is the total volume of the shell in the laboratory frame. The corresponding equations are given in Ruffini et al. [142]. Having defined all its governing equations we can now return to the description of the different eras of the GRB phenomena.

VII. THE ERA I: THE PEM PULSE

We have assumed that, following the gravitational collapse process, a region of very low baryonic contamination exists in the dyadosphere all the way to the remnant of the progenitor star.

Recalling Eq.(9) the limit on such baryonic contamination, where ρ_{B_c} is the mass-energy density of baryons, is given by

$$\rho_{B_c} \ll m_p n_{e^+e^-}(r) = 3.2\cdot 10^8 \left(\frac{r_{ds}}{r}\right)^2 \left[1 - \left(\frac{r}{r_{ds}}\right)^2\right] (g/cm^3). \tag{70}$$

Near the horizon $r \simeq r_+$, this gives

$$\rho_{B_c} \ll m_p n_{e^+e^-}(r) = 1.86\cdot 10^{14}\left(\frac{\xi}{\mu}\right)(g/cm^3)\,, \tag{71}$$

and near the radius of the dyadosphere r_{ds}:

$$\rho_{B_c} \ll m_p n_{e^+e^-}(r) = 3.2 \cdot 10^8 \left[1 - \left(\frac{r}{r_{ds}}\right)^2\right]_{r \to r_{ds}} (g/cm^3)\,. \tag{72}$$

Such conditions can be easily satisfied in the collapse to an EMBH, but not necessarily in a collapse to a neutron star.

Consequently we have solved the equations governing a plasma composed solely of e^+e^--pairs and electromagnetic radiation, starting at time zero from the dyadosphere configurations corresponding to constant density in Fig. 17. The Livermore code (Ruffini et al. [142]) has shown very clearly the self organization of the expanding plasma in a very sharp pulse which we have defined as the pair-electromagnetic pulse (PEM pulse), in analogy with the EM pulse observed in nuclear explosions. In order to further examine the structure of the PEM pulse with the simpler procedures of the Rome codes we have assumed (Ruffini et al. [142]) three alternative patterns of expansion of the PEM pulse on which to try the simplified special relativistic treatment and then compared the results with the fully general relativistic hydrodynamical results:

- Spherical model: we assume the radial component of the four-velocity $U_r(r) = U\frac{r}{\mathcal{R}}$, where U is the radial component of the four-velocity at the moving outer surface $r = \mathcal{R}(t)$ of the PEM pulse and the $\bar{\gamma}$-factor and the velocity V_r are

$$\begin{aligned} \bar{\gamma} &= \frac{3}{8U^3}\Big[2U(1+U^2)^{\frac{3}{2}} - U(1+U^2)^{\frac{1}{2}} \\ &- \ln(U + \sqrt{1+U^2})\Big], \quad V_r = \frac{U_r}{\bar{\gamma}}\ ; \end{aligned} \tag{73}$$

  this distribution expands keeping an uniform density profile which decreases with time similar to a portion of a Friedmann Universe.

- Slab 1: we assume $U(r) = U_r = \text{const.}$, the constant width of the expanding slab $\mathcal{D} = R_\circ$ in the laboratory frame of the PEM pulse, while $\bar{\gamma}$ and V_r are

$$\bar{\gamma} = \sqrt{1+U_r^2}, \quad V_r = \frac{U_r}{\bar{\gamma}}\ ; \tag{74}$$

  this distribution does not need any averaging process.

- Slab 2: we assume a constant width $R_2 - R_1 = R_\circ$ of the expanding slab in the comoving frame of the PEM pulse, while $\bar{\gamma}$ and V_r are

$$\bar{\gamma} = \sqrt{1+U_r^2(\tilde{r})}, \quad V_r = \frac{U_r}{\bar{\gamma}}, \tag{75}$$

  This distribution needs an averaging procedure and $R_1 < \tilde{r} < R_2$, i.e. $\tilde{r}$ is an intermediate radius in the slab.

These different assumptions lead to three different distinct slopes for the monotonically increasing $\bar{\gamma}$-factor as a function of the radius (or time) in the laboratory frame, having assumed for the energy of dyadosphere $E_{dya} = 3.1\times10^{54}$ erg (see Fig. 19). In principle, we could have an infinite number of models by defining arbitrarily the geometry of the expanding fluid in the special relativistic treatment given above. To find out which expanding pattern of PEM pulses is the physically realistic one, we need to compare and contrast the results of our simplified models (performed in Rome) with the numerical results based on the hydrodynamic Eqs.(56,57,59) (obtained at Livermore) (Ruffini et al. [142]). Details of the iterative method used to solve the special relativistic equation can be found in Ruffini et al. [142].

It is manifest from the results (see Fig. 19) that the slab 1 approximation (constant thickness in the laboratory frame) is in excellent agreement with the Livermore results (open squares).

The remarkable validation of the special relativistic treatment of the PEM pulse (Ruffini et al. [142]), allows us to easily estimate the related quantities of physical and astrophysical interest in the model, like the e^+e^--pair densities as a function of the laboratory time, the temperature of the plasma in the comoving and laboratory frames, the reheating ratio as a function of the e^+e^--pair annihilation for a variety of initial conditions (Ruffini et al. [142]).

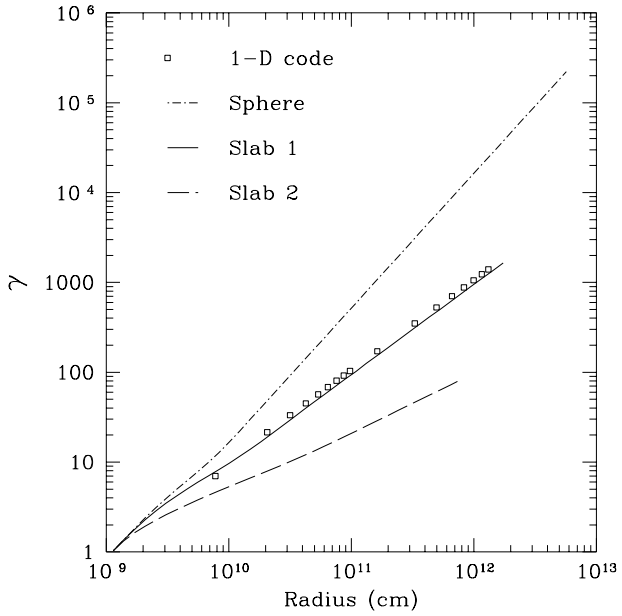

Figure 19: gamma factor as a function of radius. Three models for the expansion pattern of the PEM-pulse are compared with the results of the one dimensional hydrodynamic code for an energy of dyadosphere $E_{dya} = 3.1 \times 10^{54}$ erg. The 1-D code has an expansion pattern that strongly resembles that of a shell with constant thickness in the laboratory frame.

VIII. THE ERA II: THE INTERACTION OF THE PEM PULSE WITH THE REMNANT OF THE PROGENITOR STAR

The PEM pulse expands initially in a region of very low baryonic contamination created by the process of gravitational collapse. As it moves further out the baryonic remnant (see Fig. 1) of the progenitor star is encountered. As discussed in section XXVI below, the existence of such a remnant is necessary in order to guarantee the overall charge neutrality of the system: the collapsing core has the opposite charge of the remnant and the system as a whole is clearly neutral. The number of extra charges in the baryonic remnant negligibly affects the overall charge neutrality of the PEM pulse (Ruffini [139], Ruffini et al. [159]).

The baryonic matter remnant is assumed to be distributed well outside the dyadosphere in a shell of thickness Δ between an inner radius $r_{\rm in}$ and an outer radius $r_{\rm out} = r_{\rm in} + \Delta$ at a distance from the EMBH at which the original PEM pulse expanding in vacuum has not yet reached transparency. For the sake of an example we choose

$$r_{\rm in} = 100 r_{\rm ds}, \qquad \Delta = 10 r_{\rm ds}. \tag{76}$$

The total baryonic mass $M_B = N_B m_p$ is assumed to be a fraction of the dyadosphere initial total energy ($E_{\rm dya}$). The total baryon-number N_B is then expressed as a function of the dimensionless parameter B given by

$$B = \frac{N_B m_p c^2}{E_{\rm dya}}, \tag{77}$$

where B is a parameter in the range $10^{-8} - 10^{-2}$ and m_p is the proton mass. We shall see below the paramount importance of B in the determination of the features of the GRBs. We will see in section X the sense in which B and E_{dya} can be considered to be the only two free parameters of the EMBH theory for the entire GRB family, the so called "long bursts". We shall see in section XII that for the so called "short bursts" the EMBH theory depends on the two other parameters μ, ξ, since in that case $B = 0$. The baryon number density n_B° is assumed to be a constant

$$\bar{n}_B^\circ = \frac{N_B}{V_B}, \qquad \bar{\rho}_B^\circ = m_p \bar{n}_B^\circ c^2. \tag{78}$$

As the PEM pulse reaches the region $r_{\rm in} < r < r_{\rm out}$, it interacts with the baryonic matter which is assumed to be at rest. In our simplified quasi-analytic model we make the following assumptions to describe this interaction:

- the PEM pulse does not change its geometry during the interaction;
- the collision between the PEM pulse and the baryonic matter is assumed to be inelastic,
- the baryonic matter reaches thermal equilibrium with the photons and pairs of the PEM pulse.

These assumptions are valid if: (i) the total energy of the PEM pulse is much larger than the total mass-energy of baryonic matter M_B, $10^{-8} < B < 10^{-2}$, (ii) the ratio of the comoving number density of pairs and baryons at the moment of collision $n_{e^+e^-}/n_B^\circ$ is very high (e.g., $10^6 < n_{e^+e^-}/n_B^\circ < 10^{12}$) and (iii) the PEM pulse has a large value of the gamma factor ($100 < \bar{\gamma}$).

In the collision between the PEM pulse and the baryonic matter at $r_{\rm out} > r > r_{\rm in}$, we impose total conservation of energy and momentum. We consider the collision process between two radii r_2, r_1 satisfying $r_{\rm out} > r_2 > r_1 > r_{\rm in}$ and $r_2 - r_1 \ll \Delta$. The amount of baryonic mass acquired by the PEM pulse is

$$\Delta M = \frac{M_B}{V_B}\frac{4\pi}{3}(r_2^3 - r_1^3), \tag{79}$$

where M_B/V_B is the mean-density of baryonic matter at rest. The conservation of total energy leads to the estimate of the corresponding quantities before (with "$\circ$") and after such a collision

$$(\Gamma\bar{\epsilon}_\circ + \bar{\rho}_B^\circ)\bar{\gamma}_\circ^2\mathcal{V}_\circ + \Delta M = (\Gamma\bar{\epsilon} + \bar{\rho}_B + \frac{\Delta M}{V} + \Gamma\Delta\bar{\epsilon})\bar{\gamma}^2\mathcal{V}, \tag{80}$$

where $\Delta\bar{\epsilon}$ is the corresponding increase of internal energy due to the collision. Similarly the momentum-conservation gives

$$(\Gamma\bar{\epsilon}_\circ + \bar{\rho}_B^\circ)\bar{\gamma}_\circ U_r^\circ\mathcal{V}_\circ = (\Gamma\bar{\epsilon} + \bar{\rho}_B + \frac{\Delta M}{V} + \Gamma\Delta\bar{\epsilon})\bar{\gamma}U_r\mathcal{V}, \tag{81}$$

where the radial component of the four-velocity of the PEM pulse is $U_r^\circ = \sqrt{\bar{\gamma}_\circ^2 - 1}$ and Γ is the thermal index. We then find

$$\Delta\bar{\epsilon} = \frac{1}{\Gamma}\left[(\Gamma\bar{\epsilon}_\circ + \bar{\rho}_B^\circ)\frac{\bar{\gamma}_\circ U_r^\circ\mathcal{V}_\circ}{\bar{\gamma}U_r\mathcal{V}} - (\Gamma\bar{\epsilon} + \bar{\rho}_B + \frac{\Delta M}{V})\right], \tag{82}$$

$$\bar{\gamma} = \frac{a}{\sqrt{a^2-1}}, \quad a \equiv \frac{\bar{\gamma}_\circ}{U_r^\circ} + \frac{\Delta M}{(\Gamma\bar{\epsilon}_\circ + \bar{\rho}_B^\circ)\bar{\gamma}_\circ U_r^\circ\mathcal{V}_\circ}. \tag{83}$$

These equations determine the gamma factor $\bar{\gamma}$ and the internal energy density $\bar{\epsilon} = \bar{\epsilon}_\circ + \Delta\bar{\epsilon}$ in the capture process of baryonic matter by the PEM pulse.

The effect of the collision of the PEM pulse with the remnant leads to the following results (Ruffini et al. [143]) as a function of the B parameter defined in Eq.(77):
1) an abrupt decrease of the gamma factor given by

$$\gamma_{coll} = \gamma_\circ\frac{1+B}{\sqrt{{\gamma_\circ}^2\,(2B+B^2)+1}}\,, \tag{84}$$

where $\gamma_\circ$ is the gamma factor of the PEM pulse prior to the collision and B is given by Eq.(77),
2) an increase of the internal energy in the comoving frame E_{coll} developed in the collision given by

$$\frac{E_{coll}}{E_{dya}} = \frac{\sqrt{{\gamma_\circ}^2\,(2B+B^2)+1}}{\gamma_\circ} - \left(\frac{1}{\gamma_\circ} + B\right)\,, \tag{85}$$

3) a corresponding reheating of the plasma in the comoving frame but not in the laboratory frame, an increase of the number of e^+e^- pairs and correspondingly an overall increase of the opacity of the pulse. See details in section XI.

IX. THE ERA III: THE PEMB PULSE

After the engulfment of the baryonic matter of the remnant the plasma formed of e^+e^--pairs, electromagnetic radiation and baryonic matter expands again as a sharp pulse, namely the PEMB pulse. The calculation is continued as the plasma fluid expands, cools and the e^+e^- pairs recombine until it becomes optically thin:

$$\int_R dr(n_{e^\pm} + \bar{Z}n_B)\sigma_T \simeq O(1), \tag{86}$$

where $\sigma_T = 0.665 \cdot 10^{-24}\mathrm{cm}^2$ is the Thomson cross-section and the integration is over the radial interval of the PEMB pulse in the comoving frame. We have first explored the general problem of the PEMB pulse evolution by integrating the general relativistic hydrodynamical equations with the Livermore codes, for a total energy in the dyadosphere of 3.1×10^{54} erg and a baryonic shell of thickness $\Delta = 10 r_{\rm ds}$ at rest at a radius of $100 r_{\rm ds}$ and $B \simeq 1.3 \cdot 10^{-4}$.

In total analogy with the special relativistic treatment for the PEM pulse, presented in section VII (see also Ruffini et al. [142]), we obtain for the adiabatic expansion of the PEMB pulse in the constant-slab approximation described by the Rome codes the following hydrodynamical equations with $\rho_B \neq 0$

$$\frac{\bar{n}_B^\circ}{\bar{n}_B} = \frac{V}{V_\circ} = \frac{\mathcal{V}\bar{\gamma}}{\mathcal{V}_\circ \bar{\gamma}_\circ}, \tag{87}$$

$$\frac{\bar{\epsilon}_\circ}{\bar{\epsilon}} = \left(\frac{V}{V_\circ}\right)^\Gamma = \left(\frac{\mathcal{V}}{\mathcal{V}_\circ}\right)^\Gamma \left(\frac{\bar{\gamma}}{\bar{\gamma}_\circ}\right)^\Gamma, \tag{88}$$

$$\bar{\gamma} = \bar{\gamma}_\circ \sqrt{\frac{(\Gamma\bar{\epsilon}_\circ + \bar{\rho}_B^\circ)\mathcal{V}_\circ}{(\Gamma\bar{\epsilon} + \bar{\rho}_B)\mathcal{V}}}, \tag{89}$$

$$\frac{\partial}{\partial t}(N_{e^\pm}) = -N_{e^\pm}\frac{1}{\mathcal{V}}\frac{\partial \mathcal{V}}{\partial t} + \overline{\sigma v}\frac{1}{\bar{\gamma}^2}(N_{e^\pm}^2(T) - N_{e^\pm}^2). \tag{90}$$

In these equations ($r > r_{\rm out}$) the comoving baryonic mass- and number densities are $\bar{\rho}_B = M_B/V$ and $\bar{n}_B = N_B/V$, where V is the comoving volume of the PEMB pulse.

We compare and contrast (see Fig. 5) the bulk gamma factor as computed from the Rome and Livermore codes, where excellent agreement has been found. This validates the constant-thickness approximation in the case of the PEMB pulse as well. On this basis we easily estimate a variety of physical quantities for an entire range of values of B.

For the same EMBH we have considered five different cases: a shell of baryonic mass with (1) $B \simeq 1.3 \cdot 10^{-4}$; (2) $B \simeq 3.8 \cdot 10^{-4}$; (3) $B \simeq 1.3 \cdot 10^{-3}$; (4) $B \simeq 3.8 \cdot 10^{-3}$; (5) $B \simeq 1.3 \cdot 10^{-3}$). The results of the integration given in detail in Ruffini et al. [143] show that for the first parameter range the PEMB pulse propagates as a sharp pulse of constant thickness in the laboratory frame, but already for $B \simeq 1.3 \cdot 10^{-2}$ the expansion of the PEMB pulse becomes much more complex and the constant-thickness approximation ceases to be valid; see Ruffini et al. [143] for details.

It is particularly interesting to evaluate the final value of the gamma factor of the PEMB pulse when the transparency condition given by Eq.(86) is reached as a function of B, see Fig. 20. For a given EMBH, there is a *maximum* value of the gamma factor at transparency. By further increasing the value of B the entire E_{dya} is transferred into the kinetic energy of the baryons; see also section XII. Details are given in Ruffini et al. [143].

In Fig. 20 we plot the gamma factor of the PEMB pulse versus the radius for different amounts of baryonic matter. The diagram extends to values of the radial coordinate at which the transparency condition given by Eq.(86) is reached. The "asymptotic" gamma factor

$$\bar{\gamma}_{\rm asym} \equiv \frac{E_{\rm dya}}{M_B c^2} \tag{91}$$

is also shown for each curve. The closer the gamma value approaches the "asymptotic" value (91) at transparency, the smaller the intensity of the radiation emitted in the burst and the larger the amount of kinetic energy left in the baryonic matter.

X. THE IDENTIFICATION OF THE FREE PARAMETERS OF THE EMBH THEORY

Within the approximation presented in section III the EMBH is characterized by two parameters: μ and ξ. The energy of the dyadosphere is expressed in terms of these two parameters by Eq.(12).

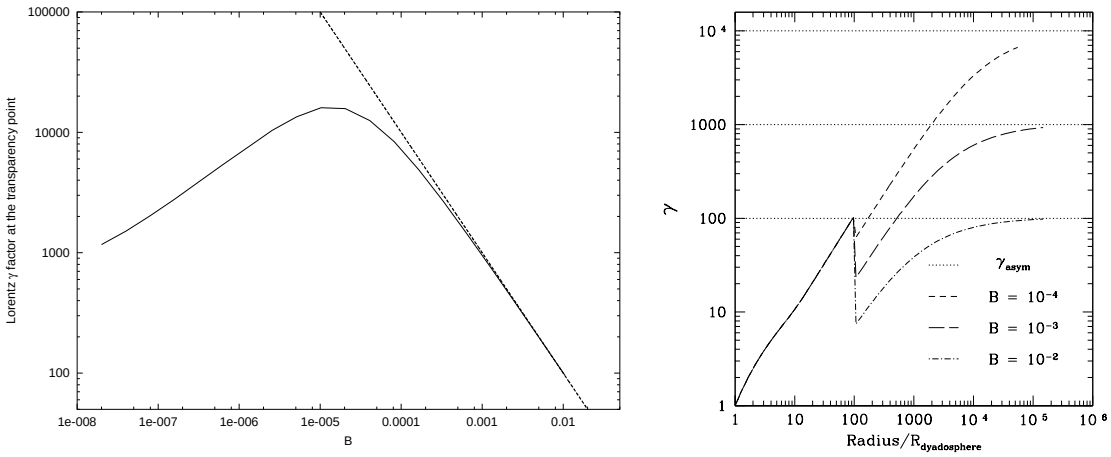

Figure 20: **Left)** The gamma factor (the solid line) at the transparent point is plotted as a function of the B parameter. The asymptotic value (the dashed line) $E_{\rm dya}/(M_Bc^2)$ is also plotted. **Right)** The gamma factors are given as functions of the radius in units of the dyadosphere radius for selected values of B for the typical case $E_{dya} = 3.1 \times 10^{54}$ erg. The asymptotic values $\gamma_{\rm asym} = E_{\rm dya}/(M_Bc^2) = 10^4, 10^3, 10^2$ are also plotted. The collision of the PEM pulse with the baryonic remnant occurs at $r/r_{ds} = 100$ where the jump occurs and the PEMB pulse starts.

There is an entire family of EMBH solutions with different values of μ and ξ corresponding to the same value of E_{dya} (see Fig. 17). These solutions are physically different with respect to the density of electron-positron pair distributions given by Eq.(9), as well as to their energy density given by Eq.(11). A clear example of such a degeneracy is given in Fig. 21 where the two limiting energy density profiles approximating the dyadosphere as introduced in Fig. 17 are given for three different EMBH configurations corresponding to the same value of $E_{dya} = 3.1 \times 10^{54}$ erg. The three configurations correspond respectively to the three different pairs (μ, ξ): $(10, 0.76)$, $\left(10^2, 0.27\right)$, $\left(10^3, 0.10\right)$.

The corresponding dynamical evolution of the PEM pulse introduced in section VII and Ruffini et al. [142] is clearly different in the three cases. It is remarkable that when the collision with the remnant of the progenitor star is considered all these differences disappear. As usual (see section VIII) we describe the baryonic content of the remnant by the parameter B. The PEMB pulse generated after the collision with the baryonic matter depends uniquely on the two parameters E_{dya} and B. In Fig. 22 the temperature in the laboratory frame is given for the PEM pulse and the PEMB pulse corresponding to the three configurations of Fig.21 and $B = 4 \times 10^{-3}$. It is clear that while for the PEM pulse era the three configurations are markedly different, they do converge to a common behaviour in the PEMB pulse era.

If we turn now to the effect of the distance between the EMBH and the baryonic remnant, we see that this degeneracy is further extended: while the three PEM pulse eras are quite different, the common PEMB pulse era is largely insensitive to the location of the baryonic remnant, see Fig. 23. We have plotted the three gamma factors in the PEM pulse era corresponding to the different configurations of Fig. 21 and $B = 10^{-2}$, in the two cases the baryonic remnant is positioned at different distances from the EMBH.

If the PEM pulse has reached extreme relativistic regimes, the common value γ_{coll} to which the three gamma factors drop in the collision with the baryonic matter of the remnant can be simply expressed by the large gamma limit of Eq.(84)

$$\gamma_{coll} = \frac{B+1}{\sqrt{B^2+2B}}\,, \tag{92}$$

while the internal energy E_{coll} developed in that collision is simply given by the corresponding limit of Eq.(85)

$$\frac{E_{coll}}{E_{dya}} = -B + \sqrt{B^2+2B}\,. \tag{93}$$

This approximation applies when the final gamma factor at the end of the PEM pulse era is larger than γ_{coll}, upper panel in Fig. 23.

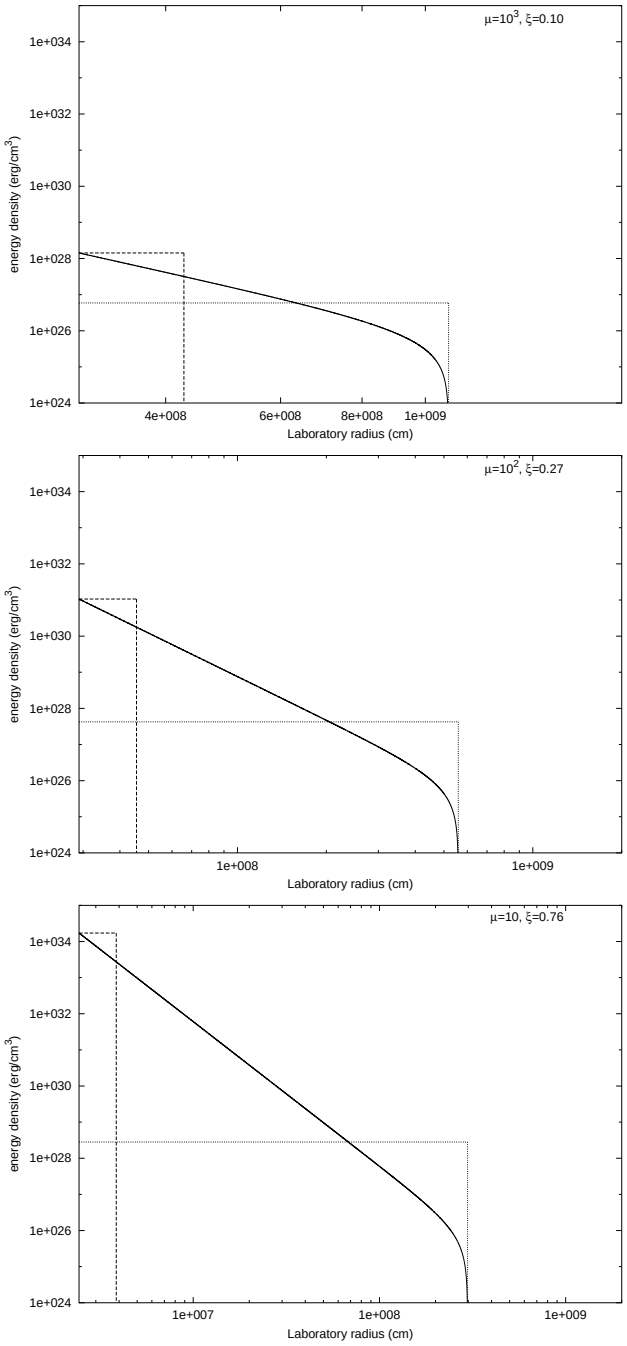

Figure 21: Three different dyadospheres corresponding to the same value of $E_{dya} = 3.1 \times 10^{54}$ erg and with different values of the two parameters μ and ξ are given. The three different configurations are markedly different in their spatial extent as well as in their energy-density distribution.

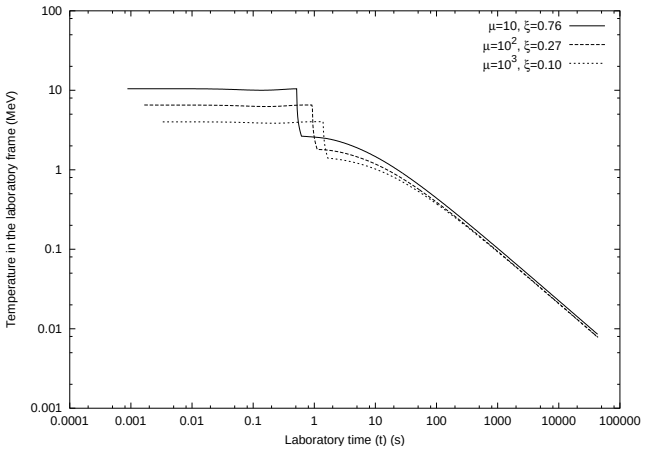

Figure 22: The temperature of the plasma during the PEM pulse and PEMB pulse eras, measured in the laboratory frame, corresponding to the three configurations presented in Fig. 21 is given as a function of the laboratory time. The three different curves converge to a common one in the PEMB pulse era, which is therefore only a function of the E_{dya} and B. The difference among the three curves in the early part of the PEMB pulse follows from having located the baryonic matter at a distance of $50(r_{\rm ds} - r_+)$, which is different in the three cases. Such difference become negligible at large distances in the later phases of the evolution.

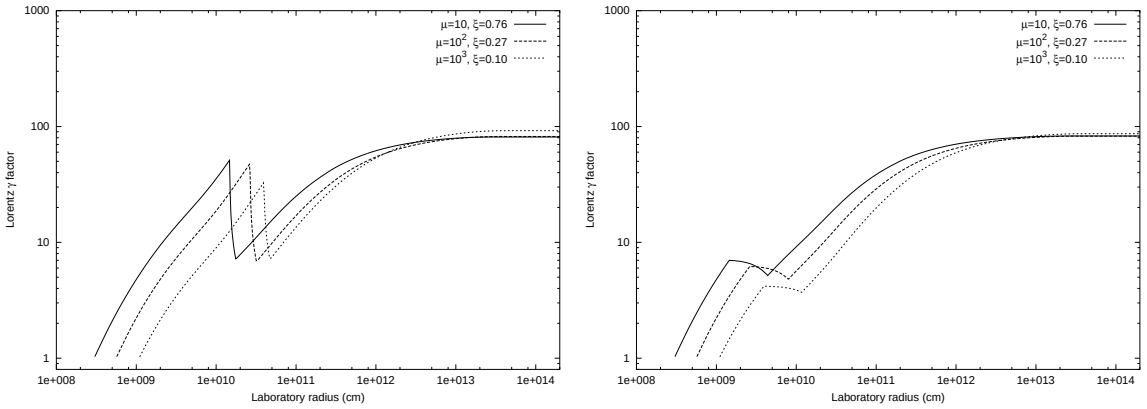

Figure 23: The gamma factors for the three configurations considered in Fig. 21 are given as a function of the radial coordinate in the laboratory frame. The two figures correspond to a baryonic remnant positioned respectively at $r_{in} = 50(r_{\rm ds} - r_+)$ (left) and at $r_{in} = 5(r_{\rm ds} - r_+)$ (right). Again the convergence to a common behaviour, uniquely a function of E_{dya} and B for the late stages of the PEMB pulse, is manifest.

Turning from these general considerations to the GRB data, this degeneracy in the PEMB pulse eras and their dependence on only two parameters E_{dya} and B has far reaching astrophysical implications for the identification of the source of GRBs. As we will see in the conclusions all the information obtainable from GRBs with a large value of the parameter B will lead to the determination of the above two parameters. An entire family of degenerate astrophysical solutions in the range of charges and masses given in Fig. 17 are possible. The direct knowledge of the mass and charge of the EMBH can only be gained from the PEM pulse or from GRBs with very small values of B — the so called "short bursts", see section XII and the conclusions.

XI. THE APPROACH TO TRANSPARENCY: THE THERMODYNAMICAL QUANTITIES

As the condition of transparency expressed by Eq.(86) is reached the *injector phase* terminates. The electromagnetic energy of the PEMB pulse is released in the form of free-streaming photons — the proper GRB. The remaining energy of the PEMB pulse is released as an accelerated-baryonic-matter (ABM) pulse.

We now proceed to the analysis of the approach to the transparency condition. It is then necessary to turn from the pure dynamical description of the PEMB pulse described in the previous sections to the relevant thermodynamic parameters. Also such a description at the time of transparency needs the knowledge of the thermodynamical parameters in all previous eras of the GRB.

As above we shall consider as a typical case an EMBH of $E_{dya} = 3.1 \times 10^{54}$ erg and $B = 10^{-2}$. The considerations will refer to a dyadosphere configuration described by the two limiting approximations shown in Fig. 17.

One of the key thermodynamical parameters is represented by the temperature of the PEM and PEMB pulses. It is given as a function of the radius both in the comoving and in the laboratory frames in Fig. 24. Before the collision the PEM pulse expands keeping its temperature in the laboratory frame constant while its temperature in the comoving frame falls (see Ruffini et al. [142]). In fact Eqs.(66,67) are equivalent to

$$\frac{d(\epsilon\gamma^2\mathcal{V})}{dt} = 0, \tag{94}$$

where the baryon mass-density is $\rho_B = 0$ and the thermal energy-density of photons and e^+e^--pairs is $\epsilon = \sigma_B T^4(1 + f_{e^+e^-})$, σ_B is the Boltzmann constant and $f_{e^+e^-}$ is the Fermi-integral for e^+ and e^-. This leads to

$$\epsilon\gamma^2\mathcal{V} = E_{\rm dya}, \quad T^4\gamma^2\mathcal{V} = \text{const.} \tag{95}$$

Since e^+ and e^- in the PEM pulse are extremely relativistic, we have the equation of state $p \simeq \epsilon/3$ and the thermal index (22) $\Gamma \simeq 4/3$ in the evolution of PEM pulse. Eq.(95) is thus equivalent to

$$T^3\bar{\gamma}\mathcal{V} \simeq \text{const.} \tag{96}$$

These two equations (94) and (96) result in the constancy of the laboratory temperature $T\bar{\gamma}$ in the evolution of the PEM pulse.

It is interesting to note that Eqs.(95) and (96) hold as well in the cross-over region where $T \sim m_e c^2$ and e^+e^- annihilation takes place. In fact from the conservation of entropy it follows that asymptotically we have

$$\frac{(VT^3)_{T<m_ec^2}}{(VT^3)_{T>m_ec^2}} = \frac{11}{4}\ , \tag{97}$$

exactly for the same reasons and physics scenario discussed in the cosmological framework by Weinberg, see e.g. Eq. (15.6.37) of Weinberg (1972). The same considerations when repeated for the conservation of the total energy $\epsilon\gamma V = \epsilon\gamma^2\mathcal{V}$ following from Eq. (94) then lead to

$$\frac{(VT^4\gamma)_{T<m_ec^2}}{(VT^4\gamma)_{T>m_ec^2}} = \frac{11}{4}\ . \tag{98}$$

The ratio of these last two quantities gives asymptotically

$$T_\circ = (T\gamma)_{T>m_ec^2} = (T\gamma)_{T<m_ec^2}, \tag{99}$$

where $T_\circ$ is the initial average temperature of the dyadosphere at rest.

During the collision of the PEM pulse with the remnant we have an increase in the number density of e^+e^- pairs (see Fig. 24). This transition corresponds to an *increase* of the temperature in the comoving frame and a *decrease* of the temperature in the laboratory frame as a direct effect of the dropping of the gamma factor (see Fig. 20).

After the collision we have the further acceleration of the PEMB pulse (see Fig. 20). The temperature now decreases both in the laboratory and the comoving frame (see Fig. 24). Before the collision the total energy of the e^+e^- pairs and the photons is constant and equal to $E_{\rm dya}$. After the collision

$$E_{\rm dya} = E_{\rm Baryons} + E_{e^+e^-} + E_{\rm photons}, \tag{100}$$

which includes both the total energy $E_{e^+e^-} + E_{\rm photons}$ of the nonbaryonic components and the kinetic energy $E_{\rm Baryons}$ of the baryonic matter

$$E_{\rm Baryons} = \bar{\rho}_B V(\bar{\gamma} - 1). \tag{101}$$

In Fig. 25 we plot both the total energy $E_{e^+e^-} + E_{\rm photons}$ of the nonbaryonic components and the kinetic energy $E_{\rm Baryons}$ of the baryonic matter as functions of the radius for the typical case $E_{\rm dya} = 3.1 \times 10^{54}$ erg and $B = 10^{-2}$. Further details are given in Ruffini et al. [143].

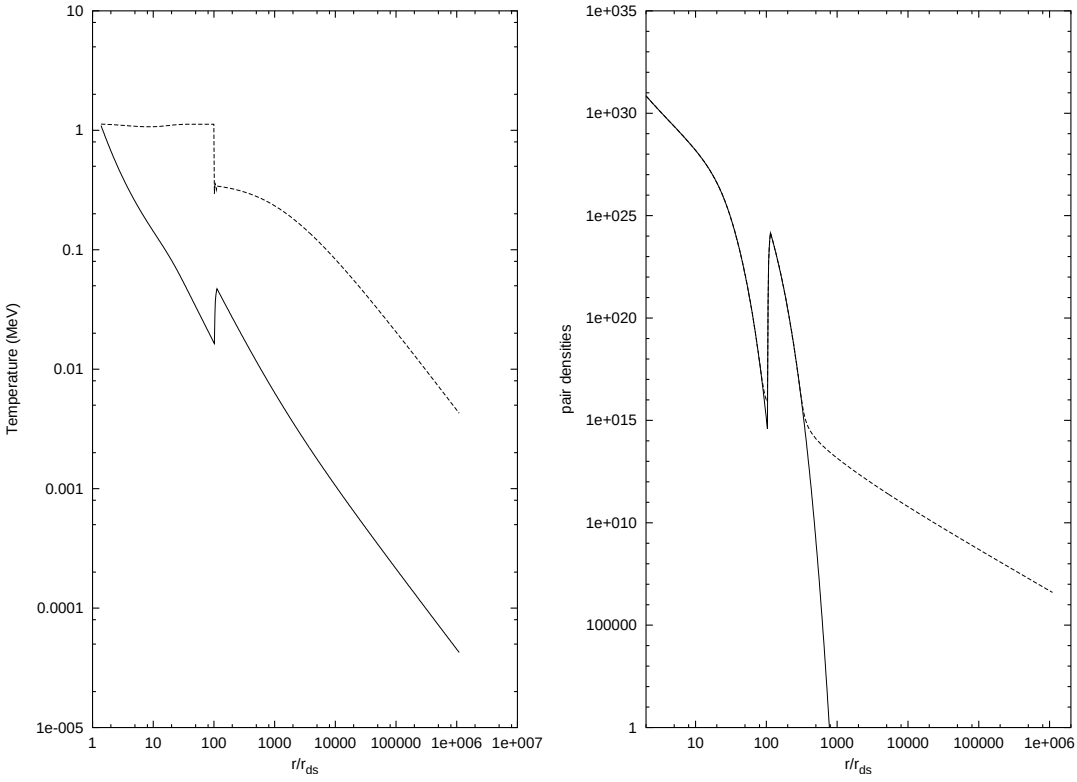

Figure 24: **Left)** The temperature of the plasma in the comoving frame T'(MeV) (the solid line) and in the laboratory frame $\bar{\gamma}T'$ (the dashed line) are plotted as functions of the radius in the unit of the dyadosphere radius $r_{\rm ds}$. **Right)** The number densities $n_{e^+e^-}(T)$ (the solid line) computed by the Fermi integral and $n_{e^+e^-}$ (the dashed line) computed by the rate equation (see section IV) are plotted as functions of the radius. $T' \ll m_e c^2$, two curves strongly divergent due to e^+e^--pairs frozen out of the thermal equilibrium. The peak at $r \simeq 100 r_{\rm ds}$ is due to the internal energy developed in the collision.

XII. THE P-GRBS AND THE "SHORT BURSTS". THE END OF THE INJECTOR PHASE.

We now analyze the approach to the transparency condition given by Eq.(86). For selected values of B we give the energy $E_{P\text{-}GRB}$ of the P-GRB, and $E_{\rm Baryons}$ of the ABM pulse. We clearly have

$$E_{dya} = E_{P\text{-}GRB} + E_{\rm Baryons}\,. \tag{102}$$

Taking into account the results shown in Figs. 24–25, we can repeat all the considerations for selected values of B. We shall examine values of B ranging from $B = 10^{-8}$ only up to $B = 10^{-2}$: for larger values of B our constant slab approximation breaks down. We will see in the following that this range does indeed cover the most relevant observational features of the GRBs.

As clearly shown in Fig. 20 both the final value of the gamma factor and the radial coordinate at which the transparency condition is reached depend very strongly on B. Therefore a strong dependence on B is also found in the relative values of $E_{P\text{-}GRB}$ and $E_{\rm Baryons}$.

We are now finally ready to give in Fig. 6 the crucial diagram representing the values of $E_{P\text{-}GRB}$ and $E_{\rm Baryons}$ in units of the E_{dya} as functions of B. This diagram, a universal one, is very important and is essential for the understanding of the GRB structure.

We find that for small values of B (around 10^{-8}) almost all the E_{dya} is emitted in the P-GRB (see also our previous paper Ruffini et al. [142]) and very little energy is left in the baryons. While for $B \simeq 10^{-2}$ roughly only 10^{-2} of the total initial energy of the dyadosphere is radiated away in the P-GRB and almost all energy is transferred to the baryons.

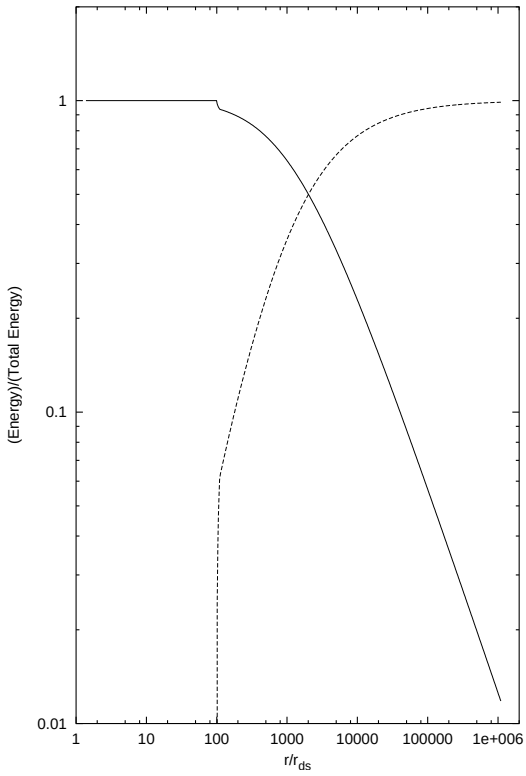

Figure 25: The energy of the non baryonic components of the PEMB pulse (the solid line) and the kinetic energy of the baryonic matter (the dashed line) in unit of the total energy are plotted as functions of the radius in the unit of the dyadosphere radius $r_{\rm ds}$.

This behaviour is at the heart of the fundamental difference between the so called *short bursts* and *long bursts*. We have proposed in Ruffini et al. [145] that the *short bursts* must be identified with the P-GRBs in the case of very small B. There are a variety of reasons supporting this identification:

1. For small values of B, $E_{\rm Baryons}$ is negligible, see Fig. 6, and consequently the intensity of the afterglow is also negligible and the entire energy E_{dya} is released into the P-GRB. This is clearly consistent with the absence of observed afterglows in the short bursts.

2. The temperature of the P-GRB in the laboratory frame $\bar{\gamma}T$ at the transparency point is a strongly decreasing function of B, see Fig. 6. $\bar{\gamma}T$ is related to the energy corresponding to the peak of the photon-number spectrum, as described in Ruffini et al. [142]. This is also in very good agreement with the observed decrease of the hardness ratio between the *short bursts* and the *long bursts* (Kouveliotou et al. [84]).

3. The time T_{90}, the duration of 90% of the energy emission as used in the current literature and discussed in Ruffini et al. [143] is plotted in Fig. 26 for selected values of E_{dya} and for different values of B.

Before concluding a word of caution is needed about how to use the above results: all these considerations are based on the drastic approximations in the description of the dyadosphere presented in section III, see also Fig. 21. This treatment is very appropriate in estimating the general dependence of the energy of the P-GRB, the kinetic energy of the ABM pulse and consequently the intensity of the afterglow. Especially powerful is the establishment of the dependence of $E_{P\text{-}GRB}$ and $E_{\rm Baryons}$ on B (see Fig. 6). As we will see in the next sections, this approximation is similarly powerful in determining the overall time structure of the GRB and especially the time of the release of the P-GRB with respect to the moment of gravitational collapse and the afterglow.

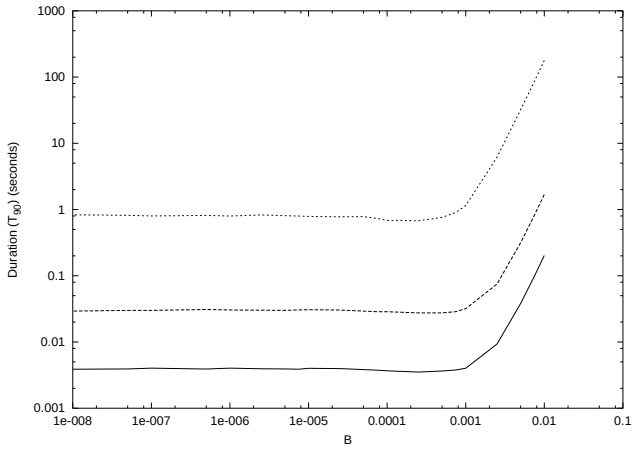

Figure 26: The duration computed with the T_{90} criterion is represented as a function of the B parameter for three selected EMBH respectively with $E_{dya} = 4.4 \times 10^{52}$ erg, $E_{dya} = 3.1 \times 10^{54}$ erg, $E_{dya} = 4.1 \times 10^{58}$ erg going from the lower curve to the upper one.

If, however, we turn to the detailed temporal structure of the P-GRB and its detailed spectral distribution, it is clear that the approximations given in section III is no longer valid. The detailed description of the formation of the dyadosphere as qualitatively expressed in Fig. 48 is now needed in all mathematical rigour with the full development of all its governing equations. Progress in this direction is being made at this moment (Cherubini et al. [28], Ruffini & Vitagliano [156, 157], Ruffini et al. [159]). This situation, however, provides a unique opportunity to follow in real time the general relativistic effects of the approach to the EMBH horizon as it occurs. In other words all direct general relativistic effects of the GRBs are encoded in the fine structure of the P-GRB. For the reasons given in section X the information on the EMBH mass and charge can only come from the short bursts.

This terminates the *injector phase*. We now turn to the *Beam-Target phase* in which the ABM pulse collides with the interstellar medium target and the afterglow is generated. We shall in the following sections review the basic theoretical treatment necessary for the description of these remaining eras and proceed then to the confrontation of the EMBH theory with the data.

XIII. THE ERA IV: THE ULTRARELATIVISTIC AND RELATIVISTIC REGIMES IN THE AFTERGLOW

In the introduction we have already expressed the basic assumptions which we have adopted for the description of the collision of the ABM pulse with the ISM. In analogy and by extension of the results obtained for the PEM and PEMB pulse cases, we also assume that the expansion of the ABM pulse through the ISM occurs keeping its width constant in the laboratory frame, although the results are quite insensitive to this assumption. We assume then that this interaction can be represented by a sequence of inelastic collisions of the expanding ABM pulse with a large number of thin and cold ISM spherical shells at rest with respect to the central EMBH. Each of these swept up shells of thickness Δr has a mass $\Delta M_{\rm ism}$ and is assumed to be located between two radial distances r_1 and r_2 (where $r_2 - r_1 = \Delta r \ll r_1$) in the laboratory frame. These collisions create an internal energy $\Delta E_{\rm int}$.

We indicate by $\Delta\epsilon$ the increase in the proper internal energy density due to the collision with a single shell and by ρ_B the proper energy density of the swept up baryonic matter. This includes the baryonic matter composing the remnant around the central EMBH, already swept up in the PEMB pulse formation, and the baryonic matter from the ISM swept up by the ABM pulse:

$$\rho_B = \frac{(M_B + M_{\rm ism})\, c^2}{V}. \tag{103}$$

Here V is the ABM pulse volume in the comoving frame, M_B is the mass of the baryonic remnant and $M_{\rm ism}$ is the

ISM mass swept up from the transparency point through the r in the laboratory frame:

$$M_{\rm ism} = m_p n_{\rm ism} \frac{4\pi}{3} \left(r^3 - {r_\circ}^3 \right) , \tag{104}$$

where m_p the proton mass and $n_{\rm ism}$ the number density of the ISM in the laboratory frame.

The energy conservation law in the laboratory frame at a generic step of the collision process is given by

$$\rho_{B_1} {\gamma_1}^2 \mathcal{V}_1 + \Delta M_{\rm ism} c^2 = \left(\rho_{B_1} \frac{V_1}{V_2} + \frac{\Delta M_{\rm ism} c^2}{V_2} + \Delta\epsilon \right) {\gamma_2}^2 \mathcal{V}_2, \tag{105}$$

where the quantities with the index "1" are calculated before the collision of the ABM pulse with an elementary shell of thickness Δr and the quantities with "2" after the collision, γ is the gamma factor and $\mathcal{V}$ the volume of the ABM pulse in the laboratory frame so that $V = \gamma \mathcal{V}$.

The momentum conservation law in the laboratory frame is given by

$$\rho_{B_1} \gamma_1 U_{r_1} \mathcal{V}_1 = \left(\rho_{B_1} \frac{V_1}{V_2} + \frac{\Delta M_{\rm ism} c^2}{V_2} + \Delta\epsilon \right) \gamma_2 U_{r_2} \mathcal{V}_2, \tag{106}$$

where $U_r = \sqrt{\gamma^2 - 1}$ is the radial covariant component of the four-velocity vector (see Ruffini et al. [142, 143] and Eq.53).

We thus obtain

$$\Delta\epsilon = \rho_{B_1} \frac{\gamma_1 U_{r_1} \mathcal{V}_1}{\gamma_2 U_{r_2} \mathcal{V}_2} - \left(\rho_{B_1} \frac{V_1}{V_2} + \frac{\Delta M_{\rm ism} c^2}{V_2} \right), \tag{107}$$

$$\gamma_2 = \frac{a}{\sqrt{a^2 - 1}}, \qquad a \equiv \frac{\gamma_1}{U_{r_1}} + \frac{\Delta M_{\rm ism} c^2}{\rho_{B_1} \gamma_1 U_{r_1} \mathcal{V}_1}. \tag{108}$$

We can use for $\Delta\varepsilon$ the following expression

$$\Delta\varepsilon = \frac{E_{\rm int_2}}{V_2} - \frac{E_{\rm int_1}}{V_1} = \frac{E_{\rm int_1} + \Delta E_{\rm int}}{V_2} - \frac{E_{\rm int_1}}{V_1} = \frac{\Delta E_{\rm int}}{V_2} \tag{109}$$

because we have assumed a "fully radiative regime" and so $E_{\rm int_1} = 0$. Substituting Eq.(108) in Eq.(107) and applying Eq.(109), we obtain:

$$\Delta E_{\rm int} = \rho_{B_1} V_1 \sqrt{1 + 2\gamma_1 \frac{\Delta M_{\rm ism} c^2}{\rho_{B_1} V_1} + \left(\frac{\Delta M_{\rm ism} c^2}{\rho_{B_1} V_1} \right)^2} - \rho_{B_1} V_1 \left(1 + \frac{\Delta M_{\rm ism} c^2}{\rho_{B_1} V_1} \right) , \tag{110}$$

$$\gamma_2 = \frac{\gamma_1 + \frac{\Delta M_{\rm ism} c^2}{\rho_{B_1} V_1}}{\sqrt{1 + 2\gamma_1 \frac{\Delta M_{\rm ism} c^2}{\rho_{B_1} V_1} + \left(\frac{\Delta M_{\rm ism} c^2}{\rho_{B_1} V_1} \right)^2}} . \tag{111}$$

These relativistic hydrodynamic (RH) equations have to be numerically integrated.

These are the actual set of equations we have integrated in the EMBH theory. In order to compare and contrast our results with the ones in the current literature, in section XVIII we have introduced the continuous limit of our equations and proceeded to have piecewise approximate power law solutions. We examine as well in section XX still under the above assumptions, the effects of a possible departure from homogeneity in the interstellar medium, still keeping the average density $n_{ism} = const.$ Although these inhomogeneities are not relevant for the overall behaviour of the afterglow which we address here, they are indeed important for the actual observed flux and its temporal structures (see Ruffini et al. [147]). Also these considerations are affected by the angular spreading (Ruffini et al. [148]).

XIV. THE ERA V: THE APPROACH TO THE NONRELATIVISTIC REGIMES IN THE AFTERGLOW

The only reason for addressing this last era is that the issue of the approach to nonrelativistic behaviour has been extensively discussed in the literature. In our treatment these results do not show any particular problems and the

relativistic equations of the previous section continue to hold. In the specific example of GRB 991216 we will present in section XVIII some analytic asymptotic expansions of these equations.

This concludes the exposition of the different eras of the EMBH theory. It goes without saying that for the description of each era, all the preceding eras must necessarily be known in order to determine the space-time grid in the laboratory frame and its relation to the arrival times as seen by a distant observer. This is the basic message expressed in the RSTT paradigm.

We can now turn to the comparison of the EMBH theory with the observational data.

XV. THE BEST FIT OF THE EMBH THEORY TO THE GRB 991216: THE GLOBAL FEATURES OF THE SOLUTION

For reasons already explained in the introduction, we use the GRB 991216 as a prototype. We will then later apply the EMBH theory to other GRBs. The relevant data of GRB 991216 are reproduced in Fig. 3: the data on the burst as recorded by BATSE Rapid Burst Response [6] and the data on the afterglow from the RXTE satellite (Corbet & Smith [31]) and the Chandra satellite (Piro et al., [120]), see also Halpern et al. [73].

The data fitting procedure relies on three basic assumption:

1. In the E-APE region, the source luminosity is mainly in the energy band 50–300 KeV, so we consider the flux observed by BATSE a good approximation of the total flux.

2. In the decaying part of the afterglow, we assume that during the R-XTE and Chandra observations the source luminosity is mainly in the energy band 2–10 KeV, so we can again assume that the flux observed by these satellites is a good approximation of the total one.

3. We have neglected in this paper the optical and radio emissions, since they are always negligible with respect to the X and γ ray fluxes. In fact, even in the latest afterglow phases up to where the X-ray data are available, they are one order of magnitude smaller then the X-ray flux.

These assumptions were initially adopted for the sake of simplicity, but have now also been justified on the basis of the spectral description of the afterglow (Ruffini et al. [150]).

As already emphasized in the previous sections, in the EMBH theory there are only two free parameters characterising the afterglow: the energy of the dyadosphere, E_{dya}, and the baryonic matter in the remnant of the progenitor star, parametrized by the dimensionless parameter B. The location of the remnant has been assumed $\sim 10^{10}$ cm. As discussed in Ruffini et al. [144] and section X, the results are rather insensitive to the actual density and location of the baryonic component but they are very sensitive to the value of B (Ruffini et al. [143]).

In Fig. 7 we present the actual first results of fitting our EMBH theory to the data from the R-XTE and Chandra satellites, corresponding to selected values of E_{dya} and B. There are three distinct features which are clearly evident as a function of the arrival time at the detector: an initial rising part in the afterglow luminosity which reaches a peak followed by a monotonically decreasing part.

We have then proceeded to fine tune the two parameters in Fig. 27. The main conclusions from our model are the following:

1) The slope of the afterglow in the region where the experimental data are present is $n = -1.6$ and is in perfect agreement with the observational data. The index n in this region is rather insensitive to the values of the parameters E_{dya} and B. The physical reason for this universality of the slope is rather remarkable since it depends on a variety of factors including the ultrarelativistic energy of the baryons in the ABM pulse, the assumption of constant average density in the ISM, the "fully radiative" conditions leading predominantly to X-ray emission, as well as all the different relativistic effects described in the RSTT paradigm (see also section XVIII).

2) The afterglow fit does not depend directly on the parameters μ, ξ but only through their combination E_{dya}. Thus there is a 1-parameter family of values of the pair (μ, ξ) allowed by a given viable value of E_{dya} (see Fig 17 and section X).

3) By fine tuning the parameters of the best fit of the luminosity profile and time evolution of the afterglow the following parameters have been found:

$$E_{dya} = 4.83 \times 10^{53} erg, \quad B = 3 \times 10^{-3} \; . \tag{112}$$

After fixing in Eq.(112) the two free parameters of the EMBH theory, modulo the mass-charge relationship which fixes E_{dya}, we can derive all the space-time parameters of the GRB 991216 (see Tab. I) as well as the explicit dependence of the gamma factor as a function of the radial coordinate (see Fig. 8).

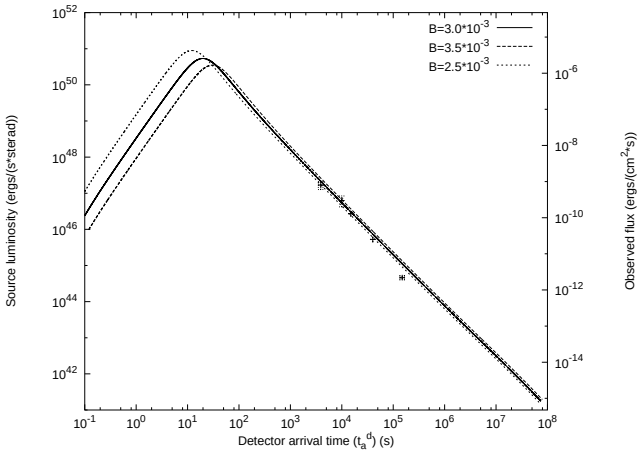

Figure 27: Fine tuning of the best fit of the afterglow data of Chandra, RXTE as well as of the range of variability of the BATSE data on the major burst by a unique afterglow curve leading to the parameter values $E_{dya} = 4.83 \times 10^{53} erg, B = 3 \times 10^{-3}$.

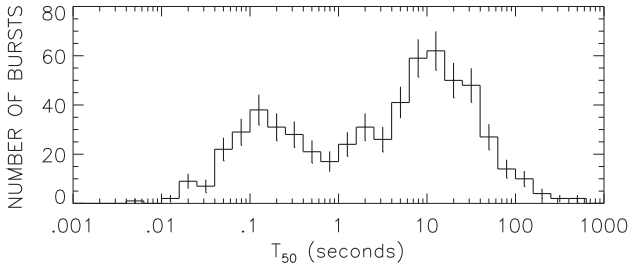

Figure 28: The distribution of the burst durations clearly shows two different classes of events: the "short bursts" and the "long bursts" (reproduced from Paciesas et al. [107]).

Of special interest is the fundamental diagram of Fig. 9. Its role is essential in interpreting all quantities measured in arrival time (the time of an observer in an inertial frame at the detector) and their relations to the ones measured in the laboratory time by an observer in an inertial frame at the GRB source. The two times are clearly related by light signals (see Fig. 18) and expressed by the integral Eq.(37) and are also affected by the cosmological expansion (see section V).

XVI. THE EXPLANATION OF THE "LONG BURSTS" AND THE IDENTIFICATION OF THE PROPER GAMMA RAY BURST (P-GRB)

Having determined the two free parameters of the EMBH theory, any other feature is a new prediction. An unexpected result soon became apparent, namely that the average luminosity of the main burst observed by BATSE can be fit by the afterglow curve (see Fig. 10). This led us to the identification of the long bursts observed by BATSE with the extended afterglow peak emission (E-APE). The peak of this E-APE occurs at $\sim 19.87\, s$ and its intensity and time scale are in excellent agreement with the BATSE observations (see also Ruffini et al. [147]). It is clear that this E-APE is *not* a burst, but is seen as such by BATSE due to its high noise threshold (see also Ruffini et al. [147]). Thus the outstanding unsolved problem of explaining the long GRBs (see e.g. Piran [117], Salmonson et al. [162], Wilson et al. [187]) is radically resolved: the so called "long bursts" do not exist, they are just E-APEs (see Fig. 28).

We now turn to the most cogent question to be asked: where does one find the burst which is emitted when the

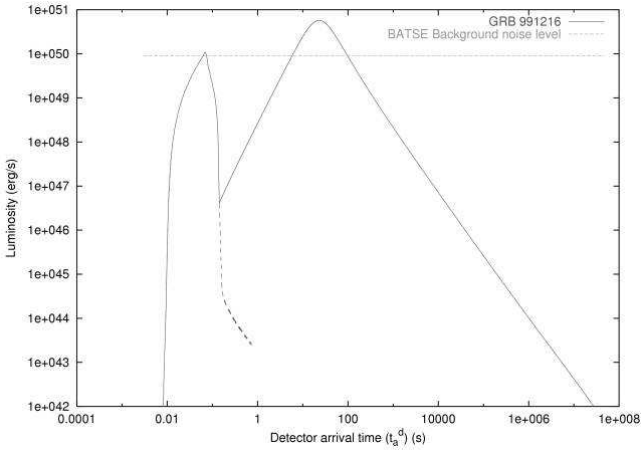

Figure 29: A qualitative diagram showing the full picture of the model, with both P-GRB and E-APE.

condition of transparency against Thomson scattering is reached? We have referred to this as the proper gamma ray burst (P-GRB) in order to distinguish it from the global GRB phenomena (see Bianco et al. [13], Ruffini et al. [144]). We are guided in this search by two fundamental diagrams (see Fig. 11 and Fig. 11):

1. In Ruffini et al. [143] it is shown that for a fixed value of E_{dya} the value of B uniquely determines the energy $E_{P\text{-}GRB}$ of the P-GRB and the kinetic energy $E_{Baryons}$ of the ABM pulse which gives origin to the afterglow (see Fig. 11). For the particular values of the parameters given in Eq. (112), we find

$$E_{P\text{-}GRB} = 7.54 \times 10^{51} erg\,, \quad E_{Baryons} = 9.43 \times 10^{52} erg \tag{113}$$

and then:

$$\frac{E_{P\text{-}GRB}}{E_{Baryons}} = 1.58 \times 10^{-2}\,. \tag{114}$$

2. One important additional piece of information comes from the differences in arrival time between the P-GRB and the peak of the E-APE, see Fig. 11. Using the results of this figure and the numerical values given in Tab. I, we can retrace the P-GRB by reading off the time parameters of point 4 in Fig. 8. Transparency is reached at $21.57\,s$ in comoving time at a radial coordinate $r = 1.94 \times 10^{14}$ cm in the laboratory frame and at $8.41 \times 10^{-2}\,s$ in arrival time at the detector.

All this, namely the energy predicted in Eq.(113) for the intensity of the burst and its time of arrival, leads to the unequivocal identification of the P-GRB with the apparently inconspicuous initial burst in the BATSE data. We have estimated from the BATSE data the ratio of the P-GRB to the E-APE over the noise threshold to be $\sim 10^{-2}$, in excellent agreement with the result in Eq. (114), see Fig. 29.

It is important to emphasize that the diagrams in Fig. 6 and Fig. 11 are not universal, but depend on the dyadosphere energy. The corresponding diagrams for three selected E_{dya} values ($E_{dya} = 5.29 \times 10^{51}$ erg, $E_{dya} = 4.83 \times 10^{53}$ erg and $E_{dya} = 4.49 \times 10^{55}$ erg) are given in Fig. 30a where we have plotted the energy of the P-GRB and of the E-APE as a function of B. The crossing of the intensity of P-GRB and E-APE occurs respectively at $B_1 = 6.0 \times 10^{-5}$, $B_2 = 2.5 \times 10^{-5}$ and $B_3 = 1.2 \times 10^{-5}$ where $B_1 > B_2 > B_3$. In Fig. 30b the same quantities are plotted as a function of the baryon mass M_B in units of solar masses and the opposite dependence occurs: $M_1 < M_2 < M_3$.

The physical reasons beyond these results is the following. We recall that the kinetic energy $E_{Baryons}$ and mass M_B of PEMB pulse are

$$E_{Baryons} = (\gamma - 1) M_B \quad M_B \equiv B E_{dya} \tag{115}$$

at the crossing point defined by

$$E_{Baryons} = E_{P\text{-}GRB} = \frac{1}{2} E_{dya}. \tag{116}$$

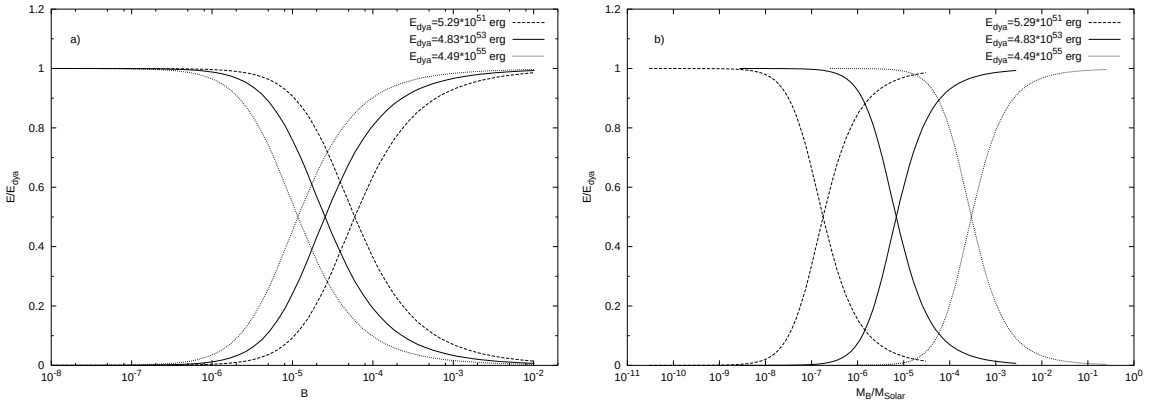

Figure 30: **a)** The same diagram of Fig. 6 is plotted for three different E_{dya} values: $E_{dya} = 5.29 \times 10^{51}$ erg (dashed lines), $E_{dya} = 4.83 \times 10^{53}$ erg (solid lines) and $E_{dya} = 4.49 \times 10^{55}$ erg (dotted lines). **b)** Same as in a) but plotted as a function of the baryonic mass M_B in units of solar masses instead of B.

From these two equations, we obtain

$$B = \frac{1}{2(\gamma_\circ - 1)} \simeq \frac{1}{2\gamma_\circ}, \tag{117}$$

$\gamma_\circ$ is the Lorentz gamma factor of the PEMB pulse at the transparency point, where (see section XI)

$$(n_{pair} + n_B)\sigma_T \simeq n_B \sigma_T = 1, \quad n_B = \frac{M_B}{4\pi r_\circ^2 \Delta \gamma_\circ}, \tag{118}$$

Δ_t is the PEMB pulse thickness and $r_\circ$ the radial position at the transparency point. In addition, from the total energy conservation, we have

$$(\epsilon + n_B)\gamma_\circ^2 4\pi r_\circ^2 \Delta = const., \tag{119}$$

where ϵ is the thermal energy of the PEMB pulse. In the regime $n_B \gg \epsilon$, we have

$$\gamma_\circ \simeq \frac{E_{dya}}{M_B}, \tag{120}$$

and in the regime $n_B \ll \epsilon$, we have

$$\gamma_\circ \sim r_\circ. \tag{121}$$

Considering the crossing point to occur in the second regime, we obtain at the crossing point

$$B \sim (E_{dya})^{-\frac{1}{4}}, \quad M_B \sim (E_{dya})^{\frac{3}{4}}. \tag{122}$$

These results are plotted in Figs. 31a–b. The agreement with the computed results is quite satisfactory. The differences can be attributed to the approximation adopted in Eq.(121) which is modified for high B values.

The conclusion is that for increasing E_{dya} also the baryonic mass corresponding to the cross increases, but in percentage it increases less than E_{dya}.

XVII. CONSIDERATIONS ON THE P-GRB SPECTRUM AND THE HARDNESS OF THE SHORT BURSTS

Regarding the P-GRB spectrum, the initial energy of the electron-positron pairs and photons in the dyadosphere for given values of the parameters can be easily computed following the work of Preparata et al. [124]. We obtain

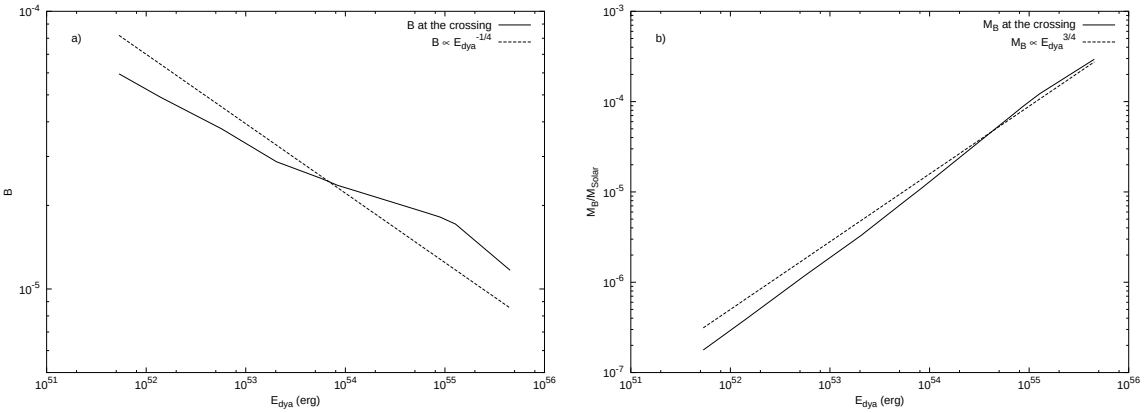

Figure 31: **a)** The B values corresponding to the crossings in Fig. 30a are plotted versus E_{dya} (solid line). The function $B \propto E_{dya}^{-1/4}$ obtained from a qualitative theoretical estimate (see Eq.(122)) is also plotted (dashed line). **b)** The M_B values corresponding to the crossings in Fig. 30b are plotted versus E_{dya} (solid line). The function $M_B \propto E_{dya}^{3/4}$ obtained from a qualitative theoretical estimate (see Eq.(122)) is also plotted (dashed line).

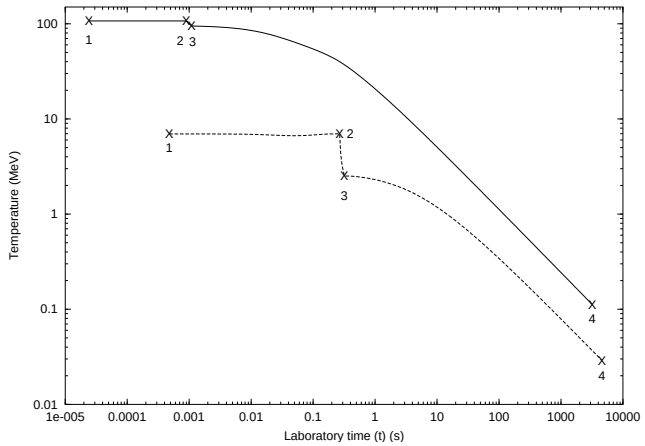

Figure 32: The temperature of the pulse in the laboratory frame for the first three eras of Fig. 1 of Ruffini et al. [144] is given as a function of the laboratory time. The numbers 1, 2, 3, 4 represent the beginning and end of each era. The two curves refer to two extreme approximations adopted in the description of the dyadosphere. Details are given in Ruffini et al. [143] and in section X.

respectively $T = 1.95$ MeV and $T = 29.4$ MeV in the two approximations we have used for the average energy density of the dyadosphere (see section X). It is then possible to follow in the laboratory frame the time evolution of the temperature of the electron-positron pairs and photons through the different eras, see Fig. 32. The condition of transparency is reached at temperatures in the range of $\sim 15 - 55$ KeV at the detector, in agreement with the BATSE results. We emphasize that in the limit of B going to 10^{-8} in which the P-GRB coincides with the "short bursts" the spectrum of the P-GRB becomes harder in agreement with the observational data (see Fig. 6 and Band et al. [4], Dermer et al. [40], Frontera et al. [56], Norris et al. [105]).

All the above are average values derived from the two approximations used in Fig. 17. If one wishes to compare the EMBH theoretical results with the fine temporal details of the observational data on the P-GRB, a departure from this average approach will be needed and the fully time varying relativistic analysis outlined in Fig. 48 applies as will be further discussed in section XXVI.

XVIII. APPROXIMATIONS AND POWER LAWS IN THE DESCRIPTION OF THE AFTERGLOW

In addition to the BATSE data, there is also clearly perfect agreement with the decaying part of the afterglow data from the RXTE and Chandra satellites.

We can also establish at this point a first set of conclusions on the luminosity power law index "n" which is a function depending strongly on the transformation $t \to t_a \to t_a^d$ (see Fig. 9). In the current literature such transformations and the corresponding n values are incorrect. Our theoretical value $n_{theo} = -1.6$ obtained for spherical symmetry for fully radiative conditions and constant density of the ISM is in agreement with observed $n_{obs} = -1.616 \pm 0.067$. No evidence of beaming is found in GRB 991216. We shall return to this point in the conclusions.

An extremely large number of papers in the literature deal with the power law index in the afterglow era. This issue has been particularly debated in connection with the aim of decreasing the energy requirements of GRBs by the effect of beaming (see e.g. Davies et al. [34], Mao & Yi [91]). It is currently very popular to infer the existence of beaming from the direct observations of breakings in the power-law index of the afterglow (see e.g. Dermer & Chiang [39], Gou et al. [71], Halpern et al. [73], Mészáros & Rees [95], Mészáros et al. [97], Panaitescu et al. [112], Panaitescu & Mészáros [115], Rhoads [129, 131], Sari, at al. [167]). Our aim here is to underline an often neglected point that the power law index of the afterglow is the result of a variety of factors including the very different regimes in the relation between the laboratory time t and the detector arrival time t_a^d presented in Fig. 9. No meaningful statements on the values of the power-law index of the afterglow can be made neglecting these necessary considerations expressed in the RSTT paradigm. This becomes particularly transparent from the power law expansion in the semianalytic treatments we present below. It is therefore not so surprising, as we will show in the next session, that the results obtained in the EMBH theory differ from the ones in the current literature.

A. The approximate expression of the hydrodynamic equations

We proceed to a first approximation and expand Eqs.(110, 111) to second order in the quantity

$$\frac{\Delta M_{\rm ism} c^2}{\rho_{B_1} V_1} \ll 1 \,. \tag{123}$$

We obtain the following expressions:

$$\Delta E_{\rm int} = (\gamma_1 - 1)\, \Delta M_{\rm ism} c^2 - \frac{1}{2} \frac{\gamma_1^2 - 1}{M_B + M_{\rm ism}} \left(\Delta M_{\rm ism}\right)^2 c^2 \,, \tag{124}$$

$$\Delta\gamma = -\frac{\gamma_1^2 - 1}{M_B + M_{\rm ism}} \Delta M_{\rm ism} + \frac{3}{2} \gamma_1 \frac{\gamma_1^2 - 1}{\left(M_B + M_{\rm ism}\right)^2} \left(\Delta M_{\rm ism}\right)^2 \,, \tag{125}$$

where we set $\Delta\gamma \equiv \gamma_2 - \gamma_1$ and have used the fact that $\rho_{B_1} V_1 \equiv (M_B + M_{\rm ism})\, c^2$. In the limit $\Delta E_{\rm int} \to dE_{\rm int}$, $\Delta\gamma \to d\gamma$, and $\Delta M_{\rm ism} \to dM_{\rm ism}$, neglecting also second order terms, where

$$dM_{\rm ism} = 4\pi r^2 m_p n_{\rm ism} dr = 4\pi r^2 m_p n_{\rm ism} v dt, \quad v = \frac{dr}{dt}, \tag{126}$$

and where the ISM number density $n_{\rm ism}$ is assumed for simplicity to be $n_{\rm ism} = 1\,{\rm cm}^{-3}$, we obtain:

$$dE_{\rm int} = (\gamma - 1)\, dM_{\rm ism} c^2 \,, \tag{127}$$

$$d\gamma = -\frac{\gamma^2 - 1}{M_B + M_{\rm ism}} dM_{\rm ism} \,. \tag{128}$$

Eqs.(127, 128) are limiting cases of Taub's hydrodynamical equations (Boccaletti et al. [22], Landau & Lifshitz [87], Taub [177]). They have been at times referred into the GRB literature as the Blandford-McKee equations (see Blandford & McKee [17]). It is clear that the application of these equations holds if Eq.(123) applies. The behaviour of $\frac{\Delta M_{\rm ism} c^2}{\rho_{B_1} V_1}$ as a function of the radius when $M_{\rm ism} \ll M_B$ is:

$$\frac{\Delta M_{\rm ism} c^2}{\rho_{B_1} V_1} \sim \frac{r^2 \Delta r}{M_B}. \tag{129}$$

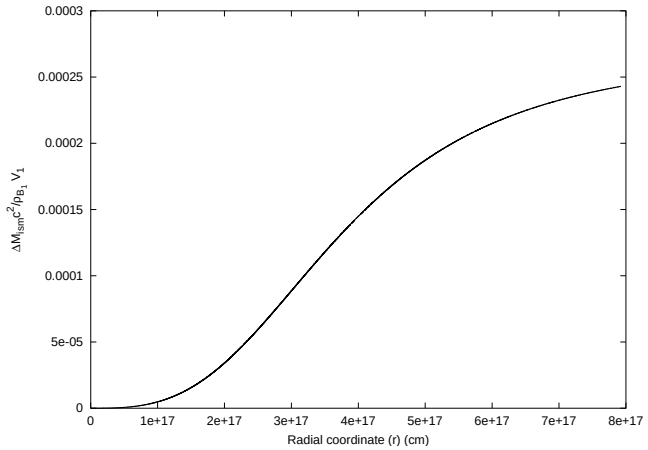

Figure 33: The factor $\frac{\Delta M_{\rm ism}c^2}{\rho_{B_1} V_1}$ is represented as a function of the radial coordinate. It is manifestly an increasing function.

The condition $M_{\rm ism} \ll M_B$ holds for GRB 991216 during the entire evolution of the system and so Eq.(123) is valid (see Fig. 33).

Eqs.(127,128) can be simply solved analytically (see e.g. Blandford & McKee [17]). We then have:

$$\gamma = \frac{(M_B + M_{\rm ism})^2 + C}{(M_B + M_{\rm ism})^2 - C}, \tag{130}$$

where

$$C = {M_B}^2 \frac{\gamma_\circ - 1}{\gamma_\circ + 1}, \tag{131}$$

where we recall that $r_\circ$ and $\gamma_\circ$ are the radial coordinate and the gamma factor at the transparency point and M_B is the initial baryonic mass of the ABM pulse.

Eq.(130) is a differential equation for $r\,(t)$, namely

$$1 - \left(\frac{dr}{cdt}\right)^2 = \left[\frac{(M_B + M_{\rm ism})^2 + C}{(M_B + M_{\rm ism})^2 - C}\right]^{-2}, \tag{132}$$

which can be integrated analytically with solution (see e.g. Abramowitz & Stegun [1])

$$\begin{aligned} 2c\sqrt{C}\,(t - t_\circ) = (M_B - m_i^\circ)\,(r - r_\circ) + \frac{1}{4} m_i^\circ r_\circ \left[\left(\frac{r}{r_\circ}\right)^4 - 1\right] + \frac{C r_\circ}{6 m_i^\circ B^2} \ln\left[\frac{\left(B + \frac{r}{r_\circ}\right)^3}{B^3 + \left(\frac{r}{r_\circ}\right)^3} \frac{B^3 + 1}{(B+1)^3}\right] \\ + \frac{C r_\circ}{3 m_i^\circ B^2}\left[\sqrt{3}\arctan\frac{2\frac{r}{r_\circ} - B}{B\sqrt{3}} - \sqrt{3}\arctan\frac{2 - B}{B\sqrt{3}}\right], \end{aligned} \tag{133}$$

where $m_i^\circ = \frac{4}{3}\pi m_p n_{\rm ism} r_\circ^3$, $B = \left(\frac{M_B - m_i^\circ}{m_i^\circ}\right)^{1/3}$ and we recall that $t_\circ$ is the laboratory time at the transparency point. Clearly the fulfilment of Eq.(123) has to be checked to ensure the validity of this solution.

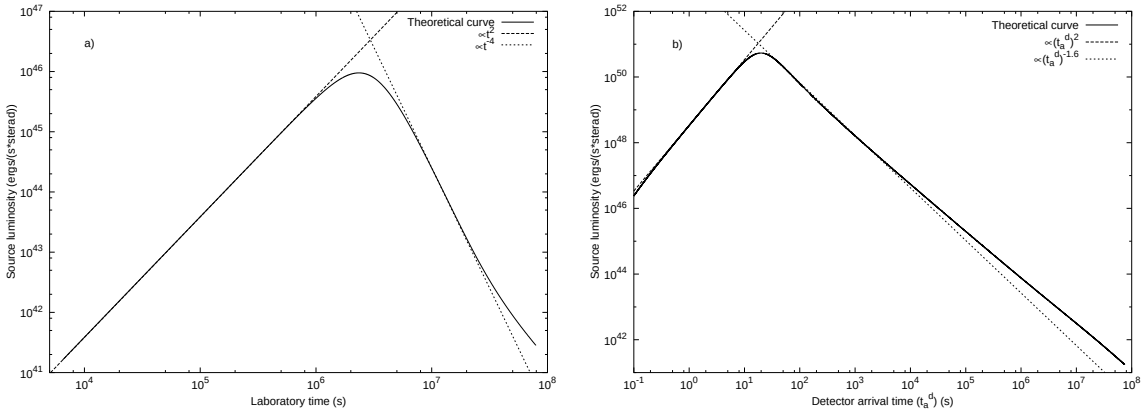

Figure 34: **a)** The GRB flux emitted in laboratory time. **b)** the flux emitted in the arrival time, measured by an observer at rest with respect to the detector (see section XVIII).

B. The approximate expression of the emitted flux

From Eqs.(127,128), it follows that the emitted flux in the laboratory frame is given by (see Fig. 34a)

$$\frac{dE}{dt} = 4\pi r^2 n_{\rm ism} m_p v\gamma\left(\gamma-1\right)c^2, \tag{134}$$

and the corresponding flux in detector arrival time (see Fig. 34b) by

$$\frac{dE}{dt_a^d} = \left[\frac{dt}{dt_a^d}\frac{dE}{dt}\right]_{t=t(t_a^d)} = 4\pi n_{\rm ism} m_p c^2\left[vr^2\gamma\left(\gamma-1\right)\frac{dt}{dt_a^d}\right]_{t=t(t_a^d)}. \tag{135}$$

For the solution of these equations we distinguish four different phases (A–D). The first two correspond to era V.

Phase A

Just after the transparency condition is reached, the ISM matter involved is so small that we can approximately neglect the $M_{\rm ism}$ term in Eq.(130) and we have:

$$\gamma \simeq \gamma_\circ. \tag{136}$$

In the specific case of GRB 991216 we have $\gamma_\circ = 310.1$, $r_\circ = 1.94\times10^{14}\,cm$, $t_\circ = 6.48\times10^3\,s$, $t_{a_\circ} \simeq 4.21\times10^{-2}\,s$ and $t^d_{a_\circ} \simeq 8.41\times10^{-2}\,s$, where the index "$\circ$" refers to the quantities at the transparency point. We can then establish the following equation describing the ABM pulse motion in this phase: $r\left(t\right) = vt$ with $v \simeq c$. We can than use the following relation between laboratory time and arrival time:

$$t = 2{\gamma_\circ}^2 t_a = \frac{2{\gamma_\circ}^2}{1+z}t_a^d, \tag{137}$$

which is in perfect agreement with the full numerical computation (see Fig. 9).

We can substitute these equations into Eqs.(134,135), obtaining:

$$\frac{dE}{dt} \propto \gamma_\circ^2 n_{\rm ism} t^2 \tag{138}$$

in laboratory time and

$$\frac{dE}{dt_a^d} \propto \frac{\gamma_\circ^8 n_{\rm ism}}{(1+z)^3}\left(t_a^d\right)^2 \tag{139}$$

in arrival time, assuming $\gamma\left(\gamma-1\right) \simeq \gamma^2$. The results of the numerical integration of Eqs.(107,108) are in perfect agreement with these approximations (see Fig. 34).

Points P – the two maxima of the energy flux

Since the contribution of the ISM mass in Eqs.(130–131) can no longer be neglected, the value of γ starts to significantly decrease (see Fig. 8) and the flux reaches a maximum value. We integrate Eq.(134) and Eq.(135) using Eq.(130) for γ, assuming $r\left(t\right) = vt$ with $v \simeq c$ and Eq.(137) for the relation between the laboratory time and the arrival time (see Figs. 35–9). We can now obtain the point where the emitted flux reaches its maximum. In general, the location of the maximum of the flux, point P in Ruffini et al. [144], will occur at different events, if considered in the arrival time (P_A) or in the laboratory time (P_L). In this second case, the point P_L is determined by equating to zero the first derivative of Eq.(134), and we have:

$$\gamma_{P_L} \simeq \frac{2}{3}\gamma_\circ, \quad \left.\frac{M_B}{M_{\rm ism}}\right|_{P_L} \simeq 2\gamma_\circ, \tag{140}$$

which in the case of GRB 991216 gives $\gamma_{P_L} = 206.7$ and $\left.\frac{M_B}{M_{\rm ism}}\right|_{P_L} \simeq 620.2$. The maximum of the observed flux is determined by equating to zero the first derivative of Eq.(135). We obtain:

$$\gamma_{P_A} \simeq \frac{5}{6}\gamma_\circ, \quad \left.\frac{M_B}{M_{\rm ism}}\right|_{P_A} \simeq 5\gamma_\circ, \tag{141}$$

which in the case of GRB 991216 gives $\gamma_{P_A} \simeq 258.4$ and $\left.\frac{M_B}{M_{\rm ism}}\right|_{P_A} \simeq 1550.5$.

The results of the numerical integration of Eqs.(107,108) are in perfect agreement with these approximations (see Fig. 34).

Phase B – the "golden value" $n = -1.6$

In this phase γ can no longer be considered constant and strongly decreases (see Fig. 8). $M_{\rm ism}$ is increasing, but v is still almost constant, equal to c. As a consequence, we can still say that $r\left(t\right) = vt$ with $v = c$, but the relation between laboratory time and arrival time given in Eq.(137) is no longer valid, and also Eq.(41) is no longer applicable in this phase (see Fig. 9). We can instead write the following "effective" relation:

$$t \propto \left(t_a^d\right)^{0.20}, \tag{142}$$

which is a result of a best fit of the numerical data in this region. Expanding the squares in Eq.(130), neglecting $M_{\rm ism}^2$ with respect to M_B^2 but retaining the terms in $M_{\rm ism}$ and assuming $\gamma_\circ \gg 1$ we obtain:

$$\gamma \sim \frac{M_B}{M_{\rm ism}} \sim \gamma_{P_L}\frac{r_{P_L}^3}{r^3} = \gamma_{P_L}\frac{t_{P_L}^3}{t^3}, \tag{143}$$

where r_{P_L} and t_{P_L} are the values of r and t at point P_L. Substituting this result into Eqs.(134), we obtain the emitted flux in the laboratory frame, given by

$$\frac{dE}{dt} \propto \gamma_P^2 t_P^6 n_{\rm ism} t^{-4}, \tag{144}$$

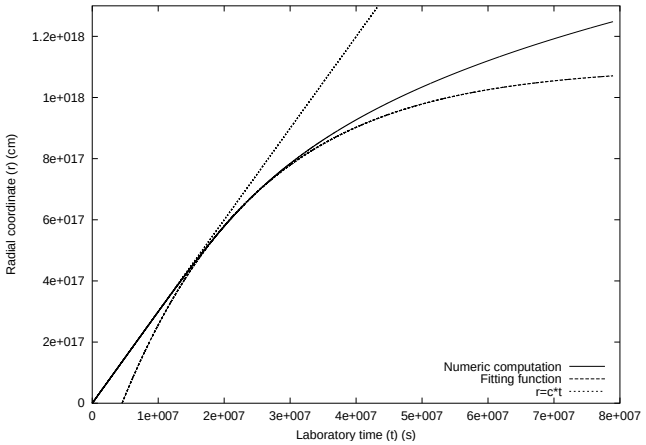

Figure 35: The exact numerical solution for $r\,(t)$ (solid line), together with the line $r = ct$ (dotted line) and the fitting function given in Eq.(149) (dashed line).

and this is in good agreement with the full numerical computation (see Fig. 34).

To obtain an analytic formula for the observed flux on the detector, we can still try to use the approximate relation between t and t_a^d given by Eq.(41):

$$t = 2\gamma\,(t)^2 t_a = \frac{2\gamma\,(t)^2}{1+z} t_a^d, \tag{145}$$

where $\gamma\,(t)$ is given by Eq.(143). We obtain:

$$t = \left(\frac{2\gamma_{P_L}^2 t_{P_L}^6}{1+z} t_a^d\right)^{1/7}. \tag{146}$$

Using this formula in Eq.(135), we finally obtain:

$$\frac{dE}{dt_a^d} \propto \frac{\gamma_P^{\frac{8}{7}} t_P^{\frac{24}{7}} n_{\rm ism}}{(1+z)^{-\frac{17}{7}}} \left(t_a^d\right)^{-\frac{10}{7}} \tag{147}$$

where we again assumed $\gamma\,(\gamma-1) \simeq \gamma^2$. This results are not in agreement with the observational data, because the power-law index for the observed flux is $-10/7 \simeq -1.43$, instead of the observed value -1.6.

This is a confirmation that Eq.(145) cannot be applied in this phase, as instead has been done by many authors in the current literature. We instead have to use Eq.(142). In fact, doing so we obtain the correct value:

$$\frac{dE}{dt_a^d} \propto n_{\rm ism} \left(t_a^d\right)^{-1.6}, \tag{148}$$

The results of the numerical integration of Eqs.(107,108) are in perfect agreement with these approximations (see Fig. 34), which implies that the approximate Eq.(127,128) can still be used in this regime, but not Eq.(41), which has to be replaced by an "effective" local power-law behaviour (see Eq.(142)).

Phase C

This new phase begins when γ has decreased so much that the approximation $r = ct$ is no longer valid (see Fig. 35). In the case of GRB 991216 this happens when $\gamma \simeq 3.0$, $t \simeq 1.5 \times 10^7$ s, $t_a^d \simeq 2.9 \times 10^5$ s and $r \simeq 4.4 \times 10^{17}$ cm. In this entire phase, $r\,(t)$ manifests the following behaviour typical of damped motion:

$$r\left(t\right)=\hat{r}\left(1-e^{-\frac{t-t^{\star}}{\tau}}\right), \tag{149}$$

where $\hat{r}$, $t^{\star}$ and τ are constants that can be determined by the best fit of the numerical solution. In the present case of GRB 991216 we obtain:

$$\hat{r}\simeq 1.101\times 10^{18}cm,\quad \tau\simeq 2.072\times 10^{7}s,\quad t^{\star}\simeq 4.52\times 10^{6}s. \tag{150}$$

It is important to note that this interesting behaviour, typical of a damped motion, does not lead to any power-law relationship for the emitted flux as a function of the laboratory time (see Fig. 34). However, if we look at the observed flux as a function of the detector arrival time, we see that a power-law relationship still can be established, fitting the numerical solution. The result is:

$$\frac{dE}{dt_{a}^{d}}\propto\left(t_{a}^{d}\right)^{-1.36}. \tag{151}$$

This quite unexpected result can be explained because the relation between t and t_a^d depends on $r\left(t\right)$ in a nonpower-law behaviour. This fact balances the complex behaviour of the emitted flux as a function of the laboratory time, leading finally again to a power-law behaviour arrival time.

In this last phase, however, the flux decreases markedly, and from the point of view of the GRB observations, the most relevant regions are phases A and B described above, as well as the peak separating them.

Phase D

This last phase starts when the system approaches a Newtonian regime. In the case of GRB 991216 this occurs when $\gamma\simeq 1.05$, $t\simeq 5.0\times 10^{7}$ s, $t_a^d\simeq 3.1\times 10^{7}$ s and $r\simeq 1.0\times 10^{18}$ cm. In this phase $r\left(t\right)$ is again approaching a linear behaviour, due to the velocity decreasing less steeply than in Phase C. The emitted flux as a function of the laboratory time still does not show a power-law behaviour, while the observed flux as a function of detector arrival time does, with an index $n=-1.45$ (see Fig. 34).

XIX. THE POWER-LAW INDEX OF THE AFTERGLOW AND INFERENCES ON BEAMING IN GRBS

The results obtained in the previous sections have emphasized the relevance of the proper application of the RSTT paradigm to the determination of the power-law index of the afterglow. Particularly interesting is the subtle interplay between the different regimes in the relation between the laboratory time and the arrival time at the detector clearly expressed by Fig. 9 and the corresponding different regimes encountered in the first order expansion of the relativistic hydrodynamic equations of Taub [177] (see section XVIII). It is interesting to compare and contrast our treatment with selected results of the current literature, in order to illustrate some relevant points (see Tab. III). We will consider the results in the literature only with reference to the limiting case which we address in our work: the condition of fully radiative emission.

The first line of Tab. III describes the ultrarelativistic regime, corresponding to an increasing energy flux of the afterglow as a function of the arrival time (phase A in previous section). Our treatment and the results in the literature by Dermer et al. (see e.g. Böttcher & Dermer [20], Chiang & Dermer [29], Dermer et al. [41]) coincide. They agree as well with the results by Piran et al. (see e.g. Piran [116, 117], Sari & Piran [168]).

The second line corresponds to the relativistic regime, in which the energy flux of the afterglow, after having reached the maximum (point P in previous section), monotonically decreases (phase B in previous section). The dependence we have found of the gamma factor on the radial coordinate of the expanding ABM pulse does coincide with the one given by Dermer et al. and Piran et al. Our power law index n in this regime, which perfectly fits the data, however, is markedly different from the others. Particularly interesting is the difference between our results and those of Dermer et al: the two treatments coincide up to the last relation between the laboratory time and the arrival time at the detector. As explained in Eqs.(147-148), the two treatments differ in the approximation adopted in relating the laboratory time to the arrival time at the detector, illustrated in Fig. 9. Dermer et al. incorrectly adopted the approximation represented by the lower curve in Fig. 9 and consequently they do not find agreement with the observational data. We have not been able to retrace in the treatment by Piran et al. the steps which have led to their different results. Special mention must be made of a result stated by Halpern et al. [73], the last entry in line 2,

Table III: We compare and contrast the results on the power-law index n of the afterglow in the EMBH theory with other treatments in the current literature, in the limit of high energy and fully radiative conditions. The differences between the values of $-10/7 \sim -1.43$ (Dermer) and the results -1.6 in the EMBH theory can be retraced to the use of the two different approximation in the arrival time versus the laboratory time given in Fig. 9. See details in section XVIII.

	EMBH theory	Chiang & Dermer [29] Dermer et al. [41] Böttcher & Dermer [20]	Piran [116] Sari & Piran [168] Piran [117]	Vietri [180]	Halpern et al. [73]
Ultra-relativistic	$\gamma = \gamma_\circ$ $\gamma_\circ = 310.1$ $n = 2$	$\gamma = \gamma_\circ$ $n = 2$	$\gamma = \gamma_\circ$ $n \simeq 2$		
Relativistic	$\gamma \simeq r^{-3}$ $3.0 < \gamma < 258.5$ $n = -1.6$	$\gamma \sim r^{-3}$ $n = -\frac{10}{7} = -1.43$	$\gamma \sim r^{-3}$ $n = -\frac{5.5}{4} = -1.375$		$n > -1.47$
Non-relativistic	$n = -1.36$ $1.05 < \gamma < 3.0$			$n = -1.7$	
Newtonian	$n = -1.45$ $1 < \gamma < 1.05$				

that an absolute lower limit for the power-law index $n - 1.47$ can be established on theoretical grounds. Such a result, clearly not correct also on the basis of our analysis, has been erroneously used ti support the existence of beaming in GRBs, as we will see below.

The third line in Tab. III is also interesting, treating the nonrelativistic limit (Phase C in previous section). This regime has been analysed by Vietri [180], avoiding the exact integration of the equations and relying on simple qualitative arguments. These results are not confirmed by the integration of the equations we have performed. This is an interesting case to be examined for its pedagogical consequences. Having totally neglected the relation between the laboratory time and the time of arrival at the detector, which we have illustrated in Fig. 9, and identifying $t_a^d \equiv t$, Vietri reaches a very different power law from our. Moreover, his solution brings to an underestimation of the radial coordinate: he estimated a radial coordinate of $1.1 \times 10^{15}\, cm$ at $t_a^d = 3.5 \times 10^4\, s$, while the exact computation shows a result greater than $3.0 \times 10^{17}\, cm$ (see Tab. I). On the other hand if one assumes, from the above mentioned identity $t_a^d \equiv t$, $t = 3.5 \times 10^4\, s$, one obtains a gamma factor of ~ 300 (see Tab. I) in total disagreement with the nonrelativistic approximation adopted by Vietri. Quite apart from this pedagogical value, this nonrelativistic phase is of little interest from the observational point of view, due to the smallness of the flux emitted.

For completeness, we have also shown our estimates of the index n as the Newtonian phase approaches in the last line of Tab. III.

The perfect agreement between our theoretically predicted value for the power-law index, n_{theo}, and the observed one, n_{obs},

$$n_{theo} = -1.6, \quad n_{obs} = -1.616 \pm 0.067, \tag{152}$$

confirms the validity of our major assumptions:

1. The fully radiative regime.
2. The constant average density of the ISM ($n_{ism} = 1\, proton/cm^3$).
3. The spherical symmetry of the emission and the absence of beaming in GRB 991216.

After the work of Mao & Yi [91] pointing to the possibility of introducing beaming to reduce the energetics of GRBs and after the discovery of the afterglow, many articles have appeared trying to obtain theoretical and observational evidence for beamed emission in GRBs. The observations have ranged from radio (see e.g. Frail et al. [54], Rol et al. [134]) to optical (see e.g. Garnavich, et al [63], Halpern et al. [73], Sagar et al. [161], Schaefer [169]) all the way to X-rays. Particular attention has been devoted to relating the existence of beaming to possible breaks in the light curve slope, generally expected at a value of the gamma factor

$$\gamma = \frac{1}{\vartheta_0}, \tag{153}$$

where ϑ_0 is the beam opening angle. There are many articles on this subject; to mention only the most popular ones, we recall Mészáros et al. [97], Panaitescu & Mészáros [115], Rhoads [129, 130, 131], Sari, at al. [167]. Far from having reached a standard formulation, these approaches differ from each other in the expected time at which the break should take place up to a factor of 20 (see e.g. Sari, at al. [167]). They differ as well for the opening angle of the beam, up to a factor of 3 (see e.g. Sari, at al. [167]). Disagreement still exists on the number of breaking points: two in the case of Panaitescu & Mészáros [115], one in the case of Sari, at al. [167], one again in the case of Rhoads [129, 130, 131] but differing in position from the one of Sari, at al. [167]. It has also been noticed that other authors have shown through numerical simulations that such a transition, if visible at all, is not very sharp (see e.g. Halpern et al. [73]).

Ample observational data have been obtained for the GRB 991216, in addition to the X-ray band, also in the optical and radio. For the reason mentioned at the beginning of section XV, we only address in this article the problem of the γ- and the X-ray emission. In that respect, the main article addressing the issue of beaming in the X-rays for GRB 991216 is the one of Halpern et al. [73]. The key argument is based on the theoretical inequality claimed to exist for the power-law index $n > -1.47$ (see above). The fact that the observed X-ray decay rate is found to be $n_{obs} = 1.616 \pm 0.067$ is interpreted by the authors as evidence for beaming. Moreover, the fact that the decay rate $n = -1.6$ has been observed before a steepening in the optical decay occurred at approximately 1 day of arrival time authorized an even more extreme proposal of a narrower beam in the X-rays within the optical beam.

It is clear from the entire treatment which we have presented and the results of the EMBH theory given by $n_{theo} = -1.6$ that there is no evidence for such a beaming, as already stated above. The motivation by Halpern et al. [73] stems from the incorrect theoretical assumption of the existence of a lower limit in the afterglow power-law index $n > -1.47$. From our theoretical analysis the existence of $n = -1.6$ is clear proof of isotropic emission in the GRB 991216 and a clear test of the complete relativistic treatment of the source. The fact that the break in the index should be "achromatic" and the absence of beaming in the X-rays imply an absence of beaming also in the optical and radio bands. The observed steepening in the optical decay has to find an alternative explanation. Although this is not the subject of our present work for the above mentioned reasons, we have found interesting the considerations by Panaitescu & Kumar [111], which find that "there are some major difficulties to apply a jet model to GRB 991216". They also state, still for GRB 991216, that "the steepening of the optical decay of a few days is not due to a jet effect, as suggested by Halpern et al. [73], but to the passage of a spectral break".

Concerning our own position on the possibility of beaming in GRBs, we would like just to remark that, from a preliminary analysis of beamed emission within the EMBH model, we have found some new features which are not encompassed by the results in the current literature, and they could become a distinctive signature for the discrimination of the existence or nonexistence of beaming (Ruffini et al. [151]). The study of the steepening in the optical and radio decay is addressed within the EMBH theory in Ruffini et al. [150].

XX. SUBSTRUCTURES IN THE E-APE DUE TO INHOMOGENEITIES IN THE INTERSTELLAR MEDIUM

The afterglow is emitted as the ABM pulse plows through the interstellar matter engulfing new baryonic material. In our previous articles we were interested in explaining the overall energetics of the GRB phenomena and in this sense, we have adopted the very simplified assumption that the interstellar medium is a constant density medium with $n_{ism} = 1/cm^3$. Consequently, the afterglow emission obtained is very smooth in time. We are now interested in seeing if in this framework we can also explain most of the time variability observed by BATSE (see e.g. Fishman & Meegan [53]), all of which except for the P-GRB should correspond to the beam-target phase in the IBS paradigm.

We pursue this treatment neglecting the angular spreading due to off-axis scattering in the radiation of the afterglow, which will be presented in sections XXI–XXIII.

Our goal is to focus in this simplified model on the basic energetic parameters as well as on the drastic consequences of the space-time variables expressed in the RSTT paradigm.

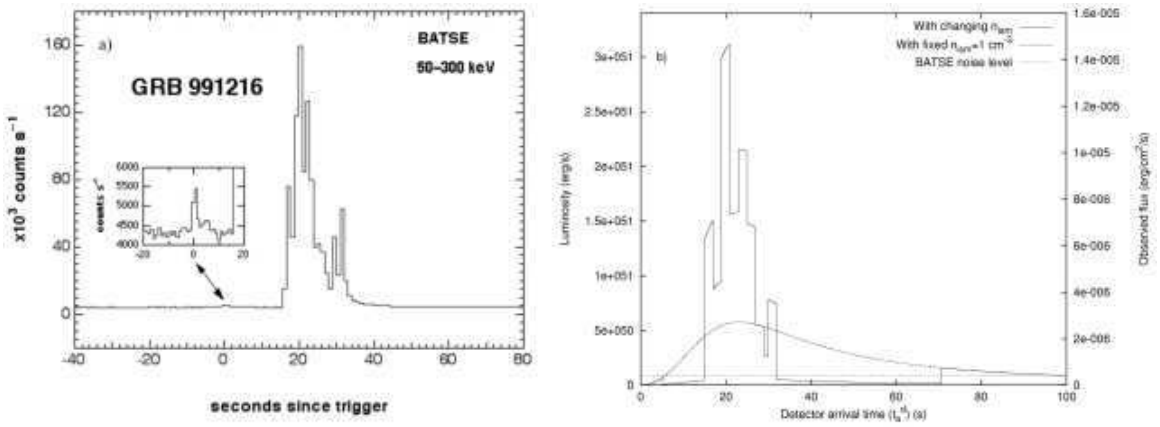

Figure 36: **a)** Flux of GRB 991216 observed by BATSE. The enlargement clearly shows the P-GRB (see Ruffini et al. [145]). **b)** Flux computed in the collision of the ABM pulse with an ISM cloud with the density profile given in Fig. 37. The dashed line indicates the emission from an uniform ISM with $n = 1cm^{-3}$. The dotted line indicates the BATSE noise level.

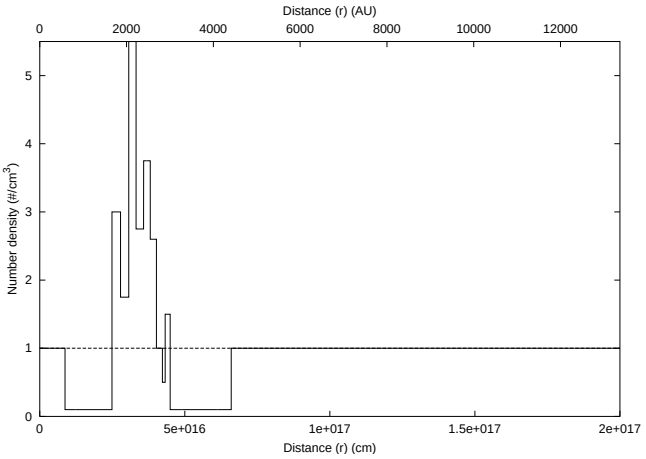

Figure 37: The density contrast of the ISM cloud profile introduced in order to fit the observation of the burst of GRB991216. The dashed line indicates the average uniform density $n = 1cm^{-3}$.

Having obtained the two results presented in Fig. 8 and Fig. 34, we can proceed to attack the specific problem of the time variability observed by BATSE.

The fundamental point is that in both regimes *the flux observed in the arrival time is proportional to the interstellar matter density*: any inhomogeneity in the interstellar medium $\Delta n_{ism}/\overline{n}_{ism}$ will lead correspondingly to a proportional variation in the intensity $\Delta I/\overline{I}$ of the afterglow. This result has been erroneously interpreted in the current literature as a burst originating in an unspecified "inner engine".

In particular, for the main burst observed by BATSE (see Fig. 36a) we have

$$\left(\Delta I/\overline{I}\right) = \left(\Delta n_{ism}/n_{ism}\right) \sim 5. \tag{154}$$

There are still a variety of physical circumstances which may lead to such density inhomogeneities.

The additional crucial parameter in understanding the physical nature of such inhomogeneities is the time scale of the burst observed by BATSE. Such a burst lasts $\Delta t_a \simeq 20s$ and shows substructures on a time scale of $\sim 1s$ (see Fig. 36a). In order to infer the nature of the structure emitting such a burst we must express these times scales in the

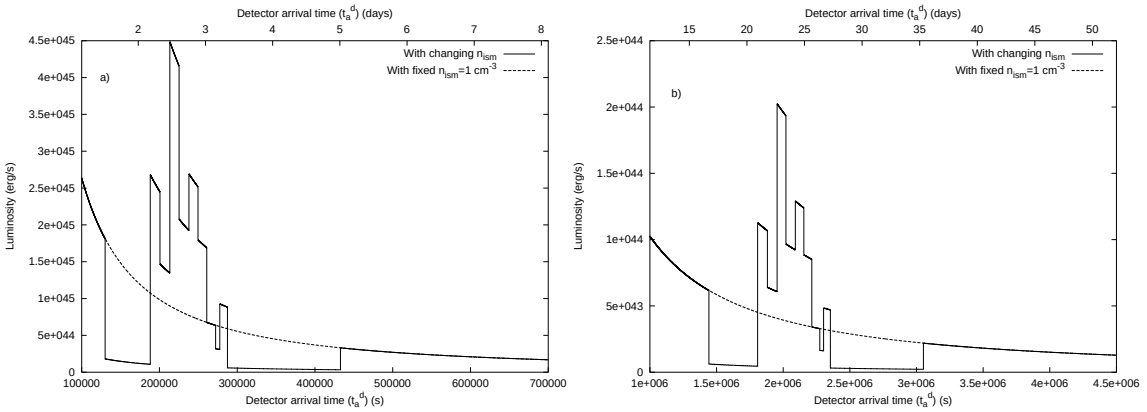

Figure 38: **a)** Same as Fig. 36b with the ISM cloud located at a distance of $3.17 \times 10^{17} cm$ from the EMBH, the time scale of the burst now extends to $\sim 1.58 \times 10^5 s$. **b)** Same as a) with the ISM cloud at a distance of $4.71 \times 10^{17} cm$ from the EMBH, the time scale of the burst now extends to $\sim 1.79 \times 10^6 s$.

laboratory time (see Ruffini et al. [144]). Since we are at the peak of the GRB we have $\gamma_{P_A} \sim 258.5$ (see Eq.(141)) and Δt_a corresponds in the laboratory time to an interval

$$\Delta t \sim 1.0 \times 10^6 s, \tag{155}$$

which determines the characteristic size of the inhomogeneity creating the burst $\Delta L \sim 5.0 \times 10^{16} cm$ (see Tab. I and Fig. 9).

It is immediately clear from Eq.(154) and Eq.(155) that these are the typical dimensions and density contrasts corresponding to a small interstellar cloud. As an explicit example we have shown in Fig. 37 the density contrasts and dimensions of an interstellar cloud with an *average density* $< n >= 1/cm^3$. Such a cloud is located at a distance of $\sim 8.7 \times 10^{15} cm$ from the EMBH, gives rise to a signal similar to the one observed by BATSE (see Fig. 36b).

It is now interesting to see the burst that would be emitted, if our present approximation would still apply, by the interaction of the ABM pulse with the same ISM cloud encountered at later times during the evolution of the afterglow. Fig. 38a shows the expected structure of the burst at a distance $4.1 \times 10^{17} cm$, corresponding to an arrival time delay of ~ 2 days, where the gamma factor is now $\gamma_\star \sim 3.6$. It is interesting that the overall intensity would be smaller, the intensity ratio of the burst relative to the average emission would remains consistent with Eq.(154), but the time scales of the burst would be longer by a factor $\left(\frac{\gamma_{P_A}}{\gamma_\star}\right)^2 \simeq 5 \times 10^3$. Fig. 38b shows the corresponding quantities for the same ISM cloud located at a distance $6.4 \times 10^{17} cm$ from the EMBH, corresponding to an arrival time delay of ~ 1 month, where the gamma factor is ~ 1.5.

We are going to analyze in the coming sections the modifications of this basic theory by the effect of the angular spreading: it will increase the accuracy of the fit obtained in Fig. 36 and will wash away all the features at late arrival time in the afterglow (see Fig. 38).

XXI. CONSIDERATIONS ON THE RELATIVISTIC BEAMING ANGLES AND ON THE ARRIVAL TIME

We now generalize the results obtained in section V to consider also the effects due to the size of the emitting surface and of its curvature. The frequency ω and wave-vector $\mathbf{k}$ of photons emitted from the ABM pulse (see Fig. 39) expressed in the laboratory frame are:

$$\mathbf{k} = \frac{\omega}{c} \left(-\sin\vartheta \mathbf{u} + \cos\vartheta \mathbf{v} \right) , \quad |\mathbf{k}| = \frac{\omega}{c} , \tag{156}$$

where ϑ is the angle (in the laboratory frame) between the radial expansion velocity and the line of sight, $\mathbf{v}$ is a unit vector along the radial expansion velocity of the ABM pulse, and $\mathbf{u}$ is a unit vector orthogonal to $\mathbf{v}$ oriented toward

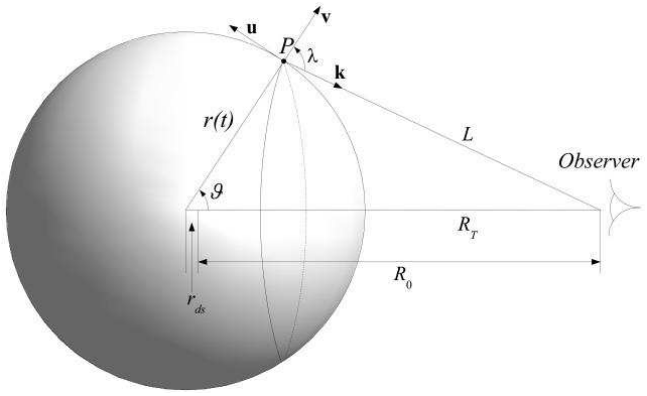

Figure 39: Qualitative description of the kinematics of the system. The big sphere is the expanding ABM pulse interacting with the ISM (not shown in the picture). The radius of the ABM pulse at time t is $r\,(t)$. The generic point P on the ABM pulse, from which the photon is emitted, corresponds to a displacement angle ϑ from the line of sight. L is the distance of P from the observer. $R_{\rm T}$ is the distance of the EMBH from the observer. $r_{\rm ds}$ is the dyadosphere radius. R_0 is defined by $R_0 \equiv R_{\rm T} - r_{\rm ds}$. $\mathbf{v}$ is a unit vector along the radial expansion velocity. $\mathbf{u}$ is a unit vector orthogonal to $\mathbf{v}$ oriented toward rising ϑ. $\mathbf{k}$ is the momentum of the photons emitted toward the observer. Note that we have assumed $\vartheta \equiv \lambda$, i.e. $\mathbf{k} \parallel R_{\rm T}$ (see text).

rising ϑ. We are assuming here that $\mathbf{k}$ and $R_{\rm T}$ are parallel, also for photons emitted with $\vartheta \neq 0$, so that $\lambda \equiv \vartheta$. This is clearly a good approximation, because the distance $R_{\rm T}$ corresponds to a redshift $z \sim 1$, while the radius of the emitting region is less than a light year in order of magnitude. Then the Lorentz boost along $\mathbf{v}$ to the comoving frame of the ABM pulse yields the corresponding comoving quantities:

$$\omega_\circ = \gamma\omega\left(1 - \frac{v}{c}\cos\vartheta\right), \quad \omega_\circ = |\mathbf{k}_\circ|\, c, \tag{157}$$

$$\mathbf{k}_\circ = -\,|\mathbf{k}|\sin\vartheta\mathbf{u} + \gamma\,|\mathbf{k}|\left(\cos\vartheta - \frac{v}{c}\right)\mathbf{v}, \tag{158}$$

In the comoving frame photons radiating out of the ABM pulse must have (see Eq.(158)):

$$\cos\vartheta \geq \frac{v}{c}, \tag{159}$$

because the component of the photon momentum in the comoving frame along the radial expansion velocity direction must be positive in order to escape. There will then be a maximum allowed ϑ value ϑ_{max} defined by $\cos\vartheta_{max} = (v/c)$ (see Figs. 40–41).

Due to the high value of the Lorentz gamma factor (~ 300) for the bulk motion of the expanding ABM pulse, the spherical waves emitted from its external surface appear extremely distorted to a distant observer. Let us indicate by t_a the arrival time at a detector of a photon emitted at a laboratory time t by the spherical surface of the relativistically expanding shell (see also section V). Photons arriving at the same time t_a will be emitted at different t as a function of the angle ϑ (see Fig. 39). The relation between t and $t_{\rm a}$ in the case of a constant $\gamma \sim 5$ for expanding radio sources was found by Rees (see Rees [127]):

$$t_{\rm a} = t\left(1 - \frac{v}{c}\cos\vartheta\right). \tag{160}$$

For a constant expansion speed, the radius $r\,(t)$ of the source is given by:

$$r\,(t) = vt\,. \tag{161}$$

From Eqs.(160–161) we find the equation describing the "surface" emitting the photons detected at arrival time $t_{\rm a}$:

$$r = \frac{v\,t_{\rm a}}{1 - \frac{v}{c}\cos\vartheta}, \tag{162}$$

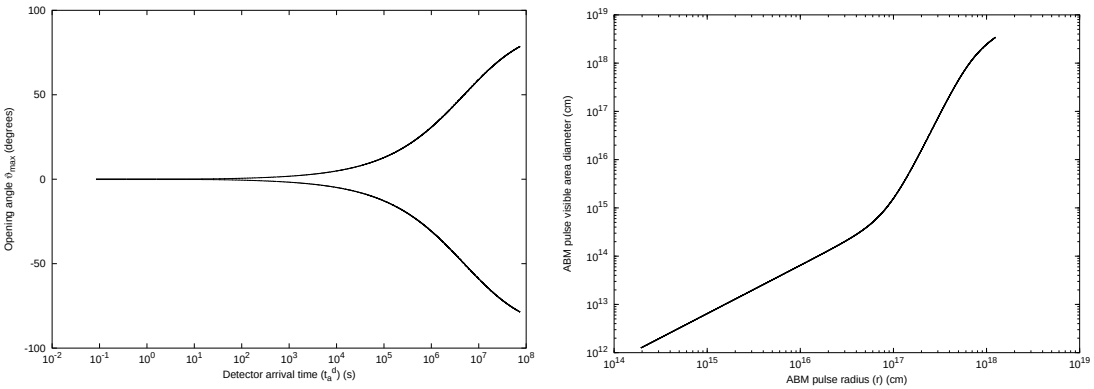

Figure 40: **Left)** Not all values of ϑ are allowed. Only photons emitted at an angle such that $\cos\vartheta \geq (v/c)$ can be viewed by the observer. Thus the maximum allowed ϑ value ϑ_{max} corresponds to $\cos\vartheta_{max} = (v/c)$. In this figure we represent ϑ_{max} (i.e. the angular amplitude of the visible area of the ABM pulse) in degrees as a function of the arrival time at the detector for the photons emitted along the line of sight (see text). In the earliest GRB phases $v \sim c$ and so $\vartheta_{max} \sim 0$. On the contrary, in the latest phases of the afterglow the ABM pulse velocity decreases and ϑ_{max} tends to the maximum possible value, i.e. 90°. **Right)** The diameter of the visible area is represented as a function of the ABM pulse radius. In the earliest expansion phases ($\gamma \sim 310$) ϑ_{max} is very small (see left pane and Fig. 41), so the visible area is just a small fraction of the total ABM pulse surface. On the other hand, in the final expansion phases $\vartheta_{max} \to 90^\circ$ and almost all the ABM pulse surface becomes visible.

which describes an ellipsoid of eccentricity $\frac{v}{c}$ (see Rees [127]).

In our case the ABM pulse Lorentz gamma factor is not constant (see Fig. 8), and so we must generalize Eqs.(160,162) to nonconstant expansion velocity. This can be done using the geometry of Fig. 39. We set $t = 0$ when the plasma starts to expand, so that $r(0) = r_{\rm ds}$, i.e. the dyadosphere radius. Let a photon be emitted at time t from the point P. Its distance from the observer is L. The time it takes to arrive at the detector is of course $\frac{L}{c}$. Thus its arrival time, measured from the arrival of the first photon a time $\frac{R_0}{c}$ after its emission at $t = 0$, is:

$$t_{\rm a} = t + \frac{L}{c} - \frac{R_0}{c}\,, \tag{163}$$

where we have defined $t_{\rm a} = 0$ when a photon emitted at $t = 0$ and $\vartheta = 0$ reaches the observer. L is clearly given by:

$$L = \sqrt{R_{\rm T}^2 + r(t)^2 - 2\,R_{\rm T}\,r(t)\cos\vartheta}\,, \tag{164}$$

where at any given value of emission time t, $\cos\vartheta$ can assume any value between $\left(\frac{v(t)}{c}\right)$ and 1 as noted above, where $v(t)$ is the expansion speed of the ABM pulse at time t (see Eq.(159)). Now $r(t)$ is less than one light year in order of magnitude while $R_{\rm T}$ corresponds to a redshift $z \sim 1$. Thus we can expand the right hand side of equation (164) in powers of $\frac{r(t)}{R_{\rm T}}$ to first order:

$$L \simeq R_{\rm T}\left(1 - \frac{r(t)}{R_{\rm T}}\,\cos\vartheta\right)\,, \tag{165}$$

which corresponds to assuming L to be equal to its projection on the line of sight (see Fig. 39). Substituting (165) into (163) yields:

$$t_{\rm a} = t + \frac{r_{\rm ds}}{c} - \frac{r(t)}{c}\cos\vartheta\,, \tag{166}$$

where we have used the fact that $R_{\rm T} = R_0 + r_{\rm ds}$ (see Fig. 39). For $r(t)$ we can use the following expression:

$$r(t) = \int_0^t v(t')\,dt' + r_{\rm ds}, \tag{167}$$

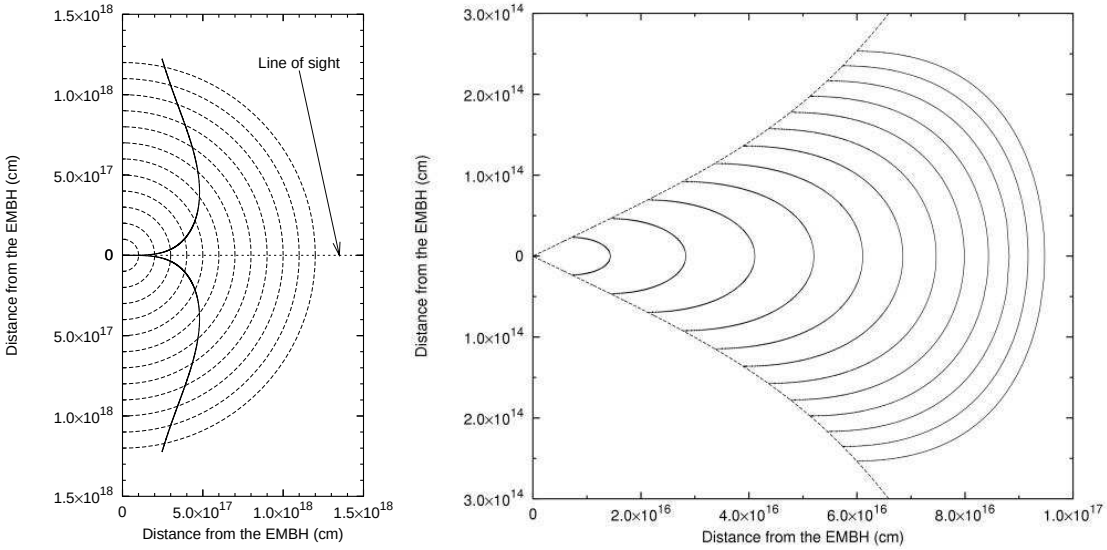

Figure 41: **Left)** This figure shows the temporal evolution of visible area of the ABM pulse. The dashed half-circles are the expanding ABM pulse at radii corresponding to different laboratory times. The black curve marks the boundary of the visible region. The EMBH is located at position (0,0) in this plot. Again, in the earliest GRB phases the visible region is squeezed along the line of sight, while in the final part of the afterglow phase almost all the emitted photons reach the observer. This time evolution of the visible area is crucial to the explanation of the GRB temporal structure. **Right)** Due to the extremely high and extremely varying Lorentz gamma factor, photons reaching the detector on the Earth at the same arrival time are actually emitted at very different times and positions. We represent here the surfaces of photon emission corresponding to selected values of the photon arrival time at the detector: the *equitemporal surfaces* (EQTS). Such surfaces differ from the ellipsoids described by Rees in the context of the expanding radio sources with typical Lorentz factor $\gamma \sim 4$ and constant. In fact, in GRB 991216 the Lorentz gamma factor ranges from 310 to 1. The EQTSes represented here (solid lines) correspond respectively to values of the arrival time ranging from $5\,s$ (the smallest surface on the left of the plot) to $60\,s$ (the largest one on the right). Each surface differs from the previous one by $5\,s$. To each EQTS contributes emission processes occurring at different values of the Lorentz gamma factor. The dashed lines are the boundaries of the visible area of the ABM pulse and the EMBH is located at position $(0, 0)$ in this plot. Note the different scale on the two axes, indicating the very high EQTS "effective eccentricity". The time interval from 5 s to 60 s has been chosen to encompass the E-APE emission, ranging from $\gamma = 308.8$ to $\gamma = 56.84$.

so that equation (166) can be written in the form:

$$t_{\rm a} = t - \frac{\int_0^t v\,(t')\,dt' + r_{\rm ds}}{c}\cos\vartheta + \frac{r_{\rm ds}}{c}, \tag{168}$$

which reduces to Eq.(160) only if v is constant and $r_{\rm ds}$ is negligible with respect to $r\,(t)$.

Also from Eq.(168) we can obtain the equation describing the surface that emits the photons detected at an arrival time $t_{\rm a}$. In this case, we no longer have ellipsoids of constant eccentricity $\frac{v}{c}$. Since the velocity is strongly varying from point to point, we have more complicated surfaces like the profiles reported in Fig. 41 where at every point there will be a tangent ellipsoid of a given eccentricity, but such an ellipsoid varies in eccentricity from point to point.

For a fixed time t of emission in Eq.(168), the allowed angular interval $\frac{v}{c} \leq \cos\vartheta \leq 1$ leads to a corresponding smearing of the arrival time t_a over the interval

$$\Delta t_a = \frac{r}{\gamma^2 c\left(1+\frac{v}{c}\right)}\,. \tag{169}$$

We need now to correct Eq.(168) for the cosmological expansion effects to get the wanted relation between t and t_a^d. We recall that (see section V)

$$t_a^d = (1+z)\,t_a\,, \tag{170}$$

where z is the cosmological redshift. Our final relation is therefore:

$$t_a^d = (1+z)\left(t - \frac{\int_0^t v\,(t')\,dt' + r_{\rm ds}}{c}\cos\vartheta + \frac{r_{\rm ds}}{c}\right). \tag{171}$$

XXII. THE EMISSION PROCESS TAKING OFF-AXIS CONTRIBUTIONS INTO ACCOUNT

We now take into consideration the contributions of the off-axis emission to the afterglow to see if the previous positive results still hold and if some of the problems just stated can be overcome by a more detailed and relativistic treatment. The corresponding computation for the P-GRB structure will be presented elsewhere, where the time evolutions of the dyadosphere formation and its consequences on the P-GRB structures are presented following the work of Cherubini et al. [28], Ruffini & Vitagliano [156, 157], Ruffini et al. [159]. The effects on the P-GRB structure of the dyadosphere formation dominate those due to the angular spreading.

Following Eqs.(110–111), we recall that in the comoving frame of the expanding ABM pulse we suppose that the internal energy due to kinetic collision is instantly radiated away and that the corresponding emission is isotropic. As in section II, let $\Delta\varepsilon$ be the internal energy density developed in the collision. In the comoving frame the energy per unit of volume and per solid angle is simply

$$\left(\frac{dE}{dV\,d\Omega}\right)_\circ = \frac{\Delta\varepsilon}{4\pi} \tag{172}$$

due to the fact that the emission is isotropic in this frame. The total number of photons emitted is an invariant quantity independent of the frame used. Thus we can compute this quantity as seen by an observer in the comoving frame (which we denote with the subscript "$\circ$") and by an observer in the laboratory frame (which we denote with no subscripts). Doing this we find

$$\frac{dN_\gamma}{dt d\Omega d\Sigma} = \int_{shell}\left(\frac{dN_\gamma}{dt d\Omega d\Sigma}\right)_\circ \Lambda^{-3}\cos\vartheta\,, \tag{173}$$

where $\cos\vartheta$ comes from the projection of the elementary surface of the shell on the direction of propagation and $\Lambda = \gamma(1-\beta\cos\vartheta)$ is the Doppler factor introduced in the two following differential transformation

$$d\Omega_\circ = d\Omega \times \Lambda^{-2} \tag{174}$$

for the solid angle transformation and

$$dt_\circ = dt \times \Lambda^{-1} \tag{175}$$

for the time transformation. The integration in $d\Sigma$ is performed over the visible area of the ABM pulse at laboratory time t, namely with $0 \le \vartheta \le \vartheta_{max}$ and ϑ_{max} defined in section XXI (see Eq.(159) and Figs. 40–41). An extra Λ factor comes from the energy transformation:

$$E_\circ = E \times \Lambda\,. \tag{176}$$

See also Chiang & Dermer [29]. Thus finally we obtain:

$$\frac{dE}{dt d\Omega d\Sigma} = \int_{shell}\left(\frac{dE}{dt d\Omega d\Sigma}\right)_\circ \Lambda^{-4}\cos\vartheta\,. \tag{177}$$

Doing this we clearly identify $\left(\frac{dE}{dt d\Omega d\Sigma}\right)_\circ$ as the energy density in comoving frame up to a factor $\frac{v}{4\pi}$ (see Eq.(172)). Then we have:

$$\frac{dE}{dt d\Omega} = \int_{shell}\frac{\Delta\varepsilon}{4\pi}\,v\,\cos\vartheta\,\Lambda^{-4}\,d\Sigma\,, \tag{178}$$

where the integration in $d\Sigma$ is performed over the ABM pulse visible area at laboratory time t, namely with $0 \le \vartheta \le \vartheta_{max}$ and ϑ_{max} defined in section XXI.

Eq.(178) gives us the energy emitted toward the observer per unit solid angle and per unit laboratory time t in the laboratory frame. But what we really need is the energy emitted per unit solid angle and per unit detector arrival

time t_a^d, so we must use the complete relation between t_a^d and t given in Eq.(171). First we have to multiply the integrand in Eq.(178) by the factor $\left(dt/dt_a^d\right)$ to transform the energy density generated per unit of laboratory time t into the energy density generated per unit arrival time t_a^d. Then we have to integrate with respect to $d\Sigma$ over the *equitemporal surface* (EQTS, see section XXI) of constant arrival time t_a^d instead of the ABM pulse visible area at laboratory time t. The analog of Eq.(178) for the source luminosity in detector arrival time is then:

$$\frac{dE_\gamma}{dt_a^d d\Omega} = \int_{EQTS} \frac{\Delta\varepsilon}{4\pi}\, v\, \cos\vartheta\, \Lambda^{-4}\, \frac{dt}{dt_a^d} d\Sigma\,. \tag{179}$$

It is important to note that, in the present case of GRB 991216, the Doppler factor Λ^{-4} in Eq.(179) enhances the apparent luminosity of the burst, as compared to the intrinsic luminosity, by a factor which at the E-APE is in the range between 10^{10} and 10^{12}!

To perform the numerical integration of Eq.(179) we have implemented the following procedure for each fixed value of the laboratory time t:

1. We fix the laboratory time t.

2. We divide the interval of the allowed values $(v\,(t)\,/c) \leq \cos\vartheta \leq 1$ into N small steps, each one of amplitude

$$\Delta_N\,(\cos\vartheta) = \frac{1-(v\,(t)\,/c)}{N}\,. \tag{180}$$

3. We select n directions defined by:

$$\cos\vartheta_n = 1 - n\Delta\,(\cos\vartheta)\ , \tag{181}$$

   where n is an integer, $0 \leq n \leq N$ and so $\vartheta_0 = 0$ and $\vartheta_n = \vartheta_{max}$.

4. For each ϑ_n we compute with Eq.(179) the contribution to the afterglow luminosity arising from an angular aperture corresponding to $\Delta_N\,(\cos\vartheta)$ around such a direction.

5. We compute for each value of n the corresponding values of the arrival time t_a^d using Eq.(171).

To obtain the total luminosity at arrival time t_a^d we sum together all the above contributions corresponding to the same t_a^d.

We first apply this treatment to the analysis of the afterglow using assumptions 1 and 2 of section. II, namely that the ISM density is constant $n_{ism} =< n_{ism} >= 1\,\text{particle/cm}^3$ and that the ABM is spherically symmetric.

Fig. 42 compares the new result for the afterglow luminosity as a function of the detector arrival time with the previous one obtained in section XV by neglecting off-axis emission. The main conclusions are:

1. The total energy emitted both in the radial approximation and in the full computation with the off-axis emission is conserved. This is a necessary condition for checking the consistency of the model.

2. The slope of the decreasing part of the afterglow is unchanged. We emphasize once more the great advantage of the radial approximation which has allowed to obtain an analytic expression for this slope.

3. The final phase of the afterglow ($\gamma < 2$) is largely affected by the late arrival of the radiation emitted at large angles. In fact in the radial approximation the luminosity goes abruptly to zero when γ reaches 1 while in the new complete treatment the behavior is much smoother due to the delayed arrival of the radiation emitted at large angles. Consequently, enforcing the energy conservation, in the rising part of the afterglow the luminosity in the new treatment is shown to be slightly smaller than in the radial case.

In order to acquire a better understanding of the effects of angular spreading, we have found it helpful to analyze the radiation emitted from selected angles ϑ between 0 and ϑ_{max}. This is in addition to the integration results presented in Fig. 42. In Fig. 42 we show the results of such an analysis plotting the contributions to the total luminosity corresponding to selected values of n in Eq.(181). We easily see that radiation emitted at large angles is time shifted with respect to that emitted near the line of sight. In fact the afterglow peak occurs later going to higher n values (see Fig. 42).

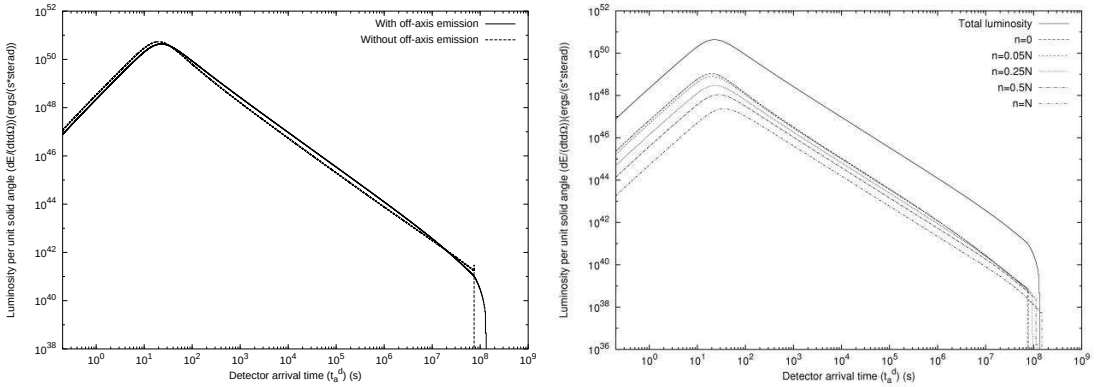

Figure 42: **Left)** The predicted afterglow curve for GRB 991216 assuming a constant ISM density equal to $1\,\text{particle/cm}^3$ and taking into account all the effects due to off-axis emission (solid line). For comparison we plot also the corresponding curve obtained in the simple radial approximation (dashed line). We see that this last curve falls sharply to zero when the ABM pulse reaches $\gamma = 1$, while the first one has a much smoother behavior due to the time delay in the arrival of the photons emitted at large ϑ. Recall that when γ tends to 1, the maximum allowed values of ϑ tend to 90°. **Right)** This figure shows how the radiation emitted from different angles contributes to the afterglow luminosity. The solid line on the top of the picture is the total luminosity as in the previous plots. The other dashed and dotted curves represent the radiation components corresponding to selected values of n in Eq.(181). From the upper to the lower one they corresponds respectively to $n = 0$, $n = 0.05N$, $n = 0.25N$, $n = 0.5N$, $n = N$, where in this plot $N = 200$. We can easily see that the radiation emitted at large angles ($n = N$) is time shifted with respect to that emitted near the line of sight ($n = 0$).

Table IV: For each ISM density peak represented in Fig. 43 we give the initial radius r, the corresponding comoving time τ, laboratory time t, arrival time at the detector t_a^d, diameter of the ABM pulse visible area d_v, Lorentz factor γ and observed duration Δt_a^d of the afterglow luminosity peaks generated by each density peak. In the last column, the apparent motion in the radial coordinate, evaluated in the arrival time at the detector, leads to an enormous "superluminal" behavior, up to $9.5 \times 10^4\, c$.

Peak	$r(cm)$	$\tau(s)$	$t(s)$	$t_a^d(s)$	$d_v(cm)$	$\Delta t_a^d(s)$	γ	"Superluminal" $v \equiv \frac{r}{t_a^d}$
A	4.50×10^{16}	4.88×10^3	1.50×10^6	15.8	2.95×10^{14}	0.400	303.8	$9.5 \times 10^4 c$
B	5.20×10^{16}	5.74×10^3	1.73×10^6	19.0	3.89×10^{14}	0.622	265.4	$9.1 \times 10^4 c$
C	5.70×10^{16}	6.54×10^3	1.90×10^6	22.9	5.83×10^{14}	1.13	200.5	$8.3 \times 10^4 c$
D	6.20×10^{16}	7.64×10^3	2.07×10^6	30.1	9.03×10^{14}	5.16	139.9	$6.9 \times 10^4 c$
E	6.50×10^{16}	9.22×10^3	2.17×10^6	55.9	2.27×10^{15}	10.2	57.23	$3.9 \times 10^4 c$
F	6.80×10^{16}	1.10×10^4	2.27×10^6	87.4	2.42×10^{15}	10.6	56.24	$2.6 \times 10^4 c$

XXIII. THE E-APE TEMPORAL SUBSTRUCTURES TAKING INTO ACCOUNT THE OFF-AXIS EMISSION

We are now ready to reconsider the problem of the ISM inhomogeneity generating the temporal substructures in the E-APE by integrating on the EQTS surfaces and improving on the considerations based on the purely radial approximation. We have created (see details in Ruffini et al. [153]) an ISM inhomogeneity "mask" (see Fig. 43 and Tab. IV) with the main criteria that the density inhomogeneities and their spatial distribution still fulfill $< n_{ism} >= 1\,\text{particle/cm}^3$.

The results are given in Fig. 44. We obtain, in perfect agreement with the observations:

1. the theoretically computed intensity of the A, B, C peaks as a function of the ISM inhomogneities;
2. the fast rise and exponential decay shape for each peak;
3. a continuous and smooth emission between the peaks.

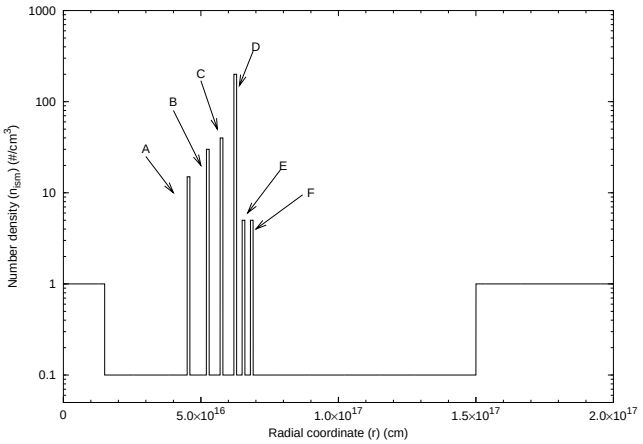

Figure 43: The density profile ("mask") of an ISM cloud used to reproduce the GRB 991216 temporal structure. As before, the radial coordinate is measured from the black hole. In this cloud we have six "spikes" with overdensity separated by low density regions. Each spike has the same spatial extension of 10^{15} cm. The cloud average density is $< n_{ism} >= 1\,\mathrm{particle/cm^3}$.

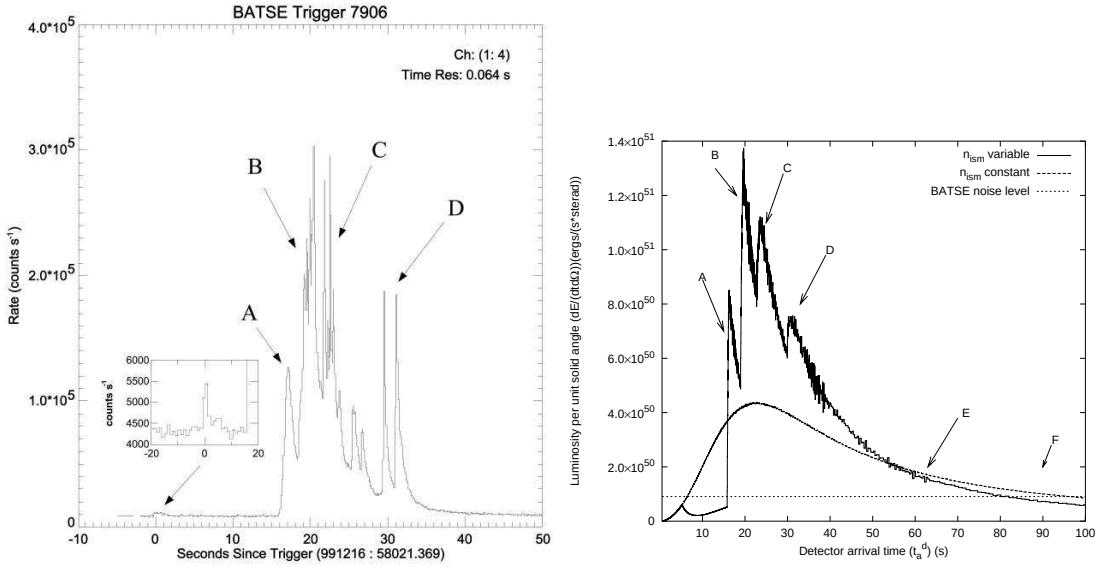

Figure 44: **Left)** The BATSE data on the E-APE of GRB 991216 (source: BATSE GRB light curves [5]) together with an enlargement of the P-GRB data (source: BATSE Rapid Burst Response [6]). For convenience each E-APE peak has been labeled by a different uppercase Latin letter. **Right)** The source luminosity connected to the mask in Fig. 43 is given as a function of the detector arrival time (solid "spiky" line) with the corresponding curve for the case of constant $n_{ism} = 1\,\mathrm{particle/cm^3}$ (dashed smooth line) and the BATSE noise level (dotted horizontal line). The "noise" observed in the theoretical curves is due to the discretization process adopted, described in Ruffini et al. [153], for the description of the angular spreading of the scattered radiation. For each fixed value of the laboratory time we have summed 500 different contributions from different angles. The integration of the equation of motion of this system is performed in $22,314,500$ contributions to be considered. An increase in the number of steps and in the precision of the numerical computation would lead to a smoother curve.

Interestingly, the signals from shells E and F, which have a density inhomogeneity comparable to A, are undetectable. The reason is due to a variety of relativistic effects and partly to the spreading in the arrival time, which for A, corresponding to $\gamma = 303.8$ is $0.4s$ while for E (F) corresponding to $\gamma = 57.23$ (56.24) is of 10.2 s (10.6 s) (see Tab. IV and Ruffini et al. [148, 153]).

In the case of D, the agreement with the arrival time is reached, but we do not obtain the double peaked structure. The ABM pulse visible area diameter at the moment of interaction with the D shell is $\sim 1.0 \times 10^{15}$ cm, equal to the extension of the ISM shell (see Tab. IV and Ruffini et al. [148, 153]). Under these conditions, the concentric shell approximation does not hold anymore: the disagreement with the observations simply makes manifest the need for a more detailed description of the three dimensional nature of the ISM cloud.

The physical reasons for these results can be simply summarized: we can distinguish two different regimes corresponding in the afterglow of GRB 991216 respectively to $\gamma > 150$ and to $\gamma < 150$. For different sources this value may be slightly different. In the E-APE region ($\gamma > 150$) the GRB substructure intensities indeed correlate with the ISM inhomogeneities. In this limited region (see peaks A, B, C) the Lorentz gamma factor of the ABM pulse ranges from $\gamma \sim 304$ to $\gamma \sim 200$. The boundary of the visible region is smaller than the thickness ΔR of the inhomogeneities (see Fig. 41 and Tab. IV). Under this condition the adopted spherical approximation is not only mathematically simpler but also fully justified. The angular spreading is not strong enough to wipe out the signal from the inhomogeneity spike.

As we descend in the afterglow ($\gamma < 150$), the Lorentz gamma factor decreases markedly and in the border line case of peak D $\gamma \sim 140$. For the peaks E and F we have $\gamma \sim 50$ and, under these circumstances, the boundary of the visible region becomes much larger than the thickness ΔR of the inhomogeneities (see Fig. 41 and Tab. IV). A three dimensional description would be necessary, breaking the spherical symmetry and making the computation more difficult. However we do not need to perform this more complex analysis for peaks E and F: any three dimensional description would *a fortiori* augment the smoothing of the observed flux. The spherically symmetric description of the inhomogeneities is already enough to prove the overwhelming effect of the angular spreading (Ruffini et al. [153]).

On this general issue of the possible explanation of the observed substructures with the ISM inhomogeneities, there exists in the literature two extreme points of view: the one by Fenimore and collaborators (see e.g. Fenimore et al. [48], Fenimore [49], Fenimore et al. [50]) and Piran and collaborators (see e.g. Piran [116, 117], Piro et al., [120], Sari & Piran [165]) on one side and the one by Dermer and collaborators (Dermer [38], Dermer et al. [40], Dermer & Mitman [42]) on the other.

Fenimore and collaborators have emphasized the relevance of a specific signature to be expected in the collision of a relativistic expanding shell with the ISM, what they call a fast rise and exponential decay (FRED) shape. This feature is confirmed by our analysis (see peaks A, B, C in Fig. 44). However they also conclude, sharing the opinion by Piran and collaborators, that the variability observed in GRBs is inconsistent with causally connected variations in a single, symmetric, relativistic shell interacting with the ambient material ("external shocks") (Fenimore et al. [50]). In their opinion the solution of the short time variability has to be envisioned within the protracted activity of an unspecified "inner engine" (Sari & Piran [165]); see as well Mészáros & Rees [98, 99], Mészáros [100], Panaitescu & Mészáros [113], Rees & Mészáros [128].

On the other hand, Dermer and collaborators, by considering an idealized process occurring at a fixed $\gamma = 300$, have reached the opposite conclusions and they purport that GRB light curves are tomographic images of the density distributions of the medium surrounding the sources of GRBs (Dermer & Mitman [42]).

From our analysis we can conclude that Dermer's conclusions are correct for $\gamma \sim 300$ and do indeed hold for $\gamma > 150$. However, as the gamma factor drops from $\gamma \sim 150$ to $\gamma \sim 1$ (see Fig 8), the intensity due to the inhomogeneities markedly decreases also due to the angular spreading (events E and F). The initial Lorentz factor of the ABM pulse $\gamma \sim 310$ decreases very rapidly to $\gamma \sim 150$ as soon as a fraction of a typical ISM cloud is engulfed (see Tab. IV). We conclude that the "tomography" is indeed effective, but uniquely in the first ISM region close to the source and for GRBs with $\gamma > 150$.

One of the most striking feature in our analysis is clearly represented by the fact that the inhomogeneities of a mask of radial dimension of the order of 10^{17} cm give rise to arrival time signals of the order of 20 s. This outstanding result implies an apparent "superluminal velocity" of $\sim 10^5 c$ (see Tab. IV). The "superluminal velocity" here considered, first introduced in Ruffini et al. [144], refers to the motion along the line of sight. This effect is proportional to γ^2. It is much larger than the one usually considered in the literature, within the context of radio sources and microquasars (see e.g. Mirabel & Rodriguez [101]), referring to the component of the velocity at right angles to the line of sight (see details in Ruffini et al. [153]). This second effect is in fact proportional to γ (see Rees [127]). We recall that this "superluminal velocty" was the starting point for the enunciation of the RSTT paradigm (Ruffini et al. [144]), emphasizing the need of the knowledge of the *entire* past worldlines of the source. This need has been further clarified here in the determination of the EQTS surfaces (see Fig. 41 which indeed depend on an integral of the Lorentz gamma factor extended over the *entire* past worldlines of the source. In turn, therefore, the agreement between the observed structures and the theoretical predicted ones (see Figs. 3–44) is also an extremely stringent additional test on the

values of the Lorentz gamma factor determined as a function of the radial coordinate within the EMBH theory (see Fig. 8).

XXIV. ON THE ISTANTANEOUS SPECTRUM OF GRBS

Variability on the shortest time scale ever observed in nature is the main message we have acquired from the theoretical understanding of GRB astrophysical phenomena (see sections V,VII–XI). This situation is made even more extreme by the fact that astronomical and astrophysical observations are carried out in the "pathological" time coordinate of the photon arrival time at the detector (see section V), whereby the first 10^4 seconds of the GRB phenomena are further compressed in ~ 0.1 seconds (see Tab. I) and further enhanced. The understanding that in these first 10^4 seconds four different physical eras of the GRB phenomena occur has led us to a sentiment of natural skepticism toward any global or average description of the GRB phenomenon. We start to realize that such average descriptions mediate on totally different physical processes and lead to very questionable results. Such skepticism was even strengthened as soon as we realized that the characteristic quantities usually adopted for the description of the bursts, e.g. T_{50} and T_{90}, which so many tried for years to explain within the context of the internal shock model (see e.g. Fenimore [49], Fenimore et al. [50], Paczyński & Xu [109], Piran [116], Rees & Mészáros [128], Sari & Piran [165] and references therein) were actually referring not at all to the bursts but to the extended emission from the peak of the afterglow: the E-APE! In this sense they were quite irrelevant for understanding the nature of the GRB source and were at most of interest for inquiring the structure of the ISM a few light months away from the source! It has been then with this sentiment of marked skepticism toward a global approach that we have started to consider the problem of the spectrum of GRBs and the validity of the band relation (Band et al. [7]). To attempt an integral description of the spectra of the GRBs extending over 10^6 seconds in arrival time is clearly meaningless. It mediates on two conceptually physically different phases of GRBs: the injector phase and the beam-target phase (Ruffini et al. [145]). In addition, in each of these phases many specific eras are present and each one of these eras needs due attention and can lead in principle to a different instantaneous spectrum. The fact that the spectral distribution observed by Band was a non-thermal one has been a very strong objection to consider any thermal spectrum. The situation became so extreme in the recent years that the sole appearance of a thermal spectrum in any part of a theoretical paper was considered a good reason for rejecting the paper by a refereed journal and to discard the validity of that work.

Having developed the very powerful theoretical tool of the EQTS surfaces (see section XXI and Ruffini et al. [148, 153]) and having been successful in having established the substructure of the E-APE, in addition to the features of the afterglow, we have decided to approach the instantaneous spectra of the GRBs in Ruffini et al. [150]. In the abstract of that paper, we summarize as follows the results: *"A theoretical attempt to identify the physical process at the basis of the afterglow emission of GRBs is presented, assuming GRB 991216 as a prototype. Such a physical process is identified in a mechanism leading to a thermal emission occurring in the comoving frame of the shock wave originating the GRBs. For the determination of the actually observed GRB luminosities and spectra at a given arrival time, the concept of equitemporal surfaces (EQTS, see Ruffini et al. [148]) has to be implemented: the final results comprehend an integration over an infinite number of planckian spectra, weighted by appropriate relativistic transformations, each one corresponding to a different viewing angle in the past light cone of the observer. The relativistic transformations have been computed on the ground of the knowledge of the already determined equations of motion of GRBs within the EMBH theory (Ruffini et al. [144, 145, 148]). The only free parameter of the present theory is then the dimension of the "effective cavity" where the thermalization process occurs. A precise fit* $\left(\chi^2 \simeq 1.08\right)$ *of the observed luminosity in the* 2–10 *keV band of GRB 991216 is presented as well as a detailed estimate of the observed luminosity in the* 50–300 *keV band and of the expected one in the* 10–50 *keV band. The long awaited explanation of the observed hard-to-soft transition in GRBs is also presented"* (Ruffini et al. [150]). It is interesting that this theoretical result, which up to few years ago were hardly testable due to the paucity of photons collected by the detectors, have now become a necessity in order to interpret the splendid observational results of the new families of space observatory like Chandra and XMM (see e.g. Borozdin & Trudolyubov [23], Watson et al. [184, 185]).

Prior to our work, the possibility that the non-thermal looking spectrum of GRBs can be found as a superposition of a set of thermal blackbody spectrum was forcefully expressed in a simple paper by Blinnikov, Kozyreva & Panchenko [18]. These three authors have expressed in an analytic treatment that indeed the time integration of the black body planckian spectrum with a temperature varying with time following a simple power-law and expanding with another power-law can lead to a non-thermal spectrum in agreement with the observed Band relations. To obtain this result, they use two indexes for their qualitative analysis to be fitted by the observational data. Toward the end of their paper they finally quoted *"In reality, not only time, but also space integration takes place. As shown by Rees [127], (see also Drozdova & Panchenko [44], Sari [164]) in the case of an expanding emitting shell an observer simultaneously detects radiation produced in different moments of time (thus, with different temperatures) on the ellipsoidal or egg-like surface. The integration over this surface can give the same effect as the integration over time*

done in this paper, but we do not perform this here because the result strongly depends on the unknown geometry of the emitting surface" (Blinnikov, Kozyreva & Panchenko [18]). This treatment which they outline but they discard due to the difficulty of defining the geometry of the EQTS is exactly what we have done. Our treatment has only one free parameter and can fit the data of GRBs in a range between a few seconds all the way up to 10^6 seconds. There is a basic observational feature between our treatment and the one by Blinnikov, Kozyreva & Panchenko [18]: their instantaneous spectral distribution has necessarily to be a blackbody one, while in our case is represented by an integration over an infinite number of planckian spectra, weighted by appropriate relativistic transformations, each one corresponding to a different viewing angle in the past light cone of the observer. The difference between such unique spectra should be simply discernible using the observations of XMM, Chandra, and of future space observatories.

XXV. THE OBSERVATION OF THE IRON LINES IN GRB 991216: ON A POSSIBLE GRB-SUPERNOVA TIME SEQUENCE

We have seen in the previous sections how the time structure of the E-APE gives information on the composition of the interstellar matter at distances of the order of 5×10^{16} cm from the source. We would like now to point out that the data on the iron lines from the Chandra satellite on the GRB 991216 (Piro et al., [120]) and similar observations from other sources (Amati et al. [3], Piro et al. [119], Piro et al., [120]) make it possible to extend this analysis to a larger distance scale, possibly all the way out to a few light years, and consequently probe the distribution of stars in the surroundings of the newly formed EMBH.

Most importantly, these considerations lead to a new paradigm for the interpretation of the supernova-GRB correlation (see Ruffini et al. [146]). Indeed a correlation between the occurrence of GRBs and supernova events exists and has been established by the works of Bloom et al. [19], Galama et al. [58, 59, 60], Kulkarni et al. [85], Piran [116], Piro et al. [118], Rhoads [131], van Paradijs et al. [179].

Such an association has been assumed to indicate that GRBs are generated by supernova explosions (see e.g. Kulkarni et al. [85]). In turn, such a point of view has implied further consequences: the optical and radio data of the supernova have been attributed to the GRB afterglow, and many theorists have tried to encompass these data and explain them as a genuine component of the GRB scenario.

We propose instead an alternative point of view implying a very clear distinction between the GRB phenomenon and the supernova: if relativistic effects presented in the RSTT paradigm are properly taken into account, then a kinematically viable explanation can be given of the supernova-GRB association. We still use GRB 991216 as a prototypical case.

The GRB-Supernova Time Sequence paradigm, which we have indicated for short as GSTS paradigm (see Ruffini et al. [146]), states that: *A massive GRB-progenitor star P_1 of mass M_1 undergoes gravitational collapse to an EMBH. During this process a dyadosphere is formed and subsequently the P-GRB and the E-APE are generated in sequence. They propagate and impact, with their photon and neutrino components, on a second supernova-progenitor star P_2 of mass M_2. Assuming that both stars were generated approximately at the same time, we expect to have $M_2 < M_1$. Under some special conditions of the thermonuclear evolution of the supernova-progenitor star P_2, the collision of the P-GRB and the E-APE with the star P_2 can induce its supernova explosion.*

Especially relevant to our paradigm are the following data from the Chandra satellite (see Piro et al., [120]):

1. At the arrival time of 37 hr after the initial burst there is evidence of iron emission lines for GRB 991216.

2. The emission lines are present during the entire observation period of 10^4 s. The iron lines could also have been produced earlier, before Chandra was observing. Thus the times used in these calculations are not unique: they do serve to provide an example of the scenario.

3. The emission lines appear to have a peak at an energy of 3.49 ± 0.06 keV which, at a redshift $z = 1.00 \pm 0.02$ corresponds to an hydrogen-like iron line at 6.97 keV at rest. This source does not appear to have any significant motion departing from the cosmological flow. The iron lines have a width of 0.23 keV consistent with a radial velocity field of $0.1c$. The iron lines are only a small fraction of the observed flux.

On the basis of the explicit computations of the different eras presented in the above sections, we make three key points:

1. An arrival time of 37 hr in the detector frame corresponds to a radial distance from the EMBH travelled by the ABM pulse of 3.94×10^{17} cm in the laboratory frame (see Tab. I).

2. It is likely that a few stars are present within that radius as members of a cluster. It has become evident from observations of dense clusters of star-forming regions that a stellar average density of typically $10^2 \mathrm{pc}^{-3}$ (Beck

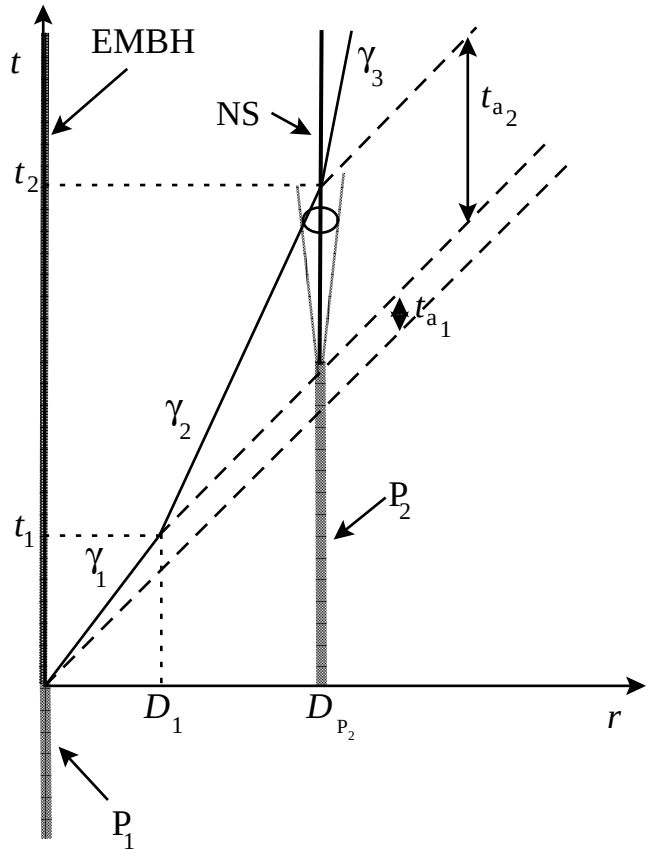

Figure 45: A qualitative simplified space-time diagram (in arbitrary units) illustrating the GSTS paradigm. The EMBH, originating from the gravitational collapse of a massive GRB-progenitor star P_1, and the massive supernova-progenitor star P_2-neutron star (P_2-NS) system, separated by a radial distance D_{P_2}, are assumed to be at rest in in the laboratory frame. Their worldlines are represented by two parallel vertical lines. The supernova shell moving at $0.1c$ generated by the P_2-NS transition is represented by the dotted line cone. The solid line represents the motion of the pulse, as if it would move with an "effective" constant gamma factor γ_1 during the eras reaching the condition of transparency. Similarly, another "effective" constant gamma factor $\gamma_2 < \gamma_1$ applies during era IV up to the collision with the P_2-NS system. A third "effective" constant gamma factor $\gamma_3 < \gamma_2$ occurs during era V after the collision as the nonrelativistic regime of expansion is reached. The dashed lines at 45 degrees represent signals propagating at speed of light.

et al. [9]) should be expected. There is also the distinct possibility for this case and other systems that the stars P_1 and P_2 are members of a binary system.

3. The possible observations at different wavelengths of the supernova crucially depend on the relative intensities between the GRB and the supernova as well as on the value of the distance and the redshift of the source. In the present case of GRB 991216, the expected optical and radio emission from the supernova are many orders of magnitude smaller than the GRB intensity. The opposite situation will be encountered in GRB 980425 (Ruffini et al. [152]).

In order to reach an intuitive understanding of these complex computations we present a schematic very simplified diagram (not to scale) in Fig. 45.

We now describe the sequence of events and the specific data corresponding to the GSTS paradigm:

1. The two stars P_1 and P_2 are separated by a distance $D_{P_2} = 3.94 \times 10^{17}$ cm in the laboratory frame, see Fig. 45. Both stars are at rest in the inertial laboratory frame. At laboratory time $t = 0$ and at comoving time

$\tau = 0$, the gravitational collapse of the GRB-progenitor star P_1 occurs, and the initial emission of gravitational radiation or a neutrino burst from the event then synchronizes this event with the arrival times $t_a = 0$ at the supernova-progenitor star P_2 and $t_a^d = 0$ for the distant observer at rest with the detector. The electromagnetic radiation emitted by the gravitational collapse process is instead practically zero, due to the optical thickness of the material at this stage (Bianco et al. [13], see Tab. I).

2. From Tab. I, at laboratory time $t_1 = 6.48 \times 10^3\, s$ and at a distance from the EMBH of $D_1 = 1.94 \times 10^{14}\, cm$, the condition of transparency for the PEMB pulse is reached and the P-GRB is emitted (see section IX). This time is recorded in arrival time at the detector $t_{a_1}^d = 8.41 \times 10^{-2}\, s$, and, at P_2, at $t_{a_1} = 4.20 \times 10^{-2}\, s$. The fact that the PEMB pulse in an arrival time of $8.41 \times 10^{-2}\, s$ covers a distance of $1.94 \times 10^{14}\, cm$ gives rise to an apparent "superluminal" effect. This apparent paradox can be straightforwardly explained by introducing an "effective" gamma factor, see Ruffini et al. [146].

3. At laboratory time $t = 1.73 \times 10^6\, s$ and at a distance from the EMBH of $5.18 \times 10^{16}\, cm$ in the laboratory frame, the peak of the E-APE is reached which is recorded at the arrival time $t_a = 9.93\, s$ at P_2 and $t_a^d = 19.87\, s$ at the detector. This also gives rise to an apparent "superluminal" effect.

4. At a distance $D_{P_2} = 3.94 \times 10^{17}\, cm$, the two bursts described in the above points 2) and 3) collide with the supernova-progenitor star P_2 at arrival times $t_{a_1} = 4.20 \times 10^{-2}\, s$ and $t_a = 9.93\, s$ respectively. They can then induce the supernova explosion of the massive star P_2.

5. The associated supernova shell expands with velocity $0.1c$.

6. The expanding supernova shell is reached by the ABM pulse generating the afterglow with a delay of $t_{a_2} = 18.5\, hr$ in arrival time following the arrival of the P-GRB and the E-APE. This time delay coincides with the interval of laboratory time separating the two events, since the P_2 is at rest in the inertial laboratory frame (see Ruffini et al. [146]). The ABM pulse has travelled in the laboratory frame a distance $D_{P_2} - D_1 \simeq D_{P_2} = 3.94 \times 10^{17}\, cm$ in a laboratory time $t_2 - t_1 \simeq t_2 = 1.32 \times 10^7\, s$ (neglecting the supernova expansion).

The collision of the pulse with the supernova shell occurs at $\gamma \simeq 4.0$. By this time the supernova shell has reached a dimension of $1.997 \times 10^{14}\, cm$, which is consistent with the observations from the Chandra satellite.

In these considerations on GRB 991216 the supernova remnant has been assumed to be close to but not exactly along the line of sight extending from the EMBH to the distant observer. If such an alignment should exist for other GRBs, it would lead to an observation of iron absorption lines as well as to an increase in the radiation observed in the afterglow corresponding to the crossing of the supernova shell by the ABM pulse. In fact, as the ABM pulse engulfs the baryonic matter of the remnant, above and beyond the normal interstellar medium baryonic matter, the conservation of energy and momentum implies that a larger amount of internal energy is available and radiated in the process (see section XIII). This increased energy-momentum loss will generally affect the slope of the afterglow decay, approaching more rapidly a nonrelativistic expansion phase (details are given in section XVIII).

It is quite clear that as soon as the relativistic transformations of the RSTT paradigm are duly taken into account, the sequence of events between the supernova and the GRB occurrences are exactly the opposite of the one postulated in the so-called "supranova" scenario (Vietri & Stella [181, 182], Vietri et al. [183]). This can be considered a very appropriate pedagogical example of how classical nonrelativistic applied to ultrarelativistic regimes can indeed subvert the very causal relation between events.

If we now turn to the possibility of dynamically implementing the scenario, there are at least three different possibilities:

1. Particularly attractive is the possibility that a massive star P_2 has rapidly evolved during its thermonuclear evolution to a white dwarf (see e.g. Chandrasekhar [26]). It it then sufficient that the P-GRB and the E-APE implode the star sufficiently as to reach a central density above the critical density for the ignition of thermonuclear burning. Consequently, the explosion of the star P_2 occurs, and a significant fraction of a solar mass of iron is generated. These configurations are currently generally considered precursors of some type I supernovae (see e.g. Filippenko [52] and references therein).

2. Alternatively, the massive star P_2 can have evolved to the condition of being close to the point of gravitational collapse, having developed the formation of an iron-silicon core, type II supernovae. The above transfer of energy momentum from the P-GRB and the E-APE may enhance the capture of the electrons on the iron nuclei and consequently decrease the Fermi energy of the core, leading to the onset of gravitational instability (see e.g. Bethe [12] p. 270 and followings). Since the time for the final evolution of a massive star with an iron-silicon core is short, this event requires a well tuned coincidence.

3. The pressure wave may trigger massive and instantaneous nuclear burning process, with corresponding changes in the chemical composition of the star, leading to the collapse.

The GSTS paradigm has been applied to the case of the GRB 980425 - SN1998bw which, with a red shift of 0.0083, is one of the closest and weaker GRBs observed. In this case, the radio and the optical emission of the supernova is distinctively observed. For this particular case, the EMBH appears to have a significantly lower value of the parameter ξ and the validity of the GSTS paradigm presented here is confirmed (see Ruffini et al. [152]).

XXVI. GENERAL CONSIDERATIONS ON THE EMBH FORMATION

Before concluding let us consider the problem of the EMBH formation. Such a problem has been debated for many years since the earliest discussions in 1970 in Princeton and has been finally clarified and addressed in general terms to justify the plausibility of the hypothesis in Ruffini [139]. There has been a basic change of paradigm. All the considerations on the electric charge of stars were traditionally directed, following the classical work by Shvartsman [174] all the way to the fundamental book by Punsly [126], to the presence of a net charge on the star surface in a steady state condition. The star can be endowed of rotation and magnetic field and surrounded by plasma, like in the case of Goldreich & Julian [70], or, in the case of absence of both magnetic field and rotation, the electrostatic processes can be related to the depth of the gravitational well, like in the treatment of Shvartsman [174]. However, in neither cases it is possible to reach the condition of the overcritical field needed for pair creation nor have the condition of no baryonic contamination discussed in sections III, VII and essential for the dyadosphere formation. The basic conceptual point is that GRBs are maybe the most violent transient phenomenon occurring in the universe and so the condition for the dyadosphere creation have to be searched in a transient phenomenon. The solution is related to the most transient phenomenon occurring in the life of a star: the process of gravitational collapse.

Having acquired such a fundamental understanding, the next step is to estimate the amount of polarization needed in order to reach the fully relativistic condition

$$\frac{Q}{M\sqrt{G}} = 1 \, . \tag{182}$$

Recalling that the charge to mass ratio of a proton is $q_p/\left(m_p\sqrt{G}\right) = 1.1 \times 10^{18}$, it is enough to have an excess of one quantum of charge every 10^{18} nucleons in the core of the collapsing star to obtain an extreme EMBH after the occurrence of the gravitational collapse. Physically this means that we are dealing with a process of charge segregation between the core and the outer part of the star which has the opposite sign of net charge in order to enforce the overall charge neutrality condition. We here emphasize the name "charge segregation" instead of the name "charge separation" in order to contrast a very mild charge surplus created in different part of the star, keeping the overall charge neutrality, from the much more extreme condition of charge separation in which all the charges of the atomic component of the star are separated. It is indeed reassuring that such a core, endowed with charge segregation, is indeed stable with respect to the Fermi-Chandrasekhar criteria for the stability of self-gravitating stars duly extended from the magnetic to the electric case: the electric energy of such a core is consistently smaller than its gravitational energy (see Boccaletti et al. [22]).

Such a condition of charge segregation between the core and the oppositely charged star surface layer can be reached under a very large number of physical conditions. We consider, for simplicity, one of the oldest example: the one of a star endowed with both a magnetic field and rotation. It is proved that a typical magnetic field expected for the ISM is $B_\circ \sim 10^{-5}\, G$ (Ferrière [51]). We further assume, consistently with the data which we have acquired and verified in the present article (see sections XIII, XIX), that also in the galaxy where GRB 991216 occurred the ISM has an average density of $n_{ism} = 1\, proton/cm^3$. From this value of density we have that an ISM cloud with mass $M \sim 10 M_\odot$ occupies a sphere of radius $R_\circ \sim 1.4 \times 10^{19}\, cm$. If this sphere collapse to a star with radius $R = R_\odot$, from the flux conservation we obtain that it is enough for this star to rotate with the most reasonable angular speed

$$\Omega \sim \frac{\xi M c \sqrt{G}}{R_\odot R_\circ^2 B_\circ} \tag{183}$$

to conclude that the progenitor star core is endowed of a charge to mass ratio equal to ξ. In the extreme case of Eq.(182) we have $\xi = 1$ and so the angular speed is $\Omega \sim 1.1 \times 10^{-3}\, rad/s$ — i.e. one round in $1.5\, hr$ — and correspondingly we have smaller Ω values for $\xi < 1$ (see Boccaletti et al. [22]). Clearly the overall neutrality is guaranteed by the oppositely charged baryonic matter which is the one measured by the B parameter in the EMBH model (see sections VIII–IX). The smallness of the B value clearly points to the absence of an extended envelope of the progenitor star.

The formation process of such an electromagnetised progenitor star will be clearly affected by the presence of differential rotation, the consequent amplification of the magnetic field and a variety of magnetohydrodynamical problems which will affect somewhat the simplicity of the heuristic Eq.(183). Similarly the process of gravitational collapse of such a progenitor star endowed with rotation will lead to complex phenomena of "gravitationally induced electromagnetic radiation" (Johnston et al. [81]) and of "electromagnetically induced gravitational radiation" (Johnston et al. [82]) which will tend to reduce both the eccentricity and the angular velocity of the collapsing core. The general outcome of gravitational collapse will be a Kerr-Newmann spacetime. It is interesting that such a general case will break the degeneracy in (μ, ξ) described in section X (see Ruffini et al. [153]). In this article we have addressed the much simpler case of a solution in which $(cL) / \left(GM^2\right) \ll 1$ and the treatment can be well approximated by a collapse described by a Reissner-Nordström geometry.

In addition to this scenario, based on the role of magnetic field and rotation, we are as well pursuing the possible generation of the charge segregation by quantum effects at the surface of the Fermi semi-degenerate core. In this framework, it is particularly interesting to consider the purely electric analog of the Chandrasekhar & Fermi [27] paper on the gravitational stability of self-gravitating magnetized stars. The stability condition, based on the virial theorem, is simply that the Coulomb energy of the inner core of a charged star should be smaller or equal than the gravitational energy of the star (Boccaletti et al. [22]). Previous to the collapse, the gravitational energy can be much smaller than the rest energy of the star and be amplified during the process of gravitational collapse reaching overcritical intensity of the electric field (see Fig. 46 and Ruffini [139]). It is interesting that the Chandrasekhar-Fermi inequality just leads to an extreme Reissner-Nordström solution.

In both these cases the Reissner-Nordström geometry appears indeed to be the relevant model for GRB 991216 as discussed in the previous sections. We shall return to non spherical configuration in forthcoming publications and/or when requested by observational evidence (see Ruffini et al. [153]).

XXVII. SOME PROPAEDEUTIC ANALYSIS FOR THE DYNAMICAL FORMATION OF THE EMBH

While the formation in time of the dyadosphere is the fundamental phenomena we are interested in, we can get an insight on the issue of gravitational collapse of an electrically charged star core studying in details a simplified model, namely a thin shell of charged dust. In De la Cruz & Israel [35], Israel [80] it is shown that the problem of a collapsing charged shell in general relativity can be reduced to a set of ordinary differential equations. We reconsider here the following relativistic system: a spherical shell of electrically charged dust which is moving radially in the Reissner-Nordström background of an already formed nonrotating EMBH of mass M_1 and charge Q_1, with $Q_1 \leq M_1$.

The world surface spanned by the shell divides the space-time into two regions: an internal one $\mathcal{M}_-$ and an external one $\mathcal{M}_+$. The line element in Schwarzschild like coordinate is (Cherubini et al. [28])

$$ds^2 = \begin{cases} -f_+ dt_+^2 + f_+^{-1} dr^2 + r^2 d\Omega^2 & \text{in } \mathcal{M}_+ \\ -f_- dt_-^2 + f_-^{-1} dr^2 + r^2 d\Omega^2 & \text{in } \mathcal{M}_- \end{cases}, \tag{184}$$

where $f_+ = 1 - \frac{2M}{r} + \frac{Q^2}{r^2}$, $f_- = 1 - \frac{2M_1}{r} + \frac{Q_1^2}{r^2}$ and t_- and t_+ are the Schwarzschild-like time coordinates in $\mathcal{M}_-$ and $\mathcal{M}_+$ respectively. M is the total mass-energy of the system formed by the shell and the EMBH, measured by an observer at rest at infinity and $Q = Q_0 + Q_1$ is the total charge: sum of the charge Q_0 of the shell and the charge Q_1 of the internal EMBH.

Indicating by R the radius of the shell and by $T_\pm$ its time coordinate, the equations of motion of the shell become (Ruffini & Vitagliano [156])

$$\begin{aligned} \left(\tfrac{dR}{d\tau}\right)^2 &= \tfrac{1}{M_0^2}\left(M - M_1 + \tfrac{M_0^2}{2R} - \tfrac{Q_0^2}{2R} - \tfrac{Q_1 Q_0}{R}\right)^2 - f_-(R) \\ &= \tfrac{1}{M_0^2}\left(M - M_1 - \tfrac{M_0^2}{2R} - \tfrac{Q_0^2}{2R} - \tfrac{Q_1 Q_0}{R}\right)^2 - f_+(R), \end{aligned} \tag{185}$$

$$\tfrac{dT_\pm}{d\tau} = \tfrac{1}{M_0 f_\pm(R)}\left(M - M_1 \mp \tfrac{M_0^2}{2R} - \tfrac{Q_0^2}{2R} - \tfrac{Q_1 Q_0}{R}\right), \tag{186}$$

where M_0 is the rest mass of the shell and τ is its proper time. Eqs.(185,186) (together with Eq.(184)) completely describe a 5-parameter (M, Q, M_1, Q_1, M_0) family of solutions of the Einstein-Maxwell equations. Note that Eqs.(185,186) imply that

$$M - M_1 - \tfrac{Q_0^2}{2R} - \tfrac{Q_1 Q_0}{R} > 0 \tag{187}$$

holds for $R > M + \sqrt{M^2 - Q^2}$ if $Q < M$ and for $R > M_1 + \sqrt{M_1^2 - Q_1^2}$ if $Q > M$.

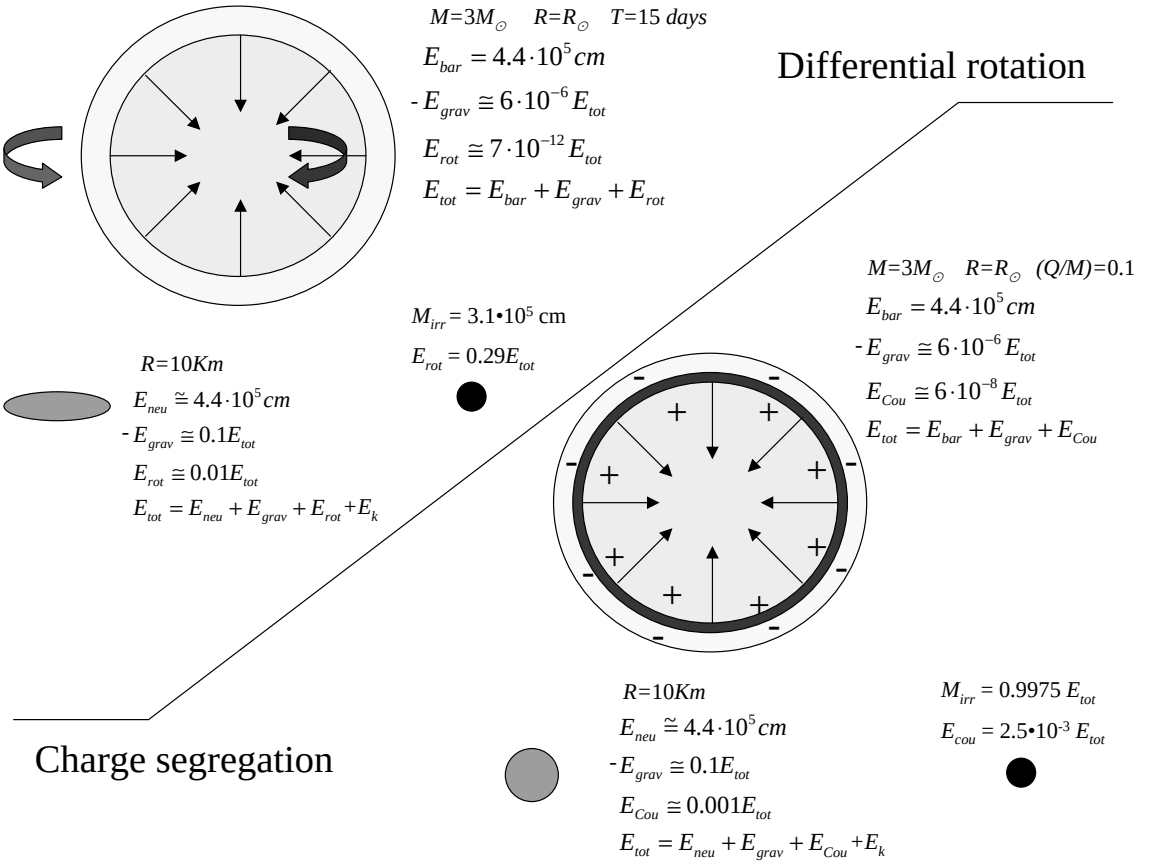

Figure 46: Quantitative description of the gravitational collapse to a neutron star and to a black hole of the core of a rotating progenitor rotating. The core is estimated to have a mass equal to $3M_\odot$, to have an initial radius $r = r_\odot$ and a rotation period of 15 days. Although the initial rotational energy is of the order of 10^{-11} of the total energy, the total rotational energy, in principle extractable, of the rotating black hole can be as high as of the order of 29%. On the lower-right side the same considerations are applied to the case of a neutral star formed by a core oppositely charged from its outermost envelope. The core is expected to have a mass of $3M_\odot$, a radius equal to $r_\odot$ and electromagnetic energy $Q/M = 0.1$. Although the initial Coulomb energy is only $\sim 10^{-7}$ of the total energy, which is in turn hundred times smaller than the gravitational energy, the final Coulomb energy can be as high as 2.5×10^{-3} of the total energy. In both cases, the amplification of the rotational energy and of the Coulomb energy, which indeed are the only two extractable forms of energy from a black hole, is due to the process of gravitational collapse.

For astrophysical applications (Ruffini et al. [159]) the trajectory of the shell $R = R(T_+)$ is obtained as a function of the time coordinate T_+ relative to the space-time region $\mathcal{M}_+$. In the following we drop the + index from T_+. From Eqs.(185,186) we have

$$\frac{dR}{dT} = \frac{dR}{d\tau}\frac{d\tau}{dT} = \pm\frac{F}{\Omega}\sqrt{\Omega^2 - F}, \tag{188}$$

where

$$F \equiv f_+(R) = 1 - \frac{2M}{R} + \frac{Q^2}{R^2}, \tag{189}$$

$$\Omega \equiv \Gamma - \frac{M_0^2 + Q^2 - Q_1^2}{2M_0 R}, \tag{190}$$

$$\Gamma \equiv \frac{M - M_1}{M_0}. \tag{191}$$

Since we are interested in an imploding shell, only the minus sign case in (188) will be studied. We can give the following physical interpretation of Γ. If $M - M_1 \geq M_0$, Γ coincides with the Lorentz γ factor of the imploding shell at infinity; from Eq.(188) it satisfies

$$\Gamma = \frac{1}{\sqrt{1-\left(\frac{dR}{dT}\right)^2_{R=\infty}}} \geq 1. \tag{192}$$

When $M - M_1 < M_0$ then there is a *turning point* R^*, defined by $\frac{dR}{dT}\big|_{R=R^*} = 0$. In this case Γ coincides with the "effective potential" at R^* :

$$\Gamma = \sqrt{f_-\left(R^*\right)} + M_0^{-1}\left(-\frac{M_0^2}{2R^*} + \frac{Q_0^2}{2R^*} + \frac{Q_1 Q_0}{R^*}\right) \leq 1. \tag{193}$$

The solution of the differential equation (188) is given by:

$$\int dT = -\int \frac{\Omega}{F\sqrt{\Omega^2 - F}} dR. \tag{194}$$

The functional form of the integral (194) crucially depends on the degree of the polynomial $P\left(R\right) = R^2\left(\Omega^2 - F\right)$, which is generically two, but in special cases has lower values. We therefore distinguish the following cases:

1. $\boldsymbol{M = M_0 + M_1}$; $\boldsymbol{Q_1 = M_1}$; $\boldsymbol{Q = M}$: $P\left(R\right)$ is equal to 0, we simply have

$$R(T) = \text{const}. \tag{195}$$

2. $\boldsymbol{M = M_0 + M_1}$; $\boldsymbol{M^2 - Q^2 = M_1^2 - Q_1^2}$; $\boldsymbol{Q \neq M}$: $P\left(R\right)$ is a constant, we have

$$\begin{aligned} T = \text{const} + \frac{1}{2\sqrt{M^2-Q^2}}\left[\left(R+2M\right)R\right. \\ \left. + r_+^2 \log\left(\frac{R-r_+}{M}\right) + r_-^2 \log\left(\frac{R-r_-}{M}\right)\right]. \end{aligned} \tag{196}$$

3. $\boldsymbol{M = M_0 + M_1}$; $\boldsymbol{M^2 - Q^2 \neq M_1^2 - Q_1^2}$: $P\left(R\right)$ is a first order polynomial and

$$\begin{aligned} T = \text{const} + 2R\sqrt{\Omega^2 - F}\left[\frac{M_0 R}{3\left(M^2-Q^2-M_1^2+Q_1^2\right)}\right. \\ \left. + \frac{\left(M_0^2+Q^2-Q_1^2\right)^2 - 9MM_0\left(M_0^2+Q^2-Q_1^2\right) + 12M^2M_0^2 + 2Q^2M_0^2}{3\left(M^2-Q^2-M_1^2+Q_1^2\right)^2}\right] \\ - \frac{1}{\sqrt{M^2-Q^2}}\left[r_+^2 \operatorname{arctanh}\left(\frac{R}{r_+}\frac{\sqrt{\Omega^2-F}}{\Omega_+}\right)\right. \\ \left. - r_-^2 \operatorname{arctanh}\left(\frac{R}{r_-}\frac{\sqrt{\Omega^2-F}}{\Omega_-}\right)\right], \end{aligned} \tag{197}$$

   where $\Omega_\pm \equiv \Omega\left(r_\pm\right)$.

4. $\boldsymbol{M \neq M_0 + M_1}$: $P\left(R\right)$ is a second order polynomial and

$$\begin{aligned} T = \text{const} - \frac{1}{2\sqrt{M^2-Q^2}}\left\{\frac{2\Gamma\sqrt{M^2-Q^2}}{\Gamma^2-1}R\sqrt{\Omega^2-F}\right. \\ + r_+^2 \log\left[\frac{R\sqrt{\Omega^2-F}}{R-r_+} + \frac{R^2\left(\Omega^2-F\right) + r_+^2\Omega_+^2 - \left(\Gamma^2-1\right)\left(R-r_+\right)^2}{2\left(R-r_+\right)R\sqrt{\Omega^2-F}}\right] \\ - r_-^2 \log\left[\frac{R\sqrt{\Omega^2-F}}{R-r_-} + \frac{R^2\left(\Omega^2-F\right) + r_-^2\Omega_-^2 - \left(\Gamma^2-1\right)\left(R-r_-\right)^2}{2\left(R-r_-\right)R\sqrt{\Omega^2-F}}\right] \\ - \frac{\left[2MM_0\left(2\Gamma^3-3\Gamma\right) + M_0^2 + Q^2 - Q_1^2\right]\sqrt{M^2-Q^2}}{M_0\left(\Gamma^2-1\right)^{3/2}} \log\left[\frac{R\sqrt{\Omega^2-F}}{M}\right. \\ \left.\left. + \frac{2M_0\left(\Gamma^2-1\right)R - \left(M_0^2+Q^2-Q_1^2\right)\Gamma + 2M_0M}{2M_0M\sqrt{\Gamma^2-1}}\right]\right\}. \end{aligned} \tag{198}$$

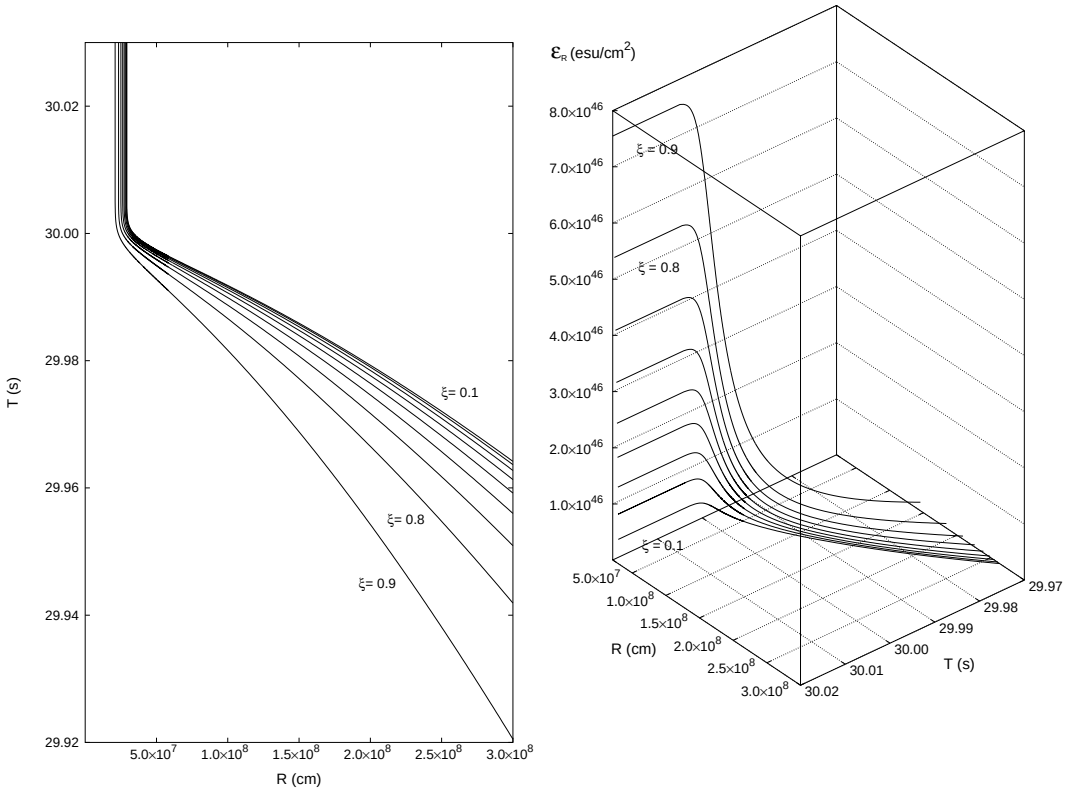

Figure 47: **Left)** Collapse curves in the plane (T, R) for $M = 20M_\odot$ and for different values of the parameter ξ. The asymptotic behavior is the clear manifestation of general relativistic effects as the horizon of the EMBH is approached. **Right)** Electric field behaviour at the surface of the shell for $M = 20M_\odot$ and for different values of the parameter ξ. The asymptotic behavior is the clear manifestation of general relativistic effects as the horizon of the EMBH is approached.

Of particular interest is the time varying electric field $\mathcal{E}_R = \frac{Q}{R^2}$ on the external surface of the shell. In order to study the variability of $\mathcal{E}_R$ with time it is useful to consider in the tridimensional space of parameters $(R, T, \mathcal{E}_R)$ the parametric curve $\mathcal{C} : \left(R = \lambda, \quad T = T(\lambda), \quad \mathcal{E}_R = \frac{Q}{\lambda^2}\right)$. In astrophysical applications (Ruffini et al. [159]) we are specially interested in the family of solutions such that $\frac{dR}{dT}$ is 0 when $R = \infty$ which implies that $\Gamma = 1$. In Fig. 47 we plot the collapse curves in the plane (T, R) for different values of the parameter $\xi \equiv \frac{Q}{M}$, $0 < \xi < 1$. The initial data (T_0, R_0) are chosen so that the integration constant in equation (197) is equal to 0. In all the cases we can follow the details of the approach to the horizon which is reached in an infinite Schwarzschild time coordinate. In Fig. 47 we plot the parametric curves $\mathcal{C}$ in the space $(R, T, \mathcal{E}_R)$ for different values of ξ. Again we can follow the exact asymptotic behavior of the curves $\mathcal{C}$, $\mathcal{E}_R$ reaching the asymptotic value $\frac{Q}{r_+^2}$. The detailed knowledge of this asymptotic behavior is of great relevance for the observational properties of the EMBH formation (see e.g. Ruffini & Vitagliano [156]).

In the case of a shell falling in a flat background ($M_1 = Q_1 = 0$) Eq.(185) reduces to

$$\left(\frac{dR}{d\tau}\right)^2 = \frac{1}{M_0^2}\left(M + \frac{M_0^2}{2R} - \frac{Q^2}{2R}\right)^2 - 1. \tag{199}$$

Introducing the total radial momentum $P \equiv M_0 u^r = M_0 \frac{dR}{d\tau}$ of the shell, we can express the kinetic energy of the shell as measured by static observers in $\mathcal{M}_-$ as $T \equiv -M_0 u_\mu \xi_-^\mu - M_0 = \sqrt{P^2 + M_0^2} - M_0$. Then from equation (199) we

have

$$M = -\frac{M_0^2}{2R} + \frac{Q^2}{2R} + \sqrt{P^2 + M_0^2} = M_0 + T - \frac{M_0^2}{2R} + \frac{Q^2}{2R}. \tag{200}$$

where we choose the positive root solution due to the constraint (187). Eq.(200) is the *mass formula* of the shell, which depends on the time-dependent radial coordinate R and kinetic energy T. If $M \geq Q$, an EMBH is formed and we have

$$M = M_0 + T_+ - \frac{M_0^2}{2r_+} + \frac{Q^2}{2r_+}\,, \tag{201}$$

where $T_+ \equiv T\left(r_+\right)$ and $r_+ = M + \sqrt{M^2 - Q^2}$ is the radius of external horizon of the EMBH. We know from the Christodoulou-Ruffini EMBH mass formula that

$$M = M_{\rm irr} + \frac{Q^2}{2r_+}, \tag{202}$$

so it follows that

$$M_{\rm irr} = M_0 - \frac{M_0^2}{2r_+} + T_+, \tag{203}$$

namely that $M_{\rm irr}$ is the sum of only three contributions: the rest mass M_0, the gravitational potential energy and the kinetic energy of the rest mass evaluated at the horizon. $M_{\rm irr}$ is independent of the electromagnetic energy, a fact noticed by Bekenstein (Bekenstein [10]). We have taken one further step here by identifying the independent physical contributions to $M_{\rm irr}$.

Next we consider the physical interpretation of the electromagnetic term $\frac{Q^2}{2R}$, which can be obtained by evaluating the conserved Killing integral

$$\begin{aligned}\int_{\Sigma_t^+} \xi_+^\mu T_{\mu\nu}^{(\rm em)} d\Sigma^\nu &= \int_R^\infty r^2 dr \int_0^1 d\cos\theta \int_0^{2\pi} d\phi\; T^{(\rm em)}{}_0{}^0 \\ &= \frac{Q^2}{2R}\,,\end{aligned} \tag{204}$$

where Σ_t^+ is the space-like hypersurface in $\mathcal{M}_+$ described by the equation $t_+ = t = \text{const}$, with $d\Sigma^\nu$ as its surface element vector and where $T_{\mu\nu}^{(\rm em)} = -\frac{1}{4\pi}\left(F_\mu{}^\rho F_{\rho\nu} + \frac{1}{4} g_{\mu\nu} F^{\rho\sigma} F_{\rho\sigma}\right)$ is the energy-momentum tensor of the electromagnetic field. The quantity in Eq.(204) differs from the purely electromagnetic energy

$$\int_{\Sigma_t^+} n_+^\mu T_{\mu\nu}^{(\rm em)} d\Sigma^\nu = \frac{1}{2}\int_R^\infty dr \sqrt{g_{rr}} \frac{Q^2}{r^2},$$

where $n_+^\mu = f_+^{-1/2} \xi_+^\mu$ is the unit normal to the integration hypersurface and $g_{rr} = f_+$. This is similar to the analogous situation for the total energy of a static spherical star of energy density ϵ within a radius R, $m\left(R\right) = 4\pi \int_0^R dr\; r^2 \epsilon$, which differs from the pure matter energy $m_{\rm p}\left(R\right) = 4\pi \int_0^R dr \sqrt{g_{rr}} r^2 \epsilon$ by the gravitational energy (see Misner, Thorne, & Wheeler [103]). Therefore the term $\frac{Q^2}{2R}$ in the mass formula (200) is the *total* energy of the electromagnetic field and includes its own gravitational binding energy. This energy is stored throughout the region Σ_t^+, extending from R to infinity.

We now turn to the problem of extracting the electromagnetic energy from an EMBH see (see Christodoulou & Ruffini [30]). We can distinguish between two conceptually physically different processes, depending on whether the electric field strength $\mathcal{E} = \frac{Q}{r^2}$ is smaller or greater than the critical value $\mathcal{E}_{\rm c} = \frac{m_e^2 c^3}{e\hbar}$. Here m_e and e are the mass and the charge of the electron. As already mentioned in this paper an electric field $\mathcal{E} > \mathcal{E}_{\rm c}$ polarizes the vacuum creating electron-positron pairs (see Heisenberg & Euler [78]). The maximum value $\mathcal{E}_+ = \frac{Q}{r_+^2}$ of the electric field around an EMBH is reached at the horizon. We then have the following:

1. For $\mathcal{E}_+ < \mathcal{E}_{\rm c}$ the leading energy extraction mechanism consists of a sequence of discrete elementary decay processes of a particle into two oppositely charged particles. The condition $\mathcal{E}_+ < \mathcal{E}_{\rm c}$ implies

$$\begin{aligned}\xi &\equiv \frac{Q}{\sqrt{G}M} \\ &\lesssim \begin{cases} \frac{GM/c^2}{\lambda_{\rm C}} \frac{\sqrt{G} m_e}{e} \sim 10^{-6} \frac{M}{M_\odot} & \text{if } \frac{M}{M_\odot} \leq 10^6 \\ 1 & \text{if } \frac{M}{M_\odot} > 10^6 \end{cases},\end{aligned} \tag{205}$$

where $\lambda_{\rm C}$ is the Compton wavelength of the electron. Denardo & Ruffini [36] and Denardo et al. [37] have defined as the *effective ergosphere* the region around an EMBH where the energy extraction processes occur. This region extends from the horizon r_+ up to a radius

$$r_{\rm Eerg} = \frac{GM}{c^2}\left[1+\sqrt{1-\xi^2\left(1-\frac{e^2}{Gm_e^2}\right)}\right] \simeq \frac{e}{m_e}\frac{Q}{c^2}\,. \tag{206}$$

The energy extraction occurs in a finite number $N_{\rm PD}$ of such discrete elementary processes, each one corresponding to a decrease of the EMBH charge. We have

$$N_{\rm PD} \simeq \frac{Q}{e}\,. \tag{207}$$

Since the total extracted energy is (see Eq. (202)) $E^{\rm tot} = \frac{Q^2}{2r_+}$, we obtain for the mean energy per accelerated particle $\langle E\rangle_{\rm PD} = \frac{E^{\rm tot}}{N_{\rm PD}}$

$$\langle E\rangle_{\rm PD} = \frac{Qe}{2r_+} = \frac{1}{2}\frac{\xi}{1+\sqrt{1-\xi^2}}\frac{e}{\sqrt{G}m_e}\; m_e c^2 \simeq \frac{1}{2}\xi\frac{e}{\sqrt{G}m_e}\; m_e c^2, \tag{208}$$

which gives

$$\langle E\rangle_{\rm PD} \lesssim \begin{cases} \left(\frac{M}{M_\odot}\right)\times 10^{21} eV & \text{if } \frac{M}{M_\odot}\leq 10^6 \\ 10^{27} eV & \text{if } \frac{M}{M_\odot} > 10^6 \end{cases}\,. \tag{209}$$

One of the crucial aspects of the energy extraction process from an EMBH is its back reaction on the irreducible mass expressed in Christodoulou & Ruffini [30]. Although the energy extraction processes can occur in the entire effective ergosphere defined by Eq. (206), only the limiting processes occurring on the horizon with zero kinetic energy can reach the maximum efficiency while approaching the condition of total reversibility (see Fig. 2 in Christodoulou & Ruffini [30] for details). The farther from the horizon that a decay occurs, the more it increases the irreducible mass and loses efficiency. Only in the complete reversibility limit (Christodoulou & Ruffini [30]) can the energy extraction process from an extreme EMBH reach the upper value of 50% of the total EMBH energy.

2. For $\mathcal{E}_+ \geq \mathcal{E}_{\rm c}$ the leading extraction process is a *collective* process based on an electron-positron plasma generated by the vacuum polarization, (see Fig. 4) as discussed in section III The condition $\mathcal{E}_+ \geq \mathcal{E}_{\rm c}$ implies

$$\frac{GM/c^2}{\lambda_{\rm C}}\left(\frac{e}{\sqrt{G}m_e}\right)^{-1} \simeq 2\cdot 10^{-6}\frac{M}{M_\odot} \leq \xi \leq 1\,. \tag{210}$$

This vacuum polarization process can occur only for an EMBH with mass smaller than $2\cdot 10^6 M_\odot$. The electron-positron pairs are now produced in the dyadosphere of the EMBH, (note that the dyadosphere is a subregion of the effective ergosphere) whose radius r_{ds} is given in Eq.(8). We have $r_{ds} \ll r_{\rm Eerg}$. The number of particles created and the total energy stored in dyadosphere are given in Eqs.(10,12) respectively and we have approximately

$$N^\circ_{e^+e^-} \simeq \left(\frac{r_{ds}}{\lambda_{\rm C}}\right)\frac{Q}{e}\,, \tag{211}$$

$$E_{dya} \simeq \frac{Q^2}{2r_+} \tag{212}$$

The mean energy per particle produced in the dyadosphere $\langle E\rangle_{\rm ds} = \frac{E_{dya}}{N^\circ_{e^+e^-}}$ is then

$$\langle E\rangle_{\rm ds} \simeq \frac{3}{8}\left(\frac{\lambda_{\rm C}}{r_{ds}}\right)\frac{Qe}{r_+}\,, \tag{213}$$

which can be also rewritten as

$$\langle E\rangle_{\rm ds} \simeq \frac{1}{2}\left(\frac{r_{\rm ds}}{r_+}\right)\; m_e c^2 \sim \sqrt{\frac{\xi}{M/M_\odot}}10^5 keV\,. \tag{214}$$

Such a process of vacuum polarization, occurring not at the horizon but in the extended dyadosphere region ($r_+ \leq r \leq r_{\rm ds}$) around an EMBH, has been observed to reach the maximum efficiency limit of 50% of the total

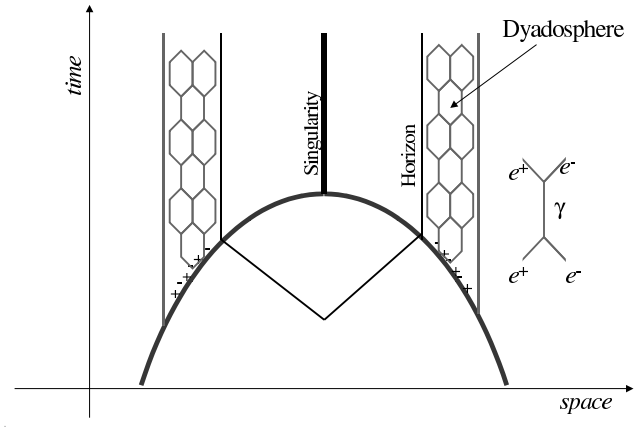

Figure 48: Space-time diagram of the collapse process leading to the formation of the dyadosphere. As the collapsing core crosses the dyadosphere radius the pair creation process starts, and the pairs thermalize in a neutral plasma configuration. Then also the horizon is crossed and the singularity is formed.

mass-energy of an extreme EMBH (see e.g. Preparata et al. [124]). The conceptual justification of this result follows from the present work: the e^+e^- creation process occurs at the expence of the Coulomb energy given by Eq. (204) and does not affect the irreducible mass given by Eq. (203), which indeed, as we have proved, does not depend of the electromagnetic energy. In this sense, $\delta M_{\rm irr} = 0$ and the transformation is fully reversible. This result will be further validated by the study of the dynamical formation of the dyadosphere, which we have obtained using the present work and Cherubini et al. [28] (see Ruffini et al. [159]).

Let us now compare and contrast these two processes. We have

$$r_{\rm Eerg} \simeq \left(\frac{r_{ds}}{\lambda_C}\right) r \tag{215}$$

$$N_{\rm dya} \simeq \left(\frac{r_{ds}}{\lambda_C}\right) N_{\rm PD}, \tag{216}$$

$$\langle E\rangle_{\rm dya} \simeq \left(\frac{\lambda_C}{r_{ds}}\right) \langle E\rangle_{\rm PD}\,. \tag{217}$$

Moreover we see (Eqs. (209), (214)) that $\langle E\rangle_{\rm PD}$ is in the range of energies of UHECR, while for $\xi \sim 0.1$ and $M \sim 10 M_\odot$, $\langle E\rangle_{\rm ds}$ is in the gamma ray range. In other words, the discrete particle decay process involves a small number of particles with ultra high energies ($\sim 10^{21} eV$), while vacuum polarization involves a much larger number of particles with lower mean energies ($\sim 10 MeV$).

Having so established and clarified the basic conceptual processes of the energetic of the EMBH, we are now ready to approach, using the new analytic solution obtained, the dynamical process of vacuum polarization occurring during the formation of an EMBH as qualitatively represented in Fig. 48. The study of the dyadosphere dynamical formation as well as of the electron-positron plasma dynamical evolution will lead to the first possibility of directly observing the general relativistic effects approaching the EMBH horizon.

Before closing we would like to emphasize once more a basic point: all the considerations presented in the description of the preceding eras are based on the approximations in the description of the dyadosphere presented in section III. This treatment is very appropriate in estimating the general dependence of the energy of the P-GRB, the kinetic energy of the ABM pulse and consequently the intensity of the afterglow, as well as the overall time structure of the GRB and especially the time of the release of the P-GRB in respect to the moment of gravitational collapse and its relative intensity with respect to the afterglow. If, however, is addressed the issue of the detailed temporal structure of the P-GRB and its detailed spectral distribution, the above dynamical considerations on the dyadosphere formation are needed (see also Ruffini et al. [159]). In turn, this detailed analysis is needed if the general relativistic effects close to the horizon formation have to be followed. As expressed already in section. XII, all general relativistic quantum field theory effects are encoded in the fine structure of the P-GRB. As emphasized in section X, the only way to differentiate between solutions with same E_{dya} but different EMBH mass and charge is to observe the P-GRBs in the limit $B \to 0$, namely, to observe the short GRBs.

XXVIII. CONTRIBUTION OF THE EMBH MODEL TO THE BLACK HOLE THEORY

The aim of this section is to point out how the knowledge obtained from the EMBH model is of relevance also for the basic theory of black holes and further how very high precision verification of general relativistic effects in the very strong field near the formation of the horizon should be expected in the near future.

We shall first see how Eq.(203) for $M_{\rm irr}$,

$$M_{\rm irr} = M_0 - \frac{M_0^2}{2r_+} + T_+ \,, \tag{218}$$

leads to a deeper physical understanding of the role of the gravitational interaction in the maximum energy extraction process of an EMBH. This formula can also be of assistance in clarifying some long lasting epistemological issue on the role of general relativity, quantum theory and thermodynamics.

It is well known that if a spherically symmetric mass distribution without any electromagnetic structure undergoes free gravitational collapse, its total mass-energy M is conserved according to the Birkhoff theorem: the increase in the kinetic energy of implosion is balanced by the increase in the gravitational energy of the system. If one considers the possibility that part of the kinetic energy of implosion is extracted then the situation is very different: configurations of smaller mass-energy and greater density can be attained without violating Birkhoff theorem.

We illustrate our considerations with two examples: one has found confirmation from astrophysical observations, the other promises to be of relevance for gamma ray bursts (GRBs) (see Ruffini & Vitagliano [156]). Concerning the first example, it is well known from the work of Landau [86] that at the endpoint of thermonuclear evolution, the gravitational collapse of a spherically symmetric star can be stopped by the Fermi pressure of the degenerate electron gas (white dwarf). A configuration of equilibrium can be found all the way up to the critical number of particles

$$N_{\rm crit} = 0.775 \frac{m_{Pl}^3}{m_0^3}, \tag{219}$$

where the factor 0.775 comes from the coefficient $\frac{3.098}{\mu^2}$ of the solution of the Lane-Emden equation with polytropic index $n = 3$, and $m_{Pl} = \sqrt{\frac{\hbar c}{G}}$ is the Planck mass, m_0 is the nucleon mass and μ the average number of electrons per nucleon. As the kinetic energy of implosion is carried away by radiation the star settles down to a configuration of mass

$$M = N_{\rm crit} m_0 - U, \tag{220}$$

where the gravitational binding energy U can be as high as $5.72 \times 10^{-4} N_{\rm crit} m_0$.

Similarly Gamov (see Gamow & Critchfield [61]) has shown that a gravitational collapse process to still higher densities can be stopped by the Fermi pressure of the neutrons (neutron star) and Oppenheimer (Oppenheimer & Volkoff [106]) has shown that, if the effects of strong interactions are neglected, a configuration of equilibrium exists also in this case all the way up to a critical number of particles

$$N_{\rm crit} = 0.398 \frac{m_{Pl}^3}{m_0^3}, \tag{221}$$

where the factor 0.398 comes now from the integration of the Tolman-Oppenheimer-Volkoff equation (see e.g. Harrison et al. [75]). If the kinetic energy of implosion is again carried away by radiation of photons or neutrinos and antineutrinos the final configuration is characterized by the formula (220) with $U \lesssim 2.48 \times 10^{-2} N_{\rm crit} m_0$. These considerations and the existence of such large values of the gravitational binding energy have been at the heart of the explanation of astrophysical phenomena such as red-giant stars and supernovae: the corresponding measurements of the masses of neutron stars and white dwarfs have been carried out with unprecedented accuracy in binary systems (Gursky & Ruffini [72]).

From a theoretical physics point of view it is still an open question how far such a sequence can go: using causality nonviolating interactions, can one find a sequence of braking and energy extraction processes by which the density and the gravitational binding energy can increase indefinitely and the mass-energy of the collapsed object be reduced at will? This question can also be formulated in the mass-formula language of a black hole given in Christodoulou & Ruffini [30] (see also Ruffini & Vitagliano [156]): given a collapsing core of nucleons with a given rest mass-energy M_0, what is the minimum irreducible mass of the black hole which is formed?

Following Cherubini et al. [28] and Ruffini & Vitagliano [156], consider a spherical shell of rest mass M_0 collapsing in a flat space-time. In the neutral case the irreducible mass of the final black hole satisfies the equation (see Ruffini & Vitagliano [156])

$$M_{\rm irr} = M = M_0 - \frac{M_0^2}{2r_+} + T_+, \tag{222}$$

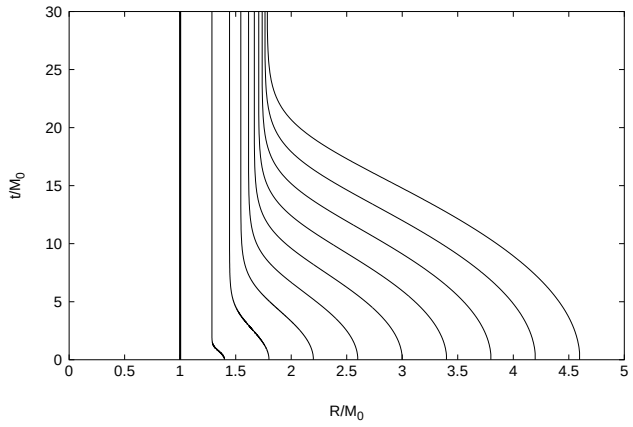

Figure 49: Collapse curves for neutral shells with rest mass M_0 starting at rest at selected radii R^* computed by using the exact solutions given in Cherubini et al. [28]. A different value of $M_{\rm irr}$ (and therefore of r_+) corresponds to each curve. The time parameter is the Schwarzschild time coordinate t and the asymptotic behaviour at the respective horizons is evident. The limiting configuration $M_{\rm irr} = \frac{M_0}{2}$ (solid line) corresponds to the case in which the shell is trapped, at the very beginning of its motion, by the formation of the horizon.

where M is the total energy of the collapsing shell and T_+ the kinetic energy at the horizon r_+. Recall that the area S of the horizon is (Christodoulou & Ruffini [30])

$$S = 4\pi r_+^2 = 16\pi M_{\rm irr}^2 \tag{223}$$

where $r_+ = 2M_{\rm irr}$ is the horizon radius. The minimum irreducible mass $M_{\rm irr}^{(\rm min)}$ is obtained when the kinetic energy at the horizon T_+ is 0, that is when the entire kinetic energy T_+ has been extracted. We then obtain the simple result

$$M_{\rm irr}^{(\rm min)} = \frac{M_0}{2}. \tag{224}$$

We conclude that in the gravitational collapse of a spherical shell of rest mass M_0 at rest at infinity (initial energy $M_{\rm i} = M_0$), an energy up to 50% of M_0c^2 can in principle be extracted, by braking processes of the kinetic energy. In this limiting case the shell crosses the horizon with $T_+ = 0$. The limit $\frac{M_0}{2}$ in the extractable kinetic energy can further increase if the collapsing shell is endowed with kinetic energy at infinity, since all that kinetic energy is in principle extractable.

In order to illustrate the physical reasons for this result, using the formulas of Cherubini et al. [28], we have represented in Fig. 49 the world lines of spherical shells of the same rest mass M_0, starting their gravitational collapse at rest at selected radii R^*. These initial conditions can be implemented by performing suitable braking of the collapsing shell and concurrent kinetic energy extraction processes at progressively smaller radii (see also Fig. 50). The reason for the existence of the minimum (224) in the black hole mass is the "self closure" occurring by the formation of a horizon in the initial configuration (thick line in Fig. 49).

Is the limit $M_{\rm irr} \to \frac{M_0}{2}$ actually attainable without violating causality? Let us consider a collapsing shell with charge Q. If $M \geq Q$ an EMBH is formed. As pointed out in Ruffini & Vitagliano [156] the irreducible mass of the final EMBH does not depend on the charge Q. Therefore Eqs. (222) and (224) still hold in the charged case with $r_+ = M + \sqrt{M^2 - Q^2}$. In Fig. 50 we consider the special case in which the shell is initially at rest at infinity, i.e. has initial energy $M_{\rm i} = M_0$, for three different values of the charge Q. We plot the initial energy M_i, the energy of the system when all the kinetic energy of implosion has been extracted as well as the sum of the rest mass energy and the gravitational binding energy $-\frac{M_0^2}{2R}$ of the system (here R is the radius of the shell). In the extreme case $Q = M_0$, the shell is in equilibrium at all radii (see Cherubini et al. [28]) and the kinetic energy is identically zero. In all three cases, the sum of the extractable kinetic energy T and the electromagnetic energy $\frac{Q^2}{2R}$ reaches 50% of the rest mass energy at the horizon, according to Eq. (224).

What is the role of the electromagnetic field here? If we consider the case of a charged shell with $Q \simeq M_0$, the electromagnetic repulsion implements the braking process and the extractable energy is entirely stored in the

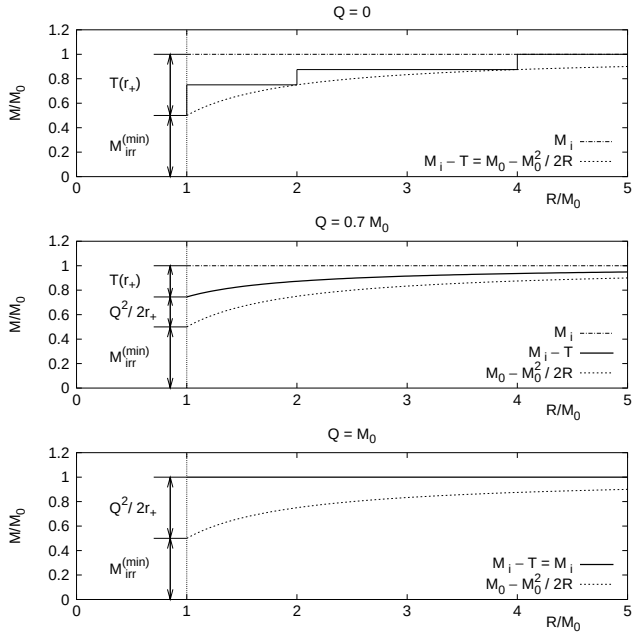

Figure 50: Energetics of a shell such that $M_{\rm i} = M_0$, for selected values of the charge. In the first diagram $Q = 0$; the dashed line represents the total energy for a gravitational collapse without any braking process as a function of the radius R of the shell; the solid, stepwise line represents a collapse with suitable braking of the kinetc energy of implosion at selected radii; the dotted line represents the rest mass energy plus the gravitational binding energy. In the second and third diagram $Q/M_0 = 0.7$, $Q/M_0 = 1$ respectively; the dashed and the dotted lines have the same meaning as above; the solid lines represent the total energy minus the kinetic energy. The region between the solid line and the dotted line corresponds to the stored electromagnetic energy. The region between the dashed line and the solid line corresponds to the kinetic energy of collapse. In all the cases the sum of the kinetic energy and the electromagnetic energy at the horizon is 50% of M_0. Both the electromagnetic and the kinetic energy are extractable. It is most remarkable that the same underlying process occurs in the three cases: the role of the electromagnetic interaction is twofold: a) to reduce the kinetic energy of implosion by the Coulomb repulsion of the shell; b) to store such an energy in the region around the EMBH. The stored electromagnetic energy is extractable as shown in Ruffini & Vitagliano [156].

electromagnetic field surrounding the EMBH (see Ruffini & Vitagliano [156]). In Ruffini & Vitagliano [156] we have outlined two different processes of electromagnetic energy extraction. We emphasize here that the extraction of 50% of the mass-energy of an EMBH is not specifically linked to the electromagnetic field but depends on three factors: a) the increase of the gravitational energy during the collapse, b) the formation of a horizon, c) the reduction of the kinetic energy of implosion. Such conditions are naturally met during the formation of an extreme EMBH but are more general and can indeed occur in a variety of different situations, e.g. during the formation of a Schwarzschild black hole by a suitable extraction of the kinetic energy of implosion (see Fig. 49 and Fig. 50).

Now consider a test particle of mass m in the gravitational field of an already formed Schwarzschild black hole of mass M and go through such a sequence of braking and energy extraction processes. Kaplan (Kaplan [83]) found for the energy E of the particle as a function of the radius r

$$E = m\sqrt{1 - \tfrac{2M}{r}}. \tag{225}$$

It would appear from this formula that the entire energy of a particle could be extracted in the limit $r \to 2M$. Such 100% efficiency of energy extraction has often been quoted as evidence for incompatibility between General Relativity and the second principle of Thermodynamics (see Bekenstein [11] and references therein). J. Bekenstein and S. Hawking have gone as far as to consider General Relativity not to be a complete theory and to conclude that in order to avoid inconsistencies with thermodynamics, the theory should be implemented through a quantum description (Bekenstein [11], Hawking [76]). Einstein himself often expressed the opposite point of view (see e.g.

Dyson [45]).

The analytic treatment presented in Cherubini et al. [28] can clarify this fundamental issue. It allows to express the energy increase E of a black hole of mass M_1 through the accretion of a shell of mass M_0 starting its motion at rest at a radius R in the following formula which generalizes Eq. (225):

$$E \equiv M - M_1 = -\frac{M_0^2}{2R} + M_0\sqrt{1-\frac{2M_1}{R}}, \tag{226}$$

where $M = M_1 + E$ is clearly the mass-energy of the final black hole. This formula differs from the Kaplan formula (225) in three respects: a) it takes into account the increase of the horizon area due to the accretion of the shell; b) it shows the role of the gravitational self energy of the imploding shell; c) it expresses the combined effects of a) and b) in an exact closed formula.

The minimum value $E_{\rm min}$ of E is attained for the minimum value of the radius $R = 2M$: the horizon of the final black hole. This corresponds to the maximum efficiency of the energy extraction. We have

$$E_{\rm min} = -\frac{M_0^2}{4M} + M_0\sqrt{1-\frac{M_1}{M}} = -\frac{M_0^2}{4(M_1+E_{\rm min})} + M_0\sqrt{1-\frac{M_1}{M_1+E_{\rm min}}}, \tag{227}$$

or solving the quadratic equation and choosing the positive solution for physical reasons

$$E_{\rm min} = \frac{1}{2}\left(\sqrt{M_1^2+M_0^2} - M_1\right). \tag{228}$$

The corresponding efficiency of energy extraction is

$$\eta_{\rm max} = \frac{M_0 - E_{\rm min}}{M_0} = 1 - \frac{1}{2}\frac{M_1}{M_0}\left(\sqrt{1+\frac{M_0^2}{M_1^2}} - 1\right), \tag{229}$$

which is strictly *smaller than* 100% for *any* given $M_0 \neq 0$. It is interesting that this analytic formula, in the limit $M_1 \ll M_0$, properly reproduces the result of equation (224), corresponding to an efficiency of 50%. In the opposite limit $M_1 \gg M_0$ we have

$$\eta_{\rm max} \simeq 1 - \frac{1}{4}\frac{M_0}{M_1}. \tag{230}$$

Only for $M_0 \to 0$, Eq. (229) corresponds to an efficiency of 100% and correctly represents the limiting reversible transformations introduced in Christodoulou & Ruffini [30]. It seems that the difficulties of reconciling General Relativity and Thermodynamics are ascribable not to an incompleteness of General Relativity but to the use of the Kaplan formula in a regime in which it is not valid. The generalization of the above results to stationary black holes is being considered.

XXIX. CONCLUSIONS

The EMBH theory has been here applied for the first time to fit the experimental data of GRB 991216. This process has given us the opportunity to rethink the entire GRB process in an unitary description starting from the moment of gravitational collapse all the way up to the latest phases of the afterglow. We have identified the three fundamental actors of the GRB phenomenon in:

1. E_{dya}. Having reanalyzed in section III the physics of the dyadosphere we have pointed out in Fig. 17 that the same value of E_{dya} can be obtained from an entire family of (μ, ξ) parameters (i.e. E_{dya} is degenerate in (μ, ξ)). We have then shown in the reexamination of all the GRB eras that all the results depend only on the value of E_{dya} and not on the particular value of (μ, ξ) (see sections VIII,IX,XIII,XIV). The only exception to this occurs in the era I (see section VII) which is the only one relevant for short GRBs.

2. B. The crucial role played by the baryonic remnant of the progenitor star in determining the relative intensity ratio and the time delay between the P-GRB and the E-APE has been summarized already in the two Figs. 11–11 in the introduction.

3. ISM. The density n_{ism} of the interstellar medium and its inhomogeneities appears to have a fundamental role in the intensity and the temporal substructures of the E-APE and the afterglow.

The observational data agree with the predictions of the model on:

1. the intensity ratio, 1.58×10^{-2}, between the P-GRB and the E-APE, which strongly depends on the parameter B;

2. the absolute intensities for both the P-GRB and the E-APE, respectively 7.54×10^{51} erg and 4.75×10^{53};

3. the arrival time of the P-GRB and the peak of the E-APE, respectively 8.41×10^{-2} s and 19.87 s;

4. the power-law index n of the afterglow, predicted $n_{theo} = -1.6$ and observed $n_{obs} = -1.616 \pm 0.067$ (see sections XVIII, XIX);

5. the temporal structure of the E-APE and its correlation with the inhomogeneity in the ISM;

6. the spectral distribution of the X-ray and γ-ray emission.

Concerning the total energy of GRB 991216, $E_{dya} = 4.83 \times 10^{53}$ erg is found in the EMBH theory. This value is systematically larger than the ones quoted in the current literature by Panaitescu & Kumar [111] and by Halpern et al. [73] due to the fact that they respectively consider beaming angles of $3^\circ - 4^\circ$ and 6°. These considerations have been shown to be untenable in section XIX. There is still a difference of $\sim 28\%$ between the total energy implied by the EMBH theory (4.83×10^{53} erg) and the value quoted by Halpern ($E_{dya} = 6.7 \times 10^{53}$ erg) in the case of spherical emission. We trust that this is a consequence of the underlying assumption of the spectral distribution of the radiation assumed by Halpern et al. [73] (see e.g. Frail et al. [55]), which should be reassessed on the ground of our theoretical results (see also Ruffini et al. [153]).

These results can certainly be considered the success of the EMBH theory.

Before closing, we like to stress how GRBs, if duly theoretically interpreted, can open a main avenue of inquiring on totally new physical and astrophysical regimes. This program is very likely one of the greatest computational efforts in physics and astrophysics and cannot be actuated using shortcuts.

From the point of view of fundamental physics new regimes are explored:

1. The process of energy extraction from black holes. It is interesting that the analysis of GRBs has promoted a new effort in developing new theoretical tools for approaching the dynamical phase of collapse as expressed in section. XXVII. These results have further clarified some basic issue related to the energy extraction process from black hole (see e.g. Ruffini [139]). It was already known from the definition of the ergosphere (see Ruffini & Wheeler [135]) that the rotational energy extraction process do occur in an extended region around the horizon of a black hole. The fortunate situation that the energy extraction process in GRBs occurs in a condition of almost perfect spherical symmetry have allowed us to focus on the second fundamental parameter of black holes, namely the electric energy. The spherical symmetry has allowed as well to develop some powerful theoretical tools (see section XXVII) which have allowed to reach a better understanding of the role of kinetic energy of implosion in the process of gravitational collapse, in the storage of electromagnetic energy in the region around black holes and to establish as well a new upper limit in the energy extraction process in the gravitational collapse up to 50% of the initial rest mass of the system (see section XXVIII). These results are of general validity and do transcend the work on the EMBH theory, although they are motivated by these researches. Interestingly this work, by giving a new expression for the efficiency of transforming gravitational energy into mechanical work (see section XXVIII), has opened up a new opportunity of debating the relation between general relativity, thermodynamics and quantum theory, which is certainly one of the most profound and important topic of research in the entire realm of fundamental physics.

2. The quantum and general relativistic effects of matter-antimatter creation near the black hole horizon. It is well known that one of the most important topics pursued in the last seventy years in physics has been the possibility, postulated by Sauter, Heisemberg, Euler, Schwinger to create matter-antimatter from the vacuum. In order to have the first experimental and observational evidence for this phenomenon, three major approaches are being followed:
a) In central collisions of heavy ions near the Coulomb barrier, as first proposed in Gerštein & Y. B. Zel'dovich [64, 65] (see also Popov & Rozhdestvenskaya [121], Popov [122], Zel'dovich & Popov [192]). Efforts in experimentally implementing this idea at GSI were made since early 80's. Despite some apparently encouraging result (Schweppe et al. [171]), such efforts have failed so far due to the small contact time of the colliding ions (see e.g. Ahmad et al. [2], Bär et al. [8], Ganz et al. [62], Heinz et al. [77], Leinberger et al. [88]). Typically the electromagnetic energy involved in the collisions of heavy ions with impact parameter $l_1 \sim 10^{-12}$cm is $E_1 \sim 10^{-6}$erg.
b) At the focus of an X-ray free electron laser (XFEL) (see Ringwald [132], Roberts et al. [133] and references therein). This idea will be possibly testable at DESY, where the XFEL is part of the design of the collider TESLA, as well as at SLAC, where the so-called Linac Coherent Light Source (LCLS) has been proposed. The electromagnetic energy at the focus of an XFEL is $E_2 \sim 10^6$erg concentrated in a region of linear extension

$l_2 \sim 10^{-8}$ cm (Ringwald [132]).
c) Around an electromagnetic black hole (EMBH) (Damour & Ruffini [33], Preparata et al. [123, 124]), giving rise to the observed phenomenon of GRBs (see e.g. Ruffini et al. [144, 145, 146, 148]). The electromagnetic energy of an EMBH of mass $M \sim 10M_\odot$ and charge $Q \sim 0.1M/\sqrt{G}$ is $E_3 \sim 10^{54}$ ergs and it is deposited in a region of linear extension $l_3 \sim 10^8$ m (Preparata et al. [124], Ruffini & Vitagliano [156]).
There is the very distinct possibility that in this race the success will be reached by the observations in relativistic astrophysics more than from the high energy experiments on the Earth. This will be certainly a splendid success which will be only second to the discovery of Helium first in the stars and then on the Earth! Quite apart from the discovery in itself, the detection of vacuum polarization in the astrophysical settings presents distinctively new physical phenomena as Ruffini et al. [160]. The very important topic to be covered in the forthcoming months is the study of the dynamical phase of gravitational collapse and to follow the effects of such process of vacuum polarization in the dynamical phase. It will be also important to follow the development of this process all the way to the emission of the P-GRB (Ruffini & Vitagliano [158]).

3. The physics of ultrarelativisitc shock waves with Lorentz gamma factor $\gamma > 100$. We are expecting much progress in this topic from the understanding of the instantaneous spectrum of GRBs. Some preliminary results along this line are presented in Ruffini et al. [150]. See also section XXIV.

From the point of view of astronomy and astrophysics also new regimes are explored:

1. The occurrence of gravitational collapse to a black hole from a critical mass core of mass $M \gtrsim 10M_\odot$, which clearly differs from the values of the critical mass encountered in the study of stars "catalyzed at the endpoint of thermonuclear evolution" (white dwarfs and neutron stars).

2. The extremely high efficiency of the spherical collapse to a black hole, where almost 99.99% of the core mass collapses leaving negligible remnant. The EMBH theory offers an unprecedented tool in order to map with great accuracy all the matter distribution around the newly formed EMBH from the horizon all the way to the ISM. This concept was pioneered by Dermer & Mitman [42] who proposed to use GRB sources as "tomographic images of the density distributions of the medium surrounding the sources of GRBs". It is important to emphasize that the very precise reading of the matter distribution encoded in the data of the P-GRB, the E-APE and the afterglow in GRB 991216 is in marked disagreement with the matter distribution postulated by the "collapsar" scenario (see MacFadyen & Woosley [90], Paczyński [110], Woosley [190]). This conclusion is evidenced not only by the absence of beaming already mentioned above, but also for the paucity of the baryonic matter encountered by the PEM pulse in its way out from the EMBH. There is no evidence for the presence either of a baryonic disk component nor of a conspicuous baryonic remnant. We actually have $B = 3.0 \times 10^{-3}$. Unlike the case of formation of a neutron star, the mass of the remnant of the progenitor star is very small indeed. This mass, determined by B, is very accurately inferable from the relative intensity and temporal distance between the P-GRB and the E-APE (see above). In the present case we have $M_B \sim 8.1 \times 10^{-4} M_\odot$. The presence of the remnant is also important for guaranteeing the overall charge neutrality of the system formed by the oppositely charged collapsing core and the remnant. It has been pointed out in section XXVI that this condition of charge separation between the collapsing core and the remnant occurs only during the relevant part of the gravitational collapse process which, we recall, for a $10M_\odot$ is of the order of 30 seconds.

3. The necessity of developing a fine tuning in the final phases of thermonuclear evolution of the stars, both for the star collapsing to the black hole and the surrounding ones, in order to explain the possible occurrence of the "induced gravitational collapse".

New regimes are as well encountered from the point of view of nature of GRBs:

1. The basic structure of GRBs is uniquely composed by a proper-GRB (P-GRB) and the afterglow. The most general GRB contains three different components: the P-GRB, the E-APE and the rest of the afterglow. The ratio between the P-GRB and the E-APE intensity and their temporal separation is a function of the B parameter (see Figs. 11–11). The best fit is obtained for $B = 3.0 \times 10^{-3}$ (see section XV). We recall that in the present case for $B < 2.5 \times 10^{-5}$ the energy of the P-GRB would be larger than the one of the E-APE and the energy of the dyadosphere would be mainly emitted in what have been called the "short bursts", while for $B > 2.5 \times 10^{-5}$ the energy of the E-APE would predominate and the energy of the dyadosphere would be mainly carried by the ABM pulse and emitted in the afterglow.

2. The long bursts are then simply explained as the peak of the afterglow (the E-APE) and their observed time variability is explained in terms of inhomogeneities in the interstellar medium (ISM). The difficulties encountered by *all* theoretical models, through the years, in order to explain the so called "long bursts" are resolved in a

drastic way (see section XVI). The so called "long bursts" are *not* bursts at all. They represent just the E-APE which was interpreted as a burst only due to the noise threshold in the BATSE observations (see Fig. 10). The E-APE is emitted at distances from the EMBH in the range $1.0 \times 10^{16} \sim 1.0 \times 10^{17}$ cm, see Tab. I, namely well outside the size of the progenitor star and already deep in interstellar space. The fact that the crossing of such distance, which is a typical dimension of an interstellar cloud, appears to occur in arrival time in only ~ 100 seconds is perfectly explained by the relativistic transformations encoded in the RSTT paradigm corresponding to a gamma factor between 100 and 300 (see section V and Tab. I). This effect would be interpreted within a classical and incorrect astronomical picture by a "superluminal" behaviour propagating at $\sim 3.6 \times 10^4 c$ (see Tab. I).

3. The short bursts are identified with the P-GRBs and the crucial information on general relativistic and vacuum polarization effects are encoded in their spectra and intensity time variability. In the limit $B \to 0$ the entire dyadosphere energy is emitted in the P-GRB. These events represents the "short bursts" class, for which the afterglow intensity is smaller than the P-GRB emission and below the actual observational limits (see section XII). It is interesting that the proposed differentiation between the "short bursts" and "long bursts" within the EMBH theory is merely due to the amount of baryonic matter in the remnant, described by the B parameter, and totally independent from the process of gravitational collapse which is clearly identical in both cases. This explains at once the recently found conclusion that the distribution of short and long GRBs have essentially the same characteristic peak luminosity (Schmidt [170]). Also the result expressed in Fig. 6 that the average temperature corresponding to the P-GRB emission does increase for decreasing values of the B parameter can explain the observed fact that the "short bursts", which are obtained in the limit $B \to 0$, are systematically harder than "long bursts" (Kouveliotou et al. [84]).

A new class of space missions to acquire information on such extreme new regimes are urgently needed. The detailed observations of the yet unexplored region in the range up to 10 seconds in Fig. 29 and the corresponding observations of the "short bursts" by a new class of space missions with higher sensitivity than the BATSE instrument appear to be of great importance. Such observations should allow to directly observe for the first time the general relativistic and extreme quantum field theory effects connected to the process of formation of the EMBH. It can be of some interest to explore the possibility of observing in these regimes the "gravitationally induced electromagnetic radiation" (Johnston et al. [81]) and the "electromagnetically induced gravitational radiation" (Johnston et al. [82]) phenomena as well as to explore the possibility of developing neutrino detectors. This will need further developments of the predictions of the EMBH theory in these general relativistic and ultra-high-energy particle phenomena.

[1] Abramowitz, M., Stegun, I.A., Editors, *Handbook of Mathematical Functions*, National Bureau of Standards, Washington, D.C., 1970
[2] Ahmad, I., et al., 1995, Phys. Rev. Lett., 75, 2658
[3] Amati, L. et al. 2000, Science, 290, 953
[4] Band, D., et al., 1993, ApJ, 413, 281
[5] BATSE GRB Light Curves, `http://gammaray.msfc.nasa.gov/batse/grb/lightcurve/`
[6] BATSE Rapid Burst Response, 1999, http://gammaray.msfc.nasa.gov∼kippen/batserbr/
[7] Band, D., et al., 1993, ApJ, 413, 281
[8] Bär, R., et al., 1995, Nucl. Phys. A, 583, 237
[9] Beck, S.C., Turner, J.L., Kovo, O., 2000, AJ, 120, 244
[10] Bekenstein, J.D., 1971, Phys. Rev. D, 4, 2185
[11] Bekenstein, J.D., 1973, Phys. Rev. D, 7, 2333
[12] Bethe, H.A., 1991, *The road from Los Alamos*, Touchstone Ed. by American Institute of Physics (New York)
[13] Bianco, C.L., Ruffini, R., Xue, S.-S., 2001a, A&A, 368, 377
[14] Bianco, C.L., Chardonnet, P., Ruffini, R., Xue, S.-S., 2002, in preparation
[15] Bini, D., Cherubini, C., Jantzen, R., Ruffini, R., 2002, Prog. Theor. Phys., 107, 967
[16] Biretta, J.A., Sparks, W.B., Macchetto, F., 1999, ApJ, 520, 621
[17] Blandford, R.D., McKee, C.F., 1976, Phys. Fluids, 19, 1130
[18] Blinnikov, S.I., Kozyreva, A.V., Panchenko, I.E., 1999, Astron. Rep., 43, 739 (preprint: astro-ph/9902378)
[19] Bloom, L. et al., 1999, Nature, 401, 453
[20] Böttcher, M., Dermer, C.D., 2000, ApJ, 532, 281
[21] Bloom, J.S., Kulkarni, S.R., Djorgowski, S.G., 2002, AJ, 123, 1111
[22] Boccaletti, D., Ohanian, H.C., Ruffini, R., 2003, in preparation
[23] Borozdin, K.N., Trudolyubov, S.P., 2003, ApJ, 583, L57
[24] Carter, B., 1997, Proceedings of the Eighth Marcel Grossmann Meeting on General Relativity, Eds. T. Piran, R. Ruffini, World Scientific, Singapore, p. 136

[25] Cavallo, G., Rees, M.J., 1978, MNRAS, 183, 359
[26] Chandrasekhar, S., *Why are the stars as they are*, in *Physics and Astrophysics of Neutron Stars and Black Holes*, R. Giacconi and R. Ruffini Eds., 1978, North Holland, Elsevier
[27] Chandrasekhar, S., Fermi, E., 1953, ApJ, 118, 116
[28] Cherubini, C., Ruffini, R., Vitagliano, L., 2002, Phys. Rev. B, 545, 226
[29] Chiang, J., Dermer, C.D., 1999, ApJ, 512, 699
[30] Christodoulou, D., Ruffini, R., 1971, Phys. Rev. D, 4, 3552
[31] Corbet, R., Smith, D.A., 2000, in Rossi2000: Astrophysics with the Rossi X-ray Timing Explorer, Greenbelt, USA
[32] Costa, E., 2002, invited talk in "IX Marcel Grossmann Meeting on General Relativity", V. Gurzadyan, R. Jantzen & R. Ruffini editors, World Scientific (Singapore)
[33] Damour, T., Ruffini, R., 1975, Phys. Rev. Lett., 35, 463
[34] Davies, M.B., Benz, W., Piran, T., Thielemann, F.K., 1994, ApJ, 431, 742
[35] De la Cruz, V., & Israel, W., 1967, Nuovo Cimento A, 51, 744.
[36] Denardo, G., Ruffini, R., 1973, Phys. Lett., 45B, 259
[37] Denardo, G., Hively, L., Ruffini, R., 1974, Phys. Lett., 50B, 270
[38] Dermer, C.D., 1998, ApJ, 501, L157
[39] Dermer, C.D., Chiang, J., 1998, in *Proceedings of High Energy Processes in Accreting Black Holes*, held Graftavallen, Sweden, June 29- July 4, 1998, J. Poutanen & R. Svensson editors (preprint: astro-ph/9810222)
[40] Dermer, C.D., Böttcher, M., Chiang J., 1999a, ApJ, 515, L49
[41] Dermer, C.D., Chiang, J., Böttcher, M., 1999b, ApJ, 513, 656
[42] Dermer, C.D., Mitman, K.E., 1999, ApJ, 513, L5
[43] Dermer, C.D., 2002, ApJ, 574, 65
[44] Drozdova, D.N., Panchenko I.E., 1997, A&A, 324, 17
[45] Dyson, F., 2002, communication at "Science and Ultimate Reality", Symposium in honour of J. A. Wheeler, Princeton
[46] Eichler, D., Livio, M., Piran, T., Schramm, D.N., 1989, Nature, 340, 126
[47] Einstein, A., 1905, Ann. Phys. (Germany), 17, 891
[48] Fenimore, E.E., Madras, C.D., Nayakshin, S., 1996, ApJ 473, 998
[49] Fenimore, E.E., 1999, ApJ, 518, 375
[50] Fenimore, E.E., Cooper C., Ramirez-Ruiz, E., Sumner, M.C., Yoshida, A., Namiki, M., 1999, ApJ, 512, 683
[51] Ferrière, K.M., 2001, Rev. Mod. Phys., 73, 1031
[52] Filippenko, A.V., 1997, Annu. Rev. Astron. Astrophys., 35, 309
[53] Fishman, G., Meegan, C., 1995, Annu. Rev. Astron. Astrophys., 33, 415
[54] Frail, D. et al., 2000, ApJ, 538, L129
[55] Frail, D. et al., 2001, ApJ, 562, L55
[56] Frontera, F., et al., 2000, ApJS, 127, 59
[57] Fryer, C.L., Woosley, S.E., Herant, M., Davies, M.B., 1999, ApJ, 520, 650
[58] Galama, T.J. et al., 1998a, IAU Circ., 6895
[59] Galama, T.J. et al., 1998b, Nature, 395, 670
[60] Galama, T.J. et al., 2000, ApJ, 536, 185
[61] Gamow, G., Critchfield, C.L., 1951, "Theory of Atomic Nucleus and Energy Sources", Clarendon Press, Oxford
[62] Ganz, R. et al., 1996, Phys. Lett. B, 389, 4
[63] Garnavich, P. et al., 2000, ApJ, 543, 61
[64] Gerštein, S.S., Zel'dovich, Y.B., 1969, Lett. Nuovo Cimento, 1, 835
[65] Gerštein, S.S., Zel'dovich, Y.B., 1970, Sov. Phys. JETP, 30, 358
[66] Giacconi, R., Ruffini, R. (Eds.), 1978, *Physics and Astrophysics of Neutron Stars and Black Holes*, North Holland, Elsevier
[67] Gibbons, G.W., 1975, Commun. Math. Phys., 44, 245
[68] Gold, T., 1968, Nature, 218, 731
[69] Gold, T., 1969, Nature, 221, 27
[70] Goldreich, P., Julian, W.H., 1969, ApJ, 157, 869
[71] Gou, L.J., Dai, Z.G., Huang, Y.F., Lu, T., 2001, A&A, 368, 464
[72] Gursky, H., Ruffini, R., editors, 1975, "Neutron Stars, Black Holes and binary X-Ray Sources", Reidel, Dordrecht
[73] Halpern, J.P., Uglesich, R., Mirabal, N., Kassin, S., Thorstensen, J., Keel, W.C., Diercks, A., Bloom, J.S., Harrison, F., Mattox, J., Eracleous, M., 2000, ApJ, 543, 697
[74] Halzen, F., "High energy neutrino astronomy" in "Weak Interactions and Neutrinos, Proceedings of the 17th International Workship. Cape Town, South Africa", Edited by C. A. Dominguez and R. D. Viollier, World Scientific Publishers (Singapore, 2000), p.123
[75] Harrison, B.K., Thorne, K.S., Wakano, M., Wheeler, J.A., 1965, "Gravitation Theory and Gravitational Collapse", University of Chicago Press, Chicago.
[76] Hawking, S.W., Nature, 1974, 248, 30
[77] Heinz, S. et al., 1998, Eur. Phys. J. A, 1, 27
[78] Heisenberg, W., Euler, H., 1935, Zeits. Phys., 98, 714
[79] Hewish, A., Bell, S.J., Pilkington, J.D., Scott, P.F., Collins, R.A., 1968, Nature, 217, 709
[80] Israel, W., 1966, Nuovo Cimento B, 44, 1
[81] Johnston, M., Ruffini, R., Zerilli, F., 1973, Phys. Rev. Lett., 31, 1317

[82] Johnston, M., Ruffini, R., Zerilli, F., 1974, Phys. Lett., 49B, 185
[83] Kaplan, S.A., 1949, Zh. Eksp. & Teor. Fiz., 19, 951
[84] Kouveliotou, C., Meegan, C.A., Fishman, G.J., Bath, N.P., Briggs, M.S., Koshut, T.M., Paciesas, W.S., Pendleton, G.N., 1993, ApJ, 413, L101
[85] Kulkarni, S.R. et al., 1998 Nature, 395, 663
[86] Landau, L., 1932, Phys. Zeits. Sowj., 1, 285
[87] Landau, L.D., Lifshitz, E.M., "Course of Theoretical Physics - Volume 6: Fluid Mechanics", 2nd edition, paperback, 1995, Butterworth Heinemann, section 135, pag. 510
[88] Leinberger, U. et al., 1997, Phys. Lett. B, 394, 16
[89] Leinberger, U. et al., 1998, Eur. Phys. J. A, 1, 249
[90] MacFadyen, A.I., Woosley, S.E., 1999, ApJ, 524, 262
[91] Mao, S., Yi, I., 1994, ApJ, 424, L131
[92] Mészáros, P., Rees, M.J., 1992a, MNRAS, 257, 29p
[93] Mészáros, P., Rees, M.J., 1992b, ApJ, 397, 570
[94] Mészáros, P., Rees, M.J., 1993, ApJ, 405, 278
[95] Mészáros, P., Rees, M.J., 1997a, ApJ, 476, 232
[96] Mészáros, P., Rees, M.J., 1997b, ApJ, 482, L29
[97] Mészáros, P., Rees, M.J., Wijers, R.A.M.J., 1998, ApJ, 499, 301
[98] Mészáros, P., Rees, M.J., 2000, ApJ, 530, 292
[99] Mészáros, P., Rees, M.J., 2001, ApJ, 556, L37
[100] Mészáros, P., 2002, Annu. Rev. Astron. Asttroph., 40, 137
[101] Mirabel, I.F., Rodriguez, L.F., 1994, Nature, 371, 46
[102] Mirabel, I.F., Rodriguez, L.F., 1999, Annu. Rev. Astron. Asttroph., 37, 409
[103] Misner, C.W., Thorne, K.S., Wheeler J.A., *Gravitation*, San Francisco: Freeman (1973), chapter 23.
[104] Narayan, R., Paczyński, B., Piran, T., 1992, ApJ, 395, L83
[105] Norris, J.P., et al., 1986, ApJ, 301, 213
[106] Oppenheimer, J.R., Volkoff, G., 1939, Phys. Rev. D, 55, 374
[107] Paciesas, W.S. et al., 1999, ApJS, 122, 465
[108] Paczyński, B., 1991, Acta Astronomica, 41, 257
[109] Paczyński, B., Xu, G., 1994, ApJ, 427, 708
[110] Paczyński, B., 1998, ApJ, 494, L45
[111] Panaitescu, A., Kumar P., 2001, ApJ, 554, 667
[112] Panaitescu, A., Mészáros, P., Rees, M.J., 1998, ApJ, 503, 314
[113] Panaitescu, A., Mészáros, P., 1998a, ApJ, 492, 683
[114] Panaitescu, A., Mészáros, P., 1998b, ApJ, 501b, 772
[115] Panaitescu, A., Mészáros, P., 1999, ApJ, 526, 707
[116] Piran, T., 1999, Phys. Rep. 314, 575
[117] Piran, T., 2001, talk at 2000 Texas Meeting (preprint: astro-ph/0104134)
[118] Piro, L. et al., 1998, GCN 155
[119] Piro, L. et al., 1999, ApJ, 514, L73
[120] Piro, L. et al., 2000, Science, 290, 955
[121] Popov, V.S., Rozhdestvenskaya, T.I., 1971, JETP Lett., 14, 177
[122] Popov, V.S., 1972, Sov. J. Nucl. Phys., 14, 257
[123] Preparata, G., Ruffini, R., Xue, S.-S., 2003, in *Proceedings of the VII Italian-Korean meeting*, ed. Journal of the Korean Physical Society, in press (preprint: astro-ph/0204080)
[124] Preparata, G., Ruffini, R., Xue, S.-S., 1998b, A&A, 338, L87
[125] Preparata, G., Ruffini, R., Xue, S.-S., 2001, in *Proceedings of the III ICRA Network Workshop and VI Italo-Korean Meeting*, C.Cherubini & R. Ruffini editors, SIF
[126] Punsly, B., "Black Hole Gravitohydromagnetics", Springer, 2001
[127] Rees M.J., 1966, Nature 211, 468
[128] Rees, M.J., Mészáros, P., 1994, ApJ, 430, L93
[129] Rhoads, J.E., 1997a, ApJ, 487, L1
[130] Rhoads, J.E., 1997b, in AIP Conf. Proc. 428, Gamma-Ray Bursts: Fourth Huntsville Symposium, ed. C. Meegan, R. Preece & T. Koshut (New York: AIP), 699
[131] Rhoads, J.E., 1999, ApJ, 525, 737
[132] Ringwald, A., 2001, Phys. Lett. B, 501, 107
[133] Roberts, C.D., Schmidt, S.M., Vinnik, D.V., 2002, Phys. Rev. Lett., 89, 153901
[134] Rol, E. et al., 1999, GCN Circ. 491 (http://gcn.gsfc.nasa.gov/gcn/gcn3/491.gcn3)
[135] Ruffini, R., Wheeler, J.A., 1971, a chapter in "The Significance of Space Research for Fundamental Physics", A.F. Moore, V. Hardy, eds., European Space Research Organization (ESRO) book No. SP-52, Paris, updated in Rees, M., Ruffini, R., Wheeler, J.A., 1974, "Black Holes, Gravitational Waves and Cosmology", Gordon and Breach Science Publisher, New York, London, Paris
[136] Ruffini, R., in *Physics and Astrophysics of Neutron Stars and Black Holes*, Giacconi, R., Ruffini, R., Ed. and coauthors, North Holland, Amsterdam, 1978

[137] Ruffini, R., 1998, in "Black Holes and High Energy Astrophysics", Proceedings of the 49th Yamada Conference Ed. H. Sato and N. Sugiyama, Universal Ac. Press, Tokyo, 1998
[138] Ruffini, R., in "Fluctuating Paths and Fields - Dedicated to Hagen Kleinert on the Occasion of His 60th Birthday", Eds. W. Janke, A. Pelster, H.-J. Schmidt, and M. Bachmann, World Scientific, Singapore, 2001, p. 771
[139] Ruffini R., 2002, in *Proceedings of the Ninth Marcel Grossmann Meeting on General Relativity*, Gurzadyan V.G., Jantzen R.T. & Ruffini R. editors, World Scientific (Singapore)
[140] Ruffini R., 2003, in *Proceedings of the 34th COSPAR Scientific Assembly - Houston, TX, USA, 2002*, Pian, E., Masetti, N., Piro, L., editors, Elsevier, in press.
[141] Ruffini, R. & Wheeler, J.A., 1971, Physics Today, 24,(1), 30
[142] Ruffini, R., Salmonson, J.D., Wilson, J.R., Xue, S.S., 1999, A&A, 350, 334, A&AS, 138, 511
[143] Ruffini, R., Salmonson, J.D., Wilson, J.R., Xue, S.S., 2000, A&A, 359, 855
[144] Ruffini, R., Bianco, C.L., Chardonnet, P., Fraschetti, F., Xue, S.-S., 2001a, ApJ, 555, L107
[145] Ruffini, R., Bianco, C.L., Chardonnet, P., Fraschetti, F., Xue, S.-S., 2001b, ApJ, 555, L113
[146] Ruffini, R., Bianco, C.L., Chardonnet, P., Fraschetti, F., Xue, S.-S., 2001c, ApJ, 555, L117
[147] Ruffini, R., Bianco, C.L., Chardonnet, P., Fraschetti, F., Xue, S.-S., 2001e, Nuovo Cimento, 116, 99
[148] Ruffini, R., Bianco, C.L., Chardonnet, P., Fraschetti, F., Xue, S.-S., 2002, ApJ, 581, L19
[149] Ruffini, R., Bianco, C.L., Chardonnet, P., Fraschetti, F., Xue, S.-S., 2003a, Int. Journ. Mod. Phys. D, to appear
[150] Ruffini, R., Bianco, C.L., Chardonnet, P., Fraschetti, F., Xue, S.-S., 2003b, ApJ, submitted to
[151] Ruffini, R., Bianco, C.L., Chardonnet, P., Fraschetti, F., Xue, S.-S., 2003c, in preparation
[152] Ruffini, R., Bianco, C.L., Chardonnet, P., Fraschetti, F., Xue, S.-S., 2003d, in preparation
[153] Ruffini, R., Bianco, C.L., Chardonnet, P., Fraschetti, F., Xue, S.-S., 2003e, A&A, submitted to
[154] Ruffini, R., Bianco, C.L., Chardonnet, P., Fraschetti, F., Xue, S.-S., 2003f, in preparation
[155] Ruffini, R., Bianco, C.L., Chardonnet, P., Fraschetti, F., Xue, S.-S., 2003g, in preparation
[156] Ruffini, R., Vitagliano, L., 2002a, Phys. Lett. B, 545, 233
[157] Ruffini, R., Vitagliano, L., 2003a, Int. Journ. Mod. Phys. D, 12, 121
[158] Ruffini, R., Vitagliano, L., 2003b, in preparation
[159] Ruffini, R., Vitagliano, L., Xue, S.-S., 2003h, in preparation
[160] Ruffini, R., Vitagliano, L., Xue, S.-S., 2003i, in preparation
[161] Sagar, R. et al., 2000, Bull Astron. Soc. India, 28, 15
[162] Salmonson, J.D., Wilson, J.R., Mathews, G.J, 2001, ApJ, 553, 471
[163] Sari, R., 1997, ApJ, 489, L37
[164] Sari, R., 1998, ApJ, 494, L49
[165] Sari, R., Piran, T., 1997, ApJ, 485, 270
[166] Sari, R., Piran, T., Narayan, R., 1998, ApJ, 497, L17
[167] Sari, R., Piran, T., Halpern, J.P., 1999, ApJ, 519, L17
[168] Sari, R., Piran, T., 1999, ApJ, 520, 641
[169] Schaefer, B., 2000, GCN Circ. 517 (http://gcn.gsfc.nasa.gov/gcn/gcn3/517.gcn3)
[170] Schmidt, M., 2001, ApJ, 559, L79
[171] Schweppe, J., et al., 1983, Phys. Rev. Lett., 51, 2261
[172] Schwinger, J., 1951, Phys. Rev., 98, 714
[173] Shemi, A., Piran, T., 1990, ApJ, 365, L55
[174] Shvartsman, V.F., 1097, Soviet Physics JETP, 33, 475
[175] Strong, I.B., in "Neutron Stars, Black Holes and Binary X-Ray Sources", Gursky, H. and Ruffini, R., editors, D. Reidel Publishing Company, 1975
[176] Takeshima, T., Markwardt, C., Marshall, F., Giblin, T., Kippen, R.M., 1999, GCN Circ. 478 (http://gcn.gsfc.nasa.gov/gcn/gcn3/478.gcn3)
[177] Taub, A.H., 1948, Phys. Rev., 74, 328
[178] van Dick, R.S., Schwinberg, P.B., Dehmelt, H.G., 1977, Phys. Rev. Lett., 38, 310
[179] van Paradijs, J., Kouveliotou, C., Wijers, R.A.M.J., 2000, Annu. Rev. Astron. Astrophys., 38, 379
[180] Vietri, M., 1997, ApJ, 478, L9
[181] Vietri, M., Stella, L., 1998, ApJ, 507, L45
[182] Vietri, M., Stella, L., 1999, ApJ, 527, L43
[183] Vietri, M., Perola, C., Piro, L., Stella, L., 1999, MNRAS 308, L29
[184] Watson, D., Reeves, J.N., Osborne, J.P., Tedds, J.A., O'Brien, P.T., Tomas, L., Ehle, M., 2002a, A&A, 395, L41
[185] Watson, D., Reeves, J.N., Osborne, J., O'Brien, P.T., Pounds, K.A., Tedds, J.A., Santos-Lleó, M., Ehle, M., 2002b, A&A, 393, L1
[186] Waxman, E., 1997, ApJ, 491, L19
[187] Wilson, J.R., Mathews, G.J., Marronetti, P., 1996, Phys. Rev. D, 54, 1317
[188] Wilson, J.R., Salmonson, J.D., Mathews, G.J., 1997, in Gamma-Ray Bursts: 4th Huntsville Symposium, ed. C. A. Meegan, R. D. Preece, T. M. Koshut (American Institute of Physics)
[189] Wilson, J.R., Salmonson, J.D., Mathews, G.J., 1998, in 2nd Oak Ridge Symposium on Atomic and Nuclear Astrophysics (IOP Publishing Ltd).
[190] Woosley, S.E., 1993, ApJ, 405, 273
[191] Zaumen, W.T., 1974, Nature, 247, 530

[192] Zel'dovich, Y.B., Popov, V.S., 1972, Sov. Phys. Usp., 14, 673
[193] Zel'dovich, Ya.B. & Rayzer, Yu.R., 1966, *Physics of shock waves and high-temperature hydrodynamic phenomena*, Ed. by Wallace D. Hayes and Ronald F. Probstein, Academic press (New York and London)

15 Appendix 8

TITLE
ASP Conference Series, Vol. **VOLUME***, **YEAR OF PUBLICATION**
NAMES OF EDITORS

The EMBH model in GRB 991216 and GRB 980425

R. Ruffini, C.L. Bianco, P. Chardonnet, F. Fraschetti, S.-S. Xue

ICRA — International Center for Relativistic Astrophysics and Dipartimento di Fisica, Università di Roma "La Sapienza", Piazzale Aldo Moro 5, I-00185 Roma, Italy; ruffini@icra.it, bianco@icra.it, chardon@lapp.in2p3.fr, fraschetti@icra.it, vitagliano@icra.it, xue@icra.it

Abstract. This is a summary of the two talks presented at the Rome GRB meeting by C.L. Bianco and R. Ruffini. It is shown that by respecting the Relative Space-Time Transformation (RSTT) paradigm and the Interpretation of the Burst Structure (IBS) paradigm, important inferences are possible: a) in the new physics occurring in the energy sources of GRBs, b) on the structure of the bursts and c) on the composition of the interstellar matter surrounding the source.

The understanding of new astrophysical phenomena is reached as soon as its energy source has been identified. This has been the case for pulsars (see Hewish et al., 1968) where the rotational energy of the neutron star was identified as the energy source (see e.g. Gold, 1968, 1969). Similarly, in binary X-ray sources the accretion process from a normal companion star in the deep potential well of a neutron star or a black hole has clearly pointed to the gravitational energy of the accreting matter as the basic energy source and consequently all the main features of the light curves of the sources have been clearly understood (Giacconi & Ruffini, 1978). In this spirit, our work in the field of Gamma-Ray Bursts (GRBs) has focused on identifing the energy extraction process from the black hole (Christodoulou & Ruffini, 1971) as the basic energy source for the GRB phenomenon. The distinguishing feature of this approach is a theoretically predicted source energetics all the way up to $1.8 \times 10^{54} \, (M_{BH}/M_{\odot})$ ergs for $3.2 M_{\odot} \leq M_{BH} \leq 7.2 \times 10^{6} M_{\odot}$ (Damour & Ruffini, 1975). In particular, the formation of a "dyadosphere", during the gravitational collapse leading to a black hole endowed with electromagnetic structure (EMBH) has been indicated as the initial boundary conditions of the GRB process (Ruffini, 1998; Preparata et al., 1998). Our model has been referred as "the EMBH model for GRBs", although the EMBH physics only determines the initial boundary conditions of the GRB process by specifying the physical parameters and spatial extension of the neutral electron positron plasma originating the phenomenon.

Traditionally, following the observations of the *Vela* (Strong, 1975) and *CGRO*[1] satellites, GRBs have been characterized by few parameters such as the fluence, the characteristic duration (T_{90} or T_{50}) and the global time averaged

[1] see http://cossc.gsfc.nasa.gov/batse/

spectral distribution (Band et al., 1993). With the observations of *BeppoSAX*[2] and the discovery of the afterglow, and the consequent optical identification, the distance of the GRB source has been determined and consequently the total energetics of the source has been added as a crucial parameter.

The observed energetics of GRBs computed for spherically symmetric explosions do coincide with the ones theoretically predicted in Damour & Ruffini (1975). This fact has convinced us of the necessity to develop in full details the EMBH model. For simplicity, we have considered the vacuum polarization process occurring in an already formed Riessner-Nordström black hole (Ruffini, 1998; Preparata et al., 1998), whose dyadosphere has an energy E_{dya}. It is clear, however, that this is only an approximation to the real dynamical description of the process of gravitational collapse to an EMBH. In order to prepare the background for attacking this extremely complex dynamical process, we have clarified some basic theoretical issues, necessary to implement the description of the fully dynamical process of gravitational collapse to an EMBH (see Ruffini & Vitagliano, 2002, 2003; Cherubini et al., 2002). We have then given the constitutive equations for the five eras in our model. *The Era I*: the e^+e^- pairs plasma, initially at $\gamma = 1$, self propels itself away from the dyadosphere as a sharp pulse (the PEM pulse), reaching Lorentz gamma factor of the order of 100 (Ruffini et al., 1999). *The Era II*: the PEM pulse, still optically thick, engulfs the remnant left over in the process of gravitational collapse of the progenitor star with a drastic reduction of the gamma factor; the mass M_B of this engulfed baryonic material is expressed by the dimensionless parameter $B = M_B c^2/E_{dya}$ (Ruffini et al., 2000). *The Era III*: the newly formed pair-electromagnetic-baryonic (PEMB) pulse, composed of e^+e^- pair and of the electrons and baryons of the engulfed material, self-propels itself outward reaching in some sources Lorentz gamma factors of 10^3–10^4; this era stops when the transparency condition is reached and the emission of the proper-GRB (P-GRB) occurs (Bianco et al., 2001). *The Era IV*: the resulting accelerated baryonic matter (ABM) pulse, ballistically expanding after the transparency condition has been reached, collides at ultrarelativistic velocities with the baryons and electrons of the interstellar matter (ISM) which is assumed to have a average constant number density, giving origin to the afterglow. *The Era V*: this era represents the transition from the ultrarelativistic regime to the relativistic and then to the non relativistic ones (Ruffini et al., 2003a).

Our approach differs in many respect from the ones in the current literature. The major difference consists in the appropriate theoretical description of all the above five eras, as well as in the evaluation of the process of vacuum polarization originating the dyadosphere. The dynamical equations as well as the description of the phenomenon in the laboratory time and the time sequence carried by light signals recorded at the detector have been explicitly integrated (see e.g. Ruffini et al., 2003a, 2003b). In doing so we have also corrected a basic conceptual inadequacy, common to all the current works on GRBs, which led to an improper spacetime parametrization of the GRB phenomenon, preempting all these works from their predictive power: the relation between the photon arrival time at the detector and their emission time in the laboratory frame, expressed in our

[2]see http://www.asdc.asi.it/bepposax/

approach by an integral of a function of the Lorentz gamma factor extended over all the past source worldlines, has been in the current literature expressed as a function of an instantaneous value of the Lorentz gamma factor. This two approaches are conceptually very different and lead to significant qualtitative differences (Ruffini et al., 2003a, 2003b). The description of the inner engine originating the GRBs described has never been addressed in the necessary details in the literature. Only the treatment of the afterglow has been widely considered in the literature by the so-called "fireball model" (see e.g. Mészáros & Rees, 1992, 1993; Rees & Mészáros, 1994; Piran, 1999 and references therein).

However, also in the description of the afterglow, there are major differences between the works in the literature and our approach:
a) Processes of synchrotron radiation and inverse Compton as well as an adiabatic expansion in the source generating the afterglow are usually adopted in the current literature. On the contrary, in our approach: 1) a "fully radiative" condition is systematically adopted in the description of the X-ray and γ-ray emission of the afterglow; 2) the basic microphysical emission process is traced back to the physics of shock waves as considered by Zel'dovich & Rayzer (1966); and 3) a special attention is given to identify such processes in the comoving frame of the shock front generating the observed spectra of the afterglow (see Ruffini et al., 2003c).
b) In the current literature the variation of the gamma Lorentz factor during the afterglow is expressed by a unique power-law of the radial co-ordinate of the source and a similar power-law relation is assumed also between the radial coordinate of the source and the asymptotic observer frame time. Such simple approximations appear to be quite inadequate and do contrast with the almost hundred pages summarizing the needed computations which we have recently presented in four long articles (Ruffini et al., 2002a, 2003a, 2003b, 2003d). In our approach the dynamical equations of the source are integrated self-consistently with the constitutive equations relating the observer frame time to the laboratory time and the boundary conditions are adopted and uniquely determined by each previous era of the GRB source (see e.g. Ruffini et al., 2002b, 2003a, 2003b, 2003c).
c) At variance with the many power-laws for the observed afterglow flux found in the literature, our treatment naturally leads to a "golden value" for the bolometric luminosity power-law index $n = -1.6$.

The fit of the EMBH model to the observed afterglow data fixes the only two free parameters of our theory: the E_{dya} and the B parameter, measuring the remnant mass left over by the gravitational collapse of the progenitor star (Ruffini et al., 2002b, 2003a, 2003b, 2003c).

It is not surprising that such large differences in the theoretical treatment have led to a different interpretation of the GRB phenomenon as well as to the identification of new fundamental physical regimes. The introduction of new interpretative paradigms has been necessary and the theory has been confirmed by the observation to extremely high accuracy.

In particular from the definition of the complete space-time coordinates of the GRB phenomenon as a function of the radial coordinate, the comoving time, the laboratory time, the arrival time and the arrival time at the detector, expressed in Tab. 1 of Ruffini et al. (2002a, 2003a, 2003d), it has been concluded

that in no way a description of a given era is possible in the GRB phenomena without the knowledge of the previous ones. Therefore the afterglow as such cannot be interpreted unless all the previous eras have been correctly computed and estimated. It has also become clear that a great accuracy in the analysis of each era is necessary in order to identify the theoretically predicted features with the observed ones. If this is done, the GRB phenomena presents an extraordinary precise correspondence between the theoretically predicted features and the observations leading to the exploration of totally new physical and astrophysical process with unprecedented accuracy. This has been expressed in the relative space-time transformation (RSTT) paradigm: "the necessary condition in order to interpret the GRB data, given in terms of the arrival time at the detector, is the knowledge of the *entire* worldline of the source from the gravitational collapse. In order to meet this condition, given a proper theoretical description and the correct constitutive equations, it is sufficient to know the energy of the dyadosphere and the mass of the remnant of the progenitor star" (Ruffini et al., 2001a).

Having determined the two independent parameters of the EMBH model, namely E_{dya} and B, by the fit of the afterglow we have introduced a new paradigm for the Interpretation of the Burst Structure: the IBS paradigm (Ruffini et al., 2001b). In it we reconsider the relative roles of the afterglow and the burst in the GRBs by defining in this complex phenomenon two new phases:
1) the *injector phase* starting with the process of gravitational collapse, encompassing the above Eras I, II, III and ending with the emission of the Proper-GRB (P-GRB);
2) the *beam-target phase* encompassing the above Eras IV and V giving rise to the afterglow. In particular in the afterglow three different regimes are present for the average bolometric intensity : one increasing with arrival time, a second one with an Extended Afterglow Peak Emission (E-APE) and finally one decreasing as a function of the arrival time. Only this last one appears to have been considered in the current literature (Ruffini et al., 2001b).

We have applied the EMBH model to GRB 991216 as a prototype. We think that this source will play for GRBs a role similar to the one of NP0532 (the Crab pulsar) in the understanding of the pulsar phenomenon. The GRB 991216 presents clearly the three fundamental aspects: the P-GRB, the E-APE and the late phases of the afterglow (Ruffini et al., 2001a,b). What makes this system so unique are the outstanding data obtained by BATSE in the P-GRB and in the E-APE and concurrently the very high quality ones on the afterglow obtained by R-XTE and Chandra. It is the simultaneous occurrence of these three features which makes this source so attractive and becoming the prototype for GRBs. We have computed the intensity ratio of the afterglow to the P-GRB ($1.45 \cdot 10^{-2}$), and the arrival time of the P-GRB ($8.413 \cdot 10^{-2}$s) as well as the arrival time of the peak of the afterglow (19.87s) (see Fig. 1 and Ruffini et al., 2001b, 2002a, 2003a, 2003d). The fact that the theoretically predicted intensities coincide within a few percent with the observed ones and that the arrival time of the P-GRB and the peak of the afterglow also do coincide within a tenth of millisecond with the observed one can be certainly considered a clear success of the predictive power of the EMBH model.

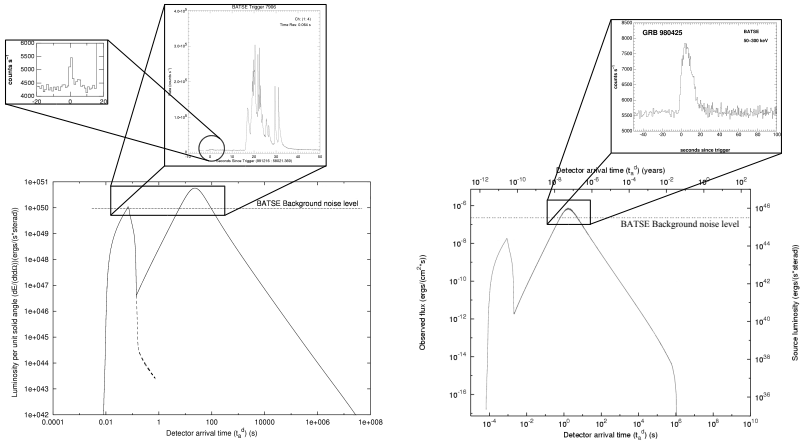

Figure 1. The EMBH theory applied to GRB 991216 (left) and GRB 980425 (right). Note the structure of the P-GRB and the E-APE with respect to the BATSE noise threshold.

As a by-product of this successful analysis, we have reached the following conclusions:
a) The most general GRB is composed by a P-GRB, an E-APE and the rest of the afterglow. The ratio between the P-GRB and the E-APE intensities is a function of the B parameter.
b) In the limit B=0 all the energy is emitted in the P-GRB. These events represent the "short burst" class, for which no afterglows has been observed.
c) The "long bursts" do not exist, they are just part of the afterglow, the E-APEs.

Our model has been also applied to GRB 980425 showing not only the agreement with the observed luminosity but also, in particular, that in both sources there is not significant departure from spherical symmetry (see Fig. 1).

While the aboce analysis of the average bolometric luminosity of GRB was performed in the radial approximation, we have also developed the full non-radial approximation, taking into account all the relativistic corrections for the off-axis emission from the spherically symmetric expansion of the ABM pulse (Ruffini et al., 2002b, 2003b). We have so defined the temporal evolution of the ABM pulse visible area, as well as the equitemporal surfaces (see Fig. 2 and Ruffini et al., 2002b, 2003b).

Having satisfactorily identified the average intensity distribution of the afterglow and the relative position of the P-GRB, in Ruffini et al. (2001c) we have addressed the issue whether the fast temporal variation observed in the so-called long bursts, on time scales as short as fraction of a second (see e.g. Fishman & Meegan, 1995), can indeed be explained as an effect of inhomogeneities in the interstellar medium. Such a possibility was pioneered in the work by Dermer & Mitman (1999), purporting that such a time variability corresponds to a tomographic analysis of the ISM. In order to probe the validity of such an explanation,

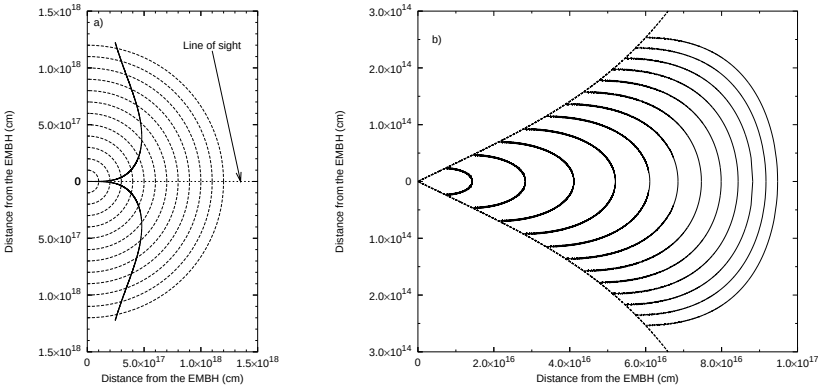

Figure 2. The temporal evolution of the visible area of the ABM pulse external surface (left) and the equitemporal surfaces for selected values of the detector arrival time encompassing the E-APE (right) for the case of GRB 991216. Details in Ruffini et al. (2002b, 2003b, 2003d).

we have first considered the simplified case of the radial approximation (Ruffini et al., 2001c). The aim has been to explain the observed fluctuation in intensity on a fraction of a second as originated from inhomogeneities in ISM, typically of the order of 10^{16} due to apparent "superluminal" behavior of roughly 10^5c. These "superluminal" effects can be derived consistently from the dynamics of the source. After this successful attempt, we have proceeded to the non-radial approximation, taking into account all the relativistic corrections for the off-axis emission from the spherically symmetric expansion of the ABM pulse (Ruffini et al. 2002b, 2003b). We have so defined the temporal evolution of the ABM pulse visible area, as well as the equitemporal surfaces (EQTS, Ruffini et al. 2002b, 2003b). We have then described the inhomogeneities of the ISM by an appropriate density profile (mask) of an ISM cloud. Of course at this stage, for simplicity, only the case of spherically symmetric "spikes" with over-density separated by low-energy regions, has been considered. Each spike has been assumed to have the spatial extension of 10^{15}cm. The cloud average density is $< n_{ism} >= 1\,\mathrm{particle/cm^3}$. The corresponding analysis for GRB 980425 has been presented in Ruffini (2003e).

We can distinguish two different regimes corresponding respectively to $\gamma > 150$ and to $\gamma < 150$. In the E-APE region ($\gamma > 150$) the GRB substructure intensities indeed correlate with the ISM inhomogeneities. In this limited region (see peaks A, B, C) the Lorentz gamma factor of the ABM pulse ranges from $\gamma \sim 304$ to $\gamma \sim 200$. The boundary of the visible region is smaller than the thickness ΔR of the inhomogeneities (see Figs. 2,3 and Ruffini et al., 2002b, 2003b). Under these conditions the adopted spherical symmetry for the density spikes is not only mathematically simpler but also fully justified. The angular spreading is not strong enough to wipe out the signal from the inhomogeneity spike. The observational results reproduced in Fig. 3 present a remarkably

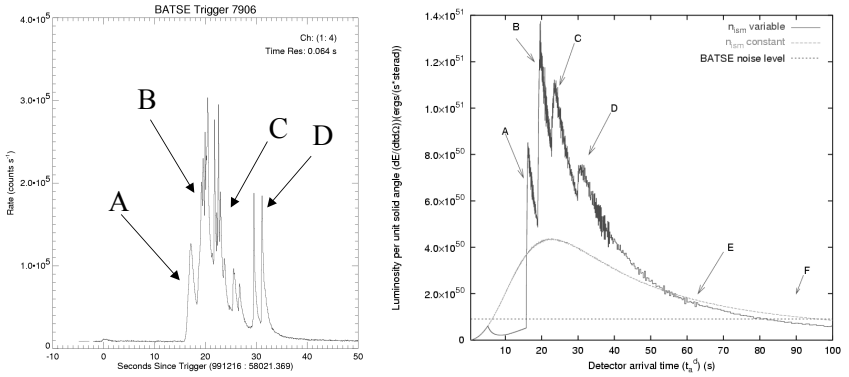

Peak	r (cm)	τ (s)	t (s)	t_a (s)	t_a^d (s)	Δt_a^d (s)	γ	"Superluminal" $v \equiv \frac{r}{t_a^d}$
A	4.50×10^{16}	4.88×10^{3}	1.50×10^{6}	7.90	15.8	0.400	303.8	$9.5 \times 10^{4}c$
B	5.20×10^{16}	5.74×10^{3}	1.73×10^{6}	9.50	19.0	0.622	265.4	$9.1 \times 10^{4}c$
C	5.70×10^{16}	6.54×10^{3}	1.90×10^{6}	11.4	22.9	1.13	200.5	$8.3 \times 10^{4}c$
D	6.20×10^{16}	7.64×10^{3}	2.07×10^{6}	15.0	30.1	5.16	139.9	$6.9 \times 10^{4}c$
E	6.50×10^{16}	9.22×10^{3}	2.17×10^{6}	27.9	55.9	10.2	57.23	$3.9 \times 10^{4}c$
F	6.80×10^{16}	1.10×10^{4}	2.27×10^{6}	43.7	87.4	10.6	56.24	$2.6 \times 10^{4}c$

Figure 3. Details of the fit of the E-APE structure of GRB 991216 in the EMBH theory. Details in Ruffini et al. (2002b, 2003b, 2003d)

improved fit, both in intensity, time scale and general morfology, with respect to the one considered in Ruffini et al. (2001c).

Finally we then conclude:
a) the informations carried by the afterglow, including the E-APE, are relevant for determining the structure of the ISM (Dermer's tomography);
b) the main general relativistic effects are contained in the P-GRB. A new family of space missions are therefore urgently needed;
c) for the first time we are witnessing the energy extraction from black holes.

References

Band, D., et al., 1993, ApJ, 413, 281

Bianco, C.L., Ruffini, R., Xue, S.-S., 2001, A&A, 368, 377

Cherubini, C., Ruffini, R., Vitagliano, L., 2002, Phys.Rev.B, 545, 226

Christodoulou, D., Ruffini, R., 1971, Phys.Rev.D, 4, 3552

Damour, T., Ruffini, R., 1975, Phys.Rev.Lett, 35, 463

Dermer, C.D., Mitman, K.E., 1999, ApJ, 513, L5

Fishman, G., Meegan, C., 1995, ARA&A, 33, 415

Giacconi, R., Ruffini, R. (Eds.), 1978, *Physics and Astrophysics of Neutron Stars and Black Holes*, North Holland, Elsevier

Gold, T., 1968, Nature, 218, 731

Gold, T., 1969, Nature, 221, 27

Hewish, A., Bell, S.J., Pilkington, J.D., Scott, P.F., Collins, R.A., 1968, Nature, 217, 709

Mészáros, P., Rees, M.J., 1992, MNRAS, 257, 29p

Mészáros, P., Rees, M.J., 1993, ApJ, 405, 278

Piran, T., 1999, Phys. Rep, 314, 575

Preparata, G., Ruffini, R., Xue, S.-S., 1998, A&A, 338, L87

Rees, M.J., Mészáros, P., 1994, ApJ, 430, L93

Ruffini, R., 1998, in "Black Holes and High Energy Astrophysics", Proceedings of the 49th Yamada Conference Ed. H. Sato and N. Sugiyama, Universal Ac. Press, Tokyo

Ruffini, R., Bianco, C.L., Chardonnet, P., Fraschetti, F., Xue, S.-S., 2001a, ApJ, 555, L107

Ruffini, R., Bianco, C.L., Chardonnet, P., Fraschetti, F., Xue, S.-S., 2001b, ApJ, 555, L113

Ruffini, R., Bianco, C.L., Chardonnet, P., Fraschetti, F., Xue, S.-S., 2001c, Nuovo Cimento, 116, 99

Ruffini, R., Bianco, C.L., Chardonnet, P., Fraschetti, F., Xue, S.-S., 2002a, A&A, submitted to

Ruffini, R., Bianco, C.L., Chardonnet, P., Fraschetti, F., Xue, S.-S., 2002b, ApJ, 581, L19

Ruffini, R., Bianco, C.L., Chardonnet, P., Fraschetti, F., Xue, S.-S., 2003a, Int. Journ. Mod. Phys. D, 12, 173

Ruffini, R., Bianco, C.L., Chardonnet, P., Fraschetti, F., Xue, S.-S., 2003b, A&A, submitted to

Ruffini, R., Bianco, C.L., Chardonnet, P., Fraschetti, F., Xue, S.-S., 2003c, ApJ, submitted to

Ruffini, R., Bianco, C.L., Chardonnet, P., Fraschetti, F., Xue, S.-S., 2003d, in "Proceedings of the X^{th} Brazilian School of Cosmology and Gravitation", M. Novello, S.E. Perez Bergliaffa, editors, AIP Conference proceedings 668, p. 16

Ruffini R., 2003e, in *Proceedings of the 34th COSPAR Scientific Assembly - Houston, TX, USA, 2002*, Pian, E., Masetti, N., Piro, L., editors, Elsevier, in press.

Ruffini, R., Salmonson, J.D., Wilson, J.R., Xue, S.S., 1999, A&A, 350, 334, A&AS, 138, 511

Ruffini, R., Salmonson, J.D., Wilson, J.R., Xue, S.S., 2000, A&A, 359, 855

Ruffini, R., Vitagliano, L., 2002, Phys. Lett. B, 545, 233

Ruffini, R., Vitagliano, L., 2003, Int. Journ. Mod. Phys. D, 12, 121

Strong, I.B., 1975, in "Neutron Stars, Black Holes and Binary X-Ray Sources", Gursky, H. and Ruffini, R., editors, D. Reidel Publishing Company

Zel'dovich, Ya.B. & Rayzer, Yu.R., 1966, *Physics of shock waves and high-temperature hydrodynamic phenomena*, Ed. by Wallace D. Hayes and Ronald F. Probstein, Academic press (New York and London)

16 Appendix 9

GRB 980425, SN1998BW AND THE EMBH MODEL

R. Ruffini[1], M.G. Bernardini[1], C.L. Bianco[1], P. Chardonnet[2], F. Fraschetti[3], S.-S. Xue[1]

[1] *ICRA - International Centre for Relativistic Astrophysics and Dipartimento di Fisica, Università di Roma "La Sapienza", Piazzale Aldo Moro 5, I-00185 Roma, Italy*
[2] *Université de Savoie, LAPTH - LAPP, BP 110, F-74941 Annecy-le-Vieux Cedex, France*
[3] *Università di Trento, Via Sommarive 14, I-38050 Povo (Trento), Italy.*

ABSTRACT

The EMBH model, previously developed using GRB 991216 as a prototype, is here applied to GRB 980425. We fit the luminosity observed in the 40–700 keV, 2–26 keV and 2–10 keV bands by the BeppoSAX satellite. In addition we present a novel scenario in which the supernova SN1998bw is the outcome of an "induced gravitational collapse" triggered by GRB 980425, in agreement with the GRB-Supernova Time Sequence (GSTS) paradigm (Ruffini et al. 2001c). A further outcome of this astrophysically exceptional sequence of events is the formation of a young neutron star generated by the SN1998bw event. A coordinated observational activity is recommended to further enlighten the underlying scenario of this most unique astrophysical system.

INTRODUCTION

The aim of this talk is to present the application of the EMBH theory, previously successfully applied to GRB 991216 used as a prototype, to the case of GRB 980425 (Pian et al., 2000) and SN1998bw (Galama et al., 1998). This is a particularly important test for the validity of the EMBH theory over a range of energies of 6 orders of magnitude: as we will see, both sources appear to be spherically symmetric and the respective total energies are $E_{tot} \simeq 5 \times 10^{53}$ ergs and $E_{tot} \simeq 10^{48}$ ergs. We recall that the EMBH theory (see Ruffini et al., 2003b) depends only on three parameters, the energy of the dyadosphere E_{dya}, the B parameter and the factor $\mathcal{R}$ describing the interstellar medium (ISM) porosity. The theory, therefore, explains all the observed features of the bolometric intensity variations of the afterglow as well as the spectral properties of the source and, in the specific case of GRB 980425, it also allows to clarify the general astrophysical scenario in which the GRB actually occurs. In this system, in fact, we propose that GRB 980425 has been the trigger of a phenomenon of "induced gravitational collapse" (Ruffini et al., 2001c) originating the supernova explosion and we also witness the birth of a young neutron star out of the supernova event. This extraordinary coincidence of these three astrophysical events represents an unprecedented scenario of fundamental importance in the field of relativistic astrophysics. Using the EMBH theory we shall explore: **a)** the process of black hole formation in the event GRB 980425 (Pian et al., 2000), **b)** the concept of "induced gravitational collapse", introduced in the GRB-Supernova Time Sequence (GSTS) paradigm (Ruffini et al., 2001c), and its link to a very special supernova type in SN1998bw (Galama et al., 1998), and finally **c)** the observation for the first time of the cooling of a hot newly formed neutron star.

The observational situation of this system is quite complex. In addition to the source GRB 980425 and the supernova SN1998bw, two X-ray sources have been found by BeppoSAX in the error box for the location of GRB 980425: a source *S1* and a source *S2* (Pian et al., 2000). Since the nature of the two sources S1 and S2 was not clear, a variety of slopes in the decaying part of the afterglow have been proposed (see Fig. 1). Kulkarni et al. (1998) have proposed to explain both the supernova SN1998bw and the GRB 980425 observations by a new class of GRBs, distinctly different from the cosmological ones, both

originated by a single unusual supernova event. Similarly, Iwamoto et al. (1998) have tried to explain both the supernova event and the GRB with a new kind of supernova with an extremely large explosion energy, larger than 10^{52} ergs, which they identify with the "hypernovae" predicted by Paczyński (1998). In this approach a totally novel concept is introduced: the supernova itself is assumed to originate in the process of gravitational collapse to a black hole of a massive progenitor star ($\sim 40 M_\odot$) with a particularly large angular momentum and strong magnetic field. A large rotational energy of the black hole extracted with a strong magnetic field is called in, by these authors, to explain the successful explosion of this "hypernova" leading both to the GRB and the supernova.

Our approach is drastically different. We first interpret the GRB 980425 within the EMBH theory. This allows the computation of the luminosity, spectra, Lorentz gamma factors, and more generally all the dynamical aspects of the source. Having characterized the features of GRB 980425, we can gradually approach the remaining part of the scenario, disentangling the GRB observations from the supernova ones and from the sources S1 and S2. This leads to a natural time sequence of events and to their autonomous astrophysical characterization.

THE ENERGETICS, DYNAMICAL PARAMETERS AND SPACE-TIME PARAMETRIZATION OF GRB 980425

Our approach has focused on identifying the energy extraction process from the black hole (Christodoulou & Ruffini, 1971) as the basic energy source for the GRB phenomenon. The distinguishing feature is a theoretically predicted source energetics all the way up to $1.8 \times 10^{54} \, (M_{BH}/M_\odot)$ ergs for $3.2 M_\odot \leq M_{BH} \leq 7.2 \times 10^6 M_\odot$ (Damour & Ruffini, 1975). In particular, the formation of a "dyadosphere", during the gravitational collapse leading to a black hole endowed with electromagnetic structure (EMBH) has been indicated as the initial boundary conditions of the GRB process (Ruffini, 1998; Preparata et al., 1998). Our model has been referred as "the EMBH model", although the EMBH physics only determines the initial boundary conditions of the GRB process by specifying the physical parameters and spatial extension of the neutral electron positron plasma originating the phenomenon created in the dyadosphere. The creation of this plasma is due to the vacuum polarization process occurring in a supercritical field by the Heisenberg-Euler-Schwinger process (see Heisenberg & Euler, 1935; Schwinger, 1951; Damour & Ruffini, 1975; Preparata et al., 1998).

Traditionally, following the observations of the *Vela* (Strong, 1975) and *CGRO*[1] satellites, GRBs have been characterized by few parameters such as the fluence, the characteristic duration (T_{90} or T_{50}) and the global time averaged spectral distribution (Band et al., 1993). With the observations of *BeppoSAX*[2] and the discovery of the afterglow, and the consequent optical identification, the distance of the GRB source has been determined and consequently the total energetics of the source has been added as a crucial parameter.

The observed energetics of GRBs, computed for spherically symmetric explosions, do coincide with the ones theoretically predicted in Damour & Ruffini (1975). This has been the major reason which has motivated us to reconsider and develop in full details the EMBH model. For simplicity, we have considered the vacuum polarization process occurring in an already formed Reissner-Nordström black hole (Ruffini, 1998; Preparata et al., 1998), whose dyadosphere has an energy E_{dya}. It is clear, however, that this is only an approximation to the real dynamical description of the process of gravitational collapse to an EMBH. In order to prepare the background for attacking this extremely complex dynamical process, we have clarified some basic theoretical issues, necessary to implement the description of the fully dynamical process of gravitational collapse to an EMBH (see Ruffini & Vitagliano, 2002,2003; Cherubini et al., 2002).

We have then given the constitutive equations for the five eras in the EMBH model (see for details Ruffini et al., 2003a and references therein). *The Era I*: the e^+e^- pairs plasma, initially at $\gamma = 1$, self propels itself away from the dyadosphere as a sharp pulse (the PEM pulse), reaching Lorentz gamma factor of the order of 100 (Ruffini et al., 1999). *The Era II*: the PEM pulse, still optically thick, engulfs the remnant left over in the process of gravitational collapse of the progenitor star with a drastic reduction of the gamma factor; the mass M_B of this engulfed baryonic material is expressed by the dimensionless parameter $B = M_B c^2/E_{dya}$ (Ruffini et al., 2000). *The Era III*: the newly formed pair-electromagnetic-baryonic (PEMB) pulse, composed

[1] see http://cossc.gsfc.nasa.gov/batse/
[2] see http://www.asdc.asi.it/bepposax/

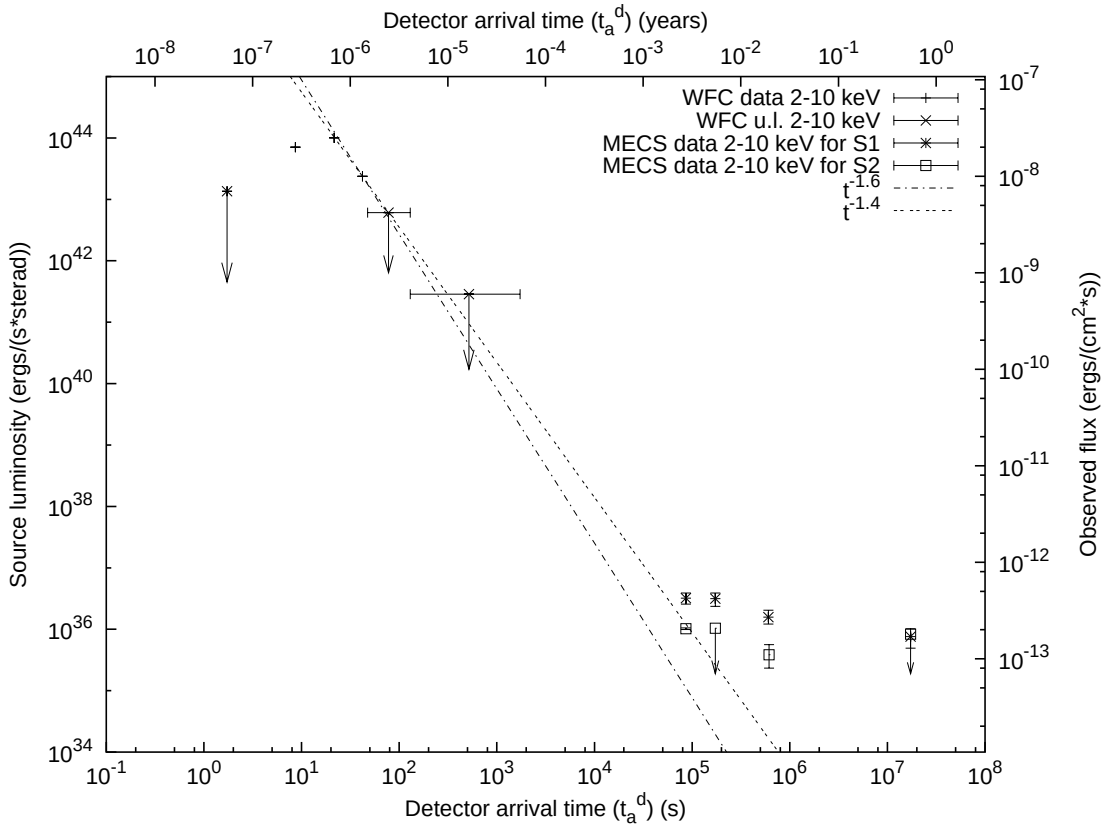

Fig. 1. The BeppoSAX MECS light curves in the 2-10 keV band of the X-ray sources S1 and S2 from Pian et al. (2000) detected in the GRB 980425 fields are shown. The WFC early measurement and 3σ upper limits in the same band are also shown. The dotted lines represent the power laws of indexes $\simeq 1.4$ and $\simeq 1.6$ connecting the last WFC measurement and the first and last of the first 5 MECS points of S2 which are in this picture replaced by the first point that has been obtained by integrating and averaging the flux in shorter time interval, as in Pian et al. (2000). In the vertical axis is reported (left) the luminosity of the source and (right) the observed flux as a function of the arrival time at the detector in seconds (bottom) and in years (top).

of e^+e^- pair and of the electrons and baryons of the engulfed material, self-propels itself outward reaching in some sources Lorentz gamma factors of 10^3–10^4; this era stops when the transparency condition is reached and the emission of the proper-GRB (P-GRB) occurs (Bianco et al., 2001). *The Era IV*: the resulting accelerated baryonic matter (ABM) pulse, ballistically expanding after the transparency condition has been reached, collides at ultrarelativistic velocities with the baryons and electrons of the interstellar matter (ISM) which is assumed to have a average constant number density, giving origin to the afterglow. *The Era V*: this era represents the transition from the ultrarelativistic regime to the relativistic and then to the non relativistic ones (see Ruffini et al., 2003a,2003b and references therein).

The EMBH model differs in many respects from the models in the current literature. The major difference consists in the following points:
a) The appropriate theoretical description of all the above mentioned five eras is implemented, as well as the evaluation of the process of vacuum polarization originating the dyadosphere. The description of the inner engine originating the GRBs has never been addressed in the necessary details in the literature;
b) The dynamical equations as well as the description of the phenomenon in the laboratory time and the time sequence carried by light signals recorded at the detector have been explicitly integrated (see e.g. Ruffini et al., 2003a, 2003b). In doing so we have also corrected a basic conceptual inadequacy, common to all the current works on GRBs, which led to an improper spacetime parametrization of the GRB phenomenon, preempting all these works from their predictive power: the relation between the photon arrival time at the detector and their emission time in the laboratory frame, expressed in our approach by an integral of a function of the Lorentz gamma factor extended over all the past source worldlines, has been in the current literature expressed as a function of an instantaneous value of the Lorentz gamma factor. These two approaches are conceptually very different and lead to significant qualitative differences (Ruffini et al., 2003a, 2003b and references therein).
c) The treatment of the afterglow has been widely considered in the literature by the so-called "fireball model" (see e.g. Mészáros & Rees, 1992, 1993; Rees & Mészáros, 1994; Piran, 1999 and references therein). However, also in the description of the afterglow, there are major differences between the works in the literature and our approach (Ruffini et al., 2003b).

The equations of motion in our model depend only on two free parameters: the total energy E_{tot}, which coincides with the dyadosphere energy E_{dya}, and the amount M_B of baryonic matter left over from the gravitational collapse of the progenitor star, which is determined by the dimensionless parameter $B = M_B c^2/E_{dya}$. The best fit of GRB 980425 is reproduced in Tab. 1. It correspond to $E_{dya} = 1.1 \times 10^{48}$ ergs, $B = 7\times10^{-3}$ and the ISM average density is found to be $\langle n_{ism}\rangle = 0.02\text{particle/cm}^3$. The plasma temperature and the total number of pairs in the dyadosphere are respectively $T = 1.028\,\text{MeV}$ and $N_{e^\pm} = 5.3274 \times 10^{53}$.

THE GRB 980425 LUMINOSITY IN SELECTED ENERGY BANDS PREDICTED BY THE EMBH MODEL

Recently, within the EMBH model, we have developed an attempt to theoretically derive the GRB spectra out of first principles as well as the GRB luminosity in fixed energy bands (Ruffini et al. 2003c). We have adopted three basic assumptions: **a)** the resulting radiation as viewed in the comoving frame during the afterglow phase has a thermal spectrum and **b)** the ISM swept up by the front of the shock wave, with a Lorentz gamma factor between 300 and 2, is responsible for this thermal emission. **c)** We also adopt, like in our previous papers (Ruffini et al., 2001a,2001b,2002,2003b), that the expansion occurs with spherical symmetry. This three assumptions are different from the ones adopted in the GRB literature, in which the afterglow emission is believed to originate from synchrotron emission in the production of a shock or reverse shock generated when the assumed jet-like ejecta encounter the external medium (see e.g. Giblin et al., 2002 and references therein).

In the EMBH model the structure of the shock is determined by mass, momentum and energy conservation: the constancy of the specific enthalpy, which is a standard condition in shock rest frames (Zel'dovich & Rayzer, 1966) and have been used in our derivation (Ruffini et al., 2003b). The only free parameter of our model is the size of the "effective emitting area" in the shock wave front: A_{eff}. Since the determination of this free parameter is performed here by empirically fitting the observational data, we avoid ambiguities due to the absence of relevant theoretical and laboratory results on relativistic shocks for Lorentz factor

Table 1. Gamma factor for selected events and their space-time coordinates: r is the radial coordinate in the laboratory frame, t is the laboratory time and t_a^d is the photon arrival time at the detector. The points $1, 2, 3, 4$ mark the beginning of first four "eras" (see Ruffini et al., 2003a,2003b) until the transparency point (point 4). The points A, B, C correspond to three events respectively before, during and after the peak of the E-APE. The points D, E, F, G, H, I, J are taken in the decaying part of the afterglow. The last column shows how the apparent motion in the radial coordinate, evaluated in the arrival time at the detector, leads to an enormous apparent "superluminal" behaviour. This illustrates the impossibility of using such a classical estimate in regimes of high gamma Lorentz factor.

Point	$r(cm)$	$t(s)$	$t_a^d(s)$	γ	"Superluminal" $v \equiv \frac{r}{t_a^d}$
1	8.79×10^6	2.60×10^{-5}	2.03×10^{-5}	1.027	$14c$
2	2.89×10^8	9.56×10^{-3}	2.13×10^{-4}	28.423	$47c$
3	3.45×10^8	1.14×10^{-2}	2.19×10^{-4}	8.647	$53c$
4	4.31×10^{11}	14.4	7.65×10^{-4}	138.863	$1.9 \times 10^4 c$
A	4.01×10^{15}	1.34×10^5	3.65	129.819	$3.7 \times 10^4 c$
B	6.00×10^{15}	2.00×10^5	5.87	115.309	$3.4 \times 10^4 c$
C	6.50×10^{15}	2.17×10^5	6.98	84.704	$3.1 \times 10^4 c$
D	1.02×10^{16}	3.40×10^5	19.2	53.982	$1.8 \times 10^4 c$
E	1.07×10^{16}	3.57×10^5	98.5	6.510	$3.6 \times 10^3 c$
F	1.12×10^{16}	3.74×10^5	3.00×10^2	6.469	$1.2 \times 10^3 c$
G	1.17×10^{16}	3.90×10^5	5.00×10^2	6.426	$7.8 \times 10^2 c$
H	1.29×10^{16}	4.30×10^5	1.00×10^3	6.309	$4.3 \times 10^2 c$
I	2.67×10^{16}	8.99×10^5	1.00×10^4	4.101	$89c$
J	4.31×10^{16}	1.49×10^6	5.00×10^4	2.097	$29c$

$\gamma \sim 300$.

The temperature T of the black body in the comoving frame is then

$$T = \left(\frac{\Delta E_{\rm int}}{16\pi r^2 \gamma \Delta t \sigma \mathcal{R}} \right)^{1/4}, \tag{1}$$

where

$$\mathcal{R} = \frac{A_{eff}}{A_{abm}} \tag{2}$$

is the ratio between the "effective emitting area" and the ABM pulse surface A_{abm}, σ is the Stefan-Boltzmann constant and $\Delta E_{\rm int}$ is the proper internal energy developed in the collision between the ABM pulse and the ISM (see Ruffini et al., 2003b,2003c). The ratio $\mathcal{R}$, which is a priori a function that varies as the system evolves, is evaluated at every given value of the laboratory time t.

All the subsequent steps are now uniquely determined by the equations of motion of the system. The basic tool in this calculation involves the definition of the EQuiTemporal Surfaces (EQTS) for the relativistic expanding ABM pulse as seen by an asymptotic observer. The key to determining such EQTS (see Fig. 1 in Ruffini et al., 2002) is the relation between the time t in the laboratory frame at which a photon is emitted from the ABM pulse external surface and the arrival time t_a^d at which it reaches the detector. We have instead adopted the equations (see Ruffini et al., 2002,2003b):

$$\begin{aligned} t_a^d &= (1+z)\left(t - \frac{r\,(t)}{c}\cos\vartheta + \frac{r_0}{c}\right) = (1+z)\left(t - \frac{\int_0^t v\,(t')\,dt' + r_0}{c}\cos\vartheta + \frac{r_0}{c}\right) \\ &= (1+z)\left(t - \cos\vartheta \int_0^t \sqrt{1 - \frac{1}{\gamma^2\,(t')}}\,dt' + \frac{r_0}{c}\,(1-\cos\vartheta)\right), \end{aligned} \tag{3}$$

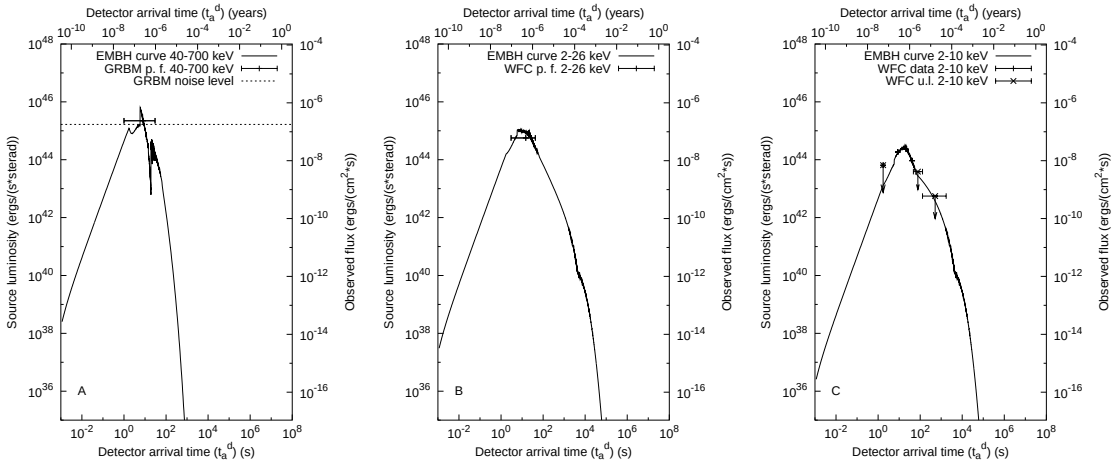

Fig. 2. **a)** The light curve computed within the EMBH model in γ-ray (40-700 keV) is represented; the horizontal bar represents the peak flux in the 40–700 keV band measured by the GRBM (Frontera et al., 2000). The horizontal dotted line represents the noise level of the GRBM detector. **b)** The light curve computed within the EMBH model in hard X-rays in the 2–26 keV band with the peak flux and time duration from WFC (Frontera et al., 2000). **c)** The light curve computed within the EMBH model in hard X-rays in the 2–10 keV band with the experimental data in the same band from WFC (Pian et al., 2000)

where z is the cosmological redshift of the source, $r_0 \equiv r\,(t=0)$ and ϑ is the angle subtended by the emission point of the photon on the ABM pulse external surface, having defined $\vartheta = 0$ along the line of sight. For such a relation, different approximations exist in the literature (see e.g. Fenimore et al., 1996; Sari, 1997,1998, Rees & Mészáros, 1998; Fenimore et al., 1999; Granot et al., 1999 and see also the reviews by Piran, 1999; Mészáros, 2002). There are both quantitative and qualitative important differences in the use of Eq.(3) instead of the ones usually adopted in the literature (Ruffini et al., 2003b). It is a matter of fact that only the use of the EQTS defined by Eq.(3) allows to fit the observational data and that even a very minor departure from it leads to unacceptable results. It is also important to recall that this inadequacy in the current literature between in the relation between the arrival time and the laboratory time has affected also all the estimates of the power-law slopes in the afterglow, preempting all current theoretical considerations in the literature of their predictive power. All the considerations about beaming in GRBs existing in the current literature have to be reformulated on the ground of the proper theoretical treatment and of Eq.(3) (see Ruffini et al., 2003b). Having so determined the EQTS we have been able to evaluate the source luminosity in a given energy band, in agreement with the above mentioned new assumptions (Ruffini et al., 2003c).

We can now proceed to the best fit of the GRB 980425 observed data. The best fit of the observed luminosity in selected energy bands has been obtained for the above mentioned values of the parameters E_{dya}, B and for $\mathcal{R} = 6.63 \times 10^{-15}$. The results are given in Fig. 2 where the luminosity is computed as a function of the arrival time for three selected energy bands.

We can then conclude:

1. The best fit is obtainable under almost perfect spherical symmetry. This has been proven as a result of an analysis of unprecedented redundancy: the luminosity curves are obtained from an integration over almost 10^7 different paths, relating the observer to the EQTS. This procedure tests, to a very high level of accuracy, any departure from spherical symmetry as well as any departure from the computed equations of motion of the source (Ruffini et al., 2003b). This same circumstance was encountered in GRB 991216 (Ruffini et al., 2003b).

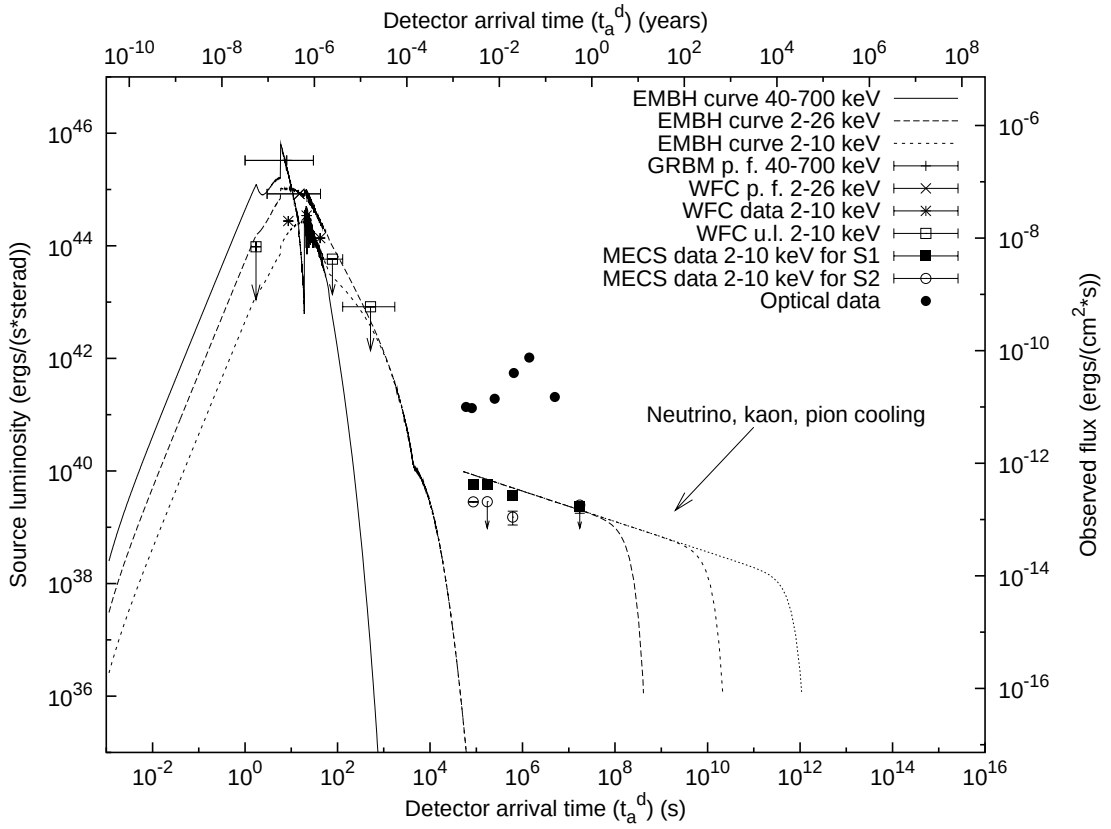

Fig. 3. The light curves in selected bands are reported as well as the MECS light curves in the 2-10 keV band of S1 and S2 (Pian et al. 2000) as well as the optical data (Iwamoto, 1999). Here are also reported theoretical models of neutron star cooling (Canuto, 1978).

2. Each luminosity curve as a function of the arrival time presents complex behavior, which could be erroneously interpreted as evidence for breaks in the power-law indexes leading to erroneous inferences on the possible existence of jets (Ruffini et al., 2003c).

3. Although each luminosity curve presents some special features, the bolometric luminosity has a very clear and simple power-law behavior with the "golden value" index $n = -1.6$ (Ruffini et al., 2003b).

THE NEW ASTROPHYSICAL SCENARIO AND THE NEWLY BORN NEUTRON STAR

In Fig. 3 the luminosities in the three bands are represented together with the optical data of SN1998bw (black dots), the source S1 (black squares) and the source S2 (open circles). It is then clear that GRB 980425 is separated both from the supernova data and from the sources S1 and S2.

While the occurrence of the supernova in relation to the GRB has already been discussed with the GRB-Supernova Time Sequence (GSTS) paradigm (Ruffini et al. 2001c), we like to address here a different fundamental issue: the possibility of observing the birth of a newly formed neutron star out of the supernova event, which in turn has been triggered by the GRB 980425.

In the early days of neutron star physics it was clearly shown by Gamow & Schoenberg (1940,1941) that the URCA processes are at the very heart of the supernova explosions. The neutrino-antineutrino emission described in the URCA process is the essential cooling mechanism necessary for the occurrence of

the process of gravitational collapse of the imploding core. Since then, it has become clear that the newly formed neutron star can be still significantly hot and in its early stages will be associated to three major radiating processes (Tsuruta, 1964,1979,2002; Canuto, 1978): **a)** the thermal radiation from the surface, **b)** the radiation due to neutrino, kaon, pion cooling, and **c)** the possible influence in both these processes of the superfluid nature of the supra-nuclear density neutron gas. Qualitative representative curves for these cooling processes, which are still today very undetermined due to the lack of observational data, are shown in Fig. 3.

It is of paramount importance to follow the further time history of the two sources S1 and S2. If, as we propose, S2 is a background source, its flux should be practically constant in time and this source has nothing to do with the GRB 980425 / SN1998bw system. If S1 is indeed the cooling radiation emitted by the newly born neutron star, it should be possible to notice a very drastic behavior in its luminosity as qualitatively expresses in Fig. 3.

CONCLUSIONS

It is particularly attractive, in conclusion, to emphasize some of the analogies and the differences between the case of GRB 991216 and the one of GRB 980425:

1. In both these sources a GRB and, independently, a supernova event are present. In the case of GRB 991216 the inferences of the supernova can be obtained only on the ground of the emission of iron lines (Piro et al., 2000; Ruffini et al., 2001c). In the present case of GRB 98025 we have a very fortunate circumstance: the GRB source is much weaker and is much closer to us ($z = 1.0$ for GRB 991216 and $z = 0.00835$ for GRB 980425). This situation is particularly important for obtaining detailed data on the supernova and on the possible occurrence of a newly born neutron star. This occurrence could not be observed in GRB 991216 due to the very large distance and to the overwhelming X-ray luminosity of the afterglow (see Ruffini et al., 2003b).

2. The energetics of GRB 991216 is $E_{dya} = 4.83 \times 10^{53}$ ergs, while the one of GRB 980425 is $E_{dya} = 1.1 \times 10^{48}$ ergs. It is very impressive that the EMBH model applies over a range of more than 6 orders of magnitude, giving important inferences on the source as well as on the structure of the ISM surrounding the source. It is significant that in both sources the condition of spherical symmetry appears to be strongly implemented and this fact is a very clear discriminant among all possible sources of energy for GRBs.

3. The main difference between GRB 991216 and GRB 980425 is then traced back, within the EMBH model, to the different parameters occurring in the dyadosphere and to the nature of the "effective" Reissner-Nordström geometry which we have used as a reliable estimate for the dynamical processes of gravitational collapse leading to the formation of the EMBH. For GRB 991216 we have a ratio between the electromagnetic energy and the total mass of the imploding core, described by the parameter Q/M, given by $Q/M = 0.23$ while for GRB 980425 we have $Q/M = 6.5 \times 10^{-4}$. In both cases a reasonable mass of the black hole is $M_{BH} \simeq 10 M_{\odot}$ (Ruffini et al., 2003b).

An dedicated observational campaign, both with XMM and Chandra, to follow the cooling of the newly formed neutron star is needed in order to gain for the first time information on this extremely important astrophysical process.

REFERENCES

Band, D., et al., BATSE observations of Gamma-Ray Bursts spectra. I. Spectral diversity, *Astroph. Journ.*, **413**, 281, 1993

Bianco, C.L., R. Ruffini, and S.-S. Xue, The elementary spike produced by a pure e^+e^- pair-electromagnetic pulse from a Black Hole: The PEM Pulse, *Astron. & Astroph.*, **368**, 377–390, 2001

Canuto, V., Neutron Stars, Physics and astrophysics of neutron stars and black holes - Proceedings of the International School of Physics "Enrico Fermi", ed. R. Giacconi and R. Ruffini, pp. 448-527, Bologna, Società Italiana di Fisica; Amsterdam, North Holland Publishing Co., 1978

Cherubini, C., R. Ruffini, and L. Vitagliano, On the electromagnetic field of a charged collapsing spherical shell in general relativity, *Phys. Lett. B*, **545**, 226–232, 2002

Christodoulou, D., and R. Ruffini, Reversible transformations of a charged black hole, *Phys. Rev. D*, **4**, 3552, 1971

Damour, T., and R. Ruffini, Quantum electrodynamical effects in Kerr-Newmann geometries, *Phys. Rev. Lett.*, **35**, 463, 1975

Fenimore, E.E., C.D. Madras, and S. Nayakshin, Expanding Relativistic Shells and Gamma-Ray Burst Temporal Structure, *Astroph. Journ.*, **473**, 998, 1996

Fenimore, E.E., C. Cooper, E. Ramirez-Ruiz, M.C. Sumner, A. Yoshida, and M. Namiki, Gamma-Ray Bursts and Relativistic Shells: The Surface Filling Factor, *Astroph. Journ.*, **512**, 683, 1999

Frontera, F., et al., Prompt and delayed emission properties of Gamma-Ray Bursts observed with BeppoSAX, *Astroph. Journ. Suppl. Ser.*, **127**, 59–78, 2000

Galama, T.J., et al., An unusual supernova in the error box of the γ-ray burst of 25 April 1998, *Nature*, **395**, 670–672, 1998

Gamow, G., and M. Schoenberg, The Possible Role of Neutrinos in Stellar Evolution, *Phys. Rev.*, **58**, 1117, 1940

Gamow, G., and M. Schoenberg, Neutrino theory of stellar collapse, *Phys. Rev.*, **59**, 539–547, 1941

Giblin, T.W., et al., Extended Power-Law Decays in BATSE Gamma-Ray Bursts: Signatures of External Shocks?, *Astroph. Journ.*, **570**, 573, 2002

Granot, J., T. Piran, and R. Sari, Images and Spectra from the Interior of a Relativistic Fireball, *Astroph. Journ.*, **513**, 679, 1999

Heisenberg, W., and H. Euler, Folgerungen aus der Diracschen Theorie des Positrons, *Zeits. fur Phys.*, **98**, 714–732, 1935

Iwamoto et al., A hypernova model for the supernova associated with the gamma-ray burst of 25 April 1998, *Nature*, **395**, 672, 1998

Iwamoto K., On the radio-to-X-ray light curves of SN 1998bw and GRB 980425, *Astroph. Journ.*, **512**, L47–L50, 1999

Kulkarni, et al., Radio emission from the unusual supernova 1998bw and its association with the γ-ray burst of 15 April 1998, *Nature*, **395**, 663–669, 1998

Mészáros, P., and M. Rees, High-entropy fireballs and jets in gamma-ray burst sources, *MNRAS*, **257**, 29p, 1992

Mészáros, P., and M. Rees, Relativistic fireballs and their impact on external matter - Models for cosmological gamma-ray bursts, *Astroph. Journ.*, **405**, 278, 1993

Paczyński, B., Are Gamma-Ray Bursts in star forming regions?, *Astroph. Journ.*, **494**, L45–L48, 1998

Pian, E., et al., BeppoSAX observations of GRB 980425: detection of the prompt event and monitoring of the error box, *Astroph. Journ.*, **536**, 778–787, 2000

Piran, T., Gamma-ray bursts and the fireball model, *Phys. Rep.*, **314**, 575, 1999

Piro, L., et al., Observation of X-ray lines from a gamma-ray burst (GRB991216): evidence of moving ejecta from the progenitor, *Science*, **290**, 955, 2000

Preparata, G., R. Ruffini, and S.-S. Xue, The dyadosphere of black holes and Gamma-Ray Bursts, *Astron. & Astroph.*, **338**, L87, 1998

Rees, M., and P. Mészáros, Unsteady outflow models for cosmological gamma-ray bursts, *Astroph. Journ.*, **430**, L93, 1994

Rees, M.J., and P. Mészáros, Refreshed Shocks and Afterglow Longevity in Gamma-Ray Bursts, *Astroph. Journ.*, **496**, L1, 1998

Ruffini, R., On the dyadosphere of black holes, in Black Holes and High Energy Astrophysics, Proceedings of the 49th Yamada Conference, ed. H. Sato and N. Sugiyama, Universal Ac. Press, Tokyo, 1998

Ruffini, R., J.D. Salmonson, J.R. Wilson, and S.-S. Xue, On the Pair Electromagnetic Pulse of a Black Hole with Electromagnetic Structure, *Astron. & Astroph.*, **350**, 334–343, 1999

Ruffini, R., J.D. Salmonson, J.R. Wilson, and S.-S. Xue, On the pair-electromagnetic pulse from an electromagnetic Black Hole surrounded by a Baryonic Remnant, *Astron. & Astroph.*, **359**, 855–864, 2000

Ruffini, R., C.L. Bianco, P. Chardonnet, F. Fraschetti, and S.-S. Xue, Relative space-time transformations in GRBs, *Astroph. Journ.*, **555**, L107–L111, 2001a

Ruffini, R., C.L. Bianco, P. Chardonnet, F. Fraschetti, and S.-S. Xue, On the interpretation of the burst

structure of GRBs, *Astroph. Journ.*, **555**, L113–L116, 2001b

Ruffini, R., C.L. Bianco, P. Chardonnet, F. Fraschetti, and S.-S. Xue, On a possible GRB-supernova time sequence, *Astroph. Journ.*, **555**, L117–L120, 2001c

Ruffini, R., C.L. Bianco, P. Chardonnet, F. Fraschetti, and S.-S. Xue, On the structures in the afterglow peak emission of gamma ray bursts, *Astroph. Journ.*, **581**, L19–L22, 2002

Ruffini, R., C.L. Bianco, P. Chardonnet, F. Fraschetti, and S.-S. Xue, On the structure of the burst and afterglow of Gamma-Ray Bursts I: the radial approximation, *Int. Journ. Mod. Phys. D*, **12**, 173–270, 2003a

Ruffini, R., C.L. Bianco, P. Chardonnet, F. Fraschetti, L. Vitagliano, and S.-S. Xue, New perspectives in physics and astrophysics from the theoretical understanding of Gamma-Ray Bursts, in Proceedings of the X^{th} Brazilian School of Cosmology and Gravitation, ed. M. Novello and S.E. Perez Bergliaffa, pp. 16–108, AIP Conference Proceedings **668**, 2003b

Ruffini, R., C.L. Bianco, P. Chardonnet, F. Fraschetti, V. Gurzadyan, and S.-S. Xue, On the instantaneous spectrum of gamma ray bursts, *Astroph. Journ.*, submitted to, 2003c

Ruffini, R., and L. Vitagliano, Irreducible mass and energetics of an electromagnetic black hole, *Phys. Lett. B*, **545**, 233–237, 2002

Ruffini, R., and L. Vitagliano, Energy Extraction From Gravitational Collapse to Static Black Holes, *Int. Journ. Mod. Phys. D*, **12**, 121–128, 2003

Sari, R., Hydrodynamics of Gamma-Ray Burst Afterglow, *Astroph. Journ.*, **489**, L37, 1997

Sari, R., The Observed Size and Shape of Gamma-Ray Burst Afterglow, *Astroph. Journ.*, **494**, L49, 1998

Schwinger, J., On Gauge Invariance and Vacuum Polarization, *Phys. Rev.*, **82**, 664–679, 1951

Strong, I.B., Cosmic Gamma-Ray Bursts, in Neutron Stars, Black Holes and Binary X-Ray Sources, ed. H. Gursky and R. Ruffini, pp. 47–58, D. Reidel Publishing Company, 1975

Tsuruta, S., Ph.D. Thesis, Columbia University, 1964

Tsuruta, S., Thermal properties and detectability of neutron stars I - cooling and heating of neutron stars, *Phys. Rep.*, **56**, 237–278, 1979

Tsuruta, S., M.A. Teter, T. Takatsuka, T. Tatsumi, and R. Tamagaki, Confronting Neutron stars cooling with new observations, *Astroph. Journ*, **571**, L143–L146, 2002

Zel'dovich, Ya.B., Yu.P. Rayzer, Physics of shock waves and high-temperature hydrodynamic phenomena, ed. W.D. Hayes and R.F. Probstein, Academic press, New York and London, 1966

17 Appendix 10

International Journal of Modern Physics D
Vol. 13, No. 5 (2004) 843–851

World Scientific
www.worldscientific.com

ON THE INSTANTANEOUS SPECTRUM OF GAMMA-RAY BURSTS

REMO RUFFINI, CARLO LUCIANO BIANCO and SHE-SHENG XUE

ICRA — International Center for Relativistic Astrophysics and Dipartimento di Fisica, Università di Roma "La Sapienza", Piazzale Aldo Moro 5, I-00185 Roma, Italy

PASCAL CHARDONNET

ICRA — International Center for Relativistic Astrophysics and Université de Savoie, LAPTH — LAPP, BP 110, F74941 Annecy-le-Vieux Cedex, France

FEDERICO FRASCHETTI

ICRA — International Center for Relativistic Astrophysics and Università di Trento, Via Sommarive 14, I-38050 Povo (Trento), Italy

VAHE GURZADYAN

ICRA — International Center for Relativistic Astrophysics and Yerevan Physics Institute, Alikhanian Brothers Street 2, 375036, Yerevan-36, Armenia

Received 17 April 2004
Communicated by L. Z. Fang

A theoretical attempt to identify the physical process responsible for the afterglow emission of Gamma-Ray Bursts (GRBs) is presented, leading to the occurrence of thermal emission in the comoving frame of the shock wave which gives rise to the bursts. The determination of the luminosities and spectra involves integration over an infinite number of Planckian spectra, weighted by appropriate relativistic transformations, each one corresponding to a different viewing angle in the past light cone of the observer. The relativistic transformations have been computed using the equations of motion of GRBs within our theory, giving special attention to the determination of the equitemporal surfaces. The only free parameter of the present theory is the "effective emitting area" in the shock wave front. A self-consistent model for the observed hard-to-soft transition in GRBs is also presented. When applied to GRB 991216 a precise fit ($\chi^2 \simeq 1.078$) of the observed luminosity in the 2–10 keV band is obtained. Similarly, detailed estimates of the observed luminosity in the 50–300 keV and in the 10–50 keV bands are obtained.

Keywords: Black hole physics; gamma rays; gamma rays bursts; burst observations; radiation mechanisms; thermal mechanisms.

1. Introduction

Gamma-Ray Bursts (GRBs), following the observations by the BATSE instrument,[1] have been characterized by a few global parameters (see e.g. Ref. 2) such as the

fluence, the characteristic duration (T_{90} or T_{50}), and the global spectral distribution, given e.g. by the Band relation.[3] After the discovery of the afterglow,[4] two additional important parameters have been added: the power-law indexes of the afterglow and the source luminosity.

It has become clear that a variety of different eras are present in the GRB data and that GRBs quite possibly have the most extreme time-variation of any phenomena in nature (see e.g. Ref. 5 and references therein). We present here an attempt to derive from first principles the instantaneous GRB luminosity in selected energy bands and the GRB spectra. We use GRB 991216 as the prototype (see Ref. 6) since this source offers a superb set of data by BATSE in the 50–300 keV band (see BATSE Rapid Burst Response)[7] and by R-XTE and Chandra in the 2–10 keV band (see Refs. 8 and 9) to be compared to the theoretically predicted ones in the 2–300 keV range. We also give physical reasons for the often mentioned hard-to-soft transition observed in the majority of GRBs (see e.g. Refs. 10–13).

2. The Model

The complete dynamics of GRB 991216 has been computed (see Ref. 5). The initial conditions we adopted for this source at $t = 10^{-21}$ s ~ 0 s are a spherical shell of $e^+ - e^-$-photon neutral plasma lying between the radii $r_0 = 6.03 \times 10^6$ cm and $r_1 = 2.35 \times 10^8$ cm: the temperature of such a plasma is 2.2 MeV, the total energy $E_{\rm tot} = 4.83 \times 10^{53}$ erg and the total number of pairs $N_{e^+e^-} = 1.99 \times 10^{58}$. These conditions have been derived from vacuum polarization processes occurring in the dyadosphere of an ElectroMagnetic Black Hole (EMBH).[14,15]

The optically thick electron–positron plasma self-propels itself outward reaching ultrarelativistic velocities,[16] then interacts with the remnant of the progenitor star and, by further expansion, becomes optically thin.[17] As the transparency condition is reached, the *Proper*-GRB (P-GRB) is emitted with an extremely relativistic shell of Accelerated Baryonic Matter (the ABM pulse, see Ref. 18). It is this ABM pulse which gives origin to the afterglow through its interaction with the ISM, whose average density is assumed to be $\langle n_{\rm ism}\rangle = 1$ particle/cm^3. In such a collision the "fully radiative condition" is implemented (see Ref. 5 for details): the internal energy $\Delta E_{\rm int}$ which results is instantaneously radiated away.

The equations of motion in our model depend only on two free parameters: the total energy $E_{\rm tot}$, which coincides with the dyadosphere energy $E_{\rm dya}$, and the amount M_B of baryonic matter left over from the gravitational collapse of the progenitor star, which is determined by the dimensionless parameter $B = M_B c^2/E_{\rm dya}$. These two parameters have been determined by fitting, with high accuracy, the bolometric intensity and the slope of the afterglow.[18] We have also fit, again with high accuracy, the substructures observed in the E-APE which result from inhomogeneities in the ISM, still maintaining an average density distribution of $\langle n_{\rm ism}\rangle = 1$ particle/cm^3 (Ref. 19).

3. The Newly Assumed Origin of the Afterglow X- and γ-Ray Radiation

Here we adopt three basic assumptions: (a) the resulting radiation as viewed in the comoving frame during the afterglow phase has a thermal spectrum and (b) the ISM swept up by the front of the shock wave, with a Lorentz gamma factor between 300 and 2, is responsible for this thermal emission. We also adopt, like in our previous papers,[5,18–20] that (c) the expansion occurs with spherical symmetry. These three assumptions are different from the ones adopted in the GRB literature, in which the afterglow emission is believed to originate from synchrotron emission in the production of the shock or reverse shock generated when the assumed jet-like ejecta encounter the external medium (see e.g. Ref. 21 and references therein).

The structure of the shock is determined by mass, momentum and energy conservation, i.e. the constancy of the specific enthalpy, which are standard conditions in shock rest frames[22] and have already been used in our derivation.[5] The only additional free parameter of our model is the size of the "effective emitting area" in the shock wave front: $A_{\rm eff}$.

The temperature T of the black body in the co-moving frame is then

$$T = \left(\frac{\Delta E_{\rm int}}{4\pi r^2 \Delta\tau \sigma \mathcal{R}} \right)^{1/4} , \tag{1}$$

where

$$\mathcal{R} = \frac{A_{\rm eff}}{A_{\rm abm}} \tag{2}$$

is the ratio between the "effective emitting area" and the ABM pulse surface $A_{\rm abm}$, $\Delta E_{\rm int}$ is the internal energy developed in the collision with the ISM in a time interval $\Delta\tau$ in the co-moving frame and σ is the Stefan–Boltzmann constant. The ratio $\mathcal{R}$, which is *a priori* a function that varies as the system evolves, is evaluated at every given value of the laboratory time t.

All the subsequent steps are now uniquely determined by the equations of motion of the system. The basic tool in this calculation involves the definition of the EQuiTemporal Surfaces (EQTS) for the relativistic expanding ABM pulse as seen by an asymptotic observer. See Fig. 1 in Ref. 19, and Refs. 23 and 24.

We are now ready to evaluate the source luminosity in a given energy band. The source luminosity at a detector arrival time t_a^d, per unit solid angle $d\Omega$ and in the energy band $[\nu_1, \nu_2]$ is given by:[5]

$$\frac{dE_\gamma^{[\nu_1,\nu_2]}}{dt_a^d d\Omega} = \int_{\rm EQTS} \frac{\Delta\varepsilon}{4\pi}\, v\cos\vartheta \Lambda^{-4} \frac{dt}{dt_a^d} W(\nu_1, \nu_2, T_{\rm arr}) d\Sigma\,, \tag{3}$$

where $\Delta\varepsilon = \Delta E_{\rm int}/V$ is the energy density released in the interaction of the ABM pulse with the ISM inhomogeneities measured in the comoving frame, $\Lambda = \gamma(1 - (v/c)\cos\vartheta)$ is the Doppler factor, $W(\nu_1, \nu_2, T_{\rm arr})$ is an "effective weight" required to evaluate only the contributions in the energy band $[\nu_1, \nu_2]$, $d\Sigma$ is the surface element

of the EQTS at detector arrival time t_a^d on which the integration is performed (see also Ref. 19) and $T_{\rm arr}$ is the observed temperature of the radiation emitted from $d\Sigma$:

$$T_{\rm arr} = \frac{T}{\gamma\left(1 - \frac{v}{c}\cos\vartheta\right)} \frac{1}{(1+z)} \,. \tag{4}$$

The "effective weight" $W(\nu_1, \nu_2, T_{\rm arr})$ is given by the ratio of the integral over the given energy band of a Planckian distribution at a temperature $T_{\rm arr}$ to the total integral $aT_{\rm arr}^4$:

$$W(\nu_1, \nu_2, T_{\rm arr}) = \frac{1}{aT_{\rm arr}^4} \int_{\nu_1}^{\nu_2} \rho(T_{\rm arr}, \nu) d\left(\frac{h\nu}{c}\right)^3 , \tag{5}$$

where $\rho(T_{\rm arr}, \nu)$ is the Planckian distribution at temperature $T_{\rm arr}$:

$$\rho(T_{\rm arr}, \nu) = \frac{2}{h^3} \frac{h\nu}{\exp^{h\nu/(kT_{\rm arr})} - 1} \,. \tag{6}$$

4. The Best Fit of the Observed Flux in Selected Energy Bands

We can now proceed to the best fit of the observed data using GRB 991216 as the prototype. Such an estimate is perfectly well defined from a theoretical point of view, although from a numerical point of view the integration on all the EQTS and the associated relativistic transformations have raised unprecedented and time consuming difficulties. Almost 10^8 paths with different temperatures and different Lorentz boosts had to be considered in the integration over the EQTS. We give in Figs. 1 and 2 the results for the three energy bands 50–300 keV (BATSE), 2–10 keV (R-XTE, Chandra) and 10–50 keV. It is most remarkable that the best fit is obtained simply by a factor $\mathcal{R}$, which is monotonically varying in the range:

$$3.01 \times 10^{-8} \geq \mathcal{R} \geq 5.01 \times 10^{-12} \tag{7}$$

respectively in correspondence with the beginning of the afterglow emission and the last observation by Chandra at $\sim$ 37 hr after the GRB. We point out the perfect agreement with the data obtained by BATSE Rapid Burst Response[7] in the energy range 50–300 keV (see dashed line in Fig. 1). Very impressive is the fit of the data obtained by the R-XTE and Chandra satellites (see Ref. 25) in the energy range 2–10 keV (see dotted line in Figs. 1 and 2). These data are fitted with a $\chi^2 \simeq 1.078$. This fit covers a time span of $\sim 10^6$ s and is impressive if we recall that it is a function of the single parameter $\mathcal{R}$. The fit can be further improved, reaching a $\chi^2 \simeq 0.48$, when a radial dependence in $\langle n_{\rm ism}\rangle$ is introduced, ranging from $\langle n_{\rm ism}\rangle \simeq 1$ particle/cm^3 in the E-APE region ($r \simeq 5 \times 10^{16}$ cm) to $\langle n_{\rm ism}\rangle \simeq 3$ particle/cm^3 in the latest afterglow phases ($r \simeq 4 \times 10^{17}$ cm). Both in Figs. 1 and 2 the solid line gives the bolometric luminosity (see details in Ref. 5).

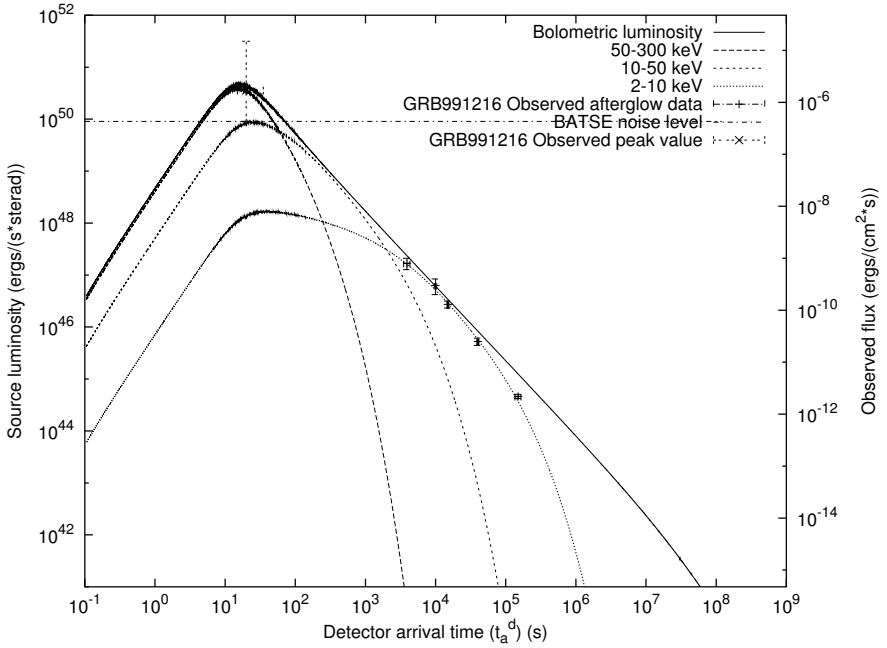

Fig. 1. Best fit of the afterglow data of GRB 991216. The solid curve is the bolometric luminosity. See Ref. 18 for the radial approximation and Refs. 5 and 19 for the relativistic analysis of the off-axis contributions. The three dotted curves correspond to the luminosities in the bands 50–300 keV, 10–50 keV and 2–10 keV respectively. Near the E-APE, where the BATSE data are present, almost all the luminosity is in the 50–300 keV band. The afterglow data from R-XTE and Chandra (see Ref. 25) in the 2–10 keV are perfectly fit by the corresponding luminosity curve (see also Fig. 2).

5. On the Time Integrated Spectra and the Hard-to-Soft Spectral Transition

We turn now to the much debated issue of the origin of the observed hard-to-soft spectral transition during the GRB observations (see e.g. Refs. 10–13). We consider the instantaneous spectral distribution of the observed radiation for three different EQTS:

- $t_a^d = 10$ s, in the early radiation phase near the peak of the luminosity,
- $t_a^d = 1.45 \times 10^5$ s, in the last observation of the afterglow by the Chandra satellite, and
- $t_a^d = 10^4$ s, chosen in between the other two (see Fig. 3).

The observed hard-to-soft spectral transition is then explained and traced back to:

(1) a time decreasing temperature of the thermal spectrum measured in the co-moving frame,
(2) the GRB equations of motion,
(3) the corresponding infinite set of relativistic transformations.

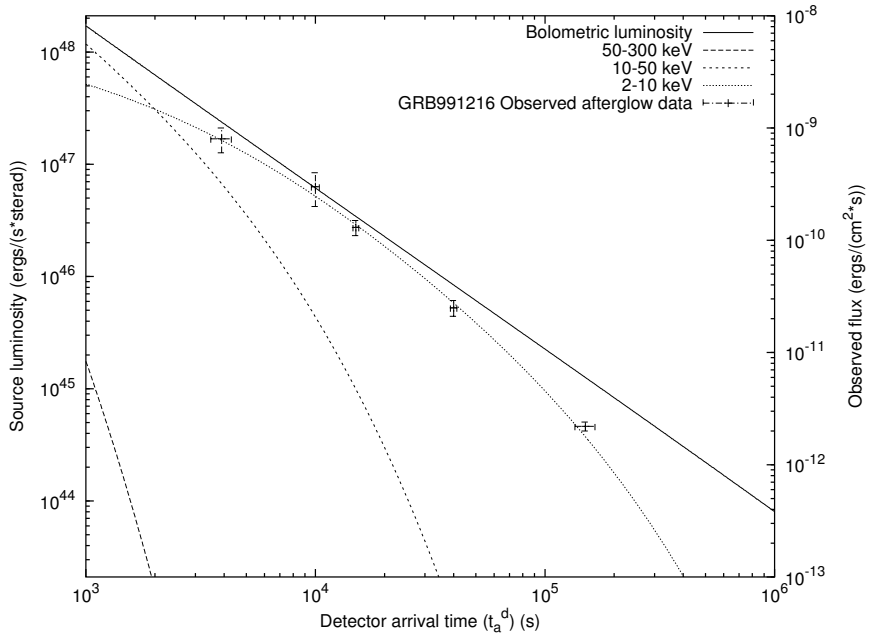

Fig. 2. This is an enlargement of Fig. 1 in the region of the afterglow data in the 2–10 keV band from the R-XTE and Chandra satellites, showing the perfect agreement between the theoretical curve and the observational data. The reduced χ^2 value for this fit is $\chi^2 \simeq 1.078$.

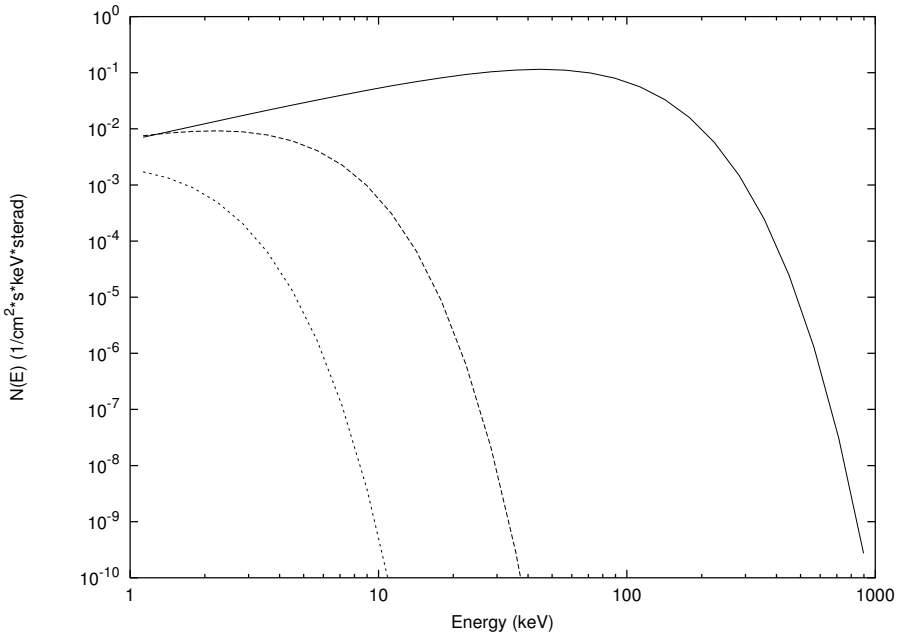

Fig. 3. The instantaneous spectra of the radiation observed in GRB 991216 at three different EQTS respectively, from top to bottom, for $t_a^d = 10$ s, $t_a^d = 10^4$ s and $t_a^d = 1.45 \times 10^5$ s. These diagrams have been computed assuming a constant $\langle n_{\rm ism} \rangle \simeq 1$ particle/cm^3 and clearly explains the often quoted hard-to-soft spectral evolution in GRBs.

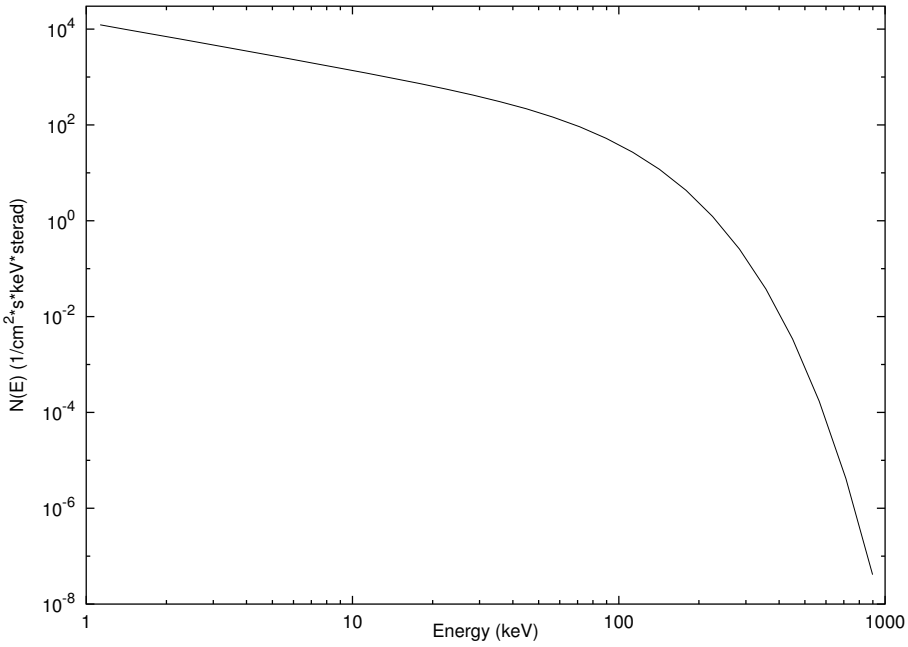

Fig. 4. The time-integrated spectrum of the radiation observed in GRB 991216. The low energy part of the curve below 10 keV is fit by a power-law with index $\alpha = -1.05$ and the high energy part above 500 keV is fit by a power-law with an index $\beta < -16$.

A clear signature of our model is the existence of a common low-energy behavior of the instantaneous spectrum represented by a power-law with index $\alpha = +0.9$. This prediction will be possibly verified in future observations.

Starting from these instantaneous values, we integrate the spectra in arrival time obtaining what is usually fit in the literature by the "Band relation."[3] Indeed we find for our integrated spectra a low energy spectral index $\alpha = -1.05$ and an high energy spectral index $\beta < -16$ when interpreted within the framework of a Band relation (see Fig. 4). This theoretical result can be submitted to a direct confrontation with the observations of GRB 991216 and, most importantly, the entire theoretical framework which we have developed can now be applied to any GRB source. The so-obtained theoretical predictions on the luminosity in fixed energy bands can then be straightforwardly confronted with the observational data.

6. Conclusions

In addition to the above results, we have also applied our model to GRB 980425, which is one of the weakest GRBs observed, with an energy of the order of $\sim 10^{48}$ ergs (see Refs. 26–28). Our model then applies over a range of energies spanning 6 orders of magnitude.

The fundamental novel point here is the assumption of the thermal origin of the X and γ radiation of the afterglow in the comoving frame of the shock front. The

fit of the data in Figs. 1 and 2 gives a clearest and unambiguous support from the observations to this theoretical approach.

All the works in the current literature tries to explain the afterglow emission by a very complex process implying magnetic fields, jet-like ejecta, emission by a forward shock and a reverse shock (see e.g. Refs. 12, 29 and 30 and references therein). In our approach we evidence the existence of a much simpler process, directed forward, basically spherically symmetric and originating by a simple thermal emission in the comoving frame of the shock.

We are grateful to an anonymous referee for pointing out that Blinnikov *et al.*[31] did argue that nonthermally looking GRB spectra can indeed be formed by a superposition of a set of thermal black body spectra with a temporal power-law evolution of the temperature. In our treatment not only time but also space integration on the EQTS takes place. This effect was explicitly omitted in the interesting paper of Blinnikov *et al.*:[31] while their instantaneous GRB spectra are thermal, in our approach each instantaneous spectrum is derived from an infinite set of foliations of events on the EQTS, each one characterized by a different thermal spectrum in the comoving frame boosted by a different relativistic transformation obtained from the EOM.

We emphasize that these results are extremely sensitive to the structure of the EQTS and to the theoretical assumptions adopted for each GRB era (see examples in Refs. 5, 23 and 24). Due to the enormous redundancy built into the almost 10^8 different paths mentioned above, possibly unprecedented in physics and astrophysics, we can assert the uniqueness of the solution. We also conclude that there is a marked difference (see Fig. 1) between the bolometric intensity of the afterglow, with a simple power-law behavior with an index $n = -1.6$ in the decreasing part, and the actual luminosity in a fixed bandwidth, which can have a complex dependence on time. Such a complex behavior could be erroneously interpreted as a broken power-law supporting the existence of jet-like structures in GRBs.

The physical reasons justifying the assumptions in Eqs. (1) and (2) are presented in Ruffini *et al.*[32]

References

1. W. S. Paciesas *et al.*, *Astrophys. J. Suppl.* **122**, 465 (1999).
2. G. J. Fishman and C. A. Meegan, *Ann. Rev. Astron. Astrophys.* **33**, 415 (1995).
3. D. Band *et al.*, *Astrophys. J.* **413**, 281 (1993).
4. E. Costa *et al.*, *Nature* **387**, 783 (1997).
5. R. Ruffini, C. L. Bianco, P. Chardonnet, F. Fraschetti, L. Vitagliano and S.-S. Xue, in *Proceedings of the Xth Brazilian School of Cosmology and Gravitation*, eds. M. Novello, and S. E. Perez Bergliaffa, AIP Conference Proceedings 668, (2003), p. 16.
6. R. Ruffini, C. L. Bianco, P. Chardonnet, F. Fraschetti and S.-S. Xue, in *Proceedings of Gamma-Ray Burst in the Afterglow Era*: *3rd Workshop*, eds. G. Chincarini, E. Costa, F. Frontera and L. Piro (ASP, 2003), in press.
7. BATSE Rapid Burst Response (1999), http://gammaray.msfc.nasa.gov/∼kippen/batserbr/

8. L. Piro *et al.*, *Science* **290**, 955 (2000).
9. R. Corbet and D. A. Smith, in *Rossi2000*: *Astrophysics with the Rossi X-ray Timing Explorer* (Greenbelt, USA, 2000).
10. F. Frontera *et al.*, *Astrophys. J. Suppl.* **127**, 59 (2000).
11. G. Ghirlanda, A. Celotti and G. Ghisellini, *Astron. & Astrophys.* **393**, 409 (2002).
12. T. Piran, *Phys. Rep.* **314**, 575 (1999).
13. L. Piro *et al.*, *Astrophys. J. Lett.* **514**, L73 (1999).
14. R. Ruffini, Black holes and high energy astrophysics, in *Proceedings of the 49th Yamada Conference*, eds. H. Sato and N. Sugiyama (Universal Academic Press, Tokyo, 1998).
15. G. Preparata, R. Ruffini and S.-S. Xue, *Astron. & Astrophys.* **338**, L87 (1998).
16. R. Ruffini, J. D. Salmonson, J. R. Wilson and S.-S. Xue, *Astron. & Astrophys.* **350**, 334 (1999); *Astron. & Astrophys. Suppl. Series* **138**, 511 (1999).
17. R. Ruffini, J. D. Salmonson, J. R. Wilson and S.-S. Xue, *Astron. & Astrophys.* **359**, 855 (2000).
18. R. Ruffini, C. L. Bianco, P. Chardonnet, F. Fraschetti and S.-S. Xue, *Astrophys. J. Lett.* **555**, L113 (2001).
19. R. Ruffini, C. L. Bianco, P. Chardonnet, F. Fraschetti and S.-S. Xue, *Astrophys. J. Lett.* **581**, L19 (2002).
20. R. Ruffini, C. L. Bianco, P. Chardonnet, F. Fraschetti and S.-S. Xue, *Astrophys. J. Lett.* **555**, L107 (2001).
21. T. W. Giblin *et al.*, *Astrophys. J.* **570**, 573 (2002).
22. Ya. B. Zel'dovich and Yu. P. Rayzer, *Physics of Shock Waves and High-Temperature Hydrodynamic Phenomena*, eds. D. H. Wallace and R. F. Probstein (Academic Press, New York and London, 1966).
23. C. L. Bianco and R. Ruffini, *Astrophys. J. Lett.* **605**, L1 (2004).
24. C. L. Bianco and R. Ruffini, submitted to *Astron. & Astrophys.* (2004).
25. J. P. Halpern *et al.*, *Astrophys. J.* **543**, 697 (2000).
26. R. Ruffini, C. L. Bianco, P. Chardonnet, F. Fraschetti and S.-S. Xue, in *Proceedings of the 34th COSPAR Scientific Assembly* (Elsevier, 2003).
27. R. Ruffini, M. G. Bernardini, C. L. Bianco, P. Chardonnet, F. Fraschetti and S.-S. Xue, in *Proceedings of the Tenth Marcel Grossmann Meeting on General Relativity*, eds. M. Novello, S. E. Perez-Bergliaffa and R. Ruffini (World Scientific, Singapore, 2004).
28. R. Ruffini, in *Proceedings of the 6th RESCEU International Symposium* (Universal Academy Press, Tokyo, 2004).
29. J. van Paradijs, C. Kouveliotou and R. A. M. J. Wijers, *Ann. Rev. Astron. Astrophys.* **38**, 379 (2000).
30. P. Mészáros, *Ann. Rev. Astron. Astrophys.* **40**, 137 (2002).
31. S. I. Blinnikov, A. V. Kozyreva and I. E. Panchenko, *Astron. Rep.* **43**, 739 (1999).
32. R. Ruffini, C. L. Bianco, P. Chardonnet, F. Fraschetti, V. Gurzadyan and S.-S. Xue, submitted to *Astrophys. J. Lett.* (2004).

18 Appendix 11

The GRB 980425-SN1998bw Association in the EMBH Model

F. Fraschetti*, M.G. Bernardini†, C.L. Bianco†, P. Chardonnet**, R. Ruffini† and S.-S. Xue†

*Università di Trento, Via Sommarive 14, I-38050 Povo (Trento), Italy
†ICRA - International Centre for Relativistic Astrophysics and Dipartimento di Fisica, Università di Roma "La Sapienza", Piazzale Aldo Moro 5, I-00185 Roma, Italy
**Université de Savoie, LAPTH - LAPP, BP 110, F-74941 Annecy-le-Vieux Cedex, France

Abstract. Our GRB theory, previously developed using GRB 991216 as a prototype, is here applied to GRB 980425. We fit the luminosity observed in the 40–700 keV, 2–26 keV and 2–10 keV bands by the BeppoSAX satellite. In addition the supernova SN1998bw is the outcome of an "induced gravitational collapse" triggered by GRB 980425, in agreement with the GRB-Supernova Time Sequence (GSTS) paradigm (Ruffini et al. [1]). A further outcome of this astrophysically exceptional sequence of events is the formation of a young neutron star generated by the SN1998bw event (Ruffini et al. [2]). A coordinated observational activity is recommended to further enlighten the underlying scenario of this most unique astrophysical system.

Our GRB theory (Ruffini et al. [3, 4, 1, 5, 6] and references therein), previously successfully applied to GRB 991216 used as a prototype, is applied to GRB 980425 (Pian et al. [7]) and SN1998bw (Galama and et al. [8]). This event allows to test the validity of the theory over a range of energies of 6 orders of magnitude: both sources appear to be spherically symmetric and the respective total energies are $E_{tot} \simeq 5 \times 10^{53}$ ergs and $E_{tot} \simeq 10^{48}$ ergs.

The theory, therefore, explains all the observed features of the bolometric intensity variations of the afterglow as well as the spectral properties of the source and, in the specific case of GRB 980425 (Ruffini et al. [2]), it also allows to clarify the general astrophysical scenario in which the GRB actually occurs. In this system, in fact, we propose that GRB 980425 has been the trigger of a phenomenon of "induced gravitational collapse" (Ruffini et al. [1]) originating the supernova explosion and we also witness the birth of a young neutron star out of the supernova event. This extraordinary coincidence of these three astrophysical events represents an unprecedented scenario of fundamental importance in the field of relativistic astrophysics.

The observational situation of this system is quite complex. In addition to the source GRB 980425 and the supernova SN1998bw, two X-ray sources have been found by BeppoSAX in the error box for the location of GRB 980425: a source *S1* and a source *S2* (Pian et al. [7]). Our approach is the following. We first interpret the GRB 980425 within the EMBH theory. This allows the computation of the luminosity, spectra, Lorentz gamma factors, and more generally all the dynamical aspects of the source. Having characterized the features of GRB 980425, we can gradually approach the remaining part of the scenario, disentangling the GRB observations from the supernova ones and

from the sources *S1* and *S2*. This leads to a natural time sequence of events and to their autonomous astrophysical characterization.

Our approach has focused on identifying the energy extraction process from the black hole (Christodoulou and Ruffini [9]) as the basic energy source for the GRB phenomenon. The distinguishing feature is a theoretically predicted source energetics all the way up to $1.8\times10^{54}\,(M_{BH}/M_{\odot})$ ergs for $3.2M_{\odot}\leq M_{BH}\leq 7.2\times10^{6}M_{\odot}$ (Damour and Ruffini [10]). In particular, the formation of a "dyadosphere", during the gravitational collapse leading to a black hole endowed with electromagnetic structure (EMBH) has been indicated as the initial boundary conditions of the GRB process (Ruffini [11], Preparata et al. [12]).

The equations of motion in our theory depend only on two free parameters: the total energy E_{tot}, which coincides with the dyadosphere energy E_{dya}, and the amount M_B of baryonic matter left over from the gravitational collapse of the progenitor star, which is determined by the dimensionless parameter $B=M_Bc^2/E_{dya}$. Our best fit corresponds to $E_{dya}=1.1\times10^{48}$ ergs, $B=7\times10^{-3}$ and the ISM average density is found to be $\langle n_{ism}\rangle=0.02$ particle/cm^3. The plasma temperature and the total number of pairs in the dyadosphere are respectively $T=1.028$ MeV and $N_{e^{\pm}}=5.3274\times10^{53}$.

Recently, within the EMBH theory, we have developed an attempt to theoretically derive the GRB spectra out of first principles as well as the GRB luminosity in fixed energy bands (Ruffini et al. [13]). We have adopted three basic assumptions: **a)** the resulting radiation as viewed in the comoving frame during the afterglow phase has a thermal spectrum and **b)** the ISM swept up by the front of the shock wave, with a Lorentz gamma factor between 300 and 2, is responsible for this thermal emission. **c)** We also assume, like in our previous papers (Ruffini et al. [3, 4, 5, 6]), that the expansion occurs with spherical symmetry.

The temperature T of the black body in the comoving frame is then

$$T=\left(\frac{\Delta E_{\rm int}}{4\pi r^2\Delta\tau\sigma\mathscr{R}}\right)^{1/4}, \tag{1}$$

where $\mathscr{R}=A_{eff}/A_{abm}$ is the ratio between the "effective emitting area" and the ABM pulse surface A_{abm} (in this case the best fit value of $\mathscr{R}$ is monotonically decreasing from 4.81×10^{-10} to 2.65×10^{-12}), σ is the Stefan-Boltzmann constant and $\Delta E_{\rm int}$ is the proper internal energy developed in the collision between the ABM pulse and the ISM in the proper time interval $\Delta\tau$ (see Ruffini et al. [6, 13]). The ratio $\mathscr{R}$, which is a priori a function that varies as the system evolves, is evaluated at every given value of the laboratory time t.

All the subsequent steps are now uniquely determined by the equations of motion of the system. The basic tool in this calculation involves the definition of the EQuiTemporal Surfaces (EQTS) for the relativistic expanding ABM pulse as seen by an asymptotic observer. The key to determining such EQTS (see Fig. 1 in Ruffini et al. [5]) is the relation between the time t in the laboratory frame at which a photon is emitted from the ABM pulse external surface and the arrival time t_a^d at which it reaches the detector.

The results are given in Fig. 1 where the luminosity is computed as a function of the arrival time for three selected energy bands.

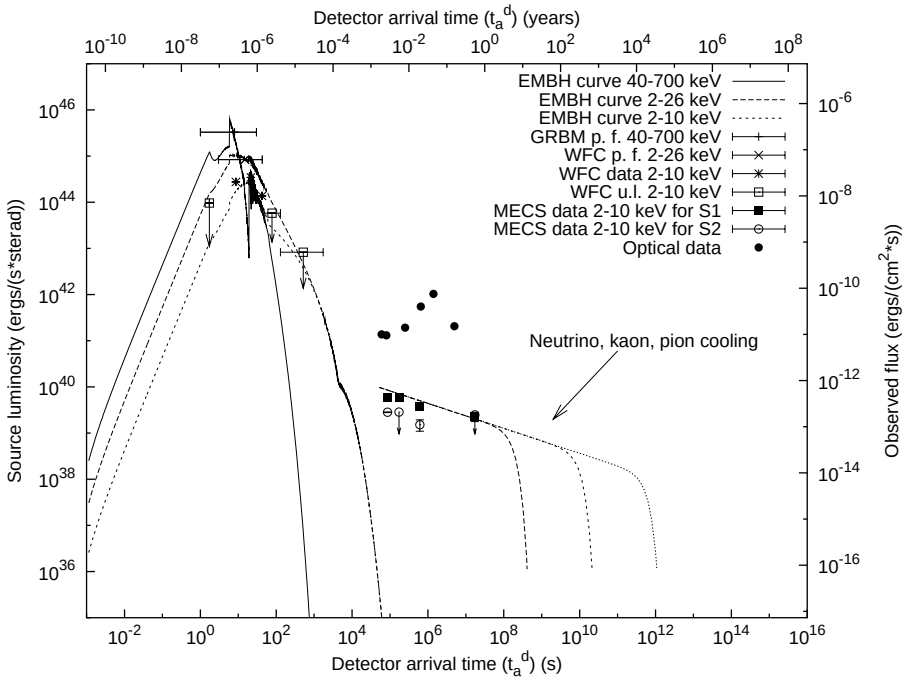

FIGURE 1. The light curves in selected bands are reported as well as the MECS light curves in the 2-10 keV band of S1 and S2 (Pian et al. [7]) as well as the optical data (Iwamoto [14]). Here are also reported theoretical models of neutron star cooling (Canuto [15]).

In Fig. 1 the luminosities in the three bands are represented together with the optical data of SN1998bw (black dots), the source S1 (black squares) and the source S2 (open circles). It is then clear that GRB 980425 is separated both from the supernova data and from the sources *S1* and *S2*.

While the occurrence of the supernova in relation to the GRB has already been discussed with the GRB-Supernova Time Sequence (GSTS) paradigm (Ruffini et al. [1]), we like to address here a different fundamental issue: the possibility of observing the birth of a newly formed neutron star, possibly pulsating, out of the supernova event, which in turn has been triggered by the GRB 980425.

In the early days of neutron star physics it was clearly shown by (Gamow and Schoenberg [16]) that the URCA processes are at the very heart of the supernova explosions. The neutrino-antineutrino emission described in the URCA process is the essential cooling mechanism necessary for the occurrence of the process of gravitational collapse of the imploding core. Since then, it has become clear that the newly formed neutron star can be still significantly hot and in its early stages will be associated to three major radiating processes (Tsuruta [17, 18], Tsuruta et al. [19], Canuto [15]): **a)** the thermal radiation from the surface, **b)** the radiation due to neutrino, kaon, pion

cooling, and **c)** the possible influence in both these processes of the superfluid nature of the supra-nuclear density neutron gas. Qualitative representative curves for these cooling processes, which are still today very undetermined due to the lack of observational data, are shown in Fig. 1.

It is of paramount importance to follow the further time history of the two sources *S1* and *S2*. If, as we propose, *S2* is a background source, its flux should be practically constant in time and this source has nothing to do with the GRB 980425 / SN1998bw system. If S1 is indeed the cooling radiation emitted by the newly born neutron star, it should be possible to notice a very drastic behavior in its luminosity as qualitatively expresses in Fig. 1.

The complete details on the source with all numerical values and explicit relations is going to appear in (Ruffini et al. [20]).

REFERENCES

1. Ruffini, R., Bianco, C. L., Chardonnet, P., Fraschetti, F., and Xue, S.-S., *ApJ Lett.*, **555**, L117 (2001).
2. Ruffini, R., Bernardini, M. G., Bianco, C. L., Chardonnet, P., Fraschetti, F., and Xue, S.-S., "GRB 980425, SN1998bw and the EMBH Model," in *Proceedings of the 34th COSPAR Scientific Assembly*, edited by E. Pian, N. Masetti, and L. Piro, Elsevier, 2003, in press.
3. Ruffini, R., Bianco, C. L., Chardonnet, P., Fraschetti, F., and Xue, S.-S., *ApJ Lett.*, **555**, L107 (2001).
4. Ruffini, R., Bianco, C. L., Chardonnet, P., Fraschetti, F., and Xue, S.-S., *ApJ Lett.*, **555**, L113 (2001).
5. Ruffini, R., Bianco, C. L., Chardonnet, P., Fraschetti, F., and Xue, S.-S., *ApJ Lett.*, **581**, L19 (2002).
6. Ruffini, R., Bianco, C. L., Chardonnet, P., Fraschetti, F., Vitagliano, L., and Xue, S.-S., "New Perspectives in Physics and Astrophysics from the Theoretical Understanding of Gamma-Ray Bursts," in *COSMOLOGY AND GRAVITATION: X^{th} Brazilian School of Cosmology and Gravitation; 25^{th} Anniversary (1977-2002)*, edited by M. Novello and S. E. P. Bergliaffa, AIP, New York, 2003, vol. 668, p. 16, Allegato 8.
7. Pian, E., Amati, L., Antonelli, L., Butler, R., Costa, E., Cusumano, G., Danziger, J., Feroci, M., Fiore, F., Frontera, F., Giommi, P., Masetti, N., Muller, J., Nicastro, L., Oosterbroek, T., Orlandini, M., Owens, A., Palazzi, E., Parmar, A., Piro, L., in 't Zand, J., Castro-Tirado, A., Coletta, A., Fiume, D. D., Sordo, S. D., Heise, J., Soffitta, P., and Torroni, V., *ApJ*, **536**, 778 (2000).
8. Galama, T., and et al., *Nature*, **59**, 395 (1998).
9. Christodoulou, D., and Ruffini, R., *Phys. Rev. D*, **4**, 3552 (1971).
10. Damour, T., and Ruffini, R., *Phys. Rev. Lett.*, **35**, 463 (1975).
11. Ruffini, R., "Beyond the Critical Mass: The Dyadosphere of Black Holes," in *Black Holes and High Energy Astrophysics, Proceedings of the 49th Yamada Conference*, edited by H. Sato and N. Sugiyama, Universal Ac. Press, Tokyo, 1998.
12. Preparata, G., Ruffini, R., and Xue, S.-S., *A&A*, **338**, L87 (1998).
13. Ruffini, R., Bianco, C. L., Chardonnet, P., Fraschetti, F., Gurzadyan, V., and Xue, S.-S., On the instantaneous spectrum of gamma-ray bursts (2004), iJMPD, in press.
14. Iwamoto, K., *ApJ Lett.*, **512**, L47 (1999).
15. Canuto, V., "Neutron Stars, Physics and astrophysics of neutron stars and black holes," in *Proceedings of the International School of Physics "Enrico Fermi"*, edited by R. Giacconi and R. Ruffini, Amsterdam, North Holland Publishing Co., 1978.
16. Gamow, G., and Schoenberg, M., *Phys. Rev.*, **59**, 539 (1941).
17. Tsuruta, S., Ph.D. thesis, Columbia University (1964).
18. Tsuruta, S., *Phys. Rep.*, **56**, 237 (1979).
19. Tsuruta, S., Teter, M. A., Takatsuka, T., Tatsumi, T., and Tamagaki, R., *ApJ*, **571**, L143 (2002).
20. Ruffini, R., Bernardini, M. G., Bianco, C. L., Chardonnet, P., Fraschetti, F., and Xue, S.-S. (2004), in preparation.

19 Appendix 12

GRB 970228 Within the EMBH Model

A. Corsi*, M.G. Bernardini*, C.L. Bianco*, P. Chardonnet†, F. Fraschetti**, R. Ruffini* and S.-S. Xue*

*ICRA - International Center for Relativistic Astrophysics and Dipartimento di Fisica, Università di Roma "La Sapienza", Piazzale Aldo Moro 5, I-00185 Roma, Italy.
†Université de Savoie, LAPTH - LAPP, BP 110, F-74941 Annecy-le-Vieux Cedex, France.
**Università di Trento, Via Sommarive 14, I-38050 Povo (Trento), Italy.

Abstract. We consider the gamma-ray burst of 1997 February 28 (GRB 970228) within the ElectroMagnetic Black Hole (EMBH) model. We first determine the value of the two free parameters that characterize energetically the GRB phenomenon in the EMBH model, that is to say the dyadosphere energy, $E_{dya} = 5.1 \times 10^{52}$ ergs, and the baryonic remnant mass M_B in units of E_{dya}, $B = M_B c^2/E_{dya} = 3.0 \times 10^{-3}$. Having in this way estimated the energy emitted during the beam-target phase, we evaluate the role of the InterStellar Medium (ISM) number density (n_{ISM}) and of the ratio $\mathscr{R}$ between the effective emitting area and the total surface area of the GRB source, in reproducing the observed profiles of the GRB 970228 prompt emission and X-ray (2-10 keV energy band) afterglow. The importance of the ISM distribution three-dimensional treatment around the central black hole is also stressed in this analysis.

The GRB 970228 [1] had an important role in solving the origin of GRBs through the first detection of counterparts at other wavelengths: the afterglow phenomenon, long-lived multi-wavelength emission, was discovered following GRB 970228 at X-ray ([2], Costa et al. [3]) and optical ([4], van Paradijs et al. [5]) wavelengths. We consider of great interest to compare the predictions of the ElectroMagnetic Black Hole (EMBH) theory (see Ruffini et al. [6] and references therein) with the first afterglow observed by the Beppo-SAX satellite. We are also interested in testing the efficiency of the model in reproducing the GRB 970228 prompt emission: in the 40-700 keV energy band the burst was characterized by an initial 5 s strong pulse followed, after about 30 s, by three additional pulses of decreasing intensity (Frontera et al. [7]). The InterStellar Medium (ISM) number density (n_{ISM}) inhomogeneities have an important role in interpreting this profile within the EMBH model.

Our analysis starts establishing the value of the two free parameters that determine energetically the GRB phenomenon in the EMBH model: the total energy deposited in the dyadosphere E_{dya} (Ruffini et al. [8]) and the amount of the baryonic matter left over in the collapse process of the EMBH progenitor star (Ruffini et al. [8]), that can be parametrized by the dimensionless parameter $B = M_B c^2/E_{dya}$. With the choice of $E_{dya} = 5.1 \times 10^{52}$ ergs and $B = 3.0 \times 10^{-3}$, the EMBH model predicts that a 98% of the total energy E_{dya} is emitted during the so-called beam-target phase (Ruffini et al. [9]), that is to say during the collision of the Accelerated Baryonic Matter-pulse (ABM-pulse) with the ISM (Ruffini et al. [6]). During this phase, the internal energy developed in the collision is instantaneously radiated away (fully radiative condition)

and, as a consequence, the resulting shape of the light curve is strictly linked to the ISM distribution and number density (Ruffini et al. [10]). We use a one-dimensional treatment of the ISM, where the n_{ISM} is a function of the radial distance from the central black hole (Ruffini et al. [10]). In order to reproduce the observed profile of the GRB 970228, n_{ISM} has to range between the values of 10^{-2} particles/cm^3 and 200 particles/cm^3 in the region of space within 2.00×10^{15} cm and 4.95×10^{16} cm from the central black hole. Since 2.00×10^{15} cm and beyond 4.95×10^{16} cm, the ISM number density has a constant value of 1 particle/cm^3 (details are given in Ruffini et al. [11], Ruffini et al. [12]). The correct spectral distribution of the energy emitted during the the beam-target phase depends on the $\mathscr{R}$ parameter (Ruffini et al. [13]). As a consequence, the theoretical curves in selected energy bands are strictly related to this parameter. $\mathscr{R}$ is a function of the radial distance from the EMBH and it represents the ratio between the effective emitting area of the ABM-pulse and its total surface area:

$$\mathscr{R} = A_{eff}/A_{ABM} \tag{1}$$

According to Ruffini et al. [13], by assuming a black-body spectrum in the co-moving frame for the radiation emitted during the collision with the ISM, the spectral distribution of the energy emitted results to be dependent on the temperature of the emitting black body (Ruffini et al. [13], Ruffini et al. [14]):

$$T = \left(\frac{\Delta E_{int}}{4\pi r^2 \Delta\tau \sigma \mathscr{R}} \right)^{1/4} \tag{2}$$

where ΔE_{int} is the proper internal energy developed in the collision of the ABM-pulse with the ISM in the proper time interval $\Delta\tau$, r is the radial coordinate of the ABM-pulse, t is the laboratory time (Ruffini et al. [15]), σ is the Stefan-Boltzmann constant. In the case of GRB 970228 we find $\mathscr{R}$ monotonically varying from 3.7×10^{-12} to 8.8×10^{-11} when the radial coordinate r goes from 7.0×10^{14} cm to 5.0×10^{17} cm. With this result, the first peak in the 40-700 keV observed light curve is correctly reproduced by the model (details are given in Ruffini et al. [11], Ruffini et al. [12]). The three additional pulses, that follow the first one after a gap in the emission, are reproduced by the model in terms of the mean luminosity. The Fast Rise Exponential Decay (FRED) shape that emerges in the theoretical light curve is a consequence of the one-dimensional treatment of the ISM. To solve this problem, a three-dimensional treatment of the ISM distribution is required (details are given in Ruffini et al. [11], Ruffini et al. [12]).

About the X-ray afterglow, in Fig.1 we present the theoretical curve in the 2-10 keV energy band compared with the observed data by Beppo-SAX (Costa et al. [3]) and ASCA [16]. The afterglow phase corresponds to the ABM-pulse expansion in the region beyond 4.95×10^{16} cm, where the number density of the ISM has a constant value, n_{ISM} =1particle/cm^3. We can see that there is a good agreement (χ^2=0.5) between the theoretical light curve in the 2-10 keV energy band and the observed data by Beppo-SAX and ASCA. From this analysis we conclude that:

- a mask of density inhomogeneities of the ISM is needed in the region of space between 2.00×10^{15} cm and 4.95×10^{16} cm from the black hole, in order to reproduce the structure of the GRB 970228 prompt emission;

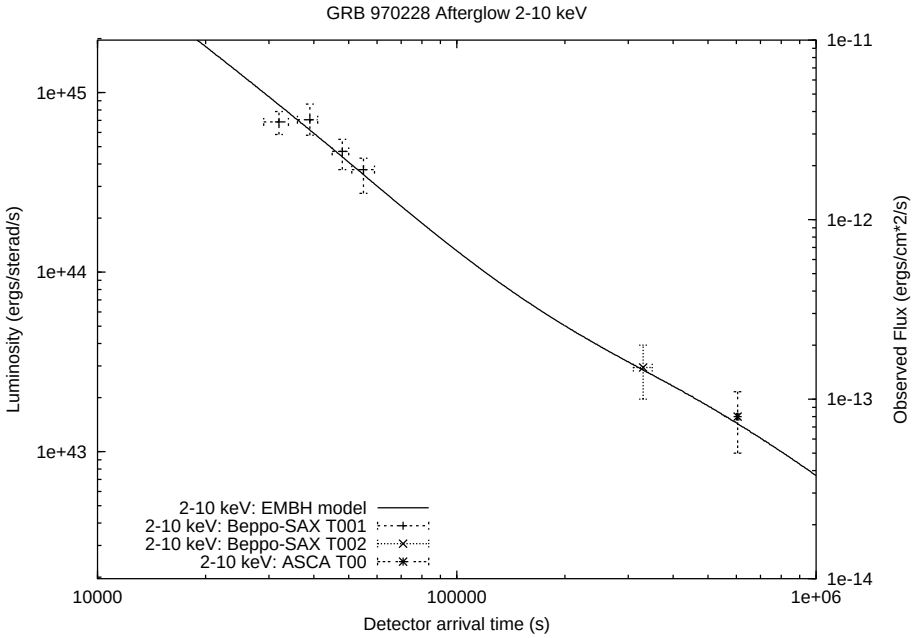

FIGURE 1. Afterglow 2-10 keV: the solid line represents the theoretical light curve for the 2-10 keV emission in the EMBH model. The points are the GRB 970228 2-10 keV afterglow data observed by Beppo-SAX (Costa et al. [3]) and ASCA ([16])

- a three-dimensional treatment of the ISM is required in order to improve the theoretical predictions of the model (details are given in Ruffini et al. [11], Ruffini et al. [12]);
- finally, a good result is obtained with a constant value of the $n_{ISM} = 1 \text{particle/cm}^3$ for the 2-10 keV afterglow emission.

REFERENCES

1. IAU Circ. 6572 (1997).
2. IAU Circ. 6576 (1997).
3. Costa, E., Frontera, F., Heise, J., Feroci, M., in't Zand, J., Fiore, F., Cinti, M. N., Dal Fiume, D., Nicastro, L., Orlandini, M., Palazzi, E., Rapisarda, M., Zavattini, G., Jager, R., Parmar, A., Owens, A., Molendi, S., Cusumano, G., Maccarone, M. C., Giarrusso, S., Coletta, A., Antonelli, L. A., Giommi, P., Muller, J. M., Piro, L., and Butler, R. C., *Nature*, **387**, 783 (1997).
4. IAU Circ. 6584 (1997).
5. van Paradijs, J., Groot, P. J., Galama, T., Kouvelioutou, C., Strom, R. G., Telting, J., Rutten, R. G. M., Fishman, G. J., Meegan, C. A., Pettini, M., Tanvir, N., Bloom, J., Pedersen, H., Nørdgaard-Nielsen, H. U., Linden-Vørnle, M., Melnick, J., van der Steene, G., Bremer, M., Naber, R., Heise, J., in't Zand, J., Costa, E., Feroci, M., Piro, L., Frontera, F., Zavattini, G., Nicastro, L., Palazzi, E., Bennet, K., Hanlon, L., and Parmar, A., *Nature*, **386**, 686 (1997).

6. Ruffini, R., Bianco, C. L., Chardonnet, P., Fraschetti, F., Vitagliano, L., and Xue, S.-S., "New Perspectives in Physics and Astrophysics from the Theoretical Understanding of Gamma-Ray Bursts," in *COSMOLOGY AND GRAVITATION: Xth Brazilian School of Cosmology and Gravitation; 25th Anniversary (1977-2002)*, edited by M. Novello and S. E. P. Bergliaffa, AIP, New York, 2003, vol. 668, p. 16.
7. Frontera, F., Costa, E., Piro, L., Muller, J. M., Amati, L., Feroci, M., Fiore, F., Pizzichini, G., Tavani, M., Castro-Tirado, A., Cusumano, G., Dal Fiume, D., Heise, J., Hurley, K., Nicastro, L., Orlandini, M., Owens, A., Palazzi, E., Parmar, A. N., in't Zand, J., and Zavattini, G., *ApJ*, **493**, L67 (1998).
8. Ruffini, R., Salmonson, J. D., Wilson, J., and Xue, S.-S., *A&A*, **855**, 359 (2000).
9. Ruffini, R., Bianco, C. L., Chardonnet, P., Fraschetti, F., and Xue, S.-S., *ApJ Lett.*, **555**, L113 (2001).
10. Ruffini, R., Bianco, C. L., Chardonnet, P., Fraschetti, F., and Xue, S.-S., *ApJ Lett.*, **581**, L19 (2002).
11. Ruffini, R., Bianco, C. L., Bernardini, M. G., Corsi, A., Chardonnet, P., Fraschetti, F., and Xue, S.-S. (2003a), in preparation.
12. Ruffini, R., Bernardini, M. G., Bianco, C. L., Bernardini, M. G., Corsi, A., Chardonnet, P., Fraschetti, F., and Xue, S.-S., "," in *Proceedings of the 10th Marcell Grossmann Meeting*, 2003b, in preparation.
13. Ruffini, R., Bianco, C. L., Chardonnet, P., Fraschetti, F., Gurzadyan, V., and Xue, S.-S., *IJMPD* (2004), in press.
14. Ruffini, R., Bernardini, M. G., Bianco, C. L., Chardonnet, P., Fraschetti, F., and Xue, S.-S., "GRB 980425, SN1998bw and the EMBH Model," in *Proceedings of the 34th COSPAR Scientific Assembly*, edited by E. Pian, N. Masetti, and L. Piro, Elsevier, 2003, in press.
15. Ruffini, R., Bianco, C. L., Chardonnet, P., Fraschetti, F., and Xue, S.-S., *ApJ Lett.*, **555**, L107 (2001).
16. IAU Circ. 6593 (1997).

20 Appendix 13

A New Astrophysical "Triptych": GRB030329/SN2003dh/URCA-2

M.G. Bernardini*, C.L. Bianco*, P. Chardonnet†, F. Fraschetti**, R. Ruffini* and S.-S. Xue*

*ICRA - International Center for Relativistic Astrophysics and Dipartimento di Fisica, Università di Roma "La Sapienza", Piazzale Aldo Moro 5, I-00185 Roma, Italy.
†Université de Savoie, LAPTH - LAPP, BP 110, F-74941 Annecy-le-Vieux Cedex, France.
**Università di Trento, Via Sommarive 14, I-38050 Povo (Trento), Italy.

Abstract. We analyze the data of the Gamma-Ray Burst/Supernova GRB030329/SN2003dh system obtained by HETE-2 (gcn [1]), R-XTE (gcn [2]), XMM (Tiengo et al. [3]) and VLT (Hjorth et al. [4]) within our theory (Ruffini et al. [5] and references therein) for GRB030329. By fitting the only three free parameters of the EMBH theory, we obtain the luminosity in fixed energy bands for the prompt emission and the afterglow (see Fig. 1). Since the Gamma-Ray Burst (GRB) analysis is consistent with a spherically symmetric expansion, the energy of GRB030329 is $E = 2.1 \times 10^{52}$ erg, namely $\sim 2 \times 10^3$ times larger than the Supernova energy. We conclude that either the GRB is triggering an induced-supernova event or both the GRB and the Supernova are triggered by the same relativistic process. In no way the GRB can be originated from the supernova. We also evidence that the XMM observations (Tiengo et al. [3]), much like in the system GRB980425/SN1998bw (Ruffini et al. [6], Pian and et al. [7]), are not part of the GRB afterglow, as interpreted in the literature (Tiengo et al. [3]), but are associated to the Supernova phenomenon. A dedicated campaign of observations is needed to confirm the nature of this XMM source as a newly born neutron star cooling by generalized URCA processes.

A distinctive feature of our model, developed in the framework of the three interpretational paradigms (Ruffini et al. [8, 9, 10]), has been the relation between the photon arrival time at the detector t_a^d and the photon emission time t (see Ruffini et al. [5, 9, 11]):

$$t_a^d = (1+z)\left(t - \frac{\int_0^t v(t')\,dt' + r^\star}{c}\cos\vartheta + \frac{r^\star}{c}\right), \qquad (1)$$

where $r(t)$, $v(t)$ and $\gamma(t)$ are the radial coordinate, the velocity and the Lorentz gamma factor of the expanding shell, $r^\star = r(t=0)$, ϑ is the angle between the velocity of the emission point of the photon and the line of sight and z is the cosmological redshift of the source.

In contrast with the relation between t_a^d and t used in the literature, which depends on an instantaneous value of the Lorentz γ factor (see e.g. Rees and Mészáros [12], Eq.(30) in Piran [13]], Eq.(2) in van Paradijs et al. [14], Eq.(2) in Mészáros [15]), Eq.(1) contains an integral which is a function of all previous values of the Lorentz gamma factor along the source world-line since the time $t = 0$. Therefore the knowledge of the Equations Of Motion (EOM) of the source is crucial to the evaluation of Eq.(1). In turns all the quantities which are computed using the EQuiTemporal Surfaces (EQTS, Ruffini et al. [5, 11], Bianco and Ruffini [16]) determined from Eq.(1) become themselves very

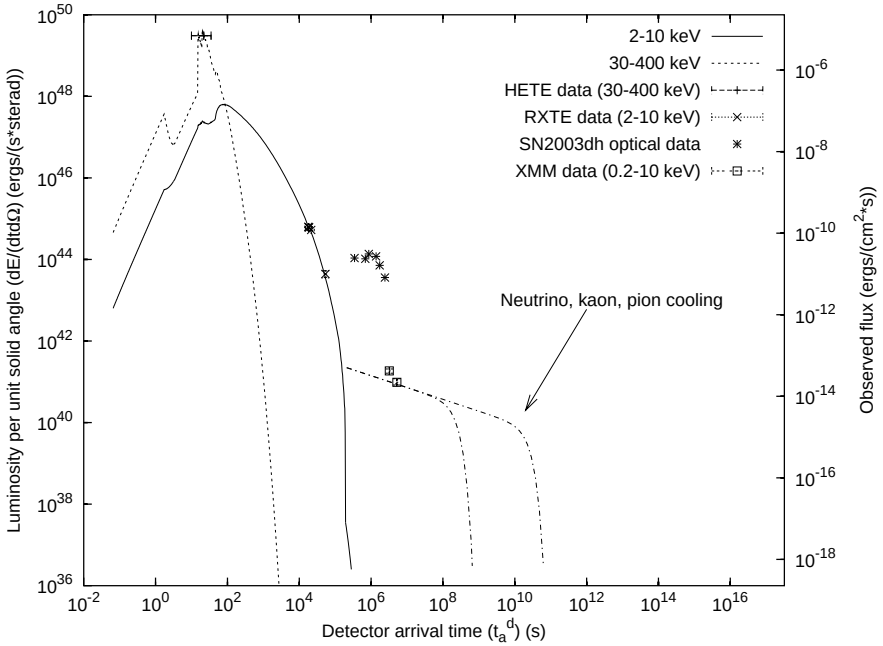

FIGURE 1. The dotted line represents our theoretically predicted GRB030329 light curve in γ-rays (30-400 keV) with the horizontal bar corresponding to the mean peak flux from HETE-2 (gcn [1]). The solid line represents the corresponding one in X-rays (2-10 keV) with the experimental data obtained by R-XTE (gcn [2]). The remaining points refer respectively to the optical VLT data (Hjorth et al. [4]) of SN2003bw and to the X-ray XMM data (Tiengo et al. [3]) of URCA-2. The dash-dotted lines corresponds to cooling theoretical curves of young neutron stars by generalized URCA processes. It is interesting to compare and contrast these results with the ones for GRB980425/SN1998bw (see Fig. 3 in Ruffini et al. [6])

sensitive functions of the EOM. This includes the slope of the afterglow (Ruffini et al. [5]), which is essential in assessing the possible presence of beaming in the source (Ruffini et al. [17]), the luminosity in fixed energy bands and the spectral analysis (Ruffini et al. [18]).

The determination of the EOM leads to a quite complex treatment, which starts from a very special set of initial conditions, proven to be unique. This treatment fits the observed luminosities with a large number of redundancy checks on the EOM (see Fig. 1). It fits as well the time variability in the prompt radiation self-consistently with the determination of the EOM [19].

We have adopted a spherically symmetric distribution for the GRB source and, as initial conditions at $t = 10^{-21}$ s, an e^+-e^--photon neutral plasma lying between the radii $r_1 = 2.9 \times 10^6$ cm and $r_2 = 9.0 \times 10^7$ cm. The temperature of such a plasma is 2.1 MeV, the total energy $E_{tot} = 2.1 \times 10^{52}$ erg and the total number of pairs $N_{e^+e^-} = 1.1 \times 10^{57}$. These conditions have been derived evaluating the vacuum polarization processes (Damour and Ruffini [20]) occurring in the dyadosphere of an EMBH (Ruffini

[21], Preparata et al. [22], Cherubini et al. [23], Ruffini and Vitagliano [24, 25], Ruffini et al. [26]). The total energy E_{tot} coincides with the dyadosphere energy E_{dya} which is the first independent parameter of the EMBH theory. The optically thick electron-positron plasma created in the dyadosphere self-propels itself outward reaching ultrarelativistic velocities (Ruffini et al. [27]) and then interacts with the baryonic matter of the remnant of the progenitor star. The baryonic matter component M_B is the second free parameter of the EMBH theory: $B = M_B c^2/E_{dya} = 4.8 \times 10^{-3}$. The $e+$-e^--photon-baryon plasma by further expansion becomes optically thin (Ruffini et al. [28]). As the transparency condition is reached, the Proper-GRB (P-GRB) is emitted with an extremely relativistic shell of Accelerated Baryonic Matter (the ABM pulse) with initial Lorentz gamma factor of $\gamma = 183.6$. It is this ABM pulse which produces the afterglow through its interaction with the ISM, whose average density is best fitted by $< n_{ism} >= 1$ particle/cm^3. In such a collision the "fully radiative condition" is implemented (for details see Ruffini et al. [5]): the internal energy ΔE_{int} which results is instantaneously radiated away.

We have recently assumed that the radiation emitted in the collision between the ABM pulse and the ISM has a thermal spectrum measured in the ABM pulse comoving frame (Ruffini et al. [18]). In our approach the source luminosity is derived from an infinite set of foliations of events on the EQTS, each one characterized by a different thermal spectrum in the comoving frame boosted by a different relativistic transformation obtained from the EOM. The third free parameter of the EMBH theory describes this process of generating the thermal spectrum in the comoving frame. It is given by $1.1 \times 10^{-7} < R = A_{eff}/A_{abm} < 5.0 \times 10^{-11}$, where A_{abm} is the ABM pulse external surface area and A_{eff} is the ABM pulse effective emitting area.

We can then obtain for the GRB030329 the luminosities in given energy bands, computed in the range 2-400 keV with very high accuracy. Fig. 1 shows the results for the luminosities in the 30-400 keV and 2-10 keV bands. Subsequently, the theoretically predicted GRB spectra have been evaluated at selected values of the arrival time [19].

We can now compare these results with those for GRB980425/SN1998bw (Ruffini et al. [6]). We conclude that:

a) The intensity of the GRB versus the Supernova, comparable in the case of GRB980425, becomes 2×10^3 times larger in the case of GRB030329. This crucial fact clearly indicates beyond any doubt the independence of the GRB phenomenon from the Supernova (Ruffini et al. [10]). Moreover, the GRB is generally energetically dominant on the supernova; either the GRB is triggering an induced-supernova event or both the GRB and the Supernova are triggered by the same relativistic process. In no way the GRB can originate from the supernova.

b) In both systems the XMM observations point to the existence of an additional X-ray source, which we consider related to the Supernova phenomenon and not to the GRB. There is the distinct possibility that this source originates from the emission of a newly formed hot neutron star, cooling via generalized URCA processes (Ruffini et al. [6]). It has been recently proposed (Ruffini et al. [29]) to indicate this new physical and astrophysical systems as URCA-1 for GRB980425/SN1998bw and URCA-2 for GRB030329/SN2003dh. A dedicated campaign of observations with XMM is urgently needed in order to explore this unprecedented "triptych" astrophysical systems, formed by a GRB, an induced-supernova and possibly a newly born pulsating hot neutron star.

Details of this results are going to be published in [19].

REFERENCES

1. GCN Circ. 1997 (2003).
2. GCN Circ. 1996 (2003).
3. Tiengo, A., Mereghetti, S., Ghisellini, G., Rossi, E., Ghirlanda, G., and Schartel, N., *A&A*, **409**, 983 (2003).
4. Hjorth, J., Sollerman, J., Møller, P., Fynbo, J. P. U., Woosley, S. E., Kouveliotou, C., Tanvir, N. R., Greiner, J., Andersen, M. I., Castro-Tirado, A. J., Cerón, J. M. C., Fruchter, A. S., Gorosabel, J., Jakobsson, P., Kaper, L., Klose, S., Masetti, N., Pedersen, H., Pedersen, K., Pian, E., Palazzi, E., Rhoads, J. E., Rol, E., van den Heuvel, E. P. J., Vreeswijk, P. M., Watson, D., and Wijers, R. A. M. J., *Nature*, **423**, 847 (2003).
5. Ruffini, R., Bianco, C. L., Chardonnet, P., Fraschetti, F., Vitagliano, L., and Xue, S.-S., "New Perspectives in Physics and Astrophysics from the Theoretical Understanding of Gamma-Ray Bursts," in *COSMOLOGY AND GRAVITATION: X^{th} Brazilian School of Cosmology and Gravitation; 25^{th} Anniversary (1977-2002)*, edited by M. Novello and S. E. P. Bergliaffa, AIP, New York, 2003, vol. 668, p. 16.
6. Ruffini, R., Bernardini, M. G., Bianco, C. L., Chardonnet, P., Fraschetti, F., and Xue, S.-S., "GRB 980425, SN1998bw and the EMBH Model," in *Proceedings of the 34th COSPAR Scientific Assembly*, edited by E. Pian, N. Masetti, and L. Piro, Elsevier, 2003, in press.
7. Pian, E., and et al., "," in *Proceedings of the 34th COSPAR Scientific Assembly*, edited by E. Pian, N. Masetti, and L. Piro, Elsevier, 2003, in press.
8. Ruffini, R., Bianco, C. L., Chardonnet, P., Fraschetti, F., and Xue, S.-S., *ApJ Lett.*, **555**, L107 (2001).
9. Ruffini, R., Bianco, C. L., Chardonnet, P., Fraschetti, F., and Xue, S.-S., *ApJ Lett.*, **555**, L113 (2001).
10. Ruffini, R., Bianco, C. L., Chardonnet, P., Fraschetti, F., and Xue, S.-S., *ApJ Lett.*, **555**, L117 (2001).
11. Ruffini, R., Bianco, C. L., Chardonnet, P., Fraschetti, F., and Xue, S.-S., *ApJ Lett.*, **581**, L19 (2002).
12. Rees, M. J., and Mészáros, P., *MNRAS*, **258**, 41p (1992).
13. Piran, T., *Phys. Rep.*, **314**, 575–667 (1999).
14. van Paradijs, J., Kouveliotou, C., and Wijers, R. A. M. J., *Ann. Rev. Astron. Astroph.*, **38**, 379 (2000).
15. Mészáros, P., *Ann. Rev. Astron. Astroph.*, **40**, 137 (2002).
16. Bianco, C. L., and Ruffini, R., On the analytic expressions for the equitemporal surfaces in gamma-ray burst afterglows (2004), submitted to A&A.
17. Ruffini, R., Bianco, C. L., Chardonnet, P., Fraschetti, F., and Xue, S.-S., Is there any beaming in GRBs? (2003), submitted to Phys. Rev. Lett.
18. Ruffini, R., Bianco, C. L., Chardonnet, P., Fraschetti, F., Gurzadyan, V. G., and Xue, S.-S., On the instantaneous spectrum of gamma-ray bursts (2004), iJMPD in press.
19. Ruffini, R., Bernardini, M. G., Bianco, C. L., Chardonnet, P., Fraschetti, F., and Xue, S.-S. (2004), in preparation.
20. Damour, T., and Ruffini, R., *Phys. Rev. Lett.*, **35**, 463–466 (1975).
21. Ruffini, R., "Beyond the Critical Mass: The Dyadosphere of Black Holes," in *Black Holes and High Energy Astrophysics, Proceedings of the 49th Yamada Conference*, edited by H. Sato and N. Sugiyama, Universal Ac. Press, Tokyo, 1998.
22. Preparata, G., Ruffini, R., and Xue, S.-S., *A&A*, **338**, L87–L90 (1998).
23. Cherubini, C., Ruffini, R., and Vitagliano, L., *Phys. Lett. B*, **545**, 226 (2002).
24. Ruffini, R., and Vitagliano, L., *Phys. Lett. B*, **545**, 233 (2002).
25. Ruffini, R., and Vitagliano, L., *Int. Journ. Mod. Phys. D*, **12**, 121 (2003).
26. Ruffini, R., Vitagliano, L., and Xue, S.-S., *Phys. Lett. B*, **559**, 12 (2003).
27. Ruffini, R., Salmonson, J. D., Wilson, J. R., and Xue, S.-S., *A&A*, **350**, 334–343 (1999).
28. Ruffini, R., Salmonson, J. D., Wilson, J. R., and Xue, S.-S., *A&A*, **359**, 855 (2000).
29. Ruffini, R., Bernardini, M. G., Bianco, C. L., Chardonnet, P., Fraschetti, F., and Xue, S.-S., "," in *Proceedings of the Tenth Marcel Grossmann Meeting on General Relativity*, edited by V. G. Gurzadyan, R. T. Jantzen, and R. Ruffini, World Scientific, Singapore, 2003.

21 Appendix 14

International Journal of Modern Physics D

Observational signatures of an electromagnetic overcritical gravitational collapse

REMO RUFFINI

ICRA — International Center for Relativistic Astrophysics and Dipartimento di Fisica, Università di Roma "La Sapienza", Piazzale Aldo Moro 5, I-00185 Roma, Italy.

FEDERICO FRASCHETTI

ICRA — International Center for Relativistic Astrophysics and Dipartimento di Fisica, Università di Trento, Via Sommarive 14, I-38050 Povo (Trento), Italy.

LUCA VITAGLIANO

ICRA — International Center for Relativistic Astrophysics and Dipartimento di Fisica, Università di Roma "La Sapienza", Piazzale Aldo Moro 5, I-00185 Roma, Italy.

SHE-SHENG XUE

ICRA — International Center for Relativistic Astrophysics and Dipartimento di Fisica, Università di Roma "La Sapienza", Piazzale Aldo Moro 5, I-00185 Roma, Italy.

Received Day Month Year
Revised Day Month Year

We present theoretical predictions for the spectral, temporal and intensity signatures of the electromagnetic radiation emitted during the process of the gravitational collapse of a stellar core to a black hole, during which electromagnetic field strengths rise over the critical value for e^+e^- pair creation. The last phases of this gravitational collapse are studied, leading to the formation of a black hole with a subcritical electromagnetic field, likely with zero charge, and an outgoing pulse of initially optically thick e^+e^--photon plasma. Such a pulse reaches transparency at Lorentz gamma factors of 10^2–10^4. We find a clear signature in the outgoing electromagnetic signal, drifting from a soft to a hard spectrum, on very precise time-scales and with a very specific intensity modulation. The relevance of these theoretical results for the understanding of short gamma-ray bursts is outlined.

Keywords: EMBH — electron-positron plasma — gravitational collapse — gamma-ray bursts

1. Introduction

The discovery in 1997 of the afterglows of Gamma-Ray Bursts (GRBs) [1] has evidenced the cosmological nature of these sources. By the analysis of the first and second BATSE catalogs[a] Tavani in 1998 [2] confirmed the existence of two families of

[a]see http://cossc.gsfc.nasa.gov/batse/

GRBs: the so-called "long-bursts" with a soft spectrum and duration $\Delta t > 2.5$sec and the "short-bursts" with harder spectrum and duration $\Delta t < 2.5$sec. In 2001 the theory was advanced [3] that both short-bursts and long-bursts originate from the same underlying physical process due to the vacuum polarization of electromagnetic overcritical gravitational collapse leading to the creation of $e^+ - e^-$ pairs at the expenses of the extractable energy of a black hole [4]. The difference between the short-bursts and long-bursts in this theory is mainly due to the amount of baryonic matter encountered by the e^+e^- pairs in their relativistic expansion. A support of such a theory was given by Schmidt [5] showing that short-bursts and long-bursts have the same isotropic-equivalent characteristic peak luminosity.

In recent work we have systematically developed the theoretical background of a process of gravitational collapse of matter involving an electromagnetic field with field strength higher than the critical value for e^+e^- pair creation [6,7,8,9,10,11]. The goal has been to clarify the physical nature of the process of extracting the mass energy of a black hole by the creation of e^+e^- matter pairs [4] and to analyze the electromagnetic radiation emission process during the transient dynamical phases of the gravitational collapse leading to the final formation of the black hole.

In this letter we conclude this analysis by making precise predictions for the spectra, the energy fluxes and characteristic time-scales of the radiation for short-bursts. If the precise luminosity variation and spectral hardening of the radiation we have predicted will be confirmed by observations of short-bursts, these systems will play a major role as standard candles in cosmology.

These considerations will also be relevant for the analysis of the long-bursts when the baryonic matter contribution will be taken into account.

2. The model

The idea that the origin of GRBs is related to the energy extractable from a black hole [4] by process of vacuum polarization [12,13,14] and the creation of e^+e^- plasma was advanced in 1974 by Damour and Ruffini [16]. The basic considerations on the dynamics of the e^+e^- plasma in the context of GRBs were outlined in 1978 by Cavallo and Rees [15], without addressing the issue of the origin of this plasma. In 1998 [17] these concepts were further evolved by the identification of the region around an already formed black hole in which such e^+e^- plasma can be created and the concept of "dyadosphere" was introduced.

In this letter for the first time we present progress in describing the expected radiation from the dynamical formation of the dyadosphere in the process of gravitational collapse.

The dynamics of the collapse of an electrically-charged stellar core, separating itself from an oppositely charged remnant in an initially neutral star, was first modelled by an exact solution of the Einstein-Maxwell equations corresponding to a shell of charged matter in Ref. [6]. The fundamental dynamical equations and their analytic solutions were obtained, revealing the amplification of the electromagnetic

field strength during the process of collapse and the asymptotic approach to the final static configuration. The results, which properly account for general relativistic effects, are summarized in Fig. 1 and Fig. 2 of Ref. [6].

A first step toward the understanding of the process of extracting energy from a black hole was obtained in Ref. [7], where it was shown how the extractable electromagnetic energy is not stored behind the horizon but is actually distributed all around the black hole. Such a stored energy is in principle extractable, very efficiently, on time-scales $\sim \hbar/m_e c^2$, by a vacuum polarization process *à là* Sauter-Heisenberg-Euler-Schwinger [12,13,14]. Such a process occurs if the electromagnetic field becomes larger than the critical field strength $\mathcal{E}_{\rm c}$ for e^+e^- pair creation. In Ref. [7] we followed the approach of Damour and Ruffini [16] in order to evaluate the energy density and the temperature of the created e^+e^--photon plasma. As a byproduct, a formula for the irreducible mass of a black hole was also derived solely in terms of the gravitational, kinetic and rest mass energies of the collapsing core. This surprising result allowed us in Ref. [8] to obtain a deeper understanding of the maximum limit for the extractable energy during the process of gravitational collapse, namely 50% of the initial energy of the star: the well known result of a 50% maximum efficiency for energy extraction in the case of a Reissner-Nordström black hole [4] then becomes a particular case of a process of much more general validity.

The crucial issue of the survival of the electric charge of the collapsing core in the presence of a copious process of e^+e^- pair creation was addressed in Refs. [9,10]. By using theoretical techniques borrowed from plasma physics and statistical mechanics [19,20,21,22,23,24,25] based on a generalized Vlasov equation, it was possible to show that while the core keeps collapsing, the created e^+e^- pairs are entangled in the overcritical electric field. The electric field itself, due to the back reaction of the created e^+e^- pairs, undergoes damped oscillations in sign finally settling down to the critical value $\mathcal{E}_{\rm c}$. The pairs fully thermalize to an e^+e^--photon plasma on time-scales typically of the order of 10^2–$10^4\hbar/m_e c^2$. During this characteristic damping time, which we recall is much larger than the pair creation time-scale $\hbar/m_e c^2$, the core moves inwards, collapsing with a speed 0.2–0.8c, further amplifying the electric field strength at its surface and enhancing the pair creation process.

Turning now to the dynamical evolution of such an e^+e^- plasma we recall that, after some original attempt to consider a steady state emission [26,27], the crucial progress was represented by the understanding that during the optically thick phase such a plasma expands as a thin shell. There exists a fundamental relation between the width of the expanding shell and the Lorentz gamma factor. The shell expands, but the Lorentz contraction is such that its width in laboratory frame appears to be constant. Such a result was found in [28] on the basis of a numerical approach, further analyzed in Bisnovatyi-Kogan and Murzina [29] on the basis of an analytic approach. Attention to the role of the rate equations governing the e^+e^- annihilation were given in [30], where approximations to the full equation were introduced. These results were improved in two important respects in 1999 and 2000 [31,32]: the initial conditions were made more accurate by the considerations

of the dyadosphere as well as the dynamics of the shell was improved by the self-consistent solution of the hydrodynamical equation and the rate equation for the e^+e^- plasma following both an analytic and numerical approach.

We are now ready to report in this letter the result of using the approach in [31,32] in this general framework describing the dynamical formation of the dyadosphere.

The first attempt to analyze the expansion of the newly generated and thermalized e^+e^--photon plasma was made in Ref. [11]. The initial dynamical phases of the expansion were analyzed, using the general relativistic equations of Ref. [6] for the gravitational collapse of the core. A *separatrix* was found in the motion of the plasma at a critical radius $\bar{R}$: the plasma created at radii larger than $\bar{R}$ expands to infinity, while the one created at radii smaller than $\bar{R}$ is trapped by the gravitational field of the collapsing core and implodes towards the black hole. The value of $\bar{R}$ was found in Ref. [11] to be $\bar{R} = 2GM/c^2[1 + \left(1 - 3Q^2/4GM^2\right)^{1/2}]$, where M and Q are the mass and the charge of the core, respectively.

In this letter we pursue further the evolution of such a system, describing the dynamical phase of the expansion of the pulse of the optically thick plasma all the way to the point where the transparency condition is reached. Some pioneering work in this respect were presented in Goodman in 1986 [33]. In this process the pulse reaches ultrarelativistic regimes with Lorentz factor $\gamma \sim 10^2$–10^4. The spectra, the luminosities and the time-sequences of the electromagnetic signals captured by a far-away observer are analyzed here in detail for the first time. The relevance of these theoretical results for short-bursts is then discussed.

3. The expansion of the $e^+e^-\gamma$ plasma as a discrete set of elementary slabs

We discretize the gravitational collapse of a spherically symmetric core of mass M and charge Q by considering a set of events along the world line of a point of fixed angular position on the collapsing core surface. Between each of these events we consider a spherical shell slab of plasma of constant coordinate thickness Δr so that:

(1) Δr is assumed to be a constant which is small with respect to the core radius;
(2) Δr is assumed to be large with respect to the mean free path of the particles so that the statistical description of the $e^+e^-\gamma$ plasma can be used;
(3) There is no overlap among the slabs and their union describes the entirety of the process.

We check that the final results are independent of the special value of the chosen Δr.

In order to describe the dynamics of the expanding plasma pulse the energy-momentum conservation law and the rate equation for the number of pairs in the Reissner-Nordström geometry external to the collapsing core have to be integrated:

$$T^{\mu\nu}{}_{;\mu} = 0, \tag{1}$$

$$\left(n_{e^+e^-}u^\mu\right)_{;\mu} = \overline{\sigma v}\left[n^2_{e^+e^-}\left(T\right) - n^2_{e^+e^-}\right], \tag{2}$$

where $T^{\mu\nu} = \left(\epsilon + p\right)u^\mu u^\nu + pg^{\mu\nu}$ is the energy-momentum tensor of the plasma with proper energy density ϵ and proper pressure p, u^a is the fluid 4-velocity, $n_{e^+e^-}$ is the pair number density, $n_{e^+e^-}\left(T\right)$ is the equilibrium pair number density at the temperature T of the plasma and $\overline{\sigma v}$ is the mean of the product of the e^+e^- annihilation cross-section and the thermal velocity of the pairs. We use Eqs. (1) and (2) to study the expansion of each slab, following closely the treatment developed in Refs [31,32] where it was shown how a homogeneous slab of plasma expands as a pair-electromagnetic pulse (PEM pulse) of constant thickness in the laboratory frame. Two regimes can be identified in the expansion of the slabs:

(1) In the initial phase of expansion the plasma experiences the strong gravitational field of the core and a fully general relativistic description of its motion is needed. The plasma is sufficiently hot in this first phase that the e^+e^- pairs and the photons remain at thermal equilibrium in it. As shown in Ref. [11], under these circumstances, the right hand side of Eqs. (2) is effectively 0 and Eqs. (1) and (2) are equivalent to:

$$\begin{aligned}\left(\frac{dr}{cdt}\right)^2 &= \alpha^4\left[1 - \left(\frac{n_{e^+e^-}}{n_{e^+e^-0}}\right)^2\left(\frac{\alpha_0}{\alpha}\right)^2\left(\frac{r}{r_0}\right)^4\right], \\ \left(\frac{r}{r_0}\right)^2 &= \left(\frac{\epsilon+p}{\epsilon_0}\right)\left(\frac{n_{e^+e^-0}}{n_{e^+e^-}}\right)^2\left(\frac{\alpha}{\alpha_0}\right)^2 - \frac{p}{\epsilon_0}\left(\frac{r}{r_0}\right)^4,\end{aligned} \tag{3}$$

where r is the radial coordinate of a slab of plasma, $\alpha = \left(1 - 2MG/c^2r + Q^2G/c^4r^2\right)^{1/2}$ is the gravitational redshift factor and the subscript "0" refers to quantities evaluated at the initial time.

(2) At asymptotically late times the temperature of the plasma drops below an equivalent energy of 0.5 MeV and the e^+e^- pairs and the photons can no longer be considered to be in equilibrium: the full rate equation for pair annihilation needs to be used. However, the plasma is so far from the central core that gravitational effects can be neglected. In this new regime, as shown in Ref. [31], Eqs. (1) and (2) reduce to:

$$\begin{aligned}\frac{\epsilon_0}{\epsilon} &= \left(\frac{\gamma\mathcal{V}}{\gamma_0\mathcal{V}_0}\right)^\Gamma, \\ \frac{\gamma}{\gamma_0} &= \sqrt{\frac{\epsilon_0\mathcal{V}_0}{\epsilon\mathcal{V}}}, \\ \frac{\partial}{\partial t}N_{e^+e^-} &= -N_{e^+e^-}\frac{1}{\mathcal{V}}\frac{\partial\mathcal{V}}{\partial t} + \overline{\sigma v}\frac{1}{\gamma^2}\left[N^2_{e^+e^-}\left(T\right) - N^2_{e^+e^-}\right],\end{aligned} \tag{4}$$

where $\Gamma = 1 + p/\epsilon$, $\mathcal{V}$ is the volume of a single slab as measured in the laboratory frame by an observer at rest with the black hole, $N_{e^+e^-} = \gamma n_{e^+e^-}$ is the pair number density as measured in the laboratory frame by an observer at rest with the black hole, and $N_{e^+e^-}\left(T\right)$ is the equilibrium laboratory pair number density.

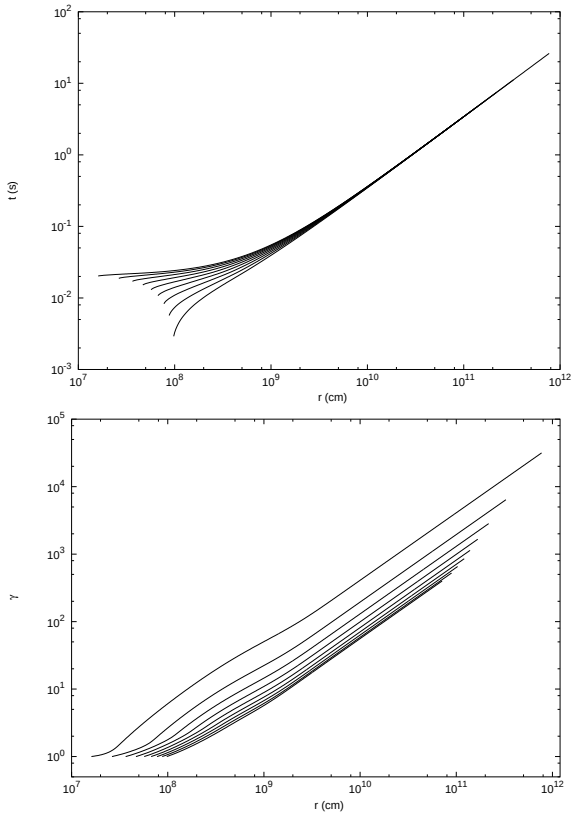

Fig. 1. Expansion of the plasma created around an overcritical collapsing stellar core with $M = 10M_\odot$ and $Q = 0.1\sqrt{G}M$. Upper diagram: world lines of the plasma. Lower diagram: Lorentz γ factor as a function of the radial coordinate r.

4. The reaching of transparency and the signature of the outgoing gamma ray signal

Eqs. (3) and (4) must be separately integrated and the solutions matched at the transition between the two regimes. The integration stops when each slab of plasma reaches the optical transparency condition given by

$$\int_0^{\Delta r} \sigma_T n_{e^+e^-} dr \sim 1\,, \tag{5}$$

where σ_T is the Thomson cross-section and the integral extends over the radial thickness Δr of the slab. The evolution of each slab occurs without any collision

or interaction with the other slabs; see the upper diagram in Fig. 1. The outer layers are colder than the inner ones and therefore reach transparency earlier; see the lower diagram in Fig. 1. In Fig. 1, Eqs. (3) and (4) have been integrated for a core with

$$M = 10M_{\odot}, \quad Q = 0.1\sqrt{G}M; \tag{6}$$

the upper diagram represents the world lines of the plasma as functions of the radius, while the lower diagram shows the corresponding Lorentz γ factors. The overall independence of the result of the dynamics on the number N of the slabs adopted in the discretization process or analogously on the value of Δr has also been checked. We have repeated the integration for $N = 10$, $N = 100$ reaching the same result to extremely good accuracy. The results in Fig. 1 correspond to the case $N = 10$.

We now turn to the results in Fig. 2, where we plot both the theoretically predicted luminosity L and the spectral hardness of the signal reaching a far-away observer as functions of the arrival time t_a. Since all three of these quantities depend in an essential way on the cosmological redshift factor z, see Refs. [35,36], we have adopted a cosmological redshift $z = 1$ for this figure.

As the plasma becomes transparent, gamma ray photons are emitted. The energy $\hbar\omega$ of the observed photon is $\hbar\omega = k\gamma T/(1+z)$, where k is the Boltzmann constant, T is the temperature in the comoving frame of the pulse and γ is the Lorentz factor of the plasma at the transparency time. We also recall that if the initial zero of time is chosen as the time when the first photon is observed, then the arrival time t_a of a photon at the detector in spherical coordinates centered on the black hole is given by [35,36]:

$$t_a = (1+z)\left[t + \tfrac{r_0}{c} - \tfrac{r(t)}{c}\cos\theta\right] \tag{7}$$

where $(t, r(t), \theta, \phi)$ labels the laboratory emission event along the world line of the emitting slab and r_0 is the initial position of the slab. The projection of the plot in Fig. 2 onto the t_a-L plane gives the total luminosity as the sum of the partial luminosities of the single slabs. The sudden decrease of the intensity at the time $t = 0.040466$ s corresponds to the creation of the *separatrix* introduced in Ref. [10]. We find that the duration of the electromagnetic signal emitted by the relativistically expanding pulse is given in arrival time by

$$\Delta t_a \sim 5 \times 10^{-2}\mathrm{s}. \tag{8}$$

The projection of the plot in Fig. 2 onto the kT_{obs}, t_a plane describes the temporal evolution of the spectral hardness. We observe a precise soft-to-hard evolution of the spectrum of the gamma ray signal from $\sim 10^2$ KeV monotonically increasing to ~ 1 MeV. We recall that $kT_{\mathrm{obs}} = k\gamma T/(1+z)$.

The above quantities are clearly functions of the cosmological redshift z, of the charge Q and the mass M of the collapsing core. We present in Fig. 3 the arrival

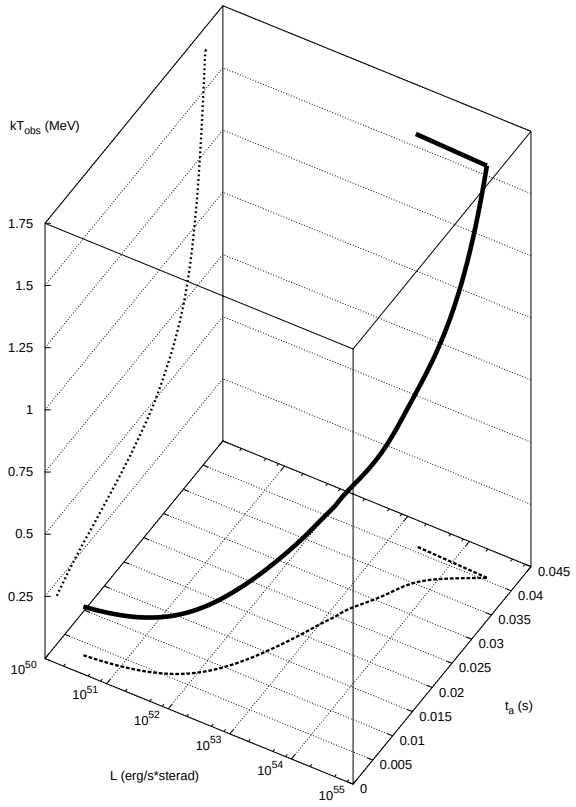

Fig. 2. Predicted observed luminosity and observed spectral hardness of the electromagnetic signal from the gravitational collapse of a collapsing core with $M = 10M_\odot$, $Q = 0.1\sqrt{G}M$ at $z = 1$ as functions of the arrival time t_a.

time interval for M ranging from $M \sim 10M_\odot$ to $10^3 M_\odot$, keeping $Q = 0.1\sqrt{G}M$. The arrival time interval is very sensitive to the mass of the black hole:

$$\Delta t_a \sim 10^{-2} - 10^{-1}\mathrm{s}\,. \tag{9}$$

Similarly the spectral hardness of the signal is sensitive to the ratio $Q/\sqrt{G}M$ [37]. Moreover the duration, the spectral hardness and luminosity are all sensitive to the cosmological redshift z (see Ref. [37]). All the above quantities can also be sensitive to a possible baryonic contamination of the plasma due to the remnant of the progenitor star which has undergone the process of gravitational collapse.

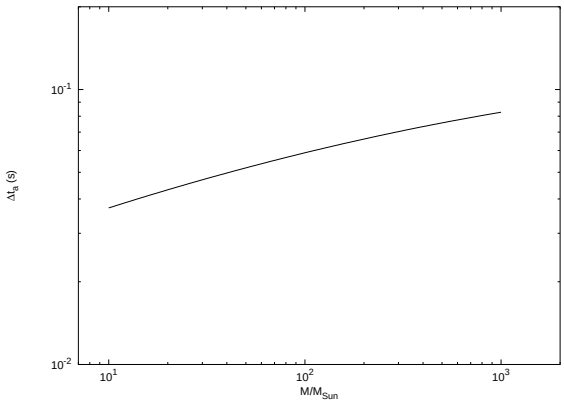

Fig. 3. Arrival time duration of the electromagnetic signal from the gravitational collapse of a stellar core with charge $Q = 0.1\sqrt{G}M$ as a function of the mass M of the core.

5. Conclusions

The above results were obtained considering e^+e^- plasma without any baryonic contamination and are therefore directly relevant for short-bursts [3]. The characteristic spectra, time variabilities and luminosities of the electromagnetic signals from collapsing overcritical stellar cores, here derived from first principles, agrees very closely with the observations of short-bursts [38]. New space missions must be planned, with temporal resolution down to fractions of μs and higher collecting area and spectral resolution than at present, in order to verify the detailed agreement between our model and the observations. It is now clear that if our theoretical predictions will be confirmed, we would have a very powerful tool for cosmological observations: the independent information about luminosity, time-scale and spectrum can uniquely determine the mass, the electromagnetic structure and the distance from the observer of the collapsing core, see e.g. Fig. 3 and Ref. [37]. In that case short-bursts may become the best example of standard candles in cosmology [39]. The introduction we are currently analysing is the introduction of baryonic matter in the optically thick phase of the expansion of the e^+e^- plasma which can affect the structure of the Proper-GRB (P-GRB) [40] as well as the structure of the long-bursts [41].

An interesting proposal was advanced in 2002 [42] that the e^+e^- plasma may have a fundamental role as well in the physical process generating jets in the extragalactic radio sources. The concept of dyadosphere originally introduced in Reissner-Nordström black hole in order to create the e^+e^- plasma relevant for GRBs can also be generalized to the process of vacuum polarization originating in a Kerr-Newman black hole due to magneto-hydrodynamical process of energy extraction

(see e.g. [43] and references therein). The concept therefore introduced in this letter becomes relevant for both the extraction of rotational and electromagnetic energy from the most general black hole [4].

After the submission of this letter we have become aware that Ghirlanda et al. [44] have given evidence for the existence of an exponential cut off at high energies in the spectra of short bursts. We are currently comparing and contrasting these observational results with the predicted cut off in Fig. 2 which results from the existence of the separatrix introduced in [9]. The observational confirmation of the results presented in Fig. 2 would lead for the first time to the identification of a process of gravitational collapse and its general relativistic self-closure as seen from an asymptotic observer.

References

1. E. Costa et al., *Nature* **387** 783 (1997).
2. M. Tavani, *ApJ Lett.* **497** L21 (1998).
3. R. Ruffini, C.L. Bianco, P. Chardonnet, F. Fraschetti, S.-S. Xue, *ApJ Lett.* **555** L113 (2001)
4. D. Christodoulou, R. Ruffini, *Phys. Rev. D* **4** 3552 (1971).
5. M. Schmidt, *ApJ Lett.* **559** L79 (2001).
6. C. Cherubini, R. Ruffini, L. Vitagliano, *Phys. Lett. B* **545** 226 (2002).
7. R. Ruffini, L. Vitagliano, *Phys. Lett. B* **545** 233 (2002).
8. R. Ruffini, L. Vitagliano, *Int. J. Mod. Phys. D* **12** 121 (2003).
9. R. Ruffini, L. Vitagliano, S.-S. Xue, *Phys. Lett.* **B573** 33 (2003).
10. R. Ruffini, L. Vitagliano, S.-S. Xue, Quantum Aspects of Beam Physics, *28th Advanced IFCA Beam Dynamics Workshop*, Ed. Pisin Chen, (World Scientific, Singapore, 2003) *in press*; astro-ph/0304306.
11. R. Ruffini, L. Vitagliano, S.-S. Xue, *Phys. Lett. B* **559** 12 (2003).
12. F. Sauter, *Zeits. Phys.* **69** 742 (1931).
13. W. Heisenberg, H. Euler, *Zeits. Phys.* **98** 714 (1935).
14. J. Schwinger, *Phys. Rev.* **82** 664 (1951).
15. G. Cavallo, M. Rees, *Mon. Not. R. Astron. Soc.* **183** 359 (1978).
16. T. Damour, R. Ruffini, *Phys. Rev. Lett.*, **35** 463 (1975).
17. G. Preparata, R. Ruffini, S.-S. Xue, *A&A* **338** L87 (1998).
18. K. Kajantie, T. Matsui, *Phys. Lett. B* **164** 373 (1985).
19. G. Gatoff, A. K. Kerman, T. Matsui, *Phys. Rev. D* **36** 114 (1987).
20. Y. Kluger, J. M. Eisenberg, B. Svetitsky, F. Cooper, E. Mottola, *Phys. Rev. Lett.* **67** 2427 (1991).
21. Y. Kluger, J. M. Eisenberg, B. Svetitsky, F. Cooper, E. Mottola, *Phys. Rev. D* **45** 4659 (1992).
22. F. Cooper, J. M. Eisenberg, Y. Kluger, E. Mottola, B. Svetitsky, *Phys. Rev. D* **48** 190 (1993).
23. Y. Kluger, E. Mottola and J.M. Eisenberg, *Phys. Rev. D* **58** 125015 (1998).
24. S. M. Schmidt et al., *Int. J. Mod. Phys. E* **7** 709 (1998).
25. J. C. R. Bloch et al., *Phys. Rev. D* **60** 116011 (1999).
26. B. Paczyński, *ApJ Lett.* **308** L43 (1986).
27. B. Paczyński, *ApJ Lett.* **363** 218 (1990).
28. T. Piran, A. Shemi, R. Narayan, *Mon. Not. R. Astron. Soc.* **263** 861 (1993).
29. G. S. Bisnovatyi-Kogan, M. V. A. Murzina, *Phys. Rev. D* **52** 4380 (1995).

30. O.M. Grimsrud, I Wasserman, *Mon. Not. R. Astron. Soc.* **300** 1158 (1998).
31. R. Ruffini, J. D. Salmonson, J. R. Wilson, S.-S. Xue, *A&A* **350** 334 (1999).
32. R. Ruffini, J. D. Salmonson, J. R. Wilson, S.-S. Xue, *A&A* **359** 855 (2000).
33. J. Goodman *ApJ Lett.* **308** L47 (1986).
34. G. Preparata, R. Ruffini, S.-S. Xue, *J. Korean Phys. Soc.* **42** S99 (2003).
35. C. L. Bianco, R. Ruffini, S.-S. Xue, *A&A* **368** 377 (2001).
36. R. Ruffini, C. L. Bianco, P. Chardonnet, F. Fraschetti, S.-S. Xue, *Int. J. Mod. Phys. D* **12** 173 (2003).
37. R. Ruffini, F. Fraschetti, L. Vitagliano, S.-S. Xue, *in preparation.*
38. W. S. Paciesas et al. *ApJ Suppl.* **122** 465 (1999).
39. R. Ruffini, invited talk at "Frontiers in Astroparticle Physics and Cosmology", *6th RESCEU International Symposium*, Tokyo 2003.
40. R. Ruffini, C.L. Bianco, P. Chardonnet, F. Fraschetti, S.-S. Xue, *ApJ Lett.* **555** L107 (2001).
41. R. Ruffini, C.L. Bianco, P. Chardonnet, F. Fraschetti, L. Vitagliano and S.-S. Xue, in *Proceedings of the* X^{th} *Brazilian School of Cosmology and Gravitation*, M. Novello, S.E. Perez Bergliaffa, editors, AIP Conference proceedings 668, 16 (2003).
42. S. Iwamoto and F. Takahara, *ApJ* **565** 163 (2002).
43. B. Punsly, *Black Hole Gravitohydromagnetics, (Astronomy and Astrophysics Library)*, Springer-Verlag (2001).
44. G. Ghirlanda, G. Ghisellini and A. Celotti, pre-print: astro-ph/0310861.